frontiers | Research Topics

Molecular advances in diagnosis and treatment of CNS tumors, volume II

Edited by
Liam Chen and Zhaohui Zhang

Published in
Frontiers in Oncology
Frontiers in Neurology

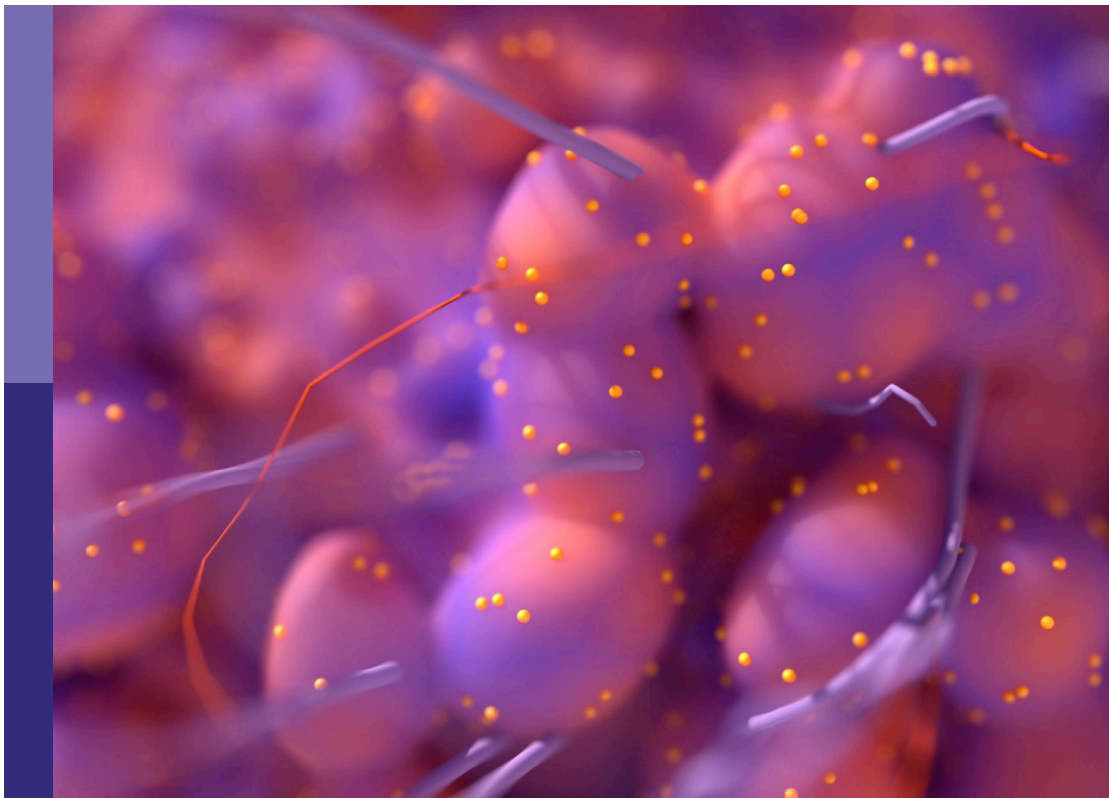

ISSN 1664-8714
ISBN 978-2-83251-655-3
DOI 10.3389/978-2-83251-655-3

About Frontiers

Frontiers is more than just an open access publisher of scholarly articles: it is a pioneering approach to the world of academia, radically improving the way scholarly research is managed. The grand vision of Frontiers is a world where all people have an equal opportunity to seek, share and generate knowledge. Frontiers provides immediate and permanent online open access to all its publications, but this alone is not enough to realize our grand goals.

Frontiers journal series

The Frontiers journal series is a multi-tier and interdisciplinary set of open-access, online journals, promising a paradigm shift from the current review, selection and dissemination processes in academic publishing. All Frontiers journals are driven by researchers for researchers; therefore, they constitute a service to the scholarly community. At the same time, the *Frontiers journal series* operates on a revolutionary invention, the tiered publishing system, initially addressing specific communities of scholars, and gradually climbing up to broader public understanding, thus serving the interests of the lay society, too.

Dedication to quality

Each Frontiers article is a landmark of the highest quality, thanks to genuinely collaborative interactions between authors and review editors, who include some of the world's best academicians. Research must be certified by peers before entering a stream of knowledge that may eventually reach the public - and shape society; therefore, Frontiers only applies the most rigorous and unbiased reviews. Frontiers revolutionizes research publishing by freely delivering the most outstanding research, evaluated with no bias from both the academic and social point of view. By applying the most advanced information technologies, Frontiers is catapulting scholarly publishing into a new generation.

What are Frontiers Research Topics?

Frontiers Research Topics are very popular trademarks of the *Frontiers journals series*: they are collections of at least ten articles, all centered on a particular subject. With their unique mix of varied contributions from Original Research to Review Articles, Frontiers Research Topics unify the most influential researchers, the latest key findings and historical advances in a hot research area.

Find out more on how to host your own Frontiers Research Topic or contribute to one as an author by contacting the Frontiers editorial office: frontiersin.org/about/contact

Molecular advances in diagnosis and treatment of CNS tumors, volume II

Topic editors

Liam Chen — University of Minnesota, United States

Zhaohui Zhang — Renmin Hospital of Wuhan University, China

Citation

Chen, L., Zhang, Z., eds. (2023). *Molecular advances in diagnosis and treatment of CNS tumors, volume II*. Lausanne: Frontiers Media SA.

doi: 10.3389/978-2-83251-655-3

Table of contents

frontiers | Frontiers in Oncology

TYPE Editorial
PUBLISHED 30 January 2023
DOI 10.3389/fonc.2023.1146805

OPEN ACCESS

EDITED AND REVIEWED BY
David D. Eisenstat,
Royal Children's Hospital, Australia

*CORRESPONDENCE
Liam Chen
llchen@umn.edu

SPECIALTY SECTION
This article was submitted to Neuro-Oncology and Neurosurgical Oncology, a section of the journal Frontiers in Oncology

RECEIVED 17 January 2023
ACCEPTED 23 January 2023
PUBLISHED 30 January 2023

CITATION
Chen C and Chen L (2023) Editorial: Molecular advances in diagnosis and treatment of CNS tumors, volume II. *Front. Oncol.* 13:1146805. doi: 10.3389/fonc.2023.1146805

Editorial: Molecular advances in diagnosis and treatment of CNS tumors, volume II

Clark Chen[1] and Liam Chen[2]*

[1]Department of Neurosurgery, University of Minnesota Medical School, Minneapolis, MN, United States, [2]Department of Pathology, University of Minnesota Medical School, Minneapolis, MN, United States

KEYWORDS

brain tumor, glioblastoma, glioma, astrocytic, embryonal

Editorial on the Research Topic
Molecular advances in diagnosis and treatment of CNS tumors, volume II

It's been barely two years since the publication of the first volume of the Research Topic "*Molecular advances in diagnosis and treatment of CNS tumors*" (Zhang et al.). In the last two years, researchers across the world continue to make great strides in the fight against the brain and spinal cord tumors. Here we are delighted to present the second volume of this research topic which includes ten original research articles, four review articles and one meta-analysis that cover several important themes:

Some of the manuscripts published in this volume concern studies that further elucidate the molecular pathobiology of particular CNS tumors. For IDH-wildtype diffuse astrocytic tumors in adults, the fifth edition of the WHO classification of CNS tumors considers IDH-wild type lower-grade glioma (LGG) as a provisional entity as tumors that conform to this diagnosis most likely can be reclassified as other tumors with additional genetic analyses. Indeed, Wang et al. showed that the differentially expressed genes in LGG patients were mainly enriched in metabolic pathways and pathways in cancer and in the function of signal transduction and positive regulation of GTPase activity, whereas in glioblastoma (GBM) patients, they were mainly enriched in the PI3K-Akt signaling pathway and in the functions of apoptotic process and oxidation-reduction process. Wang et al. studied the role of cancer-derived immunoglobulin G (cancer-IgG) in glioma which has been known to be associated with several malignancies such as breast cancer, colorectal cancer, and lung cancer. They found that the expression of cancer-IgG was higher in glioma and molecular subtypes with poor prognosis. The overall survival of patients with a high expression of cancer-IgG was worse in the stratified analysis. In addition, cancer-IgG may function in phagosome, antigen processing and presentation, extracellular matrix structural constituent, antigen binding, and collagen-containing extracellular matrix. Traditionally, the histology-based glioma classification is composed of multiple different molecular subtypes with distinct behavior,

prognosis, and response to therapy, and now each aspect can be assessed by corresponding emerging MR sequences like amide proton transfer-weighted MRI, inflow-based vascular-space-occupancy MRI, and radiomics informed algorithms. Indeed, Wei and Wei discussed these recent advances in MRI in their timely review to demonstrate that preoperative diagnosis of glioma has stepped into molecular and algorithm-assisted levels.

Epilepsy is a common clinical symptom in patients with glioma, which can impair neurocognitive function and quality of life. In the only meta-analysis study accepted in the second volume, Song et al. investigated the relationship between five commonly used tumor molecular markers and the incidence of perioperative epilepsy in patients with glioma. Their findings showed that isocitrate dehydrogenase 1 (IDH1) mutation was significantly correlated with the incidence of preoperative epilepsy, but not with intraoperative and postoperative epilepsy. There was no correlation between O6-methylguanine-DNA methyltransferase methylation and 1p/19q deletion and the incidence of perioperative epilepsy.

The rest of the accepted manuscripts studied other common CNS tumors. Liang et al. discovered that aurora kinase A and kinesin family member 20A may be involved in the initiation and development of medulloblastoma. Liu et al. studied the expression of tumor biomarkers and evaluate their clinical significance in non-functioning pituitary adenomas with different invasion patterns. Cathepsin K has the potential as a marker for sphenoid sinus invasion, whereas MMP9 and MMP2 may be markers for cavernous sinus invasion. Two comprehensive reviews, one by Zhang et al. on biomarkers associated with vestibular schwannoma growth, the other one by Ferguson et al. on the advances in leptomeningeal disease diagnosis with a focus on the role of circulating tumor DNA, have been included for readers' interests.

While CNS tumors can now be much more precisely characterized than a few years ago, the translation of this increased knowledge into more effective treatments is still seriously lagging behind. Three studies explored the benefits of promising antitumor therapeutic agents. Tsai et al. analyzed the impact of valproic acid (VPA) on GBM patient survival and its possible correlation with temozolomide (TMZ) treatment and p53 gene mutation. Their analysis of clinical data indicates that the survival benefit of a combined TMZ and VPA treatment in GBM patients is dependent on their p53 gene status. In cellular experiments, VPA enhanced the antineoplastic effect of TMZ by enhancing p53 activation and promoting the expression of its downstream pro-apoptotic protein, PUMA. Thus GBM patients with wild-type p53 may benefit from a combined TMZ+VPA treatment. In their seminal review, Bonafé et al. presented mounting evidence to argue that the effectiveness of four natural plant compounds, namely caffeine, dipotassium glycyrrhizinate (DPG), curcumin, and euphol is likely achieved through enhancing apoptosis-related pathways and cell cycle impairment in GBM cell lines. Furthermore, antitumoral effect of these plant compounds on GBM cell lines through microRNAs (miRNAs) modulation was investigated. Interestingly, only DPG and curcumin were found to be effective on miRNA modulation. The same group further evaluated in a separate study the expression profiles of miRNAs related to NF-κB suppression in the T98G GBM cell line after DPG exposure. The most over-expressed miRNAs were miR-4443 and miR-3620. Their results suggest that DPG inhibits cell viability by activating apoptosis and inhibiting cell proliferation and stem cell subpopulation formation through miR-4443 and miR-3620 upregulation. Both miRNAs are responsible for the post-transcriptional inhibition of NF-κB by CD209 and TNC modulation.

One study focused on identifying novel therapeutic targets for glioma. Through analysis of The Cancer Genome Atlas (TCGA) data, Ma et al. identified that OLFML2A is a key promotor of gliomagenesis. OLFML2A expression was significantly upregulated in glioma specimens and positively correlated with pathological grades and shorter overall survival in glioma patients. Mechanistically, OLFML2A downregulation inhibits Wnt/β-catenin signaling by upregulating amyloid precursor protein expression and reducing stabilized β-catenin levels, leading to the repression of MYC, CD44, and CSKN2A2 expression. By uncovering the oncogenic effects in human and rodent gliomas, their data support OLFML2A as a potential therapeutic target for glioma.

Finally, this volume includes three studies investigating the independent prognostic markers in CNS tumor. Primary central nervous system diffuse large B-cell lymphoma (PCNS-DLBCL) is an uncommon non-Hodgkin lymphoma subtype, and its clinical and pathological characteristics remain unclear. Qi et al. retrospectively evaluated PCNS-DLBCL patient data to determine clinical and pathological characteristics and prognostic factors. Multivariate analysis identified Ki-67 and CD3 as independent prognostic factors for survival. Moreover, multifocal lesions and deep brain involvement were unfavorable independent prognostic markers for progression-free survival. This study indicates that targeted drug development for adverse prognostic factors is possible and provides guidance for clinical treatment decision-making. He et al. showed that higher prognostic nutrition index (PNI) was an independent prognostic factor for grade IV glioma. Interestingly, they found that the nomogram including preoperative PNI, age, extent of resection, number of gliomas, and MGMT methylation status could predict the prognosis of patients with grade IV glioma well. Wang et al. selected five DNA damage repair genes (DDRGs) including CDK4, HMGB2, WEE1, SMC3 and GADD45G to construct a DDRGs signature for glioma. The survival analysis showed that the DDRGs signature could differentiate the outcome of the low- and high-risk groups. The immune microenvironment analysis revealed that more immunosuppressive cells, such as tumor associated macrophages and regulatory T cells, were recruited in the high-risk group. Therefore, the five DDRGs signature and its impact on the infiltration of immunosuppressive cells could potentially predict the prognosis.

In summary, in the second volume of the Research Topic entitled "Molecular Advances in Diagnosis and Treatment of CNS Tumors" a tremendous amount of information with relevance for neurooncology has been published. Hopefully, this collection of knowledge can be

exploited to help drastically improve the lives of patients that suffer from a CNS tumor.

Author contributions

All authors listed have made a substantial, direct, and intellectual contribution to the work and approved it for publication.

Acknowledgments

We are very grateful to all the authors who contributed to this Research Topic and for the interest shown by the scientific community.

Conflict of interest

The authors declare that the research was conducted in the absence of any commercial or financial relationships that could be construed as a potential conflict of interest.

Publisher's note

frontiers in Oncology

ORIGINAL RESEARCH
published: 28 May 2021
doi: 10.3389/fonc.2021.682932

A Prognostic DNA Damage Repair Genes Signature and Its Impact on Immune Cell Infiltration in Glioma

Guohui Wang[1,2†], Huandi Zhou[1,3†], Lei Tian[1†], Tianfang Yan[4], Xuetao Han[1], Pengyu Chen[5], Haonan Li[1], Wenyan Wang[1], Zhiqing Xiao[1], Liubing Hou[1,3] and Xiaoying Xue[1]*

[1] Department of Radiotherapy, The Second Hospital of Hebei Medical University, Shijiazhuang, China, [2] Department of Radiation Oncology, Peking University China-Japan Friendship School of Clinical Medicine, Beijing, China, [3] Department of Central Laboratory, The Second Hospital of Hebei Medical University, Shijiazhuang, China, [4] Department of Neurological Diagnosis and Restoration, Osaka University Graduate School of Medicine, Suita, Japan, [5] Department of Neurosurgery, Third Affiliated Hospital, Southern Medical University, Guangzhou, China

OPEN ACCESS

Edited by:
Liam Chen, University of Minnesota, United States

Reviewed by:
Antonino Scibilia, Universitaire de Strasbourg, France
Carlos Velásquez, Marqués de Valdecilla University Hospital, Spain

***Correspondence:**
Xiaoying Xue
xxy0636@163.com

†These authors have contributed equally to this work

Specialty section:
This article was submitted to Neuro-Oncology and Neurosurgical Oncology, a section of the journal Frontiers in Oncology

Received: *19 March 2021*
Accepted: *10 May 2021*
Published: *28 May 2021*

Citation:
Wang G, Zhou H, Tian L, Yan T, Han X, Chen P, Li H, Wang W, Xiao Z, Hou L and Xue X (2021) A Prognostic DNA Damage Repair Genes Signature and Its Impact on Immune Cell Infiltration in Glioma. Front. Oncol. 11:682932. doi: 10.3389/fonc.2021.682932

Objective: Glioma is the most frequent type of malignant cerebral tumors. DNA damage repair genes (DDRGs) play a crucial role in the development of cancer. In this study, we constructed a DDRGs signature and investigated the potential mechanisms involved in this disease.

Methods: RNA sequence data, microarray data, and corresponding clinical information of gliomas were downloaded from The Cancer Genome Atlas (TCGA), Chinese Glioma Genome Atlas (CGGA), and Gene Expression Omnibus (GEO). Subsequently, we identified candidate genes by differential analysis and Cox regression analysis. The least absolute shrinkage and selection operator Cox regression model was utilized to construct a DDRGs signature using TCGA training dataset. According to this signature, patients with glioma were divided into low- and high-risk groups. The predictive ability of the signature was validated by prognostic analysis, receiver operating characteristic curves, principal component analysis, and stratification analysis in TCGA testing and CGGA verification datasets. CIBERSORT and single-sample gene set enrichment analysis (ssGSEA) were used to evaluate the immune microenvironment of glioma. Moreover, we conducted GSEA to determine the functions and pathways in the low- and high-risk groups. Finally, a nomogram was constructed by combining the signature and other clinical features.

Results: A total of 1,431 samples of glioma (592 from TCGA, 686 from the CGGA, and 153 from the GEO) and 23 samples of normal brain tissue from the GEO were analyzed in this study. There were 51 prognostic differentially expressed DDRGs. Additionally, five DDRGs (CDK4、HMGB2、WEE1、SMC3 and GADD45G) were selected to construct a DDRGs signature for glioma, stratifying patients into low- and high-risk groups. The survival analysis showed that the DDRGs signature could differentiate the outcome of the low- and high-risk groups, showing that high-risk gliomas were associated with shorter overall survival. The immune microenvironment analysis revealed that more immunosuppressive cells, such as tumor associated macrophages and regulatory

T cells, were recruited in the high-risk group. GSEA also showed that high-risk glioma was correlated with the immune and extracellular matrix pathways.

Conclusion: The five DDRGs signature and its impact on the infiltration of immunosuppressive cells could precisely predict the prognosis and provide guidance on the treatment of glioma.

Keywords: glioma, DNA repair, tumor microenvironment, prognosis, immune cells

INTRODUCTION

Glioma is the most common type of primary tumors of the central nervous system (CNS), accounting for approximately 70% of cases. It is also a major cause of death among patients with intracranial tumors (1). Patients with glioma are primarily treated with surgical resection, radiotherapy, chemotherapy, and a combination of different therapies. The National Comprehensive Cancer Network guideline recommends chemoradiation with or without tumor-treating fields (TTF) for the adjuvant treatment of primary glioblastoma (GBM). However, the prognosis of GBM remains poor, mainly due to the high risk of recurrence and resistance to chemoradiotherapy (2–4). In addition, gliomas do not have clear boundaries and are characterized by high degrees of infiltration *via* diffusion and a high proliferation rate, thereby complicating surgical resection (5). Recently, some new therapies have been proposed for numerous types of cancer, including immunotherapy and molecular targeted therapy. Randomized controlled clinical studies have shown that these treatments could significantly improve the survival of patients with lung cancer, colorectal cancer, and numerous other types of tumors (6–8). However, some clinical trials have found that these therapeutic modalities are not as effective in patients with glioma. Some researchers argued that this may be attributed to differences in the microenvironments of gliomas and other types of cancer (9).

Radiotherapy and chemotherapy can cause DNA double-strand breaks in tumor cells, which in turn trigger cell apoptosis and death. The DNA damage repair mechanism of tumor cells is abnormally activated; it mainly repairs damaged DNA by homologous recombination and non-homologous end joining. Following DNA double-strand breakage, DNA damage receptors are activated and damage repair proteins, such as BRCA1 DNA repair associated (BRCA1), BRCA2, and RAD51 recombinase (RAD51), are recruited at the damaged sites to repair damaged DNA this process leads to complete resistance to the tumoricidal effect of chemoradiotherapy (10). The alkylating agent temozolomide (TMZ), which can induce DNA breaks in glioma cells and subsequently lead to cell death, is one of the major therapeutic approaches used in patients with glioma. O-6-methylguanine-DNA methyltransferase (MGMT) encodes a DNA damage repair protein that protects tumor cells against DNA double-strand breaks caused by alkylating agents, such as TMZ. Some researchers have demonstrated that the expression levels of MGMT could predict sensitivity to TMZ in patients with glioma (11). Therefore, DNA damage repair genes (DDRGs) play an important role in tumor resistance to chemoradiotherapy.

DNA repair deficiency is also an emerging biomarker of response to immune checkpoint blockade (12). Alterations in DDRGs are associated with genomic instability and increased somatic tumor mutational burden, which in turn promote the generation of tumor-specific neoantigens. The continuous stimulation of the body by tumor antigens generates a persistent immune activation response. This effect depletes or remodels the related effector cells in the tumor microenvironment, thereby impairing their normal functions. In turn, an immunosuppressive microenvironment is generated that promotes tumorigenesis and progression (13). Thus, the tumor microenvironment contains more neoantigens and the function of immune cells of the tumor microenvironment becomes more complex, especially with regards to immunosuppressive cell infiltration. At present, there are few studies on the interaction between DDRGs and the tumor microenvironment of gliomas.

In this study, we collected RNA sequencing data, microarray data, and corresponding clinical information of gliomas from The Cancer Genome Atlas (TCGA), Chinese Glioma Genome Atlas (CGGA), and Gene Expression Omnibus (GEO) databases. Next, we identified survival-related DDRGs by univariate regression analysis. Subsequently, a DDRGs signature for prognostic prediction was constructed using least absolute shrinkage and selection operator (LASSO) regression and Cox proportional hazards regression. The DDRGs signature composed of CDK4, HMBG2, WEE1, SMC3 and GADD45G could accurately predict the prognosis of gliomas. More importantly, we found that the DDRGs signature was strongly associated with immunosuppressive cell infiltration in the microenvironment of gliomas. Our results demonstrated that the DDRGs signature was closely related to prognosis and provided reliable clues for elucidating the microenvironment of glioma.

MATERIALS AND METHODS

Data Acquisition and Identification of Candidate Genes

RNA sequencing data and corresponding clinical information from TCGA LGG and GBM datasets were downloaded from TCGA data portal (https://portal.gdc.cancer.gov/) updated to July 19, 2019. Gene expression profiling and corresponding clinical features of gliomas were obtained from the CGGA database (http://www.cgga.org.cn/) up to May 6, 2020,

including the datasets mRNAseq-693 and mRNAseq-325. The microarray dataset GSE4290 for differential gene analysis was downloaded from the GEO database (https://www.ncbi.nlm.nih.gov/geo). RNA sequencing data from TCGA (LGG and GBM datasets) and CGGA (693 and 325 datasets) were normalized and batched using the limma R package. All data were screened to remove samples with missing clinical information. The clinicopathological characteristics of patients in this study are presented in **Table 1**. A total of 513 DDRGs were retrieved from the molecular signature database (MSigDB) (https://www.gsea-msigdb.org/gsea/msigdb) and previous literature (14) (**Supplementary Table S1**). Differentially expressed DDRGs between gliomas and normal brain tissues the GSE4290 dataset were identified using the limma R package and the following criteria: |logFC|>1; false discovery rate <0.05. Next, data from TCGA were randomly divided into the training and testing datasets. Candidate genes in TCGA training dataset were identified through univariate Cox analysis with cut-off values of P<0.001. An interaction network of candidate genes was constructed using the Search Tool for the Retrieval of Interacting Genes (STRING) database (version 11.0) (15).

Construction and Validation of a DDRGs Signature

Candidate genes were analyzed using LASSO regression and Cox proportional hazards regression. The independent variable in the regression was the expression of candidate DDRGs, and the response variable was the prognosis of patients in the training set. Subsequently, the DDRGs signature was constructed by a linear combination of the regression coefficient multiplied by its mRNA expression level:

$$riskScore = \sum_{j=1}^{n}(Coefj * Xj)$$

Using the formula shown above, we can calculate the risk score for each patient with glioma. Patients were separated into high- and low-risk groups according to the median score. Prognostic analysis was performed with the survminer package in R.

Principal component analysis (PCA) was performed to explore the distribution in the low- and high-risk groups using the Rtsne package, an established dimensionality reduction method (16). Using the survivalROC R package, we constructed a time-dependent receiver operating characteristic (ROC) curve and Harrell's concordance index to assess the predictive value of the DDRGs signature for prognosis. The online database Gene Expression Profiling Interactive Analysis (GEPIA; http://gepia.cancer-pku.cn/index.html) (17) was used to analyze the expression and prognosis of genes constituting the DDRGs signature in glioma. In addition, the protein expression levels of these genes were determined using the Human Protein Atlas (http://www.proteinatlas.org) online database (18).

Internal and External Validation of the DDRGs Signature

TCGA testing and CGGA datasets were used for internal and external validation, and a risk score could be calculated for each patient with glioma using the formula shown above. Based on the

TABLE 1 | Clinicopathological characteristics of glioma patients from the TCGA, CGGA and GEO databases.

	TCGA-Training cohort N = 294	TCGA-Testing cohort N = 298	CGGA validation cohort N = 686	GSE4290 N = 176
Age				
<42	114	129	307	NA
≥42	180	169	379	NA
Gender				
Male	173	171	399	NA
Female	121	127	287	NA
Normal Tissue	NA	NA	NA	23
Grade				
II	101	110	177	45
III	116	122	226	31
IV	77	66	283	77
IDH				
Wild	116	104	315	NA
Mutation	178	194	371	NA
1p/19q				
Codel	69	80	141	NA
Non-codel	225	218	545	NA
MGMT				
Methylated	NA	NA	386	NA
un-methylated	NA	NA	300	NA
Status				
Dead	91	82	457	NA
Alive	203	216	229	NA
RiskScore				
Low	141	151	343	NA
High	153	147	343	NA

median values, patients were divided into high- and low-risk groups. Next, the prognostic analysis, PCA, and construction of the time-dependent ROC curve of each patient were performed using R. Univariate and Multivariate Cox regression analyses were used to identify independent prognostic factors.

Survival Analysis of the DDRGs Signature in Stratified Patients With Glioma

In this study, patients with glioma were stratified according to their clinicopathological features including age, sex, primary-recurrent-secondary (PRS) type, grade, IDH, 1p19q, and MGMT status. The Kaplan–Meier survival analysis was implemented to calculate the survival rates in the low- and high-risk groups of stratified patients.

Construction of a Predictive Nomogram

In clinical research, nomograms are widely used to predict the outcomes of patients with cancer (19). In the CGGA cohort, all clinical features were utilized for the construction of a nomogram to investigate the probability of 1-, 2-, and 3-year overall survival (OS) of patients with glioma using the rms R package. A calibration curve was used to compare the predictions of this nomogram with the actual rates using the rms package. Specifically, the C-index was used as a discrimination measure considering the censored data in this survival analysis study. To demonstrate the incremental value of the DDRGs signature over the clinicopathological characteristic for individualized assessment of OS, the decision curve was constructed.

Evaluation of the Glioma Microenvironment Through CIBERSORT and Single-Sample Gene Set Enrichment Analysis (ssGSEA)

CIBERSORT (20) utilizes a deconvolution algorithm to predict the percentages of 22 phenotypes of immune cells in tumor tissue. This method was used to estimate the population fractions of immunocytes in the low- and high-risk groups. Violin plots were generated using the vioplot package to show differences in the infiltration of immunocytes between the high- and low-risk groups. In addition, the degree of immune cell infiltration was quantified using enrichment scores calculated through ssGSEA of the Gene Set Variation Analysis package of the R software. This analysis yielded 29 immune infiltration-related information, including immune cell species, immune function, and immune-related pathways. The patients of glioma were hierarchically clustered to high, medium or low immune group based on ssGSEA scores for those 29 immune infiltration related information.

Gene Set Enrichment Analyses

Finally, we searched for the underlying molecular mechanism through which the DDRGs signature indicated worse prognosis in patients with glioma using the GSEA 4.0.2 software (21). We used the MsigDB, c2.cp.kegg.v7.2.symbols.gmt and c5.go.bp.v7.2.symbols.gmt as the functional gene sets. Default weighted enrichment statistics were used, and the number of random combinations was set to 1,000. A normalized enrichment score (NES) >1 and false discovery rate <0.05 denoted statistical significance.

Statistical Analysis

The R software (4.0.0) with corresponding packages and GraphPad Prism 7 (GraphPad Software Inc., San Diego, CA, USA) were used for statistical analyses. Unless specified otherwise above, $P<0.05$ denoted statistically significant differences.

RESULTS

Characteristics of Patients With Glioma

The flow chart of this research study is shown in **Figure 1**. Gene expression profile and clinical information of gliomas were obtained from clinical databases with large sample sizes. Patients with incomplete clinical information were removed. In total, 1,431 samples of glioma and 23 normal brain tissues were obtained from TCGA-LGG, TCGA-GBM, CGGA, and GSE4290 datasets. The detailed clinical features of gliomas collected from the articles are summarized in **Table 1**.

Data Preprocessing and Identification of Candidate Genes

We analyzed differentially expressed genes (DEGs) between gliomas and normal brain tissues in the GSE4290 cohort using the Wilcoxon test; the microarray data included a total of 153 samples of glioma and 23 normal brain tissues. According to the screening criteria (|logFC|>1, false discovery rate <0.05), a total of 2,450 DEGs were identified. Among those, 1,450 were upregulated and 1,425 were downregulated (**Figure 2A**). In addition, 513 DDRGs were retrieved from the MSigDB (https://www.gsea-msigdb.org/gsea/msigdb) and previous literature (14) (**Supplementary Table S1**). We found that 51 genes were both DEGs and DDRGs (**Figure 2B**). The gene expression profiles of these genes are displayed through heatmaps (**Figure 2C**). **Figure 2D** illustrates the interaction of these 51 genes in the protein–protein interaction network. Next, TCGA data were randomly divided into two datasets (294 and 298 patients in the training and testing datasets, respectively) (**Table 1**). Univariate independent prognostic analysis was performed for these 51 genes in TCGA training dataset. A total of 43 genes were significantly associated with prognosis (**Figure 2E**). In addition, we used the Metascape website to analyze the function of these genes. As expected, these 43 DDRGs were involved in DNA damage repair processes and cell cycle pathways (**Supplementary Figure S1**).

Construction of a Prognostic Model Using the Training Dataset

The 43 candidate genes were subsequently analyzed using LASSO regression and Cox proportional hazards regression. The independent variable in the regression was the expression profiles of these candidate genes, and the response variables were the clinical features of gliomas in TCGA training dataset (**Figures 2F, G**). Next, five risk genes

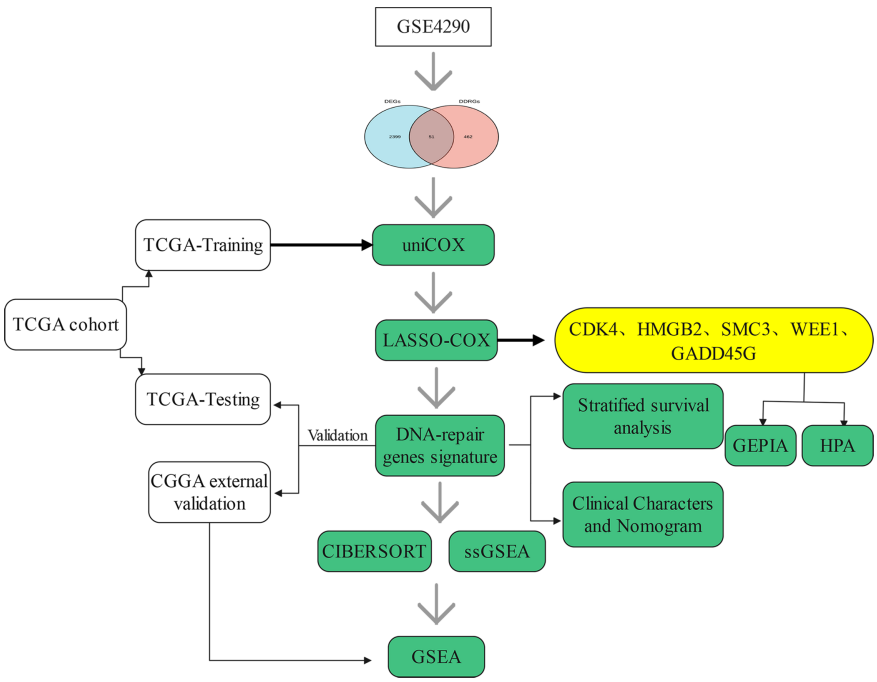

FIGURE 1 | Flow chart of this study.

(CDK4, HMGB2, WEE1, SMC3, and GADD45G) were identified (**Table 2**). The DDRGs signature was calculated as follows: RiskScore=0.307*$CDK4_{expression}$+0.356*$HMGB2_{expression}$+0.445*$WEE1_{expression}$+(−0.453*$SMC3_{expression}$)+(−0.371*$GADD45G_{expression}$). The forest map of Cox regression analysis indicated that SMC3 and GADD45G were positively correlated with the prognosis of patients with glioma, whereas CDK4, WEE1, and HMGB2 were negatively correlated with prognosis (**Figure 2H**). To further investigate the properties of these five DDRGs, we retrieved their expression levels and impact on the prognosis of patients with glioma in the GEPIA website. In agreement with the results of a previous differential analysis, the expression levels of these five genes were higher in both LGG and GBM than in normal brain tissue (**Supplementary Figures S2A–E**). In terms of prognostic analysis, consistent with our previous results, high expression of CDK4, HMGB2, and WEE1 could lead to poor prognosis of glioma; however, gliomas with high expression of SMC3 and GADD45G were linked to longer survival (**Supplementary Figures S2F–J**). Subsequently, we investigated the proteins encoded by these five genes in patients with glioma using the Human Protein Atlas database. The previously described protein expression profile and gene expression levels were similar, and CDK4, HMGB2, WEE1, SMC3, and GADD45G exhibited medium staining intensity. However, their corresponding expression levels in normal brain tissues were not detected, or the staining intensity was low (**Supplementary Figures S3A–E**). Each patient could be scored according to this formula; patients with glioma in TCGA training dataset were divided into high-risk and low-risk groups (n=147, respectively) according to the median score (**Figure 3A**). A heatmap was used to describe the expression of these five DDRGs in different groups (**Figure 3B**). In the high-risk group, CDK4, HMGB2, and WEE1 were upregulated, whereas SMC3 and GADD45G were downregulated. **Figure 3C** suggests that patients in the high-risk group were associated with a higher mortality rate and shorter survival than those in the low-risk group. Consistently, based on the Kaplan–Meier curve, patients in the low-risk group had a significantly better OS (hazard ratio [HR] =8.17, 95% confidence interval [CI]: 4.53–14.73, P<0.001) than those in the high-risk group (P<0.01) (**Figure 3D**). Following the classification of patients with glioma into high- and low-risk groups according to the risk model, PCA was performed. The results revealed that the patients in different risk groups were distributed in two directions (**Figure 3E**). Time-dependent ROC curves were constructed to further evaluate the accuracy of the DDRGs signature for predicting prognosis. The area under the curve values for 1-, 2-, and 3-year survival were 0.913, 0.929, and 0.918, respectively (**Figure 3F**). The calculated C index was to be 0.769 in the training TCGA cohort.

Analysis of the DDRGs Signature Using TCGA Testing and CGGA Validation Datasets

We further clarified the role of the DDRGs signature in predicting prognosis in patients with glioma by performing analysis using TCGA testing and CGGA validation datasets. Scores for each patient were calculated using the formula shown

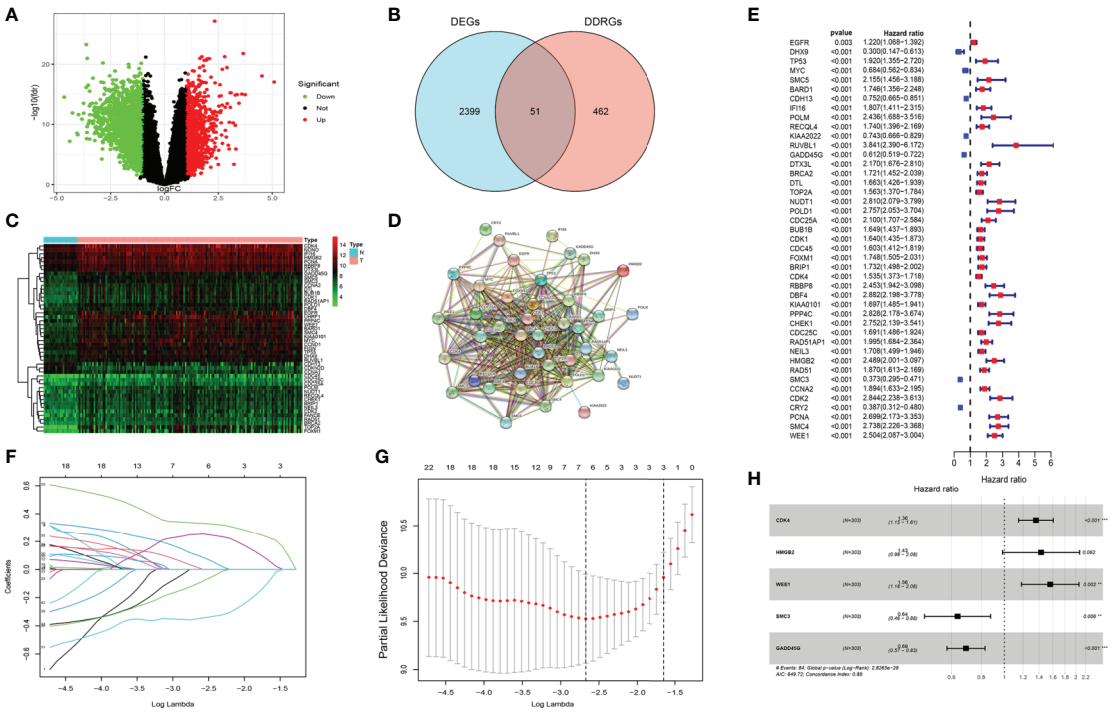

FIGURE 2 | Screening candidate genes and construction a DNA damage repair genes (DDRGs) signature using LASSO regression and Cox proportional hazards regression. **(A)** Volcano plot of differentially expressed genes (DEGs) between gliomas and normal brain tissues. **(B)** Venn diagram showing the intersection of DEGs and DDRGs. **(C)** Heatmap was used to show the expression of the genes at the intersection. **(D)** The protein–protein interaction (PPI) network downloaded from the STRING database indicated the interactions among the candidate genes. **(E)** Forest plot showing the hazard ratios from the univariate Cox regression analysis. **(F)** LASSO coefficient profiles of the 43 candidate genes in TCGA training dataset. **(G)** A coefficient profile plot was generated against the log (lambda) sequence. Selection of the optimal parameter (lambda) in the LASSO model for TCGA training dataset. **(H)** Forest plot showing the five genes that composed the DDRGs signature. LASSO, least absolute shrinkage and selection operator; STRING, Search Tool for the Retrieval of Interacting Genes; TCGA, The Cancer Genome Atlas. $^{**}p < 0.01$,$^{***}p < 0.001$.

above, and patients were divided into high- and low-expression groups based on the corresponding median score (**Supplementary Figures S4A–D**). The distribution of patients in TCGA testing and CGGA cohorts was presented in **Figures 4A, B**. High-risk patients in the TCGA training dataset had a shorter OS (HR=9.96, 95% CI: 5.47–18.13, P<0.001), in the external CGGA validation dataset were same as TCGA dataset (HR=4.74, 95% CI: 3.87–5.80, P<0.001) (**Figures 4C, D**). PCA revealed that patients in the two subgroups were distributed in discrete directions in both TCGA testing and CGGA datasets (**Figures 4E, F**). In addition, in the TCGA testing dataset, the area under the curve values of the DDRGs signature for 1, 2, and 3 years were 0.826, 0.920, and 0.948, respectively; in the CGGA dataset, these values were 0.740, 0.814, and 0.815, respectively (**Figures 4G, H**). The C-indexes were 0.722 and 0.819 in testing TCGA and validation CGGA sets.

Independent Prognostic Value of the DDRGs Signature

Univariate and multivariate Cox regression analyses were performed to assess whether DDRGs signature was an independent prognostic indicator. In the TCGA database, Univariate Cox regression analysis demonstrated that the risk scores were associated with the overall survival rate of glioma patients(HR=5.103, 95%CI=3.407-7.620, P<0.001). Multivariate

TABLE 2 | The information of 5 DNA repair genes constructing the prognostic risk model.

Gene symbol	Description	Ensemble ID	Category	Coeffcient	HR (95%CI)	Pvalue
CDK4	Cyclin Dependent Kinase 4	ENSG00000135446	Protein Coding	0.31	1.36 (1.15-1.61)	<0.01
HMGB2	High Mobility Group Box 2	ENSG00000164104	Protein Coding	0.36	1.43 (0.98-2.08)	0.06
WEE1	WEE1 G2 Checkpoint Kinase	ENSG00000166483	Protein Coding	0.45	1.56 (1.18-2.06)	<0.01
SMC3	Structural Maintenance Of Chromosomes 3	ENSG00000108055	Protein Coding	-0.45	0.64 (0.46-0.88)	0.01
GADD45G	Growth Arrest And DNA Damage Inducible Gamma	ENSG00000130222	Protein Coding	-0.37	0.69 (0.57-0.83)	<0.01

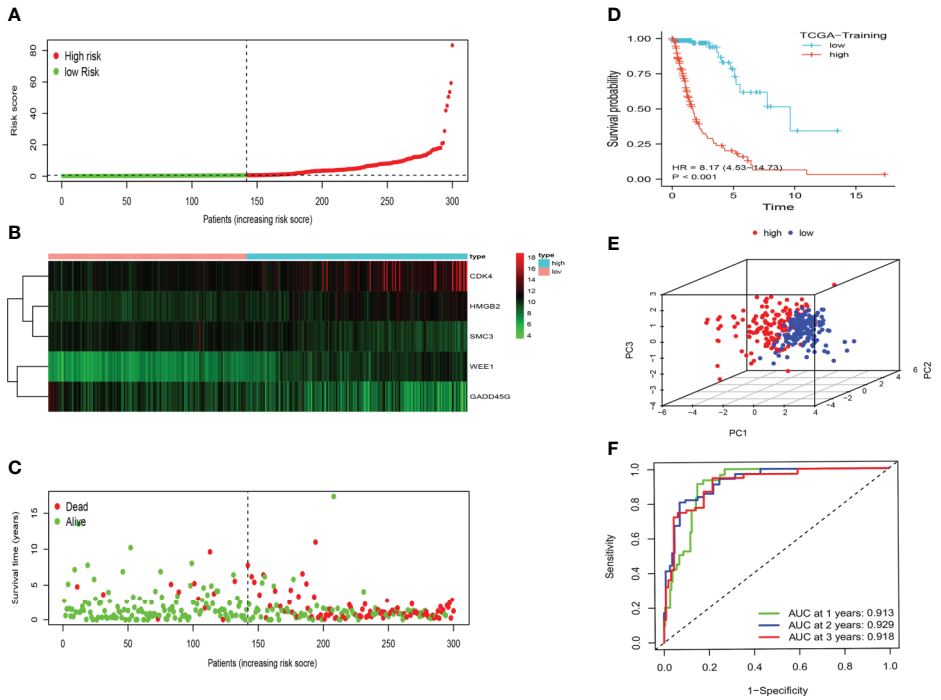

FIGURE 3 | Prognostic analysis of the DDRG signature in TCGA training set. **(A)** The distribution and median value of the risk scores in TCGA training dataset. **(B)** The distributions of status, OS, and risk score in TCGA training dataset. **(C)** Heatmap showing the expression of five genes in the low- and high-risk groups. **(D)** Survival curve was used to analyze OS of the low- and high-risk groups in TCGA training dataset. **(E)** Principal components analysis (PCA) of the DDRGs signature. **(F)** The AUC values of time-dependent ROC curves verify the prognostic performance of the risk score in TCGA training dataset. AUC, area under the curve; DDRGs, DNA damage repair genes; OS, overall survival; ROC, receiver operating characteristic; TCGA, The Cancer Genome Atlas.

Cox regression analysis revealed that the risk scores were independent risk factors for predicting the overall survival rate of glioma patients(HR=2.967, 95%CI=1.627-4.823, P<0.001). The results were validated in the CGGA (**Supplementary Figures S5A–D**).

Prediction of Outcome by the DDRGs Signature in Stratified Patients

We subsequently sought to validate the prognostic role of the DDRGs signature in gliomas with different clinical characteristics. Survival analysis was performed for patients from the CGGA dataset who were divided according to their age (<42, ≥42), sex (female, male), PRS type (primary, recurrent), grade (II, III, IV), IDH (mutation, wild), 1p19q (co-deletion [codel], non-codel), and MGMT status (methylated, unmethylated). The Kaplan–Meier analysis showed that a low risk score was linked to longer OS than a high risk score in all stratified patients (**Figures 5A–O**). Consistent results were obtained from TCGA dataset (**Supplementary Figures S6A–J**). Interestingly, we noted that all stratified patients with grade IV disease in TCGA dataset were in the high-risk subgroup. Moreover, the risk scores were significantly higher in GBM than LGG in the GSE4290, TCGA, and CGGA cohorts (**Supplementary Figures S7A–C**). These results suggested that the DDRGs signature could precisely predict the prognosis of gliomas, linking patients with a high-risk score to poor survival.

Relationship Between the DDRGs Signature and Clinical Characteristics of Gliomas

To examine the association between this DDRGs signature and clinical characteristics of gliomas in CGGA cohort, we investigated potential positive correlations of the risk score with age and grade of glioma. We also explored that the risk score was lower in IDH mutation, 1p19q codel and MGMT methylated significantly which were the clinical features with good prognosis of glioma (**Figure 6**).

Relationship Between the DDRGs Signature and Immune Cell Infiltration in the Tumor Microenvironment

Next, we performed CIBERSORT and ssGSEA to evaluate the relationship between the DDRGs signature and immune cell infiltration in the tumor microenvironment of gliomas. The 686 glioma samples obtained from the CGGA dataset were segregated into low- and high-risk group using the formula shown above. CIBERSORT was used to analyze the RNA sequencing data of these selected patients and evaluate the

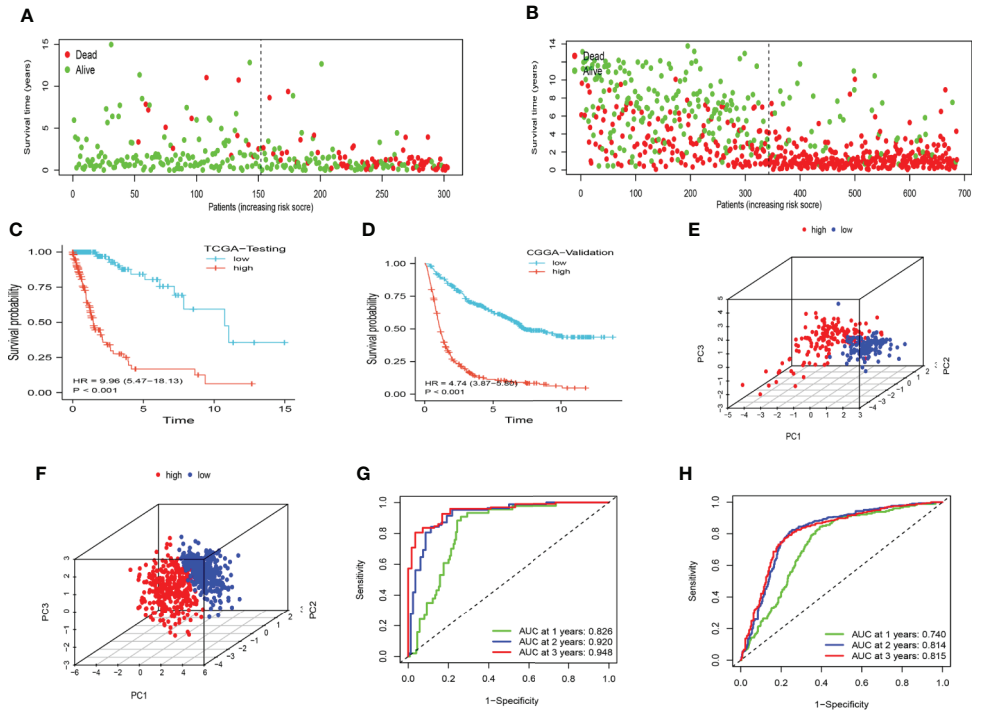

FIGURE 4 | The accuracy of the DDRGs signature was verified using internal and external validation. **(A, B)** Scatter plots depicting the survival and status of patients in the high- and low-risk groups in TCGA testing and CGGA validation datasets. **(C, D)** Survival curve was used to analyze OS in the low- and high-risk groups in TCGA testing and CGGA sets. **(E, F)** Principal component analysis (PCA) of the DDRG signature in TCGA testing and CGGA sets. **(G, H)** ROC curves were constructed for TCGA testing and CGGA sets. CGGA, Chinese Glioma Genome Atlas; DDRG, DNA damage repair gene; OS, overall survival; ROC, receiver operating characteristic; TCGA, The Cancer Genome Atlas.

fractions of 22 immune cell types in the high- and low-risk groups. Surprisingly, the risk score was positively correlated with T follicular helper cells, regulatory T (Treg) cells, and macrophages M0 (P<0.01). In contrast, it was negatively correlated with CD4 naïve T cells, CD4 memory resting T cells, gamma-delta T cells, monocytes, and activated mast cells (P<0.01) (**Supplementary Figures S8A, B**). Subsequently, we also conducted ssGSEA to determine the degree of immune cell infiltration. We similarly observed that the risk score was positively correlated with activated dendritic cells, B cells, CD8+ T cells, dendritic cells, macrophages, mast cells, plasmacytoid dendritic cells, T helper (Th) cells, Th2 cells, tumor-infiltrating lymphocytes, and Treg cells; in contrast, the risk score was negatively correlated with neutrophils and Th1 cells. Moreover, we found that the risk score was correlated with immune processes, such as CCR, check-point, cytolytic activity, etc. (**Supplementary Figures S8C, D**). According to these results, we divided patients with glioma into high- group, medium-, and low-immunity groups. As expected, patients with higher risk scores tended to be in the high-immunity group (**Supplementary Figure S8E**). In addition, the present study revealed that the risk score was negatively correlated with tumor purity, and positively correlated with immune score and stroma score. These findings indicated that the risk score was closely related to the tumor microenvironment (**Figures 7A–E**).

Next, we analyzed the relationship between the risk score and immune checkpoints (programmed cell death 1 [PD1], programmed cell death 1 ligand 1 [PDL1], T-cell immunoglobulin mucin family member 3 [TIM3], cytotoxic T-lymphocyte associated protein 4 [CTLA4], B7-H3, and lymphocyte activating 3 [LAG3]) through correlation analysis. The Pearson analysis showed that the risk score was strongly positively correlated with B7-H3 (r=0.720), moderately and weakly correlated with PDL1 (r=0.443), TIM3 (r=0.330), LAG3 (r=0.210), and CTLA4 (r=0.190), and moderately negatively correlated with PD1 (r=−0.320) (**Figures 8A–F**).

Identification of Involved Signaling Pathways

GSEA was performed to further examine the mechanism of DDRGs and poor prognosis of patients with glioma. In the c2.cp.kegg dataset, we found that the high-risk group was significantly associated with the following pathways: antigen processing and presentation (NES=2.80, P<0.0001), cytokine-cytokine receptor interaction (NES=1.937, P=0.0039), extracellular matrix receptor interaction (NES=1.90, P=0.0059), and T cell receptor signaling pathway (NES=1.703, P=0.017). Gene Ontology analysis showed that high risk was closely associated with the following pathways: activation of immune response (NES=2.79, P<0.0001), antigen receptor-mediated

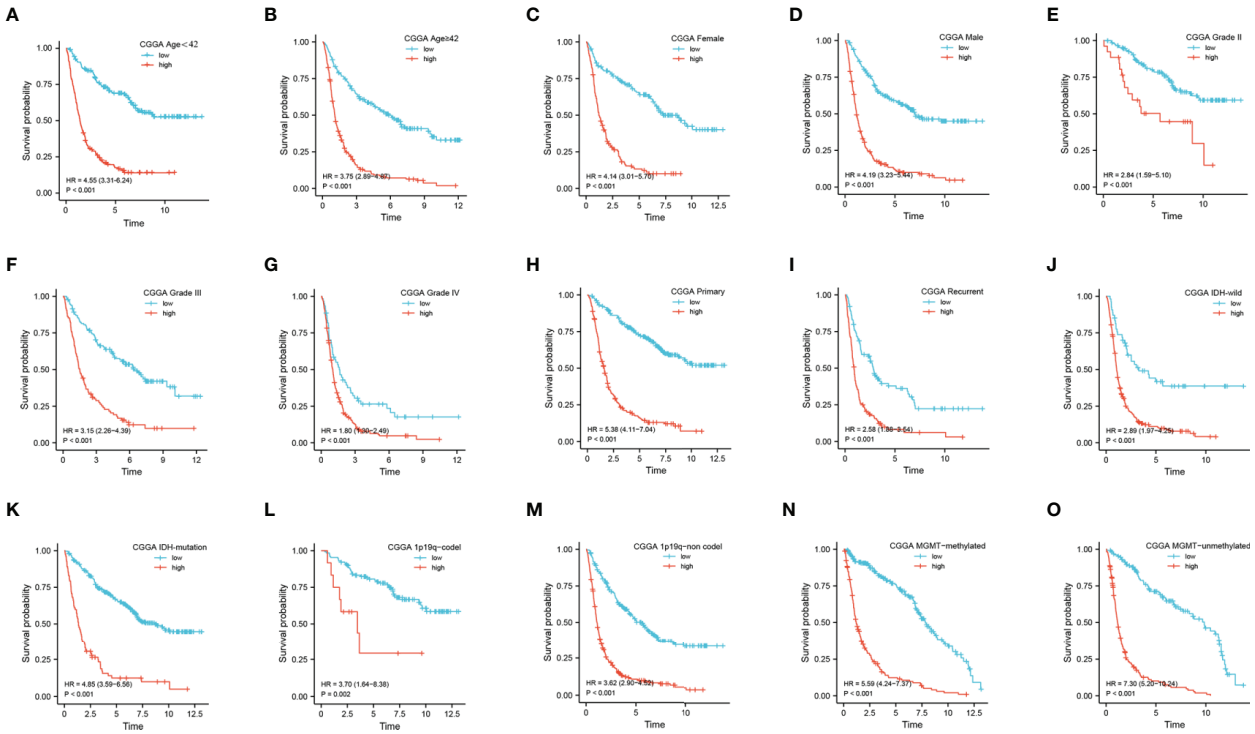

FIGURE 5 | Prediction of outcome of the DDRGs signature in stratified patients in the CGGA dataset. **(A–O)** Survival analysis of the signature in patients stratified by age, sex, PRS type, grade, IDH, 1p19q status, and MGMT promoter. CGGA, Chinese Glioma Genome Atlas; DDRG, DNA damage repair gene; IDH, isocitrate dehydrogenase; MGMT, O-6-methylguanine-DNA methyltransferase; PRS, primary-recurrent-secondary.

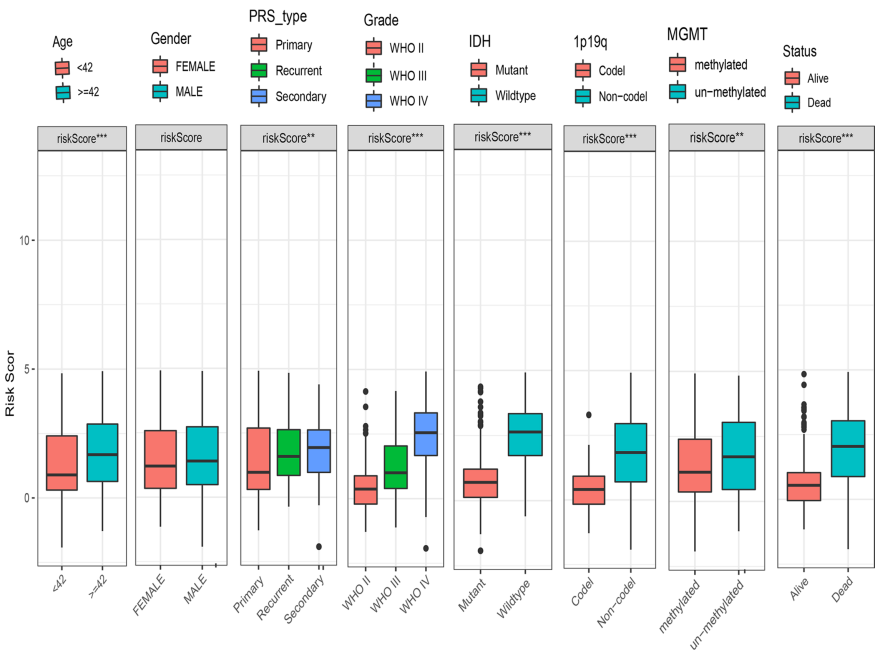

FIGURE 6 | Box charts showing the characteristics of patients in different risk groups, including age, sex, PRS type, grade, IDH, 1p19q, MGMT, and survival status. IDH, isocitrate dehydrogenase; MGMT, O-6-methylguanine-DNA methyltransferase; PRS, primary-recurrent-secondary.

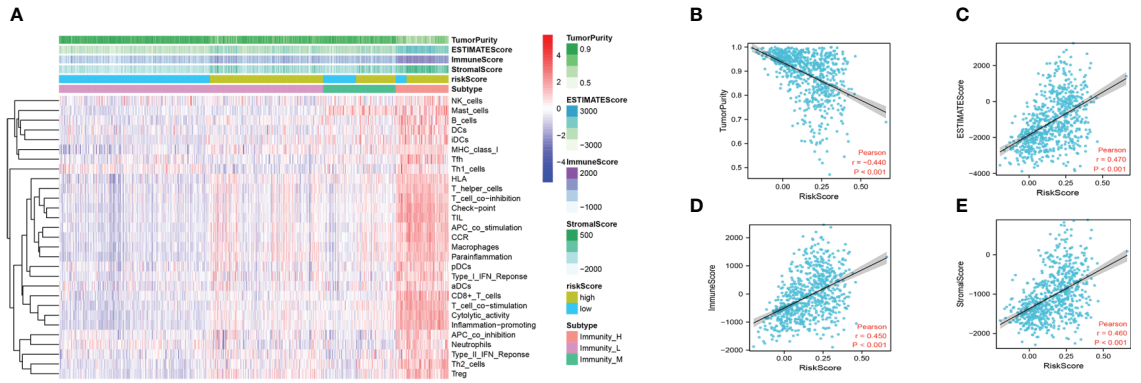

FIGURE 7 | Immune infiltration patterns of low- and high-risk score analyzed by ssGSEA methods in glioma from the CGGA dataset. **(A)** Heatmap revealing the scores of immune cells in low, middle, and high immunities. **(B–E)** Scatter plot showing the correlation between risk score and tumor purity, ESTIMATE, immune and stromal score. CGGA, Chinese Glioma Genome Atlas; ssGSEA, single-sample gene set enrichment analysis.

signaling pathway (NES=1.96, P<0.0012), lymphocyte-mediated immunity (NES=2.13, P<0.0001), and regulation of lymphocyte activation (NES=2.330, P<0.0001) (**Figures 9A, B**).

A Personalized Prognostic Prediction Model

The nomogram can conveniently and rapidly predict the prognosis of patients with cancer; hence, it is widely used in clinical research on cancer (19). According to the clinical information and risk model score of patients with glioma, a nomogram model was established to predict the prognosis of patients, including age, PRS type, grade, IDH, 1p19q, MGMT status, and risk score. Each patient was scored according to their respective different clinical traits and risk score; subsequently, the 1-, 2-, and 3-year survival rates of patients with glioma were predicted according to the prediction line at the bottom of the nomogram (**Figure 10A**). Calibration curves indicated that actual and predicted survival matched well (**Figure 10B**), particularly for 3-year survival. Meanwhile, the calculated C index was to be 0.785. The decision curves shown in **Figure 10C** demonstrated the clinical usefulness of the prediction models, indicating that the DDRGs nomogram

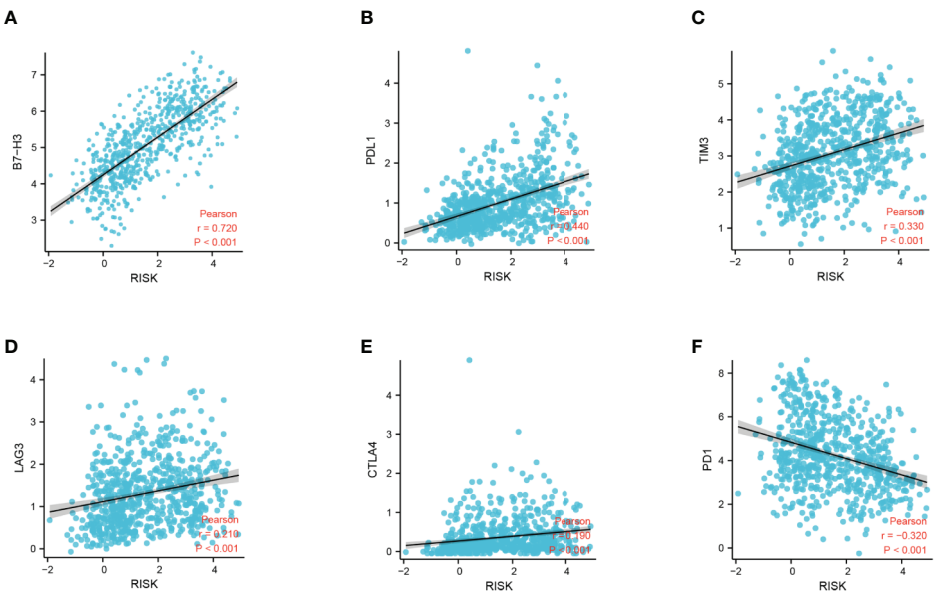

FIGURE 8 | Correlation analysis between the DDRG signature and immune checkpoints. **(A–F)** Relationship between the DDRG signature and B7-H3, PDL1, TIM3, LAG3, CTLA4, and PD1, respectively. CTLA4, cytotoxic T-lymphocyte associated protein 4; DDRG, DNA damage repair gene; LAG3, lymphocyte activating 3; PD1, programmed cell death 1; PDL1, programmed cell death 1 ligand 1; TIM3, T-cell immunoglobulin mucin family member 3.

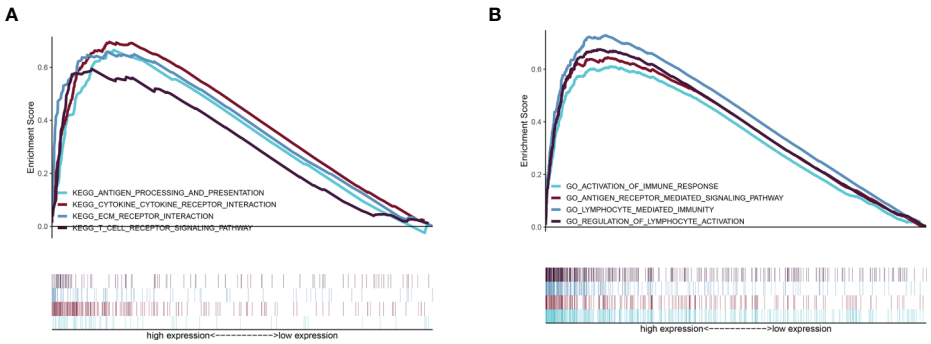

FIGURE 9 | GSEA of the relevant mechanisms involved in the DDRG signature. KEGG **(A)** and GO **(B)**. DDRGs, DNA damage repair genes; GSEA, gene set enrichment analysis; KEGG, Kyoto Encyclopedia of Genes and Genomes; GO, Gene Ontology.

achieved a higher overall net benefit than the clinicopathologic nomogram within most range of threshold probabilities.

DISCUSSION

In 2020, the number of new CNS tumor cases was 308,102, accounting for 1.6% of the total number of new tumor cases, worldwide. Moreover, 251,329 deaths due to brain tumors were reported, accounting for 2.5% of cancer-related deaths globally (22). Gliomas constitute approximately 70% of intracranial malignancy cases and are the leading cause of death among these patients. The prognosis of patients with gliomas, particularly GBM, is poor; median survival after the postoperative administration of concurrent chemoradiotherapy is <2 years (23). The main reasons for the poor prognosis of gliomas are the aggressive proliferation, invasive growth and chemoradiotherapy resistance of glioma cells (24).

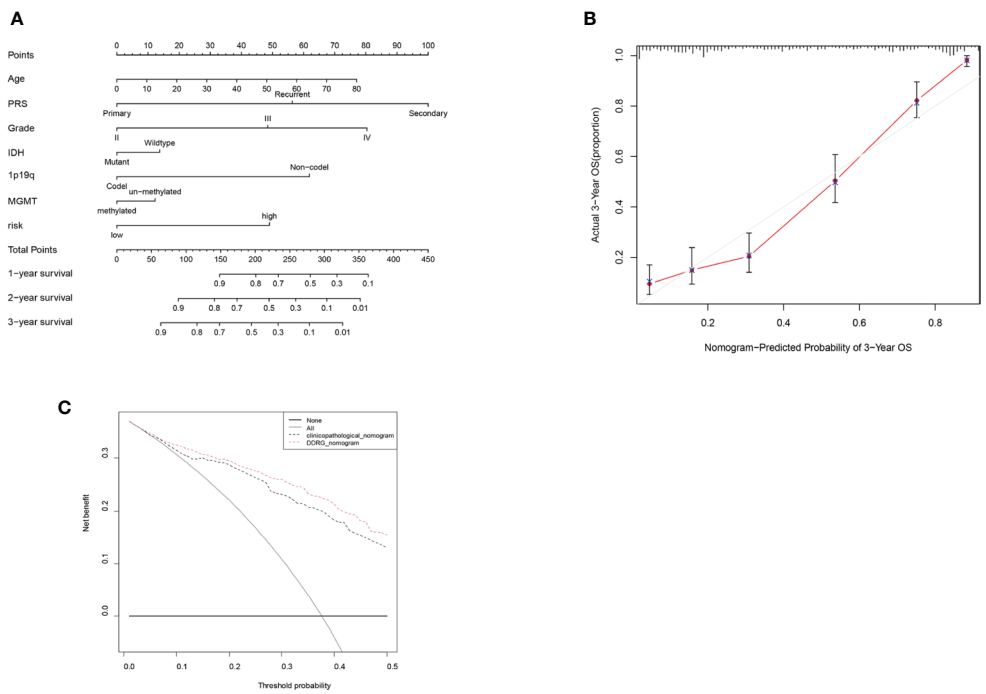

FIGURE 10 | Nomogram for the prediction of prognostic probabilities in the CGGA dataset. **(A)** The nomogram for the prediction of OS was developed using the CGGA dataset. **(B)** The calibration plots for predicting 3-year survival. **(C)** Decision curve analysis for the DDRGs signature nomogram and the clinicopathological nomogram to estimate the OS. CGGA, Chinese Glioma Genome Atlas; OS, overall survival; DDRGs, DNA damage repair genes.

It has been proved that DDRGs are closely related to chemoradiotherapy resistance of tumors (25, 26). In this study, we investigated DDRGs and constructed a risk model consisting of five such genes (CDK4, HMGB2, WEE1, SMC3, and GADD45G) by differential analysis using LASSO regression and Cox proportional hazards regression. We validated the accuracy of this model for predicting the prognosis of gliomas by internal and external validation and stratification analysis. In the TCGA cohort, we found that all GBM patients were in high-risk subgroup. But we did not observe it in the CGGA set. Nevertheless, we found that most of the patients with GBM in the CGGA set were still in high-risk subgroup and had statistical significance. Further, we also explored that the risk score of LGG was significantly lower than GBM in TCGA, CGGA and GSE4290 databases. Moreover, by analyzing the clinical characteristics of patients with glioma, we found that the risk score was positively correlated with malignancy and negatively correlated with protective factors (e.g., IDH mutation, 1p19q codel, and MGMT methylation). Collectively, these results suggest that this risk model is significantly associated with the prognosis of patients with glioma.

The CDK4 promotes tumor cell differentiation from G1 to S phase and increases proliferation. Schmidt et al. (27) were the first to report that amplification of the CDK4 gene occurs in highly malignant GBMs and anaplastic astrocytomas, whereas there are alterations observed in benign astrocytomas. Additionally, recent studies have shown that overexpression of the CDK4 gene was closely related to poor prognosis of patients with glioma (28). HMGB2 is a member of the high mobility group of the nonhistone chromatin-associated proteins that regulate the processes of transcription, replication, recombination, and DNA repair (29). HMGB2 is highly expressed during embryonic development, but lowly expressed in adult organs; it is mainly detected in lymphoid organs and testes. HMGB2 is highly expressed in most tumor tissues (30). As a target gene of mi-R130a, HMGB2 controls the proliferation and epithelial mesenchymal transition of glioma cells (31). WEE1 is a nuclear kinase belonging to the serine/threonine protein kinase family. It is a key regulator of cell cycle progression and maintenance of genomic stability. WEE1 can control the cell cycle by phosphorylating CDK1 and regulating the activity of the CDK1/cyclin B complex. As an integral part of the G2/M phase checkpoint, WEE1 determines the time point of entry into mitosis and inhibits the early progression of the cell cycle, while also participating in the cellular response to DNA damage (32). Shahryar et al. (33) reported that inhibition of WEE1 expression increased the sensitivity of GBM to radiation. This effect may be related to the blockage of WEE1 in the G2M phase of GBM. SMC3 is an essential component of the cohesin family. Studies found that SMC3 activates nuclear factor-κB (NF-κB) through autocrine tumor necrosis factor-α (TNF-α), which inhibits apoptosis in cancer cells. However, it also can activate the AKT pathway, thereby promoting cancer growth (34). GADD45G (relative molecular mass: 18,000 Da) is an evolutionarily conserved protein among members of the growth arrest and DNA damage-inducible protein 45 family. Its expression is elevated in response to a variety of exogenous genotoxic and oncogenic stimuli. Li et al. (35) found that knockdown of GADD45G expression increased the proliferative and migratory ability of esophageal cancer cells. It has also been shown that overexpression of GADD45G reverses resistance to sorafenib both *in vitro* and *in vivo*. Moreover, the proapoptotic effect of sorafenib on sorafenib-sensitive cells is partially abolished by inhibiting the expression of GADD45G using siRNA (36). The traditional view that the CNS is an immune privileged organ arose from the fact that the blood–brain barrier can selectively block the delivery of immune cells and immune macromolecules from the periphery to the CNS. Nonetheless, this is not absolute, and recent studies suggested that lymphatic vessels existing in the brain can also generate an immune response (37). The use of immunotherapy has resulted in significant breakthroughs in the therapeutic landscape of cancer, particularly in the treatment of tumors, such as lung cancer, melanoma, and colorectal cancer. Nevertheless, in gliomas, immunotherapy has not achieved good outcomes, mainly because glioma gradually develops a multifactorial, multicellular complex suppressive immune microenvironment during growth (9, 38). Infiltration of immunosuppressive cells in the tumor microenvironment is key to the efficacy of immunotherapy and tumor immune evasion; the major immunosuppressive cells include tumor-associated macrophages (TAMs) and Treg cells (39). In this study, the infiltration of immune cells in each patient was determined through CIBERSORT and ssGSEA; the high-risk group had more immunosuppressive cells, such as TAMs and Treg cells. Patients were divided into high-, moderate-, and low-immunity groups, according to the degree of immune cell infiltration. Unexpectedly, we observed a trend of positive association between patients in the high-risk group and high-immunity group. It has also been shown that patients with glioma and high immunity are associated with worse prognosis (40). The present findings are consistent with those of previous studies. This also explains the poorer prognosis of patients in the high-risk group.

Chemoradiotherapy can cause double-strand breaks in the DNA of cancer cells, thereby initiating a series of reexamined biochemical reactions for the repair of damaged DNA. Failure to efficiently repair damage or correctly modify DNA can lead to gene mutations, chromosomal rearrangements, or even cell death. Therefore, DNA damage repair is intimately linked to genomic instability. Genomic instability in cells can result in the production of a large number of neoantigens that are more easily recognized by the immune system, which in turn leads to the infiltration of more immune cells in the tumor microenvironment. The infiltrating immune cells are reprogramed by various tumor-derived cytokines and chemokines, acquiring unique functional phenotypes and transforming into tumor-related immune cells. The tumor microenvironment of glioma is particular owing to the unique brain immunology. As the essence of blood–brain barrier, the immune privilege of CNS can inhibit and delay the immune response. The occurrence, development, and immune evasion of

gliomas are closely related to this physiological state (i.e., the tumor immunosuppressive microenvironment), which markedly limits the effectiveness of immunotherapy. In addition to the inherent immunosuppressive microenvironment of glioma, the infiltration of immunosuppressive cells (e.g., TAMs, myeloid-derived suppressor cells, tumor-associated neutrophils, and Treg cells) is also closely related to the tumor immunosuppressive microenvironment (41). Glioma cells interact with various components in their microenvironment, jointly inducing the formation of the immunosuppressive microenvironment and promoting the progression of glioma. Therefore, elucidation of the mechanism of the immunosuppressive microenvironment of glioma may provide an important theoretical basis for improving immunotherapy strategies against glioma. Of the various immunotherapies, checkpoint blockade is currently the most widely applied in clinical practice; however, it may not be the most promising treatment for glioma. Effector T cells can be reactivated by binding to specific antibodies and checkpoint molecules, thereby performing their cytotoxic role against tumor cells.

PD1 and its ligand PDL1/2 are the most widely studied immune checkpoint molecules thus far. These molecules can negatively regulate the signal transduction pathway mediated by T cell receptors. By binding to PDL1, PD1 suppresses the proliferation and differentiation of T cell, blocks the production of inflammatory factors, and leads to T cell inactivation. CTLA4, a member of the immunoglobulin superfamily, is a glycoprotein expressed on the surface of activated clusters of differentiated CD4 and CD8 T cells. It is an important negative regulator in the immune system and the first immunomodulatory molecule to be used in targeted therapy. CTLA4 inhibits T cell activation and induces T cell incompetence by binding the natural CD80 and CD86 ligands expressed on antigen-presenting cells. LAG3 is a member of the immunoglobulin superfamily and exerts an inhibitory effect on lymphocytes. It can enhance the negative regulatory function of Treg cells, which play an important role in the immune response. In addition, it is involved in the immune evasion of various tumor cells. TIM3 is a negative immune checkpoint molecule that can be expressed in T cells, monocyte macrophages, Treg cells, natural killer cells, and tumor cells. The binding of TIM3 to its ligand galectin 9 (LGALS9) induces the depletion of T cells, which cannot be activated and are unable to secrete cytokines, leading to tumor immunosuppression and immune evasion (42). As a newly discovered member of the B7-CD28 checkpoint pathway, B7-H3 plays an extremely important role in the process of tumor immunity. Numerous studies have shown that B7-H3 is highly expressed in most tumors and associated with tumor immune evasion, which is inextricably linked to tumor stemness, invasion, and metastasis (43). B7-H3 is highly expressed in patients with glioma, positively correlated with tumor pathological grade, and negatively correlated with survival (44). In this study, we found that the DDRGs signature was positively correlated with these immune checkpoints, particularly B7-H3, which could serve as a potential approach to enhancing immunotherapy for glioma.

The present study was characterized by some limitations. Firstly, despite the use of the GEO, TCGA, and CGGA databases for validation, there is a lack of multicenter data. In future studies, we plan to analyze data of patients with glioma from our hospital and other hospitals. Secondly, our results warrant further validation *in vitro* and *in vivo*. Further validation of this risk model could lead to precise prediction of the prognosis of patients with glioma and provide guidance for treatment.

In this study, we analyzed the differential expression of DDRGs between gliomas and normal brain tissues and constructed a signature composed of five such genes. The DDRGs signature could accurately predict the prognosis of patients with glioma, which was validated using data obtained from both TCGA and CGGA databases. Most importantly, immune cell infiltration analysis revealed that the DDRGs signature was closely related to inhibitory immune cell infiltration in the microenvironment of glioma. These findings provide a new potential approach and strategy for improving immunotherapy against glioma.

DATA AVAILABILITY STATEMENT

The datasets presented in this study can be found in online repositories. The names of the repository/repositories and accession number(s) can be found in the article/**Supplementary Material**

ETHICS STATEMENT

Ethical review and approval was not required for the study on human participants in accordance with the local legislation and institutional requirements. Written informed consent for participation was not required for this study in accordance with the national legislation and the institutional requirements.

AUTHOR CONTRIBUTIONS

XX was responsible for the overall design of this study. GW, HZ, and LT analyzed the data and edited the manuscript. TY revised the images and tables of this article. XH and PC performed R language modification. HL validated the data analysis. WW and ZX revised the discussion of the article. LH contributed to the study design. All authors contributed to the article and approved the submitted version.

FUNDING

This study was supported by the Key R&D program of Hebei Province (Grant number: 19277737D).

SUPPLEMENTARY MATERIAL

The Supplementary Material for this article can be found online at: https://www.frontiersin.org/articles/10.3389/fonc.2021.682932/full#supplementary-material

Supplementary Figure 1 | Metascape dataset showing the interaction and enrichment pathways of candidate genes.

Supplementary Figure 2 | The gene expression of the constructed risk model and its prognostic impact on glioma patients were analyzed through the GEPIA online website. Figure 2 A-E exhibited the differential expression of CDK4, HGMB2, WEE1, SMC3, GADD45G respectively in LGG and GBM. Figure 2 F-J revealed the overall survival of low and high expression of CDK4, HGMB2, WEE1, SMC3, GADD45G in glioma, respectively. GEPIA, Gene Expression Profiling Interactive Analysis; LGG, lower grade glioma; GBM, glioblastoma.

Supplementary Figure 3 | Protein expression of the genes used for the construction of risk models by the Human Protein Atlas. A-E: immunohistochemical assay in normal and tumor tissue of CDK4, HGMB2, WEE1, SMC3, GADD45G, respectively.

Supplementary Figure 4 | TCGA testing and CGGA datasets were used to verify the accuracy of the DDRGs signature. **(A, B)** Scatterplots illustrating the risk scores for patients with glioma in TCGA testing and CGGA datasets. **(C, D)** The Heatmap illustrating the expression of the five genes in the high- and low-risk groups. TCGA, The Cancer Genome Atlas; CGGA, Chinese Glioma Genome Atlas; DDRGs, DNA damage repair genes.

Supplementary Figure 5 | Univariate and multivariate Cox analysis of prognostic risk scores for gliomas. Univariate Cox regression analysis. Forest plot of associations between risk factors and the survival of gliomas in the TCGA **(A)**, and CGGA **(B)**. Multiple Cox regression analysis. The DDRGs signature is an independent predictor of gliomas in the TCGA **(C)**, and CGGA **(D)**. TCGA, The Cancer Genome Atlas; CGGA, Chinese Glioma Genome Atlas.

Supplementary Figure 6 | Prediction of outcome of the DDRGs signature in stratified patients in TCGA dataset. Survival analysis of the signature in patients stratified by age **(A, B)**, gender **(C, D)**, grade **(E, F)**, IDH **(G, H)**, and 1p19q status **(I, J)**. DDRGs, DNA damage repair genes; TCGA, The Cancer Genome Atlas; IDH, isocitrate dehydrogenase.

Supplementary Figure 7 | Comparison of risk scores in GBM and LGG in the TCGA **(A)**, CGGA **(B)**, and GSE4290 **(C)**. TCGA, The Cancer Genome Atlas; CGGA, Chinese Glioma Genome Atlas.

Supplementary Figure 8 | Relationship between the DDRGs signature and immune infiltrating cells in the tumor microenvironment. **(A)** CIBERSORT was used to analyze the types and proportion of infiltrating immune cells in the tumor microenvironment of patients with glioma. **(B)** Differences in immune infiltrating cells between high- and low-risk groups determined by CIBERSORT. **(C, D)** Differences in immune infiltrating cells and immune related pathways between high- and low-risk groups determined by ssGSEA. **(E)** Violin diagram showing the relationship between immune grouping and risk score. DDRGs, DNA damage repair genes; ssGSEA, single-sample gene set enrichment analysis.

REFERENCES

1. Ostrom QT, Gittleman H, Xu J, Kromer C, Wolinsky Y, Kruchko C, et al. Cbtrus Statistical Report: Primary Brain and Other Central Nervous System Tumors Diagnosed in the United States in 2009-2013. *Neuro Oncol* (2016) 18: v1–75. doi: 10.1093/neuonc/now207
2. Ostrom QT, Cioffi G, Gittleman H, Patil N, Waite K, Kruchko C, et al. Cbtrus Statistical Report: Primary Brain and Other Central Nervous System Tumors Diagnosed in the United States in 2012-2016. *Neuro Oncol* (2019) 21:v1–100. doi: 10.1093/neuonc/noz150
3. Porter KR, McCarthy BJ, Freels S, Kim Y, Davis FG. Prevalence Estimates for Primary Brain Tumors in the United States by Age, Gender, Behavior, and Histology. *Neuro Oncol* (2010) 12:520–7. doi: 10.1093/neuonc/nop066
4. Savage N. Searching for The Roots of Brain Cancer. *Nature* (2018) 561:S50–1. doi: 10.1038/d41586-018-06709-2
5. Huse JT, Holland EC. Targeting Brain Cancer: Advances in The Molecular Pathology of Malignant Glioma and Medulloblastoma. *Nat Rev Cancer* (2010) 10:319–31. doi: 10.1038/nrc2818
6. Faivre-Finn C, Vicente D, Kurata T, Planchard D, Paz-Ares L, Vansteenkiste JF, et al. Brief Report: Four-Year Survival With Durvalumab After Chemoradiotherapy in Stage III NSCLC - An Update From The Pacific Trial. *J Thorac Oncol* (2021) 16:860–7. doi: 10.1016/j.jtho.2020.12.015
7. Woolston A, Khan K, Spain G, Barber LJ, Griffiths B, Gonzalez-Exposito R, et al. Genomic and Transcriptomic Determinants of Therapy Resistance and Immune Landscape Evolution During Anti-EGFR Treatment in Colorectal Cancer. *Cancer Cell* (2019) 36:35–50.e9. doi: 10.1016/j.ccell.2019.05.013
8. Llosa NJ, Luber B, Siegel N, Awan AH, Oke T, Zhu Q, et al. Immunopathologic Stratification of Colorectal Cancer for Checkpoint Blockade Immunotherapy. *Cancer Immunol Res* (2019) 7:1574–9. doi: 10.1158/2326-6066.CIR-18-0927
9. Garner H, de Visser KE. Immune Crosstalk in Cancer Progression and Metastatic Spread: A Complex Conversation. *Nat Rev Immunol* (2020) 20:483–97. doi: 10.1038/s41577-019-0271-z
10. Xu R, Yu S, Zhu D, Huang X, Xu Y, Lao Y, et al. Hcinap Regulates the DNA-damage Response and Mediates the Resistance of Acute Myelocytic Leukemia Cells to Therapy. *Nat Commun* (2019) 10:3812. doi: 10.1038/s41467-019-11795-5
11. Stupp R, Hegi ME, Gilbert MR, Chakravarti A. Chemoradiotherapy in Malignant Glioma: Standard of Care and Future Directions. *J Clin Oncol* (2007) 25:4127–36. doi: 10.1200/JCO.2007.11.8554
12. Mouw KW, Goldberg MS, Konstantinopoulos PA, D'Andrea AD. Dna Damage and Repair Biomarkers of Immunotherapy Response. *Cancer Discovery* (2017) 7:675–93. doi: 10.1158/2159-8290.CD-17-0226
13. Turley SJ, Cremasco V, Astarita JL. Immunological Hallmarks of Stromal Cells in The Tumour Microenvironment. *Nat Rev Immunol* (2015) 15:669–82. doi: 10.1038/nri3902
14. Yang X, Wang G, Gu R, Xu X, Zhu G. A Signature of Tumor Dna Repair Genes Associated With The Prognosis of Surgically-resected Lung Adenocarcinoma. *PeerJ* (2020) 8:e10418. doi: 10.7717/peerj.10418
15. Szklarczyk D, Franceschini A, Kuhn M, Simonovic M, Roth A, Minguez P, et al. The STRING Database in 2011: Functional Interaction Networks of Proteins, Globally Integrated and Scored. *Nucleic Acids Res* (2011) 39:D561–8. doi: 10.1093/nar/gkq973
16. Toghi Eshghi S, Au-Yeung A, Takahashi C, Bolen CR, Nyachienga MN, Lear SP, et al. Quantitative Comparison of Conventional and T-SNE-Guided Gating Analyses. *Front Immunol* (2019) 10:1194. doi: 10.3389/fimmu.2019.01194
17. Tang Z, Li C, Kang B, Gao G, Li C, Zhang Z. Gepia: A Web Server for Cancer and Normal Gene Expression Profiling and Interactive Analyses. *Nucleic Acids Res* (2017) 45:W98–102. doi: 10.1093/nar/gkx247
18. Pontén F, Schwenk JM, Asplund A, Edqvist PH. The Human Protein Atlas as A Proteomic Resource for Biomarker Discovery. *J Intern Med* (2011) 270:428–46. doi: 10.1111/j.1365-2796.2011.02427.x
19. Iasonos A, Schrag D, Raj GV, Panageas KS. How to Build and Interpret A Nomogram for Cancer Prognosis. *J Clin Oncol* (2008) 26:1364–70. doi: 10.1200/JCO.2007.12.9791
20. Chen B, Khodadoust MS, Liu CL, Newman AM, Alizadeh AA. Profiling Tumor Infiltrating Immune Cells With CIBERSORT. *Methods Mol Biol* (2018) 1711:243–59. doi: 10.1007/978-1-4939-7493-1_12
21. Subramanian A, Tamayo P, Mootha VK, Mukherjee S, Ebert BL, Gillette MA, et al. Gene Set Enrichment Analysis: A Knowledge-Based Approach for Interpreting Genome-Wide Expression Profiles. *Proc Natl Acad Sci USA* (2005) 102:15545–50. doi: 10.1073/pnas.0506580102
22. Sung H, Ferlay J, Siegel RL, Laversanne M, Soerjomataram I, Jemal A, et al. Global Cancer Statistics 2020: GLOBOCAN Estimates of Incidence and

Mortality Worldwide for 36 Cancers in 185 Countries. *CA Cancer J Clin* (2021) 71:209–49. doi: 10.3322/caac.21660
23. Stupp R, Hegi ME, Mason WP, van den Bent MJ, Taphoorn MJ, Janzer RC, et al. Effects of Radiotherapy With Concomitant and Adjuvant Temozolomide Versus Radiotherapy Alone on Survival in Glioblastoma in A Randomised Phase III Study: 5-Year Analysis of The Eortc-NCIC Trial. *Lancet Oncol* (2009) 10:459–66. doi: 10.1016/S1470-2045(09)70025-7
24. Van Meir EG, Hadjipanayis CG, Norden AD, Shu HK, Wen PY, Olson JJ. Exciting New Advances in Neuro-oncology: The Avenue to A Cure for Malignant Glioma. *CA Cancer J Clin* (2010) 60:166–93. doi: 10.3322/caac.20069
25. Kojima T, Shah MA, Muro K, Francois E, Adenis A, Hsu CH, et al. Randomized Phase Iii KEYNOTE-181 Study of Pembrolizumab Versus Chemotherapy in Advanced Esophageal Cancer. *J Clin Oncol* (2020) 38:4138–48. doi: 10.1200/JCO.20.01888
26. Turner KM, Sun Y, Ji P, Granberg KJ, Bernard B, Hu L, et al. Genomically Amplified Akt3 Activates Dna Repair Pathway and Promotes Glioma Progression. *Proc Natl Acad Sci USA* (2015) 112:3421–6. doi: 10.1073/pnas.1414573112
27. Schmidt EE, Ichimura K, Reifenberger G, Collins VP. CDKN2 (P16/MTS1) Gene Deletion or CDK4 Amplification Occurs in The Majority of Glioblastomas. *Cancer Res* (1994) 54:6321–4.
28. Moradimotlagh A, Arefian E, Rezazadeh Valojerdi R, Ghaemi S, Jamshidi Adegani F, Soleimani M. microRNA-129 Inhibits Glioma Cell Growth by Targeting CDK4, CDK6, and MDM2. *Mol Ther Nucleic Acids* (2020) 19:759–64. doi: 10.1016/j.omtn.2019.11.033
29. Thomas JO. HMG1 and 2: Architectural DNA-Binding Proteins. *Biochem Soc Trans* (2001) 29:395–401. doi: 10.1042/bst0290395
30. Rhodes DR, Yu J, Shanker K, Deshpande N, Varambally R, Ghosh D, et al. Large-Scale Meta-analysis of Cancer Microarray Data Identifies Common Transcriptional Profiles of Neoplastic Transformation and Progression. *Proc Natl Acad Sci USA* (2004) 101:9309–14. doi: 10.1073/pnas.0401994101
31. Tang C, Yang Z, Chen D, Xie Q, Peng T, Wu J, et al. Downregulation of Mir-130a Promotes Cell Growth and Epithelial to Mesenchymal Transition by Activating HMGB2 in Glioma. *Int J Biochem Cell Biol* (2017) 93:25–31. doi: 10.1016/j.biocel.2017.08.010
32. Sasaki M, Terabayashi T, Weiss SM, Ferby I. The Tumor Suppressor MIG6 Controls Mitotic Progression and the G2/M DNA Damage Checkpoint by Stabilizing the WEE1 Kinase. *Cell Rep* (2018) 24:1278–89. doi: 10.1016/j.celrep.2018.06.064
33. Mir SE, De Witt Hamer PC, Krawczyk PM, Balaj L, Claes A, Niers JM, et al. In Silico Analysis of Kinase Expression Identifies WEE1 as A Gatekeeper Against Mitotic Catastrophe in Glioblastoma. *Cancer Cell* (2010) 18:244–57. doi: 10.1016/j.ccr.2010.08.011
34. Bai L, Xu S, Chen W, Li Z, Wang X, Tang H, et al. Blocking NF-κb and Akt by Hsp90 Inhibition Sensitizes Smac Mimetic Compound 3-Induced Extrinsic Apoptosis Pathway and Results in Synergistic Cancer Cell Death. *Apoptosis* (2011) 16:45–54. doi: 10.1007/s10495-010-0542-4
35. Li T, Xu L, Teng J, Ma Y, Liu W, Wang Y, et al. Gadd45g Interacts With E-cadherin to Suppress the Migration and Invasion of Esophageal Squamous Cell Carcinoma. *Dig Dis Sci* (2020) 65:1032–41. doi: 10.1007/s10620-019-05836-8
36. Ou DL, Shyue SK, Lin LI, Feng ZR, Liou JY, Fan HH, et al. Growth Arrest DNA Damage-inducible Gene 45 Gamma Expression as A Prognostic and Predictive Biomarker in Hepatocellular Carcinoma. *Oncotarget* (2015) 6:27953–65. doi: 10.18632/oncotarget.4446
37. Louveau A, Smirnov I, Keyes TJ, Eccles JD, Rouhani SJ, Peske JD, et al. Structural and Functional Features of Central Nervous System Lymphatic Vessels. *Nature* (2015) 523:337–41. doi: 10.1038/nature14432
38. Zhao J, Chen AX, Gartrell RD, Silverman AM, Aparicio L, Chu T, et al. Immune and Genomic Correlates of Response to Anti-PD-1 Immunotherapy in Glioblastoma. *Nat Med* (2019) 25:462–9. doi: 10.1038/s41591-019-0349-y
39. Quail DF, Joyce JA. The Microenvironmental Landscape of Brain Tumors. *Cancer Cell* (2017) 31:326–41. doi: 10.1016/j.ccell.2017.02.009
40. Wang X, Gao M, Ye J, Jiang Q, Yang Q, Zhang C, et al. An Immune Gene-Related Five-LncRNA Signature for to Predict Glioma Prognosis. *Front Genet* (2020) 11:612037. doi: 10.3389/fgene.2020.612037
41. Galon J, Bruni D. Tumor Immunology and Tumor Evolution: Intertwined Histories. *Immunity* (2020) 52:55–81. doi: 10.1016/j.immuni.2019.12.018
42. Qi Y, Liu B, Sun Q, Xiong X, Chen Q. Immune Checkpoint Targeted Therapy in Glioma: Status and Hopes. *Front Immunol* (2020) 11:578877. doi: 10.3389/fimmu.2020.578877
43. Ruggeri L, Capanni M, Urbani E, Perruccio K, Shlomchik WD, Tosti A, et al. Effectiveness of Donor Natural Killer Cell Alloreactivity in Mismatched Hematopoietic Transplants. *Science* (2002) 295:2097–100. doi: 10.1126/science.1068440
44. Baral A, Ye HX, Jiang PC, Yao Y, Mao Y. B7-H3 and B7-H1 Expression in Cerebral Spinal Fluid and Tumor Tissue Correlates With The Malignancy Grade of Glioma Patients. *Oncol Lett* (2014) 8:1195–201. doi: 10.3892/ol.2014.2268

Conflict of Interest: The authors declare that the research was conducted in the absence of any commercial or financial relationships that could be construed as a potential conflict of interest.

frontiers in Oncology

ORIGINAL RESEARCH
published: 07 July 2021
doi: 10.3389/fonc.2021.696214

Integrated Analysis of the Clinical and Molecular Characteristics of IDH Wild-Type Gliomas in the Chinese Glioma Genome Atlas

Peng Wang[1†], *Yanwei Liu*[1], *Lin Zhi*[1] *and Xiaoguang Qiu*[1,2*†]

[1] Department of Radiation Oncology, Beijing Tiantan Hospital, Capital Medical University, Beijing, China, [2] Department of Molecular Neuropathology, Beijing Neurosurgery Institute, Capital Medical University, Beijing, China

OPEN ACCESS

Edited by:
Zhaohui Zhang,
Renmin Hospital of Wuhan University, China

Reviewed by:
Julie J. Miller,
Massachusetts General Hospital and Harvard Medical School, United States
Hans Binder,
Leipzig University, Germany
Changxiang Yan,
Capital Medical University, China

***Correspondence:**
Xiaoguang Qiu
qiuxiaoguang@bjtth.org

†ORCID:
Peng Wang
orcid.org/0000-0002-5808-4265
Xiaoguang Qiu
orcid.org/0000-0002-6806-9827

Specialty section:
This article was submitted to Neuro-Oncology and Neurosurgical Oncology, a section of the journal Frontiers in Oncology

Received: *16 April 2021*
Accepted: *16 June 2021*
Published: *07 July 2021*

Citation:
Wang P, Liu Y, Zhi L and Qiu X (2021) Integrated Analysis of the Clinical and Molecular Characteristics of IDH Wild-Type Gliomas in the Chinese Glioma Genome Atlas. Front. Oncol. 11:696214. doi: 10.3389/fonc.2021.696214

Purpose: Current studies and guidelines suggest that the biobehavior of IDH-wild type (IDH-wt) lower-grade glioma (LGG, WHO II-III) is similar to IDH-wt glioblastoma (GBM). However, differences in their clinical and molecular characteristics have not been reported. This study aimed to analyze the clinical and genetic information of gliomas with IDH-wt.

Methods: 389 patients with IDH-wt were enrolled in the study (LGG=165, GBM=224), and their clinical and genetic information was collected from the Chinese Glioma Genome Atlas (CGGA). We conducted an analysis of this information between the two groups of patients and drew conclusions thereof.

Results: The median age of the LGG patients was 42 (18–74) years, whereas that of the GBM patients was 51 (18–79) years ($P < 0.010$). GBM patients were more likely to undergo total resection ($P = 0.018$) and had fewer epileptic seizure symptoms ($P < 0.001$). The median overall survival (OS) was 55 months for the LGG patients and only 14.83 months for the GBM patients ($P < 0.01$). The median progression-free survival (PFS) was 44 months for the LGG patients and only 9.767 months for the GBM patients ($P < 0.001$). GBM patients were more prone to PETN mutations ($P = 0.010$). Transcriptome analysis showed that the differentially expressed genes in LGG patients were mainly enriched in metabolic pathways and pathways in cancer and in the function of signal transduction and positive regulation of GTPase activity, whereas in GBM patients, they were mainly enriched in the PI3K-Akt signaling pathway and in the functions of apoptotic process and oxidation-reduction process.

Conclusions: Our data indicate that these two groups of patients should be re-evaluated and treated differently, despite both having IDH wild type.

Keywords: Lower-grade glioma, Glioblastoma, IDH wild-type, molecular pathology, whole exome sequencing

INTRODUCTION

Gliomas are the most common and lethal type of primary malignant central nervous system (CNS) tumor, with an extremely poor prognosis. They comprise approximately 30% of all brain tumors and 80% of all malignant brain tumors (1). According to the World Health Organization (WHO) classification of tumors of the CNS, malignant adult diffuse gliomas are classified into grades II to IV based on their histologic features. In the 2016 edition of the classification, gliomas were subdivided into more subtypes based on molecular features, such as 1p/19q codeletion and IDH mutational status (2–4). With the addition of molecular pathology to the diagnosis of glioma by the WHO in 2016, the classification of glioma has undergone new changes, providing a new basis for the prediction of patient treatment and prognosis, thus improving the accuracy of treatment (5, 6). With the newly proposed molecular pathology-based diagnosis, IDH, as a very important classification standard, has been widely used in the classification and diagnosis of glioma (7). According to Yan et al.'s research, more than 80% of LGGs harbor an IDH mutation, including diffuse astrocytoma (grade II, 90%), pleomorphic xanthoastrocytoma (grade II, 14%), and anaplastic astrocytoma (grade III, 73%), whereas only 5% of primary GBMs contain IDH mutations (2, 3, 8).

Current studies have mainly focused on a comparison between IDH mutant-type LGG and GBM. Few studies have been conducted on glioma with IDH-wt. According to the latest studies by the RTOG 9802 and Kosuke et al., the prognosis of IDH-wt LGG is substantially poor, with a median OS and PFS of 22.8 and 8.4 months, respectively, close to those of GBM (9, 10). In addition, in terms of molecular genetic background, IDH-wt LGG and GBM are similar, and some researchers believe that IDH-wt GBM may develop from IDH-wt LGG (11). In addition, in the third cIMPACT-NOW report, the committee recommended reclassifying IDH1/2 wild-type diffuse lower-grade gliomas of WHO grade II and III (LGG) as diffuse astrocytic glioma, IDH1/2-wt with molecular features of glioblastoma (12). Moreover, NCCN guidelines recommend that IDH wild-type LGG be treated using therapy typical for GBM (13). However, according to the abovementioned reports and the latest literature, as well as our data, we found that IDH-wt LGG and IDH-wt GBM may have differences in their prognoses and molecular features, such as TERT promoter mutation and EGFR amplification, which may lead to differences in treatment (12, 14).

Our study explored the differences between the two types of glioma by comparing the clinical and genetic information of 389 patients, which will provide a theoretical basis for better distinguishing the two types of patients and future precision medicine.

METHODS

Patients

We screened 850 IDH wild-type glioma patients from 2546 glioma patients in the Chinese Glioma Genome Atlas (CGGA) database (http://cgga.org.cn/), and a further 389 patients were obtained according to the following conditions: they have complete clinical information, older than 18 years, newly diagnosed, and received the standard treatment regimen. All patients were followed up until May 2019 or death, after they received the first operation. Their clinical characteristics, such as age, sex, resection range, survival, and chemotherapy regimen, and molecular pathological information, such as 1p/19q co-deletion, MGMT methylation status, and PTEN mutational status, were collected for subsequent analysis. We also selected 140 of the 389 patients to collect their mRNA sequencing (mRNA-seq) data. All patients received the treatment regimen based on the NCCN guideline and received the MRI examination within 24 h after the operation to assess the extent of resection (15). All research performed was approved by the Tiantan Hospital Institutional Review Board (IRB). All the subjects were diagnosed with glioma by consensus, according to central pathology reviews by independent board-certified neuropathologists and further graded based on the 2007/2016 WHO classification. Written informed consent was obtained from all patients.

Identification of Molecular Alterations

IDH1/2 (IDH) mutational status and the methylation status of the O6-methylguanine-DNA methyl-transferase (MGMT) promoter were detected by pyrosequencing. We predicted 1p/19q codeletion status by FISH. To determine the mutation status of P53 and PTEN, we used an immunohistochemical method (16–19).

Data Analysis

To identify the gene sets related to particular biological processes present in IDH-wt LGG and GBM, we screened 140 patients from 398 patients (61LGG, 79GBM), and collected their WEseq data, then gene expression profiling and gene set enrichment analysis (GSEA) were performed as described previously (20). The analysis we conducted was based on that found on the Database for Annotation, Visualization, and Integrated Discovery (DAVID) website (21, 22). Survival distributions were estimated with Kaplan-Meier survival analysis, and log-rank analysis was used to assess the significance of differences between stratified survival groups using GraphPad Prism 8.0 statistical software. The χ^2 test was performed by SPSS software (IBM SPSS Statistics 24). We found the gene sequencing data of the enrolled patients through the CGGA database, calculated the mean value of each gene, and then used unpaired *t* test grouping to select genes of interest in IDH-wt LGG and GBM. We used R Studio to perform supervised cluster analysis on the screened differential genes to identify whether they were different from each other.

RESULTS

Clinical Information Analysis

In this study, we enrolled 165 LGG patients and 224 GBM patients. In terms of clinical information, LGG cohort has 99

male and 66 female, GBM cohort has 146 male and 78 female patients. In terms of clinical information, we found that the median age of the IDH wild-type LGG and GBM patients was 42 years (range, 18–74 years; primarily 40–47 years, with a median age of 42 years) and 51 years (range, 18–79 years; primarily 47–53 years; with a median age of 51 years), respectively ($P < 0.010$). 135 (60.3%) IDH-wt GBM patients and 77 (46.7%) LGG patients underwent total resection ($P = 0.018$). Epileptic symptoms were noted for 50 (22.3%) IDH-wt GBM patients and 82 (49.7%) IDH-wt LGG patients ($P < 0.001$). There was no significant difference in the extent of invasion (multilobe LGG, 56 patients (33.9%); multilobe GBM, 74 patients (33%); $P = 0.264$) or sex ($P = 0.296$) between the two groups of patients. Data for all of the above patients are shown in **Table 1**. As to therapy, 134 LGG patients (81.2%) received radiotherapy and 190 GBM patients (84.8%) received radiotherapy ($P = 0.072$). 80 LGG patients (48.5%) received chemotherapy and 159 GBM patients (71.0%) received chemotherapy ($P < 0.001$).

Molecular Pathological Characteristics

Among the patient information we collected, 1p/19q codeletion occurred in none of the IDH-wt GBM patients (0%) or IDH-wt LGG patients (0%). About 5% LGG patients have PTEN mutation versus 11.6% GBM patients ($P = 0.010$). However, in our data, there was no significant difference in MGMT methylation status (15.2% LGG has methylation and 30.8% GBM has methylation, $P = 0.520$), P53 mutational status (7.9% LGG was mutant, 7.6% GBM was mutant, $P = 0.518$), TERT promoter mutations (7.3% LGG was mutant, 9.8% GBM was mutant, $P = 0.991$), and EGFR amplification (4.2% LGG was amplification and 6.3% GBM was amplification, P=0.204) between the two groups of patients (**Table 1**).

Survival Analysis

To understand patient prognosis, we collected survival data from the enrolled cohort. The overall survival (OS) was 55 months for the IDH-wt LGG patients and only 14.83 months for the IDH-wt GBM patients (Hazard ratio, 0.3213; 95% CI of hazard ratio, 0.2543-0.4060; P < 0.001). The median progression-free survival (PFS) was 44 months for IDH-wt LGG and only 9.767 months for GBM (HR, 0.3535; 95% CI, 0.2826-0.4421; P < 0.001) (**Figure 1**). By Kaplan-Meier survival analysis, we found significant differences in survival between the two groups, even though the treatment strategy for IDH-wt LGG was less aggressive than that for IDH-wt GBM. We performed univariable Cox regression analysis on the patient prognostic data and found that in LGG, patients with MGMT methylation had a better prognosis ($P < 0.001$). The prognosis of LGG patients who did not undergo radiotherapy or chemotherapy was better ($P = 0.038$). In LGG, the prognosis of grade 2 glioma was significantly better than that of grade 3 glioma ($P < 0.001$). In GBM, patients without PTEN mutations had a better prognosis ($P = 0.023$). Intraoperative total tumor resection ($P = 0.015$), postoperative radiotherapy ($P = 0.034$), and postoperative acceptance with chemotherapy ($P < 0.001$) were associated with a better prognosis. Then we performed a multivariate analysis using the SPSS software and found that the prognostic factors were different between the two groups of patients. In LGG, the OS and PFS were mainly affected by MGMT methylation ($P < 0.001$), TERT promoter mutation ($P = 0.005$), TP53 ($P = 0.002$), and the onset age ($P < 0.001$). While in GBM, the OS and PFS were more likely to be affected by interoperative resection ($P = 0.004$), radiotherapy ($P = 0.006$), chemotherapy ($P = 0.001$), and onset age ($P = 0.03$).

TABLE 1 | Characteristics of clinical and molecular in this study.

Characteristics	II-III grade (IDH wild-type)	Primary GBM (IDH wild-type)	P value
Total	165 (42.4%)	224 (56%)	NA
Age	42 (18-74)	51 (18-79)	<0.01
Gender			0.296
Male	99 (60.0%)	146 (65.2%)	
Female	66 (40.0%)	78 (34.8)	
Resection			0.018
Total resection	77 (46.7%)	135 (60.3%)	
Subtotal resection	74 (44.8%)	78 (34.8%)	
NA	14 (8.5%)	11 (4.9%)	
Tumor location			0.264
Multi lobe	56 (33.9%)	74 (33.0%)	
Single lobe	78 (47.3%)	79 (35.3%)	
NA	31 (18.8%)	71 (31.7%)	
Symptom			<0.001
Seizure	82 (49.7%)	50 (22.3%)	
No seizure	69 (41.8%)	153 (68.3%)	
NA	14 (8.5%)	21 (9.4%)	
Radiotherapy			0.072
Yes	134 (81.2%)	190 (84.8%)	
No	27 (16.4%)	22 (9.8%)	
NA	4 (2.4%)	12 (5.4%)	
Chemotherapy			<0.001
Yes	80 (48.5%)	159 (71.0%)	
No	78 (47.3%)	56 (25.0%)	
NA	7 (4.2%)	9 (4%)	
Median PFS (Mo)	44	9.767	<0.001
Median OS (Mo)	55	14.83	<0.001
1p/19q codeletion			NA
Yes	0 (0%)	0 (0%)	
No	51 (30.9%)	106 (47.3%)	
NA	114 (69.1%)	118 (52.7%)	
MGMT methylation			0.520
Yes	25 (15.2%)	69 (30.8%)	
No	42 (25.5%)	140 (62.5%)	
NA	98 (59.4%)	15 (6.7%)	
PETN			0.010
Yes (wild)	88 (53.3%)	79 (35.3%)	
No (mutant)	8 (5.0%)	26 (11.6%)	
NA	69 (41.7%)	119 (53.1%)	
P53			0.518
Yes (wild)	87 (52.7%)	88 (39.3%)	
No (mutant)	13 (7.9%)	17 (7.6%)	
NA	65 (39.4%)	119 (53.1%)	
TERT			0.991
Mutant	12 (7.3%)	22 (9.8%)	
Wild	17 (10.3%)	31 (13.8%)	
NA	136 (82.4%)	171 (76.4%)	
EGFR			0.204
Amplification	7 (4.2%)	14 (6.3%)	
Wild	125 (75.8%)	138 (61.6%)	
NA	33 (20%)	72 (32.1%)	

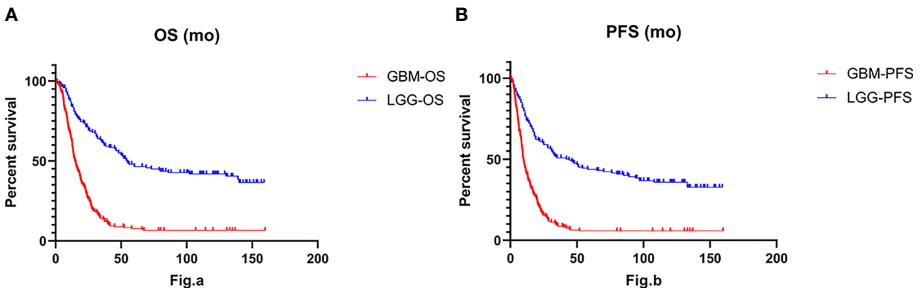

FIGURE 1 | The Log-rank test and Gehan-Breslow-Wilcoxon test for overall survival (OS) **(A)** and progression-free survival (PFS) **(B)** indicate that IDH-wt LGG was associated with longer overall survival ($P < 0.001$) and longer progression-free survival ($P < 0.001$) than IDH-wt GBM.

Gene Expression Analysis

We used R Studio to perform supervised cluster analysis on the 140 patient gene sequencing data (61 LGG and 79 GBM) and obtained gene heat maps describing the levels of gene expression in the different patient groups (**Figure 2**). Through the obtained gene heat map, it can be seen that there are obvious differences in the gene expression levels and gene expression types between IDH-wt LGG patients and IDH-wt GBM patients. Gene expression in LGG patients was more concentrated in the upper left corner of the picture, the first quarter of the list of genes, this part of the gene is low expressed in GBM patients. We screened the IDH-wt LGG and GBM genes from the database and performed Gene Ontology (GO) analysis. The results of the analysis were completely different for gliomas of different grades (**Figure 3**). The differentially expressed genes in patients with IDH-wt LGG were mainly enriched in the signal transduction

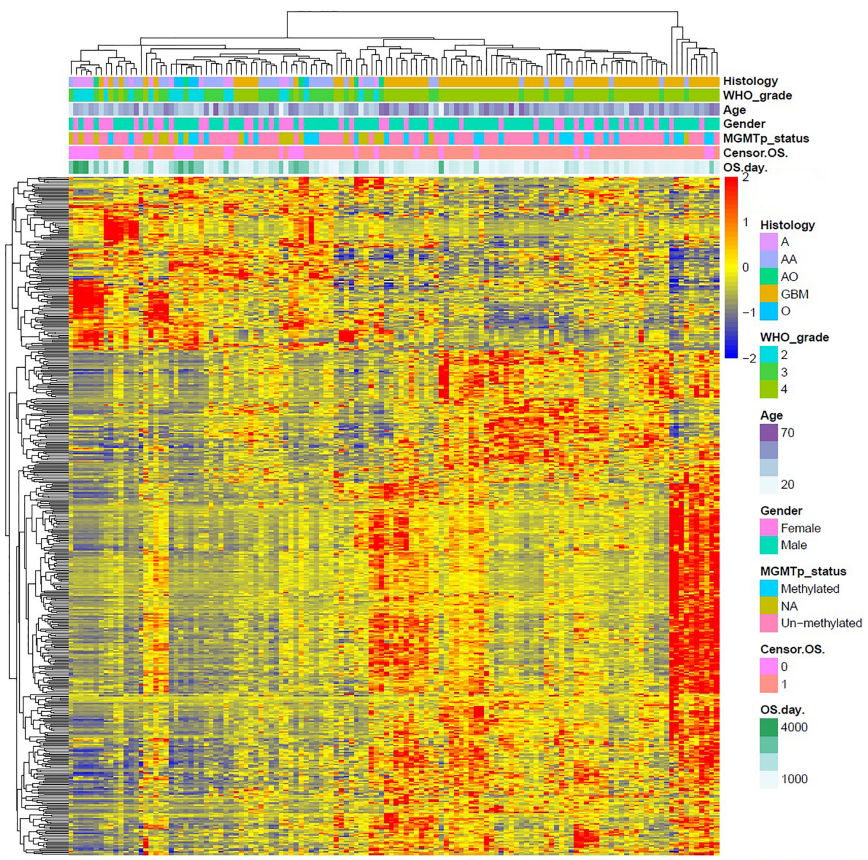

FIGURE 2 | Supervised cluster analysis of the gene sequencing data. We obtained gene heat maps describing gene expression in the different patient groups and found that there were obvious differences in gene expression levels and gene expression types between IDH-wt LGG patients and IDH-wt GBM patients.

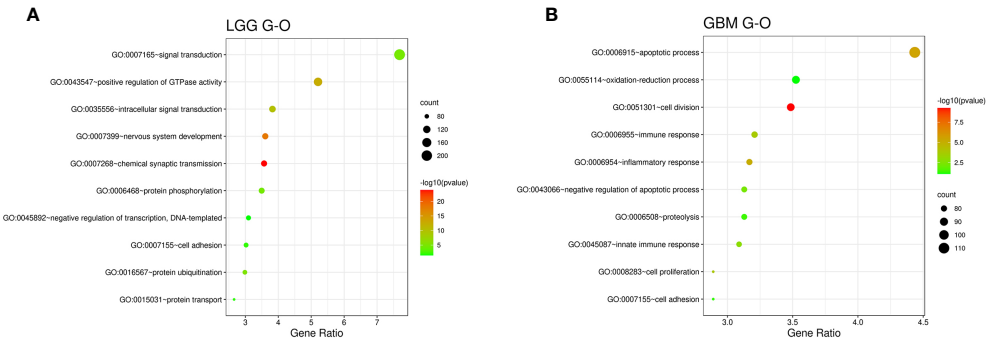

FIGURE 3 | Functional enrichment analysis of associated genes for LGG **(A)** and GBM **(B)**, indicating the functional roles of the gene sets in the different subgroups. Enrichment results for biological processes were obtained from the GO database. The orders of the biological processes listed in the bubble chart are based on the number of targets annotated in biological process (BP).

and positive regulation of GTPase activity functions, whereas those in patients with IDH-wt GBM were mainly enriched in the functions of apoptotic process and oxidation–reduction process.

We compared the gene expression of the patients and used the Kyoto Encyclopedia of Genes and Genomes (KEGG) database provided by the DAVID website for correlation analysis and found that the cellular pathways of IDH wild-type LGG and GBM were completely different in terms of magnitude and function (21, 22). The differentially expressed genes in LGG were mainly enriched in metabolic pathways and MAPK signaling pathway, whereas those in GBM were mainly enriched in the Focal adhesion and HTLV-1 infection (**Figure 4**).

DISCUSSION

Following the release of the WHO's new glioma classification in 2016, there has been a growing trend toward precision medicine. Our research compared the clinical information, molecular pathology, and gene expression between IDH-wt LGG and GBM patients. According to the results of our analysis, we found that there were significant differences between the two groups in the abovementioned aspects.

Clinical Information

We use the chi-square test to analyze the two cohort patients, and we found that there is no significant difference between them in gender ($P = 0.296$). The IDH-wt LGG patients were more elderly than GBM patients in our patients ($P < 0.01$). According to Ostorm et al.'s research, GBM is mainly found in elderly patients (65-75), and LGG is mainly found in younger patients (age<65) (23). By comparing the two sets of data, we found that our conclusion is similar to them, but our patients have a younger onset age than them, this may be because our patients are all IDH-wt glioma patients, and these characteristics of molecular (IDH-wt) might lead to a tendency toward a younger age of onset in GBM, and the primary LGG patients was much more younger than the primary GBM patients. Epilepsy is one of the most common symptoms of glioma patients, so we collected the history of epilepsy of the enrolled patients. Through the chi-square test, we found that there was a significant difference between the two groups of patients ($P < 0.001$), so we believe that LGG patients are more likely to have epileptic through the course of the disease,

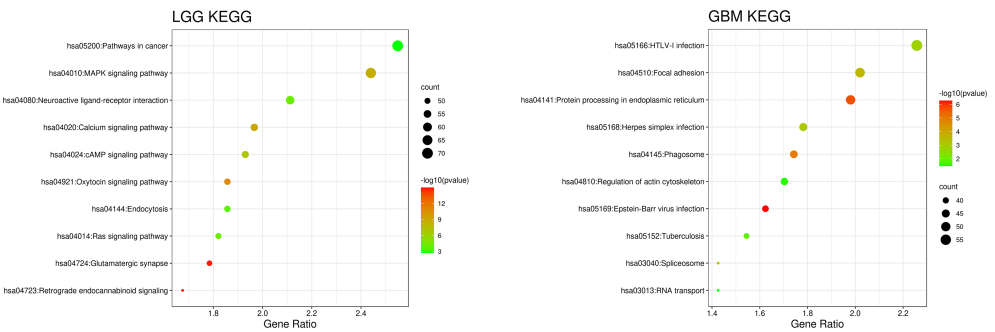

FIGURE 4 | Patient gene expression analysis was performed using the Kyoto Encyclopedia of Genes and Genomes (KEGG) database provided by the DAVID website for correlation analysis. The orders of the biological processes listed in the bubble chart are based on the number of targets annotated in biological process (BP).

which may because LGG is more incline to widespread invasion growth pattern, whereas the GBM are more likely show the characteristics of localized growth. Through the chi-square test, we found that there are no differences in the two patient groups in tumor location. In the treatment regimen, by collecting patient surgical data, we found that GBM patients are more inclined to undergo total tumor resection, and the LGG patients are more likely receive partial resection, which may because the course of LGG is longer and the scope of tumor invasion may be wider than GBM; furthermore, there is no obvious MRI enhancement boundary, so surgery for total resection may be difficult. Through the chi-square test, we found that there is a tendency that GBM patients were more likely to receive radiotherapy after the operations ($P = 0.072$). Besides, in LGG patients, 80 (48.5%) received TMZ for chemotherapy and 78 (47.3%) were not, whereas in GBM patients, 159 (71%) has TMZ for chemotherapy and 56 (25.0%) did not receive any chemotherapy. The chi-square test suggests that there have obviously been differences between them ($P < 0.001$). In summary, we concluded that there are significant differences between LGG and GBM in terms of clinical manifestations.

Molecular Pathological Characteristics

Among the patients we collected, none of the LGG or GBM patients had 1p/19q codeletion. This result is consistent with the current major view (24). In LGG patients, eight (5.0%) patients have PTEN mutation and 26 (11.6%) GBM patients have PTEN mutation, which is more than double the rate for LGG, so we conducted that GBM are more incline to PTEN mutation ($P = 0.010$). By studying the previous literature, we found that the abovementioned data are consistent with the previously reported data (25–28). In regard to p53 mutational status and MGMT methylation status, we could not find any significant differences. The chi-square test results showed that the P value for the difference in P53 mutational status between IDH-wt LGG and GBM was 0.518, whereas that for the MGMT methylation status the P value was 0.52, indicating no statistically significant difference between the groups for either condition. And the same condition is true for TERT promoter ($P = 0.991$) and EGFR amplification ($P = 0.204$). Through the abovementioned analysis, we believe that although only some of the abovementioned molecular pathological characteristics are different between IDH-wt LGG and GBM, significant differences were demonstrated in at least PETN mutational status.

Survival Analysis

By analyzing the survival data, we found that although the treatment strategy for IDH-wt LGG is less aggressive than GBM, its OS and PFS were still better ($P < 0.001$). It is generally accepted that some molecular characteristics are associated with a better prognosis, just like MGMT methylation and PTEN or P53. Combined with the molecular pathological characteristics, we believe that LGG is different from GBM. According to the research data from RTOG 9802, the OS and PFS of LGG are 7.5 and 4.4 years, respectively, which are significantly longer than what we reported. However, the RTOG 9802 was mainly focused on IDH mutation patients, whereas they found that the LGG patients have a better prognosis than GBM patients, and our study draws the same conclusion (29). Then we conducted a COX analysis and found a different conclusion about it. In LGG, the better prognosis is associated with MGMT methylation and no radiotherapy ($P = 0.199$) and no chemotherapy ($P = 0.744$). However, in GBM, the better prognosis is more inclined to NO PTEN mutation, total resection, radiotherapy, and chemotherapy. Besides, age affected both OS and PFS in LGG and GBM patients (**Table 2**).

TABLE 2 | Multivariate analysis results for LGG and GBM patients.

		Event	B	P	OR	95% CR CI
LGG	OS	MGMT	1.239	<0.001	3.453	2.007–5.940
		TERT	−1.522	0.005	0.218	0.075–0.634
		TP53	1.142	0.002	3.134	1.542–6.446
		Radiotherapy	−1.538	0.199	0.215	0.021–2.247
		Chemotherapy	0.331	0.744	1.393	0.190–10.204
		Age	0.023	0.01	1.023	1.005–1.040
	PFS	MGMT	1.249	<0.001	3.487	2.076–5.856
		TERT	−0.687	0.006	0.503	0.307–0.824
		TP53	0.445	0.012	1.561	1.104–2.208
		Radiotherapy	−1.507	0.208	0.222	0.021–2.315
		Chemotherapy	0.474	0.64	1.606	0.220–11.731
		Age	0.029	<0.001	1.03	1.013–1.047
GBM	OS	MGMT	0.76	0.013	2.139	1.174–3.897
		PTEN	−0.709	0.038	0.492	0.252–0.961
		Resection	−0.575	0.004	0.562	0.277–1.141
		Radiotherapy	−0.402	0.006	0.669	0.190–2.360
		Chemotherapy	1.395	0.001	4.037	0.890–18.302
		Age	0.014	0.026	1.014	1.002–1.027
	PFS	Resection	−0.435	0.005	0.647	0.319–1.311
		Radiotherapy	−0.391	0.009	0.677	0.190–2.406
		Chemotherapy	1.626	0.033	5.084	1.139–22.692
		Age	0.014	0.03	1.014	1.001–1.026

Gene Expression Analysis

Based on the above differences in clinical and molecular pathology, we found 3,000 differentially expressed genes from the CGGA database between the two groups through unpaired t-test analysis ($P < 0.01$). Through these differentially expressed genes, we conducted supervised clustering analysis and produced a gene heatmap. Through the heatmap, we found that the LGG patients were more concentrated in the first 700 genes. While the GBM was mainly gathering in the later 2000 genes. Since the GBM patients' heatmap clearly split into different transcriptomic classes, we also conducted a supervised cluster analysis of gene expression in GBM patients alone and found that these patients met Verhaak's classes (**Figure 5**) (30). Then we used full genes list to perform GO analysis and KEGG pathway analysis and found that there were also differences in the signaling pathways and protein expression levels between LGG and GBM patients. The differentially expressed genes in LGG patients primarily performed the function of signal transduction (GO:0007165), positive regulation of GTPase activity (GO:0043547), and so on (**Figure 3A**), according to the G-O database, we found that LGG mainly focused on the upregulate signal transduction, activation of GTPase activity, and positive regulation of guanyl-nucleotide exchange factor activity, obviously, it could help the progress of the tumor, whereas those among GBM patients primarily performed the functions of apoptotic process (GO:0006915), oxidation-reduction process (GO:0055114), cell division (GO:0051301), and so on (**Figure 3B**). which means GBM has the function of positive regulation of apoptotic process and neuron apoptotic process. Besides, although the oxidation-reduction process is obsolete, it still shows that GBM has a hypermetabolic state, this might mean that GBM is in a highly proliferative state. Regarding to KEGG pathway analysis, the differentially expressed genes in LGG were more enriched in pathways in cancer (hsa05200), MAPK signaling pathway (has04010), and so on (**Figure 4A**), which was mainly associated with various cellular functions, including cell proliferation, differentiation, migration. Besides, it is also linked to evading apoptosis, proliferation, and sustained angiogenesis. All the pathways are associated with upregulating tumor growth, whereas those in GBM were more enriched in the HTLV-1 infection pathway (hsa05166), focal adhesion (hsa04510), and so on (**Figure 4B**). HTLV-1, which is human T-cell leukemia virus type 1 in full name, is a pathogenic retrovirus that is associated with adult T-cell leukemia/

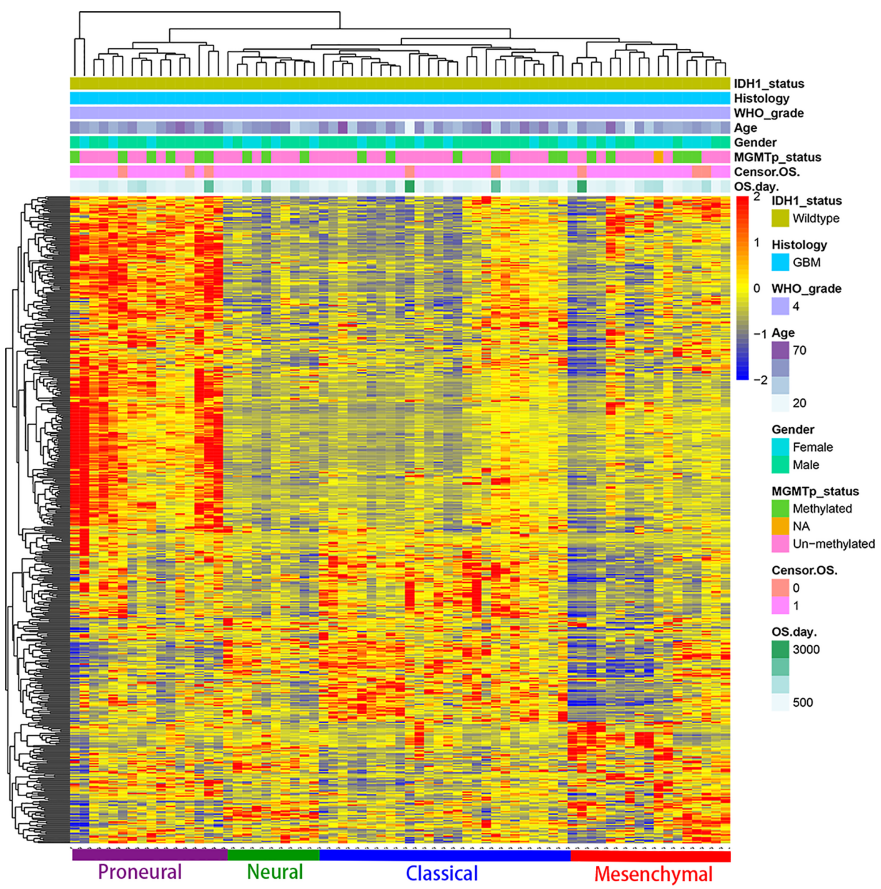

FIGURE 5 | Supervised cluster analysis of gene expression in GBM patients shows it suits the Verhaak's classes well.

lymphoma (ATL) (31). However, it is also linked to some classical pathways and genes, such as PI3K-Akt and PTEN, so we believe it has a deep impact on GBM patients. Compared with LGG, the GBM G-O analysis and KEGG express were different.

Although IDH-wt LGG and GBM have many similarities, the current data and research are insufficient to show that they are the same, nor can IDH-wt LGG be treated the same way as GBM. Further research is needed to reclassify these diseases in greater detail. However, according to the recently released NCCN 2020 treatment guidelines, IDH-wt LGG should be treated more similarly to GBM. Therefore, whether this regimen is the most suitable treatment regimen should be further analyzed (13).

Although the results of our analysis are relatively significant, this study included data from the CGGA database, which contain data only on Asians, which may cause a certain bias in the gene expression. In addition, our study only included newly diagnosed patients and excluded recurrent GBM patients, which may also produce a certain bias for this latter group. Currently, treatment regimens for IDH-wt LGG in the NCCN treatment guidelines tend to be consistent with GBM, and the 3rd version of cIMPACT-NOW indicates that when IDH-wt diffuse astrocytoma has certain molecular pathological characteristics, it can be considered a WHO grade IV glioma; however, through our analysis of clinical information, molecular pathology, and gene expression, we found that there are still many differences between IDH-wt LGG and GBM (12, 13)

CONCLUSION

Through the abovementioned analyses, we found that there are differences between LGG and GBM in terms of prognosis, epilepsy, resection range, PTEN mutational status, and biological behavior. These differences imply that whether the current treatment regimen is ideal still needs to be explored further.

DATA AVAILABILITY STATEMENT

Publicly available datasets were analyzed in this study. This data can be found here: Chinese Glioma Genome Atlas.

ETHICS STATEMENT

The studies involving human participants were reviewed and approved by Ethics Committee of Beijing Tiantan Hospital. Written informed consent to participate in this study was provided by the participants' legal guardian/next of kin.

AUTHOR CONTRIBUTIONS

PW was a major contributor in writing the manuscript. All authors contributed to the article and approved the submitted version.

FUNDING

This work was supported by the following foundations. The funding sources had no influence on the design, performance, or reporting of this study. Beijing Municipal Bureau of Health (to XQ, Grant number: N/A), Beijing Natural Science Foundation (to YL, Grant number: 7192057), Beijing Hospitals Authority Youth Programme (to YL, Grant number: QML20190506).

ACKNOWLEDGMENTS

The authors thank the participants and their colleagues, especially Yanong Li, Zheng Zhao, Jing Zhang, Shuo Zhang and Bowei Xiao for their extraordinary contributions.

REFERENCES

1. Perry A, Wesseling P. Histologic Classification of Gliomas. *Handb Clin Neurol* (2016) 134:71–95. doi: 10.1016/B978-0-12-802997-8.00005-0
2. Wang P, Dong Q, Zhang C, Kuan PF, Liu Y, Jeck WR, et al. Mutations in Isocitrate Dehydrogenase 1 and 2 Occur Frequently in Intrahepatic Cholangiocarcinomas and Share Hypermethylation Targets With Glioblastomas. *Oncogene* (2013) 32(25):3091–100. doi: 10.1038/onc.2012.315
3. De Carli E, Wang X, Puget S. IDH1 and IDH2 Mutations in Gliomas. *N Engl J Med* (2009) 360(21):2248; author reply 2249. doi: 10.1056/NEJMc090593
4. Yan H, Parsons DW, Jin G, McLendon R, Rasheed BA, Yuan W, et al. IDH1 and IDH2 Mutations in Gliomas. *N Engl J Med* (2009) 360(8):765–73. doi: 10.1016/S0513-5117(09)79085-4
5. Louis DN, Perry A, Reifenberger G, von Deimling A, Figarella–Branger D, Cavenee WK, et al. The 2016 World Health Organization Classification of Tumors of the Central Nervous System: A Summary. *Acta Neuropathol* (2016) 131(6):803–20. doi: 10.1007/s00401-016-1545-1
6. Louis DN, Ohgaki H, Wiestler OD, Cavenee WK, Burger PC, Jouvet A, et al. The 2007 WHO Classification of Tumours of the Central Nervous System. *Acta Neuropathol* (2007) 114(2):97–109. doi: 10.1007/s00401-007-0243-4
7. Camelo-Piragua S, Kesari S. Further Understanding of the Pathology of Glioma: Implications for the Clinic. *Expert Rev Neurother* (2016) 16(9):1055–65. doi: 10.1080/14737175.2016.1194755
8. Han CH, Batchelor TT. Isocitrate Dehydrogenase Mutation as a Therapeutic Target in Gliomas. *Chin Clin Oncol* (2017) 6(3):33. doi: 10.21037/cco.2017.06.11
9. Kros JM, Huizer K, Hernandez–Lain A, Marucci G, Michotte A, Pollo B, et al. Evidence-Based Diagnostic Algorithm for Glioma: Analysis of the Results of Pathology Panel Review and Molecular Parameters of EORTC 26951 and 26882 Trials. *J Clin Oncol* (2015) 33(17):1943–50. doi: 10.1200/JCO.2014.59.0166
10. Bell EH, Zhang P, Shaw EG, Buckner JC, Barger GR, Bullard DE, et al. Comprehensive Genomic Analysis in NRG Oncology/Rtog 9802: A Phase III Trial of Radiation Versus Radiation Plus Procarbazine, Lomustine (CCNU), and Vincristine in High-Risk Low-Grade Glioma. *J Clin Oncol* (2020) 38 (29):3407–17. doi: 10.1200/JCO.19.02983
11. Aoki K, Nakamura H, Suzuki H, Matsuo K, Kataoka K, Shimamura T, et al. Prognostic Relevance of Genetic Alterations in Diffuse Lower-Grade Gliomas. *Neuro Oncol* (2018) 20(1):66–77. doi: 10.1093/neuonc/nox132
12. Brat DJ, Aldape K, Colman H, Holland EC, Louis DN, Jenkins RB, et al. cIMPACT-NOW Update 3: Recommended Diagnostic Criteria for "Diffuse Astrocytic Glioma, IDH-Wildtype, With Molecular Features of Glioblastoma,

WHO Grade IV". *Acta Neuropathol* (2018) 136(5):805–10. doi: 10.1007/s00401-018-1913-0
13. Nabors LB, Portnow J, Ahluwalia M, Baehring J, Brem H, Brem S, et al. Central Nervous System Cancers, Version 3.2020, NCCN Clinical Practice Guidelines in Oncology. *J Natl Compr Canc Netw* (2020) 18(11):1537–70. doi: 10.6004/jnccn.2020.0052
14. Eckel-Passow JE, Lachance DH, Molinaro AM, Walsh KM, Decker PA, Sicotte H, et al. Glioma Groups Based on 1p/19q, IDH, and TERT Promoter Mutations in Tumors. *N Engl J Med* (2015) 372(26):2499–508. doi: 10.1056/NEJMoa1407279
15. Jiang T, Nam DH, Ram Z, Poon WS, Wang J, Boldbaatar D, et al. Clinical Practice Guidelines for the Management of Adult Diffuse Gliomas. *Cancer Lett* (2021) 499:60–72. doi: 10.1101/gr.165126.113
16. Bao ZS, Chen HM, Yang MY, Zhang CB, Yu K, Ye WL, et al. RNA-Seq of 272 Gliomas Revealed a Novel, Recurrent PTPRZ1-MET Fusion Transcript in Secondary Glioblastomas. *Genome Res* (2014) 24(11):1765–73. doi: 10.1101/gr.165126.113
17. Zhang W, Yan W, You G, Bao Z, Wang Y, Liu Y, et al. Genome-Wide DNA Methylation Profiling Identifies ALDH1A3 Promoter Methylation as a Prognostic Predictor in G-CIMP- Primary Glioblastoma. *Cancer Lett* (2013) 328(1):120–5. doi: 10.1016/j.canlet.2012.08.033
18. Cai J, Chen J, Zhang W, Yang P, Zhang C, Li M, et al. Loss of ATRX, Associated With DNA Methylation Pattern of Chromosome End, Impacted Biological Behaviors of Astrocytic Tumors. *Oncotarget* (2015) 6(20):18105–15. doi: 10.18632/oncotarget.3906
19. Hu X, Martinez–Ledesma E, Zheng S, Kim H, Barthel F, Jiang T, et al. Multigene Signature for Predicting Prognosis of Patients With 1p19q Co-Deletion Diffuse Glioma. *Neuro Oncol* (2017) 19(6):786–95. doi: 10.1093/neuonc/now285
20. Subramanian A, Tamayo P, Mootha VK, Mukherjee S, Ebert BL, Gillette MA, et al. Gene Set Enrichment Analysis: A Knowledge-Based Approach for Interpreting Genome-Wide Expression Profiles. *Proc Natl Acad Sci USA* (2005) 102(43):15545–50. doi: 10.1073/pnas.0506580102
21. Huang da W, Sherman BT, Lempicki RA. Bioinformatics Enrichment Tools: Paths Toward the Comprehensive Functional Analysis of Large Gene Lists. *Nucleic Acids Res* (2009) 37(1):1–13. doi: 10.1093/nar/gkn923
22. Huang da W, Sherman BT, Lempicki RA. Systematic and Integrative Analysis of Large Gene Lists Using DAVID Bioinformatics Resources. *Nat Protoc* (2009) 4(1):44–57. doi: 10.1038/nprot.2008.211
23. Ostrom QT, Bauchet L, Davis FG, Deltour I, Fisher JL, Langer CE, et al. The Epidemiology of Glioma in Adults: A "State of the Science" Review. *Neuro Oncol* (2014) 16(7):896–913. doi: 10.1093/neuonc/nou087
24. Jenkins RB, Blair H, Ballman KV, Giannini C, Arusell RM, Law M, et al. A T (1;19)(q10;p10) Mediates the Combined Deletions of 1p and 19q and Predicts a Better Prognosis of Patients With Oligodendroglioma. *Cancer Res* (2006) 66 (20):9852–61. doi: 10.1158/0008-5472.CAN-06-1796
25. Limam S, Missaoui N, Abdessayed N, Mestiri S, Selmi B, Mokni M, et al. Prognostic Significance of MGMT Methylation and Expression of MGMT, P53, EGFR, MDM2 and PTEN in Glioblastoma Multiforme. *Ann Biol Clin (Paris)* (2019) 77(3):307–17. doi: 10.1684/abc.2019.1448
26. Trabelsi S, Mama N, Ladib M, Karmeni N, Haddaji Mastouri M, Chourabi M, et al. MGMT Methylation Assessment in Glioblastoma: MS-MLPA Versus Human Methylation 450K Beadchip Array and Immunohistochemistry. *Clin Transl Oncol* (2016) 18(4):391–7. doi: 10.1007/s12094-015-1381-0
27. Soomro SH, Ting LR, Qing YY, Ren M, et al. Molecular Biology of Glioblastoma: Classification and Mutational Locations. *J Pak Med Assoc* (2017) 67(9):1410–4.
28. Gittleman H, Sloan AE, Barnholtz-Sloan JS. An Independently Validated Survival Nomogram for Lower-Grade Glioma. *Neuro Oncol* (2020) 22(5):665–74. doi: 10.1093/neuonc/noz191
29. Shaw EG, Wang M, Coons SW, Brachman DG, Buckner JC, Stelzer KJ, et al. Randomized Trial of Radiation Therapy Plus Procarbazine, Lomustine, and Vincristine Chemotherapy for Supratentorial Adult Low-Grade Glioma: Initial Results of RTOG 9802. *J Clin Oncol* (2012) 30(25):3065–70. doi: 10.1200/JCO.2011.35.8598
30. Verhaak RG, Hoadley KA, Purdom E, Wang V, Qi Y, Wilkerson MD, et al. Integrated Genomic Analysis Identifies Clinically Relevant Subtypes of Glioblastoma Characterized by Abnormalities in PDGFRA, Idh1, EGFR, and NF1. *Cancer Cell* (2010) 17(1):98–110. doi: 10.1016/j.ccr.2009.12.020
31. Cook L, Melamed A, Yaguchi H, Bangham CR, et al. The Impact of HTLV-1 on the Cellular Genome. *Curr Opin Virol* (2017) 26:125–31. doi: 10.1016/j.coviro.2017.07.013

Conflict of Interest: The authors declare that the research was conducted in the absence of any commercial or financial relationships that could be construed as a potential conflict of interest.

The reviewer CY declared a shared affiliation, with no collaboration, with one of the authors, XQ, to the handling editor.

frontiers in Oncology

REVIEW
published: 05 August 2021
doi: 10.3389/fonc.2021.694498

Advanced Diagnosis of Glioma by Using Emerging Magnetic Resonance Sequences

*Ruo-Lun Wei and Xin-Ting Wei**

Department of Neurosurgery, The First Affiliated Hospital of Zhengzhou University, Zhengzhou, China

Glioma, the most common primary brain tumor in adults, can be difficult to discern radiologically from other brain lesions, which affects surgical planning and follow-up treatment. Recent advances in MRI demonstrate that preoperative diagnosis of glioma has stepped into molecular and algorithm-assisted levels. Specifically, the histology-based glioma classification is composed of multiple different molecular subtypes with distinct behavior, prognosis, and response to therapy, and now each aspect can be assessed by corresponding emerging MR sequences like amide proton transfer-weighted MRI, inflow-based vascular-space-occupancy MRI, and radiomics algorithm. As a result of this novel progress, the clinical practice of glioma has been updated. Accurate diagnosis of glioma at the molecular level can be achieved ahead of the operation to formulate a thorough plan including surgery radical level, shortened length of stay, flexible follow-up plan, timely therapy response feedback, and eventually benefit patients individually.

Keywords: glioma, radiomics, preoperative grading, differential diagnosis, 7-T magnetic resonance imaging, response assessment in neuro-oncology (RANO), magnetic resonance image

OPEN ACCESS

Edited by:
Liam Chen,
University of Minnesota, United States

Reviewed by:
Kristin Huntoon,
University of Texas MD Anderson Cancer Center, United States
Remy Guillevin,
Centre Hospitalier Universitaire (CHU) de Poitiers, France
Alessia Pellerino,
University Hospital of the City of Health and Science of Turin, Italy

***Correspondence:**
Xin-Ting Wei
weixinting777@126.com
orcid.org/0000-0002-0482-2402

Specialty section:
This article was submitted to Neuro-Oncology and Neurosurgical Oncology, a section of the journal Frontiers in Oncology

Received: *13 April 2021*
Accepted: *19 July 2021*
Published: *05 August 2021*

Citation:
Wei R-L and Wei X-T (2021) Advanced Diagnosis of Glioma by Using Emerging Magnetic Resonance Sequences. Front. Oncol. 11:694498. doi: 10.3389/fonc.2021.694498

INTRODUCTION

With its heterogeneous histological and imaging features, gliomas may still be the most common primary brain tumors in adults. The prognosis of patients with gliomas is not better than that of patients with other cancers, even for glioma patients who undergo various therapies such as aggressive surgery, chemoradiotherapy, and antiangiogenic therapy. Gliomas frequently occur in brain lesions and can be difficult to discern radiologically from other brain lesions, which might influence surgical planning and the course of follow-up treatment. In recent years, the development of magnetic resonance imaging (MRI) has greatly improved the clinical treatment and management of glioma patients. Previously, clinicians could only acquire basic information of tumor mostly from contrast-enhanced T1-weighted MR sequences. However, the pathophysiological aspects of gliomas can now be directly visualized and investigated with the help of emerging functional MR sequences. Currently, MRI plays a role throughout the course of the clinical treatment cycle. In addition to allowing the identification of different lesions in the central nervous system, the therapy plan can be elaborated in light of increasingly exquisite neuro-oncological imaging. With preoperative grading and key onco-marker detection, the formulation of individual treatment plans could contribute to improving prognosis and shortening the hospital length of stay (LOS). The correct radiological

assessment during follow-up is crucial not only for the follow-up of glioma recurrence and progression but also for accurate assessment of therapeutic responses.

This review presents the frontiers of MR sequences in clinical applications relevant to the oncological imaging of glioma. The correlations between the MR sequences and their clinical applications in a glioma oncology diagnosis are discussed. Finally, the application of ultra-high-field MRI to glioma oncology is discussed.

NONINVASIVE PREOPERATIVE GRADING

Noninvasive preoperative grading and differential diagnosis of gliomas are useful for neurosurgeons. To differentiate between non-enhancing and enhancing brain tumors, amide proton transfer (APT)-weighted (APTw) MRI can be used in presurgical radiological assessments (1). As an indirect indicator of the cellular mobile protein content, APTw imaging has been well-received for its chemical exchange saturation transfer (CEST) technique, which allows visualization of changes in amide protons in the peptide bonds of mobile proteins that carry the water necessary for MRI. Routine subjoined APTw sequences in preoperative radiological examinations could be used for preliminary differentiation between low-grade (LGGs) and high-grade (HGGs) gliomas (1). The introduction of intravoxel incoherent motion (IVIM) MRI alongside APTw improved the efficiency of differentiation between LGGs and HGGs, with an area under the curve of 0.986 (2). Another systematic review that included 353 patients to evaluate the diagnostic performance of APTw MRI in differentiating between LGGs and HGGs indicated that HGGs have significantly higher amide proton-transfer signal intensity than LGGs (3). The pooled sensitivity and specificity were 88% and 91%, respectively. The clinical utility of APTw MRI was thus considered reliable.

Another powerful and advanced MRI technique is MR perfusion-weighted imaging (PWI), which can be used to visualize the aggressiveness and malignancy of a glioma. PWI facilitates the identification of the proliferation of neogenesis vessels and tumor angiogenesis in gliomas (4). Tumoral vessels can lead to hemodynamic changes in the brain due to their pathological structure, which is revealed in color maps of cerebral blood volume (CBV) and vessel wall permeability by means of PWI. This efficiency can be quantified as the relative CBV (rCBV), which is the ratio of tumoral CBV to normal-appearing white matter CBV. In PWI, increased CBV often reflects HGGs. At their first presentation, the rCBV of primary solid and non-enhancing WHO grade II gliomas on PWI was significantly lower in LGGs than that in HGGs (5). By setting the rCBV threshold at a fixed value for differentiation, dynamic susceptibility contrast-enhanced (DSC) PWI-derived rCBV is available and reliable for distinguishing newly diagnosed non-enhancing LGGs from HGGs.

As the traditional assessment for CBV, vascular-space-occupancy (VASO) MRI is impractical because of its low signal-to-noise ratio (6). Inflow-based VASO (iVASO) is improved by only inverting the blood flowing into the slice, which could reduce the partial effects of cerebrospinal fluid volume. Activating the iVASO response within a certain time window could maximize the reflection of arterial/arteriolar CBV (rCBVa) changes (7). Combining rCBVa from iVASO MRI with the minimum apparent diffusion coefficient (mADC) from diffusion-weighted imaging (DWI) shows higher preoperative grading efficiency than any sequence alone (8).

For the last decade, dynamic contrast-enhanced (DCE)-MRI has been a well-established technique for preoperative grading of gliomas (9, 10). The previous glioma grading model, mainly based on the "hot-spot" logic of DCE-MRI, recorded the average value of several well-visualized structures as the "hot-spot," which advanced mapping of tumor boundaries but was deficient in measuring its heterogeneity. To quantify spatial variation in the grayscale intensity and depict the latent imaging heterogeneity, the use of textural features in DCE-MRI has advanced preoperative glioma grading. Textural features obtained from DCE-MRI, calculated by an algorithm and screened by the model, showed good efficiency of discrimination between grade III and IV gliomas. This had been impossible in the prior "hot-spot" model because of excessive homogeneity (11, 12).

The degree of intratumoral susceptibility signal (ITSS) of susceptibility-weighted imaging (SWI) helps to visualize normal vascular brain structures and the vasculature inside the glioma (13). HGGs tend to have greater micro-hemorrhage volume and vigorous angiogenesis under 3-T conventional MRI. Using a 7-T MRI scanner has a significant advantage over using its precursor in terms of spatial resolution due to its higher signal-to-noise ratio. Moreover, local image variance (LIV) is a new complementary technique that uses 7-T MRI for the quantification of hypointense microvascular SWI structures. Using LIV-SWI for quantitative analyses in preoperative gliomas, a significantly higher value can be found in HGGs than in LGGs, making 7-T MRI practical for preoperative grading (14).

Both rCBV from PWI and ITSS from SWI are capable of grading glioma noninvasively. The rCBV achieves this through comparing the CBV of tumor with white matter, while ITSS does this through visualizing the glioma vasculature. While the study by Park et al. (15) indicates that the degree of ITSS shows a significant correlation with the value of rCBVmax in the same tumor segments and the diagnostic performance of SWI on glioma grading is comparable to that of PWI, recent research further illustrated that glioma pathological type correlated with SWI ITSS score and WHO grade correlated with rCBV ratio (16). The combination of rCBV values and ITSS scores to improve grading accuracy is recommended (17).

DIFFERENTIAL DIAGNOSIS

Glioma mostly manifests with neurological dysfunction, which can also be associated with other neoplastic and nonneoplastic

lesions such as brain inflammation, lymphoma, or brain metastasis. Certain lesions require nonoperative treatments, rendering it necessary to distinguish them from gliomas. In clinical practice, clinical symptoms and preoperative examination features of these conditions often overlap, making them indistinguishable. The lack of a clear diagnosis may lead to invasive procedures such as biopsy, surgery, or even radiotherapy that may not only be inappropriate for the primary disease treatment but also eventually aggravate a patient's condition. Therefore, it is imperative for clinicians to assess alternative noninvasive differential diagnostic tools to ensure an accurate preoperative assessment.

Differential Diagnosis of Inflammation *vs.* Glioma

In routine clinical practice, the differentiation of brain parenchyma inflammation from grade II glioma may present a dilemma for neurosurgeons. Both inflammation and glioma manifest on conventional MR sequences as lesions with a mass effect. On certain sequences, they share the same characteristics, such as hypointensity on T1-weighted imaging (T1WI), hyperintensity on T2-weighted imaging (T2WI), and no enhancement on postcontrast T1WI. Radiomics analysis, a rapidly growing method, refers to the conversion of radiological images to quantitative data using a feature extraction algorithm. The radiomics algorithm overcomes the difficulties associated with the resolution limits of the bare human eye, making it an emerging and significant approach in clinical radiological assessments. By extracting several radiomics features from routine 3-T MRI sequences and integrating them into an algorithm, a radiomics model has achieved good diagnostic efficacy for distinguishing inflammation and glioma (18).

Differential Diagnosis of Primary Central Nervous System Lymphoma *vs.* Glioma

Primary central nervous system lymphoma (PCNSL) is another common brain lesion with an increase in the incidence rate in recent decades due to the rising number of immunosuppressed and immunocompetent patients. PCNSL and HGGs share structural overlaps on MRI, both of which illustrate contrast-enhancing lesions with peritumoral edema. Quantitative APTw imaging analysis indicates that significantly higher homogeneous APTw hyperintensity, APTw min, and magnetization transfer ratio (MTR) and lower APTw max, APTw max-min, and CEST total signal intensity values can be found in PCNSLs than in HGGs. APT imaging is designed to detect free proteins and peptides in tissue. High MTR value and low CEST total signal of PCNSL lesions are often associated with a higher nuclear-to-cytoplasmic ratio. APTw max-min parameter indicates the APTw signal heterogeneity within the lesion. Significantly lower APTw max-min in PCNSL than in HGGs is consistent with the histopathological features that PCNSLs are histologically relatively homogeneous (19).

The peritumoral edematous areas of PCNSLs show significantly lower APTw value than that in HGGs, but the edema MTR values showed no statistical difference between these two types of tumors (19).

Differential Diagnosis of Brain Metastasis *vs.* Glioma

Identifying a glioma from brain metastasis is another clinical predicament due to the similar symptoms of these conditions. PWI, an MRI sequence that can characterize the peritumoral area, theoretically ensures a high diagnostic performance in differentiating glioma from brain metastasis. Several sequences from PWI can play a vital role in clinical efficiency, such as DSC, DCE, and arterial spin labeling imaging. DSC is the PWI technique that is most commonly preferred by clinicians. Researchers tend to use rCBV as a DSC parameter to distinguish gliomas from brain metastases, as gliomas tend to invade adjacent brain tissue, whereas brain metastases tend to extrude adjacent brain tissue (20). In DCE-MRI, a glioma has higher peritumoral rCBV values than those in brain metastasis, indicating that the rCBV sequence can be practically used for target identification (21).

Numerous studies have reported distinguishing HGGs with solitary brain metastasis using DWI and diffusion tensor imaging (DTI) (22, 23). The focus of this differentiation is to distinguish infiltrative edema caused by the glioma from metastatic vasogenic edema. The mean minimum peri-enhancing ADC values in HGG are significantly higher than those in brain metastases, and combining DWI and DTI has shown a moderate diagnostic performance in this peritumoral area (24–26) (**Figure 1** and **Table 1**).

KEY ONCO-MARKER DETECTION

Isocitrate Dehydrogenase

Mutation of the metabolic enzyme isocitrate dehydrogenase (IDH) is one of the earliest known genetic events in the tumorigenesis of LGGs. Recent studies indicate that IDH may be a key driver in the development of multiple subtypes of LGGs. Molecular classification of gliomas has been revised due to the discovery of the IDH1 mutation. Gliomas with IDH1 mutations tend to have a more favorable prognosis.

Radiomics models can also play a vital role in identifying IDH-mutant gliomas ahead of surgery. After extracting the mADC, relative ADC (rADC), and rCBVmax from DWI, DSC-PWI, and conventional MRI data and integrating them into a prediction model, the mADC and rADC values were found to be higher in IDH-mutant gliomas than in IDH-wild-type gliomas. IDH-mutant gliomas also presented considerably lower rCBV values. The prediction model demonstrated a moderate diagnostic performance (31–33).

From a metabolic perspective, in IDH-mutant gliomas, isocitrate is not converted to α-ketoglutarate (α-KG) as usual but is converted to a new signature metabolite, 2-hydroxyglutarate (2-HG) (34). MR spectroscopy (MRS) is a noninvasive diagnostic modality that allows the detection and quantification of metabolites in cells and patients (35). Given

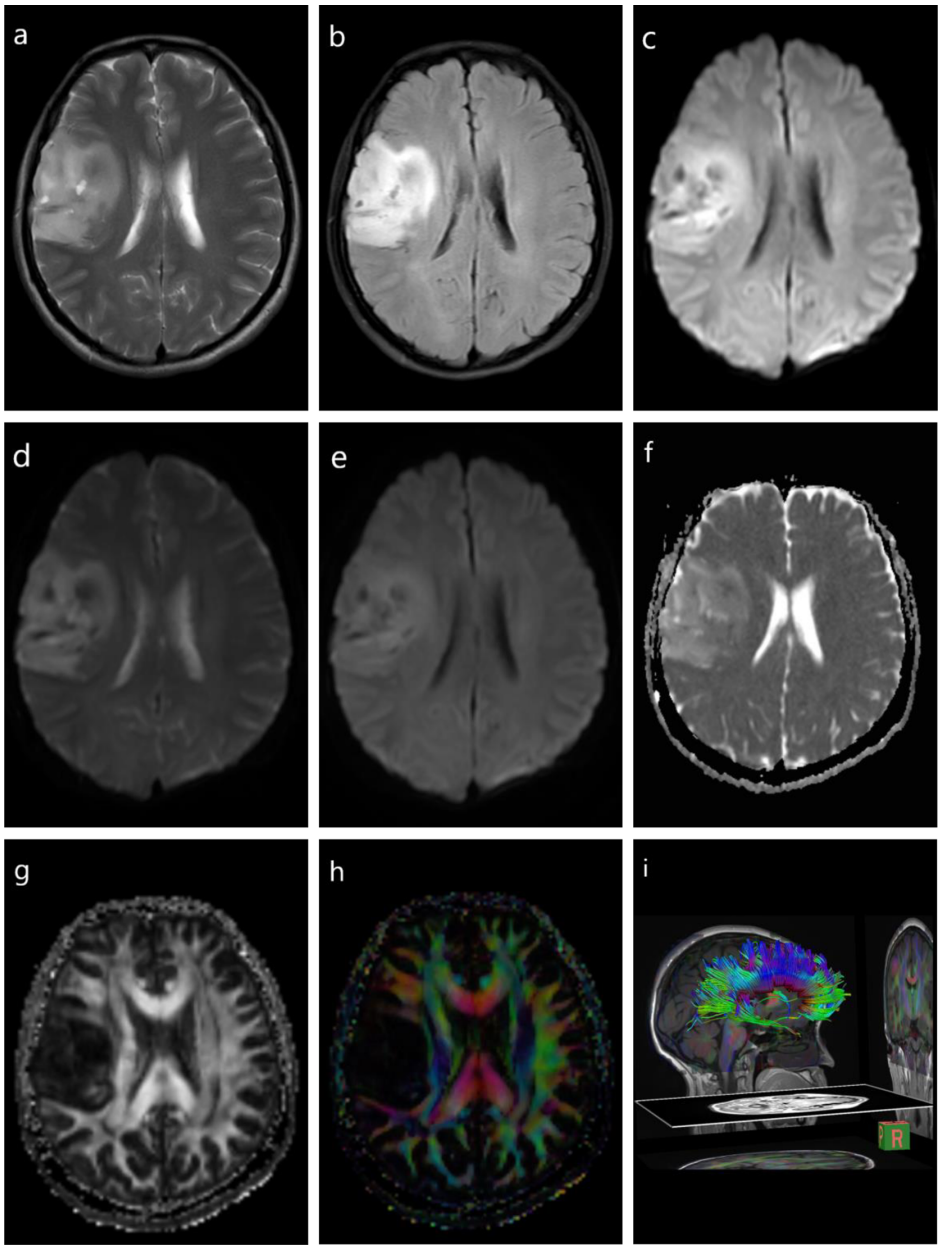

FIGURE 1 | Diffusion-weighted imaging (DWI) and diffusion tensor imaging (DTI) of a glioma. T1-weighted imaging (T1WI) **(A)**, fluid-attenuated inversion recovery (FLAIR) **(B)**, DWI **(C)**, DWI with b = 0 s/mm^2 **(D)**, DWI with b = 1,000 s/mm^2 **(E)**, DTI apparent diffusion coefficient (ADC) mapping **(F)**, DTI fractional anisotropy (FA) mapping **(G)**, DTI directional encoded color FA mapping **(H)**, diffusion tensor tractography (DTT) **(I)**.

that only IDH-mutant gliomas produce 2-HG, measuring 2-HG levels through MRS can estimate the IDH mutation status (36).

However, using MRS to identify IDH-mutant gliomas by detecting 2-HG has some drawbacks, as the process of correlating the 2-HG level and glioma tumor volume and MRS *per se* is time-consuming. Under APTw imaging, IDH-wild-type gliomas tend to demonstrate heterogeneous masses with scattered punctate or patchy high APTw signals, while IDH-mutant lesions show homogeneous iso-intensity to minimal APTw signals, making APTw a non-tumor volume-dependent and time-saving modality (37).

IDH1-R132H mutation status can also be predicted using 7-T CEST-MRI, with advanced diagnostic accuracy ($p < 0.0001$). The same MR sequence used in preoperative grading can be applied in IDH mutation status prediction, as IDH mutant gliomas manifest lower mean SWI-LIV values than IDH–wild-type gliomas (14).

TABLE 1 | MR sequence and parameter in glioma diagnosis.

Clinical application	Sequence	Parameter	Reference
Preoperative grading			
LGG *vs.* HGG	APTw	–	(1)
	PWI	rCBV	(5)
	iVASO+DWI	rCBVa+mADC	(8)
	7T-MRI	SWI-LIV	(14)
II *vs.* III (oligodendrogliomas)	DCE-MRI	Vp+Ktrans	(9)
III *vs.* IV	DCE-MRI	textural feature	(11, 12)
Differential diagnosis			
With PCNSL	APTw	–	(19)
With brain metastasis	PWI	rCBV	(20, 21)
	DWI+DTI	pADC	(22–26)
With inflammation	Radiomics (cMRI)	T1WI+T2WI	(18)
Response to therapy			
Identify tumor progression	DSC-PWI	rCBV	(27)
Response to TMZ	MRS	^{1}H MRS	(28)
Response to standard CRT	CEST-MRI	MTR+NOE+APF	(29)
	7T CEST-MRI	rNOE	(30)

LGG, low-grade glioma; HGG, high-grade glioma; APTw, amide proton transfer weighted; PWI, perfusion-weighted imaging; rCBV, relative cerebral blood volume; iVASO, inflow-based vascular-space-occupancy; DWI, diffusion-weighted imaging; mADC, minimum apparent diffusion coefficient; SWI-LIV, susceptibility-weighted imaging local image variance; DCE-MRI, dynamic contrast-enhanced MRI; Vp, plasma volume; Ktrans, volume transfer coefficient; DTI, diffusion tensor imaging; pADC, peri-enhancing apparent diffusion coefficient; cMRI, conventional MR imaging; DSC-PWI, dynamic susceptibility-weighted contrast-enhanced perfusion-weighted imaging; MRS, MR spectroscopy; CEST-MRI, chemical exchange saturation transfer MRI; MTR, magnetization transfer ratio; NOE, nuclear Overhauser effect; APF, amide proton transfer; rNOE, relayed nuclear Overhauser effect.

O6-Methylguanine-DNA Methyltransferase

Temozolomide (TMZ) is an oral alkylating agent that has been suggested to augment anti-glioma immune responses. Glioma patients may not respond to chemotherapy of alkylating agents due to the alkylator resistance caused by pivotal DNA repair enzyme such as O6-methylguanine-DNA methyltransferase (MGMT). Chemosensitivity to TMZ can be restored by methylating the MGMT promoter (MGMTpm). Therefore, MGMT promoter methylation is a robust indicator of glioma patients' sensitivity to TMZ treatment. A radiomics approach using an automated machine-learning algorithm achieved moderate discriminatory accuracy of the MGMTpm status (38). Gd-3DT1WI, T2WI, and fluid-attenuated inversion recovery sequence (Flair) from 3-T MRI scans were integrated into the algorithm, of which the kernel is formed by applying the tree-based pipeline optimization tool (TPOT). The input features can thereafter be selected and classified, and the best machine-learning pipeline can be generated.

CBVa obtained from iVASO MRI can identify the difference of tumor histogram and structural features between MGMT methylation gliomas and unmethylation ones. The root mean square and variance features from CBVa histogram and contrast-enhancing component of the tumor location from structural imaging enable the iVASO-CBVa to evaluate the MGMT methylation status in gliomas (39).

Histone H3-K27M Mutation

Compared to gliomas in other regions, diffuse midline gliomas (DMGs) mostly lead to a worse prognosis due to their diffuse growth pattern and high levels of intrinsic resistance to therapy. DMG occurs near the cerebral or infratentorial brain midline and occasionally intrudes into the spinal cord (40). DMG shares anatomical features with diffuse intrinsic pontine glioma (DIPG), a term that has now been abolished by the World Health Organization (WHO). In 2012, aberrations in a regulatory histone gene (H3) resulting in an amino acid substitution from lysine to methionine at residue 27 (K27M) were discovered in up to 40% of pediatric glioblastomas (41). Follow-up studies indicated that four out of every five childhood DIPG patients may possess H3-K27M mutations. These patients have a dismal prognosis (a mean of 0.73 years of survival), while those lacking the mutation survive for a mean of 4.6 years. Quantifying and qualifying the radiological features of the DWI in H3-K27M DMG, a moderately low ADC value compared to the H3-K27M wild type can be found in solid tumors (42). Through statistically different ADC values, several significantly lower parameters such as minimal ADC, peritumoral ADC, ratio of minimal ADC, and ratio of peritumoral ADC can be integrated to assess the H3-K27M mutational status in DMG (43).

Ki-67

Proliferation-related Ki-67 is a representative antigen in the cell cycle. It has been widely used as a proliferation marker for human tumor cells. Ki-67 maintains low expression levels in normal brain tissues but is elevated in solid glioma tumors. More malignant tumors often possess a higher Ki-67 marker index and lead to worse prognosis. Therefore, it is imperative to assess the Ki-67 level preoperatively for better individual treatment (44). Fluctuations in texture features can be found in the peritumoral area of glioma due to the expression of Ki-67. As such, a radiomics model that integrates texture features from T1WI and T2WI can effectively assess the Ki-67 level noninvasively (45).

Conventional MRI can provide information about the volume, location, and texture of the tumor and inevitably suffers bias caused by the selected region of interest (46). Multicontrast MRI, the combination of multiple conventional MRI contrast sequences, could improve the objectivity of lesion detection (47). Multicontrast radiomics provides complementary information on both geometric characteristics and molecular biological traits, which correlate significantly with tumor proliferation. Under multicontrast MRI, non-wavelet and wavelet radiomics features were found to correlate significantly with the Ki-67 labeling index. The radiomics features and related parameters extracted from multicontrast demonstrated a good prediction of the Ki-67 level (48).

P53

As a tumor suppressor gene, p53 has strong effects on gliomagenesis (49). p53 level often results in poor prognosis and malignant transformation of LGGs. Recent studies indicated that the sensitivity of gliomas to chemoradiotherapy may also be associated with the p53 level. Mutant p53 was found to be specifically associated with tumor location and enhancement texture maps in LGGs based on preoperative MRI scans (50). The least absolute shrinkage and selection operator (LASSO) method is an automated machine-learning approach that can select the best predictive features from the cohort to prevent the

bias of overfitting and under-generalization caused by human selection. By integrating p53-related first-order (including maximum, median, minimum, and uniformity), shape- and size-based, and textural (including correlation, run percentage, and sum entropy) features, p53 level can be noninvasively and preoperatively predicted (51).

Telomerase Reverse Transcriptase

The key for cancer cells to maintain their proliferative potential and avoid apoptosis is to maintain telomeres. Telomerase reverse transcriptase (TERT) is the rate-limiting catalytic subunit of telomerase. By increasing TERT expression, telomere length can be sustained (52). Mutations in the promoter region of TERT may facilitate TERT expression and serve as a crucial onco-marker in gliomas, particularly in glioblastomas (GBMs). Numerous studies have demonstrated that >80% of primary GBMs have a mutated TERT promoter (TERTpm) (53), indicating that it is fundamental to this tumor type. Volume of interest is a collection of key radiomics features selected by a specialized radiologist that can be further optimized to generate an optimal radiomics signature (Radscore). Based on a LASSO regression, multiple radiomics features, such as core necrotic volume percentages, Cho/Cr, Lac, and the Radscore, were found to be significantly higher in TERTpm than in TERT-wild-type tumors. Multiparameter models based on these statistically significant variables could predict the TERT promoter mutation status preoperatively (54).

Alpha-Thalassemia/Mental Retardation, X-Linked

The function of alpha-thalassemia/mental retardation, X-linked (ATRX), as a chromatin remodeling protein is mainly expressed through histone variant H3.3. Distributed widely in gliomas, ATRX mutations contribute to the development of alternative lengthening of telomeres (ALT), and ATRX loss-of-function mutations have been confirmed to promote ALT (55). Based on the LASSO regression model, ATRX-associated radiomics features can be auto-selected. The ATRX status affects the overall image brightness, uniformity of the gray-level distribution, coarseness of an image, and symmetry of the image (56) (**Table 2**).

Epidermal Growth Factor Receptor

The epidermal growth factor receptor (EGFR) belongs to the ERBB family of tyrosine kinase receptors. EGFR signaling cascade is a key regulator in cell proliferation, differentiation, division, survival, and cancer development (59). EGFR overexpression can promote malignant proliferation of glioma cells, and several studies have focused on suppressing malignant proliferation by inhibiting its activity (60). A radiomics algorithm formed by texture features extracted from T2WI shows a good prediction of EGFR level in lower-grade gliomas. With 41 features validated and applied, the area under the curve (AUC) of the receiver operating characteristic (ROC) prediction curve reached the value of 0.95 (57).

Another study distinguished between glioma with amplified and non-amplified EGFR under DWI. EGFR-amplified tumor shows lower mean ADC values than EGFR-non-amplified gliomas, with an AUC of 0.75. Increased EGFR amplification has been associated with increased levels of cellular growth and proliferation. Higher EGFR amplification level reflects higher cellularity, which may lead to lower ADC values; thus, the mADC could independently predict the EGFR amplification level (58).

RESPONSE TO THERAPY

In addition to overall survival, which is the gold standard of response to therapy, radiology-related measurements are increasingly favored by clinicians and radiologists. The Response Assessment in Neuro-Oncology (RANO) criteria were used for the accurate and reproducible assessment of responses to treatment in gliomas. The RANO criteria, which involve the radiology-based evaluation and measurement of tumors, can identify postsurgical progression in a timely

TABLE 2 | Detection of onco-markers preoperatively by MRI.

Onco-markers	Sequence	Parameter	AUC	Reference
IDH mutation	cMRI+DWI+DSC-PWI	mADC+rADC+rCBVmax	0.92	(31)
	MRS	2-HG	–	(35)
	APTw	–	0.89	(36)
MGMTpm	Radiomics (TPOT)	3DT1WI+Gd-3DT1WI+T2WI+FLAIR	0.951	(37)
	iVASO	CBVa	0.931	(39)
H3-K27M mutation	DWI	ADC	0.872	(41, 42)
Ki-67 level	Radiomics (cMRI)	T1WI, T2WI	0.773	(43)
	Radiomics (multicontrast MRI)	ADC+eADC+CBF+PWmap+b1000+ b0+T1FLAIR+T2FLAIR+T2FSE+T1C	0.745	(47)
p53 mutation	Radiomics (cMRI)	T2WI	0.709	(50)
TERT	Radiomics (cMRI+MRS)	CE-T1WI+Flair+T1WI+T2WI	0.955	(53)
ATRX mutation	Radiomics (cMRI)	T2WI	0.94	(56)
EGFR amplified	Radiomics (cMRI)	T2WI	0.95	(57)
	DWI	mADC	0.75	(58)

IDH, isocitrate dehydrogenase; rADC, relative apparent diffusion coefficient; 2-HG, 2-hydroxyglutarate; MGMTpm, O6-methylguanine-DNA methyltransferase promoter methylation; TPOT, tree-based pipeline optimization tool; b1,000/b0 DWI with two b-values: b = 0 and b = 1,000 s/mm^2; CE-T1WI, contrast-enhanced T1WI; TERT, telomerase reverse transcriptase; ATRX, alpha-thalassemia/mental retardation, X-linked; EGFR, epidermal growth factor receptor; mADC, minimum apparent diffusion coefficient.

manner, alter chemoradiotherapy plans, shorten clinical trial lengths, and reduce drug development costs (61).

Identification of Tumor Progression

For most glioma patients, the glioma posttreatment radiation effect (PTRE) and tumor progression tend to occur in the first 2 years after surgery. Both present enhanced lesions, peritumoral irregular edema, space-occupying effects, and cystic necrosis, similar to conventional MRI- and CT-enhanced images. The treatment and prognosis of PTRE and tumor progression are quite different. PTRE often manifests as a positive response to adjuvant treatment and typically does not require further invasive treatment. Tumor progression, on the other hand, is a sign that the previous therapy had failed and should prompt treatment changes that may provide benefit. Therefore, it is crucial for clinicians to distinguish between PTRE and tumor progression to develop a proper treatment plan. Higher perfusion was observed in regions showing glioma progression due to active cell proliferation. In regions of PTRE, a lower perfusion status tends to be present because of capillary stenosis. This hemodynamic turmoil leads to rCBV variations. Due to the refined assessment possible with rCBV, DSC-PWI is a reliable tool for the timely identification of tumor progression (27).

Temozolomide Responses

As an oral alkylating agent, TMZ is currently commonly administered to glioma patients due to it improving the adverse effects of traditional chemotherapy drugs. ^{1}H MRS is a metabolic imaging method that can noninvasively measure several tumor metabolite levels. The levels of α-ketoglutarate and glutamate, intermediate products of mutant IDH gliomas, can be detected and quantitatively assessed by ^{1}H MRS. In an *in vitro* experiment, after treatment with TMZ, the α-ketoglutarate and glutamate levels were found to be significantly lower than those in untreated glioma cells, indicating that ^{1}H MRS may be a potential assessment tool for assessing the response to TMZ treatment in IDH1-mutant gliomas (28).

Standard Chemoradiotherapy Responses

CEST is a recently emerged MR technique. Low concentrations of biomolecules can be detected using CEST by selective saturation of metabolite-bound protons and subsequent magnetization transfer to free water. This technology yields additional information about metabolic activity and the tissue microenvironment without the need for conventional contrast agents or radioactive tracers. CEST at 3-T reported good discrimination between glioma treatment responders and nonresponders. Using CEST-MRI to monitor the therapeutic response of gliomas to standard 6-week chemoradiotherapy (CRT) and several CEST matrices revealed significant differences, including in the MTR, nuclear Overhauser effect (NOE), and APT. Part of the matrix can even identify potential tumor progressors before the start of CRT (29).

The application of 7-T MRI allows the detection of more sophisticated and heterogeneous CEST effects. The relayed NOE signal in 7-T CEST-MRI scans allows direct distinction between responders and nonresponders immediately after the end of CRT. 7-T CEST-MRI enables early response assessments 4 weeks ahead of standard clinical evaluations, according to RANO (30).

CLINICAL FEASIBILITIES OF ADVANCE SEQUENCES

APT technique was firstly invented in 2003 (62), and until now, it is the only noninvasive and non-radiative MR molecular imaging technology to be used for quantification of free protein. APT is currently applied for detecting brain tumors (63), grading gliomas, distinguishing active glioma from treatment effects, identifying genetic markers in gliomas, detecting ischemic stroke (62), and detecting Alzheimer's disease (64) and Parkinson's disease (65). Thus, APT technique is worth priority recommendation for hospitals with neurology and neurosurgery specializations.

Radiomics is an emerging field in quantitative imaging. Radiomics uses high-throughput extraction of advanced quantitative features to describe tumor phenotypes objectively and quantitatively. These features could be extracted from the existing medical images by advanced mathematical algorithms to uncover tumor characteristics that one may fail to appreciate by the naked eye. Radiomics features have shown promise in the prediction of treatment response (66), differentiating benign and malignant tumors (67), and assessing cancer genetics in many cancer types (68). With no extra hardware needed, radiomics can be quickly mastered and deployed to serve clinicians.

The most evident clinical application of 7-T is the higher spatial resolution in the brain compared to 3-T. In the last few years, studies indicate new insights into the pathology of the cerebral cortex on 7-T, such as cerebrovascular related neurodegenerative disease (69), multiple sclerosis (70), cortical microinfarcts (71), and mesial temporal lobe epilepsy (72). The higher spatial resolution contributes to the imaging of microvascular structures under SWI, which helps preoperative grading, and allows direct distinction between responders and nonresponders of CRT under 7-T CEST-MRI scans. For other aspects in glioma diagnosis, the clinical utility of 7-T MRI is yet to be explored.

For other techniques that require no upgrade of existing MR equipment such as rCBV from PWI and ADC from DWI, we recommend that neurosurgeons and radiologists utilize those sequences for glioma advance diagnosis at once.

CONCLUSION AND FUTURE DIRECTIONS

Advanced MRI plays an increasingly important role in the clinical management of glioma by using emerging MR sequences to maximize safe resection, minimize surgery risk, individualize a CRT plan, shorten LOS, and ultimately prolong patients' lives (**Figure 2**). A variety of parameters in multiple MR sequences are available for clinical use. The deployment of 7-T

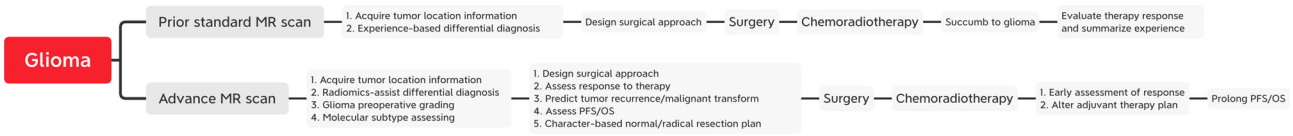

FIGURE 2 | Glioma clinical practice flow under standard MR scan and advance MR scan.

MRI with advanced morphological, functional, and metabolic imaging capabilities increasingly makes comprehensive diagnoses of gliomas possible. The correct and effective use of these MR techniques facilitates improved preoperative assessments for the accurate diagnoses and treatment responses of gliomas. Research focus on automatic machine learning and qualitative raw image data processing procedure that enables robust and thorough information for neurosurgeons will be crucial for enhancing glioma management in clinical routine. The correct and effective use of these MR techniques enables improved preoperative assessments of accurate diagnoses and treatment responses for glioma.

AUTHOR CONTRIBUTIONS

X-TW was responsible for the conception and design. R-LW wrote the manuscript. R-LW contributed to manuscript submission. All authors contributed to the article and approved the submitted version.

ACKNOWLEDGMENTS

Everyone who contributed to the article has been listed as an author.

REFERENCES

1. Durmo F, Rydhög A, Testud F, Lätt J, Schmitt B, Rydelius A, et al. Assessment of Amide Proton Transfer Weighted (APTw) MRI for Pre-Surgical Prediction of Final Diagnosis in Gliomas. *PloS One* (2020) 15(12):e0244003. doi: 10.1371/journal.pone.0244003
2. Zou T, Yu H, Jiang C, Wang X, Jiang S, Rui Q, et al. Differentiating the Histologic Grades of Gliomas Preoperatively Using Amide Proton Transfer-Weighted (APTW) and Intravoxel Incoherent Motion MRI. *NMR Biomed* (2018) 31(1):e3850. doi: 10.1002/nbm.3850
3. Suh CH, Park JE. Amide Proton Transfer-Weighted MRI in Distinguishing High- and Low-Grade Gliomas: A Systematic Review and Meta-Analysis. *Neuroradiology* (2019) 61(5):525–34. doi: 10.1007/s00234-018-02152-2
4. Sasi SD, Ramaniharan AK, Bhattacharjee R, Gupta RK, Saha I, Van Cauteren M, et al. Evaluating Feasibility of High Resolution T1-Perfusion MRI With Whole Brain Coverage Using Compressed SENSE: Application to Glioma Grading. *Eur J Radiol* (2020) 129:109049. doi: 10.1016/j.ejrad.2020.109049
5. Abrigo JM, Fountain DM, Provenzale JM, Law EK, Kwong JS, Hart MG, et al. Magnetic Resonance Perfusion for Differentiating Low-Grade From High-Grade Gliomas at First Presentation. *Cochrane Database Syst Rev* (2018) 1(1): CD011551. doi: 10.1002/14651858.CD011551.pub2
6. Hua J, Qin Q, Donahue MJ, Zhou J, Pekar JJ, van Zijl PC. Inflow-Based Vascular-Space-Occupancy (iVASO) MRI. *Magnetic Resonance Med* (2011) 66(1):40–56. doi: 10.1002/mrm.22775
7. Li X, Liao S, Hua J, Guo L, Wang D, Xiao X, et al. Association of Glioma Grading With Inflow-Based Vascular-Space-Occupancy MRI: A Preliminary Study at 3T. *J Magn Reson Imaging* (2019) 50: (6):1817–23. doi: 10.1002/jmri.26741
8. Cao H, Xiao X, Hua J, Huang G, He W, Qin J, et al. The Added Value of Inflow-Based Vascular-Space-Occupancy and Diffusion-Weighted Imaging in Preoperative Grading of Gliomas. *Neuro-Degenerative Dis* (2021) 20 (4):123–30. doi: 10.1159/000512545
9. Arevalo-Perez J, Kebede AA, Peck KK, Diamond E, Holodny AI, Rosenblum M, et al. Dynamic Contrast-Enhanced MRI in Low-Grade *Versus* Anaplastic Oligodendrogliomas. *J Neuroimaging* (2016) 26(3):366–71. doi: 10.1111/jon.12320
10. Li X, Zhu Y, Kang H, Zhang Y, Liang H, Wang S, et al. Glioma Grading by Microvascular Permeability Parameters Derived From Dynamic Contrast-Enhanced MRI and Intratumoral Susceptibility Signal on Susceptibility Weighted Imaging. *Cancer Imaging* (2015) 15(1):4. doi: 10.1186/s40644-015-0039-z
11. Xie T, Chen X, Fang J, Kang H, Xue W, Tong H, et al. Textural Features of Dynamic Contrast-Enhanced MRI Derived Model-Free and Model-Based Parameter Maps in Glioma Grading. *J Magnetic Resonance Imaging* (2018) 47 (4):1099–111. doi: 10.1002/jmri.25835
12. Raja R, Sinha N, Saini J, Mahadevan A, Rao KN, Swaminathan A. Assessment of Tissue Heterogeneity Using Diffusion Tensor and Diffusion Kurtosis Imaging for Grading Gliomas. *Neuroradiology* (2016) 58(12):1217–31. doi: 10.1007/s00234-016-1758-y
13. Liu C, Li W, Tong KA, Yeom KW, Kuzminski S. Susceptibility-Weighted Imaging and Quantitative Susceptibility Mapping in the Brain. *J Magnetic Resonance Imaging* (2015) 42(1):23–41. doi: 10.1002/jmri.24768
14. Grabner G, Kiesel B, Wöhrer A, Millesi M, Wurzer A, Göd S, et al. Local Image Variance of 7 Tesla SWI Is a New Technique for Preoperative Characterization of Diffusely Infiltrating Gliomas: Correlation With Tumour Grade and IDH1 Mutational Status. *Eur Radiol* (2017) 27(4):1556–67. doi: 10.1007/s00330-016-4451-y
15. Park MJ, Kim HS, Jahng GH, Ryu CW, Park SM, Kim SY. Semiquantitative Assessment of Intratumoral Susceptibility Signals Using non-Contrast-Enhanced High-Field High-Resolution Susceptibility-Weighted Imaging in Patients With Gliomas: Comparison With MR Perfusion Imaging. *AJNR Am J Neuroradiol* (2009) 30(7):1402–8. doi: 10.3174/ajnr.A1593
16. Aydin O, Buyukkaya R, Hakyemez B. Susceptibility Imaging in Glial Tumor Grading; Using 3 Tesla Magnetic Resonance (MR) System and 32 Channel Head Coil. *Polish J Radiol* (2017) 82:179–87. doi: 10.12659/pjr.900374
17. Saini J, Gupta PK, Sahoo P, Singh A, Patir R, Ahlawat S, et al. Differentiation of Grade II/III and Grade IV Glioma by Combining "T1 Contrast-Enhanced Brain Perfusion Imaging" and Susceptibility-Weighted Quantitative Imaging. (2018) *Neuroradiology* 60(1):43–50. doi: 10.1007/s00234-017-1942-8
18. Han Y, Yang Y, Shi ZS, Zhang AD, Yan LF, Hu YC, et al. Distinguishing Brain Inflammation From Grade II Glioma in Population Without Contrast Enhancement: A Radiomics Analysis Based on Conventional MRI. *Eur J Radiol* (2021) 134:109467. doi: 10.1016/j.ejrad.2020.109467
19. Jiang S, Yu H, Wang X, Lu S, Li Y, Feng L, et al. Molecular MRI Differentiation Between Primary Central Nervous System Lymphomas and High-Grade Gliomas Using Endogenous Protein-Based Amide Proton Transfer MR Imaging at 3 Tesla. *Eur Radiol* (2016) 26(1):64–71. doi: 10.1007/s00330-015-3805-1

20. Surendra KL, Patwari S, Agrawal S, Chadaga H, Nagadi A. Percentage Signal Intensity Recovery: A Step Ahead of rCBV in DSC MR Perfusion Imaging for the Differentiation of Common Neoplasms of Brain. *Indian J Cancer* (2020) 57(1):36–43. doi: 10.4103/ijc.IJC_421_18
21. Suh CH, Kim HS. Perfusion MRI as a Diagnostic Biomarker for Differentiating Glioma From Brain Metastasis: A Systematic Review and Meta-Analysis. (2018) *Eur Radiol* 28(9):3819–31. doi: 10.1007/s00330-018-5335-0
22. Bauer AH, Erly W, Moser FG, Maya M, Nael K. Differentiation of Solitary Brain Metastasis From Glioblastoma Multiforme: A Predictive Multiparametric Approach Using Combined MR Diffusion and Perfusion. *Neuroradiology* (2015) 57(7):697–703. doi: 10.1007/s00234-015-1524-6
23. Zhao J, Yang ZY, Luo BN, Yang JY, Chu JP. Quantitative Evaluation of Diffusion and Dynamic Contrast-Enhanced MR in Tumor Parenchyma and Peritumoral Area for Distinction of Brain Tumors. *PloS One* (2015) 10(9): e0138573. doi: 10.1371/journal.pone.0138573
24. Caravan I, Ciortea CA, Contis A, Lebovici A. Diagnostic Value of Apparent Diffusion Coefficient in Differentiating Between High-Grade Gliomas and Brain Metastases. *Acta Radiol* (2018) 59(5):599–605. doi: 10.1177/0284185117727787
25. Suh CH, Kim HS. Diffusion-Weighted Imaging and Diffusion Tensor Imaging for Differentiating High-Grade Glioma From Solitary Brain Metastasis: A Systematic Review and Meta-Analysis. (2018) *AJNR Am J Neuroradiol* 39 (7):1208–14. doi: 10.3174/ajnr.A5650
26. Han C, Huang S, Guo J, Zhuang X, Han H. Use of a High B-Value for Diffusion Weighted Imaging of Peritumoral Regions to Differentiate High-Grade Gliomas and Solitary Metastases. *J Magnetic Resonance Imaging* (2015) 42(1):80–6. doi: 10.1002/jmri.24747
27. Wang L, Wei L. Evaluation of Perfusion MRI Value for Tumor Progression Assessment After Glioma Radiotherapy: A Systematic Review and Meta-Analysis. (2020) *Medicine (Baltimore)* 99(52):e23766. doi: 10.1097/md.0000000000023766
28. Subramani E, Radoul M. Glutamate Is a Noninvasive Metabolic Biomarker of IDH1-Mutant Glioma Response to Temozolomide Treatment. *Cancer Res* (2020) 80(22):5098–108. doi: 10.1158/0008-5472.can-20-1314
29. Mehrabian H, Myrehaug S, Soliman H, Sahgal A, Stanisz GJ. Evaluation of Glioblastoma Response to Therapy With Chemical Exchange Saturation Transfer. *Int J Radiat Oncol Biol Phys* (2018) 101(3):713–23. doi: 10.1016/j.ijrobp.2018.03.057
30. Meissner JE, Korzowski A, Regnery S, Goerke S, Breitling J, Floca RO, et al. Early Response Assessment of Glioma Patients to Definitive Chemoradiotherapy Using Chemical Exchange Saturation Transfer Imaging at 7 T. *J Magn Reson Imaging* (2019) 50(4):1268–77. doi: 10.1002/jmri.26702
31. Xing Z, Yang X. Noninvasive Assessment of IDH Mutational Status in World Health Organization Grade II and III Astrocytomas Using DWI and DSC-PWI Combined With Conventional MR Imaging. *AJNR Am J Neuroradiol* (2017) 38(6):1138–44. doi: 10.3174/ajnr.A5171
32. Lee S, Choi SH, Ryoo I, Yoon TJ, Kim TM, Lee SH, et al. Evaluation of the Microenvironmental Heterogeneity in High-Grade Gliomas With IDH1/2 Gene Mutation Using Histogram Analysis of Diffusion-Weighted Imaging and Dynamic-Susceptibility Contrast Perfusion Imaging. *J Neuro-Oncol* (2015) 121(1):141–50. doi: 10.1007/s11060-014-1614-z
33. Zhang J, Chen X, Chen D, Wang Z, Li S, Zhu W. Grading and Proliferation Assessment of Diffuse Astrocytic Tumors With Monoexponential, Biexponential, and Stretched-Exponential Diffusion-Weighted Imaging and Diffusion Kurtosis Imaging. *Eur J Radiol* (2018) 109:188–95. doi: 10.1016/j.ejrad.2018.11.003
34. Bhavya B, Anand CR, Madhusoodanan UK, Rajalakshmi P, Krishnakumar K, Easwer HV, et al. To be Wild or Mutant: Role of Isocitrate Dehydrogenase 1 (IDH1) and 2-Hydroxy Glutarate (2-HG) in Gliomagenesis and Treatment Outcome in Glioma. *Cell Mol Neurobiol* (2020) 40(1):53–63. doi: 10.1007/s10571-019-00730-3
35. Tiwari V, Mashimo T, An Z, Vemireddy V, Piccirillo S, Askari P, et al. In Vivo MRS Measurement of 2-Hydroxyglutarate in Patient-Derived IDH-Mutant Xenograft Mouse Models *Versus* Glioma Patients. *Magn Reson Med* (2020) 84 (3):1152–60. doi: 10.1002/mrm.28183
36. Viswanath P, Chaumeil MM, Ronen SM. Molecular Imaging of Metabolic Reprograming in Mutant IDH Cells. *Front Oncol* (2016) 6:60. doi: 10.3389/fonc.2016.00060
37. Jiang S, Zou T, Eberhart CG, Villalobos MAV, Heo HY, Zhang Y. Predicting IDH Mutation Status in Grade II Gliomas Using Amide Proton Transfer-Weighted (APTw) MRI. *Magn Reson Med* (2017) 78(3):1100–9. doi: 10.1002/mrm.26820
38. Zhang S, Sun H, Su X, Yang X, Wang W, Wan X, et al. Automated Machine Learning to Predict the Co-Occurrence of Isocitrate Dehydrogenase Mutations and O(6) -Methylguanine-DNA Methyltransferase Promoter Methylation in Patients With Gliomas. *J Magnetic Resonance Imaging* (2021) 54(1):197–205. doi: 10.1002/jmri.27498
39. He W, Li X, Hua J, Liao S, Guo L, Xiao X, et al. Noninvasive Assessment of O(6)-Methylguanine-DNA Methyltransferase Promoter Methylation Status in World Health Organization Grade II-IV Glioma Using Histogram Analysis of Inflow-Based Vascular-Space-Occupancy Combined With Structural Magnetic Resonance Imaging. *J Magn Reson Imaging* (2021) 54(1):227–236. doi: 10.1002/jmri.27514
40. Cooney TM, Lubanszky E, Prasad R, Hawkins C, Mueller S. Diffuse Midline Glioma: Review of Epigenetics. *J Neurooncol* (2020) 150(1):27–34. doi: 10.1007/s11060-020-03553-1
41. Schwartzentruber J, Korshunov A, Liu XY, Jones DT, Pfaff E, Jacob K, et al. Driver Mutations in Histone H3.3 and Chromatin Remodelling Genes in Paediatric Glioblastoma. *Nature* (2012) 482(7384):226–31. doi: 10.1038/nature10833
42. Thust S, Micallef C, Okuchi S, Brandner S, Kumar A, Mankad K, et al. Imaging Characteristics of H3 K27M Histone-Mutant Diffuse Midline Glioma in Teenagers and Adults. *Quantitative Imaging Med Surg* (2021) 11(1):43–56. doi: 10.21037/qims-19-954
43. Chen H, Hu W, He H, Yang Y, Wen G, Lv X. Noninvasive Assessment of H3 K27M Mutational Status in Diffuse Midline Gliomas by Using Apparent Diffusion Coefficient Measurements. *Eur J Radiol* (2019) 114:152–9. doi: 10.1016/j.ejrad.2019.03.006
44. Wong E, Nahar N, Hau E, Varikatt W, Gebski V, Ng T, et al. Cut-Point for Ki-67 Proliferation Index as a Prognostic Marker for Glioblastoma. *Asia Pac J Clin Oncol* (2019) 15(1):5–9. doi: 10.1111/ajco.12826
45. Sun X, Pang P, Lou L, Feng Q, Ding Z, Zhou J. Radiomic Prediction Models for the Level of Ki-67 and P53 in Glioma. *J Int Med Res* (2020) 48 (5):300060520914466. doi: 10.1177/0300060520914466
46. Seo Y, Rollins NK, Wang ZJ. Reduction of Bias in the Evaluation of Fractional Anisotropy and Mean Diffusivity in Magnetic Resonance Diffusion Tensor Imaging Using Region-of-Interest Methodology. *Sci Rep* (2019) 9(1):13095. doi: 10.1038/s41598-019-49311-w
47. Ji S, Yang D, Lee J. Synthetic MRI: Technologies and Applications in Neuroradiology. *J Magn Reson Imaging* (2020). doi: 10.1002/jmri.27440
48. Su C, Jiang J, Zhang S, Shi J, Xu K, Shen N, et al. Radiomics Based on Multicontrast MRI can Precisely Differentiate Among Glioma Subtypes and Predict Tumour-Proliferative Behaviour. *Eur Radiol* (2019) 29(4):1986–96. doi: 10.1007/s00330-018-5704-8
49. Yang W, Wang H, Ju H, Dou C. A Study on the Correlation Between STAT−1 and Mutant P53 Expression in Glioma. *Mol Med Rep* (2018) 17(6):7807–12. doi: 10.3892/mmr.2018.8796
50. Wang YY, Zhang T, Li SW, Qian TY, Fan X, Peng XX, et al. Mapping P53 Mutations in Low-Grade Glioma: A Voxel-Based Neuroimaging Analysis. *AJNR Am J Neuroradiol* (2015) 36(1):70–6. doi: 10.3174/ajnr.A4065
51. Li Y, Qian Z, Xu K, Wang K, Fan X, Li S, et al. MRI Features Predict P53 Status in Lower-Grade Gliomas *via* a Machine-Learning Approach. *NeuroImage Clin* (2018) 17:306–11. doi: 10.1016/j.nicl.2017.10.030
52. Dratwa M, Wysoczańska B, Łacina P, Kubik T, Bogunia-Kubik K. TERT-Regulation and Roles in Cancer Formation. *Front Immunol* (2020) 11:589929. doi: 10.3389/fimmu.2020.589929
53. Hafezi F, Perez Bercoff D. The Solo Play of TERT Promoter Mutations. *Cells* (2020) 9(3):749. doi: 10.3390/cells9030749
54. Tian H, Wu H. Noninvasive Prediction of TERT Promoter Mutations in High-Grade Glioma by Radiomics Analysis Based on Multiparameter MRI. *Biomed Res Int* (2020) 2020:3872314. doi: 10.1155/2020/3872314
55. Haase S, Garcia-Fabiani MB, Carney S, Altshuler D, Núñez FJ, Méndez FM, et al. Mutant ATRX: Uncovering a New Therapeutic Target for Glioma. *Expert Opin Ther Targets* (2018) 22(7):599–613. doi: 10.1080/14728222.2018.1487953
56. Li Y, Liu X, Qian Z, Sun Z, Xu K, Wang K, et al. Genotype Prediction of ATRX Mutation in Lower-Grade Gliomas Using an MRI Radiomics Signature. *Eur Radiol* (2018) 28(7):2960–8. doi: 10.1007/s00330-017-5267-0
57. Li Y, Liu X, Xu K, Qian Z, Wang K, Fan X, et al. MRI Features can Predict EGFR Expression in Lower Grade Gliomas: A Voxel-Based Radiomic Analysis. *Eur Radiol* (2018) 28(1):356–62. doi: 10.1007/s00330-017-4964-z

58. Park YW, Ahn SS. Diffusion and Perfusion MRI may Predict EGFR Amplification and the TERT Promoter Mutation Status of IDH-Wildtype Lower-Grade Gliomas. *Eur Radiol* (2020) 30(12):6475–84. doi: 10.1007/s00330-020-07090-3
59. Sabbah DA, Hajjo R, Sweidan K. Review on Epidermal Growth Factor Receptor (EGFR) Structure, Signaling Pathways, Interactions, and Recent Updates of EGFR Inhibitors. *Curr Topics Med Chem* (2020) 20(10):815–34. doi: 10.2174/1568026620666200303123102
60. Davis SC, Samkoe KS, O'Hara JA, Gibbs-Strauss SL, Payne HL, Hoopes PJ, et al. MRI-Coupled Fluorescence Tomography Quantifies EGFR Activity in Brain Tumors. *Acad Radiol* (2010) 17(3):271–6. doi: 10.1016/j.acra.2009.11.001
61. Wen PY, Chang SM, Van den Bent MJ, Vogelbaum MA, Macdonald DR, Lee EQ. Response Assessment in Neuro-Oncology Clinical Trials. *J Clin Oncol* (2017) 35(21):2439–49. doi: 10.1200/jco.2017.72.7511
62. Zhou J, Payen JF, Wilson DA, Traystman RJ, van Zijl PC. Using the Amide Proton Signals of Intracellular Proteins and Peptides to Detect pH Effects in MRI. *Nat Med* (2003) 9(8):1085–90. doi: 10.1038/nm907
63. Eidel O, Burth S, Neumann JO, Kieslich PJ, Sahm F, Jungk C, et al. Tumor Infiltration in Enhancing and Non-Enhancing Parts of Glioblastoma: A Correlation With Histopathology. *PloS One* (2017) 12(1):e0169292. doi: 10.1371/journal.pone.0169292
64. Wang R, Li SY, Chen M, Zhou JY, Peng DT, Zhang C, et al. Amide Proton Transfer Magnetic Resonance Imaging of Alzheimer's Disease at 3.0 Tesla: A Preliminary Study. *Chin Med J* (2015) 128(5):615–9. doi: 10.4103/0366-6999.151658
65. Li C, Peng S, Wang R, Chen H, Su W, Zhao X, et al. Chemical Exchange Saturation Transfer MR Imaging of Parkinson's Disease at 3 Tesla. *Eur Radiol* (2014) 24(10):2631–9. doi: 10.1007/s00330-014-3241-7
66. Baek HJ, Kim HS, Kim N, Choi YJ, Kim YJ. Percent Change of Perfusion Skewness and Kurtosis: A Potential Imaging Biomarker for Early Treatment Response in Patients With Newly Diagnosed Glioblastomas. *Radiology* (2012) 264(3):834–43. doi: 10.1148/radiol.12112120
67. Xu R, Kido S, Suga K, Hirano Y, Tachibana R, Muramatsu K, et al. Texture Analysis on (18)F-FDG PET/CT Images to Differentiate Malignant and Benign Bone and Soft-Tissue Lesions. *Ann Nucl Med* (2014) 28(9):926–35. doi: 10.1007/s12149-014-0895-9
68. Gutman DA, Dunn WDJr., Grossmann P, Cooper LA, Holder CA, Ligon KL, et al. Somatic Mutations Associated With MRI-Derived Volumetric Features in Glioblastoma. *Neuroradiology* (2015) 57(12):1227–37. doi: 10.1007/s00234-015-1576-7
69. De Reuck J, Deramecourt V, Auger F, Durieux N, Cordonnier C, Devos D, et al. Post-Mortem 7.0-Tesla Magnetic Resonance Study of Cortical Microinfarcts in Neurodegenerative Diseases and Vascular Dementia With Neuropathological Correlates. *J Neurol Sci* (2014) 346(1-2):85–9. doi: 10.1016/j.jns.2014.07.061
70. Yao B, Hametner S, van Gelderen P, Merkle H, Chen C, Lassmann H, et al. 7 Tesla Magnetic Resonance Imaging to Detect Cortical Pathology in Multiple Sclerosis. *PloS One* (2014) 9(10):e108863. doi: 10.1371/journal.pone.0108863
71. van Veluw SJ, Zwanenburg JJ, Engelen-Lee J, Spliet WG, Hendrikse J, Luijten PR, et al. In Vivo Detection of Cerebral Cortical Microinfarcts With High-Resolution 7T MRI. *J Cereb Blood Flow Metab* (2013) 33(3):322–9. doi: 10.1038/jcbfm.2012.196
72. Springer E, Dymerska B, Cardoso PL, Robinson SD, Weisstanner C, Wiest R, et al. Comparison of Routine Brain Imaging at 3 T and 7 T. *Invest Radiol* (2016) 51(8):469–82. doi: 10.1097/rli.0000000000000256

Conflict of Interest: The authors declare that the research was conducted in the absence of any commercial or financial relationships that could be construed as a potential conflict of interest.

Publisher's Note: All claims expressed in this article are solely those of the authors and do not necessarily represent those of their affiliated organizations, or those of the publisher, the editors and the reviewers. Any product that may be evaluated in this article, or claim that may be made by its manufacturer, is not guaranteed or endorsed by the publisher.

frontiers in Neurology

SYSTEMATIC REVIEW
published: 01 September 2021
doi: 10.3389/fneur.2021.692751

Correlation Between Tumor Molecular Markers and Perioperative Epilepsy in Patients With Glioma: A Systematic Review and Meta-Analysis

Li Song[1], *Xingyun Quan*[2], *Chaoyi Chen*[3], *Ligang Chen*[4,5,6,7*†] *and Jie Zhou*[4,5,6,7*†]

[1] Department of Neurosurgery, Northwest Women's and Children's Hospital, Xi'an, China, [2] Department of Neurosurgery, Xi'an International Medical Center, Xi'an, China, [3] Anorectal Department, Affiliated Hospital of Traditional Chinese Medicine of Southwest Medical University, Lu Zhou, China, [4] Department of Neurosurgery, The Affiliated Hospital of Southwest Medical University, Lu Zhou, China, [5] Sichuan Clinical Research Center for Neurosurgery, Lu Zhou, China, [6] Academician (Expert) Workstation of Sichuan Province, Lu Zhou, China, [7] Neurological Diseases and Brain Function Laboratory, Lu Zhou, China

OPEN ACCESS

Edited by:
Zhaohui Zhang,
Renmin Hospital of Wuhan University, China

Reviewed by:
Riccardo Soffietti,
University of Turin, Italy
Kamil Krystkiewicz,
10th Military Research Hospital and Polyclinic, Poland

***Correspondence:**
Ligang Chen
chengligang.cool@163.com
Jie Zhou
zj000718@yeah.net

[†] *These authors have contributed equally to this work*

Specialty section:
This article was submitted to Neuro-Oncology and Neurosurgical Oncology, a section of the journal Frontiers in Neurology

Received: *09 April 2021*
Accepted: *20 July 2021*
Published: *01 September 2021*

Citation:
Song L, Quan X, Chen C, Chen L and Zhou J (2021) Correlation Between Tumor Molecular Markers and Perioperative Epilepsy in Patients With Glioma: A Systematic Review and Meta-Analysis. Front. Neurol. 12:692751. doi: 10.3389/fneur.2021.692751

Purpose: Tumors derived from the neuroepithelium are collectively termed gliomas and are the most common malignant primary brain tumor. Epilepsy is a common clinical symptom in patients with glioma, which can impair neurocognitive function and quality of life. Currently, the pathogenesis of glioma-related epilepsy is not fully described. Therefore, it is necessary to further understand the mechanism of seizures in patients with glioma. In this study, a comprehensive meta-analysis was conducted to investigate the relationship between five commonly used tumor molecular markers and the incidence of perioperative epilepsy in patients with glioma.

Methods: PubMed, EMBASE, and Cochrane Library databases were searched for related research studies. Odds ratio and the corresponding 95% confidence interval were used as the main indicators to evaluate the correlation between tumor molecular markers and the incidence of perioperative epilepsy in patients with glioma.

Results: A total of 12 studies were included in this meta-analysis. The results showed that isocitrate dehydrogenase 1 (IDH1) mutation was significantly correlated with the incidence of perioperative epilepsy. A subgroup analysis showed that IDH1 was significantly correlated with the incidence of preoperative epilepsy, but not with intraoperative and postoperative epilepsy. There was no correlation between O6-methylguanine-DNA methyltransferase methylation and 1p/19q deletion and the incidence of perioperative epilepsy. Tumor protein p53 and epidermal growth factor receptor could not be analyzed because of the limited availability of relevant literature. There was no significant heterogeneity or publication bias observed among the included studies.

Conclusion: The present meta-analysis confirms the relationship between tumor molecular markers and the incidence of perioperative epilepsy in patients with glioma. The present results provide more comprehensive evidence for the study of the pathogenesis of glioma-related epilepsy. Our research may offer a new method for the treatment of perioperative seizures in patients with glioma.

Keywords: tumor molecular markers, epilepsy, meta-analysis, glioma, perioperative

INTRODUCTION

Gliomas are the most common malignant tumors of the central nervous system. Seizures occur in 40–70% of patients with glioma (1). Some patients experience epilepsy as the initial symptom, leading to the diagnosis of glioma. Other patients will experience epilepsy during or after tumor resection. Epilepsy reduces the quality of life of patients with glioma and causes huge economic and emotional burdens (2). Despite the availability of antiepileptic drug treatment, approximately half of the patients will develop drug resistance; some patients also continue to experience refractory epilepsy (3). Therefore, it is necessary to systematically investigate the pathogenesis of glioma-related epilepsy.

Previous studies have shown that tumor growth stimulates seizures and *vice versa*, indicating a potential interconnection between the mechanisms of these two pathological conditions (4). A large number of studies have shown that glioma-associated

TABLE 1 | Retrieval strategy.

	Search	Query
PubMed	#1	(((((((("Isocitrate Dehydrogenase"[Mesh]) OR (Isocitrate Dehydrogenase-I[Title/Abstract])) OR (Isocitrate Dehydrogenase I[Title/Abstract])) OR (IDH[Title/Abstract])) OR (("Methyltransferases"[Mesh]) OR (MGMT))) OR (ATRX[Title/Abstract])) OR (1p/19q[Title/Abstract])) OR (P53[Title/Abstract])) OR (EGFR[Title/Abstract])
	#2	(((((((((("Glioma"[Mesh]) OR (Gliomas[Title/Abstract])) OR (Glial Cell Tumors[Title/Abstract])) OR (Glial Cell Tumor[Title/Abstract])) OR (Mixed Glioma[Title/Abstract])) OR (Mixed Gliomas[Title/Abstract])) OR (Malignant Glioma[Title/Abstract])) OR (Malignant Gliomas[Title/Abstract])) OR ((((((("Astrocytoma"[Mesh]) OR (Astrocytomas[Title/Abstract])) OR (Astroglioma[Title/Abstract])) OR (Astrogliomas[Title/Abstract])) OR (Astrocytic Glioma[Title/Abstract])) OR (Astrocytic Gliomas[Title/Abstract]))) OR (((((((((("Oligodendroglioma"[Mesh]) OR (Oligodendrogliomas[Title/Abstract])) OR (Mixed Oligodendroglioma-Astrocytoma[Title/Abstract])) OR (Mixed Oligodendroglioma Astrocytoma[Title/Abstract])) OR (Mixed Oligodendroglioma-Astrocytomas[Title/Abstract])) OR (Anaplastic Oligodendroglioma[Title/Abstract])) OR (Anaplastic Oligodendrogliomas[Title/Abstract])) OR (Oligodendroblastoma[Title/Abstract])) OR (Oligodendroblastomas[Title/Abstract]))
	#3	(((((((("Seizures"[Mesh]) OR (Seizure[Title/Abstract])) OR (Complex Partial Seizure[Title/Abstract])) OR (Complex Partial Seizures[Title/Abstract])) OR (Tonic-Clonic Seizures[Title/Abstract])) OR (Tonic Clonic Seizures[Title/Abstract])) OR (Tonic-Clonic Seizure[Title/Abstract])) OR (Clonic Seizures[Title/Abstract])) OR (((((((((("Epilepsy"[Mesh]) OR (Epilepsies[Title/Abstract])) OR (Seizure Disorder[Title/Abstract])) OR (Seizure Disorders[Title/Abstract])) OR (Awakening Epilepsy[Title/Abstract])) OR (Cryptogenic Epilepsies[Title/Abstract])) OR (Cryptogenic Epilepsy[Title/Abstract])) OR (Aura[Title/Abstract])) OR (Auras[Title/Abstract]))
Embase	#1	"isocitrate dehydrogenase":ab,ti OR "isocitrate dehydrogenase-I":ab,ti OR "isocitrate dehydrogenase I":ab,ti OR idh:ab,ti OR methyltransferases:ab,ti OR mgmt:ab,ti OR atrx:ab,ti OR "1p/19q":ab,ti OR p53:ab,ti OR egfr:ab,ti
	#2	glioma:ab,ti OR gliomas:ab,ti OR "glial cell tumors":ab,ti OR "glial cell tumor":ab,ti OR "mixed glioma":ab,ti OR "mixed gliomas":ab,ti OR "malignant glioma":ab,ti OR "malignant gliomas":ab,ti OR astrocytoma:ab,ti OR astrocytomas:ab,ti OR astroglioma:ab,ti OR astrogliomas:ab,ti OR "astrocytic glioma":ab,ti OR "astrocytic gliomas":ab,ti OR oligodendroglioma:ab,ti OR oligodendrogliomas:ab,ti OR "mixed oligodendroglioma-astrocytoma":ab,ti OR "mixed oligodendroglioma astrocytoma":ab,ti OR "mixed oligodendroglioma-astrocytomas":ab,ti OR "anaplastic oligodendroglioma":ab,ti OR "anaplastic oligodendrogliomas":ab,ti OR oligodendroblastoma:ab,ti OR oligodendroblastomas:ab,ti
	#3	seizures:ab,ti OR seizure:ab,ti OR "complex partial seizure":ab,ti OR "complex partial seizures":ab,ti OR "tonic-clonic seizures":ab,ti OR "tonic clonic seizures":ab,ti OR "tonic-clonic seizure":ab,ti OR "clonic seizures":ab,ti OR epilepsy:ab,ti OR epilepsies:ab,ti OR "seizure disorder":ab,ti OR "seizure disorders":ab,ti OR "awakening epilepsy":ab,ti OR "cryptogenic epilepsies":ab,ti OR "cryptogenic epilepsy":ab,ti OR aura:ab,ti OR auras:ab,ti
Cochrane	#1	(isocitrate dehydrogenase):ti,ab,kw OR (isocitrate dehydrogenase-i):ti,ab,kw OR (isocitrate dehydrogenase):ti,ab,kw OR (idh):ti,ab,kw OR (methyltransferases):ti,ab,kw OR (MGMT):ti,ab,kw OR (atrx):ti,ab,kw OR ("1p/19q"):ti,ab,kw OR (p53):ti,ab,kw OR (egfr):ti,ab,kw
	#2	(glioma):ti,ab,kw OR (gliomas):ti,ab,kw OR (glial cell tumors):ti,ab,kw OR (glial cell tumor):ti,ab,kw OR (mixed glioma):ti,ab,kw OR (mixed gliomas):ti,ab,kw OR (malignant glioma):ti,ab,kw OR (malignant gliomas):ti,ab,kw OR (astrocytoma):ti,ab,kw OR (astrocytomas):ti,ab,kw OR (mixed gliomas):ti,ab,kw OR (malignant glioma):ti,ab,kw OR (malignant gliomas):ti,ab,kw OR (astrocytoma):ti,ab,kw OR (astrocytomas):ti,ab,kw OR (astroglioma):ti,ab,kw OR (astrogliomas):ti,ab,kw OR (astrocytic glioma):ti,ab,kw OR (astrocytic gliomas):ti,ab,kw OR (oligodendroglioma):ti,ab,kw OR (oligodendrogliomas):ti,ab,kw OR (mixed oligodendroglioma-astrocytoma):ti,ab,kw OR (mixed oligodendroglioma astrocytoma):ti,ab,kw OR (mixed oligodendroglioma-astrocytomas):ti,ab,kw OR (anaplastic oligodendroglioma):ti,ab,kw OR (anaplastic oligodendrogliomas):ti,ab,kw OR (oligodendroblastoma):ti,ab,kw OR (oligodendroblastomas):ti,ab,kw
	#3	(Seizure):ti,ab,kw OR (Complex Partial Seizures):ti,ab,kw OR (Complex Partial Seizure):ti,ab,kw OR (Partial Seizure, Complex):ti,ab,kw OR (Partial Seizures, Complex):ti,ab,kw OR (Seizure, Complex Partial):ti,ab,kw OR (Tonic-Clonic Seizures):ti,ab,kw OR (Seizure, Tonic-Clonic):ti,ab,kw OR (Tonic Clonic Seizures):ti,ab,kw OR (Tonic-Clonic Seizure):ti,ab,kw OR (Seizures, Tonic-Clonic):ti,ab,kw OR (Clonic Seizures):ti,ab,kw OR (Seizures, Clonic):ti,ab,kw OR (Epilepsies):ti,ab,kw OR (Epilepsies):ti,ab,kw OR (Seizure Disorder):ti,ab,kw OR (Seizure Disorders):ti,ab,kw OR (Awakening Epilepsy):ti,ab,kw OR (Epilepsy, Awakening):ti,ab,kw OR (Epilepsy, Cryptogenic):ti,ab,kw OR (Cryptogenic Epilepsies):ti,ab,kw OR (Cryptogenic Epilepsy):ti,ab,kw OR (Epilepsies, Cryptogenic):ti,ab,kw OR (Aura):ti,ab,kw

epilepsy is associated with tumor grade and histopathology (4, 5). However, recent studies have shown that tumor molecular markers (TMMs), such as O6-methylguanine-DNA methyltransferase (MGMT) gene promoter methylation, 1p/19q co-deletion, and isocitrate dehydrogenase 1 mutant ($IDH1^{mut}$), also affect the occurrence of epilepsy. Nonetheless, due to the small sample size of most studies, the currently available results are inconsistent.

Studies conducted by Stockhammer et al. and Liang et al. showed that preoperative seizures are significantly related to $IDH1^{mut}$ (6, 7). However, Mullican et al. concluded the opposite (8). Yang et al. reported that patients with a low expression of the MGMT protein were linked to a higher frequency of postoperative seizures (9). In addition, Feyissa et al. showed that patients with methylation of the MGMT gene promoter were more likely to suffer from postoperative epilepsy (10). Previous studies have shown that 1p/19q co-deletion is related to epileptic seizures in adults (11, 12). Interestingly, Mulligan showed that the existence of 1p/19q co-deletion was not associated with the occurrence of preoperative seizures in patients with low-grade glioma (8). Considering these results, a systematic and comprehensive meta-analysis is required to reach a definitive conclusion. In a meta-analysis conducted in 2018, IDH1 mutations have been associated with a higher incidence of preoperative epilepsy in patients with low-grade glioma (13). However, a comprehensive meta-analysis of other genetic TMMs and glioma epilepsy is lacking. Therefore, the objective of the present study was to examine the relationship between five routinely tested TMMs and perioperative epilepsy in patients with glioma.

METHODS

Search Strategy

The PubMed, Embase, and Cochrane Library databases were searched from the establishment of each database to May 2020. The search terms used were "epilepsy", "glioma", "isocitrate dehydrogenase" or "IDH", "methyltransferase" or "MGMT",

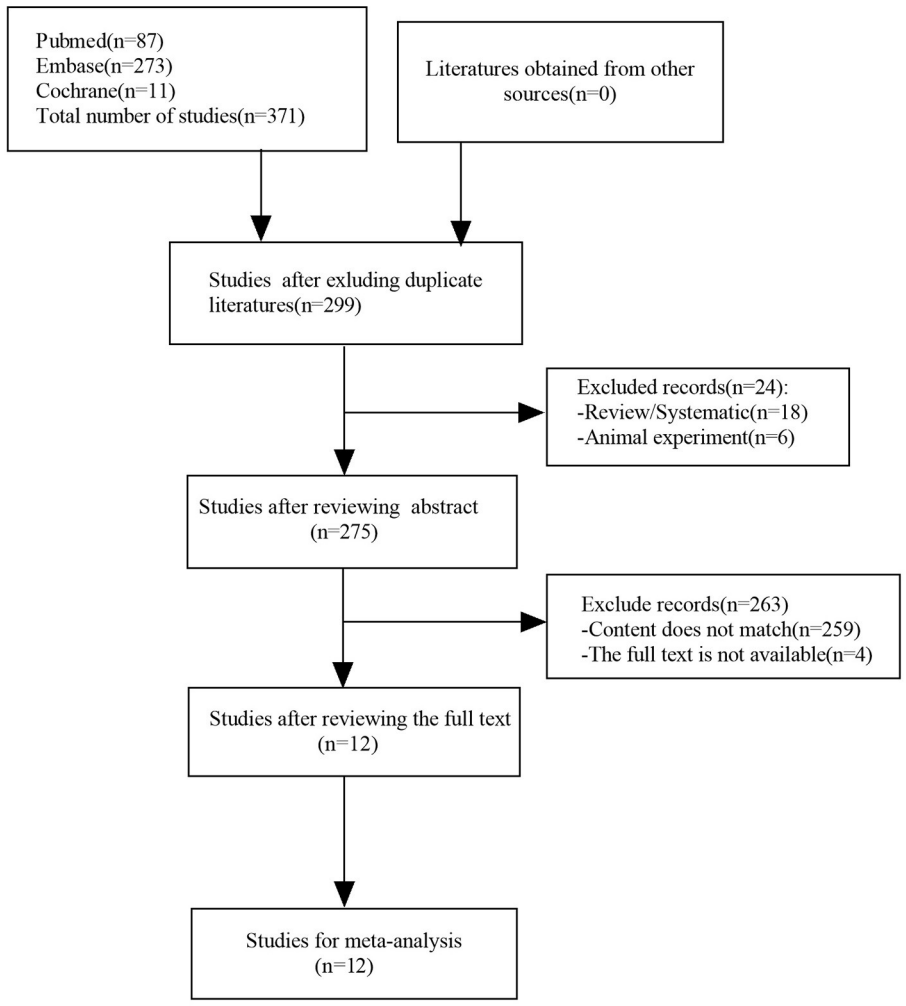

FIGURE 1 | PRISMA flow chart of the included studies.

TABLE 2 | Characteristics of the included studies.

Author	Year	Study type	Study area	Sample size, *n*		Sex, *n* (male/female)		Age, years	
				Seizure	Seizure-free	Seizure	Seizure-free	Seizure	Seizure-free
Choi et al.	2020	Retrospective	USA	98	318	59/39	185/133	49.0 ± 14.2	51.1 ± 16.0
Feyissa et al.	2019	Cohort	USA	46	22	28/18	17/5	50 ± 11	
Duan et al.	2018	Retrospective	China	73	216	45/28	120/96	48.7	48.7
Neal et al.	2018	Retrospective	China	52	48	/	/	/	/
Roberts et al.	2018	Retrospective	UK	45	18	43/20	34		
Yang et al.	2016	Retrospective	China	41	23	/	/	38 (17–72)	
Skardelly et al.	2015	Retrospective	Germany	116	218	43/73	88/130	/	/
Zhong et al.	2015	Retrospective	China	221	90	135/86	48/42	37	40.2
Mulligan et al.	2014	Retrospective	UK	48	12	/	/	42 (15–78)	
Liubinas et al.	2014	Prospective	Australia	23	7	13/9	2/5	35.4 (17–70)	
Liang et al.	2013	Retrospective	China	37	23	34/26	39.5 (17–65)		
Stockhammer et al.	2012	Retrospective	Germany	27	22	57	22	40 (13–72)	

TABLE 3 | Evaluation of the study quality.

Author	Year	Selection	Comparability	Exposure	Score
Choi et al.	2020	☆☆	☆☆	☆☆☆	7
Feyissa et al.	2019	☆☆☆	☆☆	☆☆☆	8
Duan et al.	2018	☆☆	☆☆	☆☆☆	7
Neal et al.	2018	☆☆☆	☆☆	☆☆☆	8
Roberts et al.	2018	☆☆	☆☆	☆☆☆	7
Yang et al.	2016	☆☆	☆☆	☆☆☆	7
Skardelly et al.	2015	☆☆☆	☆☆	☆☆☆	8
Zhong et al.	2015	☆☆☆	☆☆	☆☆	7
Mulligan et al.	2014	☆☆☆	☆☆	☆☆☆	8
Liubinas et al.	2014	☆☆	☆☆	☆☆☆	7
Liang et al.	2013	☆☆☆	☆☆	☆☆☆	8
Stockhammer et al.	2012	☆☆☆	☆☆	☆☆☆	8

"ATRX", "1p/19q", "P53", and "EGFR". The search strategy is shown in detail in **Table 1**.

Selection Criteria

The inclusion criteria were as follows: (1) observational studies and (2) publications in Chinese and English. The exclusion criteria were the following: (1) repeated publications, (2) studies with no full text, incomplete information, or inability to extract data, (3) a different definition of exposure from that encountered in most publications, (4) animal experiments, and (5) case reports, reviews, comments, and systematic reviews.

Data Extraction and Management

Literature retrieval, screening, and information extraction were independently performed by two researchers. In case of disagreement, a consensus was reached after a discussion with a third researcher. The extracted data included the following: author, year, research type, sample size, and clinical index.

Quality Assessment

The Newcastle–Ottawa Scale (NOS, http://www.ohri.ca/programs/clinical_epidemiology/oxford.htm) was used by the two researchers to independently evaluate the quality of the included studies. Any disagreement was resolved through a discussion with a third researcher. The NOS includes four items of "research object selection" (four points), one item of "inter-group comparability" (two points), and three items of "outcome measurement" (three points), with a maximum score of nine points; scores $\geq$7 and <7 points indicate high- and low-quality literature, respectively.

Data Analysis

Meta-analysis was performed using the R language (version 4.0). Odds ratio (OR) and 95% confidence interval (CI) were used as an effect index to evaluate the correlation between TMMs and the incidence of perioperative epilepsy in patients with glioma. I^2 was used to evaluate heterogeneity. Values of $p \geq 0.1$ and $I^2 \leq 50\%$ indicated that the studies were homogeneous, and the fixed effects model was used for a combined analysis. Furthermore, $p < 0.1$ and $I^2 > 50\%$ indicated study heterogeneity, and sensitivity analysis or subgroup analysis was used to determine the source of heterogeneity. If the heterogeneity remained large, the random effects model was utilized or a descriptive analysis was performed. When a single outcome index included more than 10 articles, funnel plot and Egger's bias test were used to analyze the publication bias of each index.

RESULTS

Study Selection

The comprehensive literature search identified 87 references from PubMed, 273 references from EMBASE, and 11 references from Cochrane (total of 371 references). After removing duplicates, 299 abstracts were reviewed and screened. Twelve studies were selected for full-text evaluation and met the inclusion criteria. **Figure 1** illustrates the flow chart.

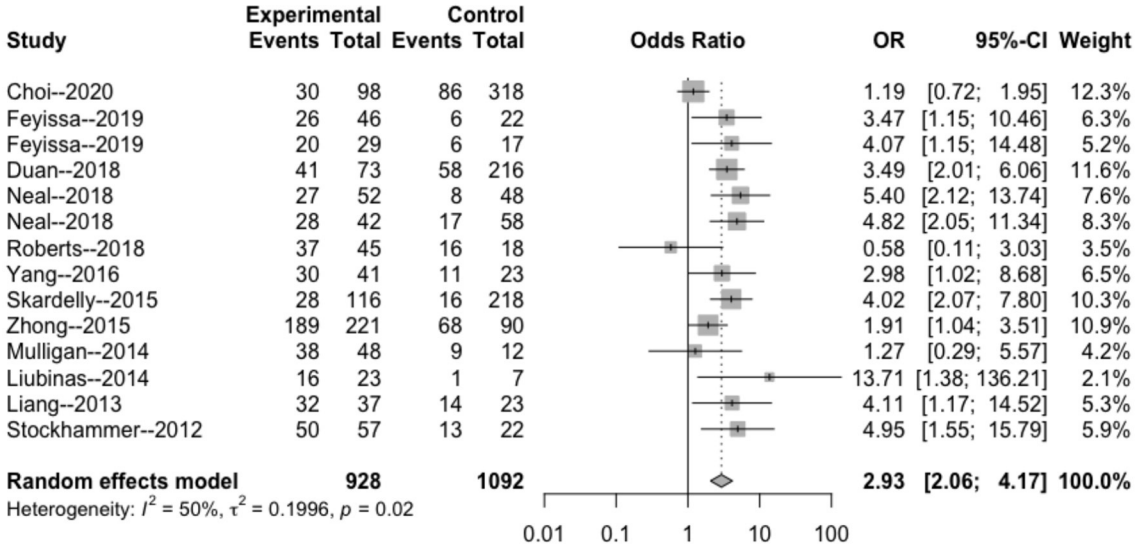

FIGURE 2 | Forest plot of the correlation between IDH mutation and perioperative epilepsy. CI, confidence interval; IDH, isocitrate dehydrogenase; OR, odds ratio.

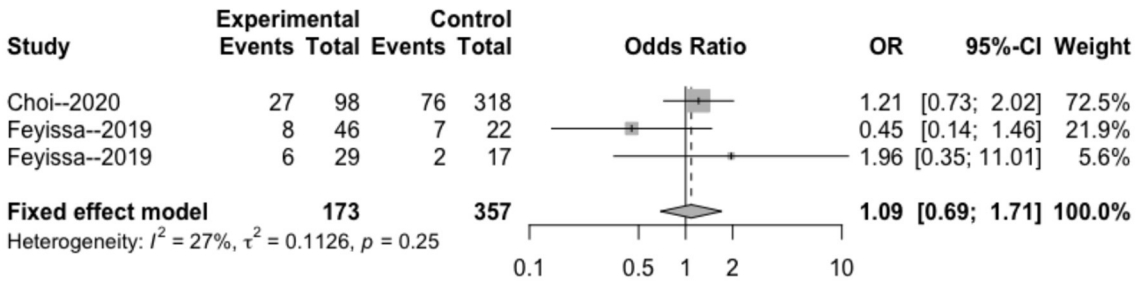

FIGURE 3 | Forest plot of the correlation between MGMT methylation and perioperative epilepsy. CI, confidence interval; MGMT, O6-methylguanine-DNA methyltransferase; OR, odds ratio.

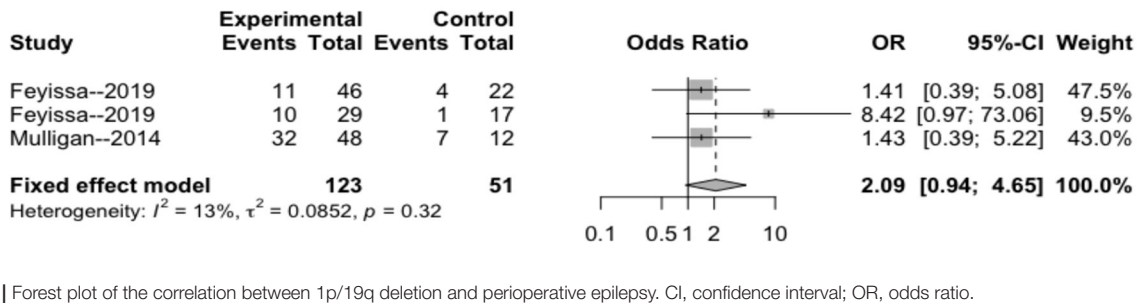

FIGURE 4 | Forest plot of the correlation between 1p/19q deletion and perioperative epilepsy. CI, confidence interval; OR, odds ratio.

Study Characteristics and Quality of Evidence

Study Characteristics

The 12 selected cohort studies were published between 2012 and 2020 and conducted in China (n = 5), Germany (n = 2), the United States of America (n = 2), the United Kingdom (n = 2), and Australia (n = 1). One and 11 studies were prospective and retrospective cohort studies, respectively. The characteristics of the included studies are shown in **Table 2**.

Quality of Evidence

All included studies had a NOS score ≥7, meeting the quality requirement. The specific results are shown in **Table 3**.

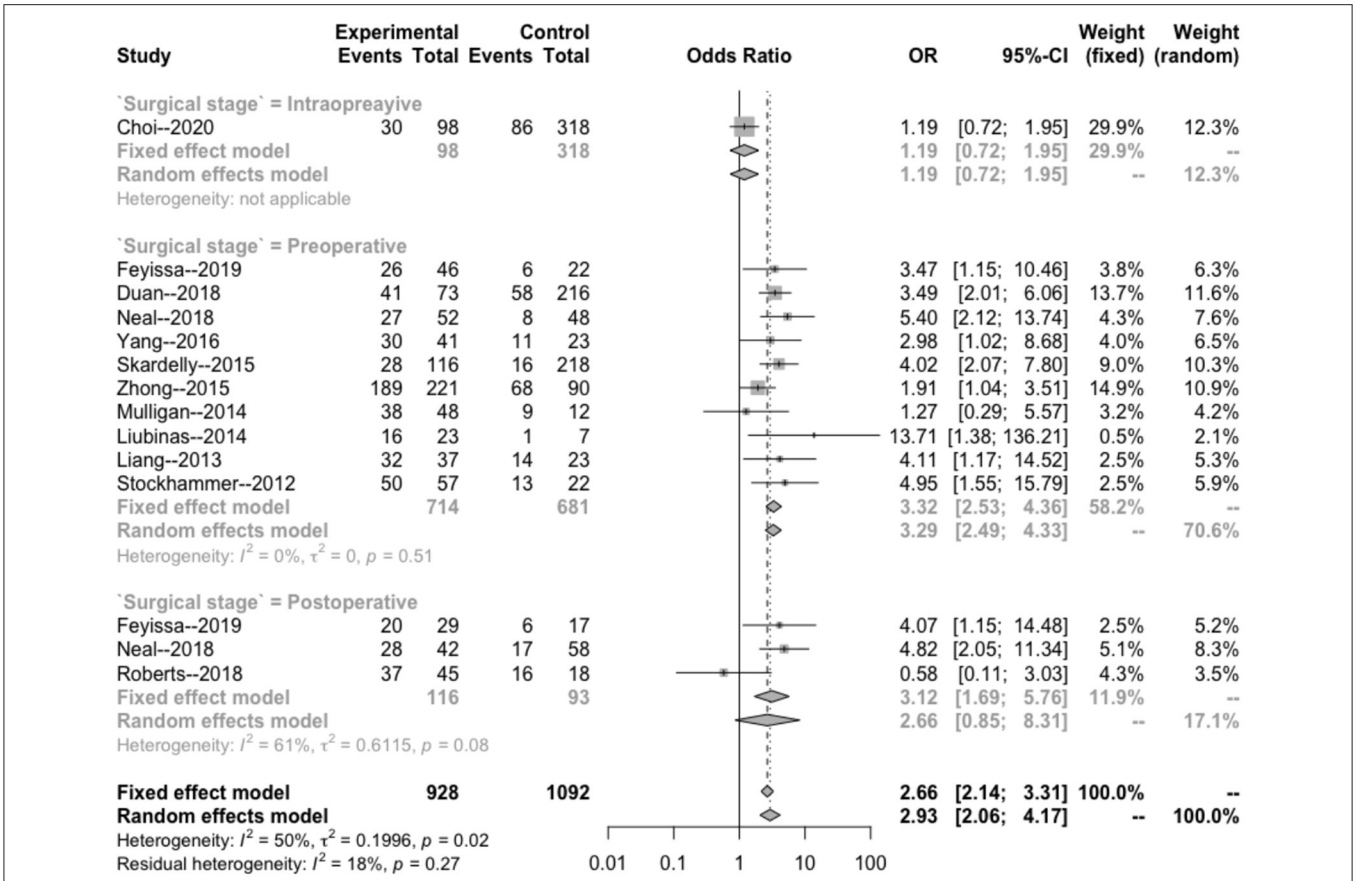

FIGURE 5 | Subgroup analysis of the relationship between IDH mutation and perioperative epilepsy. CI, confidence interval; IDH, isocitrate dehydrogenase; OR, odds ratio.

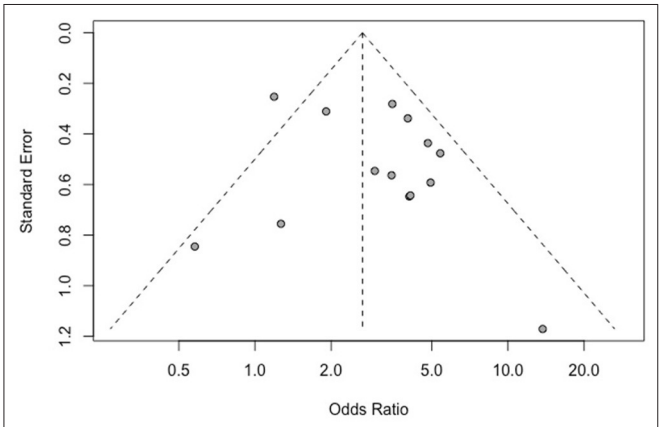

FIGURE 6 | Funnel plot of the correlation between IDH mutation and perioperative epilepsy. IDH, isocitrate dehydrogenase.

Data Analysis

IDH Mutation

The heterogeneity testing of 12 studies (I^2 = 50%, p = 0.02 < 0.1) showed slight heterogeneity and combined random effects size (OR = 2.93; 95% Cl: 2.06–4.17; p = 0.000). These findings suggested a significant correlation between IDH mutation and perioperative epilepsy (**Figure 2**).

MGMT Methylation

The heterogeneity testing of three studies (I^2 = 27 < 50%, p = 0.25 > 0.1) did not show significant heterogeneity in this study and combined fixed effects size (OR = 1.09; 95% Cl: 0.69–1.71; p = 0.720). The difference was not statistically significant. There was no correlation between MGMT methylation rate and perioperative epilepsy (**Figure 3**).

1p/19q Deletion Rate

The heterogeneity testing of three studies (I^2 = 13 < 50%, p = 0.32 > 0.1) did not show significant heterogeneity and combined fixed effect size (OR = 1.40; 95% Cl: 0.94–4.65; p = 0.087). The difference was not statistically significant. There was no significant correlation between 1p/19q deletion and perioperative epilepsy (**Figure 4**).

IDH Mutation Subgroup Analysis

The intraoperative combination combined effect (OR = 1.19; 95% Cl: 0.72–1.95) did not suggest a significant correlation between the occurrence of intraoperative epilepsy and the

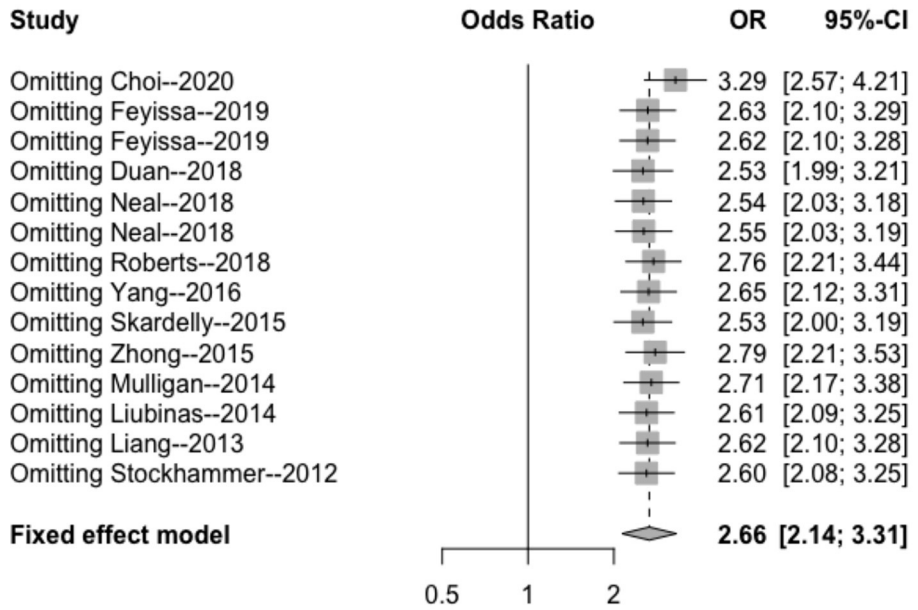

FIGURE 7 | Sensitivity analysis of the correlation between IDH mutation and perioperative epilepsy. CI, confidence interval; IDH, isocitrate dehydrogenase; OR, odds ratio.

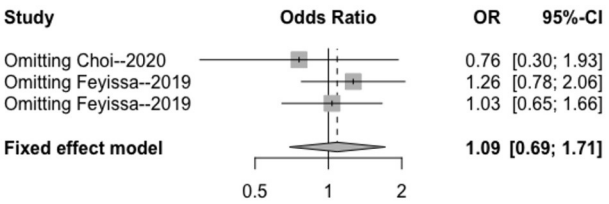

FIGURE 8 | Sensitivity analysis of the correlation between MGMT methylation and perioperative epilepsy. CI, confidence interval; MGMT, O6-methylguanine-DNA methyltransferase; OR, odds ratio.

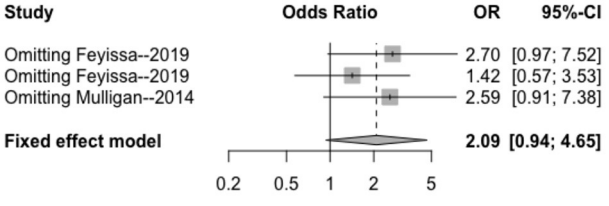

FIGURE 9 | Sensitivity analysis of the correlation between 1p/19q deletion and perioperative epilepsy. CI, confidence interval; OR, odds ratio.

presence of IDH in patients with glioma (**Figure 5**). The heterogeneity within the preoperative group ($I^2 = 0 < 50\%$, $p = 0.51 > 0.1$) and combined effects size (OR = 3.32; 95% Cl: 2.53–4.36) indicated a significant correlation between the occurrence of preoperative epilepsy and IDH in patients with glioma. The heterogeneity within the postoperative group ($I^2 = 61 > 50\%$; $p = 0.08 < 0.1$) and combined effect size (OR = 2.66; 95% Cl: 0.85–8.31) indicated that the occurrence of postoperative epilepsy in patients with glioma was not related to IDH.

Bias Test

The results of Egger's bias test based on the funnel chart of this study ($p = 0.259 > 0.05$) did not indicate an obvious publication bias (**Figure 6**).

Sensitivity Analysis

The results of the sensitivity analysis in this study are shown in **Figures 7**–**9**. After removing each article in order, it was shown that the individual studies did not have a marked influence on the results. The analysis indicated that the results of this study are relatively stable.

DISCUSSION

The present meta-analysis confirmed that IDH1 mutation was significantly associated with the incidence of perioperative epilepsy in patients with glioma. In contrast, MGMT methylation and 1p/19q deletion were not related to the incidence of perioperative epilepsy in patients with glioma. Unfortunately, it was not possible to analyze the role of tumor protein p53 (TP53) or epidermal growth factor receptor due to the lack of relevant research literature. The subgroup analysis showed that IDH1 was significantly correlated with the incidence of preoperative epilepsy in patients with glioma; however, it was not significantly correlated with the incidence of intraoperative and postoperative epilepsy. There was no significant heterogeneity and publication bias observed in the included studies, indicating that the results of this meta-analysis are stable.

Previous studies have shown that 1p/19q co-deletion is associated with a better overall survival rate in patients with low-grade glioma. TP53 mutation usually indicates a shorter survival time. IDH1 mutation, MGMT methylation, and 1p/19q co-deletion are good prognostic indicators for low-grade gliomas, being linked to a better overall survival rate (14–16). Interestingly, the combination of IDH1 mutation, MGMT methylation, and TP53 immunopositivity is associated with a faster progression to high-grade tumors (16). Thus far, tumor-related gene changes may be used as a basis for determining the prognosis of glioma. Nevertheless, this tendency has not been well investigated as a potential biomarker of epilepsy. Researchers have been committed to exploring the biochemical changes in the tumor microenvironment, searching for pathogenic and influencing factors of tumor-related epilepsy at the molecular level.

Duan et al. reported that IDH1 mutations are significantly associated with preoperative seizures in patients with glioma (17). Recently, Feyissa et al. confirmed that IDH1 mutation and MGMT methylation are associated with the occurrence of perioperative seizures (10). However, Liubinas et al. found that the presence of IDH1 mutations is not related to the incidence of epilepsy (18), though the results of that study may have been influenced by the inclusion of higher-grade tumors. Yang et al. reported that patients with a low expression of the MGMT protein were more likely to experience seizures after operation (19). In contrast, Feyissa et al. found that methylation of the MGMT gene promoter was associated with increased postoperative seizure control (10). However, they did not investigate other TMMs thought to be related to postoperative seizure control, which may have influenced their findings. Mulligan et al. showed that the combined deletion of 1p/19q was not related to the occurrence of preoperative seizures in patients with low-grade oligodendrogliomas (8). Moreover, due to the limited number of related studies, this meta-analysis could not determine the relationship between TMMs and perioperative seizures in patients with tumor-grade glioma.

The mechanism of tumor-related epilepsy remains unclear. The present findings showed that IDH1 mutations are associated with perioperative epilepsy; the subgroup analysis further showed that IDH1 is significantly related to preoperative epilepsy. The underlying mechanism of IDH mutation and perioperative seizures is unclear. This may be attributed to the activation of the receptor of N-methyl-D-aspartate (NMDA) by D-2-hydroxyglutarate (D2HG), which has a very similar structure to that of glutamate (20). Exogenous D2HG can increase the discharge of neurons in rats. The excitatory effect of D2HG could be blocked by treatment with a selective NMDA receptor antagonist (21). Numerous studies have also shown that the concentration of D2HG in glioma cells carrying IDH1 mutations is 100–300-fold higher than that measured in normal tissues (22). These studies suggested that D2HG may promote the occurrence and development of epilepsy in patients with glioma. Moreover, some studies have shown that perioperative epilepsy is not related to the location, grade, or histopathology of glioma (10, 23, 24). Previous studies have also shown that seizures may not occur in all patients with similar glioma localization and histology (24, 25). Therefore, the heterogeneity of TMM in gliomas may lead to the observed variability of epilepsy in patients with glioma. These results are important for the research and treatment of glioma-related epilepsy.

Although our results did not have any publication bias or statistically significant heterogeneity, the present analysis included 11 retrospective studies and no randomized studies. Moreover, there are still fewer TMMs other than IDH1 mutations. Hence, further studies are warranted to verify the present findings.

CONCLUSION

Our findings provide supporting evidence for the correlation between TMMs and glioma-related seizures. Future studies should include epileptic symptoms and detect more TMMs. Clarifying the mechanism of perioperative epilepsy in glioma will benefit the clinical treatment of patients with this disease and the precise treatment of epilepsy.

DATA AVAILABILITY STATEMENT

The original contributions presented in the study are included in the article/supplementary material, further inquiries can be directed to the corresponding author/s.

AUTHOR CONTRIBUTIONS

LS and XQ performed the data collection, wrote and revised the manuscript, and are co-first authors. LC designed the study. JZ contributed to conceiving and revising the manuscript. LC and JZ are co-corresponding authors. CC performed the data collection and analysis. All authors contributed to the article and approved the submitted version.

FUNDING

This work was supported by the Student Innovation and Entrepreneurship Training Program Project (201910632025), Luzhou–Southwest Medical University Scientific Research Program (2016LZXNYD-G03 and 2018LZYD-ZK50), a scientific research program of the Science and Technology Department of Sichuan (2018JY0404 and 2018JY0403), and Sichuan Province Returnees' Science and Technology Activities Project [2019(76)-72].

ACKNOWLEDGMENTS

The authors would like to thank their colleagues for helpful discussions on topics related to this work.

REFERENCES

1. Rudà R, Bello L, Duffau H, Soffietti R. Seizures in low-grade gliomas: natural history, pathogenesis, and outcome after treatments. *J Neuro Oncol.* (2012) 14(Suppl. 4):55–64. doi: 10.1093/neuonc/nos199
2. Shin JY, Kizilbash SH, Robinson SI, Uhm JH, Hammack JE, Lachance DH, et al. Seizures in patients with primary brain tumors: what is their psychosocial impact? *J Neuro Oncol.* (2016) 128:285–91. doi: 10.1007/s11060-016-2108-y
3. Vecht CJ, Kerkhof M, Duran-Pena A. Seizure prognosis in brain tumors: new insights and evidence-based management. *Oncologist.* (2014) 19:751–9. doi: 10.1634/theoncologist.2014-0060
4. Huberfeld G, Vecht CJ. Seizures and gliomas—towards a single therapeutic approach. *Nat Rev Neurol.* (2016) 12:204–16. doi: 10.1038/nrneurol.2016.26
5. Rudà R, Soffietti R. What is new in the management of epilepsy in gliomas? *J Curr Treat Options Neurol.* (2015) 17:351. doi: 10.1007/s11940-015-0351-8
6. Stockhammer F, Misch M, Helms H-J, Lengler U, Prall F, von Deimling A, et al. IDH1/2 mutations in WHO grade II astrocytomas associated with localization and seizure as the initial symptom. *Seizure.* (2012) 21:194–7. doi: 10.1016/j.seizure.2011.12.007
7. Liang R, Fan Y, Wang X, Mao Q, Liu Y. The significance of IDH1 mutations in tumor-associated seizure in 60 Chinese patients with low-grade gliomas. *Sci World J.* (2013) 2013:403942. doi: 10.1155/2013/403942
8. Mulligan L, Ryan E, O'Brien M, Looby S, Heffernan J, O'Sullivan J, et al. Genetic features of oligodendrogliomas and presence of seizures: The relationship of seizures and genetics in LGOs. *Clin Neuropathol.* (2014) 33:292–8. doi: 10.5414/NP300727
9. Yang P, You G, Zhang W, Wang Y, Wang Y, Yao K, et al. Correlation of preoperative seizures with clinicopathological factors and prognosis in anaplastic gliomas: a report of 198 patients from China. *Seizure.* (2014) 23:844–51. doi: 10.1016/j.seizure.2014.07.003
10. Feyissa AM, Worrell GA, Tatum WO, Chaichana KL, Jentoft ME, Guerrero Cazares H, et al. Potential influence of IDH1 mutation and MGMT gene promoter methylation on glioma-related preoperative seizures and postoperative seizure control. *Seizure.* (2019) 69:283–9. doi: 10.1016/j.seizure.2019.05.018
11. Mirsattari SM, Chong JJR, Hammond RR, Megyesi JF, Macdonald DR, Lee DH, et al. Do epileptic seizures predict outcome in patients with oligodendroglioma? *Epilepsy Res.* (2011) 94:39–44. doi: 10.1016/j.eplepsyres.2011.01.001
12. Chang EF, Potts MB, Keles GE, Lamborn KR, Chang SM. Seizure characteristics and control following resection in 332 patients with low-grade gliomas. *J Neurosurg.* (2008) 108:227–35. doi: 10.3171/JNS/2008/108/2/0227
13. Li Y, Shan X, Wu Z, Wang Y, Ling M, Fan X. IDH1 mutation is associated with a higher preoperative seizure incidence in low-grade glioma: a systematic review and meta-analysis. *Seizure.* (2018) 55:76–82. doi: 10.1016/j.seizure.2018.01.011
14. Kim YH, Nobusawa S, Mittelbronn M, Paulus W. Molecular classification of low-grade diffuse gliomas. *Am J Pathol.* (2010) 177:2708–14. doi: 10.2353/ajpath.2010.100680
15. Cavaliere R, Lopes MBS, Schiff D. Low-grade gliomas: an update on pathology and therapy. *Lancet Neurol.* (2005) 4:760–70. doi: 10.1016/S1474-4422(05)70222-2
16. Leu S, von Felten S, Frank S, Vassella E, Vajtai I, Taylor E, et al. IDH/MGMT-driven molecular classification of low-grade glioma is a strong predictor for long-term survival. *Neuro Oncol.* (2013) 15:469–79. doi: 10.1093/neuonc/nos317
17. Duan WC, Wang L, Li K, Wang WW, Zhan YB, Zhang FJ, et al. mutations but not TERTp mutations are associated with seizures in lower-grade gliomas. *Medicine.* (2018) 97:1–6. doi: 10.1097/MD.0000000000013675
18. Liubinas SV, D'Abaco GM, Moffat BM, Gonzales M, Feleppa F, Nowell CJ, et al. IDH1 mutation is associated with seizures and protoplasmic subtype in patients with low-grade gliomas. *Epilepsia.* (2014) 55:1438–43. doi: 10.1111/epi.12662
19. Yang Y, Mao Q, Wang X, Liu Y, Mao Y, Zhou Q, et al. An analysis of 170 glioma patients and systematic review to investigate the association between IDH-1 mutations and preoperative glioma-related epilepsy. *J Clin Neurosci.* (2016) 31:56–62. doi: 10.1016/j.jocn.2015.11.030
20. Klker S, Pawlak V, Ahlemeyer B. NMDA receptor activation and respiratory chain complex V inhibition contribute to neurodegeneration in d-2-hydroxyglutaric aciduria. *Eur J Neurosci.* (2002) 16:21–8. doi: 10.1046/j.1460-9568.2002.02055.x
21. Chen H, Judkins J, Thomas C, Wu M, Khoury L, Benjamin C. Mutant IDH1 and seizures in patients with glioma. *Neurology.* (2017) 88:1805–13. doi: 10.1212/WNL.0000000000003911
22. Reitman ZJ, Yan H. Isocitrate Dehydrogenase 1 and 2 Mutations in cancer: alterations at a crossroads of cellular metabolism. *JNCI J Natl Cancer Inst.* (2010) 102:932–41. doi: 10.1093/jnci/djq187
23. Yang P, Liang T, Zhang C, Cai J, Zhang W, Chen B, et al. Clinicopathological factors predictive of postoperative seizures in patients with gliomas. *Seizure.* (2016) 35:93–9. doi: 10.1016/j.seizure.2015.12.013
24. Pallud J, Audureau E, Blonski M, Sanai N, Bauchet L, Fontaine D, et al. Epileptic seizures in diffuse low-grade gliomas in adults. *Brain.* (2013) 137:449–62. doi: 10.1093/brain/awt345
25. Rosati A, Tomassini A, Pollo B, Ambrosi C, Schwarz A, Padovani A, et al. Epilepsy in cerebral glioma: timing of appearance and histological correlations. *J Neurooncol.* (2009) 93:395–400. doi: 10.1007/s11060-009-9796-5

Conflict of Interest: The authors declare that the research was conducted in the absence of any commercial or financial relationships that could be construed as a potential conflict of interest.

frontiers in Oncology

REVIEW
published: 27 September 2021
doi: 10.3389/fonc.2021.731441

Potential Molecular Biomarkers of Vestibular Schwannoma Growth: Progress and Prospects

Yu Zhang[1†], Jianfei Long[1†], Junwei Ren[2], Xiang Huang[2], Ping Zhong[2] and Bin Wang[1*]*

[1] Department of Pharmacy, Huashan Hospital, Fudan University, Shanghai, China, [2] Department of Neurosurgery, Huashan Hospital, Fudan University, Shanghai, China

Vestibular schwannomas (VSs, also known as acoustic neuromas) are relatively rare benign brain tumors stem from the Schwann cells of the eighth cranial nerve. Tumor growth is the paramount factor for neurosurgeons to decide whether to choose aggressive treatment approach or careful follow-up with regular magnetic resonance imaging (MRI), as surgery and radiation can introduce significant trauma and affect neurological function, while tumor enlargement during long-term follow-up will compress the adjacent nerves and tissues, causing progressive hearing loss, tinnitus and vertigo. Recently, with the deepening research of VS biology, some proteins that regulate merlin conformation changes, inflammatory cytokines, miRNAs, tissue proteins and cerebrospinal fluid (CSF) components have been proposed to be closely related to tumor volume increase. In this review, we discuss advances in the study of biomarkers that associated with VS growth, providing a reference for exploring the growth course of VS and determining the optimal treatment strategy for each patient.

Keywords: vestibular schwannoma, growth, biomarker, target therapy, merlin

OPEN ACCESS

Edited by:
Liam Chen,
University of Minnesota, United States

Reviewed by:
Emanuele La Corte,
University of Bologna, Italy
Güliz Acker,
Charité Medical University of Berlin, Germany

***Correspondence:**
Ping Zhong
zhp228899@163.com
Bin Wang
wangbin@huashan.org.cn

[†]These authors have contributed equally to this work and share first authorship

Specialty section:
This article was submitted to Neuro-Oncology and Neurosurgical Oncology, a section of the journal Frontiers in Oncology

Received: *27 June 2021*
Accepted: *06 September 2021*
Published: *27 September 2021*

Citation:
Zhang Y, Long J, Ren J, Huang X, Zhong P and Wang B (2021) Potential Molecular Biomarkers of Vestibular Schwannoma Growth: Progress and Prospects. Front. Oncol. 11:731441. doi: 10.3389/fonc.2021.731441

1 INTRODUCTION

VSs are histologically benign lesions deriving from the Schwan cells of the vestibulo-cochlear nerve commonly occur unilaterally, or bilaterally in the pathognomonic for the hereditary disorder neurofibromatosis type 2 (NF2) (1, 2). Generally, the mere presence of benign tumors is not a therapeutic indication. However, the slow but progressive growth of this intracranial tumor can confer compression to adjacent cranial nerve and brainstem, resulting in neurological deficits, balance difficulty and sensorineural hearing loss (SNHL) (3).

The goal of VS treatment has shifted from saving lives towards functional preservation, with multifaceted decision including watch-wait-rescan protocol, surgical resection and radiation (4, 5). However, surgery can be traumatic (6), while radiotherapy has a low hearing retention rate and can affect neurological function even after many years (7). We can see from the literature that two-thirds of VS did not grow during 3.6 years of follow-up, the average growth rate of sporadic VS was 1.1 mm/year diameter, and for NF2-related tumors 1.7 mm/year (8, 9), supporting the wait and watch policy in appropriate patients. A study showed that conservative management in small- to medium-sized VS (less than 2cm) can improve rates of facial nerve preservation and hearing protection in comparison to patients who undergo primary surgical treatment (10). Therefore, for stable or

involuting tumors with no mass effect, or elderly patients who will suffer higher risk of comorbidities, the continuing trend toward observation with regular follow-up imaging is reasonable (5, 11).

Nevertheless, observation policy carries the inherent risk of tumor progression and hearing deterioration in growing tumors, which emphasizing the importance of the identification of effective and convenient indicators to predict growth characteristics at the time of diagnosis to weigh the benefits and risks of active treatment against watchful observation. Previous studies have reported onset at an early age, increasing size in the first year, hearing loss, extrameatal tumor location, cerebellopontine angle extension, sway velocity with eyes open were risk factors for tumor growth (9, 12–15). Here, we provide a narrative review on the topic of biomarkers currently considered to be related to VS growth in order to assist surgeons to select the most accurate treatment approach and the development of innovative targeted therapies.

2 METHODS

The authors conducted a literature review using Web of Science and PubMed databases in order to identify important recent publications and synthesized them into a comprehensive review of potential biomarkers of VS growth. The search strategy included the search terms "growth", "expression" and "vestibular schwannoma". We have also scanned the reference lists of published articles for further potential hits of relevance to this review. Peer-reviewed full articles published in English till August 2021 were included to compile this review. Search results were judged for relevance by the research team using the title, abstract and if necessary full text. Studies were included, if they 1) explored the relationship between biomarkers and the size or growth of sporadic VS or NF2-associated VS; 2) explored molecules that aberrantly expressed in VS compared with normal tissues; 3) drug research for VS treatment. Studies were excluded, if they 1) merely found some imaging manifestations or clinical features related to VS growth; 2) case reports.

3 RESULTS

We summarized the search results into five major types of biomarkers, which are summarized in **Table 1**.

3.1 Merlin Pathway Related Proteins

Neurofibromin 2 gene mutation and the function loss of its transcription protein merlin (an acronym for moesin-ezrin-radixin-like protein) are widely regarded to play a paramount role in the pathogenesis of both sporadic and bilateral VS (46, 47). Merlin belongs to the ERM (for ezrin, radixin, moesin) family of cytoskeleton linker proteins and shares a common structural organization with it: a relatively conserved N-terminal FERM domain, followed by a α-helical region and a charged hydrophilic-COOH terminal tail (48). The *neurofibromin 2* gene encodes for two major isoforms of merlin: exon 16 skipping production isoform 1 and exon 16 retention isoform 2, both of which carry full tumor suppressive function (49).

Merlin maintains the stability of the cell membrane by the binding of integral membrane proteins and spectrin actin cytoskeleton and mediates cell contact inhibition (50). Merlin exerts its growth suppressive function by modulating the activity of intracellular promitogenic signal cascades related to tumor

TABLE 1 | Summary table of potential biomarkers related to VS growth.

Major types	Action mechanisms	Biomarkers and their characteristics	References
Merlin pathway proteins	RTK signal proteins	VEGF expression was increased in VS, and anti-VEGF therapy was effective for NF2-VS.	(16)
		Pharmaceutical inhibition of PDGFR could reduce VS growth rate.	(17, 18)
		bFGF promoted proliferation and invasion of VS cells, and also might be a hearing protector in VS.	(16, 19)
		ErbB family proteins were aberrantly expressed in VS, and its inhibition has therapeutic effects on VS.	(20)
	Ras signal proteins	Merlin inhibits Ras signal transduction by interfering with GRB2 expression and inhibiting Rac1 and PAK1 activation.	(21–23)
	CPI-17–MYPT1 switch	CPI-17–MYPT1 switch was responsible for the conformational change of merlin. CPI-17 was over-expressed in VS.	(24–26)
	Hippo signal proteins	Merlin activated LATS1/2 and inhibited the destabilization of LATS1/2 by $CRL4^{DCAF1}$. LATS1/2 promoted the degradation of YAP and inhibited the transcription of pro-proliferation and anti-apoptotic genes stimulated by YAP.	(27, 28)
Inflammatory signal	Local inflammation	The NF-κB signal activated in VS was considered to be the core of VS pathophysiology.	(29, 30)
		COX-2 was highly expressed in VS and was associated with high proliferation rate.	(31)
	Systemic inflammation	Macrophages, especially M2-type macrophages, were thought to promote VS growth.	(32, 33)
		High NLR was associated with VS growth.	(34)
Tumor miRNAs	Gene expression regulation	The upregulation of miR-29abc, miR-19, miR-340-5p, miR-21, miR-221 and downregulation of miR-744, let-7b were related to VS growth velocity.	(35, 36)
Tumor proteins	Glycoprotein	CD105 can be used as a MVD marker, and was correlated with VS size and growth rate.	(37)
	Neurotrophic factor	BDNF expression was correlated with mitotic activity in VS.	(38)
	Proteases	The expression of MMP-2 and MMP-9 was correlated with VS growth rate and was higher in cystic VS than solid VS. The proteolytic activity of MMP-14 was related to the degree of SNHL in VS patients.	(39–41)
		The expression of ADAM9 was higher in VS and related to functional impairment.	(42, 43)
CSF components	Mucopolysaccharide	HA levels were elevated in NF2-VS and correlated with the proliferation rate of schwannoma cells.	(44)
	Proteins	ABCA3, SCG1, KLF11, CA2D1, BASP1and PRDX2 were associated with VS growth.	(45)

formation, including Ras/Raf/MEK/ERK (51), PI3K/Akt (52), c-JNK (53), Hippo signaling pathway, and the overall activity of the E3 ubiquitin ligase $CRL4^{DCAF1}$ in the nucleus (54). Moreover, merlin was reported to assuming a possible role in the mediation of cell cycle progression (55).

Classically, it was considered that the activity of merlin was regulated by phosphorylation on the main regulatory Ser^{518}: dephosphorylated merlin functions as a growth inhibitor in a closed conformation formed by intramolecular association of its N-terminal domain (NTD) and carboxy-terminal domain (CTD), while phosphorylated merlin cannot form a folded state and is functionally deficient (56). However, subsequent researches have shown that transcripts of the mutated *neurofibromin 2* gene or phosphorylated merlin have a more closed form, leading to impaired contact-dependent inhibition of proliferation (57, 58). There is also a controversial view holding that merlin's tumor suppressive function is independent of its conformational change (59). The activation of receptor tyrosine kinases (RTKs), integrins, CD44 and cadherin signal are responsible for the regulation of merlin's phosphorylation *via* the downstream effector p21-activated kinase 1 (PAK1) and myosin phosphatase targeting subunit 1 (MYPT1) (**Figure 1**) (60, 61).

3.1.1 RTKs

The over-expression and over-activation of at least four types of RTKs and their ligands involved in the progression or invasion of sporadic and NF2-associated VS: ErbB (62), platelet-derived growth factor (PDGF) (63), basic fibroblast growth factor (bFGF) (19) and vascular endothelial growth factor (VEGF) (64).

VEGF is one of the most prominent angiogenesis stimulator that can regulate irregular blood vessel sprouting and growth except for simple remodeling of the capillary basement membrane (65), and lead to development of an immuno suppressive tumor microenvironment (66). Compared with normal vestibular nerve, the expression of VEGF, VEGFR-1/Flt and VEGFR-2/Flk as well as the coreceptor NP1 were considerable increased in VS tissues, suggesting at least a part of neoplastic growth was induced *via* the promotion of angiogenesis (39, 64, 67). Tissue microarray analysis of 182 sporadic VSs found significantly higher VEGF levels in the groups of recurrent and preoperatively irradiated tumors when compared to primary VS patients (67). However, there are contradictory views as to whether VEGF expression is correlated with sporadic VS growth characteristics. Koutsimpelas et al. initially found a positive correlation between VEGF expression and tumor volume, tumor growth index (calculated by dividing the maximal tumor diameter by the patient's age) and microvessel density (MVD, defined by CD31 staining) (16), but further investigation with expanded sample size demonstrated that although tumors with high proliferation index and high levels of VEGF and its receptor were more common than those with low proliferation activity expressing low levels of VEGF and its receptor, the expression of neither VEGF nor its receptors correlated with the proliferation indexes (Ki-67) or the growth characteristics of the tumors (67).

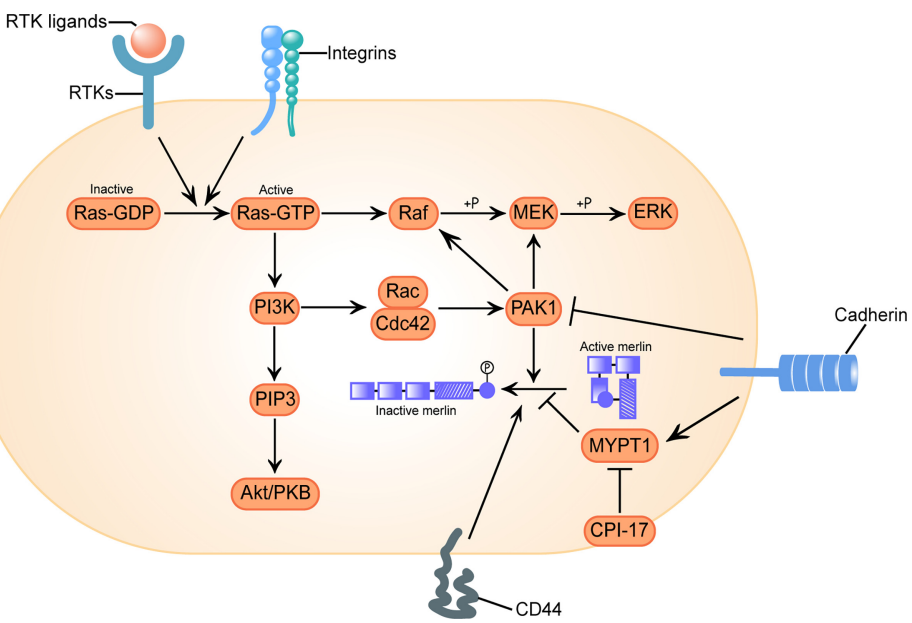

FIGURE 1 | Configurational changes of Merlin in response to receptor tyrosine kinases (RTKs), integrins, clusters of differentiation 40 (CD40) and cadherins signal stimulation. Activation of RTKs and integrins triggers GTP loading of Ras, which drives three mitogenic downstream pathways: Raf/MEK/ERK, PI3K/Rac/PAK, and PI3K/PIP3/Akt/PKB. p21-activated kinase 1 (PAK1) is an effector of the downstream pathway activated by Ras, which phosphorylates merlin at Ser^{518} and converts it to an inactive conformation. Conversely, myosin phosphatase targeting subunit 1(MYPT1) dephosphorylates and reactivates merlin. C-kinase potentiated protein phosphatase-1 inhibitor of 17 kDa (CPI-17) acts as a cellular inhibitor of MYPT1, causes loss of function of merlin. CD44 inactivates merlin. Engagement of cadherins inactivates PAK1 and activates MYPT1, inducing merlin's tumor suppressor function in a two-fold way. Here we adopt the broadly accepted hypothesis that phosphorylated merlin is the inactive form.

Multiple anti-VEGF therapy studies in patients with progressive NF2-VS have shown that bevacizumab can not only ameliorate hearing loss and reduce tumor size (68), but also normalize the tumor vasculature and reduce vasogenic edema, which improved the delivery of oxygenation, a potent radiosensitizer, and therefore reduced radiation dose and minimized radiation-related neurotoxicity (69).

As a regulator of cell growth and division, PDGF can regulate stemness in schwannoma cell lines and have a role in tumorigenesis (70). The PDGF family consists of five different disulphide-linked dimers built up of four different polypeptide chains encoded by four different genes. These isoforms, PDGF-AA, PDGF-AB, PDGF-BB, PDGF-CC and PDGF-DD, act *via* two RTKs, PDGF receptors α and β (71). Nilotinib (17) and Gleevec (18, 63, 72) pharmacologically inhibit these two receptors and their main downstream signaling pathways that have been proved to be over-expressed and activated in VS, and could also potentially reduce the angiogenic activity and growth rate of VS.

bFGF (also known as FGF-2 or FGF-β) was not only an identified angiogenic cytokine (73), but also implicated in tumor maintenance and metastasis (74). bFGF was identified as a mediator to protect auditory neurons from acoustic trauma and aminoglycoside ototoxicity, it was 3.5-fold higher in good hearing VS *versus* poor hearing VS (75), and its plasma concentration increased while patient's hearing improved after bevacizumab regimen (76). bFGF is also a known mitogen that promotes the proliferation of cell cultures derived from sporadic VS and increased the invasive phenotype mediated by Akt and ERK in HEI-193 cells (19, 77). In sporadic VS, increased levels of bFGF were positively correlated with tumor volume, tumor growth index and MVD (16). The mechanism by which bFGF stimulates mitosis might divergent from the way it modulates hearing. This notion, together with the results of cytokine array analysis where levels of ErbB, a well-established growth modulator, are not correlate with hearing status, may partly explain the irrelevance of tumor growth rate or tumor volume with VS patients' hearing outcome (75).

The ErbB family consists of four members: ErbB-1/EGFR/Her1, ErbB-2/Neu/Her2/p185, ErbB-3/Her3, and ErbB-4/Her4. ErbB family is upregulated in many malignant tumors, and also aberrantly expressed in VS. It has been reported that 68% of EGFR (62% sporadic and 75% NF2-associated VS), 84% of ErbB2 (76% sporadic and 94% NF2-related VS) and 34% of ErbB3 were upregulated in VS (20). Of EGFR ligands, EGF was up-regulated in all NF2-related VS, but none of the sporadic VS; Neuregulin was up-regulated in 86% of sporadic VS and 19% of NF2-related VS (20). In HEI-193 cells, the addition of EGF increased cellular invasion by 10-fold, which could be reduced by the inhibition of PI3K/Akt (19). Both dual small molecule inhibitor of EGFR and ErbB2 Lapatinib and the EGFR inhibitor Erlotinib demonstrated their therapeutic effects in VS (78–80).

3.1.2 Ras and Related Raf/MEK/ERK, PI3K/Akt and Rac/PAK

The small G-protein Ras, the downstream oncoprotein of RTKs that cycles between an inactive GDP-bound and an active GTP-bound state, play a role in the cascade of cell proliferation and division. In its active state, Ras can interact with several different effectors, thereby triggering an array of downstream signaling networks that responsible for promoting cellular transformation and driving tumorigenesis, such as Ras/Raf/MEK/ERK and Ras/PI3K/Akt pathways (81–83). It is well known that activation of Ras leads to subsequent activation of Rac/Cdc42 and its downstream effector PAK1, whose phosphorylation of Raf on Ser^{338} and MEK on Ser^{298} is required for effective signal transfer of Ras (**Figure 1**) (84, 85).

An increasing body of literature suggests that merlin counteract Ras-induced transformation at multiple levels. Merlin interferes with the expression of endogenous growth factor receptor binding 2 (GRB2) protein (21), directly reduces the GTP-loading of Ras and Rac to restrain their activation (86), and directly binds to the p21 binding domain (PBD) of PAK1 to interrupt PAK1 activation and its recruitment to focal adhesions (22, 87). Merlin competitively binds to angiomotin and releases the Rac1 negative regulator Rich1, which ultimately attenuates Rac1 signaling (23). Dysfunction of merlin would allow for enhanced Ras signal transduction and accelerated tumor growth rate (24).

Merlin itself is regulated by PAK reciprocally, it was phosphorylated at Ser^{518} by active PAK and therefore lose the inhibition of cell transformation. Activated Rac expression induces merlin phosphorylation and decreases the association between merlin and cytoskeleton (60). Based on the study of the role of Ras pathway signal transduction in the growth of VS, preclinical assessment of PAK inhibitors (88), MEK1/2 inhibitors (81) and Ailanthone, the down regulator of Ras and Raf, all exhibited certain antitumor properties (89).

3.1.3 MYPT1

MYPT1 is a phosphatase that forms the C-kinase potentiated protein phosphatase-1 inhibitor of 17 kDa (CPI-17)–MYPT1 switch along with its most specific and potent inhibitor CPI-17, regulating the phosphorylation of both merlin and other ERM family proteins (24, 90). Although highly homologous, the activity changes of merlin and other ERM proteins after C-terminal phosphorylation are opposite, and fulfils an antagonistic role in Ras activity control: the phosphorylation inactivates merlin, which counteracts Ras-induced transformation (91), but activates ERM proteins, which are essential for proper Ras activation (92). Thus, the oncogenic protein CPI-17 may activate Ras signaling in a two-fold way.

A previous systematically investigation on schwannomas showed that CPI-17 stained negative in non-tumor pathologies, but specifically up-regulated in over 90% of schwannomas, primarily in sporadic schwannomas (25). Moreover, high CPI-17 levels were found to correlate with higher Ki-67 proliferation indices, indicating a putative role of CPI-17 in schwannoma progression (25). Xu et al. found the over-expression of CPI-17 was a prominent feature of sporadic VS tissues, and there was a significantly positive correlation between CPI-17 expression and merlin phosphorylation (26), confirming the rationality of the causal chain CPI-17–MYPT1–merlin dysfunction in VS.

3.1.4 Yes-Associated Protein (YAP)

The deregulation of the Hippo pathway and the accompanying activation of Yes-associated protein (YAP) has been implicated in VS cell proliferation (27). As described in **Figure 2**, merlin initiate Hippo pathway to promote the phosphorylation and degradation of YAP and its homologous protein transcriptional coactivator with PDZ-binding motif (TAZ) (93, 94). In the inactivated state of merlin, YAP/TAZ migrates into the nucleus and binds to TEA domain family members (TEAD), stimulating the transcription of pro-proliferation and anti-apoptotic genes (27, 95).

The E3 ubiquitin ligase $CRL4^{DCAF1}$ can directly ubiquitinylate and destabilize LATS1/2 to activate YAP (54). Merlin can translocates into the nucleus, binds with high affinity to $CRL4^{DCAF1}$ and blocks its function (28). It is postulated that this merlin-$CRL4^{DCAF1}$-LATS1/2-YAP signaling axis might be the key mechanism of merlin's tumor suppressive effect. Although no studies have directly confirmed the correlation between VS tumorigenesis and $CRL4^{DCAF1}$ activity, targeted inhibition of the upstream activator of $CRL4^{DCAF1}$, NEDD8-activating enzyme (NAE), can induce inhibitory YAP phosphorylation and reduce cell proliferation in mouse *neurofibromin 2*-mutant schwannoma cells and human *neurofibromin 2*-mutant mesothelioma cell line (96), indicating a growth-promoting role of $CRL4^{DCAF1}$ in *neurofibromin 2*-inactivated tumors.

3.2 Inflammatory Signal

At present, there is increasing evidence that a variety of solid tumors contain a certain degree of tumor-associated inflammation that play a role in the cancer formation, progression and metastasis (97). Inflammatory response in cancer patients comprises both the local inflammatory response and the systemic response. The local inflammatory response is mediated by chemokines, cytokines, growth factors and matrix metalloproteinases (MMPs) secreted from *in situ* tumor cells, stromal cells, and infiltrating immune cells, and can became accomplices to cancer development by enhancing cell survival, invasion, neovascularization, and adaptive immunity suppression (98). Meanwhile, inflammation in the tumor microenvironment could be reflected in peripheral circulation, i.e., systemic inflammatory response that characterized by white cell components in peripheral blood, such as the platelet–to–lymphocyte ratio (PLR) and neutrophil–to–lymphocyte ratio (NLR), which have been highlighted as probable markers of pathologic responses for numerous types of solid tumors (99, 100).

It has been demonstrated that the volume increase of VS is not merely based on cell proliferation, but is also implicated with (neo)vascularization, intratumoral hemorrhage, cyst formation and inflammatory reaction (32, 101, 102).

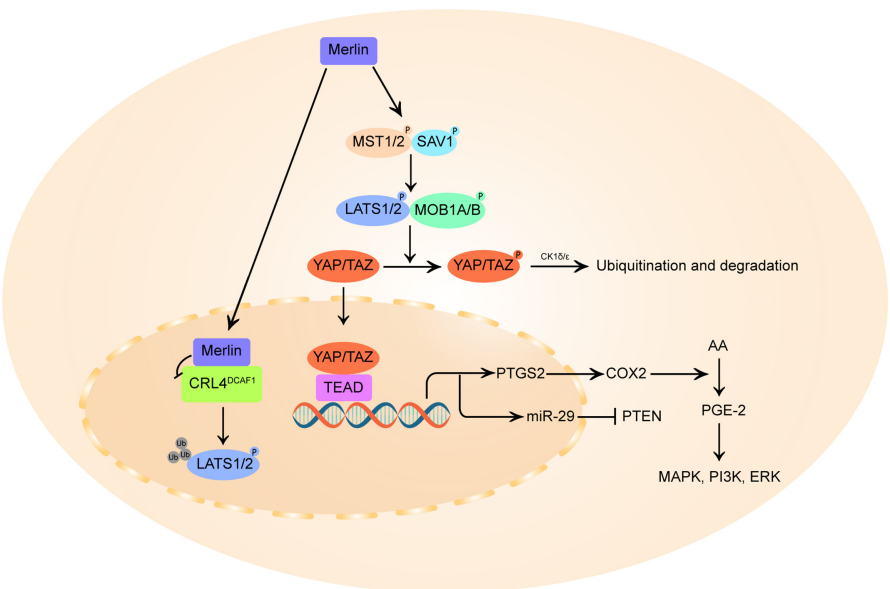

FIGURE 2 | Schematic diagram of merlin and Hippo pathway signaling. On the one hand, merlin initiates the Hippo pathway by directly activating mammalian STE20-like protein (MST1/2), which in turn phosphorylates large tumor suppressor homolog 1/2 (LATS1/2), or by recruiting LATS 1/2 to the plasma membrane for phosphorylation by MST1/2 kinases. The activated LATS1/2 directly phosphorylates Yes-associated protein (YAP) at Ser^{397} and transcriptional coactivator with PDZ-binding motif (TAZ) at Ser^{311}, priming the neighboring phosphodegron motif for phosphorylation by CK1δ/ϵ kinases and multi-level control of YAP/TAZ levels. In parallel, merlin also translocates to the nucleus and blocks the activity of the nuclear E3 ubiquitin ligase $CRL4^{DCAF1}$, which promotes the ubiquitylation of LATS1/2 to activate YAP. In merlin-deficient cells, YAP/TAZ accumulates in the nucleus and forms hybrid transcription factors with TEA domain (TEAD) family proteins to promote the transcription of pro-proliferative genes, including PTGS2 and miR-29. PTGS2 encodes cyclooxygenase-2 (COX-2) that catalyzes the conversion of arachidonic acid (AA) to prostaglandin E-2 (PGE-2), thus promoting PGE-2 mediated MAPK, ERK, PI3K pathway. By inducing miR-29, YAP can also inhibit the translation of phosphatase and tensin homolog (PTEN), a broadly downregulated tumor suppressor in vestibular schwannoma.

3.2.1 Nuclear Factor-Kappa B (NF-κB)

NF-κB is a ubiquitous, evolutionary conserved transcription factor central to cell growth, apoptosis, inflammation and various malignant diseases (103). As a group of homo- and hetero-dimeric proteins composed of members of the Rel family, NF-κB complexes includes p65/RelA, RelB, c-Rel, p50/p105 (NF-κB1), and p52/p100 (NF-κB2) five subunits (104), and resides in the cytoplasm of non-stimulating cells in the form of complexes with inhibitor of κB (IκB). The NF-κB signaling pathway is activated by inflammatory cytokines or growth factors, and induces gene transcription of these factors in a feedback-loop way (**Figure 3**) (105–107).

Studies have shown that merlin negatively regulates NF-κB signaling, and the elevated NF-κB signal was considered as the hub of the interaction network of aberrant expressed molecules in VS pathobiology (29, 30, 108). In the absence of merlin, overexpressed NIK and IKKα induced high NF-κB dependent transcription (29), while merlin expression blocks NF-κB activation by the inhibition of p65, NIK, IKKα, tumor necrosis factor-α (TNF-α)-induced IκB degradation, NF-κB–DNA binding and endogenous NF-κB signaling (30). Besides, activated NF-κB is thought to be the mechanism by which elevated $p75^{NTR}$ expression promotes cell survival in VS (109). Hyper NF-κB activity in VS potentiated hepatocyte growth factor (HGF) to c-Met autocrine feed-forward loop to promote tumor cell proliferation (108), and increased the expression of factors that reported to be increased in VS or correlated with the prognosis or absolute tumor growth rate of VS, such as matrix metalloproteinase 2 (MMP-2), MMP-9 (40), MMP-14 (41), COX-2 (110), interleukin-1 (IL-1), IL-6, TNF-α (64) and signal transducers and activators of transcription 1 (STAT1) (111).

3.2.2 Cyclooxygenase-2 (COX-2)

COX-2 is an isozyme of the COX family, catalyzes the conversion of arachidonic acid to prostaglandins, including the biosynthesis of prostaglandin E-2 (PGE-2). In a healthy state, COX-2 is involved in maintaining cell homeostasis, while its response to homeostatic dysregulation might lead to the development of cancer (112). Studies have demonstrated that COX-2 is upregulated in various solid tumors and involved in cancer inflammation (113). COX-2 is released to the cancer microenvironment by type II macrophages, cancer–associated fibroblasts and tumor cells, and can suppress tumor cell apoptosis, enhance cell adhesion to promote tumor-induced angiogenesis and achieve an aggressive phenotype (114, 115).

COX-2 presented at high levels in majority (96.67%) of VS tissue samples, and those VSs with higher COX-2 expression showed higher proliferation rate (31). Transcription of COX-2 is thought to be promoted by NF-κB. Aspirin modifies both NF-κB signaling and COX-2 expression (116), and has been shown to

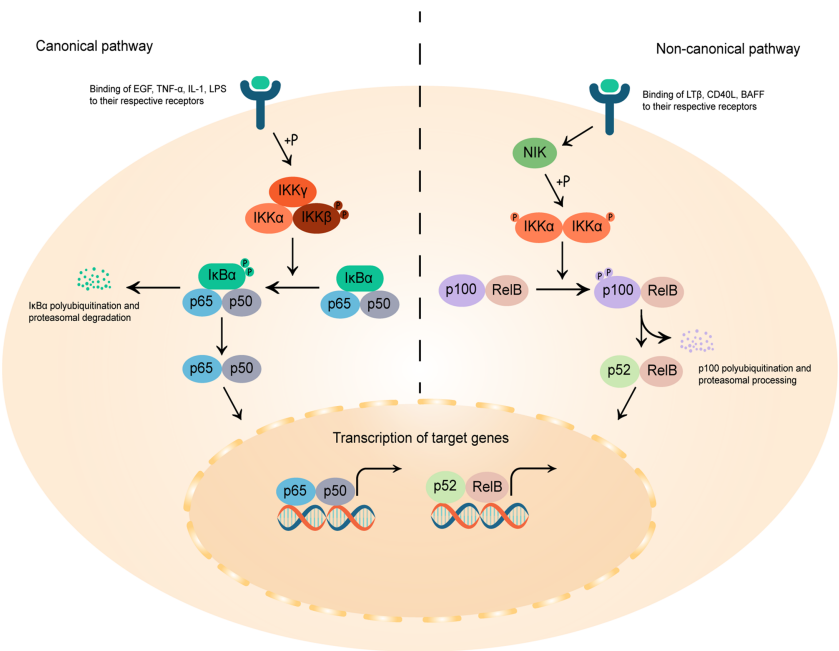

FIGURE 3 | Schematic diagram of the canonical and non-canonical NF-κB signaling pathway. In the canonical pathway, on the left, the binding of epidermal growth factor (EGF), tumor necrosis factor-α (TNF-α), interleukin-1 (IL-1) and lipopolysaccharides (LPS) to their respective receptors lead to the phosphorylation of inhibitor of κB (IκB)-kinase β (IKKβ) in the IKK complex, which in turn phosphorylates IκBα, culminating in its polyubiquitination and proteasomal degradation. The free NF-κB homo- or heterodimers, in this case p65/p50, then translocate into the nucleus to bind to κB motif and promote target gene transcription. The non-canonical pathway, on the right, is activated by the binding of lymphtoxin β (LTβ), CD40 ligand (CD40L), and B-cell activating factor (BAFF) to their respective receptors, causing IKKα dimers phosphorylation by the NF-κB-inducing kinase (NIK). Phosphorylation of p100 by activated IKKα initiates proteasomal processing of p100 N-terminal to form p52. The p52/RelB heterodimers can then undergoes nuclear translocation and modulates the gene transcription of pro-inflammatory cytokines in a feedback-loop way.

have therapeutic effects in several tumors with high COX-2 levels (117, 118). Although some studies have shown that aspirin may halt VS growth (119, 120), the latest meta-analysis disproved this viewpoint (121).

3.2.3 Macrophages

Tumor associated macrophages (TAMs) can be broadly classified into two categories, both of which are differentiated from monocytes in response to stimulus signals (122). The first type is M1-type inflammatory macrophages, also known as classically activated macrophages. M1-type macrophages are critically important in host defense and killing of tumor cells by the production of pro-inflammatory cytokines such as interferon-γ (IFN-γ), TNF-α and IL-18, which have potent microbiome-killing properties and hence are considered as 'good' macrophages (123). In order to avoid collateral damage to healthy cells/tissues by M1-type macrophages, M2-type macrophages, or alternatively activated macrophages, usually presented at the later stage of inflammatory response to suppressing destructive immunity, promoting wound repair and fibrosis. The effects of M2-type macrophages are manifested in the tumor microenvironment as inhibiting anti-tumor immunity, promoting tumor matrix remodeling and inducing angiogenesis (123). Collective data have shown that the high densities of M2-type macrophages in the tumor microenvironment are associated with the secretion of VEGF and MMP-9 (124), and worse prognosis in numerous cancer types (125, 126).

In a previous study, it was demonstrated that macrophages, rather than tumor cells, accounted for the majority of proliferating cells in the growing sporadic VS (32). Using Iba-1 as a pan-macrophage marker, the study of 24 sporadic VSs and 20 NF2-related VSs showed that the microvessel surface area was positively correlated with TAM density, and that Iba-1+ macrophages contributed significantly to VEGF production (127). This supports the idea that targeting macrophages along with vascular supply should be viewed as promising therapeutic options in both VS groups.

de Vries et al. determined the role of M2-type macrophages in promoting angiogenesis and volumetric tumor growth in sporadic VS tissue sections. They compared the expression of CD163, a specific marker for M2-type macrophages, in 10 rapidly growing VSs and 10 slow-growing VSs, and found that CD163 expression was significantly higher in fast-growing VS, and tumors with higher CD163 expression had more microvessels (as assessed by CD31). Consistent with these findings, the levels of macrophage colony-stimulating factor (M-CSF), an important cytokine that stimulates macrophage polarization into an M2-type macrophage, and its synergistic cytokine interleukin-34 (IL-34), are increased in fast-growing VS, suggesting their potential function as promoters of tumor progression (33). Recently, Bi et al. demonstrated variable expression of immune regulatory markers as well as immune infiltrates in VS (128). They found both tumor volume and volumetric growth were positively correlated with CD163 expression, and the relationship between PD-L1 and growth strengthened with increasing CD163 infiltration, suggesting a prominent role of immunotherapy in VS treatment (128).

3.2.4 Neutrophil-to-Lymphocyte Ratio (NLR)

As a representative index of systemic inflammation, preoperative peripheral blood NLR is related to the pathological characteristics of many tumors (129).The pretreatment NLR is calculated according to the absolute neutrophil count (ANC) and the absolute lymphocyte count (ALC) of routine blood tests obtained prior to any intervention. A high NLR indicated greater systemic inflammation and elevated circulating concentrations of pro-inflammatory and angiogenic cytokines, which can enhance tumor progression, immunosuppression and peritumoral stroma formation, and therefore is considered as a promising negative prognostic biomarker in solid tumors (130).

The utility of NLR has been pointed for predicting oncological growth in patients with VS. Kontorinis et al. found a significant difference of NLR between 79 growing VSs and 82 non-growing VSs, with high NLR was observed predominantly in the growing VS group (34). However, there is no such discrepancy between regressing VS and growing VS (131). A probable speculation is that NLR-associated inflammation functions not only in the pathomechanism of tumor growth, but also in the decrease of tumor size. Currently, the critical limitation needs to be obviated for NLR's clinical application and further investigation is that there is no consensus on the cutoff value of NLR (34).

3.3 miRNAs

miRNAs are small non-coding RNAs that responsible for the post-transcriptional regulation of genes by partially or perfectly complementary to the target mRNAs, leading to protein synthesis abortion or transcription inhibition (132). miRNAs play an important role in tumor initiation and development, and are potential targets for therapeutic interventions in diverse cancers.

Several differentially expressed miRNAs have been identified in VS tissues (133, 134). Using principal component analysis, affected gene ontology analysis, and analysis of miRNA expression fold changes, Sass et al. determined the relationship between rapid tumor growth and upregulation of miR-29abc, miR-19, miR-340-5p, miR-21, miR-221 and downregulation of miR-744 and let-7b (35). miR-29 fulfills controversial function in tumor progression and invasion in different tumors (135–137), and was reported to be upregulated in previous VS studies (134). Concordant with this research, Cioffi et al. demonstrated that miR-21 was over-expressed in VS compared with normal vestibular nerve tissue (36). Yang et al. found that downregulation of miR-21 by ailanthone reduced the proliferative potential of VS cells and induced apoptosis and autophagy (89). Other deregulated miRNAs also serve as modulators of tumor-related signaling pathways, such as miR-340 in Ras/Raf/MAPK (138) and let-7b in SOCS1/STAT (139). Notably, the contributions of miR-19, miR-21 and miR-221 to tumor growth are all related to their down-regulation of tumor suppressor PTEN (36, 136, 140), suggesting the role of PTEN and

its downstream PI3K/Akt/mTOR signaling pathway in VS cancerigenic process.

3.4 Proteins in Tumor Tissue

CD105, better known as endoglin, is a homodimeric transmembrane glycoprotein that highly expressed on activated angiogenic endothelial cells (141). Used as a marker of MVD, CD105 has proven itself as a potent prognostic indicator and a potential target for antiangiogenic therapy and chimeric antigen receptor-based T-cell (CAR-T) immunotherapy in several tumors (142–144). Calculated by immunohistochemically assessed CD105 expression, Gino et al. correlated the vessel cross-sectional area (VA) and vessel density (VD) with tumor dimensions and tumor growth rate in both NF2-associated VS and sporadic VS, and found a positive correlation between VD and tumor growth rate in NF2-VS, and VA and VD with tumor size in sporadic VS (37). Considering the great achievements of anti-angiogenesis therapy in VS and the specificity of CD105 to indicate the vascular front where sprouting takes place, it seems reasonable to use circulating CD105 to monitor tumor growth and to treat VS with anti-endoglin antibodies.

With several over-expressed neurotrophic factors in VS drawn attention as putative key mediators of tumor growth, Kramer et al. explored the relationship between gene expression profiles of neurotrophic factors and proliferation-associated Ki-67 labelling index, and observed significantly elevated brain derived neurotrophic factor (BDNF) expression that correlated with mitotic activity in VS (38).BDNF plays a pivotal role in myelination processing and supports the survival and synaptic integrity of the auditory nerve (145). This mitosis-promoting neurotrophic factor, together with the previously mentioned bFGF, which has the dual effects of hearing protection and growth stimulation of VS cells (16, 75), may partially explain the seemingly paradoxical phenomenon that VS patients with tumor growth do not necessarily experience hearing loss.

MMPs comprise a large family of zinc- and calcium-dependent proteolytic enzymes. Apart from their essential role in promoting cell differentiation and the reconstruction of the extracellular matrix in a regenerative milieu, MMPs play a fundamental role in tumor progression, invasion, and angiogenesis (146). Expression characteristics of several MMPs family members in VS have been explored. MMP-2 and its endogenous inhibitors tissue inhibitors of metalloproteinase (TIMP)-1 were found interstitially in sporadic solid VS, while the majority of MMP-9 was localized in tumor cells, and its concentration in tumor sample homogenates was positively correlated with the absolute tumor growth rate (40). Consistent with previous studies showing that the proteolytic activity of MMPs might degrade collagen, fibronectin, laminin and contribute to cyst formation and expansion, the expression of MMP-2 and MMP-9 were upregulated in cystic VS samples compared with solid VS (147). In cystic VS tissues, MMP-2 was localized to tumor cells on the cyst cavity inner surface and its levels were higher in the cystic fluid than in other samples (148).

Histologically, VS can be classified into two tissue types, where Antoni type A has a compact structure with interwoven bundles of long bipolar spindle cells and Antoni type B characterized by a loose texture and small, uniform satellite cells. It is known that cystic VS consist of a large mass of Antoni type B area, where the expression of MMP-14 was significantly higher than that in Antoni type A (39). The abundance and proteolytic activity of MMP-14 in VS patients was correlated with the degree of SNHL and surgical outcomes (41). Besides, MMP-2, MMP-9 and MMP-14 are all principal proteins of the MMPs family in the vasculature, implying degeneration of tumor tissues by MMPs and the accompanying increased tumor vessel permeability and adhesion to the facial nerve are critical in VS tumorigenesis, cyst formation and preoperative hearing impairment.

As a membrane-anchored protein of the A-Disintegrin and Metalloproteinase (ADAM) protein family, the overexpression of ADAM9 in solid tumors has been correlated with aggressive tumor phenotypes and unfavorable clinical prognosis (149). ADAM9 may implicated in tumor progression and invasion either *via* non-proteolytic mechanisms that include interactions between tumor cells and endothelial or peritumoral stromal cells (150), or proteolytic mechanisms that involve an enzymatic modification called "shedding" or processing of cell-surface proteins (151). The value of ADAM9 inhibition in reducing migration and invasion of different solid tumors has been established (152, 153). The earliest expression assessment of ADAM9 in VS by Breun et al. found an 8.8-fold higher ADAM9 mRNA level in VS compared with in healthy peripheral nerves, and a strong correlation between ADAM9 mRNA expression and the degree of functional impairment (42). Further, in VS primary cell cultures, ADAM9 knock down caused a 58% reduction in cell numbers, which might be a hint that ADAM9 plays a role in inducing VS progression (43).

3.5 Components in Cerebrospinal Fluid

VSs usually originate from Schwann cells of the cisternal portion of nerve rootlets exposed to CSF and may alter CSF composition by secreting proteins or altering CSF metabolism (154). CSF-based liquid biopsy approaches have been used to characterize protein expression during the pathogenesis of several brain tumors (155, 156), and differential components analyses of CSF are also expected to yielded diagnostic and therapeutic targets in VS.

Two studies have been done on CSF composition to identify biomarkers that predict VS growth. Ariyannur et al. found the levels of hyaluronan (HA) were 17-fold higher in NF2-related VS cases compared to the controls, and the rate of HA synthesis and secretion by primary schwannoma cells was commensurate with their proliferation rate (44). HA is a cell-surrounding mucopolysaccharide that binds to the Schwann cell surface CD44 receptor to trigger an uninterrupted cell proliferation cascade. Deranged HA-CD44 interaction has been identified as one of the central causative factors for schwannoma and a tumor suppressor target of merlin (157). Schwannoma cells increase their self-reproductive potential by secreting HA under the innate condition, suggesting that elevated HA in the CSF of patients with NF2-VS may be used as an indicator of tumor growth.

By characterizing the CSF proteome among VS patients with different grades, Huang et al. found that ATP-binding cassette subfamily A member 3 (ABCA3), secretogranin-1 (SCG1),

Krueppel-like factor 11 (KLF11), voltage-dependent calcium channel subunit alpha-2/delta-1 (CA2D1), brain acid soluble protein 1 (BASP1), and peroxiredoxin-2 (PRDX2) in CSF were associated with VS growth (45). It is notable that some of them did not simply increase or decrease as the tumor grows, but reached their maximum or minimum values at certain phases, suggesting that volumetric growth of VS may be driven by different signaling pathways at different tumor stages.

4 DISCUSSION

VS is a benign but potentially devastating tumor whose aggressively growth can be associated with significant morbidity including deafness and facial neuropathy. Usually, treatment of VS relies on surgery, radiation and regular follow-up. Better knowledge of the pathogenesis of VS has led to several targeted therapies with the effect of reducing tumor volume or restoring patients' hearing, of which bevacizumab has achieved the most promising results (68).

The majority of VSs may not enlarge after initial diagnosis, with an average annual growth rate of 1.11 mm (9). In order to preserve hearing function and enhance the quality of life, a substantial proportion of newly diagnosed patients will choose wait-and-scan policy, who were put at the risk of sudden tumor growth due to extremely variable growth patterns of VS. Hence, it would be helpful to identify predictive factors for VS growth at time of diagnosis. Several epidemiological, clinical, and radiological characteristics were thought to be related to the increased risk of subsequent tumor growth, such as patients' age, tumor location, hearing loss, and grow at first follow-up (9, 12–14). But there were some inconsistencies among reports of predicting growth-related factors (9), making the accuracy of this approach debatable.

From the perspective of VS growth mechanisms, numerous achievements had been obtained in exploring the relationship between tumor growth and biomarkers. The exact mechanism of VS onset and progression has remained elusive, with only a broad association with genetic and epigenetic aberrations of merlin, inflammation factors, proteolytic enzymes and nutrient supply pathways. Notably, there are mutual interactions between abnormally expressed molecules in VS biology. Merlin, whose conformational changes are regulated by RTKs and integrin signals, is also an inhibitor of the pro-inflammatory transcription factor NF-κB (30). On the other hand, high numbers of tumor infiltrating leukocytes in VS tissues can enhance cell survival, promote tumor growth and degenerative changes through the production of growth factors, cytokines, and MMPs (33, 128, 158). These evidences indicate that the progression of VS appears to be the result of interactions of these dysregulated pathways, drugs that target multiple signaling pathways simultaneously merit further investigation.

Despite the many recent advances in the identification of growth-related biomarkers, their translational researches have encountered several problems. First, current available VS animal models have some limitations. The commonly utilized animal models for the study of VS including patient-derived xenograft mice model (159), merlin-deficient Schwann cell or SC4 cells mouse model (160, 161). Nevertheless, merlin-deficient Schwann cells may not accurately reproduce VS (162), and it takes more than 2 weeks for the construction of mouse model. Recently proposed zebrafish xenograft model with shorter period of model establishment (163), as well as the application of 3D *in vitro* cell culture system (164) and *ex vivo* organ cultures (165) that fully mirror the growth patterns of VS, promise to further elucidate the role of these biomolecules in the pathogenesis of VS. Second, clinical validation of these hypotheses should take tumor diameter and clinical course into consideration. Current studies demonstrate non-linear changes of protein expression as VS size increases (45), suggesting that tumor progression at different grades might be stimulated by different signaling pathways and can therefore be predicted by different biomarkers. Along similar lines, different stages of the natural course of VS might be driven by different mechanisms either. During the enlarge of VS, accelerated growth, regression, or quiescence of the tumor can occur at any stage (2). Classifying patients according to the growth characteristics of VS and analyzing biomarker levels in different groups would shed light on which pathway induces VS initiation and which involves in VS shrinkage or growth cessation. Third, research is urgently needed to address how to obtain tissue expression data in a non-traumatic way. MRI texture analysis have been previously associated with VEGF expression in head and neck squamous cell carcinoma (166), and might also reflected VEGF levels in VS. A more precise non-invasive *in vivo* marker expression evaluation technique is targeted molecular imaging [MRI, computed tomography (CT), positron emission computed tomography/single-photon emission computed tomography (PET/SPECT) and fluorescence] (161, 167–169). Recently, Morrison et al. injected the covalently linked compounds formed by anti-VEGFR2 or anti-Her2/Neu monoclonal antibodies and near-infrared probe into Schwann cell xenograft models in mice, and observed strong correlations between day 1 tumor fluorescence and eventual maximum tumor volume (170). Apart from advanced imaging techniques, the circulating biomarkers level could also serve as convenient and reliable indicators for the prediction of subsequent tumor growth (37, 44).

We highlight some of the known and novel indicators with potential to predict VS growth enlightened therapeutic targets of VS and are critical for clinicians in stratifying patient's risk preoperatively, formulating individualized therapeutic tactics, and guiding clinical trial enrollment.

AUTHOR CONTRIBUTIONS

YZ and JL wrote the first draft of the paper. JR and XH revised the draft. PZ and BW provided approval for publication of this review. All authors contributed to the article and approved the submitted version.

FUNDING

This study was sponsored by Shanghai Science and Technology Committee Youth Sailing Program (19YF1405700), Clinical

Research Plan of Shenkang Hospital Development Center (SHDC2020CR1049B), Chinese Academy of Medical Sciences Innovation Fund for Medical Sciences (2019-I2M-5-008), National Natural Science Foundation of China (NSFC81872938, 82003864).

ACKNOWLEDGMENTS

The authors wish to acknowledge all staff of the Pharmacy Department and Neurosurgery Department of Huashan Hospital West Campus.

REFERENCES

1. Jia H, Lahlou G, Wu H, Sterkers O, Kalamarides M. Management of Neurofibromatosis Type 2 Associated Vestibular Schwannomas. *Curr Otorhinolaryngol Rep* (2021) 9(2):170–6. doi: 10.1007/s40136-021-00341-x
2. Tan D, Killeen DE, Kutz JW. The Natural History of Vestibular Schwannoma and When to Intervene. *Curr Otorhinolaryngol Rep* (2021) 9(2):134–8. doi: 10.1007/s40136-021-00337-7
3. Huang X, Xu J, Xu M, Zhou L-F, Zhang R, Lang L, et al. Clinical Features of Intracranial Vestibular Schwannomas. *Oncol Lett* (2013) 5(1):57–62. doi: 10.3892/ol.2012.1011
4. Halliday J, Rutherford SA, McCabe MG, Evans DG. An Update on the Diagnosis and Treatment of Vestibular Schwannoma. *Expert Rev Neurother* (2018) 18(1):29–39. doi: 10.1080/14737175.2018.1399795
5. Pandrangi VC, Han AY, Alonso JE, Peng KA, St John MA. An Update on Epidemiology and Management Trends of Vestibular Schwannomas. *Otol Neurotol* (2020) 41(3):411–7. doi: 10.1097/mao.0000000000002542
6. Pritchard C, Clapham L, Davis A, Lang DA, Neil-Dwyer G. Psycho-Socio-Economic Outcomes in Acoustic Neuroma Patients and Their Carers Related to Tumour Size. *Clin Otolaryngol* (2004) 29(4):324–30. doi: 10.1111/j.1365-2273.2004.00822.x
7. Hasegawa T, Kida Y, Kato T, Iizuka H, Kuramitsu S, Yamamoto T. Long-Term Safety and Efficacy of Stereotactic Radiosurgery for Vestibular Schwannomas: Evaluation of 440 Patients More Than 10 Years After Treatment With Gamma Knife Surgery Clinical Article. *J Neurosurg* (2013) 118(3):557–65. doi: 10.3171/2012.10.Jns12523
8. Suryanarayanan R, Ramsden RT, Saeed SR, Aggarwal R, King AT, Rutherford SA, et al. Vestibular Schwannoma: Role of Conservative Management. *J Laryngol Otol* (2010) 124(3):251–7. doi: 10.1017/s0022215109992362
9. Paldor I, Chen AS, Kaye AH. Growth Rate of Vestibular Schwannoma. *J Clin Neurosci* (2016) 32:1–8. doi: 10.1016/j.jocn.2016.05.003
10. Martin TPC, Tzifa K, Kowalski C, Holder RL, Walsh R, Irving RM. Conservative *Versus* Primary Surgical Treatment of Acoustic Neuromas: A Comparison of Rates of Facial Nerve and Hearing Preservation. *Clin Otolaryngol* (2008) 33(3):228–35. doi: 10.1111/j.1749-4486.2008.01715.x
11. Goshtasbi K, Abouzari M, Moshtaghi O, Sahyouni R, Sajjadi A, Lin HW, et al. The Changing Landscape of Vestibular Schwannoma Diagnosis and Management: A Cross-Sectional Study. *Laryngoscope* (2020) 130(2):482–6. doi: 10.1002/lary.27950
12. Kim JS, Cho Y-S. Growth of Vestibular Schwannoma: Long-Term Follow-Up Study Using Survival Analysis. *Acta Neurochir* (2021)163(8):2237–45. doi: 10.1007/s00701-021-04870-8. in press.
13. Roehm PC, Gantz BJ. Management of Acoustic Neuromas in Patients 65 Years or Older. *Otol Neurotol* (2007) 28(5):708–14. doi: 10.1097/01.mao.0000281805.44197.ec
14. Lee JD, Park MK, Kim JS, Cho Y-S. The Factors Associated With Tumor Stability Observed With Conservative Management of Intracanalicular Vestibular Schwannoma. *Otol Neurotol* (2014) 35(5):918–21. doi: 10.1097/mao.0000000000000338
15. Higuchi Y, Ikegami S, Horiguchi K, Aoyagi K, Nagano O, Serizawa T, et al. Predicting Potential of Rapid Tumor Growth in Small to Medium Vestibular Schwannomas on the Basis of Sway Assessed Using Posturography. *World Neurosurg* (2021) 148:E406–14. doi: 10.1016/j.wneu.2020.12.175
16. Koutsimpelas D, Stripf T, Heinrich UR, Mann WJ, Brieger J. Expression of Vascular Endothelial Growth Factor and Basic Fibroblast Growth Factor in Sporadic Vestibular Schwannornas Correlates to Growth Characteristics. *Otol Neurotol* (2007) 28(8):1094–9. doi: 10.1097/MAO.0b013e31814b2787
17. Sabha N, Au K, Agnihotri S, Singh S, Mangat R, Guha A, et al. Investigation of the In Vitro Therapeutic Efficacy of Nilotinib in Immortalized Human NF2-Null Vestibular Schwannoma Cells. *PloS One* (2012) 7(6):10. doi: 10.1371/journal.pone.0039412
18. Mukherjee J, Kamnasaran D, Balasubramaniam A, Radovanovic I, Zadeh G, Kiehl TR, et al. Human Schwannomas Express Activated Platelet-Derived Growth Factor Receptors and C-Kit and Are Growth Inhibited by Gleevec (Imatinib Mesylate). *Cancer Res* (2009) 69(12):5099–107. doi: 10.1158/0008-5472.can-08-4475
19. Blair KJ, Kiang A, Wang-Rodriguez J, Yu MA, Doherty JK, Ongkeko WM. EGF and bFGF Promote Invasion That Is Modulated by PI3/Akt Kinase and Erk in Vestibular Schwannoma. *Otol Neurotol* (2011) 32(2):308–14. doi: 10.1097/MAO.0b013e318206fc3d
20. Doherty JK, Ongkeko W, Crawley B, Andalibi A, Ryan AF. ErbB and Nrg: Potential Molecular Targets for Vestibular Schwannoma Pharmacotherapy. *Otol Neurotol* (2008) 29(1):50–7. doi: 10.1097/mao.0b013e31815d4429
21. Lim JY, Kim H, Jeun SS, Kang SG, Lee KJ. Merlin Inhibits Growth Hormone-Regulated Raf-ERKs Pathways by Binding to Grb2 Protein. *Biochem Biophys Res Commun* (2006) 340(4):1151–7. doi: 10.1016/j.bbrc.2005.12.122
22. Kissil JL, Wilker EW, Johnson KC, Eckman MS, Yaffe MB, Jacks T. Merlin, the Product of the Nf2 Tumor Suppressor Gene, the P21-Activated Is an Inhibitor of Kinase, Pak1. *Mol Cell* (2003) 12(4):841–9. doi: 10.1016/s1097-2765(03)00382-4
23. Yi C, Troutman S, Fera D, Stemmer-Rachamimov A, Avila JL, Christian N, et al. A Tight Junction-Associated Merlin-Angiomotin Complex Mediates Merlin's Regulation of Mitogenic Signaling and Tumor Suppressive Functions. *Cancer Cell* (2011) 19(4):527–40. doi: 10.1016/j.ccr.2011.02.017
24. Jin HC, Sperka T, Herrlich P, Morrison H. Tumorigenic Transformation by CPI-17 Through Inhibition of a Merlin Phosphatase. *Nature* (2006) 442 (7102):576–9. doi: 10.1038/nature04856
25. Hagel C, Dornblut C, Schulz A, Wiehl U, Friedrich RE, Huckhagel T, et al. The Putative Oncogene CPI-17 Is Up-Regulated in Schwannoma. *Neuropathol Appl Neurobiol* (2016) 42(7):664–8. doi: 10.1111/nan.12330
26. Xu JH, Zhang Y, Shi YX, Yin DM, Dai PD, Zhao WD, et al. CPI-17 Overexpression and Its Correlation With the NF2 Mutation Spectrum in Sporadic Vestibular Schwannomas. *Otol Neurotol* (2020) 41(1):E94–102. doi: 10.1097/ma0.0000000000002430
27. Zhao F, Yang ZJ, Chen Y, Zhou QY, Zhang J, Liu J, et al. Deregulation of the Hippo Pathway Promotes Tumor Cell Proliferation Through YAP Activity in Human Sporadic Vestibular Schwannoma. *World Neurosurg* (2018) 117: E269–79. doi: 10.1016/j.wneu.2018.06.010
28. Li W, Giancotti FG. Merlin's Tumor Suppression Linked to Inhibition of the E3 Ubiquitin Ligase CRL4 (Dcaf1). *Cell Cycle (Georgetown Tex)* (2010) 9 (22):4433–6. doi: 10.4161/cc.9.22.13838
29. Dilwali S, Briet MC, Kao SY, Fujita T, Landegger LD, Platt MP, et al. Preclinical Validation of Anti-Nuclear Factor-Kappa B Therapy to Inhibit Human Vestibular Schwannoma Growth. *Mol Oncol* (2015) 9(7):1359–70. doi: 10.1016/j.molonc.2015.03.009
30. Kim JY, Kim H, Jeun SS, Rha SJ, Kim YH, Ko YJ, et al. Inhibition of NF-Kappa B Activation by Merlin. *Biochem Biophys Res Commun* (2002) 296 (5):1295–302. doi: 10.1016/s0006-291x(02)02077-6
31. Hong B, Krusche CA, Schwabe K, Friedrich S, Klein R, Krauss JK, et al. Cyclooxygenase-2 Supports Tumor Proliferation in Vestibular Schwannomas. *Neurosurgery* (2011) 68(4):1112–7. doi: 10.1227/NEU.0b013e318208f5c7
32. Lewis D, Roncaroli F, Agushi E, Mosses D, Williams R, Li KL, et al. Inflammation and Vascular Permeability Correlate With Growth in Sporadic Vestibular Schwannoma. *Neuro Oncol* (2019) 21(3):314–25. doi: 10.1093/neuonc/noy177
33. de Vries WM, Briaire-de Bruijn IH, van Benthem PPG, van der Mey AGL, Hogendoorn PCW. M-CSF and IL-34 Expression as Indicators for Growth in Sporadic Vestibular Schwannoma. *Virchows Arch* (2019) 474(3):375–81. doi: 10.1007/s00428-018-2503-1

34. Kontorinis G, Crowther JA, Iliodromiti S, Taylor WAS, Locke R. Neutrophil to Lymphocyte Ratio as a Predictive Marker of Vestibular Schwannoma Growth. *Otol Neurotol* (2016) 37(5):580–5. doi: 10.1097/mao.0000000000001026
35. Sass HCR, Hansen M, Borup R, Nielsen FC, Caye-Thomasen P. Tumor miRNA Expression Profile Is Related to Vestibular Schwannoma Growth Rate. *Acta Neurochir* (2020) 162(5):1187–95. doi: 10.1007/s00701-020-04238-4
36. Cioffi JA, Yue WY, Mendolia-Loffredo S, Hansen KR, Wackym PA, Hansen MR. MicroRNA-21 Overexpression Contributes to Vestibular Schwannoma Cell Proliferation and Survival. *Otol Neurotol* (2010) 31(9):1455–62. doi: 10.1097/MAO.0b013e3181f20655
37. Marioni G, Nicol L, Cazzador D, Pavone C, D'Avella D, Martini A, et al. Endoglin (CD105) Expression in Neurofibromatosis Type 2 Vestibular Schwannoma. *Head Neck J Sci Spec* (2019) 41(10):3612–7. doi: 10.1002/hed.25881
38. Kramer F, Stoever T, Warnecke A, Diensthuber M, Lenarz T, Wissel K. BDNF mRNA Expression Is Significantly Upregulated in Vestibular Schwannomas and Correlates With Proliferative Activity. *J Neurooncol* (2010) 98(1):31–9. doi: 10.1007/s11060-009-0063-6
39. Xia L, Yang S, Wang CD, Yu EX, Zhang HL, Zhang Y, et al. Immunohistochemical Profiles of Matrix Metalloproteinases and Vascular Endothelial Growth Factor Overexpression in the Antoni B Area of Vestibular Schwannomas. *World Neurosurg* (2020) 144:E72–9. doi: 10.1016/j.wneu.2020.07.208
40. Moller MN, Werther K, Nalla A, Stangerup SE, Thomsen J, Bog-Hansen TC, et al. Angiogenesis in Vestibular Schwannomas: Expression of Extracellular Matrix Factors MMP-2, MMP-9, and TIMP-1. *Laryngoscope* (2010) 120 (4):657–62. doi: 10.1002/lary.20834
41. Ren Y, Hyakusoku H, Sagers JE, Landegger LD, Welling DB, Stankovic KM. MMP-14 (MT1-MMP) Is a Biomarker of Surgical Outcome and a Potential Mediator of Hearing Loss in Patients With Vestibular Schwannomas. *Front Cell Neurosci* (2020) 14:191. doi: 10.3389/fncel.2020.00191
42. Breun M, Schwerdtfeger A, Martellotta DD, Kessler AF, Monoranu CM, Matthies C, et al. ADAM9: A Novel Player in Vestibular Schwannoma Pathogenesis. *Oncol Lett* (2020) 19(3):1856–64. doi: 10.3892/ol.2020.11299
43. Nattmann A, Breun M, Monoranu CM, Matthies C, Ernestus RI, Lohr M, et al. Analysis of ADAM9 Regulation and Function in Vestibular Schwannoma Primary Cells. *BMC Res Notes* (2020) 13(1):528. doi: 10.1186/s13104-020-05378-7
44. Ariyannur PS, Vikkath N, Pillai AB. Cerebrospinal Fluid Hyaluronan and Neurofibromatosis Type 2. *Cancer Microenviron* (2018) 11(2-3):125–33. doi: 10.1007/s12307-018-0216-2
45. Huang X, Xu J, Shen YW, Zhang L, Xu M, Chen MY, et al. Protein Profiling of Cerebrospinal Fluid From Patients Undergoing Vestibular Schwannoma Surgery and Clinical Significance. *BioMed Pharmacother* (2019) 116:108985. doi: 10.1016/j.biopha.2019.108985
46. Asthagiri AR, Parry DM, Butman JA, Kim HJ, Tsilou ET, Zhuang Z, et al. Neurofibromatosis Type 2. *Lancet* (2009) 373(9679):1974–86. doi: 10.1016/s0140-6736(09)60259-2
47. Lee JD, Kwon TJ, Kim UK, Lee WS. Genetic and Epigenetic Alterations of the NF2 Gene in Sporadic Vestibular Schwannomas. *PloS One* (2012) 7(1):5. doi: 10.1371/journal.pone.0030418
48. Bretscher A, Edwards K, Fehon RG. ERM Proteins and Merlin: Integrators at the Cell Cortex. *Nat Rev Mol Cell Biol* (2002) 3(8):586–99. doi: 10.1038/nrm882
49. Zoch A, Mayerl S, Schulz A, Greither T, Frappart L, Rubsam J, et al. Merlin Isoforms 1 and 2 Both Act as Tumour Suppressors and Are Required for Optimal Sperm Maturation. *PloS One* (2015) 10(8):25. doi: 10.1371/journal.pone.0129151
50. Maccollin M, Ramesh V, Jacoby LB, Louis DN, Rubio MP, Pulaski K, et al. Mutational Analysis of Patients With Neurofibromatosis-2. *Am J Hum Genet* (1994) 55(2):314–20.
51. Goutagny S, Raymond E, Esposito-Farese M, Trunet S, Mawrin C, Bernardeschi D, et al. Phase II Study of Mtorc1 Inhibition by Everolimus in Neurofibromatosis Type 2 Patients With Growing Vestibular Schwannomas. *J Neurooncol* (2015) 122(2):313–20. doi: 10.1007/s11060-014-1710-0
52. Petrilli AM, Fuse MA, Donnan MS, Bott M, Sparrow NA, Tondera D, et al. A Chemical Biology Approach Identified PI3K as a Potential Therapeutic Target for Neurofibromatosis Type 2. *Am J Transl Res* (2014) 6(5):471–93.
53. Kaempchen K, Mielke K, Utermark T, Langmesser S, Hanemann CO. Upregulation of the Rac1/JNK Signaling Pathway in Primary Human Schwannoma Cells. *Hum Mol Genet* (2003) 12(11):1211–21. doi: 10.1093/hmg/ddg146
54. Li W, Cooper J, Zhou L, Yang C, Erdjument-Bromage H, Zagzag D, et al. Merlin/NF2 Loss-Driven Tumorigenesis Linked to CRL4(DCAF1)-Mediated Inhibition of the Hippo Pathway Kinases Lats1 and 2 in the Nucleus. *Cancer Cell* (2014) 26(1):48–60. doi: 10.1016/j.ccr.2014.05.001
55. Mandati V, Del Maestro L, Dingli F, Lombard B, Loew D, Molinie N, et al. Phosphorylation of Merlin by Aurora A Kinase Appears Necessary for Mitotic Progression. *J Biol Chem* (2019) 294(35):12992–3005. doi: 10.1074/jbc.RA118.006937
56. McClatchey AI, Fehon RG. Merlin and the ERM Proteins - Regulators of Receptor Distribution and Signaling at the Cell Cortex. *Trends Cell Biol* (2009) 19(5):198–206. doi: 10.1016/j.tcb.2009.02.006
57. Lallemand D, Saint-Amaux AL, Giovannini M. Tumor-Suppression Functions of Merlin Are Independent of Its Role as an Organizer of the Actin Cytoskeleton in Schwann Cells. *J Cell Sci* (2009) 122(22):4141–9. doi: 10.1242/jcs.045914
58. Sher I, Hanemann CO, Karplus PA, Bretscher A. The Tumor Suppressor Merlin Controls Growth in Its Open State, and Phosphorylation Converts It to a Less-Active More-Closed State. *Dev Cell* (2012) 22(4):703–5. doi: 10.1016/j.devcel.2012.03.008
59. Xing WC, Li M, Zhang FY, Ma X, Long JF, Zhou H. The Conformation Change and Tumor Suppressor Role of Merlin Are Both Independent of Serine 518 Phosphorylation. *Biochem Biophys Res Commun* (2017) 493 (1):46–51. doi: 10.1016/j.bbrc.2017.09.077
60. Shaw RJ, Paez JG, Curto M, Yaktine A, Pruitt WM, Saotome I, et al. The Nf2 Tumor Suppressor, Merlin, Functions in Rac-Dependent Signaling. *Dev Cell* (2001) 1(1):63–72. doi: 10.1016/s1534-5807(01)00009-0
61. Ye KQ. Phosphorylation of Merlin Regulates Its Stability and Tumor Suppressive Activity. *Cell Adhes Migr* (2007) 1(4):196–8. doi: 10.4161/cam.1.4.5192
62. Wickremesekera A, Hovens CM, Kaye AH. Expression of ErbB-1 and 2 in Vestibular Schwannomas. *J Clin Neurosci* (2007) 14(12):1199–206. doi: 10.1016/j.jocn.2007.05.009
63. Altuna X, Lopez JP, Yu MA, Arandazi MJ, Harris JP, Wang-Rodriguez J, et al. Potential Role of Imatinib Mesylate (Gleevec, STI-571) in the Treatment of Vestibular Schwannoma. *Otol Neurotol* (2011) 32(1):163–70. doi: 10.1097/MAO.0b013e3182009665
64. Taurone S, Bianchi E, Attanasio G, Di Gioia C, Ierino R, Carubbi C, et al. Immunohistochemical Profile of Cytokines and Growth Factors Expressed in Vestibular Schwannoma and in Normal Vestibular Nerve Tissue. *Mol Med Rep* (2015) 12(1):737–45. doi: 10.3892/mmr.2015.3415
65. Ebrahem Q, Chaurasia SS, Vasanji A, Qi JH, Klenotic PA, Cutler A, et al. Cross-Talk Between Vascular Endothelial Growth Factor and Matrix Metalloproteinases in the Induction of Neovascularization *In Vivo*. *Am J Pathol* (2010) 176(1):496–503. doi: 10.2353/ajpath.2010.080642
66. Tamura R, Tanaka T, Akasaki Y, Murayama Y, Yoshida K, Sasaki H. The Role of Vascular Endothelial Growth Factor in the Hypoxic and Immunosuppressive Tumor Microenvironment: Perspectives for Therapeutic Implications. *Med Oncol (Northwood London England)* (2019) 37(1):2. doi: 10.1007/s12032-019-1329-2
67. Koutsimpelas D, Bjelopavlovic M, Yetis R, Frauenknecht K, Adryan B, Schmidtmann I, et al. The VEGF/VEGF-R Axis in Sporadic Vestibular Schwannomas Correlates With Irradiation and Disease Recurrence. *Orl J Otorhinolaryngol Head Neck Surg* (2012) 74(6):330–8. doi: 10.1159/000346238
68. Alanin MC, Klausen C, Caye-Thomasen P, Thomsen C, Fugleholm K, Poulsgaard L, et al. The Effect of Bevacizumab on Vestibular Schwannoma Tumour Size and Hearing in Patients With Neurofibromatosis Type 2. *Eur Arch Otorhinolaryngol* (2015) 272(12):3627–33. doi: 10.1007/s00405-014-3398-3
69. Gao X, Zhao YC, Stemmer-Rachamimov AO, Liu H, Huang PG, Chin SM, et al. Anti-VEGF Treatment Improves Neurological Function and Augments Radiation Response in NF2 Schwannoma Model. *Proc Natl Acad Sci USA* (2015) 112(47):14676–81. doi: 10.1073/pnas.1512570112
70. Yi D, Kuo SZ, Zheng H, Abhold EL, Brown CM, Doherty JK, et al. Activation of PDGFR and EGFR Promotes the Acquisition of a Stem Cell-Like

Phenotype in Schwannomas. *Otol Neurotol* (2012) 33(9):1640–7. doi: 10.1097/MAO.0b013e31826a540d
71. Fredriksson L, Li H, Eriksson U. The PDGF Family: Four Gene Products Form Five Dimeric Isoforms. *Cytokine Growth Factor Rev* (2004) 15(4):197–204. doi: 10.1016/j.cytogfr.2004.03.007
72. Yener U, Avsar T, Akgun E, Seker A, Bayri Y, Kilic T. Assessment of Antiangiogenic Effect of Imatinib Mesylate on Vestibular Schwannoma Tumors Using *In Vivo* Corneal Angiogenesis Assay Laboratory Investigation. *J Neurosurg* (2012) 117(4):697–704. doi: 10.3171/2012.6.Jns112263
73. Thomas KA, Gimenezgallego G. Fibroblast Growth-Factors - Broad-Spectrum Mitogens With Potent Angiogenic Activity. *Trends Biochem Sci* (1986) 11(2):81–4. doi: 10.1016/0968-0004(86)90271-9
74. Labanca E, Vazquez ES, Corn PG, Roberts JM, Wang F, Logothetis CJ, et al. Fibroblast Growth Factors Signaling in Bone Metastasis. *Endocr Relat Cancer* (2020) 27(7):R255–65. doi: 10.1530/erc-19-0472
75. Dilwali S, Lysaght A, Roberts D, Barker FG, McKenna MJ, Stankovic KM. Sporadic Vestibular Schwannomas Associated With Good Hearing Secrete Higher Levels of Fibroblast Growth Factor 2 Than Those Associated With Poor Hearing Irrespective of Tumor Size. *Otol Neurotol* (2013) 34(4):748–54. doi: 10.1097/MAO.0b013e31828048ec
76. Plotkin SR, Duda DG, Muzikansky A, Allen J, Blakeley J, Rosser T, et al. Multicenter, Prospective, Phase II and Biomarker Study of High-Dose Bevacizumab as Induction Therapy in Patients With Neurofibromatosis Type 2 and Progressive Vestibular Schwannoma. *J Clin Oncol* (2019) 37 (35):3446–54. doi: 10.1200/jco.19.01367
77. Weerda HG, Gamberger TI, Siegner A, Gjuric M, Tamm ER. Effects of Transforming Growth Factor- ß 1 and Basic Fibroblast Growth Factor on Proliferation of Cell Cultures Derived From Human Vestibular Nerve Schwannoma. *Acta Otolaryngol* (1998) 118(3):337–43. doi: 10.1080/00016489850183412
78. Ahmad ZK, Brown CM, Cueva RA, Ryan AF, Doherty JK. ErbB Expression, Activation, and Inhibition With Lapatinib and Tyrphostin (AG825) in Human Vestibular Schwannomas. *Otol Neurotol* (2011) 32(5):841–7. doi: 10.1097/MAO.0b013e31821f7d88
79. Bush ML, Burns SS, Oblinger J, Davletova S, Chang L-S, Welling DB, et al. Treatment of Vestibular Schwannoma Cells With ErbB Inhibitors. *Otol Neurotol* (2012) 33(2):244–57. doi: 10.1097/MAO.0b013e31823e287f
80. Clark JJ, Provenzano M, Diggelmann HR, Xu N, Hansen SS, Hansen MR. The ErbB Inhibitors Trastuzumab and Erlotinib Inhibit Growth of Vestibular Schwannoma Xenografts in Nude Mice: A Preliminary Study. *Otol Neurotol* (2008) 29(6):846–53. doi: 10.1097/MAO.0b013e31817f7398
81. Fuse MA, Dinh CT, Vitte J, Kirkpatrick J, Mindos T, Plati SK, et al. Preclinical Assessment of MEK1/2 Inhibitors for Neurofibromatosis Type 2-Associated Schwannomas Reveals Differences in Efficacy and Drug Resistance Development. *Neuro Oncol* (2019) 21(4):486–97. doi: 10.1093/neuonc/noz002
82. Zinatizadeh MR, Momeni SA, Zarandi PK, Chalbatani GM, Dana H, Mirzaei HR, et al. The Role and Function of Ras-Association Domain Family in Cancer: A Review. *Genes Dis* (2019) 6(4):378–84. doi: 10.1016/j.gendis.2019.07.008
83. Agnihotri S, Gugel I, Remke M, Bornemann A, Pantazis G, Mack SC, et al. Gene-Expression Profiling Elucidates Molecular Signaling Networks That Can Be Therapeutically Targeted in Vestibular Schwannoma. *J Neurosurg* (2014) 121(6):1434–45. doi: 10.3171/2014.6.jns131433
84. Slack-Davis JK, Eblen ST, Zecevic M, Boerner SA, Tarcsafalvi A, Diaz HB, et al. PAKI Phosphorylation of MEK1 Regulates Fibronectin-Stimulated MAPK Activation. *J Cell Biol* (2003) 162(2):281–91. doi: 10.1083/jcb.200212141
85. Li WQ, Chong HR, Guan KL. Function of the Rho Family GTPases in Ras-Stimulated Raf Activation. *J Biol Chem* (2001) 276(37):34728–37. doi: 10.1074/jbc.M103496200
86. Morrison H, Sperka T, Manent J, Giovannini M, Ponta H, Herrlich P. Merlin/neurofibromatosis Type 2 Suppresses Growth by Inhibiting the Activation of Ras and Rac. *Cancer Res* (2007) 67(2):520–7. doi: 10.1158/0008-5472.Can-06-1608
87. Flaiz C, Chernoff J, Ammoun S, Peterson JR, Hanemann CO. PAK Kinase Regulates Rac GTPase and Is a Potential Target in Human Schwannomas. *Exp Neurol* (2009) 218(1):137–44. doi: 10.1016/j.expneurol.2009.04.019
88. Mercado-Pimentel ME, Miller C, Rolph DN, Villalobos EF, Dunn AM, Mohan PM, et al. Inhibiting P21-Activated Kinase Induces Cell Death in Vestibular Schwannoma and Meningioma *via* Mitotic Catastrophe. *Otol Neurotol* (2017) 38(1):139–46. doi: 10.1097/mao.0000000000001247
89. Yang PZ, Sun DZ, Jiang F. Ailanthone Promotes Human Vestibular Schwannoma Cell Apoptosis and Autophagy by Downregulation of miR-21. *Oncol Res* (2018) 26(6):941–8. doi: 10.3727/096504018x15149775533331
90. Riecken LB, Zoch A, Wiehl U, Reichert S, Scholl I, Cui Y, et al. CPI-17 Drives Oncogenic Ras Signaling in Human Melanomas *via* Ezrin-Radixin-Moesin Family Proteins. *Oncotarget* (2016) 7(48):78242–54. doi: 10.18632/oncotarget.12919
91. Cui Y, Groth S, Troutman S, Carlstedt A, Sperka T, Riecken LB, et al. The NF2 Tumor Suppressor Merlin Interacts With Ras and RasGAP, Which may Modulate Ras Signaling. *Oncogene* (2019) 38(36):6370–81. doi: 10.1038/s41388-019-0883-6
92. Sperka T, Geissler KJ, Merkel U, Scholl I, Rubio I, Herrlich P, et al. Activation of Ras Requires the ERM-Dependent Link of Actin to the Plasma Membrane. *PloS One* (2011) 6(11):14. doi: 10.1371/journal.pone.0027511
93. Li Y, Zhou H, Li F, Chan SW, Lin Z, Wei Z, et al. Angiomotin Binding-Induced Activation of Merlin/NF2 in the Hippo Pathway. *Cell Res* (2015) 25 (7):801–17. doi: 10.1038/cr.2015.69
94. Reginensi A, Enderle L, Gregorieff A, Johnson RL, Wrana JL, McNeill H. A Critical Role for NF2 and the Hippo Pathway in Branching Morphogenesis. *Nat Commun* (2016) 7:12309. doi: 10.1038/ncomms12309
95. Boin A, Couvelard A, Couderc C, Brito I, Filipescu D, Kalamarides M, et al. Proteomic Screening Identifies a YAP-Driven Signaling Network Linked to Tumor Cell Proliferation in Human Schwannomas. *Neuro Oncol* (2014) 16 (9):1196–209. doi: 10.1093/neuonc/nou020
96. Cooper J, Xu Q, Zhou L, Pavlovic M, Ojeda V, Moulick K, et al. Combined Inhibition of NEDD8-Activating Enzyme and mTOR Suppresses NF2 Loss-Driven Tumorigenesis. *Mol Cancer Ther* (2017) 16(8):1693–704. doi: 10.1158/1535-7163.mct-16-0821
97. Jiang XJ, Wang J, Deng XY, Xiong F, Zhang SS, Gong ZJ, et al. The Role of Microenvironment in Tumor Angiogenesis. *J Exp Clin Cancer Res* (2020) 39 (1):19. doi: 10.1186/s13046-020-01709-5
98. Wei F, Wang D, Wei JY, Tang NW, Tang L, Xiong F, et al. Metabolic Crosstalk in the Tumor Microenvironment Regulates Antitumor Immunosuppression and Immunotherapy Resisitance. *Cell Mol Life Sci* (2021) 78(1):173–93. doi: 10.1007/s00018-020-03581-0
99. Lai S, Huang L, Luo S, Liu Z, Dong J, Wang L, et al. Systemic Inflammatory Indices Predict Tumor Response to Neoadjuvant Chemoradiotherapy for Locally Advanced Rectal Cancer. *Oncol Lett* (2020) 20(3):2763–70. doi: 10.3892/ol.2020.11812
100. Sawada R, Akiyoshi T, Kitagawa Y, Hiyoshi Y, Mukai T, Nagasaki T, et al. Systemic Inflammatory Markers Combined With Tumor-Infiltrating Lymphocyte Density for the Improved Prediction of Response to Neoadjuvant Chemoradiotherapy in Rectal Cancer. *Ann Surg Oncol* (2021). doi: 10.1245/s10434-021-09975-z. in press.
101. de Vries M, Hogendoorn PCW, Briaire-de Bruyn I, Malessy MJA, van der Mey AGL. Intratumoral Hemorrhage, Vessel Density, and the Inflammatory Reaction Contribute to Volume Increase of Sporadic Vestibular Schwannomas. *Virchows Arch* (2012) 460(6):629–36. doi: 10.1007/s00428-012-1236-9
102. Han JH, Baek KH, Lee YW, Hur YK, Kim HJ, Moon IS. Comparison of Clinical Characteristics and Surgical Outcomes of Cystic and Solid Vestibular Schwannomas. *Otol Neurotol* (2018) 39(5):E381–6. doi: 10.1097/mao.0000000000001813
103. Motolani A, Martin M, Sun MY, Lu T. Phosphorylation of the Regulators, a Complex Facet of NF-Kappa B Signaling in Cancer. *Biomolecules* (2021) 11 (1):13. doi: 10.3390/biom11010015
104. Pereira SG, Oakley F. Nuclear Factor-Kappa B1: Regulation and Function. *Int J Biochem Cell Biol* (2008) 40(8):1425–30. doi: 10.1016/j.biocel.2007.05.004
105. Karin M, Delhase M. The I Kappa B Kinase (IKK) and NF-Kappa B: Key Elements of Proinflammatory Signalling. *Semin Immunol* (2000) 12(1):85–98. doi: 10.1006/smim.2000.0210
106. Sun SC. The Noncanonical NF-Kappa B Pathway. *Immunol Rev* (2012) 246:125–40. doi: 10.1111/j.1600-065X.2011.01088.x
107. Hoesel B, Schmid JA. The Complexity of NF-κb Signaling in Inflammation and Cancer. *Mol Cancer* (2013) 12(1):86. doi: 10.1186/1476-4598-12-86

108. Gehlhausen JR, Hawley E, Wahle BM, He YZ, Edwards D, Rhodes SD, et al. A Proteasome-Resistant Fragment of NIK Mediates Oncogenic NF-Kappa B Signaling in Schwannomas. *Hum Mol Genet* (2019) 28(4):572–83. doi: 10.1093/hmg/ddy361
109. Ahmad I, Yue WY, Fernando A, Clark JJ, Woodson EA, Hansen MR. P75 (NTR) Is Highly Expressed in Vestibular Schwannomas and Promotes Cell Survival by Activating Nuclear Transcription Factor Kappa B. *Glia* (2014) 62 (10):1699–712. doi: 10.1002/glia.22709
110. Behling F, Ries V, Skardelly M, Gepfner-Tuma I, Schuhmann M, Ebner FH, et al. COX2 Expression Is Associated With Proliferation and Tumor Extension in Vestibular Schwannoma But Is Not Influenced by Acetylsalicylic Acid Intake. *Acta Neuropathol Commun* (2019) 7:105. doi: 10.1186/s40478-019-0760-0
111. Xu J, Zhang Y, Shi Y, Yin D, Dai P, Zhao W, et al. Identification of Predictive Proteins and Biological Pathways for the Tumorigenicity of Vestibular Schwannoma by Proteomic Profiling. *Proteomics Clin Appl* (2019) 13 (5):1800175. doi: 10.1002/prca.201800175
112. Gong ZX, Huang WG, Wang BY, Liang N, Long SK, Li WJ, et al. Interplay Between Cyclooxygenase-2 and microRNAs in Cancer. *Mol Med Rep* (2021) 23(5):1–10. doi: 10.3892/mmr.2021.11986
113. Davila-Gonzalez D, Chang JC, Billiar TR. NO and COX2: Dual Targeting for Aggressive Cancers. *Proc Natl Acad Sci USA* (2017) 114(52):13591–3. doi: 10.1073/pnas.1717440114
114. Goradel NH, Najafi M, Salehi E, Farhood B, Mortezaee K. Cyclooxygenase-2 in Cancer: A Review. *J Cell Physiol* (2019) 234(5):5683–99. doi: 10.1002/jcp.27411
115. Montezuma MAP, Fonseca FP, Benites BM, Soares CD, do Amaral-Silva GK, de Almeida OP, et al. COX-2 as a Determinant of Lower Disease-Free Survival for Patients Affected by Ameloblastoma. *Pathol Res Pract* (2018) 214 (6):907–13. doi: 10.1016/j.prp.2018.03.014
116. Ma J, Cai ZL, Wei HL, Liu XL, Zhao QL, Zhang T. The Anti-Tumor Effect of Aspirin: What We Know and What We Expect. *BioMed Pharmacother* (2017) 95:656–61. doi: 10.1016/j.biopha.2017.08.085
117. Wang P, Shen YP, Zhao L. Chitosan Nanoparticles Loaded With Aspirin and 5-Fluororacil Enable Synergistic Antitumour Activity Through the Modulation of NF-Kappa B/COX-2 Signalling Pathway. *IET Nanobiotechnol* (2020) 14(6):479–84. doi: 10.1049/iet-nbt.2020.0002
118. Jiang W, Yan Y, Chen MY, Luo GY, Hao JJ, Pan JJ, et al. Aspirin Enhances the Sensitivity of Colon Cancer Cells to Cisplatin by Abrogating the Binding of NF-Kappa B to the COX-2 Promoter. *Aging-US* (2020) 12(1):611–27. doi: 10.18632/aging.102644
119. Kandathil CK, Dilwali S, Wu CC, Ibrahimov M, McKenna MJ, Lee H, et al. Aspirin Intake Correlates With Halted Growth of Sporadic Vestibular Schwannoma *In Vivo*. *Otol Neurotol* (2014) 35(2):353–7. doi: 10.1097/mao.0000000000000189
120. Kandathil CK, Cunnane ME, McKenna MJ, Curtin HD, Stankovic KM. Correlation Between Aspirin Intake and Reduced Growth of Human Vestibular Schwannoma: Volumetric Analysis. *Otol Neurotol* (2016) 37 (9):1428–34. doi: 10.1097/mao.0000000000001180
121. Ignacio KHD, Espiritu AI, Diestro JDB, Chan KI, Dmytriw AA, Omar AT. Efficacy of Aspirin for Sporadic Vestibular Schwannoma: A Meta-Analysis. *Neurol Sci* (2021). doi: 10.1007/s10072-021-05193-3. in press.
122. Mehraj U, Qayoom H, Mir MA. Prognostic Significance and Targeting Tumor-Associated Macrophages in Cancer: New Insights and Future Perspectives. *Breast Cancer* (2021) 28(3):1–17. doi: 10.1007/s12282-021-01231-2
123. Huang YC, Feng ZP. The Good and Bad of Microglia/Macrophages: New Hope in Stroke Therapeutics. *Acta Pharmacol Sin* (2013) 34(1):6–7. doi: 10.1038/aps.2012.178
124. Rogers TL, Holen I. Tumour Macrophages as Potential Targets of Bisphosphonates. *J Trans Med* (2011) 9:17. doi: 10.1186/1479-5876-9-177
125. Cao LL, Che XF, Qiu XS, Li Z, Yang BW, Wang S, et al. M2 Macrophage Infiltration Into Tumor Islets Leads to Poor Prognosis in Non-Small-Cell Lung Cancer. *Cancer Manage Res* (2019) 11:6125–38. doi: 10.2147/cmar.S199832
126. Hu H, Tu WZ, Chen YG, Zhu M, Jin H, Huang T, et al. The Combination of PKM2 Overexpression and M2 Macrophages Infiltration Confers a Poor Prognosis for PDAC Patients. *J Cancer* (2020) 11(8):2022–31. doi: 10.7150/jca.38981
127. Lewis D, Donofrio CA, O'Leary C, Li K-L, Zhu X, Williams R, et al. The Microenvironment in Sporadic and Neurofibromatosis Type II-Related Vestibular Schwannoma: The Same Tumor or Different? A Comparative Imaging and Neuropathology Study. *J Neurosurg* (2021) 134(5):1419–29. doi: 10.3171/2020.3.Jns193230
128. Bi WL, Gupta S, Mei Y, Al Abdulmohsen S, Larsen AG, Unadkat P, et al. Immunophenotype of Vestibular Schwannomas. *Otol Neurotol* (2020) 41 (10):E1290–E6. doi: 10.1097/mao.0000000000002782
129. Chow MT, Moeller A, Smyth MJ. Inflammation and Immune Surveillance in Cancer. *Semin Cancer Biol* (2012) 22(1):23–32. doi: 10.1016/j.semcancer.2011.12.004
130. Templeton AJ, McNamara MG, Seruga B, Vera-Badillo FE, Aneja P, Ocana A, et al. Prognostic Role of Neutrophil-To-Lymphocyte Ratio in Solid Tumors: A Systematic Review and Meta-Analysis. *J Natl Cancer Inst* (2014) 106(6):dju124. doi: 10.1093/jnci/dju124
131. Tikka T, Yiannakis CP, Stapleton E, Locke R, Crowther JA, Taylor WAS, et al. Spontaneous Vestibular Schwannoma Regression: A Case-Control Study. *Otol Neurotol* (2018) 39(10):E1118–24. doi: 10.1097/mao.0000000000001962
132. Ying SY, Lin SL. Current Perspectives in Intronic Micro RNAs (miRNAs). *J BioMed Sci* (2006) 13(1):5–15. doi: 10.1007/s11373-005-9036-8
133. Lei YH, Guo P, Li XG, Zhang YY, Du T. Identification of Differentially Expressed miRNAs and mRNAs in Vestibular Schwannoma by Integrated Analysis. *BioMed Res Int* (2019) 2019:10. doi: 10.1155/2019/7267816
134. Saydam O, Senol O, Wurdinger T, Mizrak A, Ozdener GB, Stemmer-Rachamimov AO, et al. miRNA-7 Attenuation in Schwannoma Tumors Stimulates Growth by Upregulating Three Oncogenic Signaling Pathways. *Cancer Res* (2011) 71(3):852–61. doi: 10.1158/0008-5472.Can-10-1219
135. Zhao X, Hou YX, Tuo ZZ, Wei FM. Application Values of miR-194 and miR-29 in the Diagnosis and Prognosis of Gastric Cancer. *Exp Ther Med* (2018) 15 (5):4179–84. doi: 10.3892/etm.2018.5931
136. Liu QL, Geng PS, Shi LY, Wang Q, Wang PL. miR-29 Promotes Osteosarcoma Cell Proliferation and Migration by Targeting PTEN. *Oncol Lett* (2019) 17(1):883–90. doi: 10.3892/ol.2018.9646
137. Jiang HS, Zhang G, Wu JH, Jiang CP. Diverse Roles of miR-29 in Cancer (Review). *Oncol Rep* (2014) 31(4):1509–16. doi: 10.3892/or.2014.3036
138. Strong AMP, Setaluri V, Spiegelman VS. microRNA-340 as a Modulator of RAS-RAF-MAPK Signaling in Melanoma. *Arch Biochem Biophys* (2014) 563:118–24. doi: 10.1016/j.abb.2014.07.012
139. Rong JP, Xu L, Hu YY, Liu F, Yu YR, Guo HY, et al. Inhibition of Let-7b-5p Contributes to an Anti-Tumorigenic Macrophage Phenotype Through the SOCS1/STAT Pathway in Prostate Cancer. *Cancer Cell Int* (2020) 20(1):15. doi: 10.1186/s12935-020-01563-7
140. Peng H, Yang H, Xiang X, Li SG. MicroRNA-221 Participates in Cerebral Ischemic Stroke by Modulating Endothelial Cell Function by Regulating the PTEN/PI3K/AKT Pathway. *Exp Ther Med* (2020) 19(1):443–50. doi: 10.3892/etm.2019.8263
141. Sucheta, Kataria SP, Malik S, Yadav R, Kapil R, Sen R. Histomorphological and Morphometric Evaluation of Microvessel Density in Nodal Non-Hodgkin Lymphoma Using CD34 and CD105. *J Lab Phys* (2021) 22(9):7. doi: 10.1055/s-0041-1726569
142. Burghardt I, Ventura E, Weiss T, Schroeder JJ, Seystahl K, Zielasek C, et al. Endoglin and TGF-Beta Signaling in Glioblastoma. *Cell Tissue Res* (2021) 384(3):613–24. doi: 10.1007/s00441-020-03323-5
143. Mo FZ, Duan SL, Jiang XB, Yang XM, Hou XQ, Shi W, et al. Nanobody-Based Chimeric Antigen Receptor T Cells Designed by CRISPR/Cas9 Technology for Solid Tumor Immunotherapy. *Signal Transduct Target Ther* (2021) 6(1):12. doi: 10.1038/s41392-021-00462-1
144. Liu YM, Paauwe M, Nixon AB, Hawinkels L. Endoglin Targeting: Lessons Learned and Questions That Remain. *Int J Mol Sci* (2021) 22(1):15. doi: 10.3390/ijms22010147
145. de Vries I, Schmitt H, Lenarz T, Prenzler N, Alvi S, Staecker H, et al. Detection of BDNF-Related Proteins in Human Perilymph in Patients With Hearing Loss. *Front Neurosci* (2019) 13:214. doi: 10.3389/fnins.2019.00214
146. Fields GB. Mechanisms of Action of Novel Drugs Targeting Angiogenesis-Promoting Matrix Metalloproteinases. *Front Immunol* (2019) 10:1278. doi: 10.3389/fimmu.2019.01278
147. Xu JH, Ma J, Shi YX, Yin DM, Zhang Y, Dai PD, et al. Differential Protein Expression Between Cystic and Solid Vestibular Schwannoma Using

Tandem Mass Tag-Based Quantitative Proteomic Analysis. *Proteomics Clin Appl* (2020) 14(4):1900112. doi: 10.1002/prca.201900112
148. Moon KS, Jung S, Seo SK, Jung TY, Kim IY, Ryu HH, et al. Cystic Vestibular Schwannomas: A Possible Role of Matrix Metalloproteinase-2 in Cyst Development and Unfavorable Surgical Outcome. *J Neurosurg* (2007) 106 (5):866–71. doi: 10.3171/jns.2007.106.5.866
149. Oria VO, Lopatta P, Schilling O. The Pleiotropic Roles of ADAM9 in the Biology of Solid Tumors. *Cell Mol Life Sci* (2018) 75(13):2291–301. doi: 10.1007/s00018-018-2796-x
150. Mygind KJ, Schwarz J, Sahgal P, Ivaska J, Kveiborg M. Loss of ADAM9 Expression Impairs Beta 1 Integrin Endocytosis, Focal Adhesion Formation and Cancer Cell Migration. *J Cell Sci* (2018) 131(1):jcs205393. doi: 10.1242/jcs.205393
151. Mygind KJ, Storiko T, Freiberg ML, Samsoe-Petersen J, Schwarz J, Andersen OM, et al. Sorting Nexin 9 (SNX9) Regulates Levels of the Transmembrane ADAM9 at the Cell Surface. *J Biol Chem* (2018) 293(21):8077–88. doi: 10.1074/jbc.RA117.001077
152. Chang L, Gong FC, Cai HF, Li ZH, Cui YB. Combined RNAi Targeting Human Stat3 and ADAM9 as Gene Therapy for Non-Small Cell Lung Cancer. *Oncol Lett* (2016) 11(2):1242–50. doi: 10.3892/ol.2015.4018
153. Chen WL, Lu Q, Li SY, Zhang XY, Xue XH. microRNA-1298 Inhibits the Malignant Behaviors of Breast Cancer Cells via Targeting ADAM9. *Biosci Rep* (2020) 40:12. doi: 10.1042/bsr20201215
154. Gol MAK, Lund TC, Levine SC, Adams ME. Quantitative Proteomics of Vestibular Schwannoma Cerebrospinal Fluid: A Pilot Study. *Otolaryngol Head Neck Surg* (2016) 154(5):902–6. doi: 10.1177/0194599816630544
155. Xiao F, Lv SG, Zong ZT, Wu L, Tang XP, Kuang W, et al. Cerebrospinal Fluid Biomarkers for Brain Tumor Detection: Clinical Roles and Current Progress. *Am J Transl Res* (2020) 12(4):1379–96.
156. Mattox AK, Yan H, Bettegowda C. The Potential of Cerebrospinal Fluid-Based Liquid Biopsy Approaches in CNS Tumors. *Neuro Oncol* (2019) 21 (12):1509–18. doi: 10.1093/neuonc/noz156
157. Bai Y, Liu YJ, Wang H, Xu Y, Stamenkovic I, Yu Q. Inhibition of the Hyaluronan-CD44 Interaction by Merlin Contributes to the Tumor-Suppressor Activity of Merlin. *Oncogene* (2007) 26(6):836–50. doi: 10.1038/sj.onc.1209849
158. de Vries M, Briaire-de Bruijn I, Malessy MJ, de Bruïne SF, van der Mey AG, Hogendoorn PC. Tumor-Associated Macrophages Are Related to Volumetric Growth of Vestibular Schwannomas. *Otol Neurotol* (2013) 34 (2):347–52. doi: 10.1097/MAO.0b013e31827c9fbf
159. Neff BA, Voss SG, Allen C, Schroeder MA, Driscoll CLW, Link MJ, et al. Bioluminescent Imaging of Intracranial Vestibular Schwannoma Xenografts in NOD/SCID Mice. *Otol Neurotol* (2009) 30(1):105–11. doi: 10.1097/MAO.0b013e31818b6cea
160. Bonne N-X, Vitte J, Chareyre F, Karapetyan G, Khankaldyyan V, Tanaka K, et al. An Allograft Mouse Model for the Study of Hearing Loss Secondary to Vestibular Schwannoma Growth. *J Neurooncol* (2016) 129(1):47–56. doi: 10.1007/s11060-016-2150-9
161. Szczupak M, Pena SA, Bracho O, Mei C, Bas E, Fernandez-Valle C, et al. Fluorescent Detection of Vestibular Schwannoma Using Intravenous Sodium Fluorescein *In Vivo*. *Otol Neurotol* (2021) 42(4):E503–11. doi: 10.1097/mao.0000000000002988
162. Helbing DL, Schulz A, Morrison H. Pathomechanisms in Schwannoma Development and Progression. *Oncogene* (2020) 39(32):5421–9. doi: 10.1038/s41388-020-1374-5
163. Lee HJ, Yang YJ, Jeong S, Lee JD, Choi SY, Jung DW, et al. Development of a Vestibular Schwannoma Xenograft Zebrafish Model for *In Vivo* Antitumor Drug Screening. *Laryngoscope* (2016) 126(12):E409–15. doi: 10.1002/lary.26043
164. Breun M, Martellotta DD, Leberle A, Nietzer S, Baur F, Ernestus R-I, et al. 3D *In Vitro* Test System for Vestibular Schwannoma. *J Neurosci Methods* (2020) 336:108633. doi: 10.1016/j.jneumeth.2020.108633
165. Wu L, Vasilijic S, Sun Y, Chen J, Landegger LD, Zhang Y, et al. Losartan Prevents Tumor-Induced Hearing Loss and Augments Radiation Efficacy in NF2 Schwannoma Rodent Models. *Sci Transl Med* (2021) 13(602):eabd4816. doi: 10.1126/scitranslmed.abd4816
166. Meyer HJ, Leifels L, Hamerla G, Hohn AK, Surov A. Histogram Analysis Parameters Derived From Conventional T1-And T2-Weighted Images Can Predict Different Histopathological Features Including Expression of Ki67, EGFR, VEGF, HIF-1 Alpha, and P53 and Cell Count in Head and Neck Squamous Cell Carcinoma. *Mol Imag Biol* (2019) 21(4):740–6. doi: 10.1007/s11307-018-1283-y
167. Shcherbakova DM, Baloban M, Emelyanov AV, Brenowitz M, Guo P, Verkhusha VV. Bright Monomeric Near-Infrared Fluorescent Proteins as Tags and Biosensors for Multiscale Imaging. *Nat Commun* (2016) 7:12405. doi: 10.1038/ncomms12405
168. Hessler M, Jalilian E, Xu Q, Reddy S, Horton L, Elkin K, et al. Melanoma Biomarkers and Their Potential Application for *In Vivo* Diagnostic Imaging Modalities. *Int J Mol Sci* (2020) 21(24):9583. doi: 10.3390/ijms21249583
169. Sewda K, Coppola D, Enkemann S, Yue B, Kim J, Lopez AS, et al. Cell-Surface Markers for Colon Adenoma and Adenocarcinoma. *Oncotarget* (2016) 7(14):17773–89. doi: 10.18632/oncotarget.7402
170. Morrison DR, Sorace AG, Hamilton E, Moore LS, Houson HA, Udayakumar N, et al. Predicting Schwannoma Growth in a Tumor Model Using Targeted Imaging. *Otol Neurotol* (2021) 42(5):e615–23. doi: 10.1097/MAO.0000000000003063

Conflict of Interest: The authors declare that the research was conducted in the absence of any commercial or financial relationships that could be construed as a potential conflict of interest.

Publisher's Note: All claims expressed in this article are solely those of the authors and do not necessarily represent those of their affiliated organizations, or those of the publisher, the editors and the reviewers. Any product that may be evaluated in this article, or claim that may be made by its manufacturer, is not guaranteed or endorsed by the publisher.

frontiers in Oncology

ORIGINAL RESEARCH
published: 28 September 2021
doi: 10.3389/fonc.2021.717917

OLFML2A Downregulation Inhibits Glioma Proliferation Through Suppression of Wnt/β-Catenin Signaling

Shize Ma[1,2†], Lei Duan[1,2†], Huateng Dong[3], Xiaodong Ma[1,2], Xinyu Guo[1,2], Jianli Liu[2,4], Guoqiang Li[1,2], Yue Yu[1,2], Yanlong Xu[1,2], Guoqiang Yuan[1,2], Xingkun Zhao[2], Guopeng Tian[1,2], Shijia Zhai[1,2], Yawen Pan[1,2] and Yinian Zhang[1,2*]*

[1] Department of Neurosurgery and Laboratory of Neurosurgery, Lanzhou University Second Hospital, Lanzhou, China, [2] Second Clinical School, Lanzhou University, Lanzhou, China, [3] Department of Pediatric Neurology, Gansu Provincial Maternity and Child-Care Hospital, Lanzhou, China, [4] Department of Radiology, Lanzhou University Second Hospital, Lanzhou, China

OPEN ACCESS

Edited by:
Zhaohui Zhang,
Renmin Hospital of Wuhan University, China

Reviewed by:
Gelei Xiao,
Central South University, China
Zhenchao Zhang,
Xinxiang Medical University, China

***Correspondence:**
Yinian Zhang
ery_zhangyinian@lzu.edu.cn
Yawen Pan
panyawen666@sohu.com

[†]These authors have contributed equally to this work

Specialty section:
This article was submitted to Neuro-Oncology and Neurosurgical Oncology, a section of the journal Frontiers in Oncology

Received: 31 May 2021
Accepted: 02 September 2021
Published: 28 September 2021

Citation:
Ma S, Duan L, Dong H, Ma X, Guo X, Liu J, Li G, Yu Y, Xu Y, Yuan G, Zhao X, Tian G, Zhai S, Pan Y and Zhang Y (2021) OLFML2A Downregulation Inhibits Glioma Proliferation Through Suppression of Wnt/β-Catenin Signaling. Front. Oncol. 11:717917. doi: 10.3389/fonc.2021.717917

Glioma is a highly heterogeneous and lethal tumor with an extremely poor prognosis. Through analysis of TCGA data, we identified that OLFML2A is a key promotor of gliomagenesis. However, the molecular function of OLFML2A and its underlying mechanism of action in glioma remain unclear. In this study, we found that OLFML2A expression was significantly upregulated in glioma specimens and positively correlated with pathological grades in glioma patients. Moreover, Kaplan–Meier survival analysis of TCGA data revealed that glioma patients with higher OLFML2A expression had shorter overall survival. Importantly, OLFML2A knockdown in glioma cells inhibited cell proliferation and promoted apoptosis. Mechanistically, OLFML2A downregulation inhibits Wnt/β-catenin signaling by upregulating amyloid precursor protein (APP) expression and reducing stabilized β-catenin levels, leading to the repression of MYC, CD44, and CSKN2A2 expression. Furthermore, OLFML2A downregulation suppressed the growth of transplanted glioma subcutaneously and intracranially by inhibiting Wnt/β-catenin pathway-dependent cell proliferation. By uncovering the oncogenic effects in human and rodent gliomas, our data support OLFML2A as a potential therapeutic target for glioma.

Keywords: olfactomedin-like 2A (OLFML2A), glioma, amyloid precursor protein (APP), proliferation, apoptosis, Wnt/β-catenin signaling

INTRODUCTION

Glioma is characterized by extremely poor outcomes (1). In particular, glioblastoma (GBM), a World Health Organization (WHO) grade IV tumor, is the most common and aggressive malignant brain tumor in humans, and even with radical surgery, radiation therapy, and chemotherapy, the median survival time is less than 12 months (2, 3). Studies have partly characterized the genetic basis of tumorigenesis in glioma over the past two decades (4, 5). Based on these findings, the molecular

classification standard of central nervous system tumors was established by the WHO in 2016 (6). However, glioma is a highly heterogeneous tumor (7), and there are many specific molecules that can be used for its classification. Thus, identifying the molecules that regulate glioma progression may contribute to the development of reliable therapeutic targets for glioma.

Olfactomedin-like 2A (OLFML2A) belongs to subfamily IV of olfactomedin domain-containing (OLFM) proteins (8), also known as photomedins-1, which were first identified and characterized in the mouse retina (9). In normal human tissue, OLFML2A is predominantly detected in the photoreceptor layer of the retina but is not expressed in neuronal tissues (10). In general, the function of OLFML2A remains poorly understood at present. Recent studies have shown that OLFML2A is highly expressed in triple-negative breast cancer (TNBC) and positively related to cell growth, proliferation, and migration (11). In acute myeloid leukemia, high OLFML2A expression is associated with extramedullary infiltration and predicts a poor prognosis (12). Consistent with these findings, Dai et al. showed that OLFML2A is also overexpressed in liver hepatocellular carcinoma (LIHC) and many other cancers, such as breast cancer and leukemia, by comparing the Oncomine dataset to normal samples (13). Ultimately, Kyoto Encyclopedia of Genes and Genomes (KEGG) pathway and process enrichment analysis suggested that OLFML2A regulates the tumorigenesis of LIHC through angiogenesis, negative regulation of DNA-binding transcription factor activity, regulation of neuronal differentiation, positive regulation of apoptosis, and autophagy *via* the Wnt, Notch, and hypoxia signaling pathways (13). The above observations underscore that OLFML2A may be involved in the development of many cancers. However, the detailed regulatory mechanisms have not yet been thoroughly validated, and the underlying molecular mechanisms need to be elucidated. Moreover, the role of OLFML2A in glioma has not been reported.

Therefore, to better understand the function of OLFML2A and identify new markers for targeted glioma therapy, *in vitro* and *in vivo* assays and bioinformatics analyses were performed to elucidate the function and mechanisms of OLFML2A in glioma progression.

MATERIALS AND METHODS

Cell Culture

Human glioblastoma cell lines (U87MG and U251) were purchased from GeneChem (Shanghai, China) and cultured in DMEM (HyClone, USA) supplemented with 10% fetal bovine serum (Sigma, USA) and 1% penicillin and streptomycin (Beyotime). All cells were cultured in a humidified incubator at 37°C under an atmosphere with 5% CO_2.

Abbreviations: OLFML2A, olfactomedin-like 2A; APP, amyloid precursor protein; TCGA, The Cancer Genome Atlas; LGG, low-grade glioma; TNBC, triple-negative breast cancer; LIHC, liver hepatocellular carcinoma; IHC, immunohistochemistry; DEGs, differentially expressed genes; IPA, ingenuity pathway analysis.

Lentiviral Transduction

Cells were seeded in 6-well plates at a density of 5×10^4 cells/well and incubated at 37°C until reaching 30% confluence. According to the determined multiplicity of infection, an appropriate amount of lentivirus was added to the culture medium of glioma cells for transduction, and the cells were cultured for another 14 h. Subsequently, the medium containing the lentivirus was removed, and the cells were cultured in normal medium for 58 h. GFP expression was observed under a fluorescence microscope 3 days after infection, and glioma cells with an infection efficiency of >80% were selected for subsequent analysis.

All lentiviruses were purchased from GeneChem (Shanghai, China). The forward sequences of the shRNAs targeting OLFML2A in U251 and U87MG cells were as follows: sh-OLFML2A-1 (TCTATGTCACCAACTACTA) and sh-OLFML2A-2 (GCCAAACAAACATTCACTA). The forward sequence of the shRNA targeting OLFML2A in C6 cells was as follows: AGGCCGGTGGAGTAATATGTA. To increase the efficiency of RNA interference, four shRNAs targeting amyloid precursor protein (APP) were designed, and the four plasmids carrying the different shRNAs were mixed in equal proportion for lentiviral packaging. The forward sequences of the shRNAs targeting APP in U87MG cells were as follows: psc10391 (ccCTGTTCATTGTAAGCACTT), psc10392 (gcAGACACA GACTATGCAGAT), psc11434 (ccCAAAGTTTACTCA AGACTA), and psc11435 (gcCATCTTTGACCGAAACGAA).

Immunohistochemistry (IHC)

All glioma specimens were routinely embedded in paraffin and then analyzed by immunohistochemical staining. To this end, specimens were cut into 5-μm sections and then subjected to antigen retrieval. Subsequently, the sections were incubated with primary antibodies (anti-OLFML2A, Abcam, ab75882, 1:200; anti-Ki-67, Abcam, ab15580, 1:200; anti-APP, Abcam, ab32136, 1:300; anti-β-catenin, CST, CST#8480, 1:50; anti-P-β-catenin (Ser33/37/Thr41), CST, CST#9561, 1:200; anti-GSK-3β, CST, CST#12456, 1:800; and anti-P-GSK-3β, CST, CST#9323, 1:50) overnight at 4°C and then visualized using a DAB detection kit according to the manufacturer's protocol. Then, the sections were counterstained with hematoxylin and observed under a BX-53 microscope (Olympus, Tokyo, Japan). The degree of immunostaining in the sections was reviewed and scored independently by two observers based on both the percentage of positively stained tumor cells and the staining intensity. The staining intensity was graded into four categories on a scale from 0 to 3 (intensity score): no staining (0), light-brown staining (1), brown staining (2), and dark-brown staining (3). Protein staining was evaluated using the following formula: overall staining score = intensity score × percentage score.

Cell Proliferation Analysis by Celigo Assay

Cell proliferation was analyzed using a Celigo assay as previously described (14). Briefly, cells were cultured in 96-well plates at a density of 1,000 cells/well and treated with the indicated shRNAs or control shRNA (shCtrl). The medium was changed every other day, and the cells were imaged with a Celigo Imaging Cytometer

for 5 consecutive days. For each experimental well of a 96-well plate, Celigo scans of four visual fields at each time point (40 × magnification) were performed, and the images were analyzed with the corresponding software. Each assay was conducted in triplicate. After 5 days of consecutive measurements, a cell growth curve was plotted to assess cell proliferation.

3-(4,5-Dimethylthiazol-2-yl)-2,5-Diphenyl Tetrazolium Bromide (MTT) Assay

MTT and dimethyl sulfoxide (DMSO) solutions (Sigma-Aldrich, St. Louis, MO, USA) were used to assess the cell proliferation. Specific cells (2×10^4) were seeded into 96-well plates, and sterile MTT solution (10 μl) was added to each well after for 24, 48, and 72 h of cultivation. After culturing for 4 h at 37°C, the medium was removed, and 150 μl DMSO was added to each well. Then, the absorbance at 490 nm was measured with a microplate reader (SpectraMax i3X, MOLECULAR, CA, USA).

Quantitation of Apoptosis by Flow Cytometry

An Annexin-V-APC apoptosis detection kit (eBioscience, Cat. No. 88-8007) was used to evaluate cell apoptosis according to the manufacturer's instructions. First, glioma cells were infected with a lentivirus expressing OLFML2A or a scrambled shRNA sequence (Scr-shRNA). Subsequently, after culturing for another 4 days, the cells were harvested, washed with PBS, and then resuspended in staining buffer at a final density of 1×10^6-1×10^7/ml. Then, 5 μl of Annexin-V-APC was added to 100-μl aliquots of cell suspensions and incubated at room temperature for 10–15 min. Signals were detected with a FACSCalibur instrument (Becton-Dickinson, USA).

Animal Studies

All animals were purchased from the Animal Experiment Center of Gansu College of Traditional Chinese Medicine (Lanzhou, China) and housed in a standardized specific pathogen-free animal facility. All experimental procedures were approved by the Institutional Animal Care and Use Committee of Lanzhou University Second Hospital. All mice were maintained and were used in accordance with the guidelines approved by the Institutional Animal Care and Use Committee.

For the tumor xenograft implantation model, 4-week-old mice were randomly divided into two groups (n=10 per group) and implanted with 1×10^6 U87MG cells that were previously transfected with OLFML2A shRNA lentivirus or the negative control. Then, the cells were mixed with Matrigel (50% volume) and subcutaneously implanted into the right flanks of the nude mice (BALB/c). Tumor volume was determined using an external caliper every 3–4 days and calculated using the formula (Length×Width^2)/2. Mice were sacrificed 50 days after transplantation, at which time tumors were excised and used in subsequent analyses.

For the orthotopic model, 1×10^6 C6-OLFML2A-shRNA or control cells were injected into the right corpus striatum of the brains of 6-week-old Wistar rats using a stereotactic frame (n=5 per group). Spectral computed tomography (HD750 CT scanner; GE Healthcare, Little Chalfont, UK) was performed to record tumor growth at 14 and 19 days after injection using the same scanning parameters described in a previous study (15). Rats were monitored and sacrificed when neurological signs appeared or after 35 days.

Gene Chip Microarray Analysis

Total RNA was extracted using an RNAiso Plus kit (TaKaRa Biotechnology Co., Ltd., Dalian, China) and assessed using a NanoDrop 2000 Spectrophotometer (Thermo Scientific, MA, USA) and an Agilent Bioanalyzer 2100 (Palo Alto, CA, USA) (16). Only samples of sufficient quality were used in subsequent gene chip experiments. The RNA quality control standards were as follows: 1.7<A260/A280<2.2 on the NanoDrop 2000 and an RNA integrity number (RIN)> =7.0 and a 28S/18S ratio > 0.7 on the Agilent 2100 Bioanalyzer. The microarray was processed as described in a previous study (17). Briefly, amplified RNA (aRNA) was prepared from total RNA using a GeneChip 3' IVT Express kit (Affymetrix, Santa Clara, CA, USA). Then, DNA was synthesized, after which double-stranded template DNA was synthesized. Biotin-labeled aRNA was obtained by *in vitro* transcription. Then, aRNA was purified, fragmented, labeled, and hybridized with an Affymetrix GeneChip® Human Transcriptome Array 2.0 (Affymetrix, Santa Clara, CA, USA). After hybridization, the chips were washed and stained. Finally, raw intensity data were analyzed using Affymetrix Expression Console software after the images and raw data were scanned. Genes that were up- or downregulated with fold changes of > 2.0 or < 2.0 were analyzed using Affymetrix Transcriptome Analysis Console Software.

Ingenuity Pathway Analysis

Ingenuity pathway analysis (IPA) of differentially expressed genes (DEGs) was conducted with Qiagen's Ingenuity Pathway Analysis algorithm (www.qiagen.com/ingenuity, Qiagen, Redwood City, CA, USA). Canonical pathway analysis, functional analysis, regulatory effect analysis, and interaction network analysis were performed, with activation z-scores and overlapping p-values calculated as described in a previous study (18).

Quantitative Reverse Transcription PCR

Cells in the exponential growth phase were collected and lysed with an RNAiso Plus kit (TaKaRa Biotechnology Co., Ltd., Dalian, China) to extract total RNA. A NanoDrop-2000 spectrophotometer (Thermo Scientific, MA, USA) was used to measure the purity and concentration of RNA. According to the manufacturer's protocol, total RNA was reverse-transcribed using the Prime Script RT kit (TaKaRa Biotechnology Co., Ltd.) for 15 min at 37°C before being heat inactivated for 20 s at 85°C. Subsequently, quantitative reverse transcription PCR (qRT-PCR) was performed using SYBR® Premix Ex Ta Master Mix (TaKaRa Biotechnology Co., Ltd.) and a Bio-Rad CFX96 Real-time PCR system (Bio-Rad Laboratories, Inc., Hercules, CA, USA). The primers used for qRT-PCR are shown in **Table 1**. qRT-PCR was performed in a final volume of 10 μl with the following thermocycling program: an initial denaturation at 95°C for 10 min followed by 40 cycles of 95°C for 10 s, 60°C for 30 s,

TABLE 1 | Primer sequences used in this study.

Gene	Forward primer 5'-3'	Reverse primer 5'-3'
GAPDH	*TGACTTCAACAGCGACACCCA*	*CACCCTGTTGCTGTAGCCAAA*
OLFML2A	*AACAGGCAGTAGAGTCAA*	*TTACAAGATTCCTACCAACAG*
APP	*CTGATGCGGAGGAGGATGAC*	*TCTCTGTGGCTTCTTCGTAGG*
Wnt3	*GGACGGAGAAGCGGAAGGA*	*GCGAGTTGGGTCTGGGTCAT*
Wnt5a	*TCGACTATGGCTACCGCTTTG*	*CACTCTCGTAGGAGCCCTTG*
Wnt5b	*CTGGTGGTCATTAGCTTTG*	*ATGTGCTCCTGGTACAATT*
MYC	*TGTCCGTCCAAGCAGAGG*	*CGCACAAGAGTTCCGTAGC*
CD44	*AGGCTGAGACAGGAGGTTA*	*CCTCCCTTATTTCTATCGTG*
CSNK2A2	*TGGAGTTTGGGCTGTATGTT*	*TCGTATCGCAGAAGTTTGTC*
LEF1	*AGAGCGAATGTCGTTGCTGA*	*TCGTTTTCCACCTGATGCAGA*
FZD3	*CAAATCTGGGTGTTGGGTT*	*TGAGAAAGGCTGGGCATC*
LRP6	*TGGGGAAACTATGACTAATG*	*CTGACAAAGAACTTGGGTG*
LRP1	*AGGGCGTAGGTTCCTTTCTC*	*CATTGGTCACCACGTCTTCA*
DVL3	*TACTGCGGGAGATTGTGC*	*GAACTGGTGATGGAGGAGC*
SOX4	*ACTTCGAGTTCCCGGACTACT*	*TGAAAACCAGGTTGGAGATGC*
MAP3K7	*CCGGTGAGATGATCGAAGCC*	*GCCGAAGCTCTACAATAAACGC*
AKT3	*AATGGACAGAAGCTATCCAGGC*	*TGATGGGTTGTAGAGGCATCC*
MDM2	*GAATCATCGGACTCAGGTACATC*	*TCTGTCTCACTAATTGCTCTCCT*
RARG	*ATGCTGCGTATCTGCACAAG*	*AGGCAAAGACAAGGTCTGTGA*
BTRC	*AGTTCTGCACTTGCGTTTC*	*ACTCACTACCAGCCTGTCC*
TGFBR2	*GTGCCAACAACATCAACC*	*GACTGCCACTGTCTCAAACT*
ACVR1C	*GCACCTTCCAACAGCATCAC*	*ATCCAGAGGCGGTCACATC*
ACVR2B	*AGACACGGGAGTGCATCTACT*	*GCCTATCGTAGCAGTTGAAGTC*
PPP2R2B	*ACCAGGGACTACTTGACCG*	*TCACGCTTGGTGTTTCTGT*

and 72°C for 30 s. As the reaction progressed, fluorescence signals were obtained. After amplification, a melting curve analysis was performed, the results of which were used to determine the dissociation characteristics of the PCR products. The $2^{-\Delta\Delta Cq}$ method was used to calculate the mRNA expression level relative to that of the internal reference gene GAPDH. Each sample was assayed in triplicate.

Western Blot Analysis

Cells were lysed using RIPA buffer (Beyotime Institute of Biotechnology) on ice for 30 min, after which the samples were centrifuged at 12,000×g for 45 min at 4°C. The protein concentrations of the samples were determined using a BCA protein assay kit (Solarbio, China), after which the proteins were subjected to SDS-PAGE and transferred to PVDF membranes. The membranes were then blocked with TBST containing 5% bovine serum albumin (BSA; Solarbio, China) for 2 h at room temperature and then incubated with primary antibodies against the following antigens: OLFML2A (1:500, Abcam, ab85458, UK); GAPDH (1:1,000, Abcam, ab8245, UK); APP (1:500, Abcam, ab32136, UK); β-catenin (1:500, CST, CST#8480, USA); P-β-catenin (Ser33/37/Thr41) (1:500, CST, CST#9561, USA); GSK-3β (1:500, CST, CST#12456, USA); and P-GSK-3β (1:500, CST, CST#9323, USA) overnight at 4°C. The membranes were then washed three times with TBST and incubated with a horseradish peroxidase-conjugated secondary antibody for 2 h at room temperature. The blots were visualized with an enhanced chemiluminescence (ECL) kit (Solarbio, China) and scanned with ChemImager 5500 V2.03 software. The relative integrated density values (IDVs) were calculated using Fluor Chen 2.0 software using GAPDH as an internal control.

Statistics and Data Analysis

All data are presented as means ± standard deviation (SD). Statistical analyses were performed using Prism 8 (GraphPad Software, San Diego, CA, USA). Two-tailed Student's t-test was used to assess the significance of the differences between two groups, and one-way ANOVA was used to assess the significance of the differences among multiple groups. Survival curves were analyzed using the Kaplan–Meier method and assessed by the log-rank test. P-values<0.05 were considered to indicate a significant difference.

RESULTS

OLFML2A Overexpression Is Correlated With Glioma Progression and Poor Prognosis

By analyzing datasets from The Cancer Genome Atlas (TCGA), we observed that OLFML2A expression was significantly upregulated in glioma tissues compared to normal brain tissue and that OLFML2A expression was positively correlated with glioma grades (**Figures 1A, B**). Kaplan–Meier survival analysis of TCGA data revealed that glioma patients with higher OLFML2A expression had shorter overall survival (**Figure 1C**). Real-time PCR results showed that OLFML2A expression was upregulated in four different glioma cell lines (**Figure 1D**). Taken together, these findings suggested that OLFML2A is overexpressed in human glioma.

To determine the clinical relevance of OLFML2A in glioma patients, OLFML2A expression was examined in 69 paraffin-embedded, archived glioma tissues by IHC. As expected, OLFML2A was significantly upregulated in glioma tissues (**Figure 1E**). Furthermore, OLFML2A levels were positively

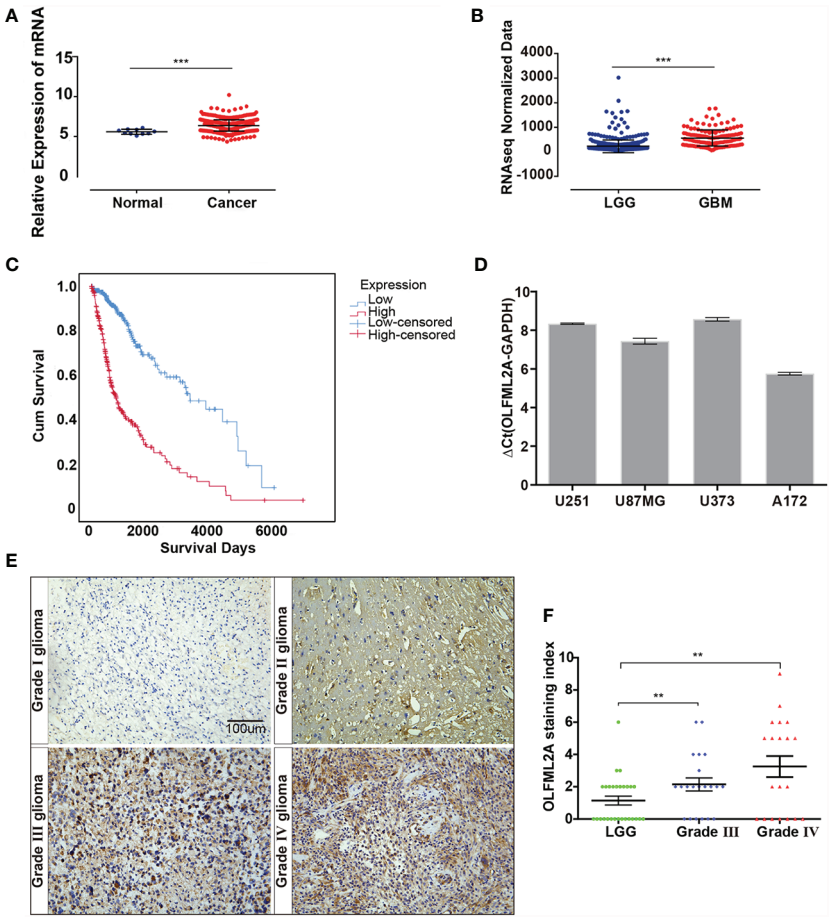

FIGURE 1 | OLFML2A expression is elevated in gliomas and correlated with tumor grade and prognosis. **(A)** Expression profile of OLFML2A mRNA in primary glioma tissues (n=548) and normal brain tissues (n=10; Mann–Whitney U test; ***P < 0.001; TCGA). **(B)** Expression profile of OLFML2A mRNA in low-grade glioma (LGG) samples (n=515) and glioblastoma (GBM) samples (n=152; Mann–Whitney U test; ***P < 0.001; TCGA). **(C)** Kaplan–Meier survival curves comparing glioma patients with low and high OLFML2A expression levels (n = 664; P < 0.001; TCGA) based on the median value of OLFML2A mRNA. **(D)** Real-time PCR analysis of OLFML2A expression in four human glioma cell lines. **(E, F)**. Immunohistochemistry (IHC) analysis of OLFML2A in 69 specimens with low- and high-grade gliomas. Scale bar=100 μm. The score was calculated according to the degree of cell staining and the proportion of positive cells. The staining index is shown as the product value of two scores. (**P < 0.01).

correlated with pathological grades in glioma patients (**Figure 1F**). Collectively, these findings confirmed the TCGA analysis results and suggested a potential association between OLFML2A upregulation and the progression of glioma.

OLFML2A Expression Is Efficiently Inhibited by Lentiviral-Based shRNA in Human Glioma Cell Lines

A positive correlation between OLFML2A expression and glioma pathological grades suggested that OLFML2A may be involved in the development and progression of glioma. To assess the biological role of OLFML2A in glioma, we used a lentivirus-based shRNA strategy to knockdown OLFML2A expression in glioma cell lines. U251 and U87MG cells were infected with a lentivirus specifically targeting human OLFML2A (OLFML2A-shrNA) or a negative control (Scr-shRNA) to evaluate the knockdown efficiency. Cells infected with the lentivirus were cultured and harvested, and total RNA/protein samples were collected. Then, the OLFML2A mRNA and protein levels were detected by qRT-PCR and Western blotting. The results demonstrated that OLFML2A mRNA expression was significantly reduced (**Figure 2A**), and OLFML2A protein was barely detectable in cells treated with OLFML2A-shRNA (**Figures 2B, C**). These results indicated that lentivirus-based shRNA strategy could inhibit OLFML2A expression at the protein and mRNA levels.

OLFML2A Knockdown Leads to Reduced Glioma Cell Proliferation *In Vitro*

U251 and U87MG cells express high levels of OLFML2A protein. To determine whether OLFML2A is required for the proliferation of these cell lines, we generated U251 and U87MG cells with lentivirus-delivered OLFML2A shRNA knockdown as previously

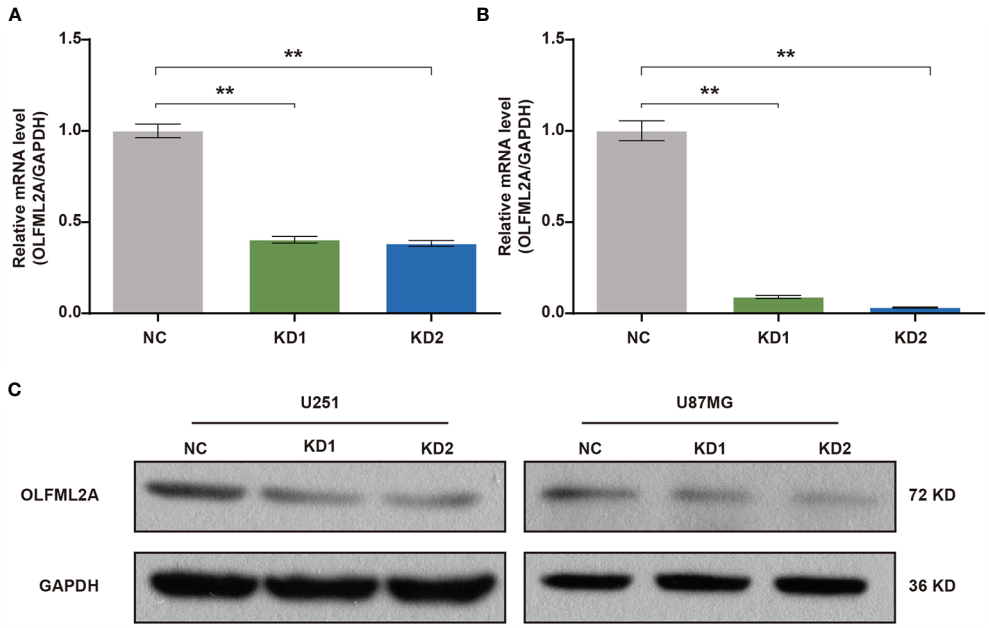

FIGURE 2 | OLFML2A expression is efficiently inhibited by lentiviral-based shRNA in human glioma cell lines. **(A, B)** OLFML2A mRNA levels were assessed by qRT-PCR in U251 **(A)** and U87MG **(B)** cells. **(C)** OLFML2A protein content in glioma cell lines was assessed by western blotting. **P < 0.01. NC, cells infected with negative control lentivirus expressing Scr-shRNA; KD1 and KD2, cells infected with an OLFML2A-knockdown lentivirus expressing OLFML2A-shRNA-1 and OLFML2A-shRNA-2, respectively.

described. Then, Celigo assays were performed to monitor cell growth for 5 days. As shown in **Figures 3A–F**, silencing OLFML2A decreased the total cell numbers and slowed the growth rate of U251 and U87MG cells. Subsequently, the MTT assay was used to further evaluate the effect of OLFML2A knockdown on the proliferation of U251 and U87MG cells. As indicated in **Figures 3G–J**, the cell proliferation rate of the OLFML2A-shRNA group was markedly reduced compared to that of the control group.

Suppression of OLFML2A Expression Leads to Increased Glioma Cell Apoptosis

The ability to resist cell death, another hallmark of cancers, is essential for tumor development (19). The reduction in cell numbers induced by OLFML2A knockdown may be attributable to cell proliferation inhibition and increased cell apoptosis. To further investigate whether OLFML2A promotes glioma cell proliferation by regulating cell apoptosis, we used Annexin-V staining to assess apoptosis in OLFML2A-knockdown and control U251 cells. OLFML2A knockdown significantly induced apoptosis in U251 cells (**Figures 4A, B**), and similar results were observed in U87MG cells following OLFML2A silencing by shRNA (**Figures 4C, D**).

Disruption of Multiple Crucial Cell Cycle Regulation Pathways Involved in Cancer Development by OLFML2A Knockdown

The results described above showed that OLFML2A is crucial for tumor development in human glioma cell lines. However, the mechanisms underlying OLFML2A-mediated glioma development and its downstream pathways have not been systematically explored. Therefore, global gene expression profiling of U87MG cells infected with lentiviruses expressing either Scr-shRNA or OLFML2A-shRNA was performed using a microarray platform, and 1,911 genes showing significant differential expression were identified (based on |fold change|≥2.0 and FDR<0.05), of which 658 were upregulated and 1,253 were downregulated (**Figures 5A, B** and **Supplementary Table 1, Supplementary Data Sheet 1**). Then, functional analysis was performed *via* IPA, and the DEGs were observed to be enriched in cancer, cell cycle, cell death and cell survival, cellular growth, and proliferation, suggesting that OLFML2A is significantly (based on a P<0.001 threshold) involved in proliferation and cell cycle regulation processes (**Figure 5C**).

Canonical pathway analysis using IPA was conducted to further evaluate potential signaling pathways, resulting in 136 pathways being identified (**Supplementary Table 2**-Canonical Pathways.xlsx), of which 117 were inhibited and 19 were activated following OLFML2A gene suppression (based on |Z-score|>0 and P<0.05). Notably, among the inhibited signaling pathways, those involved in cell proliferation and cell cycle regulation, such as Cyclins and Cell Cycle Regulation, Estrogen-mediated S-phase Entry, and Glioblastoma Multiforme Signaling, were significantly inhibited (based on |Z-score|>2 and P<0.05) (**Figure 4D**). In addition, Cell Cycle Regulation by BTG Family Proteins (Z-score=-1.633), TGF-β Signaling (Z-score=-1.387), Wnt/β-catenin Signaling (Z-score=-1.342), and Antiproliferative Role of Somatostatin Receptor 2 (Z-score=-1.265), which are important signaling pathways in glioma proliferation and cell

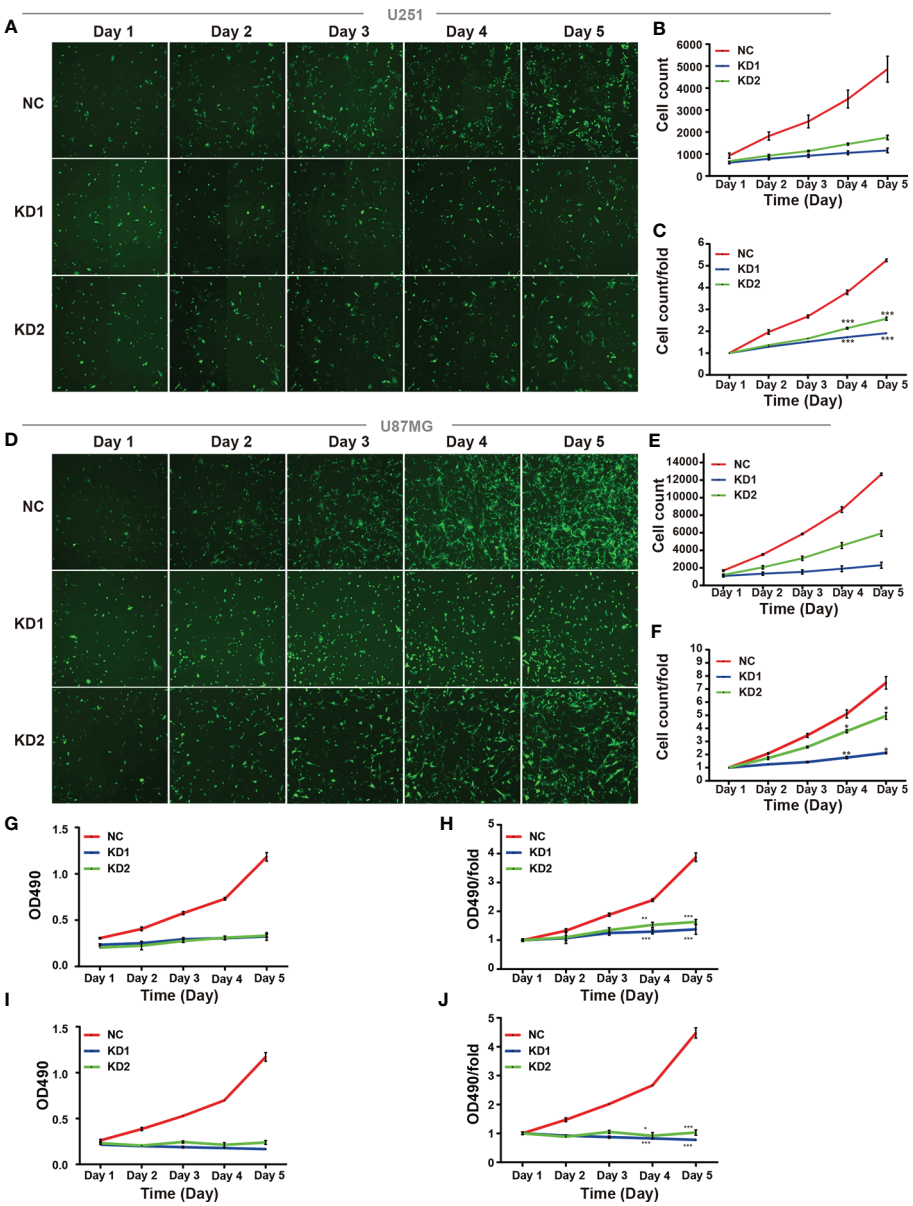

FIGURE 3 | OLFML2A knockdown inhibits cell growth and proliferation. **(A–F)** U251 and U87MG cell growth was measured by Celigo assays for 5 days. **(G–J)** U251 and U87MG cell growth was measured by the MTT assay for 5 days. The data are presented as mean ± SD. *P < 0.05, **P < 0.01, ***P < 0.001.

cycle regulation, were also inhibited (**Figure 4D**). Furthermore, Apoptosis Signaling (Z-score=1.508), Cell Cycle: G1/S Checkpoint Regulation (Z-score=1.291), and Cell Cycle: G2/M DNA Damage Checkpoint Regulation (Z-score=0.943) were activated (**Figure 5D**). Collectively, these findings provided a strong rationale for the role of OLFML2A as a crucial molecule that regulates the proliferation of glioma cells.

OLFML2A Knockdown Suppresses the Wnt/β-Catenin Pathway in Glioma Cells

The results of previous studies have shown that the Wnt/β-catenin pathway is activated in glioma and is essential for glioma growth, proliferation, cell cycle regulation, and apoptosis (20). Importantly, the IPA data showed that Wnt/β-catenin signaling was one of the inhibited pathways enriched in the OLFML2A-associated gene signatures (**Figure 5D**). The expression of 21 molecules involved in the Wnt/β-catenin pathway was altered (**Figures 6A, B**). Subsequently, we validated the expression levels of the 21 molecules by real-time PCR and observed that the expression levels of Wnt ligands (Wnt3, Wnt5a, and Wnt5b), the transcription factor LEF1, and genes downstream of Wnt (MYC, CD44, and CSKN2A2) were decreased when OLFML2A was downregulated (**Figure 6C**). The changes in the remaining molecules were generally consistent with the gene chip results

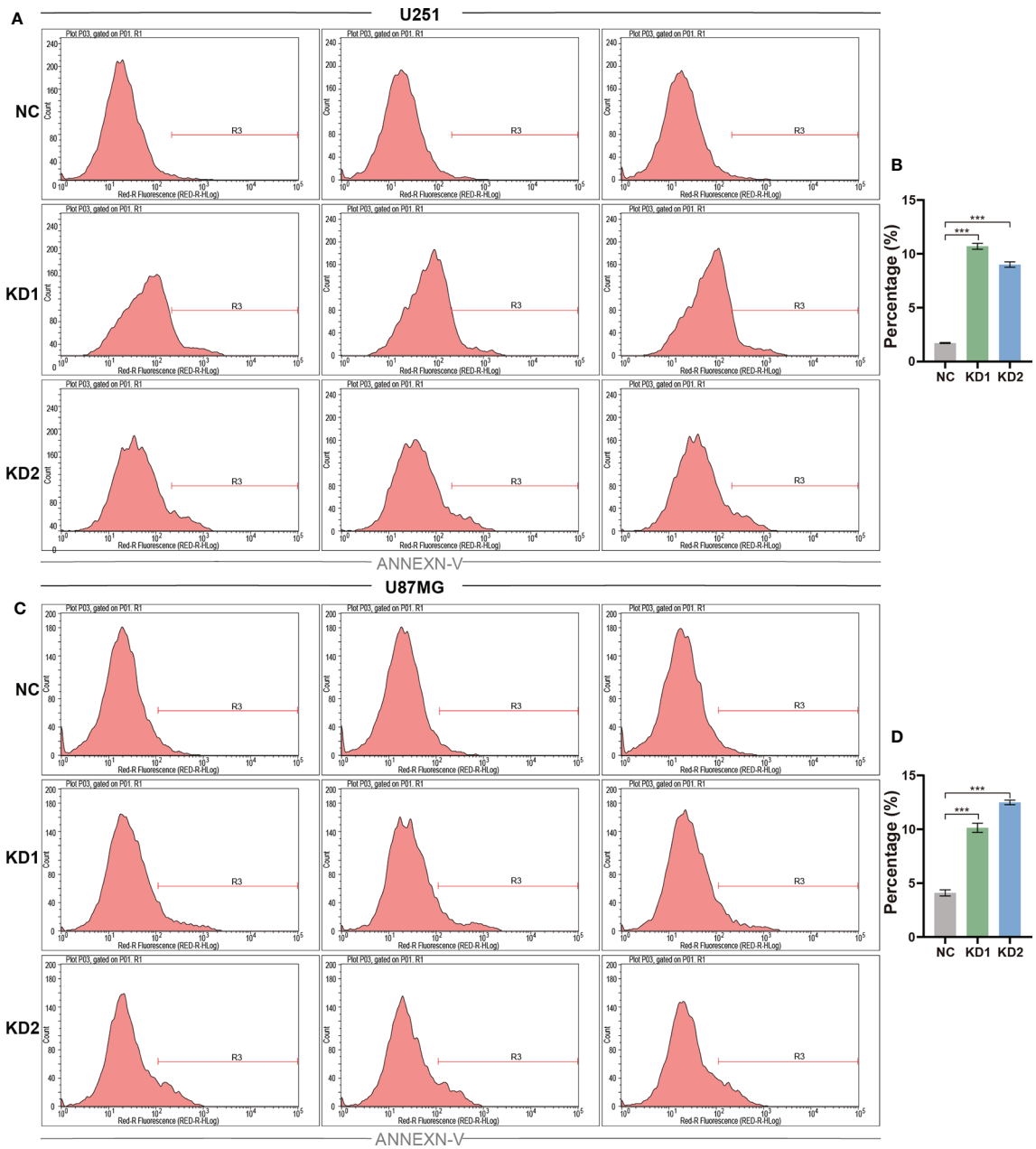

FIGURE 4 | OLFML2A suppression promotes the apoptosis of glioma cells. **(A–D)** U251 and U87MG cell apoptosis was assessed using Annexin-V staining and analyzed by flow cytometry. The rate of apoptosis is presented as the mean ± SD. ***P < 0.01.

(**Figure 6C**). These data preliminarily confirmed that Wnt activity is suppressed upon OLFML2A downregulation. Furthermore, we observed that the mRNA levels of the Wnt target genes MYC, CD44, and CSKN2A2 were significantly and positively correlated with the OLFML2A mRNA levels in GBM patients by analyzing TCGA data (**Figure 6D**). Accumulating evidence has demonstrated that the regulation of β-catenin and GSK-3β phosphorylation controls Wnt/β-catenin pathway activation (20). Therefore, we subsequently assessed the phosphorylation of β-catenin and GSK-3β in U87MG cells. The results showed that the Thr41/Ser37/Ser33 phosphorylation levels of β-catenin were significantly increased upon OLFML2A downregulation (**Figure 6E**). Conversely, stabilized β-catenin levels were decreased when OLFML2A was downregulated (**Figure 6E**). Additionally, we observed that phosphorylated GSK-3β levels were significantly decreased while total GSK-3β levels were elevated upon OLFML2A downregulation (**Figure 6E**). Thus, our results indicated that

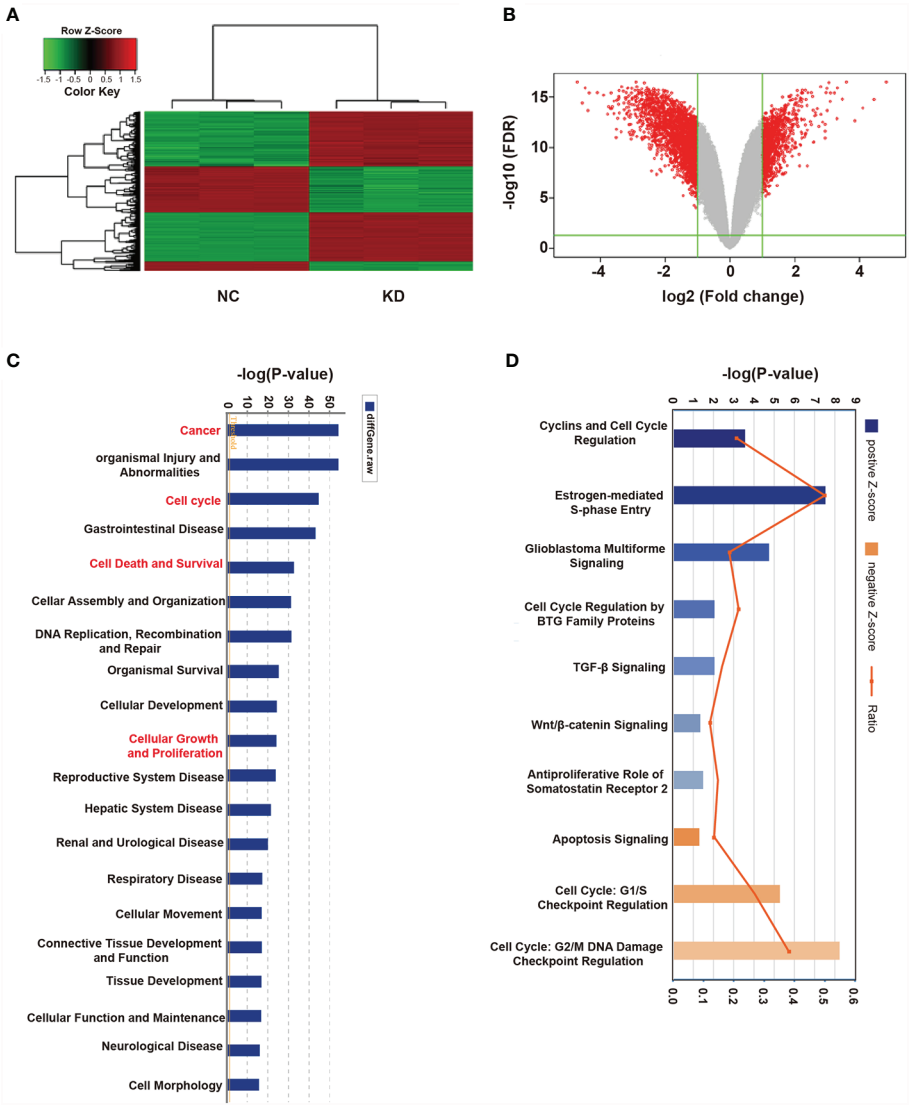

FIGURE 5 | Widespread changes in gene expression in U87MG cells with OLFML2A knockdown as determined by microarray analysis. **(A)** Heatmap representation of 1,911 genes showing significant differential expression in the human malignant glioma cell line U87MG infected with a lentivirus expressing either Scr-shRNA (NC) or OLFML2A-shRNA (KD) under the criteria P<0.05 and |fold change|>2. Genes and samples are listed in rows and columns, respectively. The color scale for the normalized expression data is shown at the bottom of the microarray heatmap (green and red represent down- and upregulated genes, respectively). **(B)** Volcano plots. The genes with significantly altered expression are marked in red. The selected thresholds were a |fold change| > 2 and P < 0.05. **(C)** Disease and function analysis was performed to classify the enriched genes after OLFML2A silencing. **(D)** Annotated classical pathway analysis indicated that multiple signaling pathways involved in cell proliferation were enriched after OLFML2A silencing. Blue and orange represent suppressed and activated signaling pathways, respectively, and the intensity of the color indicates the degree of activation or inhibition. NC, cells infected with negative control lentivirus Scr-shRNA; KD, cells infected with OLFML2A-shRNA-1.

high levels of OLFML2A expression may activate the Wnt/β-catenin pathway to promote cell proliferation and inhibit cell apoptosis.

APP Acts as an Intermediate Molecule to Mediate the Downstream Regulatory Effects of OLFML2A in Glioma

To further elucidate the regulatory mechanism of OLFML2A on the Wnt/β-catenin pathway and cell proliferation, an IPA-based interaction network analysis was performed, the results of which confirmed that APP is an important intermediate molecule that mediates the downstream regulatory effects of OLFML2A (**Figure 7A**). APP has been reported to be a negative regulator of Wnt/β-catenin signaling pathways (21). Our results showed that OLFML2A knockdown increased APP expression (**Figures 7B, C**). Furthermore, we observed that APP expression was significantly downregulated in GBM tissues compared to normal brain tissue by analyzing TCGA data (**Figure 7D**). Additionally, we demonstrated

A

	Fold change	P-value	Regulation
SOX4	2.372679	1.12E-3	UP
FZD3	2.179912	5.07E-09	UP
LRP6	2,354673	1.84E-10	UP
MDM2	2.532865	1.51E-11	UP
ACVR2B	2.270815	4.62E-09	UP
RARG	2.011163	1.6E-12	UP
TGFBR2	2.426505	2.75E-16	UP
MYC	-5.51821	1.64E-16	down
CSNK2A2	-2.25322	3.3E-13	down
PPP2R2B	-3.25051	5.72E-11	down
MAP3K7	-2.4107	1.84E-12	down
CD44	-2.15904	1.11E-15	down
AKT3	-2.33262	4.99E-10	down
DVL3	2.00553	4.35E-12	UP
LEF1	-2.17595	4.32E-08	down
BTRC	2.498081	2.83E-12	UP
ACVR1C	4.926808	5.14E-13	UP
LRP1	-0.34708	1.03E-13	UP
Wnt5B	-0.40074	2.73E-12	down
Wnt5A	-0.4544	2.28E-11	down
Wnt3	-2.55006	1.39E-12	down

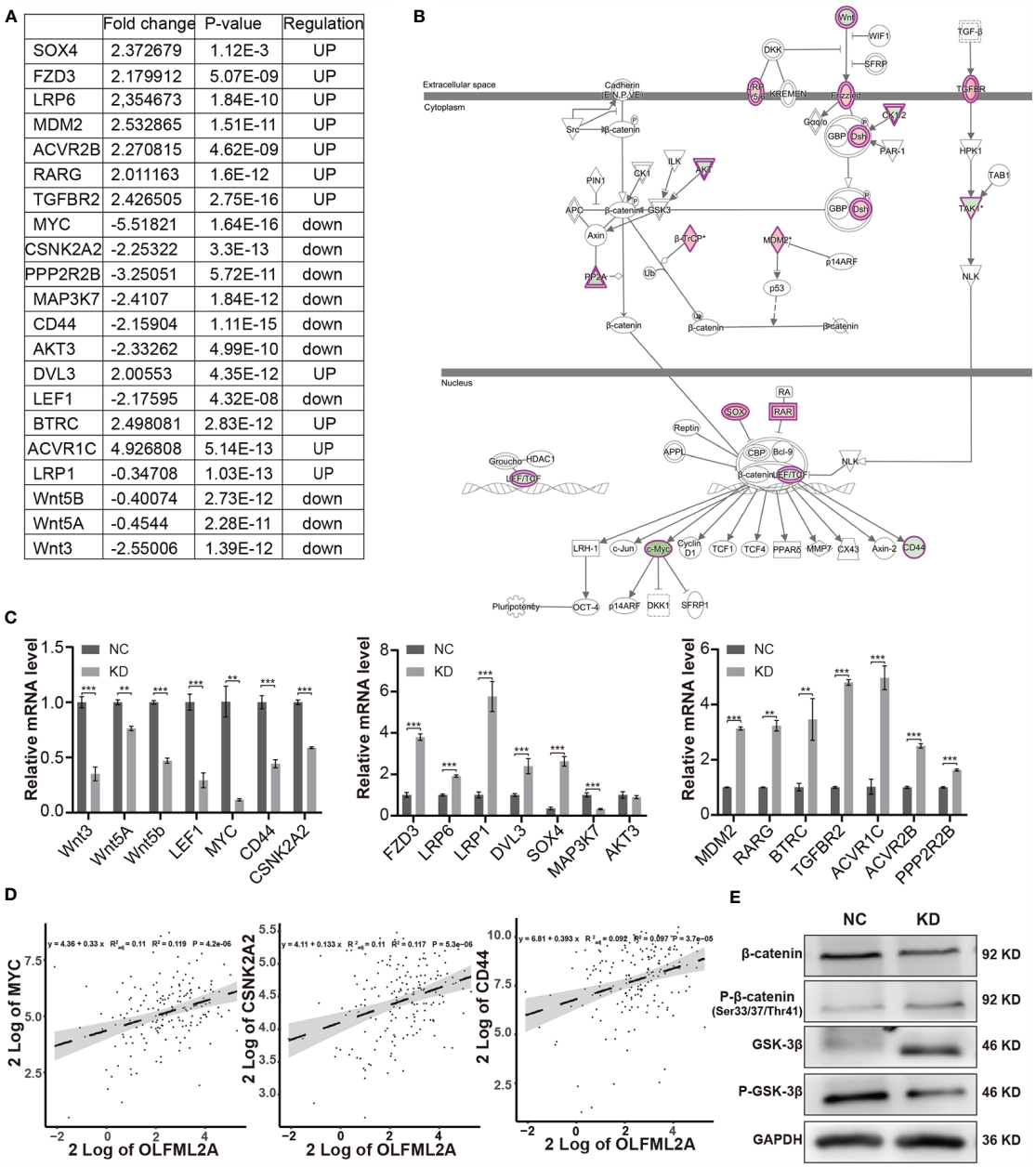

FIGURE 6 | OLFML2A knockdown suppresses the Wnt/β-catenin pathway in glioma cells. **(A)** The fold change, P-values, and regulatory effect of the molecules associated with the Wnt/β-catenin signaling pathway relative to OLFML2A knockdown are collated in the table. **(B)** The Wnt/β-catenin signaling pathway was mapped by IPA, and the 21 molecules involved in the Wnt/β-catenin pathway are included in the table **(A)**. Green: downregulated. Red: upregulated. **(C)** The expression of the 21 molecules involved in the Wnt/β-catenin pathway was verified by qRT-PCR in U87MG cells. **P < 0.01, ***P < 0.001. **(D)** The correlation of OLFML2A expression with that of MYC, CSNk2A2, and CD44 from a TCGA dataset (n = 169). **(E)** The β-catenin, p33/37/41-β-catenin, GSK-3β, and P-GSK-3β protein contents in U87MG cells were assessed by western blotting. NC, cells infected with negative control lentivirus expressing Scr-shRNA; KD, cells infected with OLFML2A-shRNA-1-expressing lentivirus.

that APP downregulation partly increases the proliferation of OLFML2A-knockdown U87MG cells (**Figures 7E, F**). These data further suggested that APP is a functional regulator that mediates the downstream regulatory effects of OLFML2A through the Wnt/β-catenin pathway in glioma.

OLFML2A Downregulation Leads to the Repression of Glioma Cell Proliferation *In Vivo*

We used a xenograft model to verify whether OLFML2A knockdown reduces tumor growth *in vivo*. U87MG cells

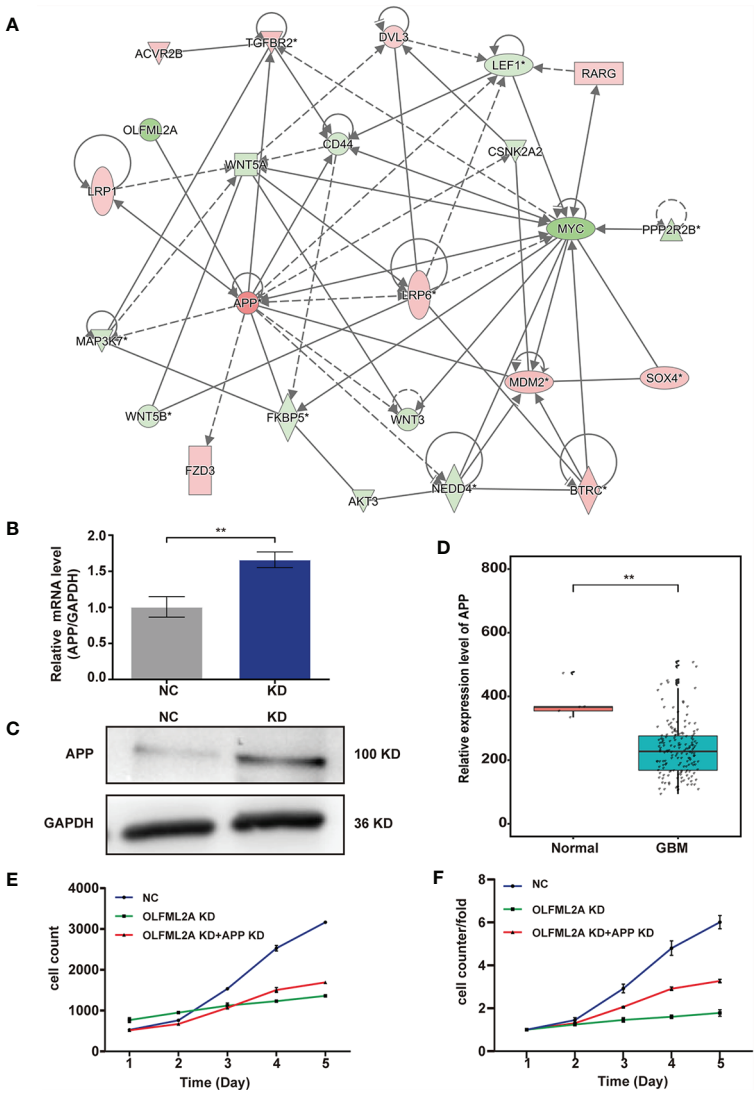

FIGURE 7 | APP acts as an intermediate molecule to mediate the downstream regulatory effects of OLFML2A in glioma. **(A)** IPA-based interaction network analysis. The interaction network analysis table shows the interactions among molecules in the datasets. **(B, C)** APP expression in U87MG cells was assessed by qRT-PCR **(B)** and western blotting **(C)**. NC, cells infected with negative control lentivirus expressing Scr-shRNA; KD, cells infected with OLFML2A-shRNA-1-expressing lentivirus. **(D)** Expression profile of APP mRNA in primary GBM tissues (n=169) and normal brain tissues (n=5; Mann–Whitney U test; **P < 0.01; TCGA). **(E, F)** U87MG cell growth was measured by Celigo assays for 5 days. NC, cells infected with negative control lentivirus expressing Scr-shRNA; OLFML2A KD, cells infected with OLFML2A-shRNA-1-expressing lentivirus; OLFML2A KD+APP KD, cells infected with OLFML2A-shRNA-1 and APP-shRNA lentiviruses.

infected with Scr-shRNA or OLFML2A-shRNA were transplanted into the right flanks of immunocompromised nude mice, and the results showed that OLFML2A knockdown led to significant decreases in tumor volume and weight (**Figures 8A–C**) (n = 10). Moreover, the IHC results showed that OLFML2A knockdown could significantly reduce the positivity rate of Ki-67 in subcutaneous tissues (**Figure 8D**). In addition, the level of APP expression was consistent with the *in vitro* results (**Figure 8E**). Furthermore, the IHC results also indicated that β-catenin phosphorylation levels were significantly elevated while stabilized β-catenin levels were markedly decreased following OLFML2A downregulation (**Figure 8E**). These results confirmed that OLFML2A functions as an oncogene in glioma by regulating the Wnt/β-catenin pathway *via* APP *in vivo*.

To further verify the effects of OLFML2A on glioma growth in immunocompetent animals, we transplanted C6 cells transfected with Scr-shRNA or OLFML2A-shRNA into the right striatum of Wistar rats (n = 5) and observed that OLFML2A downregulation strongly suppressed the growth of intracranial glioma by CT scan on days 14 and 19 after transplantation (**Figure 9A**). Similarly, gross observations also showed that OLFML2A downregulation could significantly suppress orthotopic glioma growth (**Figure 9B**), and the

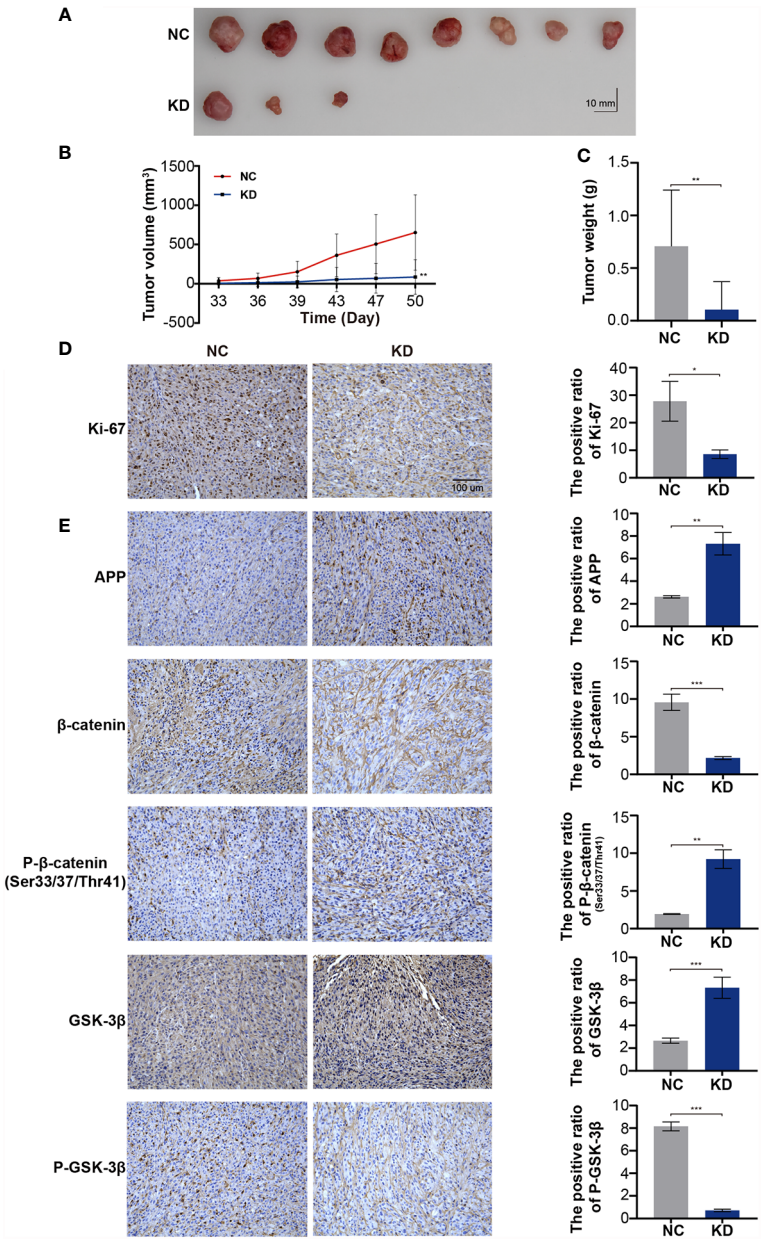

FIGURE 8 | OLFML2A downregulation leads to the repression of glioma cell proliferation and inhibition of the Wnt/β-catenin signaling pathway in xenograft implantation models. **(A–C)** Subcutaneously transplanted gliomas were utilized to analyze the effect of OLFML2A on glioma *in vivo*, and tumor values were measured every 3–4 days. **(D)** Representative IHC images of Ki67 expression in two groups of subcutaneous glioma tissues; scale bar=100 μm. **(E)** APP, p33/37/41-β-catenin, β-catenin, GSK-3β, and P-GSK-3β expression in two groups of subcutaneous glioma tissues was detected by IHC. *P < 0.05, **P < 0.01, ***P < 0.001.

positive rate of Ki-67 was also decreased after OLFML2A knockdown (**Figure 9C**).

DISCUSSION

Glioma is a very aggressive and heterogeneous tumor that lacks effective targeted therapies and has a relatively poor prognosis (22). Therefore, there is an unmet need to identify new targets to develop potential diagnostic and therapeutic strategies. In the present study, we first analyzed an available genomic database (TCGA) and identified OLFML2A as a putative molecule involved in glioma tumorigenesis. Our results indicated that OLFML2A is upregulated in glioma, positively correlated with tumor grade, and negatively correlated with the prognosis of glioma patients. In addition, we observed that the level of OLFML2A is correlated with glioma

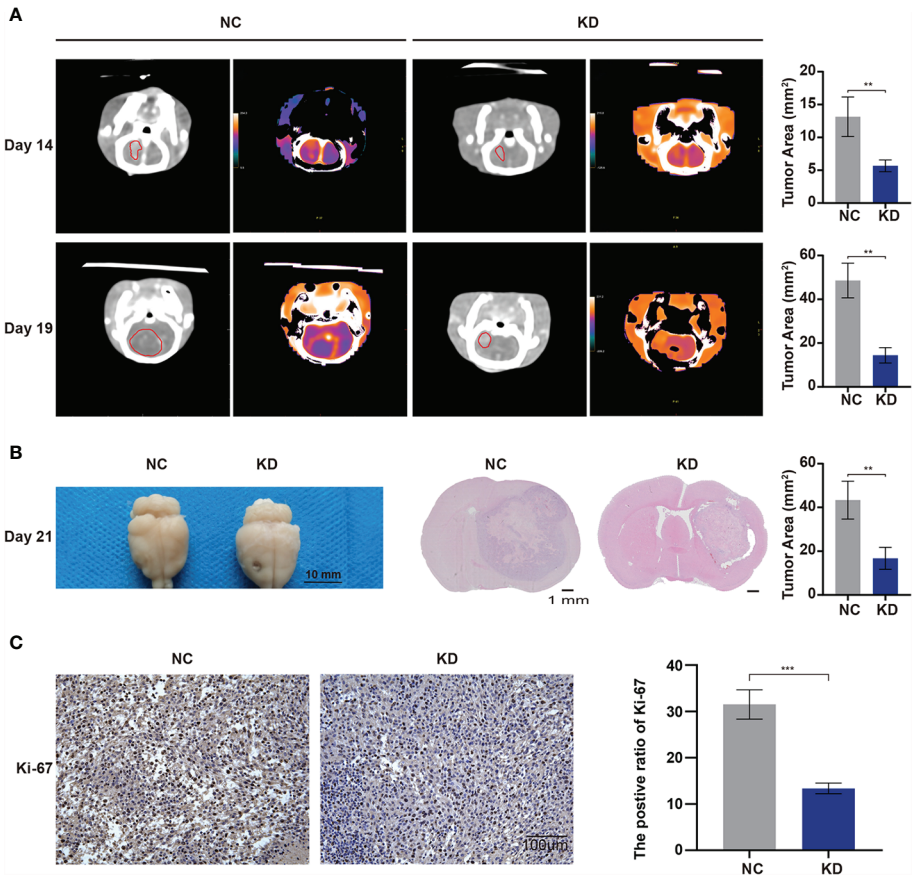

FIGURE 9 | OLFML2A knockdown inhibits cell growth and proliferation in an orthotopic model. **(A)** Intracranial xenografts of gliomas were established with C6 cells after OLFML2A downregulation, and representative spectral computed tomography images show the tumor size at 14 and 19 days after transplantation in each group. **(B)** Representative gross images of gliomas after dissection from mice in each group at 21 days. **(C)** IHC staining of Ki-67 showed the proliferation state of transplanted glioma. **P < 0.01, ***P < 0.001.

proliferation and apoptosis. Downregulation of OLFML2A expression dramatically suppressed the growth of glioma cells both *in vitro* and *in vivo*, and silencing OLFML2A significantly promoted the apoptosis of glioma cells. Furthermore, we confirmed that Wnt/β-catenin pathway activation is involved in OLFML2A-regulated glioma cell proliferation *in vitro* and *in vivo*. Finally, we demonstrated that APP is an important intermediate molecule that mediates the downstream regulatory effects of OLFML2A in glioma. Overall, OLFML2A was shown to primarily regulate glioblastoma through Wnt/β-catenin signaling by targeting APP. Our results suggested that OLFML2A promotes the progression of glioblastoma and may be a potential novel prognostic factor for glioblastoma. Importantly, OLFML2A may be a promising target gene for glioma treatment.

OLFML2A is a member of the OLF family (8). Interestingly, data obtained over the past several years demonstrated that OLF family proteins play important roles in neurogenesis, neural crest formation, dorsal ventral patterning, cell–cell adhesion, cell cycle regulation, and tumorigenesis and may act as modulators of critical signaling pathways (Wnt, BMP) (8). The human OLFML2A gene is located on chromosome 9q33.3 and encodes a secreted glycoprotein known as photomedin-1 (10). An understanding of the biological functions of proteins possessing the OLF domain has remained elusive (8, 10, 23). In the field of cancer research, the tumorigenic function of OLFM4 has been verified in many tumors (24, 25). Intriguingly, the tumorigenic function of OLFML2A is also gradually emerging. OLFML2A expression was shown to be negatively correlated with the biological progression and clinical features of TNBC, LIHC, and leukemia (11–13). Moreover, as previously reported, the Wnt/β-catenin pathway is a potential regulatory target of OLFML2A, through which OLFML2A regulates several malignant biological processes in LIHC (13). Consistent with previous studies, our results indicate that OLFML2A acts as an oncogene that exerts an important effect on glioma progression. Moreover, an IPA-based pathway enrichment analysis identified the Wnt/β-catenin pathway as being altered after OLFML2A downregulation.

Extensive studies have shown that abnormal activation of the Wnt signaling pathway leads to the malignant biological process

of glioma, including cell proliferation, cell apoptosis, and cell invasion (26). In the classic Wnt/β-catenin pathway, Wnt ligands combine with the receptor protein frizzled (Fzd) and low-density lipoprotein receptor related protein 5/6 (LRP5/6) to form a protein complex, which then activates Dishevelled (Dvl), leading to the phosphorylation and inactivation of glycogen synthase kinase 3β (GSK-3β) and preventing stabilized β-catenin from being phosphorylated and degraded (26, 27). Stable β-catenin in the cytoplasm further enters the nucleus and binds to the T-cytokine/lymph enhancer binding factor (TCF/LEF) transcription factor, resulting in the transcription of Wnt target genes such as MYC, CD44, cyclin D1, and PPAR-δ (26, 27). In our present study, we demonstrated that the expression levels of Wnt ligands (Wnt3, Wnt5a, and Wnt5b), the transcription factor LEF1, and Wnt-downstream genes (MYC and CD44) were decreased when OLFML2A was downregulated. Furthermore, total GSK-3β levels were significantly elevated, and GSK-3β phosphorylation was decreased upon OLFML2A downregulation. Additionally, the levels of stabilized β-catenin were decreased while the Thr41/Ser37/Ser33 phosphorylation levels of β-catenin were increased when OLFML2A was downregulated. Overall, the results of our present study indicate that OLFML2A downregulation can inactivate the Wnt/β-catenin pathway to inhibit cell proliferation and promote cell apoptosis.

The results of an IPA-based interaction network analysis confirmed that APP is an important intermediate molecule that mediates the downstream regulatory effects of OLFML2A in glioma. Accumulating evidence has shown that abnormal cleavage of APP is a central process in the pathological mechanisms of Alzheimer's disease (AD) (27–29), and the Wnt/β-catenin pathway is dysfunctional in AD brains (30–32). Furthermore, APP has been reported to downregulate β-catenin expression by increasing its degradation (32, 33), and overexpressed APP prevents β-catenin translocation into the nucleus through physical binding and precludes the transcription of Wnt target genes in AD disease models (21). These findings indicated a reciprocal regulation between APP and the Wnt/β-catenin signaling pathway. The results of the interaction network analysis were consistent with the function of APP acting as a suppressor of the Wnt/β-catenin pathway. In our present study, we observed that APP was expressed at low levels in glioma tissue. APP expression was observed to be negatively correlated with OLFML2A, and OLFML2A knockdown led to increased APP levels both *in vitro* and *in vivo*. Moreover, APP downregulation partially attenuated inhibitory effect of OLFML2A knockdown on cell proliferation. Therefore, we concluded that OLFML2A downregulation inhibits Wnt/β-catenin signaling by upregulating APP expression and reducing stabilized β-catenin levels.

CONCLUSION

In summary, our results suggest that OLFML2A plays a crucial role in the proliferation of glioma and acts as an oncogene to promote the progression of glioma in humans. Mechanistically, OLFML2A knockdown inhibits the Wnt/β-catenin signaling pathway by upregulating APP expression and promoting β-catenin phosphorylation, leading to repressed MYC, CD44, and CSKN2A2 expression. Our data indicate that the oncogenic effect of OLFML2A in glioma occurs through regulation of Wnt/β-catenin signaling, which may provide a new potential therapeutic target for glioma.

DATA AVAILABILITY STATEMENT

The datasets presented in this study can be found in online repositories. The names of the repository/repositories and accession number(s) can be found in the article/**Supplementary Material**.

ETHICS STATEMENT

The studies involving human participants were reviewed and approved by the ethics committee at the Lanzhou University Second Hospital (No. 2019A-077). The patients/participants provided their written informed consent to participate in this study. The animal study was reviewed and approved by the ethics committee at the Lanzhou University Second Hospital (D2019-117). Written informed consent was obtained from the individual(s) for the publication of any potentially identifiable images or data included in this article.

AUTHOR CONTRIBUTIONS

SM, LD, YP, and YZ designed the research, analyzed the data, and wrote the manuscript. SM, LD, HD, XM, XG, JL, GL, YY, YX, GY, XZ, GT, and SZ performed the experiments. All authors contributed to the article and approved the submitted version.

FUNDING

The article was supported by the National Natural Science Foundation of China (8177050431), Basic Research Innovation Group Project of Gansu Province (21JR7RA432), Special fund project for doctoral training program of Lanzhou University Second Hospital (YJS-BD-31), The Hui-Chun and Tsung Dao Lee Endowment (LZU-JZH2224), and the Cuiying Scientific and Training Program for Undergraduates of Lanzhou University Second Hospital (CYXZ-10 and CYXZ2019-08).

SUPPLEMENTARY MATERIAL

The Supplementary Material for this article can be found online at: https://www.frontiersin.org/articles/10.3389/fonc.2021.717917/full#supplementary-material

Supplementary Table 1 | Differentially expressed genes.

Supplementary Table 2 | Canonical Pathways.

Supplementary Data Sheet 1 | Heatmap.

REFERENCES

1. Weller M, Wick W, Aldape K, Brada M, Berger M, Pfister SM, et al. Glioma. *Nat Rev Dis Primers* (2015) 1:15017. doi: 10.1038/nrdp.2015.17
2. Jackson CM, Choi J, Lim M. Mechanisms of Immunotherapy Resistance: Lessons From Glioblastoma. *Nat Immunol* (2019) 20(9):1100–9. doi: 10.1038/s41590-019-0433-y
3. McKinnon C, Nandhabalan M, Murray SA, Plaha P. Glioblastoma: Clinical Presentation, Diagnosis, and Management. *BMJ* (2021) 374:n1560. doi: 10.1136/bmj.n1560
4. D'Angelo F, Ceccarelli M, Tala, Garofano L, Zhang J, Frattini V, et al. The Molecular Landscape of Glioma in Patients With Neurofibromatosis 1. *Nat Med* (2019) 25(1):176–87. doi: 10.1038/s41591-018-0263-8
5. Molinaro AM, Taylor JW, Wiencke JK, Wrensch MR. Genetic and Molecular Epidemiology of Adult Diffuse Glioma. *Nat Rev Neurol* (2019) 15(7):405–17. doi: 10.1038/s41582-019-0220-2
6. Louis DN, Perry A, Reifenberger G, von Deimling A, Figarella-Branger D, Cavenee WK, et al. The 2016 World Health Organization Classification of Tumors of the Central Nervous System: A Summary. *Acta Neuropathol* (2016) 131(6):803–20. doi: 10.1007/s00401-016-1545-1
7. Qazi MA, Bakhshinyan D, Singh SK. Deciphering Brain Tumor Heterogeneity, One Cell at a Time. *Nat Med* (2019) 25(10):1474–6. doi: 10.1038/s41591-019-0605-1
8. Tomarev SI, Nakaya N. Olfactomedin Domain-Containing Proteins: Possible Mechanisms of Action and Functions in Normal Development and Pathology. *Mol Neurobiol* (2009) 40(2):122–38. doi: 10.1007/s12035-009-8076-x
9. Furutani Y, Manabe R, Tsutsui K, Yamada T, Sugimoto N, Fukuda S, et al. Identification and Characterization of Photomedins: Novel Olfactomedin-Domain-Containing Proteins With Chondroitin Sulphate-E-Binding Activity. *Biochem J* (2005) 389(Pt 3):675–84. doi: 10.1042/bj20050120
10. Perez-Ibave DC, Gonzalez-Alvarez R, de la Luz Martinez-Fierro M, Ruiz-Ayma G, Luna-Munoz M, Martinez-De-Villarreal LE, et al. Olfactomedin-Like 2 A and B (OLFML2A and OLFML2B) Expression Profile in Primates (Human and Baboon). *Biol Res* (2016) 49(1):44. doi: 10.1186/s40659-016-0101-8
11. Wu C, Chen M, Zhang Q, Yu L, Zhu J, Gao X. Genomic and GeneChip Expression Profiling Reveals the Inhibitory Effects of Amorphophalli Rhizoma in TNBC Cells. *J Ethnopharmacol* (2019) 235:206–18. doi: 10.1016/j.jep.2019.02.004
12. Lv C, Sun L, Guo Z, Li H, Kong D, Xu B, et al. Circular RNA Regulatory Network Reveals Cell-Cell Crosstalk in Acute Myeloid Leukemia Extramedullary Infiltration. *J Transl Med* (2018) 16(1):361. doi: 10.1186/s12967-018-1726-x
13. Bai KH, He SY, Shu LL, Wang WD, Lin SY, Zhang QY, et al. Identification of Cancer Stem Cell Characteristics in Liver Hepatocellular Carcinoma by WGCNA Analysis of Transcriptome Stemness Index. *Cancer Med* (2020) 9 (12):4290–8. doi: 10.1002/cam4.3047
14. Vinci M, Gowan S, Boxall F, Patterson L, Zimmermann M, Court W, et al. Advances in Establishment and Analysis of Three-Dimensional Tumor Spheroid-Based Functional Assays for Target Validation and Drug Evaluation. *BMC Biol* (2012) 10:29. doi: 10.1186/1741-7007-10-29
15. Liu J, Zhou J, Li J, Zhang L, Zhang P, Liu B. Evaluation of Rat C6 Malignant Glioma Using Spectral Computed Tomography. *Exp Ther Med* (2017) 14 (2):1037–44. doi: 10.3892/etm.2017.4613
16. Calvano SE, Xiao W, Richards DR, Felciano RM, Baker HV, Cho RJ, et al. A Network-Based Analysis of Systemic Inflammation in Humans. *Nature* (2005) 437(7061):1032–7. doi: 10.1038/nature03985
17. Irizarry RA, Bolstad BM, Collin F, Cope LM, Hobbs B, Speed TP. Summaries of Affymetrix GeneChip Probe Level Data. *Nucleic Acids Res* (2003) 31(4):e15. doi: 10.1093/nar/gng015
18. Krämer A, Green J, Pollard J Jr, Tugendreich S. Causal Analysis Approaches in Ingenuity Pathway Analysis. *Bioinformatics* (2014) 30(4):523–30. doi: 10.1093/bioinformatics/btt703
19. Zimmermann KC, Bonzon C, Green DR. The Machinery of Programmed Cell Death. *Pharmacol Ther* (2001) 92(1):57–70. doi: 10.1016/s0163-7258(01)00159-0
20. Zhang K, Zhang J, Han L, Pu P, Kang C. Wnt/beta-Catenin Signaling in Glioma. *J Neuroimmune Pharmacol* (2012) 7(4):740–9. doi: 10.1007/s11481-012-9359-y
21. Zhang N, Parr CJC, Birch AM, Goldfinger MH, Sastre M. The Amyloid Precursor Protein Binds to β-Catenin and Modulates its Cellular Distribution. *Neurosci Lett* (2018) 685:190–5. doi: 10.1016/j.neulet.2018.08.044
22. Cuddapah VA, Robel S, Watkins S, Sontheimer H. A Neurocentric Perspective on Glioma Invasion. *Nat Rev Neurosci* (2014) 15(7):455–65. doi: 10.1038/nrn3765
23. Zeng LC, Han ZG, Ma WJ. Elucidation of Subfamily Segregation and Intramolecular Coevolution of the Olfactomedin-Like Proteins by Comprehensive Phylogenetic Analysis and Gene Expression Pattern Assessment. *FEBS Lett* (2005) 579(25):5443–53. doi: 10.1016/j.febslet.2005.08.064
24. Liu W, Li H, Hong SH, Piszczek GP, Chen W, Rodgers GP. Olfactomedin 4 Deletion Induces Colon Adenocarcinoma in Apc(Min/+) Mice. *Oncogene* (2016) 35(40):5237–47. doi: 10.1038/onc.2016.58
25. Grover PK, Hardingham JE, Cummins AG. Stem Cell Marker Olfactomedin 4: Critical Appraisal of its Characteristics and Role in Tumorigenesis. *Cancer Metastasis Rev* (2010) 29(4):761–75. doi: 10.1007/s10555-010-9262-z
26. He L, Zhou H, Zeng Z, Yao H, Jiang W, Qu H. Wnt/β-Catenin Signaling Cascade: A Promising Target for Glioma Therapy. *J Cell Physiol* (2019) 234 (3):2217–28. doi: 10.1002/jcp.27186
27. Toledo EM, Colombres M, Inestrosa NC. Wnt Signaling in Neuroprotection and Stem Cell Differentiation. *Prog Neurobiol* (2008) 86(3):281–96. doi: 10.1016/j.pneurobio.2008.08.001
28. Coronel R, Bernabeu-Zornoza A, Palmer C, Muniz-Moreno M, Zambrano A, Cano E, et al. Role of Amyloid Precursor Protein (APP) and Its Derivatives in the Biology and Cell Fate Specification of Neural Stem Cells. *Mol Neurobiol* (2018) 55(9):7107–17. doi: 10.1007/s12035-018-0914-2
29. Zhou R, Yang G, Guo X, Zhou Q, Lei J, Shi Y. Recognition of the Amyloid Precursor Protein by Human γ-Secretase. *Science* (2019) 363(6428):eaaw0930. doi: 10.1126/science.aaw0930
30. Esteve P, Rueda-Carrasco J, Inés Mateo M, Martin-Bermejo MJ, Draffin J, Pereyra G, et al. Elevated Levels of Secreted-Frizzled-Related-Protein 1 Contribute to Alzheimer's Disease Pathogenesis. *Nat Neurosci* (2019) 22 (8):1258–68. doi: 10.1038/s41593-019-0432-1
31. Boonen RA, van Tijn P, Zivkovic D. Wnt Signaling in Alzheimer's Disease: Up or Down, That Is the Question. *Ageing Res Rev* (2009) 8(2):71–82. doi: 10.1016/j.arr.2008.11.003
32. Magdesian MH, Carvalho MM, Mendes FA, Saraiva LM, Juliano MA, Juliano L, et al. Amyloid-Beta Binds to the Extracellular Cysteine-Rich Domain of Frizzled and Inhibits Wnt/beta-Catenin Signaling. *J Biol Chem* (2008) 283 (14):9359–68. doi: 10.1074/jbc.M707108200
33. Chen Y, Bodles AM. Amyloid Precursor Protein Modulates Beta-Catenin Degradation. *J Neuroinflamm* (2007) 4:29. doi: 10.1186/1742-2094-4-29

Conflict of Interest: The authors declare that the research was conducted in the absence of any commercial or financial relationships that could be construed as a potential conflict of interest.

frontiers in Oncology

ORIGINAL RESEARCH
published: 01 October 2021
doi: 10.3389/fonc.2021.722754

Valproic Acid Enhanced Temozolomide-Induced Anticancer Activity in Human Glioma Through the p53–PUMA Apoptosis Pathway

Hong-Chieh Tsai[1,2], *Kuo-Chen Wei*[1,3,4,5], *Pin-Yuan Chen*[5,6], *Chiung-Yin Huang*[3,4], *Ko-Ting Chen*[1,4], *Ya-Jui Lin*[1,5], *Hsiao-Wei Cheng*[1,7], *Yi-Rou Chen*[1] *and Hsiang-Tsui Wang*[7,8,9,10*]

[1] Department of Neurosurgery, Linkou Chang Gung Memorial Hospital, Taoyuan, Taiwan, [2] School of Traditional Chinese Medicine, Chang Gung University, Taoyuan, Taiwan, [3] Department of Neurosurgery, New Taipei Municipal TuCheng Hospital, Chang Gung Memorial Hospital, New Taipei City, Taiwan, [4] Neuroscience Research Center, Linkou Chang Gung Memorial Hospital, Taoyuan, Taiwan, [5] School of Medicine, Chang Gung University, Taoyuan, Taiwan, [6] Department of Neurosurgery, Keelung Chang Gung Memorial Hospital, Keelung, Taiwan, [7] Institute of Pharmacology, College of Medicine, National Yang-Ming University, Taipei, Taiwan, [8] Institute of Pharmacology, College of Medicine, National Yang Ming Chiao Tung University, Taipei, Taiwan, [9] Institute of Food Safety and Health Risk Assessment, National Yang Ming Chiao Tung University, Taipei, Taiwan, [10] Doctor Degree Program in Toxicology, Kaohsiung Medical University, Kaohsiung, Taiwan

OPEN ACCESS

Edited by:
Liam Chen,
University of Minnesota, United States

Reviewed by:
Bernd Kaina,
Johannes Gutenberg University Mainz, Germany
Salvatore Massimiliano Cardali,
University of Messina, Italy

***Correspondence:**
Hsiang-Tsui Wang
htwang01@nycu.edu.tw

Specialty section:
This article was submitted to Neuro-Oncology and Neurosurgical Oncology, a section of the journal Frontiers in Oncology

Received: *09 June 2021*
Accepted: *08 September 2021*
Published: *01 October 2021*

Citation:
Tsai H-C, Wei K-C, Chen P-Y, Huang C-Y, Chen K-T, Lin Y-J, Cheng H-W, Chen Y-R and Wang H-T (2021) Valproic Acid Enhanced Temozolomide-Induced Anticancer Activity in Human Glioma Through the p53–PUMA Apoptosis Pathway. Front. Oncol. 11:722754. doi: 10.3389/fonc.2021.722754

Glioblastoma (GBM), the most lethal type of brain tumor in adults, has considerable cellular heterogeneity. The standard adjuvant chemotherapeutic agent for GBM, temozolomide (TMZ), has a modest response rate due to the development of drug resistance. Multiple studies have shown that valproic acid (VPA) can enhance GBM tumor control and prolong survival when given in conjunction with TMZ. However, the beneficial effect is variable. In this study, we analyzed the impact of VPA on GBM patient survival and its possible correlation with TMZ treatment and *p53* gene mutation. In addition, the molecular mechanisms of TMZ in combination with VPA were examined using both p53 wild-type and p53 mutant human GBM cell lines. Our analysis of clinical data indicates that the survival benefit of a combined TMZ and VPA treatment in GBM patients is dependent on their *p53* gene status. In cellular experiments, our results show that VPA enhanced the antineoplastic effect of TMZ by enhancing p53 activation and promoting the expression of its downstream pro-apoptotic protein, PUMA. Our study indicates that GBM patients with wild-type *p53* may benefit from a combined TMZ+VPA treatment.

Keywords: glioblastoma, temozolomide, valproic acid, p53, PUMA, apoptosis

INTRODUCTION

Glioblastoma (GBM), the most common and most lethal type of brain tumor, accounts for 50% of malignancies in the intrinsic central nervous system and has the highest loss of potential life years compared to other cancers (1–3). Standard treatment includes surgical excision and concomitant chemoradiotherapy with temozolomide (TMZ), followed by TMZ chemotherapy. Recent studies in molecular biology have shown that, despite similarities in histological appearances, GBM harbors

significant genetic, epigenetic, and gene expression heterogeneities both interpersonally and intratumorally (4–6). The heterogeneous genetic background of GBM patients results in variable sensitivities of cancer cells to TMZ treatment and, thus, differential clinical outcomes. Hypermethylation at the promoter of O^6-methylguanine DNA methyltransferase (*MGMT*), a DNA repair gene, is associated with increased sensitivity to TMZ treatment and improved patient survival (7–11). Isocitrate dehydrogenase 1 (*IDH1*) mutant GBM patients have more favorable outcomes, partly due to the enhanced sensitivity to TMZ chemotherapy (12, 13). On the other hand, a dysfunctional p53 DNA response pathway is associated with TMZ resistance (10, 14, 15). Previous studies have shown that somatic alterations that deregulate p53 were found in 85%–90% of GBM tumors, including 27.9% of *p53* gene mutations or deletions (16). Furthermore, *p53* mutation often co-occurs with *IDH1* and *ATRX* mutations, which are critical markers defining GBM molecular classification (17, 18). These molecular alterations have significant clinical implications in that they not only define radically different subgroups of GBM but also significantly affect tumor susceptibility to treatment and, thus, patient prognosis (19–21).

Valproic acid (VPA) is an anti-epileptic drug that is widely used to treat or prevent perioperative seizures associated with GBM (22). In addition to its anti-epileptic activity, it has been shown in some retrospective studies that VPA was capable of improving GBM patient survival when given in conjunction with TMZ (23–26). However, the results of these studies are inconsistent. Multiple mechanisms of the anticancer action of VPA have been proposed, including inhibition of histone deacetylase (HDAC), alteration in the chromatin structure, disruption of DNA repair pathways or redox regulation, and induction of autophagy (27–30). Several reports have shown that VPA induces p53-dependent radiosensitization and chemosensitization *in vitro* and *in vivo* (31–34). In the present study, we attempted to identify GBM genetic alterations that are associated with favorable outcomes of VPA treatment in GBM patients and decipher the underlying mechanism. In clinical samples, GBM patient survival with respect to VPA treatment and *p53* gene status was investigated. Furthermore, the effect of TMZ alone or in combination with VPA on GBM cancer cells was examined using both p53 wild-type and p53 mutant human GBM cell lines, and its underlying molecular mechanisms were examined.

MATERIALS AND METHODS

Patient Data Collection

The institutional database of Linkou Chang-Gung Memorial Hospital was used to identify patients who underwent surgical excision of GBM between January 2015 and December 2017 following guidelines approved by the IRB board (IRB# 201701979B0). Patients who underwent standard treatment for newly diagnosed GBM, which included surgical excision, TMZ combined chemoradiotherapy (CCRT), and oral TMZ chemotherapy, and patients who underwent surgical excision for recurrent GBM were included. Patients who underwent biopsy only, did not undergo surgical excision, had a diagnosis based on imaging only, did not have histopathologically proven GBM, and did not undergo standard treatment for newly diagnosed GBM were excluded. A total of 166 patients were recruited. The medical records of these patients were reviewed and followed up until December 31, 2019. Clinical details, including immunohistochemical (IHC) staining of specific markers such as MGMT, the patient's seizure status, date of birth, date of diagnosis, date of operation, and the recorded date of disease progression or death, were recorded. Residual tumor samples were obtained from the tumor bank.

p53 and *IDH1* Mutation Analysis

Genomic DNA was extracted from frozen tissues, exon 4 of *IDH1* and *IDH2* or exons 4–9 of *p53* were PCR amplified from tumor DNA, and mutations were analyzed by sequencing analysis. The primers used in PCR and sequencing are shown in **Table 1**. All mutations were confirmed by sequencing both DNA strands.

Cell Culture and Treatment

The GBM cell lines U87, DBTRG-05MG, U118MG, and LN229 were purchased from ATCC (Manassas, VA, USA). U87 cells were grown in minimum essential medium (MEM) supplemented with 10% fetal bovine serum (FBS) at 37°C in an atmosphere of 5% CO_2. DBTRG-05MG cells were grown in RPMI-1640 supplemented with 10% FBS at 37°C in an atmosphere of 5% CO_2. U118MG and LN229 cells were maintained in Dulbecco's modified Eagle's medium (DMEM) supplemented with 10% FBS at 37°C in an atmosphere of 5% CO_2. The *p53* status of these cell lines was confirmed using DNA

TABLE 1 | The sequencing primers of exon 4 of IDH1 and IDH2 or exon 4-9 of p53.

IDH1 exon 4	Forward: TGAGCTCTATATGCCATCACTGCA Reverse: CAATTTCATACCTTGCTTAATGGG
IDH2 exon 4	Forward: GTCTGGCTGTGTTGTTGCTTG Reverse: CAGAGACAAGAGGATGGCTAGG
p53 exon 4	Forward: TGAGGACCTGGTCCTCTGAC Reverse: AGAGGAATCCCAAAGTTCCA
p53 exons 5–6	Forward: TGTTCACTTGTGCCCTGACT Reverse: TTAACCCCTCCTCCCAGAGA
p53 exon 7	Forward: AGGCACACTGGCCTCATCTT Reverse: TGTGCAGGGTGGCAAGTGGC
p53 exons 8–9	Forward: TTGGGAGTAGATGGAGCCT Reverse: AGTGTTAGACTGGAAACTTT

Sequencing of exon 4 of IDH1 and IDH2 was based on previously described (35) and sequencing of exon 4-9 of the TP53 gene was carried out following the method from IARC TP53 database (R20).

sequencing analysis (**Supplementary Figure S7**). Cells at 70% confluency were washed with phosphate-buffered saline (PBS) and treated with TMZ (0–10 mM) and/or VPA (2.5 mM) in complete culture medium at 37°C in the dark.

RNA Interference

Knockdown of *p53*, *E2F1*, or *HDAC2* in GBM cells by RNA interference with human p53 siRNA (Sigma, St. Louis, MO, USA), E2F1 Silencer Select siRNA (/N4390824; Life Technology Corporation, Carlsbad, CA, USA), or HDAC2 Silencer Select siRNA (AM51331; Life Technology Corporation) was carried out according to the manufacturer's protocol using GenMute siRNA Transfection Reagent (SignaGen Laboratories, Frederick, MD, USA). The sequence of the p53 siRNA targeting p53 mRNA (NM_000546.5) was GACUCCAGUGGUAAUCUAC, and siRNA was synthesized by Sigma (St. Louis, MO, USA). p53 siRNA, E2F1 siRNA, HDAC2 siRNA, or control siRNA was transfected at a final concentration of 30 nM for 24 h, followed by TMZ or VPA treatment as described above. Western blotting and reverse transcription PCR (RT-PCR) analyses were used to verify the efficiency of transfection.

Cell Viability Assay

GBM cells were plated in 96-well culture plates and incubated in a humidified chamber at 37°C and 5% CO_2 overnight before drug treatment. Cell viability was assessed 24 h after the addition of the drugs. The culture medium was then removed from each well and replaced with 150 µl of MTT (3-[4,5-dimethylthiazol-2-yl]-2,5 diphenyl tetrazolium bromide; 0.5 mg/ml) in complete medium. The cells were incubated for 2 h at 37°C. Formazan crystals formed in cells were dissolved in 50 µl of dimethyl sulfoxide (DMSO). The absorbance of the samples at 570 nm was measured using a microplate reader. The results were evaluated by measuring the optical density of the MTT solution at 570 nm.

Western Blot Analysis

The cell lysate was prepared by sonication in RIPA buffer with protease and phosphatase inhibitor cocktails. Proteins (30 µg) were separated by 8%–15% sodium dodecyl sulfate–polyacrylamide gel electrophoresis and transferred to polyvinylidene difluoride membranes, blocked in 5% milk, and incubated overnight at 4°C in primary antibodies including PARP (1:1,000; #9542, Cell Signaling, Danvers, MA, USA), E2F1 (1:1,000; #3742, Cell Signaling, Danvers, MA, USA), p53 (DO-1) (1:1,000;, cat. no. OP43, Calbiochem, San Diego, CA, USA), PUMA (1:1,000; #12450, Cell Signaling, Danvers, MA, USA), caspase 3 (1:1,000; #9662, Cell Signaling, Danvers, MA, USA), and caspase 9 (1:1,000; #9502, Cell Signaling, Danvers, MA, USA), followed by the respective anti-IgG secondary antibodies (1:3,000; Millipore, Burlington, MA, USA) for 1 h at room temperature. Membranes were developed for visualization and photography using enhanced chemiluminescence (ECL) (Millipore Corporation, Billerica, MA, USA). Optical band densities were quantified using ImageJ software, and the results were analyzed using Excel software.

Flow Cytometry Analysis of the Cell Cycle Phases

After harvesting, the cells were washed twice in ice-cold PBS and fixed in ice-cold 70% ethanol for 30 min or overnight at 4°C. The cells were washed in PBS and digested with DNase-free RNase A (50 U/ml) at 37°C for 30 min. Before flow cytometry analysis, the cells were resuspended in 500 µl propidium iodide (PI, 10 µg/ml; Sigma, St. Louis, MO, USA) for DNA staining. PI staining was used to measure the cell cycle status using a Becton-Dickinson FACScan instrument (Franklin Lakes, NJ, USA) and the Cell Quest software.

Quantitative Real-Time RT-PCR

Total RNA was isolated from the harvested cells using the TRIzol® Reagent (Thermo Fisher Scientific, Waltham, MA, USA) and underwent reverse transcription using RevertAid Reverse Transcriptase (Thermo Fisher Scientific) according to the manufacturer's instructions. Subsequent real-time RT-PCR analysis of cDNA was performed in triplicate using SYBR green dye on the StepOnePlus™ Real-Time PCR System (Applied Biosystems, Waltham, MA, USA). The primer sequences are shown as follows (5'–3'): PUMA, CCTGGAGGGTC CTGTACAATCTC; GCAGGCACCTAATTGGGCTC; GAPDH: CCGTCTAGAAAAACCTGCC; GCCAAATTC GTTGTCATACC. To calculate the relative mRNA expression, GAPDH was used as an internal control for all quantitative RT-PCRs and compared with the control groups.

Statistical Analyses

Student's *t*-tests were used to determine statistical significance, and two-tailed *p*-values are shown. A minimum of three independent replicate experiments were performed to justify the use of statistical tests. Survival and progression-free survival were analyzed using Kaplan–Meier survival analysis, and the log-rank test was used for comparisons between two groups. Multivariate analysis was performed using Cox regression analysis. $P < 0.05$ was considered statistically significant. All statistical analyses were performed using SPSS software version 20.0.

RESULTS

TMZ Combined with VPA Is Associated With Improved Survival in GBM Patients With Wild-Type *p53*

To evaluate the effect of VPA on the survival of GBM patients, we retrospectively reviewed patients diagnosed with primary GBM from 2015 to 2017 who underwent curative excisional surgery. Some of these patients underwent more than one surgical excision during these 2 years. For the purpose of analysis, we only included each patient's first operation. The demographic data are shown in **Table 2**. Of all 166 patients, 139 underwent surgery for newly diagnosed GBM and 27 underwent surgery for recurrent tumors. All newly diagnosed GBM patients underwent standard treatment,

TABLE 2 | Patient demographics and clinical characteristics of glioblastoma (GBM) patients.

		VPA treatment				*p*-value
		Short-term (no or <30 days)		Long-term (≥30 days)		
		Count	%	Count	%	
Age (years)	Mean ± SD	58.18 ± 14.61		54.98 ± 14.26		0.854
	<65	76	69.0	41	73.2	0.582
	≥65	34	31.0	15	26.8	
Gender	Male	71	64.5	25	44.6	0.014*
	Female	39	35.5	31	55.4	
Seizure status	Yes	41	37.2	35	62.5	0.002*
	No	69	62.8	21	37.5	
New/recurrent	Newly diagnosed	88	80.0	51	91	0.068
	Recurrent	22	20.0	5	9	

VPA, valproic acid.

**p < 0.05 (the chi-square statistic is significant at the 0.05 level).*

including surgical excision, combined chemoradiotherapy with TMZ, and TMZ chemotherapy. All recurrent GBM patients received avastin treatment after surgical excision. The median survival of all patients combined was 15.20 ± 1.17 months, with 15.67 ± 1.42 months for newly diagnosed patients and 13.10 ± 2.34 months for recurrent GBM patients.

Of these 166 patients, 51 out of 139 newly diagnosed GBM patients and 5 out of 27 recurrent GBM patients had VPA treatment for over 30 days. These patients were classified into the long-term VPA group. Patients who received long-term VPA treatment had significantly longer survival (**Figure 1A**), which is concordant with our previous report (36). Kaplan–Meier survival analyses showed that only long-term VPA treatment was associated with longer overall survival in the combined newly diagnosed and recurrent patients, while younger age (<65 years), seizure history, and long-term VPA treatment were associated with better survival in newly diagnosed GBM patients (**Figure 1B** and **Supplementary Figures S1A–C**). In the Cox regression analysis, none of these factors were independent prognostic factors (**Supplementary Tables S1** and **S2**). We further analyzed the characteristics of patient who underwent VPA treatment and their impact on the effects of VPA treatment. There were significantly more seizure patients and more female patients in the long-term VPA group (**Table 2**). The effect of VPA on median survival in the different groups is shown in **Supplementary Table S3**. Favorable outcomes with VPA treatment were observed in patients with newly diagnosed GBM (**Figure 1B**) and in patients who were under 65 years old (**Figure 1C**), but not in those with recurrent GBM (**Supplementary Figure S1D**) or older patients (≥65 years old) (**Supplementary Figure S1E**). The effect was not affected by the patient's gender or seizure status.

To further elucidate the effects of VPA on GBM subtypes, we examined the IHC staining reports of these patients to identify the expression status of MGMT and study its correlation with the VPA treatment effect. Additionally, we tried to obtain surgical specimens from these patients and evaluated their *IDH1* mutation status. *MGMT* promoter methylation inhibits DNA repair gene expression and is significantly associated with improved patient survival and TMZ sensitivity. Of the 166 patients recruited, IHC staining was available in 92 patients. No correlation was found between the expression of MGMT determined by IHC and patient survival (**Supplementary Figure S2**). Additionally, VPA treatment did not result in a statistically significant overall survival benefit in either MGMT staining-positive or MGMT staining-negative patients (**Supplementary Figure S3**), although there appears to be a trend toward better survival in long-term VPA-treated MGMT staining-negative newly diagnosed GBM patients (**Supplementary Figure S3E**).

Since several previous studies have indicated that VPA affects tumor growth *via* p53-dependent pathways (31–34), we also checked the *p53* mutation status in these tissue samples. We were able to obtain 85 tumor tissue samples from these GBM patients. The demographic data and gene analysis results are shown in **Table 3**. The majority of these samples were *IDH1* wild type, *IDH2* wild type, and *p53* wild type. Ten samples out of these 85 had $IDH1^{R132}$ mutations, while none had *IDH2* mutations. Of the *p53* mutations identified in 11 tumors, 10 were missense mutations and one was a nonsense mutation, and all of them were identified as p53-inactivating mutations in the IARC TP53 database (R20) (37) (**Supplementary Table S4** and **Supplementary Figure S4**). The mutational status of *p53* was not significantly associated with the overall survival or progression-free survival of either newly diagnosed or recurrent GBM patients (**Supplementary Figure S5**). Further analysis revealed that VPA treatment is associated with improved survival in GBM patients who were under 65 years old and had newly diagnosed *IDH* wild-type and *p53* wild-type GBM (**Figure 1D**), but not in patients who were under 65 years old and had newly diagnosed *IDH* wild-type and *p53* mutant GBM, patients who were older than 65 years with newly diagnosed *IDH* wild-type GBM, and patients with newly diagnosed *IDH* mutant GBM, with recurrent GBM regardless of the *p53* or *IDH* mutational status, and with *p53* mutant or *IDH* mutant GBM regardless of age or recurrence status (**Supplementary Figure S6**).

In conclusion, our results indicate that the survival benefit of VPA in GBM patients may be dependent on the patient's age,

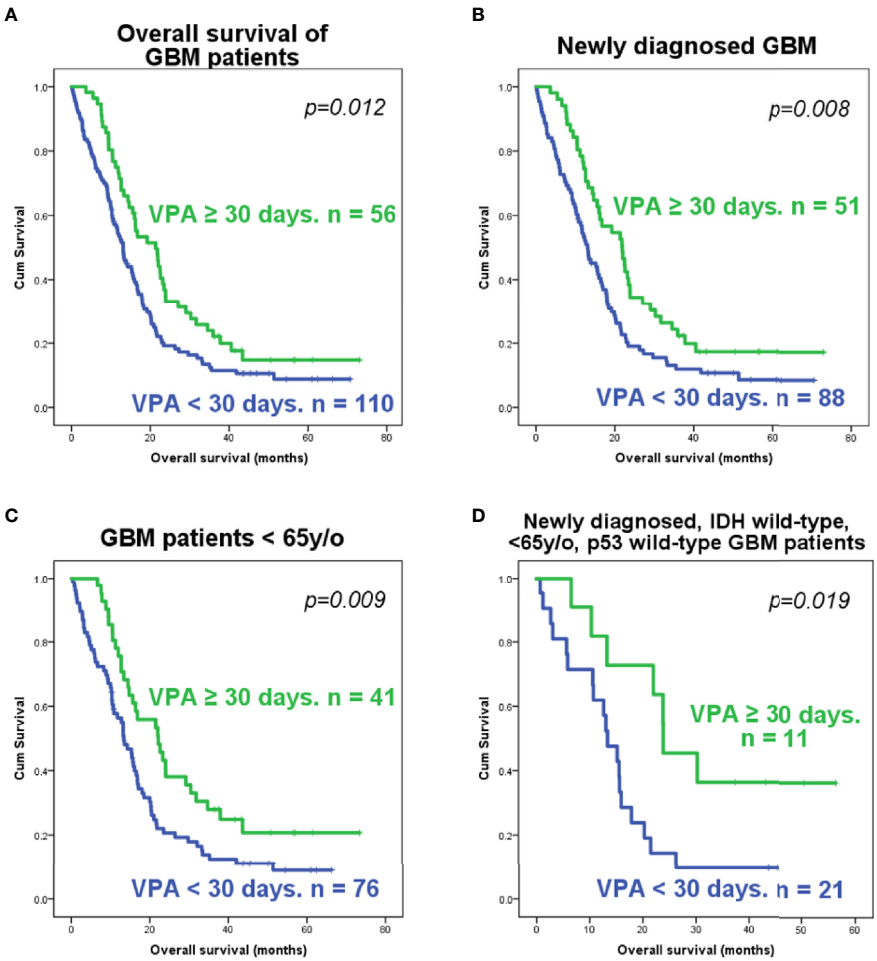

FIGURE 1 | Kaplan–Meier analysis of the survival of glioblastoma (GBM) patients according to the valproic acid (VPA) treatment group. Survival plots of all GBM patients **(A)**, newly diagnosed GBM patients **(B)**, younger GBM patients (<65 years old) **(C)**, and younger (<65 years old), newly diagnosed GBM patients with wild-type *IDH1* and wild-type *p53* **(D)**. The *p*-value was calculated using the log-rank test in SPSS software.

IDH mutation status, and *p53* mutation status. Long-term VPA treatment may confer some degree of survival benefit in newly diagnosed and *p53* wild-type GBM patients who are under 65 years old.

VPA Treatment Enhanced TMZ-Induced Cytotoxicity in GBM Cancer Cells in a p53-Dependent Manner

Since the survival benefit of TMZ combined with VPA treatment was observed in newly diagnosed GBM patients with wild-type *p53* (**Figure 1D**), we hypothesize that VPA may exert its pro-survival effect by enhancing the anticancer activity of TMZ dependent on the *p53* gene status. To determine whether VPA enhances the TMZ-mediated inhibition of GBM cancer cell proliferation and whether *p53* mutation affects susceptibility to GBM, we examined the effect of TMZ alone or in combination with VPA on GBM cancer cell lines with varying p53 status. We found that co-treatment with VPA enhanced the growth inhibitory effect of TMZ in p53 wild-type GBM cells U87 and DBTRG-05MG, but did not significantly affect the growth of p53 mutant GBM cells LN229 and U118MG (**Figures 2A, B** and **Supplementary Figure S7**). This is consistent with the cell cycle analysis showing that combined treatment with TMZ and VPA increased the sub-G1 population in U87 and DBTRG-05MG cells (**Figures 2C, D**), indicating enhanced cellular apoptosis. The effect was not apparent in LN229 and U118MG cells (**Figures 2E, F**). Western blotting analysis confirmed that VPA treatment significantly increased caspase 3 and caspase 9 cleavage in U87 and DBTRG-05MG cells and increased the expression of PUMA, a pro-apoptotic protein downstream of p53 activation, as measured 24 h after TMZ treatment, but not in LN229 and U118MG cells (**Figures 3A, B** and **Supplementary Figure S8**). These results suggest that, in TMZ-induced genotoxic events, VPA increased TMZ cytotoxicity by activating p53 and enhancing the expression of PUMA. To

TABLE 3 | Patient demographics and clinical characteristics of 85 glioblastoma (GBM) patients whose tumor samples underwent genetic evaluation.

		VPA treatment				*p*-value
		Short-term (no or <30 days)		Long-term (≥30 days)		
		Count	%	Count	%	
Age (years)	Mean ± SD					
	<65	42	68.9	21	87.5	0.101[a]
	≥65	19	31.1	3	12.5	
Gender	Male	38	62.3	12	44.6	0.335
	Female	23	37.7	12	50.0	
Seizure status	Yes	21	34.4	18	75.0	0.001*
	No	40	65.6	6	25.0	
New/recurrent	Newly diagnosed	45	73.8	20	83.3	0.409[a]
	Recurrent	16	26.2	4	16.7	
Mutation status	*IDH1* mutant	6	9.8	4	16.7	0.458
	IDH2 mutant	0	0	0	0	0.496
	p53 mutant	7	11.5	4	16.7	0.496

VPA, valproic acid.
**p < 0.05 (the chi-square statistic is significant at the 0.05 level).*
[a]Fisher's exact test.

further validate the role of p53 in VPA-induced apoptosis in combination with TMZ, we knocked down *p53* in the U87 and DBTRG-05MG cell lines and evaluated the activation of the apoptosis pathway and the expression of PUMA in response to TMZ or VPA treatment. Knockdown of *p53* expression in both cell lines significantly reduced the activation of the apoptotic pathway, as measured by caspase 9 and caspase 3 activation and enhanced PUMA expression (**Figures 3C, D**). In conclusion, our results show that the effect of VPA on GBM cancer cell proliferation is p53-dependent and that VPA enhances TMZ-induced apoptosis by promoting the expression of *PUMA*, a pro-apoptotic gene downstream of p53.

Neither *E2F1* nor *HDAC2* Further Enhanced TMZ-VPA-Induced Apoptosis in p53 Wild-Type GBM Cells

We tried to further delineate the mechanisms by which VPA enhanced p53 downstream *PUMA* expression. Previous studies have shown that abundant crosstalk exists between the p53 and E2F1 pathways (38). In genotoxic events, there is extensive crosstalk between the MDM2–p53 and Rb–E2F1 pathways, which cooperate to initiate apoptosis. We found that the expression of *E2F1* was decreased in response to TMZ or TMZ +VPA treatment after *p53* knockdown (**Figures 3C, D**). However, *E2F1* knockdown did not affect the activation of the apoptosis pathway or the expression of PUMA induced by VPA +TMZ treatment (**Supplementary Figure S9**). The results suggest that *E2F1* activation was modulated by p53 activation, but was not necessary for TMZ+VPA to exert its pro-apoptotic function. Additionally, several studies indicated that the degradation of HDAC2 is one of the anticancer actions of VPA (28, 39) and that knockdown of *HDAC2* enhances the sensitivity of GBM cancer cells to TMZ (40). Therefore, we examined the expression and the effect of HDAC2 on the apoptosis-enhancing ability of VPA+TMZ treatment. We found that HDAC2 expression did not decrease after VPA treatment for 24 h alone or in combination with TMZ (**Figures 4A, B**). Additionally, knockdown of *HDAC2* did not abrogate but further enhanced the pro-apoptotic effect of VPA +TMZ co-treatment in either p53 wild-type GBM cell line, as inferred from the increased PARP cleavage and caspase 9 and caspase 3 activation (**Figures 4A, B**). A synergistic effect was not observed in either p53 mutant GBM cell line (**Figures 4C, D**). Interestingly, knockdown of *HDAC2* in LN229 and U118MG p53 mutant cells induced cellular apoptosis without TMZ or VPA treatment (**Figures 4C, D**). Our results indicate that VPA may not exert its effect by inhibiting E2F1 activation or HDAC2 activity/expression. HDAC2 inhibition may induce apoptosis in p53 mutant cells *via* other signaling pathways.

DISCUSSION

Glioblastoma (GBM) has been shown to harbor great genetic, epigenetic, and gene expression heterogeneities in both interpersonal and intratumor tissues (4–6, 41). GBM arises *de novo* (primary GBM) or *via* the dedifferentiation of lower-grade glioma (secondary GBM) (42). While distinct mutations are predominant in each subtype, alterations of the tumor suppressor *p53* are the most common (43). These molecular alterations of GBM significantly affect tumor susceptibility to chemotherapy and, thus, patient prognosis (19–21). It has been shown that the expressions of p53 in newly diagnosed and recurrent GBM patients are inconsistent and can be altered upon recurrence (44, 45). Whether *p53* mutation affects GBM sensitivity to chemotherapy and prognosis remains controversial (46–49). In this study, our results indicate that VPA enhances TMZ cytotoxicity by promoting apoptosis through enhancing p53 pathway activation and increasing the expression of its

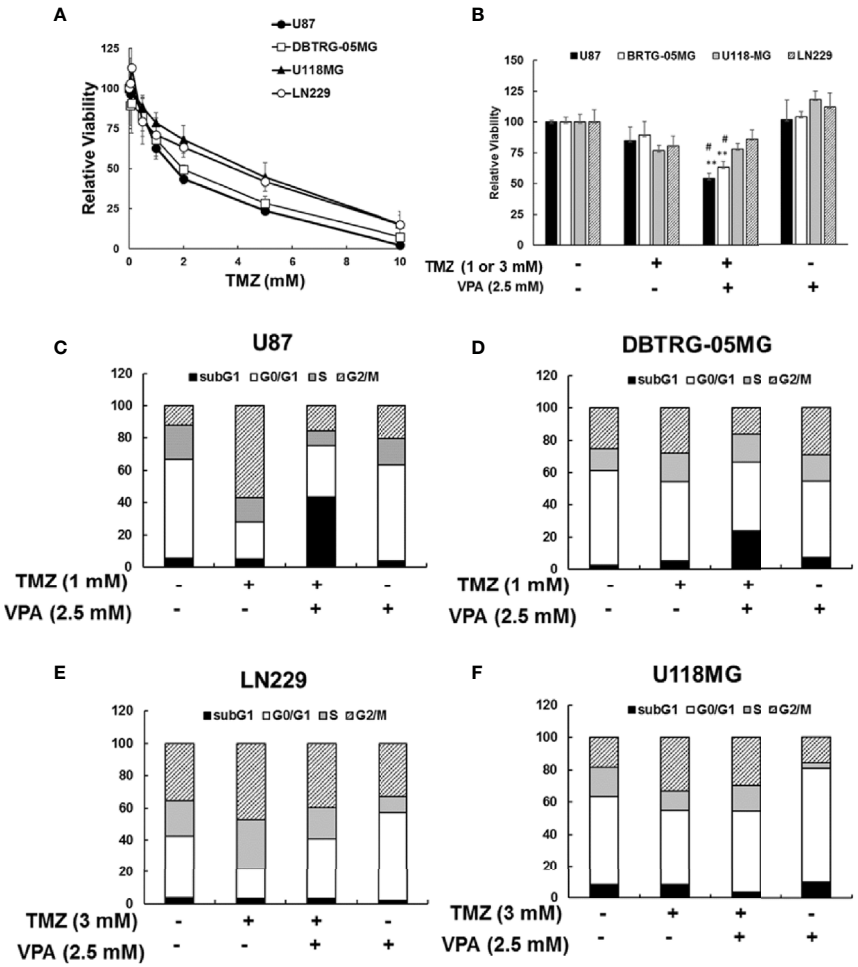

FIGURE 2 | Cytotoxicity of temozolomide (TMZ) without or with valproic acid (VPA) in glioblastoma (GBM) cell lines. **(A)** Cytotoxicity of different dosages of TMZ (0–10 mM) for 24 h in p53 wild-type GBM cells (U87 and DBTRG-05MG) and p53 mutant GBM cells (U118MG and LN229). **(B)** Cytotoxicity of TMZ (1 or 3 mM) combined with VPA (2.5 mM) for 24 h in p53 wild-type GBM cells (U87 and DBTRG-05MG) and p53 mutant GBM cells (U118MG and LN229). Cytotoxicity was analyzed using the MTT assay, as described in *Materials and Methods*. Data are the mean ± SD. $^{**}p < 0.01$ compared with cells without TMZ or VPA treatment; $^{\#}p < 0.05$ compared with cells with TMZ treatment. **(C, D)** Cell cycle analysis of TMZ (1 mM) combined with VPA (2.5 mM) for 24 h in p53 wild-type GBM cells (U87 and DBTRG-05MG). **(E, F)** Cell cycle analysis of TMZ (3 mM) combined with VPA (2.5 mM) for 24 h in p53 mutant GBM cells (U118MG and LN229). Cell cycle was analyzed using propidium iodide (PI) staining with flow cytometry, as described in *Materials and Methods*.

downstream target gene, *PUMA*. Wild-type p53 expression in GBM cells is necessary for VPA to exert its function. Screening of *p53* mutations may help identify GBM patients who will benefit from a combined VPA and TMZ treatment.

The life expectancy of GBM patients is 12–18 months, despite advances in diagnosis and treatment (50–52). Several known prognostic factors include age, preoperative functional status, history of seizure, tumor location and size, extent of surgery, use of radiotherapy, and *IDH* mutation (52–56). In our study, the median survival of newly diagnosed GBM patients was 15.67 ± 1.42 months. Younger age (<65 years), seizure history, and long-term VPA treatment (>30 days) were associated with favorable outcomes (**Supplementary Figures S1A, C** and **Figure 1A**). The results are roughly concordant with other studies (52, 54). On the other hand, the median survival of recurrent GBM patients was 13.10 ± 2.34 months, which was not significantly different from that of newly diagnosed patients ($p = 0.300$). Since all our recurrent GBM patients underwent surgical excision, it is likely that the included patients were in better physical condition capable of undergoing surgery and had tumors that were presumably located at favorable locations suited for surgical intervention, thus improving the results. When combining newly diagnosed and recurrent GBM patients, only VPA treatment was statistically significantly associated with improved survival (**Figure 1A**).

VPA is used to treat seizures in our hospital. Although it has been shown that long-term use of anticonvulsants in seizure-free patients adds no clinical benefits (57, 58), some physicians in our institute were used to keeping anticonvulsants for patients who had symptoms suspicious of complex partial seizures or absence

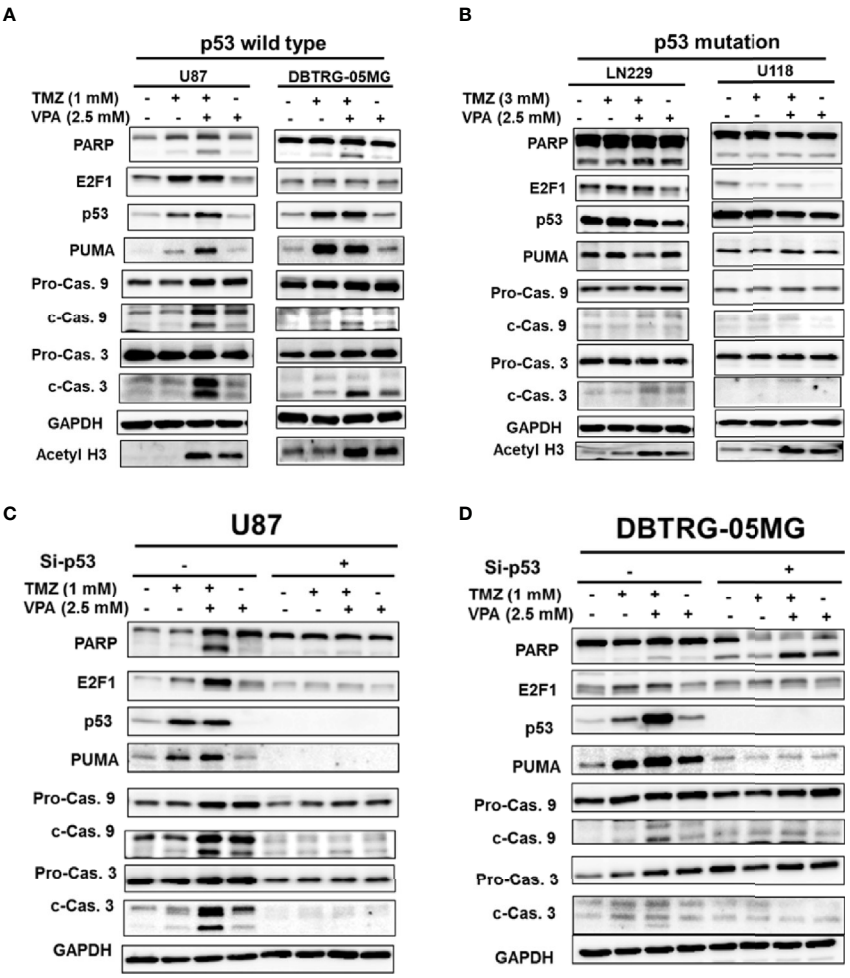

FIGURE 3 | Temozolomide (TMZ) combined with valproic acid (VPA) enhanced cellular apoptosis through the p53–PUMA pathway in GBM cell lines. Western blot analysis of apoptosis (PARP, cleavage of caspase 9 and caspase 3), *E2F1*, *p53*, and *PUMA*, a downstream target of p53, in p53 wild-type GBM cells (U87 and DBTRG-05MG) **(A)** and p53 mutant GBM cells (U118MG and LN229) **(B)**. p53 wild-type GBM cells (U87 and DBTRG-05MG) were treated with TMZ (1 mM), VPA (2.5 mM), or TMZ (1 mM) combined with VPA (2.5 mM) for 24 h, and p53 mutant GBM cells (U118MG and LN229) were treated with TMZ (3 mM), VPA (2.5 mM), or TMZ (3 mM) combined with VPA (2.5 mM) for 24 h. **(C, D)** Western blot analysis of apoptosis (PARP, cleavage of caspase 9 and caspase 3), E2F1, p53, and PUMA, a downstream target of p53, in U87 and DBTRG-05MG cells after the knockdown of *p53* with siRNA (Si-p53) followed by TMZ or VPA treatment, as described above. Note that the knockdown of *p53* reduced the apoptosis induced by TMZ combined with VPA in p53 wild-type cell lines.

of seizures until the diagnosis was excluded. Therefore, in our dataset, there were some patients who had no definite seizure diagnosis, but who received VPA for more than 1 month (**Table 2**). Although long-term VPA treatment was associated with improved survival in the single variate analysis (**Figure 1A**), multivariate Cox regression analysis did not indicate VPA use as an independent prognostic factor (**Supplementary Tables S1** and **S2**). Since VPA is used to treat seizures, which in itself is a favorable prognostic factor, evaluation of the VPA effect on the survival of GBM patient is confounded by the presence of seizures. Furthermore, there appeared to be more female patients in our long-term VPA group (**Table 2**). Gender alone does not affect treatments given to patients in our hospital. Although our seizure treatment did not differentiate between males or females, it was not shown in our study that gender significantly affected the results of GBM survival or VPA treatment (**Supplementary Figure S1B**), which indicates that there may be some degree of selection bias in our dataset. Further analysis indicated that VPA treatment appeared to be effective in newly diagnosed GBM patients and in younger patients (**Figures 1B, C**), but not in recurrent GBM or in patients over 65 years old (**Supplementary Figures S1D, E**). This result is also concordant with previous studies (59, 60). Interestingly, in our analysis, the benefit of long-term VPA treatment did not reach statistical significance in either the seizure or no-seizure group but in the combined group (**Supplementary Table S3**), indicating that the presence or absence of seizures does not significantly impact the effect of VPA. Kuo et al. reported that

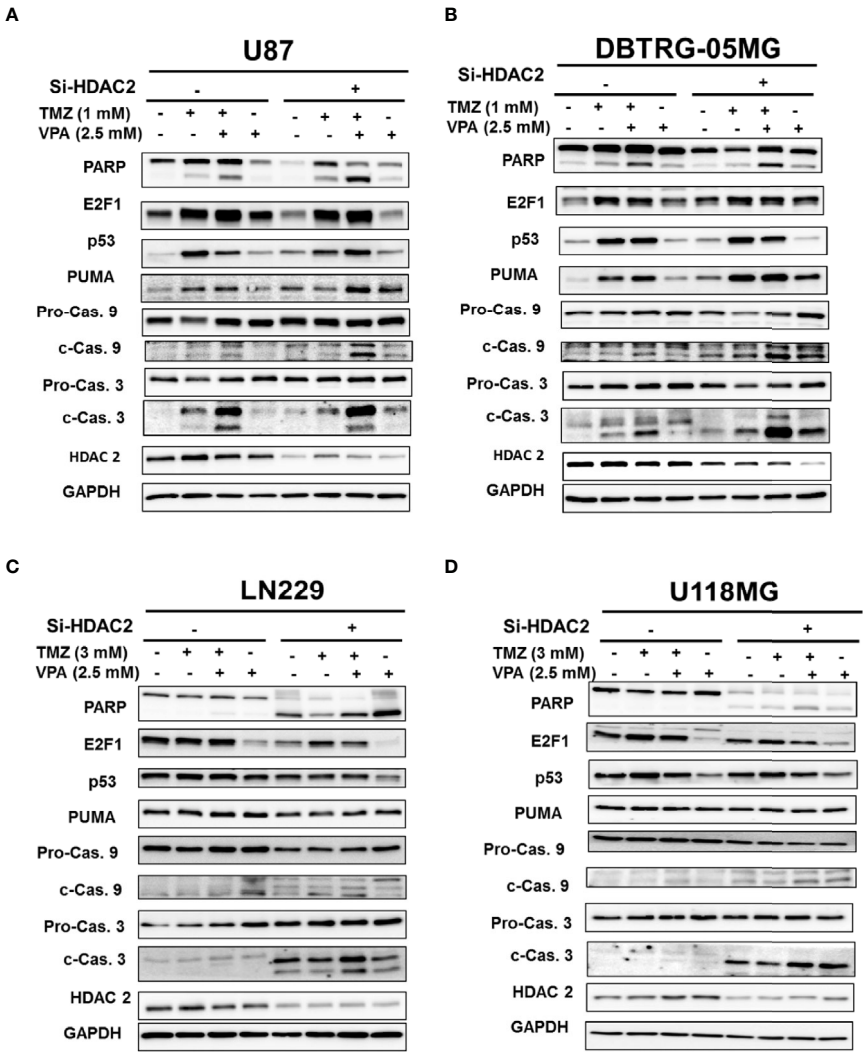

FIGURE 4 | Knockdown of *HDAC2* further enhanced the apoptosis pathway induced by temozolomide (TMZ) combined with valproic acid (VPA) in p53 wild-type cell lines. **(A)** Western blot analysis of apoptosis (PARP, cleavage of caspase 9 and caspase 3), E2F1, p53, and PUMA, a downstream target of p53, in p53 wild-type GBM cells, U87 **(A)** and DBTRG-05MG **(B)**, and in p53 mutant GBM cells, LN229 **(C)** and U118MG **(D)**, after the knockdown of *HDAC2* with siRNA (Si-HDAC2) followed by TMZ or VPA treatment, as described below. p53 wild-type GBM cells (U87 and DBTRG-05MG) were treated with TMZ (1 mM), VPA (2.5 mM), or TMZ (1 mM) combined with VPA (2.5 mM) for 24 h, and p53 mutant GBM cells (U118MG and LN229) were treated with TMZ (3 mM), VPA (2.5 mM), or TMZ (3 mM) combined with VPA (2.5 mM) for 24 h. Note that the knockdown of *HDAC2* induced cellular apoptosis in p53 mutant GBM cells.

VPA does not improve survival in patients who are seizure-free (59). This discrepancy is likely caused by our small sample size and the patient variability and requires further investigation.

The *MGMT* promoter methylation status has long been recognized as a prognostic factor of GBM patient survival (61, 62). However, it was not routinely examined in our hospital because the test was not covered by our National Health Insurance program. The Clinical Pathology Department in our institute used IHC staining to detect MGMT expression, which is known to have low specificity and undetermined thresholds and may not have a strong correlation with the outcomes of GBM patients (63–65). In this study, we did not have enough resources or patient samples to perform methylation-specific PCR. Our analysis did not demonstrate a survival benefit in either MGMT staining-positive or MGMT staining-negative patients (**Supplementary Figure S2**). We also did not detect a pro-survival effect of VPA treatment in either MGMT staining-positive or MGMT staining-negative patients (**Supplementary Figures S3A, D**). In newly diagnosed MGMT-negative GBM patients, there appeared to be a trend toward improved survival in the long-term VPA treatment group, but this trend did not reach statistical significance ($p = 0.052$) (**Supplementary Figure S3E**). Interestingly, there are some reports indicating that VPA may enhance TMZ sensitivity by downregulating MGMT expression (30). Roos et al. reported that

GBM cells with functionally intact *p53* genes were more sensitive to TMZ treatment due to the activation of the Fas/CD95/APO-1 receptor and the subsequent apoptosis triggered by O^6-methylguanine, a product of TMZ-induced DNA damage (66). Further studies evaluating the effect of *MGMT* promoter methylation on VPA treatment and its interaction with the p53 pathway may help better identify VPA-responsive patients. In conclusion, our data indicate a possible survival benefit of prolonged VPA treatment in younger, newly diagnosed GBM patients.

The molecular alterations of GBM have been shown to significantly affect tumor susceptibility to chemotherapy and, thus, patient prognosis (19–21). In this study, *p53* mutation was detected in 11 out of the 85 patients sampled. The mutational status of *p53* did not significantly affect patient survival (**Supplementary Figure S5**), which is concordant with previous studies (67). We also found that TMZ combined with long-term VPA treatment was effective in GBM patients with wild-type *p53* (**Figure 1D**). Additionally, genetic alterations affecting the function of the p53 pathway, such as CDKN2A/ARF deletion or MDM2/MDM4 amplification, could be present in ~85% of all GBM patients (16) and had similar effects on the pro-survival effect of VPA treatment. Whether these genetic alterations that impair the p53 pathway activation affect VPA-induced TMZ potentiation requires further study. Since only 11 *p53* mutant samples were identified (**Table 3**), the study may be limited by its small sample size, patient heterogeneity, and possible selection bias. However, we were able to demonstrate that VPA enhances TMZ cytotoxicity by enhancing apoptosis *via* the p53 pathway and the expression of the downstream target, *PUMA* (**Figures 3A, B** and **Supplementary Figure S8**) using p53 wild-type and p53 mutant human GBM cells.

p53 is commonly activated in response to DNA damage, genotoxicity, oncogene activation, aberrant growth signals, and hypoxia, all of which are events that can be encountered during carcinogenesis (48). p53 upregulated modulator of apoptosis (PUMA), a Bcl-2 homology 3 (BH3)-only pro-apoptotic Bcl-2 family member, was identified as a molecule that directly mediates p53-associated apoptosis (68). The PUMA protein associates with the mitochondria and induces apoptosis much earlier than the apoptosis that results from the exogenous expression of p53 when it is overexpressed in various cell lines (69). Previous studies have shown that PUMA overexpression results in massive apoptosis in GBM cells with wild-type or mutant p53, indicating that it is a therapeutic tool for GBM (70). Additionally, PUMA has been shown to increase the drug sensitivity of TMZ-resistant cells; thus, PUMA may be a suitable target for intervention to improve the therapeutic efficacy of TMZ (71). Here, we found that PUMA was further induced in p53 wild-type GBM cells, U87 cells, and DBTRG-05MG cells (**Figure 3A**). In our study, TMZ treatment induced p53 activation and apoptosis in p53 wild-type GBM cells, which was further enhanced by VPA treatment. For the *in vitro* experiments with GBM cells, we used TMZ at concentrations of 1 and 3 mM, based roughly on the IC_{50} at 24 h (**Figure 2**). This TMZ concentration induces cell death mainly *via* non-repaired *N*-alkylations, while for O^6-methylguanine-induced apoptosis, much lower doses are sufficient, which are in the range of 1–50 μM (72). Under clinical conditions, the tissue concentration of TMZ is approximately 1 μg/ml (5.2 μM) and the serum concentration about 15 μg/ml (78 μM) (73, 74). In this concentration range, the main treatment effect is achieved *via* O^6-methylguanine-induced DNA double-strand breaks and subsequent apoptosis. Whether the findings reported here are clinically relevant requires further elucidation. Additionally, there were some inconsistent reports of *p53* gene activity in LN229 cells (75, 76). The majority agrees that LN229 retains at least partial p53 activity despite the mutation. In our study, we did find a missense mutation at exon 4. Treatment with TMZ failed to induce PUMA expression in LN229 cells (**Figure 3B**), suggesting at least a possible partial loss of p53 function. We also demonstrated that the knockdown of *p53* abrogated the expression of PUMA and the cleavage of caspase 9, caspase 3, and PARP in p53 wild-type GBM cells treated with TMZ+VPA (**Figures 3C, D**) and reversed the pro-apoptotic effect of VPA in TMZ treatment, indicating that VPA enhanced TMZ-induced cell apoptosis *via* p53–PUMA pathway activation.

Several mechanisms for the anticancer effect of VPA have been proposed, including inhibition of HDAC, alteration of the chromatin structure, disruption of DNA repair pathways or redox regulation, and induction of autophagy (11, 27–30). Xie et al. reported that VPA attenuates the immunosuppressive function of myeloid-derived suppressor cells and may potentially improve the antitumor activity of $CD8^+$ T cells (77). In malignant melanoma cells, VPA was shown to enhance IFN-β-induced caspase 8 expression, thus improving its response to TMZ treatment (78). In murine limb organogenesis, VPA was shown to induce p53 hyperacetylation through its HDAC inhibitor activity, thus enhancing p53 target gene expression (79). Among these mechanisms, VPA, as an HDAC inhibitor, has been widely recognized. It induces HDAC2 degradation and inhibits HDAC2 activity (28, 39). However, our results did not show a reduction in HDAC2 expression subsequent to VPA treatment (**Figure 4**). Knockdown of HDAC2 further enhanced TMZ+VPA-induced cellular apoptosis in p53 wild-type GBM cells (**Figures 4A, B**). Interestingly, HDAC2 silencing induced cellular apoptosis in p53 mutant GBM cells (**Figures 4C, D**), which is consistent with previous studies showing that silencing *HDAC2* can suppress the proliferation of GBM cells (40). On the other hand, several potent HDAC inhibitors that entered clinical trials in recent years, such as vorinostat (SAHA) or trichostatin A (TSA), failed to demonstrate a significant survival benefit to patients in phase II clinical trials, either as single agents or in combination with standard TMZ treatment (80–82). This is consistent with our results that only VPA, but not SAHA or TSA, enhanced TMZ-induced apoptosis in U87 cells (**Supplementary Figure S10**). These results together suggest that VPA may not exert its effect by inhibiting HDAC2 activity or expression, and HDAC2 inhibition may potentiate the effect *via* other signaling pathways.

CONCLUSION

Our results indicate that the survival benefit of the combination regimen of TMZ and VPA in GBM patients is dependent on their *p53* mutation status. In cellular models, our results show that VPA enhanced the antineoplastic effect of TMZ by enhancing apoptosis *via* activation of the p53 pathway and increasing the expression of its downstream pro-apoptotic protein, PUMA. Taken together, wild-type *p53* may serve as an indicator of the effectiveness of a combined TMZ+VPA treatment in GBM.

DATA AVAILABILITY STATEMENT

The original contributions presented in the study are included in the article/**Supplementary Material**. Further inquiries can be directed to the corresponding author.

ETHICS STATEMENT

The studies involving human participants were reviewed and approved by Institutional Review Board of Chang-Gung Medical Foundation (IRB#: 201701979B0). Written informed consent for participation was not required for this study in accordance with the national legislation and the institutional requirements.

AUTHOR CONTRIBUTIONS

H-CT, K-CW, and H-TW designed, performed research, and analyzed data. H-CT, K-CW, P-YC, C-YH, K-TC, Y-JL, and Y-RC recruited, collected clinical specimens, and analyzed clinical data. H-CT and H-WC performed the experiments. H-CT and H-TW wrote the paper. All authors contributed to the article and approved the submitted version.

FUNDING

This work was funded by grants from the Ministry of Science and Technology, Taiwan [NHRI-EX110-11027PI, 109-2320-B-010-024 (H-TW) and 107-2320-B-182-044 (H-CT)], and Chang-Gung Memorial Hospital [CMRPG3K1441 (H-CT)].

ACKNOWLEDGMENTS

The authors thank all members of the Brain Tumor Team, Cancer Center, Chang-Gung Memorial Hospital, Linkou, and the Neuroscience Research Center of Chang Gung Memorial Hospital, Linkou, for their invaluable help.

SUPPLEMENTARY MATERIAL

The Supplementary Material for this article can be found online at: https://www.frontiersin.org/articles/10.3389/fonc.2021.722754/full#supplementary-material

REFERENCES

1. Louis DN, Ohgaki H, Wiestler OD, Cavenee WK, Burger PC, Jouvet A, et al. The 2007 WHO Classification of Tumours of the Central Nervous System. *Acta Neuropathol* (2007) 114(2):97–109. doi: 10.1007/s00401-007-0243-4
2. Ostrom QT, Gittleman H, Xu J, Kromer C, Wolinsky Y, Kruchko C, et al. CBTRUS Statistical Report: Primary Brain and Other Central Nervous System Tumors Diagnosed in the United States in 2009-2013. *Neuro Oncol* (2016) 18 (suppl_5):v1–75. doi: 10.1093/neuonc/now207
3. Rouse C, Gittleman H, Ostrom QT, Kruchko C, Barnholtz-Sloan JS. Years of Potential Life Lost for Brain and CNS Tumors Relative to Other Cancers in Adults in the United States, 2010. *Neuro Oncol* (2016) 18(1):70–7. doi: 10.1093/neuonc/nov249
4. Soeda A, Hara A, Kunisada T, Yoshimura S, Iwama T, Park DM. The Evidence of Glioblastoma Heterogeneity. *Sci Rep* (2015) 5:7979. doi: 10.1038/srep07979
5. Sottoriva A, Spiteri I, Piccirillo SG, Touloumis A, Collins VP, Marioni JC, et al. Intratumor Heterogeneity in Human Glioblastoma Reflects Cancer Evolutionary Dynamics. *Proc Natl Acad Sci U S A* (2013) 110(10):4009–14. doi: 10.1073/pnas.1219747110
6. Verhaak RG, Hoadley KA, Purdom E, Wang V, Qi Y, Wilkerson MD, et al. Integrated Genomic Analysis Identifies Clinically Relevant Subtypes of Glioblastoma Characterized by Abnormalities in PDGFRA, IDH1, EGFR, and NF1. *Cancer Cell* (2010) 17(1):98–110. doi: 10.1016/j.ccr.2009.12.020
7. Hegi ME, Diserens AC, Gorlia T, Hamou MF, de Tribolet N, Weller M, et al. MGMT Gene Silencing and Benefit From Temozolomide in Glioblastoma. *N Engl J Med* (2005) 352(10):997–1003. doi: 10.1056/NEJMoa043331
8. Fan CH, Liu WL, Cao H, Wen C, Chen L, Jiang G. O6-Methylguanine DNA Methyltransferase as a Promising Target for the Treatment of Temozolomide-Resistant Gliomas. *Cell Death Dis* (2013) 4:e876. doi: 10.1038/cddis.2013.388
9. Agnihotri S, Gajadhar AS, Ternamian C, Gorlia T, Diefes KL, Mischel PS, et al. Alkylpurine-DNA-N-Glycosylase Confers Resistance to Temozolomide in Xenograft Models of Glioblastoma Multiforme and is Associated With Poor Survival in Patients. *J Clin Invest* (2012) 122(1):253–66. doi: 10.1172/JCI59334
10. Bocangel DB, Finkelstein S, Schold SC, Bhakat KK, Mitra S, Kokkinakis DM. Multifaceted Resistance of Gliomas to Temozolomide. *Clin Cancer Res* (2002) 8(8):2725–34.
11. Chen CH, Chang YJ, Ku MS, Chung KT, Yang JT. Enhancement of Temozolomide-Induced Apoptosis by Valproic Acid in Human Glioma Cell Lines Through Redox Regulation. *J Mol Med (Berl)* (2011) 89(3):303–15. doi: 10.1007/s00109-010-0707-1
12. Lin L, Cai J, Tan Z, Meng X, Li R, Li Y, et al. Mutant IDH1 Enhances Temozolomide Sensitivity *via* Regulation of the ATM/CHK2 Pathway in Glioma. *Cancer Res Treat* (2021) 53(2):367–77. doi: 10.4143/crt.2020.506
13. Lu Y, Kwintkiewicz J, Liu Y, Tech K, Frady LN, Su YT, et al. Chemosensitivity of IDH1-Mutated Gliomas Due to an Impairment in PARP1-Mediated DNA Repair. *Cancer Res* (2017) 77(7):1709–18. doi: 10.1158/0008-5472.CAN-16-2773
14. Lee SY. Temozolomide Resistance in Glioblastoma Multiforme. *Genes Dis* (2016) 3(3):198–210. doi: 10.1016/j.gendis.2016.04.007
15. Forte IM, Indovina P, Iannuzzi CA, Cirillo D, Di Marzo D, Barone D, et al. Targeted Therapy Based on P53 Reactivation Reduces Both Glioblastoma Cell Growth and Resistance to Temozolomide. *Int J Oncol* (2019) 54(6):2189–99. doi: 10.3892/ijo.2019.4788
16. Brennan CW, Verhaak RG, McKenna A, Campos B, Noushmehr H, Salama SR, et al. The Somatic Genomic Landscape of Glioblastoma. *Cell* (2013) 155 (2):462–77. doi: 10.1016/j.cell.2013.09.034
17. Kloosterhof NK, Bralten LB, Dubbink HJ, French PJ, van den Bent MJ. Isocitrate Dehydrogenase-1 Mutations: A Fundamentally New Understanding

of Diffuse Glioma? [Review]. *Lancet Oncol* (2011) 12(1):83–91. doi: 10.1016/S1470-2045(10)70053-X
18. Donehower LA, Soussi T, Korkut A, Liu Y, Schultz A, Cardenas M, et al. Integrated Analysis of TP53 Gene and Pathway Alterations in The Cancer Genome Atlas. *Cell Rep* (2019) 28(5):1370–84.e5. doi: 10.1016/j.celrep.2019.07.001
19. Weller M, Stupp R, Reifenberger G, Brandes AA, van den Bent MJ, Wick W, et al. MGMT Promoter Methylation in Malignant Gliomas: Ready for Personalized Medicine? *Nat Rev Neurol* (2010) (1):39–51. doi: 10.1038/nrneurol.2009.197
20. Szopa W, Burley TA, Kramer-Marek G, Kaspera W. Diagnostic and Therapeutic Biomarkers in Glioblastoma: Current Status and Future Perspectives. *BioMed Res Int* (2017) 2017:8013575. doi: 10.1155/2017/8013575
21. Eckel-Passow JE, Lachance DH, Molinaro AM, Walsh KM, Decker PA, Sicotte H, et al. Glioma Groups Based on 1p/19q, IDH, and TERT Promoter Mutations in Tumors. *N Engl J Med* (2015) 372(26):2499–508. doi: 10.1056/NEJMoa1407279
22. Loscher W. Basic Pharmacology of Valproate: A Review After 35 Years of Clinical Use for the Treatment of Epilepsy. *CNS Drugs* (2002) 16(10):669–94. doi: 10.2165/00023210-200216100-00003
23. Ochiai S, Nomoto Y, Yamashita Y, Watanabe Y, Toyomasu Y, Kawamura T, et al. Roles of Valproic Acid in Improving Radiation Therapy for Glioblastoma: A Review of Literature Focusing on Clinical Evidence. *Asian Pac J Cancer Prev* (2016) 17(2):463–6. doi: 10.7314/APJCP.2016.17.2.463
24. Yuan Y, Xiang W, Qing M, Yanhui L, Jiewen L, Yunhe M. Survival Analysis for Valproic Acid Use in Adult Glioblastoma Multiforme: A Meta-Analysis of Individual Patient Data and a Systematic Review. *Seizure* (2014) 23(10):830–5. doi: 10.1016/j.seizure.2014.06.015
25. Kerkhof M, Dielemans JC, van Breemen MS, Zwinkels H, Walchenbach R, Taphoorn MJ, et al. Effect of Valproic Acid on Seizure Control and on Survival in Patients With Glioblastoma Multiforme. *Neuro Oncol* (2013) 15(7):961–7. doi: 10.1093/neuonc/not057
26. Watanabe S, Kuwabara Y, Suehiro S, Yamashita D, Tanaka M, Tanaka A, et al. Valproic Acid Reduces Hair Loss and Improves Survival in Patients Receiving Temozolomide-Based Radiation Therapy for High-Grade Glioma. *Eur J Clin Pharmacol* (2017) 73(3):357–63. doi: 10.1007/s00228-016-2167-1
27. Tseng JH, Chen CY, Chen PC, Hsiao SH, Fan CC, Liang YC, et al. Valproic Acid Inhibits Glioblastoma Multiforme Cell Growth *via* Paraoxonase 2 Expression. *Oncotarget* (2017) 8(9):14666–79. doi: 10.18632/oncotarget.14716
28. Kalal BS, Pai VR, Behera SK, Somashekarappa HM. HDAC2 Inhibitor Valproic Acid Increases Radiation Sensitivity of Drug-Resistant Melanoma Cells. *Med Sci (Basel)* (2019) 7(3):eng. doi: 10.3390/medsci7030051
29. Hosein AN, Lim YC, Day B, Stringer B, Rose S, Head R, et al. The Effect of Valproic Acid in Combination With Irradiation and Temozolomide on Primary Human Glioblastoma Cells. *J Neurooncol* (2015) 122(2):263–71. doi: 10.1007/s11060-014-1713-x
30. Ryu CH, Yoon WS, Park KY, Kim SM, Lim JY, Woo JS, et al. Valproic Acid Downregulates the Expression of MGMT and Sensitizes Temozolomide-Resistant Glioma Cells. *J BioMed Biotechnol* (2012) 2012:987495. doi: 10.1155/2012/987495
31. Mascaro-Cordeiro B, Oliveira ID, Tesser-Gamba F, Pavon LF, Saba-Silva N, Cavalheiro S, et al. Valproic Acid Treatment Response *In Vitro* is Determined by TP53 Status in Medulloblastoma. *Childs Nerv Syst* (2018) 34(8):1497–509. doi: 10.1007/s00381-018-3817-7
32. McCormack E, Haaland I, Venas G, Forthun RB, Huseby S, Gausdal G, et al. Synergistic Induction of P53 Mediated Apoptosis by Valproic Acid and Nutlin-3 in Acute Myeloid Leukemia. *Leukemia* (2012) 26(5):910–7. doi: 10.1038/leu.2011.315
33. Chen X, Wong P, Radany E, Wong JY. HDAC Inhibitor, Valproic Acid, Induces P53-Dependent Radiosensitization of Colon Cancer Cells. *Cancer Biother Radiopharm* (2009) 24(6):689–99. doi: 10.1089/cbr.2009.0629
34. Leitch C, Osdal T, Andresen V, Molland M, Kristiansen S, Nguyen XN, et al. Hydroxyurea Synergizes With Valproic Acid in Wild-Type P53 Acute Myeloid Leukaemia. *Oncotarget* (2016) 7(7):8105–18. doi: 10.18632/oncotarget.6991
35. Wang P, Dong Q, Zhang C, Kuan PF, Liu Y, Jeck WR, et al. Mutations in Isocitrate Dehydrogenase 1 and 2 Occur Frequently in Intrahepatic Cholangiocarcinomas and Share Hypermethylation Targets With Glioblastomas. *Oncogene* (2013) 25(25):3091–100. doi: 10.1038/onc.2012.315
36. Tsai HC, Wei KC, Tsai CN, Huang YC, Chen PY, Chen SM, et al. Effect of Valproic Acid on the Outcome of Glioblastoma Multiforme. *Br J Neurosurg* (2012) 26(3):347–54. doi: 10.3109/02688697.2011.638996
37. Bouaoun L, Sonkin D, Ardin M, Hollstein M, Byrnes G, Zavadil J, et al. TP53 Variations in Human Cancers: New Lessons From the IARC TP53 Database and Genomics Data. *Hum Mutat* (2016) 37(9):865–76. doi: 10.1002/humu.23035
38. Polager S, Ginsberg D. P53 and E2f: Partners in Life and Death. *Nat Rev Cancer* (2009) 9(10):738–48. doi: 10.1038/nrc2718
39. Kramer OH, Zhu P, Ostendorff HP, Golebiewski M, Tiefenbach J, Peters MA, et al. The Histone Deacetylase Inhibitor Valproic Acid Selectively Induces Proteasomal Degradation of HDAC2 [Research Support, Non-U.S. Gov't]. *EMBO J* (2003) 22(13):3411–20. doi: 10.1093/emboj/cdg315
40. Zhang Z, Wang Y, Chen J, Tan Q, Xie C, Li C, et al. Silencing of Histone Deacetylase 2 Suppresses Malignancy for Proliferation, Migration, and Invasion of Glioblastoma Cells and Enhances Temozolomide Sensitivity. *Cancer Chemother Pharmacol* (2016) 78(6):1289–96. doi: 10.1007/s00280-016-3188-2
41. Cancer Genome Atlas Research N. Comprehensive Genomic Characterization Defines Human Glioblastoma Genes and Core Pathways. *Nature* (2008) 455(7216):1061–8. doi: 10.1038/nature07385
42. Louis DN, Perry A, Reifenberger G, von Deimling A, Figarella-Branger D, Cavenee WK, et al. The 2016 World Health Organization Classification of Tumors of the Central Nervous System: A Summary [Review]. *Acta Neuropathol* (2016) 131(6):803–20. doi: 10.1007/s00401-016-1545-1
43. Nandeesh BN, Naskar S, Shashtri AH, Arivazhagan A, Santosh V. Recurrent Glioblastomas Exhibit Higher Expression of Biomarkers With Stem-Like Properties. *J Neurosci Rural Pract* (2018) 9(1):86–91. doi: 10.4103/jnrp.jnrp_417_17
44. Wiewrodt D, Nagel G, Dreimuller N, Hundsberger T, Perneczky A, Kaina B. MGMT in Primary and Recurrent Human Glioblastomas After Radiation and Chemotherapy and Comparison With P53 Status and Clinical Outcome [Comparative Study Research Support, Non-U.S. Gov't]. *Int J Cancer* (2008) 122(6):1391–9. doi: 10.1002/ijc.23219
45. Stark AM, Witzel P, Strege RJ, Hugo HH, Mehdorn HM. P53, Mdm2, EGFR, and Msh2 Expression in Paired Initial and Recurrent Glioblastoma Multiforme. *J Neurol Neurosurg Psychiatry* (2003) 74(6):779–83. doi: 10.1136/jnnp.74.6.779
46. Park CM, Park MJ, Kwak HJ, Moon SI, Yoo DH, Lee HC, et al. Induction of P53-Mediated Apoptosis and Recovery of Chemosensitivity Through P53 Transduction in Human Glioblastoma Cells by Cisplatin. *Int J Oncol* (2006) 28(1):119–25. doi: 10.3892/ijo.28.1.119
47. Djuzenova CS, Fiedler V, Memmel S, Katzer A, Hartmann S, Krohne G, et al. Actin Cytoskeleton Organization, Cell Surface Modification and Invasion Rate of 5 Glioblastoma Cell Lines Differing in PTEN and P53 Status. *Exp Cell Res* (2015) 330(2):346–57. doi: 10.1016/j.yexcr.2014.08.013
48. England B, Huang T, Karsy M. Current Understanding of the Role and Targeting of Tumor Suppressor P53 in Glioblastoma Multiforme [Review]. *Tumour Biol* (2013) 34(4):2063–74. doi: 10.1007/s13277-013-0871-3
49. Bieging KT, Mello SS, Attardi LD. Unravelling Mechanisms of P53-Mediated Tumour Suppression. *Nat Rev Cancer* (2014) 14(5):359–70. doi: 10.1038/nrc3711
50. Stupp R, Mason WP, van den Bent MJ, Weller M, Fisher B, Taphoorn MJ, et al. Radiotherapy Plus Concomitant and Adjuvant Temozolomide for Glioblastoma. *N Engl J Med* (2005) 352(10):987–96. doi: 10.1056/NEJMoa043330
51. Stupp R, Hegi ME, Mason WP, van den Bent MJ, Taphoorn MJ, Janzer RC, et al. Effects of Radiotherapy With Concomitant and Adjuvant Temozolomide Versus Radiotherapy Alone on Survival in Glioblastoma in a Randomised Phase III Study: 5-Year Analysis of the EORTC-NCIC Trial. *Lancet Oncol* (2009) 10(5):459–66. doi: 10.1016/S1470-2045(09)70025-7
52. Wen J, Chen W, Zhu Y, Zhang P. Clinical Features Associated With the Efficacy of Chemotherapy in Patients With Glioblastoma (GBM): A Surveillance, Epidemiology, and End Results (SEER) Analysis. *BMC Cancer* (2021) 21(1):81. doi: 10.1186/s12885-021-07800-0

53. Lamborn KR, Chang SM, Prados MD. Prognostic Factors for Survival of Patients With Glioblastoma: Recursive Partitioning Analysis. *Neuro Oncol* (2004) 6(3):227–35. doi: 10.1215/S1152851703000620
54. Berendsen S, Varkila M, Kroonen J, Seute T, Snijders TJ, Kauw F, et al. Prognostic Relevance of Epilepsy at Presentation in Glioblastoma Patients. *Neuro Oncol* (2016) 18(5):700–6. doi: 10.1093/neuonc/nov238
55. Cohen AL, Holmen SL, Colman H. IDH1 and IDH2 Mutations in Gliomas. *Curr Neurol Neurosci Rep* (2013) 13(5):345. doi: 10.1007/s11910-013-0345-4
56. Cheng HB, Yue W, Xie C, Zhang RY, Hu SS, Wang Z. IDH1 Mutation is Associated With Improved Overall Survival in Patients With Glioblastoma: A Meta-Analysis. *Tumour Biol: J Int Soc Oncodevel Biol Med* (2013) 34(6):3555–9. doi: 10.1007/s13277-013-0934-5
57. Wali AR, Rennert RC, Wang SG, Chen CC. Prophylactic Anticonvulsants in Patients With Primary Glioblastoma. *J Neurooncol* (2017) 135(2):229–35. doi: 10.1007/s11060-017-2584-8
58. Wu AS, Trinh VT, Suki D, Graham S, Forman A, Weinberg JS, et al. A Prospective Randomized Trial of Perioperative Seizure Prophylaxis in Patients With Intraparenchymal Brain Tumors. *J Neurosurg* (2013) 118(4):873–83. doi: 10.3171/2012.12.JNS111970
59. Kuo YJ, Yang YH, Lee IY, Chen PC, Yang JT, Wang TC, et al. Effect of Valproic Acid on Overall Survival in Patients With High-Grade Gliomas Undergoing Temozolomide: A Nationwide Population-Based Cohort Study in Taiwan. *Med (Baltimore)* (2020) 99(28):e21147. doi: 10.1097/MD.0000000000021147
60. Lu VM, Texakalidis P, McDonald KL, Mekary RA, Smith TR. The Survival Effect of Valproic Acid in Glioblastoma and its Current Trend: A Systematic Review and Meta-Analysis. *Clin Neurol Neurosurg* (2018) 174:149–55. doi: 10.1016/j.clineuro.2018.09.019
61. Zhao YH, Wang ZF, Cao CJ, Weng H, Xu CS, Li K, et al. The Clinical Significance of O(6)-Methylguanine-DNA Methyltransferase Promoter Methylation Status in Adult Patients With Glioblastoma: A Meta-Analysis. *Front Neurol* (2018) 9:127. doi: 10.3389/fneur.2018.00127
62. Riemenschneider MJ, Hegi ME, Reifenberger G. MGMT Promoter Methylation in Malignant Gliomas. *Target Oncol* (2010) 5(3):161–5. doi: 10.1007/s11523-010-0153-6
63. Wang L, Li Z, Liu C, Chen L, Liu L, Hu Z, et al. Comparative Assessment of Three Methods to Analyze MGMT Methylation Status in a Series of 350 Gliomas and Gangliogliomas. *Pathol Res Pract* (2017) 213(12):1489–93. doi: 10.1016/j.prp.2017.10.007
64. Rodriguez FJ, Thibodeau SN, Jenkins RB, Schowalter KV, Caron BL, O'Neill BP, et al. MGMT Immunohistochemical Expression and Promoter Methylation in Human Glioblastoma. *Appl Immunohistochem Mol Morphol* (2008) 16(1):59–65. doi: 10.1097/PAI.0b013e31802fac2f
65. Brandner S, McAleenan A, Kelly C, Spiga F, Cheng HY, Dawson S, et al. MGMT Promoter Methylation Testing to Predict Overall Survival in People With Glioblastoma Treated With Temozolomide: A Comprehensive Meta-Analysis Based on a Cochrane Review. *Neuro Oncol* (2021) 23(9):1457–69. doi: 10.1093/neuonc/noab105
66. Roos WP, Batista LF, Naumann SC, Wick W, Weller M, Menck CF, et al. Apoptosis in Malignant Glioma Cells Triggered by the Temozolomide-Induced DNA Lesion O6-Methylguanine. *Oncogene* (2007) 26(2):186–97. doi: 10.1038/sj.onc.1209785
67. Zhang Y, Dube C, Gibert MJr., Cruickshanks N, Wang B, Coughlan M, et al. The P53 Pathway in Glioblastoma. *Cancers (Basel)* (2018) 10(9):297. doi: 10.3390/cancers10090297
68. Nakano K, Vousden KH. PUMA, a Novel Proapoptotic Gene, is Induced by P53. *Mol Cell* (2001) 7(3):683–94. doi: 10.1016/s1097-2765(01)00214-3
69. Yu J, Zhang L. PUMA, a Potent Killer With or Without P53 [Research Support, N.I.H., Extramural Research Support, Non-U.S. Gov't Review]. *Oncogene* (2008) 27 Suppl 1:S71–83. doi: 10.1038/onc.2009.45
70. Ito H, Kanzawa T, Miyoshi T, Hirohata S, Kyo S, Iwamaru A, et al. Therapeutic Efficacy of PUMA for Malignant Glioma Cells Regardless of P53 Status [Research Support, N.I.H., Extramural Research Support, Non-U.S. Gov't Research Support, U.S. Gov't, P.H.S.]. *Hum Gene Ther* (2005) 16 (6):685–98. doi: 10.1089/hum.2005.16.685
71. Miao W, Liu X, Wang H, Fan Y, Lian S, Yang X, et al. P53 Upregulated Modulator of Apoptosis Sensitizes Drug-Resistant U251 Glioblastoma Stem Cells to Temozolomide Through Enhanced Apoptosis [Research Support, Non-U.S. Gov't]. *Mol Med Rep* (2015) 11(6):4165–73. doi: 10.3892/mmr.2015.3255
72. He Y, Kaina B. Are There Thresholds in Glioblastoma Cell Death Responses Triggered by Temozolomide? *Int J Mol Sci* (2019) (7):1562. doi: 10.3390/ijms20071562
73. Ostermann S, Csajka C, Buclin T, Leyvraz S, Lejeune F, Decosterd LA, et al. Plasma and Cerebrospinal Fluid Population Pharmacokinetics of Temozolomide in Malignant Glioma Patients. *Clin Cancer Res* (2004) 10 (11):3728–36. doi: 10.1158/1078-0432.CCR-03-0807
74. Portnow J, Badie B, Chen M, Liu A, Blanchard S, Synold TW. The Neuropharmacokinetics of Temozolomide in Patients With Resectable Brain Tumors: Potential Implications for the Current Approach to Chemoradiation. *Clin Cancer Res* (2009) 15(22):7092–8. doi: 10.1158/1078-0432.CCR-09-1349
75. Van Meir EG, Kikuchi T, Tada M, Li H, Diserens AC, Wojcik BE, et al. Analysis of the P53 Gene and its Expression in Human Glioblastoma Cells. *Cancer Res* (1994) 54(3):649–52.
76. Roth W, Fontana A, Trepel M, Reed JC, Dichgans J, Weller M. Immunochemotherapy of Malignant Glioma: Synergistic Activity of CD95 Ligand and Chemotherapeutics. *Cancer Immunol Immunother* (1997) 44 (1):55–63. doi: 10.1007/s002620050355
77. Xie Z, Ago Y, Okada N, Tachibana M. Valproic Acid Attenuates Immunosuppressive Function of Myeloid-Derived Suppressor Cells. *J Pharmacol Sci* (2018) 137(4):359–65. doi: 10.1016/j.jphs.2018.06.014
78. Roos WP, Jost E, Belohlavek C, Nagel G, Fritz G, Kaina B. Intrinsic Anticancer Drug Resistance of Malignant Melanoma Cells is Abrogated by IFN-Beta and Valproic Acid. *Cancer Res* (2011) 71(12):4150–60. doi: 10.1158/0008-5472.CAN-10-3498
79. Paradis FH, Hales BF. Valproic Acid Induces the Hyperacetylation of P53, Expression of P53 Target Genes, and Markers of the Intrinsic Apoptotic Pathway in Midorganogenesis Murine Limbs. *Birth Defects Res B Dev Reprod Toxicol* (2015) 104(5):177–83. doi: 10.1002/bdrb.21149
80. Gryder BE, Sodji QH, Oyelere AK. Targeted Cancer Therapy: Giving Histone Deacetylase Inhibitors All They Need to Succeed [Research Support, N.I.H., Extramural Research Support, Non-U.S. Gov't Review]. *Future Med Chem* (2012) 4(4):505–24. doi: 10.4155/fmc.12.3
81. Bailey H, Stenehjem DD, Sharma S. Panobinostat for the Treatment of Multiple Myeloma: The Evidence to Date [Review]. *J Blood Med* (2015) 6:269–76. doi: 10.2147/JBM.S69140
82. Campbell P, Thomas CM. Belinostat for the Treatment of Relapsed or Refractory Peripheral T-Cell Lymphoma [Review]. *J Oncol Pharm Practice: Off Publ Int Soc Oncol Pharm Practitioners* (2017) 23(2):143–7. doi: 10.1177/1078155216634178

Conflict of Interest: The authors declare that the research was conducted in the absence of any commercial or financial relationships that could be construed as a potential conflict of interest.

Publisher's Note: All claims expressed in this article are solely those of the authors and do not necessarily represent those of their affiliated organizations, or those of the publisher, the editors and the reviewers. Any product that may be evaluated in this article, or claim that may be made by its manufacturer, is not guaranteed or endorsed by the publisher.

frontiers in Oncology

ORIGINAL RESEARCH
published: 25 October 2021
doi: 10.3389/fonc.2021.758856

Upregulated Expression of Cancer-Derived Immunoglobulin G Is Associated With Progression in Glioma

Guohui Wang[1†], Haonan Li[1,2†], Jie Pan[3†], Tianfang Yan[4], Huandi Zhou[1,2], Xuetao Han[1], Linlin Su[1], Liubing Hou[1,2] and Xiaoying Xue[1]*

[1] Department of Radiotherapy, The Second Hospital of Hebei Medical University, Shijiazhuang, China, [2] Department of Central Laboratory, The Second Hospital of Hebei Medical University, Shijiazhuang, China, [3] Department of Pathology, Stanford University School of Medicine, Stanford, CA, United States, [4] Department of Neurological Diagnosis and Restoration, Osaka University Graduate School of Medicine, Suita, Japan

OPEN ACCESS

Edited by:
Liam Chen,
University of Minnesota, United States

Reviewed by:
Subhas K. Konar,
National Institute of Mental Health and Neurosciences (NIMHANS), India
Mohammed A. Azab,
Boise State University, United States

***Correspondence:**
Xiaoying Xue
xxy0636@163.com

[†]These authors have contributed equally to this work

Specialty section:
This article was submitted to Neuro-Oncology and Neurosurgical Oncology, a section of the journal Frontiers in Oncology

Received: 15 August 2021
Accepted: 04 October 2021
Published: 25 October 2021

Citation:
Wang G, Li H, Pan J, Yan T, Zhou H, Han X, Su L, Hou L and Xue X (2021) Upregulated Expression of Cancer-Derived Immunoglobulin G Is Associated With Progression in Glioma. Front. Oncol. 11:758856. doi: 10.3389/fonc.2021.758856

Objective: Gliomas are the most aggressive intracranial tumors accounting for the vast majority of brain tumors with very poor prognosis and overall survival (OS). Cancer-derived immunoglobulin G (cancer-IgG) has been found to be widely expressed in several malignancies such as breast cancer, colorectal cancer, and lung cancer. Cancer-IgG could promote tumorigenesis and progression. However, its role in glioma has not been revealed yet.

Methods: We mined open databases including the Chinese Glioma Genome Atlas (CGGA), The Cancer Genome Atlas (TCGA), and the Gene Expression Omnibus (GEO) to study the role of *IGHG1*, which encodes cancer-IgG in glioma. Examination of the differential expression of *IGHG1* was carried out in the GEO and TCGA databases. Furthermore, its expression in different molecular subtypes was analyzed. Stratified analysis was performed with clinical features. Subsequently, immune infiltration analysis was conducted using single-sample gene set enrichment analysis (ssGSEA). GSEA was performed to reveal the mechanisms of *IGHG1*. Lastly, immunohistochemistry was processed to validate our findings.

Results: In this study, we found that the expression of *IGHG1* was higher in glioma and molecular subtypes with poor prognosis. The overall survival of patients with a high expression of *IGHG1* was worse in the stratified analysis. Immune infiltration analysis indicated that the expression level of *IGHG1* was positively correlated with the stromal score, ESTIMATE score, and immune score and negatively correlated with tumor purity. Results from the GSEA and DAVID demonstrated that *IGHG1* may function in phagosome, antigen processing and presentation, extracellular matrix structural constituent, antigen binding, and collagen-containing extracellular matrix. Finally, immunohistochemistry assay validated our findings that patients with a high expression of cancer-IgG had poor OS and disease-free survival (DFS).

Conclusion: Cancer-IgG is a promising biomarker of diagnosis and treatment for patients with glioma.

Keywords: cancer-derived immunoglobulin G, progression, glioma, microenvironment, IGHG1

INTRODUCTION

Gliomas are the most aggressive intracranial tumors accounting for the vast majority of brain tumors with very poor prognosis and overall survival (OS) (1). According to the malignant degree of glioma, the World Health Organization (WHO) classifies it into grades I–IV. Generally, grade I and II gliomas are considered less malignant and invasive. However, grades III to IV have a higher degree of malignancy and a strong invasive ability. In recent years, the diagnosis and evaluation of glioma have changed greatly, such as the combination of histopathological diagnosis and molecular markers. In 2021, the fifth edition of the WHO Classification of Tumors of the Central Nervous System (CNS) has been published. The latest classification emphasizes the importance of molecular and integrated diagnosis in the diagnosis and treatment of glioma (2). Standard therapy includes maximal safe tumor resection and radiation therapy with oral chemotherapy (3). Recent evidence found that tumor treating fields have good prospects for the treatment of gliomas (4). But the OS of patients with glioma is still very poor. Glioblastoma (GBM) patients have the worst prognosis, with a 5-year survival rate of less than 5% and, eventually, relapse (5). Therefore, it is urgent to explore new biomarkers for the treatment of glioma.

The classical immunological theory holds that immunoglobulin G (IgG), which plays a great role in human defense against pathogenic microorganisms, is produced only by B lymphocytes and plasma cells. However, more and more studies have shown that cancer cells can also produce IgG, called cancer-derived immunoglobulin G (cancer-IgG), such as those in breast cancer, colon cancer, cervical cancer, and lung cancer (6–9). Lee et al. immunized mice with the cleavage product of the ovarian cancer cell line OC-3-VGH to obtain the monoclonal antibody (mAb) RP215, which can specifically recognize cancer-IgG by recognizing a special glycosylation site in the constant region of the IgG heavy chain (10). Liao et al. found that cancer-IgG recognized by RP215 promoted the proliferation, invasion, and metastasis of tumor cells, which is a potential tumor stem cell marker (6). Tang et al. also showed that cancer-IgG promoted the occurrence and development of lung squamous cell carcinoma by activating the focal adhesion pathway (8). Some studies have also shown that cancer-IgG induced tumor immune escape by inhibiting effector T-cell proliferation in the tumor microenvironment (TME) (11). IgG consists of two heavy chains and two light chains. Each heavy chain and light chain is composed of a constant region and a variable region. The expression of IGHG1, which encodes the constant region of immunoglobulin heavy chain, is positively correlated with cancer-IgG (12). Accumulating evidence proved that IGHG1 is highly expressed in tumors and promotes oncogenesis and progression (13, 14). However, cancer-IgG and IGHG1 have not been studied in gliomas.

In this study, we firstly analyzed the expression of *IGHG1* in glioma and its relationship with prognosis through The Cancer Genome Atlas (TCGA), Gene Expression Omnibus (GEO), and the Chinese Glioma Genome Atlas (CGGA) databases. In addition, we also analyzed its possible mechanism through immune infiltration and gene set enrichment analysis (GSEA). Finally, the expression of cancer-IgG in glioma and its relationship with OS and progression-free survival (PFS) were analyzed by immunohistochemistry.

MATERIALS AND METHODS

Data Acquisition and Processing

RNA sequencing and clinical data of patients with lower grade glioma (LGG) and GBMs were downloaded from TCGA database. We also obtained the gene expression profiling and corresponding clinical features of gliomas from the CGGA (15). The microarray dataset GSE4290 was downloaded from the GEO database (16). All RNA sequencing data downloaded from TCGA and CGGA should be standardized and batched by the R limma package. Excluding patients with unknown or incomplete clinicopathological parameters, only the gliomas with complete clinicopathological parameters and survival data in the dataset were retained.

IGHG1 Differential Expression Analysis

In the GSE4290 cohort, differences in the expression of *IGHG1* in glioma and normal brain tissues were analyzed. The expression levels of *IGHG1* in LGG, GBM, and normal brain tissues were compared in TCGA and GETx databases. Then, the patients were grouped according to the following clinical characteristics: age (≤41 and >41 years), gender (female or male), grade (grades II, III, and IV), status (alive or dead), isocitrate dehydrogenase (IDH) status (mutation or wild type), 1p19q status [co-deletion (codel) or non-codel], and O^6-methylguanine-DNA methyltransferase (MGMT) (methylated or unmethylated). Wilcoxon tests were adopted to analyze the differential expressions between the abovementioned groups.

Prognostic Analysis

Patients with glioma were divided into a high group and a low group according to the median value of the expression of *IGHG1*. Then, the patients were stratified according to their clinicopathological features, such as age (<42 and ≥42 years), gender (female or male), grade (grades II, III, and IV), IDH status (mutation or wild type), 1p19q status (codel or non-codel), and MGMT (methylated or unmethylated). Kaplan–Meier survival analysis was implemented to calculate the survival rates in the groups with low and high expressions of *IGHG1*. Then, we

analyzed the relationship between the expression of *IGHG1* and progress-free interval (PFI) in TCGA cohort.

Evaluation of the Effect of *IGHG1* on Glioma Microenvironment

Single-sample gene set enrichment Analysis (ssGSEA) was used to estimate the population fractions of immunocytes in gliomas. In addition, the degree of immune cell infiltration was quantified using enrichment scores calculated through the Gene Set Variation Analysis package of the R software. According to the degree of immune cell infiltration in the TME, glioma patients were divided into high, medium, and low immune groups. Spearman's correlation analysis was used to analyze the relationship between the expression of *IGHG1* and the tumor purity, stromal score, ESTIMATE score, and immune score.

Database for Annotation, Visualization and Integrated Discovery and GSEA

The differentially expressed genes (DEGs) between gliomas with high and low expressions of *IGHG1* in the CGGA cohort were identified using the R limma package and the following criteria: |logFC| > 1 and false discovery rate (FDR) <0.05. In order to further explore the possible mechanism of *IGHG1*, we conducted Gene Ontology (GO) and Kyoto Encyclopedia of Genes and Genomes (KEGG) pathway analysis using the Database for Annotation, Visualization and Integrated Discovery (DAVID) 6.8 online website (https://david.abcc.ncifcrf.gov/). The GSEA 4.0.2 software was also used for this purpose. A normalized enrichment score (NES) >1 and FDR <0.05 were considered meaningful.

Immunohistochemical Staining and Scoring

The tissue microarray (TMA) used in this study was purchased from Shanghai Outdo Biotech Co., Ltd. (Shanghai, China). All patients were diagnosed with glioma by pathology. The mAb RP215 (sc-69849; Santa Cruz Biotechnology, Santa Cruz, CA, USA) was used to specifically recognize cancer-IgG. Human tissues were stained using mouse and rabbit specific horseradish peroxidase (HRP)/3,3′-diaminobenzidine (DAB) Detection IHC Kit (ab64264; Abcam, Cambridge, UK) according to the manufacturer's instructions. The immunohistochemical staining score was based on previously published articles. The staining intensity was scored as follows: 0: no staining; 1: weak staining; 2: moderate staining: and 3: strong staining. The positive staining cell rate was scored as follows: 0: 0%–5%; 1: 5%–25%; 2: 26%–50%; 3: 51%–75%; and 4: >75%. A score below three points was considered negative and more than three points as positive.

Statistical Analyses

The levels of *IGHG1* in tumor and normal tissue samples were compared using the Wilcoxon signed-rank test. Spearman's rank correlation coefficients between *IGHG1* expression and the tumor purity, stromal score, ESTIMATE score, and immune score were tested. Kaplan–Meier survival curves were used to analyze the effect of *IGHG1* and tumor-derived IgG on prognosis. Statistical analyses were performed using IBM SPSS 24.0, GraphPad Prism 6, and R 4.0.1 software. $P < 0.05$ was considered statistically significant.

RESULTS

We utilized open databases to explore the expression of *IGHG1*, which encodes the heavy chain of IgG. There are 176 cases in the GSE4290 dataset, 587 in TCGA, and 686 in the CGGA database. Besides, a TMA containing 169 cases was included in our study. The clinical characteristics and molecular features are all listed in **Table 1**.

Expression of *IGHG1* Is Upregulated in Patients With Glioma

We found that the expression of *IGHG1* in patients with glioma was higher than that in normal tissues from the GEO database ($p < 0.01$; **Figure 1A**). In TCGA, the expression of this gene showed a trend to be higher in low-grade glioma, but with no statistical significance (**Figure 1B**). However, *IGHG1* was upregulated remarkably in GBM ($p < 0.001$; **Figure 1C**). From the results, we drew the conclusion that the expression of *IGHG1* is upregulated in patients with glioma.

Expression of *IGHG1* Is Correlated With Clinical Features That Predict Poor Prognosis

To examine the expression of *IGHG1* in patients with different clinical characteristics, the CGGA database was used, which contains more details on the clinical features of the patients included in our study. The results showed that the expression of *IGHG1* was upregulated in patients over 41 years ($p < 0.01$; **Figure 2A**). There was no significant gender difference (**Figure 2B**). The expression level of *IGHG1* was upregulated coupled with grade promotion ($p < 0.001$; **Figure 2C**). Deceased patients had higher expression levels than did those who are alive ($p < 0.001$; **Figure 2D**). A high expression of *IGHG1* was found in patients with the molecular subtype IDH wild type and 1p19q non-codel ($p < 0.001$; **Figures 2E, F**), but there was no significance in the status of MGMT methylation (**Figure 2G**). In short, a high expression of *IGHG1* was correlated with the characteristics that predict poor prognosis.

Glioma Patients With High Expression of *IGHG1* Had Poor Prognosis

Stratification analysis was programmed to evaluate the influence of *IGHG1* expression on the prognosis of glioma patients. The survival probability of patients with a high expression of *IGHG1* was poorer than that of those with a low expression, overall (HR = 1.97, 95%CI = 1.64–2.38, $p < 0.001$) (**Figure 3A**). We reached the same conclusions for patients younger than 41 years (HR = 1.83, 95%CI = 1.38–2.47, $p < 0.001$) (**Figure 3B**) and those over 41 years (HR = 2.01, 95%CI = 1.58–2.58, $p < 0.001$) (**Figure 3C**). The survival probability in patients with a high expression of the gene was worse in both females (HR = 2.29, 95%CI = 1.70–3.10, $p < 0.001$) (**Figure 3D**) and males (HR = 1.80, 95%CI = 1.41–2.29, $p < 0.001$) (**Figure 3E**). The survival probability of patients who were diagnosed with WHO grade III glioma (HR = 1.76, 95%CI = 1.26–2.42, $p < 0.001$) was

TABLE 1 | Clinicopathological characteristics of glioma patients from the Gene Expression Omnibus (GEO), The Cancer Genome Atlas (TCGA), and the Chinese Glioma Genome Atlas (CGGA) databases and tissue microarray.

	GSE4290 (*n* = 176)	TCGA (*n* = 587)	CGGA (*n* = 686)	Tissue microarray (*n* = 169)
Age (years)				
<42	NA	242	308	37
≥42	NA	345	378	132
Gender				
Female	NA	246	287	62
Male	NA	341	399	107
Normal tissue	23	NA	NA	NA
Grade				
II	45	211	177	97
III	31	234	226	51
IV	77	142	283	21
IDH status				
Wild type	NA	219	315	NA
Mutation	NA	368	371	NA
1p/19q				
Codel	NA	149	141	NA
Non-codel	NA	438	545	NA
MGMT				
Methylated	NA	NA	386	NA
Unmethylated	NA	NA	300	NA
Vital status				
Dead	NA	173	457	57
Alive	NA	414	229	112

IDH, isocitrate dehydrogenase; MGMT, O^6-methylguanine-DNA methyltransferase; codel, co-deletion.
NA represents No data.

significantly poor. But those with WHO grades II and IV did not reach the considered threshold (**Figures 3F–H**). Finally, patients with a high expression of *IGHG1* had a lower survival probability of reaching the threshold in the IDH mutation subgroup (HR = 2.26, 95%CI = 1.71–3.00, $p < 0.001$), the 1p19q codel subgroup (HR = 3.00, 95%CI = 1.69–5.31, $p < 0.001$), the 1p19q non-codel subgroup (HR = 1.65, 95%CI = 1.35–2.01, $p < 0.001$), the MGMT methylated subgroup (HR = 1.91, 95%CI = 1.40–2.47, $p < 0.001$), and the MGMT unmethylated subgroup (HR = 2.09, 95%CI = 1.08–2.70, $p < 0.001$), except for the IDH wild-type subgroup (**Figures 3I–N**). We also found that patients with a high expression of *IGHG1* had shorter PFI in TCGA cohort (LGG: HR = 1.44, 95%CI = 1.09–1.89, $p = 0.009$; GBM: HR = 1.41, 95% CI = 1.00–1.99, $p = 0.053$) (**Supplementary Figures S1A–D**). On the whole, patients with a high expression of *IGHG1* had poor prognosis.

High *IGHG1* Expression Was Correlated With High Immune Infiltration

ssGSEA was performed to assess immune cell infiltration. Patients were clustered into low, moderate, and high immunity groups based on the state of immune cell infiltration. Analysis revealed that patients with more immunocyte infiltration also had a higher expression of *IGHG1*. The results are demonstrated in **Figure 4A**. There was also a distinct difference in the expressions of the genes among the groups. The expression level of *IGHG1* was negatively correlated with tumor purity

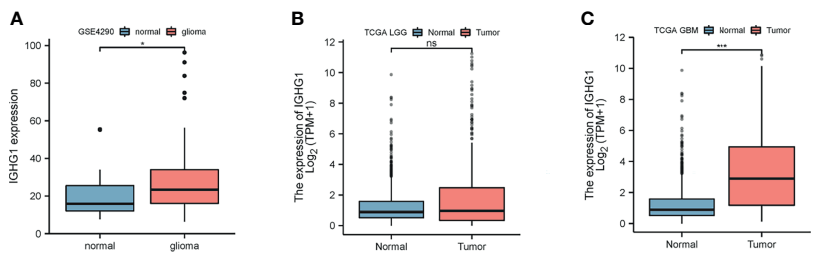

FIGURE 1 | Differences in the expression of *IGHG1* between glioma and normal brain tissues. **(A)** In the GSE4290 dataset, the expression of *IGHG1* differed between glioma and normal brain tissues. **(B)** In The Cancer Genome Atlas (TCGA) cohort, there was no significant difference in the expression of *IGHG1* in lower grade glioma (LGG) and normal brain tissues. **(C)** The expression of *IGHG1* in glioblastoma (GBM) was significantly higher than that in normal brain tissue in TCGA. * represent P < 0.01. *** represent P < 0.0001 and ns, represent no significance.

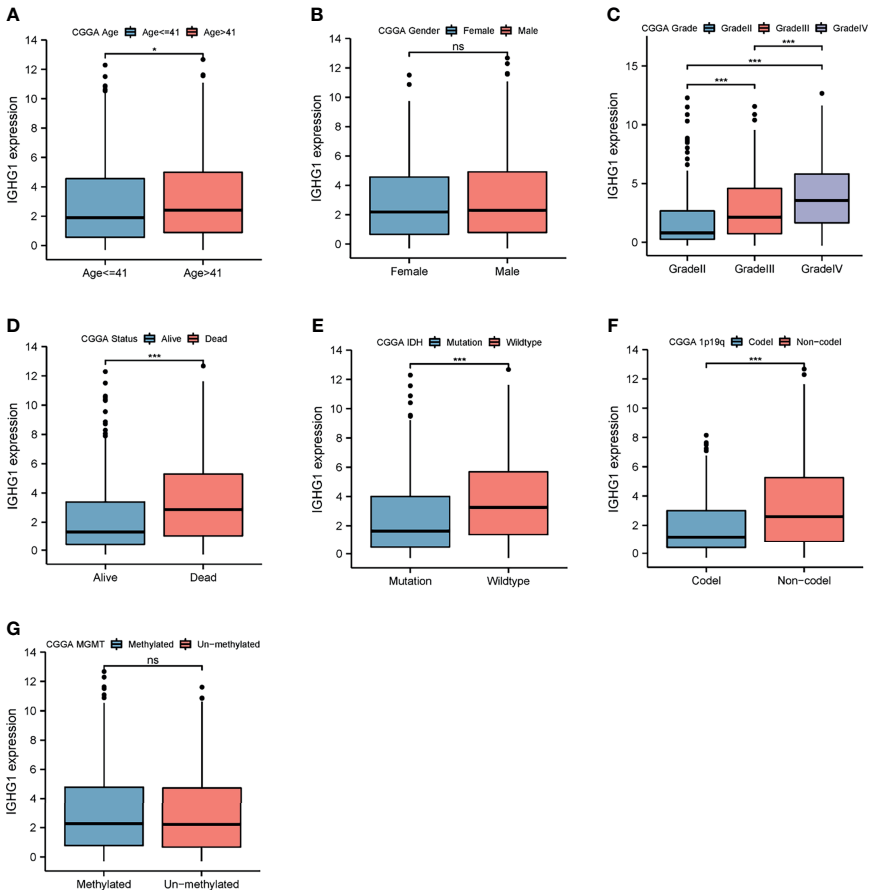

FIGURE 2 | Differences in the expression of *IGHG1* among the different clinical characteristics in patients with glioma. Expression of *IGHG1* in different ages **(A)**, genders **(B)**, grades **(C)**, living state **(D)**, isocitrate dehydrogenase (IDH) status **(E)**, 1p19q status **(F)**, and O^6-methylguanine-DNA methyltransferase (MGMT) status **(G)**. * represent P < 0.01. *** represent P < 0.0001 and ns, represent no significance.

(r = −0.610, p < 0.001) (**Figure 4B**), but it was positively correlated with the stromal score (r = 0.570, p < 0.001) (**Figure 4C**), ESTIMATE score (r = 0.610, p < 0.001) (**Figure 4D**), and immune score (r = 0.610, p < 0.001) (**Figure 4E**). In brief, *IGHG1* expression is closely relevant to the TME. A high expression of *IGHG1* indicates more immune cell infiltration in glioma (p < 0.001; **Figure 4F**).

IGHG1 Functions in Immune-Related Pathways in Glioma

To uncover the potential mechanisms of the functions of *IGHG1*, the CGGA database was analyzed to identify the DEGs. A volcano map was plotted for the DEGs (**Figure 5A**). DAVID analysis was carried out. A majority of the genes were related with immune-related functions, such as phagosome, antigen processing and presentation, extracellular matrix structural constituent, antigen binding, and collagen-containing extracellular matrix (**Figure 5B**). GO and KEGG analyses were performed using GSEA. The following were enriched in GO with thresholds of FDR < 0.05 and NES > 1: GO_ACTIVATION_OF_IMMUNE_RESPONSE, GO_ADAPTIVE_IMMUNE_RESPONSE, GO_LEUKOCYTE_PROLIFERATION, GO_REGULATION_OF_LYMPHOCYTE_ACTIVATION, and GO_T_CELL_PROLIFFERATION (**Figure 5C**). The following were enriched in KEGG analysis with thresholds of FDR < 0.05 and NES > 1: KEGG_ANTIGEN_PROCESSING_AND_PRESENTATION, KEGG_CELL_ADHESION_MELECULES_CAMS, KEGG_INTESTINAL_IMMUNE_NETWORK_FOR_IGA_PRODUCTION, and KEGG_PRIMARY_IMMUNODEFICIENCY (**Figure 5D**). To summarize, the same with ssGSEA, GO and KEGG analyses revealed that *IGHG1* plays a role in immune-related processes in glioma.

Expression of Cancer-IgG Leads to Poor Prognosis by Immunohistochemistry Assay

To back up our findings, immunohistochemistry assay was conducted with RP215, a mAb of cancer-IgG, using a TMA. **Figures 6A–C** show the weak staining, moderate staining, and strong staining intensities, respectively. Analysis of the TMA showed that OS (HR = 3.37, 95%CI = 2.21–5.14, p < 0.001) (**Figure 6D**) and disease-free survival (DFS) (HR = 6.02, 95%CI = 3.28–11.04, p < 0.001) (**Figure 6E**) were obviously poorer in

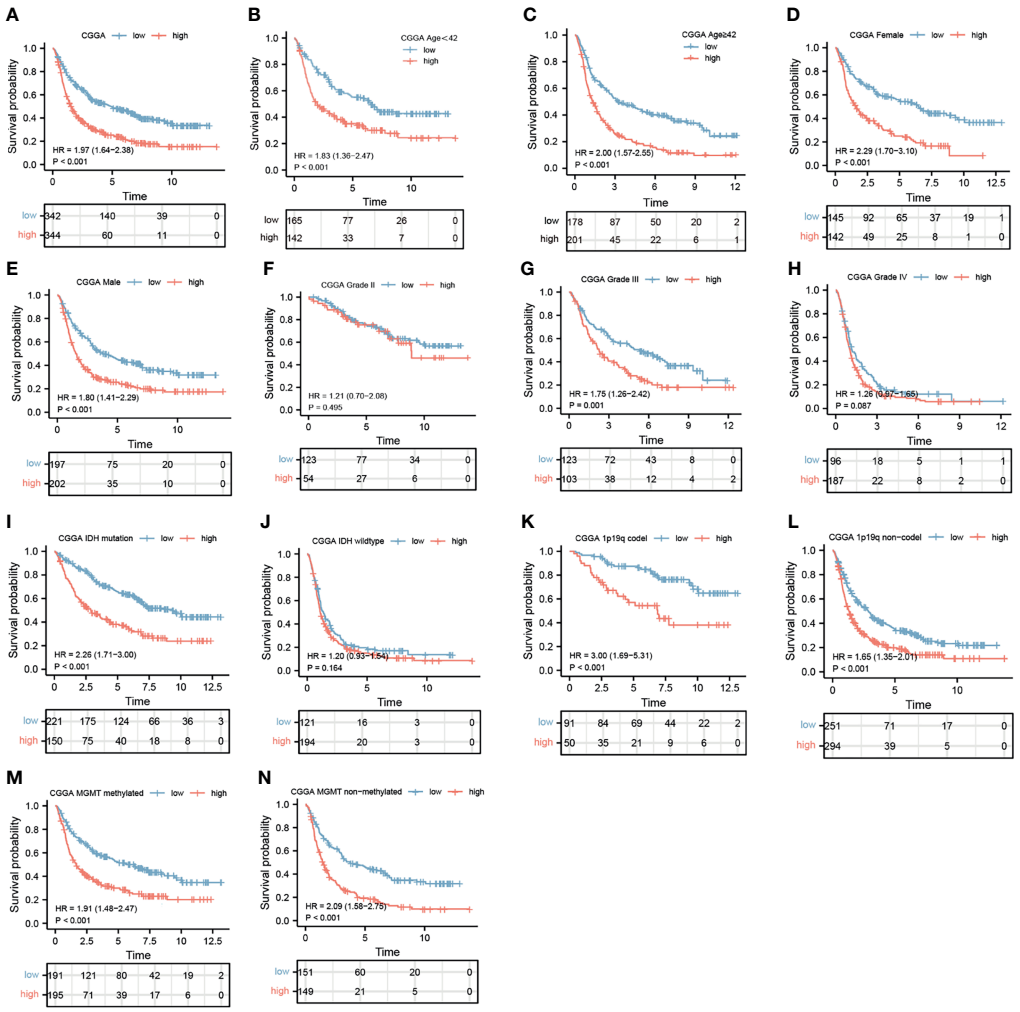

FIGURE 3 | Prediction of the outcome of *IGHG1* in stratified patients in the Chinese Glioma Genome Atlas (CGGA) dataset. **(A)** Survival curve used to analyze overall survival (OS) in the low- and high-*IGHG1* groups in the CGGA dataset. **(A–N)** Survival analysis of the signature in patients stratified by age **(B, C)**, gender **(D, E)**, grade **(F, H)**, isocitrate dehydrogenase (IDH) status **(I, J)**, 1p19q status **(K, L)**, and O^6-methylguanine-DNA methyltransferase (MGMT) promoter **(M, N)**.

patients with a high expression of cancer-IgG. In general, the expression of cancer-IgG represents poor prognosis.

DISCUSSION

Central nervous system cancer is a heterogeneous disease. Its new cases account for about 1.6% of the new tumors worldwide every year, and the mortality is about 2.5% (17). Gliomas accounting for 80% of central nervous system tumors have the characteristics of heterogeneity and complexity. Patients with glioma, especially GBM, have poor prognosis with a median survival of <2 years (5). From the initial morphological classification to the latest molecular classification in 2021, the accuracy of glioma diagnosis and prediction has been greatly improved. However, only a few of the available molecular markers truly influence clinical decision-making and treatments such as MGMT promoter methylation, co-deletion of 1p and 19q, and *IDH1*/*IDH2* mutations (18). Therefore, it is urgent to understand in depth the pathogenesis of glioma, discover new molecular targets, and develop new treatment methods.

When it comes to IgG, which is composed of two heavy chains and two light chains, we firstly hold that it is an antibody secreted by B cells that has a protective effect on the body. However, there is a growing view that tumor cells can also produce IgG by themselves, as cancer-IgG. Cancer-IgG has been widely studied in many specified epithelial tumors, such as breast cancer (6), prostate cancer (19), and bladder cancer (20). More and more evidence also showed that cancer-IgG promotes the occurrence and development and the immune escape of tumors. But the role of cancer-IgG in tumorigenesis is complex and, in glioma, is poorly understood.

In our study, we firstly analyzed the expression of *IGHG1*, the gene encoding the heavy chain of IgG, in glioma with

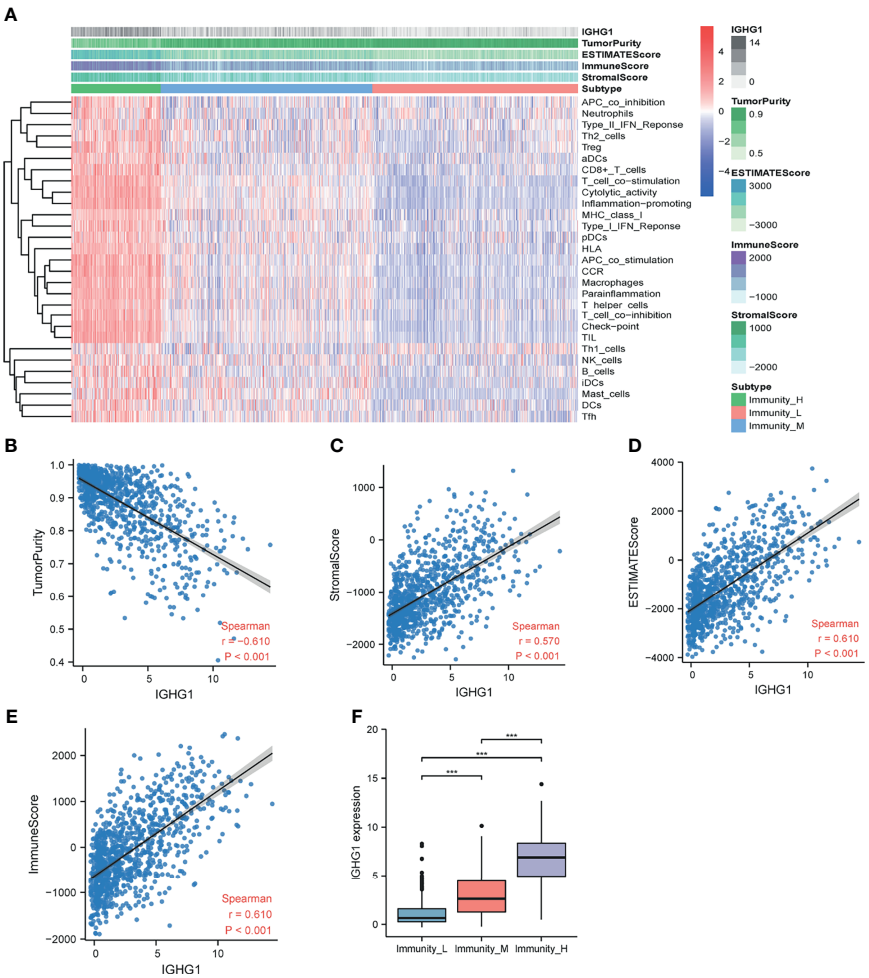

FIGURE 4 | Immune infiltration patterns of the low- and high-*IGHG1* groups analyzed using single-sample gene set enrichment analysis (ssGSEA) methods in glioma from the Chinese Glioma Genome Atlas (CGGA) dataset. **(A)** Heatmap revealing the scores of immune cells in the low, medium, and high immunity groups. **(B–E)** Scatter plot showing the correlations between *IGHG1* and tumor purity, stromal score, ESTIMATE score, and immune score. **(F)** A high expression of *IGHG1* indicates more immune cell infiltration in glioma. *** represent P < 0.0001.

bioinformatics methods. The expression level of *IGHG1* in patients with glioma was apparently upregulated from the GEO and TCGA databases, especially in GBM. The OS of patients with a higher expression of *IGHG1* had worse prognosis compared with those with a lower expression. Similar consequences have been found in some epithelial cancers. Xinyu et al. provided novel evidence that *IGHG1* acted as an oncogene by promoting gastric cancer cellular proliferation, migration, and chemoresistance (21). Jing et al. demonstrated that *IGHG1* was increased in prostate cancer tissues and promoted cell growth through activating the MEK/ERK/c-Myc pathway (22). In order to further verify the role of *IGHG1* in glioma, we performed stratified analysis. The results showed that patients with the molecular subtype IDH wild type and 1p19q non-codel had a higher expression of *IGHG1*. As is known, IDH wild type and 1p19q non-codel represent poor prognosis (23). Furthermore, our analysis showed that patients who were diagnosed with WHO grade IV glioma had the highest expressions of *IGHG1*. WHO grade II glioma patients had the lowest expressions. The expression of *IGHG1* was positively relevant to tumor grade and could predict adverse prognosis. It turns out that a high expression of *IGHG1* was associated with some of the molecular subtypes mentioned previously that represent bad prognosis.

RP215 is a mAb that specifically recognizes the sialylation site of the heavy chain of cancer-IgG (24). In the present study, we used RP215 for immunohistochemical staining, which distinguishes IgG produced by B cells. Similar to the results of the bioinformatics analysis, it was shown that a high level of cancer-IgG is significantly related to poor prognosis in glioma. Patients with a higher expression of cancer-IgG have shorter DFS. In addition, cancer-IgG expression was shown to be a powerful prognostic marker for survival. Previous researchers have discovered that cancer-IgG is an independent poor

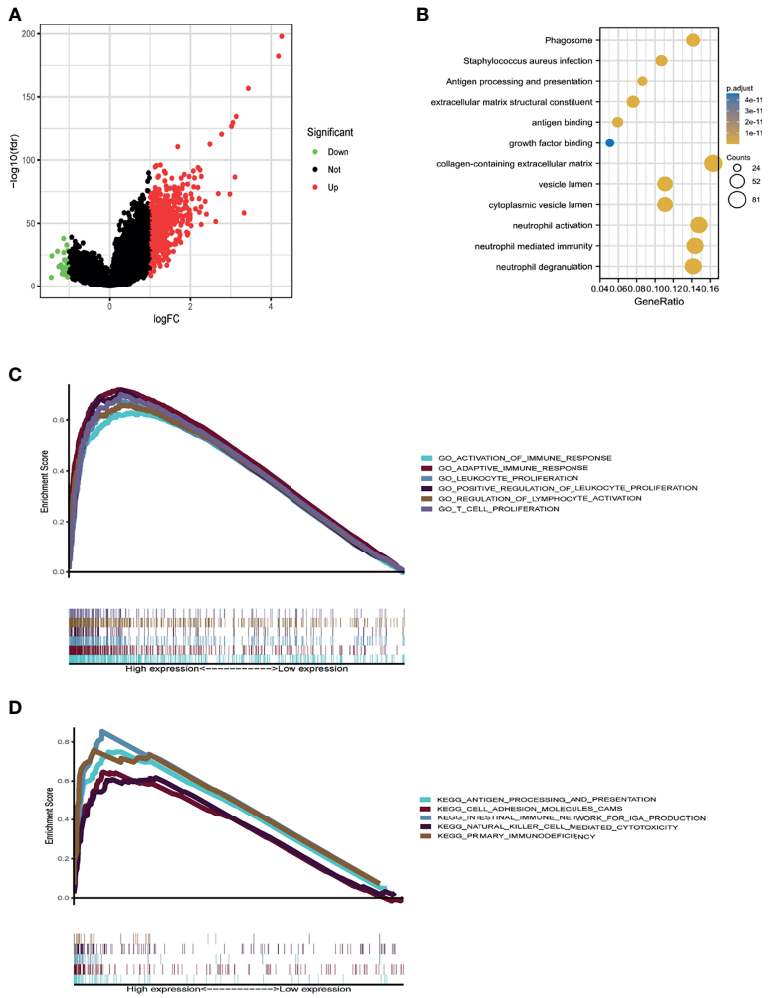

FIGURE 5 | Database for Annotation, Visualization and Integrated Discovery (DAVID) and gene set enrichment analysis (GSEA) of the relevant mechanisms involved in *IGHG1*. **(A)** Volcano map showing the differentially expressed genes. **(B–D)** DAVID **(B)**, Kyoto Encyclopedia of Genes and Genomes (KEGG) **(C)**, and Gene Ontology (GO) **(D)** were used to analyze the relevant mechanisms.

prognostic factor, as also suggested by our findings in glioma studies. Ming et al. found that a high cancer-IgG expression in pancreatic ductal adenocarcinoma and parathyroid carcinoma was related to poor DFS and OS (25, 26). Jiang et al. studied cancer-IgG in colorectal cancer. They found that the overexpression of cancer-IgG in colorectal cancer patients led to poor prognosis (27).

Many studies have concentrated on the mechanisms of cancer-IgG in carcinogenesis. Qiu et al. firstly discovered that cancer-IgG has growth factor-like activity (28). Later studies also proved this view and further found that cancer-IgG can also play the role of an oncogene through the AKT, FAK, SOX2, and other signaling pathways in cancer cells (8, 9, 19, 29). Interacting cells in the TME are considered to regulate the characteristics of cancers, such as uncontrolled proliferation, malignant metastasis, and chemoradiotherapy resistance (30). Recent studies have shown that cancer cells could secrete cancer-IgG into the TME that binds to sialic acid-binding immunoglobulin-type lectins (Siglecs) on effector $CD4^+$ and $CD8^+$ T cells. Then, cancer-IgG is secreted into the TME and promotes tumor cell immune escape (11). Xiaoyan et al. discovered that *IGHG1* in pancreatic carcinomas is associated with immune evasion (31). In our study, we explored the role of *IGHG1* in the glioma microenvironment with ssGSEA. The results illustrated that patients with a high expression of *IGHG1* were clustered into a high immunity group and those with a low expression into a low immunity group. A high expression of *IGHG1* was correlated with more immunocyte infiltration. Immune cells including the microglia and peripheral macrophages, granulocytes, myeloid-derived suppressor cells, and T lymphocytes infiltrate into the glioma. In the microenvironment of glioma, the infiltration of microglia/macrophages and myeloid-derived suppressor cells was negatively correlated with prognosis (32). Combined with our findings, this suggests that *IGHG1* could play a role in

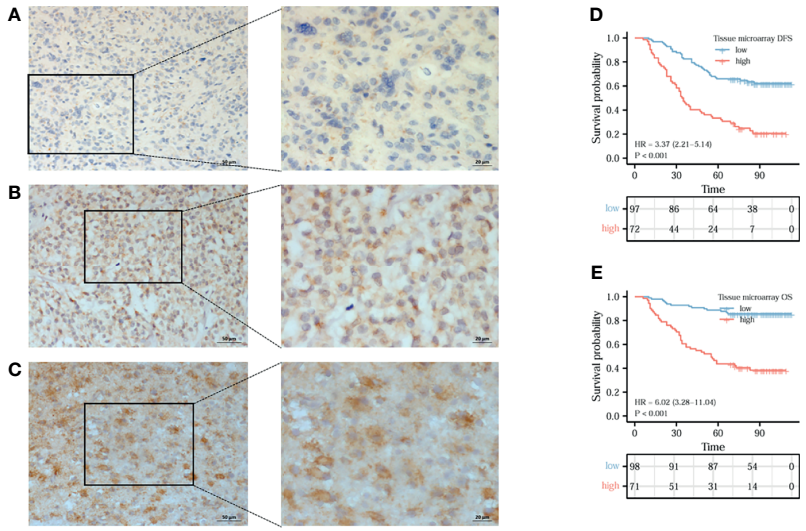

FIGURE 6 | The expression of cancer-derived immunoglobulin G (cancer-IgG) in gliomas and its prognostic significance were analyzed by immunohistochemistry. **(A–C)** Cancer-IgG is weakly, moderately, and strongly positive in gliomas, respectively. **(D, E)** A high cancer-IgG expression in glioma was Analysis of the TMA showed that disease-free survival (DFS) (HR = 6.02, 95%CI =3.28–11.04, p < 0.001) **(D)** and OS (HR = 3.37, 95%CI = 2.21–5.14, p < 0.001) **(E)** were obviously poorer in patients with a high expression of cancer-IgG.

immune-related processes, leading to poor OS. We made use of GSEA and DAVID to verify the results of the ssGSEA. We confirmed that *IGHG1* played a role in immune-related pathways. Defects of antigen processing pathways are relevant to malignant transformation, leading to the loss of major histocompatibility complex (MHC I) in cancer cells, which is one of the mechanisms of immune escape (33). Our results suggested that the expressions of *IGHG1* and cancer-IgG could induce immune escape, contributing to poor survival.

In this study, we found that the expressions of *IGHG1*/cancer-IgG were higher in glioma with poor prognosis. In addition, *IGHG1*/cancer-IgG were closely related to immune cell infiltration in the glioma microenvironment. Together, *IGHG1*/cancer-IgG are promising biomarkers of diagnosis and treatment in patients with glioma. However, the conclusion of this article, only from bioinformatics analysis and immunohistochemistry, needs to be further verified in *in vivo* and *in vitro* experiments. The detailed mechanism needs to be explored in further studies.

DATA AVAILABILITY STATEMENT

The datasets presented in this study can be found in online repositories. The names of the repository/repositories and accession number(s) can be found in the article/**Supplementary Material**.

ETHICS STATEMENT

Ethical review and approval was not required for the study on human participants, in accordance with the local legislation and institutional requirements. Written informed consent for participation was not required for this study, in accordance with the national legislation and the institutional requirements.

AUTHOR CONTRIBUTIONS

XX was responsible for the overall design of this study. GW analyzed the data and edited the manuscript. HL and JP were mainly responsible for data analysis. TY contributed to the study guidance of R software. HZ was responsible for immunohistochemical staining and scoring. XH and LS provided R language modification. LB revised the discussion of the article. All authors contributed to the article and approved the submitted version.

FUNDING

This study was supported by the Key R&D Program of Hebei Province (19277737D).

SUPPLEMENTARY MATERIAL

The Supplementary Material for this article can be found online at: https://www.frontiersin.org/articles/10.3389/fonc.2021.758856/full#supplementary-material

Supplementary Figure 1 | (A, B) Survival analysis of low- and high-IGHG1 patients in the TCGA cohorts.

REFERENCES

1. Ostrom QT, Bauchet L, Davis FG, Deltour I, Fisher JL, Langer CE, et al. The Epidemiology of Glioma in Adults: A "State of the Science" Review. *Neuro Oncol* (2014) 16:896–913. doi: 10.1093/neuonc/nou087
2. Louis DN, Perry A, Wesseling P, Brat DJ, Cree IA, Figarella-Branger D, et al. The 2021 WHO Classification of Tumors of the Central Nervous System: A Summary. *Neuro Oncol* (2021) 23:1231–51. doi: 10.1093/neuonc/noab106
3. Bell EH, Zhang P, Fisher BJ, Macdonald DR, McElroy JP, Lesser GJ, et al. Association of MGMT Promoter Methylation Status With Survival Outcomes in Patients With High-Risk Glioma Treated With Radiotherapy and Temozolomide: An Analysis From the NRG Oncology/RTOG 0424 Trial. *JAMA Oncol* (2018) 4:1405–9. doi: 10.1001/jamaoncol.2018.1977
4. Stupp R, Taillibert S, Kanner A, Read W, Steinberg D, Lhermitte B, et al. Effect of Tumor-Treating Fields Plus Maintenance Temozolomide *vs* Maintenance Temozolomide Alone on Survival in Patients With Glioblastoma: A Randomized Clinical Trial. *JAMA* (2017) 318:2306–16. doi: 10.1001/jama.2017.18718
5. Tan AC, Ashley DM, López GY, Malinzak M, Friedman HS, Khasraw M. Management of Glioblastoma: State of the Art and Future Directions. *CA Cancer J Clin* (2020) 70:299–312. doi: 10.3322/caac.21613
6. Liao Q, Liu W, Liu Y, Wang F, Wang C, Zhang J, et al. Aberrant High Expression of Immunoglobulin G in Epithelial Stem/Progenitor-Like Cells Contributes to Tumor Initiation and Metastasis. *Oncotarget* (2015) 6:40081–94. doi: 10.18632/oncotarget.5542
7. Geng ZH, Ye CX, Huang Y, Jiang HP, Ye YJ, Wang S, et al. Human Colorectal Cancer Cells Frequently Express IgG and Display Unique Ig Repertoire. *World J Gastrointest Oncol* (2019) 11:195–207. doi: 10.4251/wjgo.v11.i3.195
8. Tang J, Zhang J, Liu Y, Liao Q, Huang J, Geng Z, et al. Lung Squamous Cell Carcinoma Cells Express Non-Canonically Glycosylated IgG That Activates Integrin-FAK Signaling. *Cancer Lett* (2018) 430:148–59. doi: 10.1016/j.canlet.2018.05.024
9. Yang X, Wang G, You J, Gu R, Xu X, Xu C, et al. High Expression of Cancer-IgG Is Associated With Poor Prognosis and Radioresistance *via* PI3K/AKT/DNA-PKcs Pathway Regulation in Lung Adenocarcinoma. *Front Oncol* (2021) 11:675397. doi: 10.3389/fonc.2021.675397
10. Lee G, Ge B. Inhibition of *In Vitro* Tumor Cell Growth by RP215 Monoclonal Antibody and Antibodies Raised Against Its Anti-Idiotype Antibodies. *Cancer Immunol Immunother* (2010) 59:1347–56. doi: 10.1007/s00262-010-0864-7
11. Wang Z, Geng Z, Shao W, Liu E, Zhang J, Tang J, et al. Cancer-Derived Sialylated IgG Promotes Tumor Immune Escape by Binding to Siglecs on Effector T Cells. *Cell Mol Immunol* (2020) 17:1148–62. doi: 10.1038/s41423-019-0327-9
12. Chen Z, Gu J. Immunoglobulin G Expression in Carcinomas and Cancer Cell Lines. *FASEB J* (2007) 21:2931–8. doi: 10.1096/fj.07-8073com
13. Li Y, Wang P, Ye D, Bai X, Zeng X, Zhao Q, et al. IGHG1 Induces EMT in Gastric Cancer Cells by Regulating TGF-β/SMAD3 Signaling Pathway. *J Cancer* (2021) 12:3458–67. doi: 10.7150/jca.56056
14. Larsson C, Ehinger A, Winslow S, Leandersson K, Klintman M, Dahl L, et al. Prognostic Implications of the Expression Levels of Different Immunoglobulin Heavy Chain-Encoding RNAs in Early Breast Cancer. *NPJ Breast Cancer* (2020) 6:28. doi: 10.1038/s41523-020-0170-2
15. Zhao Z, Zhang KN, Wang Q, Li G, Zeng F, Zhang Y, et al. Chinese Glioma Genome Atlas (CGGA): A Comprehensive Resource With Functional Genomic Data From Chinese Glioma Patients. *Genomics Proteomics Bioinformatics* (2021). doi: 10.1016/j.gpb.2020.10.005
16. Sun L, Hui AM, Su Q, Vortmeyer A, Kotliarov Y, Pastorino S, et al. Neuronal and Glioma-Derived Stem Cell Factor Induces Angiogenesis Within the Brain. *Cancer Cell* (2006) 9:287–300. doi: 10.1016/j.ccr.2006.03.003
17. Sung H, Ferlay J, Siegel RL, Laversanne M, Soerjomataram I, Jemal A, et al. Global Cancer Statistics 2020: GLOBOCAN Estimates of Incidence and Mortality Worldwide for 36 Cancers in 185 Countries. *CA Cancer J Clin* (2021) 71:209–49. doi: 10.3322/caac.21660
18. Staedtke V, Dzaye O, Holdhoff M. Actionable Molecular Biomarkers in Primary Brain Tumors. *Trends Cancer* (2016) 2:338–49. doi: 10.1016/j.trecan.2016.06.003
19. Qin C, Sheng Z, Huang X, Tang J, Liu Y, Xu T, et al. Cancer-Driven IgG Promotes the Development of Prostate Cancer Though the SOX2-CIgG Pathway. *Prostate* (2020) 80:1134–44. doi: 10.1002/pros.24042
20. Sheng Z, Liu Y, Qin C, Liu Z, Yuan Y, Yin H, et al. Involvement of Cancer-Derived IgG in the Proliferation, Migration and Invasion of Bladder Cancer Cells. *Oncol Lett* (2016) 12:5113–21. doi: 10.3892/ol.2016.5350
21. Li X, Chen W, Yang C, Huang Y, Jia J, Xu R, et al. IGHG1 Upregulation Promoted Gastric Cancer Malignancy *via* AKT/GSK-3β/β-Catenin Pathway. *Cancer Cell Int* (2021) 21:397. doi: 10.1186/s12935-021-02098-1
22. Chu J, Li Y, Deng Z, Zhang Z, Xie Q, Zhang H, et al. IGHG1 Regulates Prostate Cancer Growth *via* the MEK/ERK/c-Myc Pathway. *BioMed Res Int* (2019) 2019:7201562. doi: 10.1155/2019/7201562
23. Eckel-Passow JE, Lachance DH, Molinaro AM, Walsh KM, Decker PA, Sicotte H, et al. Glioma Groups Based on 1p/19q, IDH, and TERT Promoter Mutations in Tumors. *N Engl J Med* (2015) 372:2499–508. doi: 10.1056/NEJMoa1407279
24. Lee G, Zhu M, Ge B, Cheung AP, Chien CH, Chow SN, et al. Carbohydrate-Associated Immunodominant Epitope(s) of CA215. *Immunol Invest* (2012) 41:317–36. doi: 10.3109/08820139.2011.633141
25. Cui M, You L, Zheng B, Huang X, Liu Q, Huang J, et al. High Expression of Cancer-Derived Glycosylated Immunoglobulin G Predicts Poor Prognosis in Pancreatic Ductal Adenocarcinoma. *J Cancer* (2020) 11:2213–21. doi: 10.7150/jca.39800
26. Cui M, Hu Y, Zheng B, Zhang S, Zhang X, Wang M, et al. Cancer-Derived Immunoglobulin G: A Novel Marker for Differential Diagnosis and Relapse Prediction in Parathyroid Carcinoma. *Clin Endocrinol (Oxf)* (2020) 92:461–7. doi: 10.1111/cen.14158
27. Jiang H, Kang B, Huang X, Yan Y, Wang S, Ye Y, et al. Cancer IgG, a Potential Prognostic Marker, Promotes Colorectal Cancer Progression. *Chin J Cancer Res* (2019) 31:499–510. doi: 10.21147/j.issn.1000-9604.2019.03.12
28. Qiu X, Zhu X, Zhang L, Mao Y, Zhang J, Hao P, et al. Human Epithelial Cancers Secrete Immunoglobulin G With Unidentified Specificity to Promote Growth and Survival of Tumor Cells. *Cancer Res* (2003) 63(19):6488–95.
29. Peng J, Wang HC, Liu Y, Jiang JH, Lv WQ, Yang Y, et al. Involvement of non-B Cell-Derived Immunoglobulin G in the Metastasis and Prognosis of Salivary Adenoid Cystic Carcinoma. *Oncol Lett* (2017) 14:4491–8. doi: 10.3892/ol.2017.6782
30. Quail DF, Joyce JA. Microenvironmental Regulation of Tumor Progression and Metastasis. *Nat Med* (2013) 19:1423–37. doi: 10.1038/nm.3394
31. Li X, Ni R, Chen J, Liu Z, Xiao M, Jiang F, et al. The Presence of IGHG1 in Human Pancreatic Carcinomas Is Associated With Immune Evasion Mechanisms. *Pancreas* (2011) 40:753–61. doi: 10.1097/MPA.0b013e318213d51b
32. Gieryng A, Pszczolkowska D, Walentynowicz KA, Rajan WD, Kaminska B. Immune Microenvironment of Gliomas. *Lab Invest* (2017) 97:498–518. doi: 10.1038/labinvest.2017.19
33. Reeves E, James E. Antigen Processing and Immune Regulation in the Response to Tumours. *Immunology* (2017) 150:16–24. doi: 10.1111/imm.12675

Conflict of Interest: The authors declare that the research was conducted in the absence of any commercial or financial relationships that could be construed as a potential conflict of interest.

frontiers in Oncology

REVIEW
published: 12 January 2022
doi: 10.3389/fonc.2021.800053

Challenges and Advances in Diagnosis and Treatment of Leptomeningeal Disease (LMD)

Sherise D. Ferguson[1]*, *Elena I. Fomchenko*[1], *Renato A. Guerrieri*[2] *and Isabella C. Glitza Oliva*[2]

[1] Department of Neurosurgery, University of Texas, MD Anderson Cancer Center, Houston, TX, United States,
[2] Department of Melanoma Medical Oncology, University of Texas, MD Anderson Cancer Center, Houston, TX, United States

Leptomeningeal disease (LMD) is a devastating category of CNS metastasis with a very poor prognosis and limited treatment options. With maximal aggressive therapy, survival times remain short and, without treatment, prognosis is measured in weeks. Both LMD diagnosis and treatment are challenging topics within neuro-oncology. In this review, we discuss the advances in LMD diagnosis with a focus on the role of circulating tumor DNA (ctDNA) and discuss the role of targeted and immunotherapy in LMD treatment.

Keywords: leptomeningeal disease, ctDNA = circulating tumor DNA, targeted therapy, immunothearpy, intrathecal therapy

OPEN ACCESS

Edited by:
Liam Chen,
University of Minnesota, United States

Reviewed by:
Christine Marosi,
Medical University of Vienna, Austria
Rajiv Magge,
Cornell University, United States

***Correspondence:**
Sherise D. Ferguson
sdferguson@mdanderson.org

Specialty section:
This article was submitted to Neuro-Oncology and Neurosurgical Oncology, a section of the journal Frontiers in Oncology

Received: *22 October 2021*
Accepted: *06 December 2021*
Published: *12 January 2022*

Citation:
Ferguson SD, Fomchenko EI, Guerrieri RA and Glitza Oliva IC (2022) Challenges and Advances in Diagnosis and Treatment of Leptomeningeal Disease (LMD). Front. Oncol. 11:800053. doi: 10.3389/fonc.2021.800053

INTRODUCTION

Leptomeningeal disease (LMD) is a dire category of central nervous system (CNS) metastasis that entails tumor cell dissemination to the cerebrospinal fluid (CSF) and/or leptomeninges and often results in significant neurological morbidity. It occurs in approximately 5-15% of patients with solid tumors, and the incidence is rising (1–8). Among solid malignancies, lung cancer, breast cancer and melanoma are most frequently associated with LMD. Further within each primary malignancy, specific subtypes have been linked with an increased propensity for LMD. In patients with non-small cell lung cancer (NSCLC), those harboring an epidermal growth factor receptor (EGFR) mutation have a higher risk of LMD; specifically 9.4% in EGFR-mutant tumors versus 1.7% in wild-type tumors in a retrospective analysis of patients with NSCLC LMD (9). Similarly in breast cancer, tumor subtype, specifically HER2 (human epidermal growth factor receptor 2) status has been described to impact LMD propensity and outcome (10, 11). For example, the triple negative molecular subtype (*estrogen/progesterone/HER2 negative*) accounts for approximately 40% of breast cancer LMD cases, however only is diagnosed in 10% of all breast cancer patients, indicating a clear overrepresentation of this subtype among LMD patients. Furthermore, the time from breast cancer diagnosis to the development of LMD is shorter in hormone receptor negative cases (12–14).

As mentioned, the incidence of LMD is rising across various tumor types, possibly due to the fact that patients live longer with both extracranial and intracranial parenchymal metastatic disease due to advances in systemic therapy and improved imaging. Autopsy reports suggest that the actual frequency of LMD may be underestimated. In fact, one postmortem analysis of patients with cancer who exhibited neurologic symptoms revealed that 18% had evidence of leptomeningeal infiltration (15). The spread of cancer cells can be local or disseminated through the entire CNS, and LMD

almost always results in rapid neurologic disability and death. If untreated, survival can be as short at 4-6 weeks (5). However, even with currently available treatment options, prognosis remains dismal, and therefore, LMD represents one of the most challenging disease processes in neuro-oncology. In this review we will discuss advances in the diagnosis and treatment of LMD with a focus on targeted and immunotherapy.

CHALLENGES IN LMD DIAGNOSIS AND THE ROLE OF ctDNA

The diagnosis of LMD is currently based on neurological symptoms, contrast-enhanced magnetic resonance imaging (MRI) or computed tomography (CT) imaging characteristics and CSF cytopathology analysis. Since CSF tumor spread can propagate to the entire CNS, LMD can present with a wide constellation of neurological symptoms and signs from invasion of the brain, spine and/or cranial nerves. As such, symptoms may include (but not limited to) headache (from meningeal irritation), cranial nerve palsies, altered mental status, bowel or bladder dysfunction and/or extremity weakness. Furthermore, some patients may develop symptoms of elevated intracranial pressure from LMD induced aberrations in CSF dynamics. Radiographically, LMD may present with a variety of enhancement patterns on MRI. Classically, MRIs show linear or nodular enhancement along the cerebral sulci, dura, cerebellar folia, spinal cord/cauda equina and/or cranial nerves (16) (**Figure 1**). LMD disease can also cause abnormalities in CSF dynamics resulting in ventriculomegaly and potentially increased intracranial pressure. Finally, CSF analysis is critical in the diagnosis of LMD and is currently considered the gold standard. CSF is most commonly acquired *via* lumbar puncture and cytology may show the presence of malignant cells. In addition to cytology, CSF cell count and chemistry (particularly protein levels) are abnormal in 90% of LMD patients, aiding in diagnosis (17, 18).

Despite these approaches, the definitive diagnosis of LMD can still be quite challenging due to the limited sensitivity of initial CSF cytology and MRI and the high variability of presentation between patients. MRI has the benefit of being non-invasive, so it is typically the first diagnostic step; however, the sensitivity and specificity are 75% and 77%, respectively (19). Several clinical scenarios, including recent radiation or surgery, infection and intracranial hypotension, can resemble LMD by also causing abnormal enhancement. Furthermore, adjacent parenchyma metastasis can also cause localized sulcal/leptomeningeal enhancement. In situations where imaging is unclear or equivocal, CSF analysis is required; however, in many cases, CSF analysis is performed as an additional confirmatory step even when radiographic findings are consistent with LMD. Despite CSF analysis being the diagnostic gold standard, it still has significant limitations. First, CSF cytology has lower sensitivity than MRI, with malignant cells reportedly detected in only 50-67% of patients (17, 20–22). Frequently, two or three CSF samples are required to establish the diagnosis of LMD, as the sensitivity rises to 80-90% with a second and third lumbar puncture (17). In most cases, CSF chemistry, specifically elevated protein, can be observed, but these abnormalities are also non-specific. Finally, CSF cytological analysis may suffer from inter-observer variability and may depend on the experience of the pathologist (16).

Prompt diagnosis of LMD is critical, and improved diagnostics could potentially improve the outcome of these patients. Further, none of the currently available diagnostic modalities can provide reliable information on disease burden or (early) response to treatment. As such, novel molecular tools have emerged to address these issues. Considering the pathogenesis of LMD remains elusive, these tools also provide the opportunity to assess specific and potentially actionable therapeutic targets.

Among recent molecular advancements, circulating tumor DNA (ctDNA) has provided an avenue to address the above concerns. ctDNA are short, double stranded tumor DNA fragments that are released by tumor cells as a result of cell apoptosis and or necrosis. ctDNA are different from so called circulating tumor cells (CTCs), which are intact tumor cells (23, 24). The role of ctDNA has been demonstrated in multiple studies across different solid tumor types and includes aiding early diagnosis, monitoring treatment response and monitoring patients for early recurrence in the adjuvant setting (23, 25–27). Further, tumor-specific genomic abnormalities can be detected in ctDNA using next-generation sequencing techniques or PCR-based options, and this assay has demonstrated a strong concordance with the genomic profile of malignant tissue, making ctDNA a potentially powerful biomarker (23, 28).

In the setting of neurological malignancies, the utility of plasma-derived ctDNA is suboptimal (29–32). However, recent studies have shown that CSF is a promising platform for ctDNA analysis in the setting of intracranial pathology (31). For example, Mattos-Arruda et al., performed targeted sequencing and/or exome sequencing coupled with droplet digital PCR (ddPCR) on matched CSF-derived ctDNA, plasma-derived ctDNA, and tumor tissue deposits in patients with both primary and metastatic brain tumors (31). These authors reported significantly higher genomic alteration sensitivity in CSF-derived ctDNA than in plasma-derived ctDNA in patients with CNS tumors. Furthermore, this same study observed treatment-associated changes in CSF ctDNA signatures through longitudinal collection of CSF, potentially identifying new therapeutic targets. This finding has also been consistent in patients with LMD. In a study of patients with NSCLC LMD, Ying et al. performed sequencing on 72 matched CSF and plasma samples. Mutation detections rates were 81% in CSF versus only 62% in plasma. Moreover, the average maximum allelic frequency in plasma was 4.6% versus 44% in CSF, demonstrating that CSF is superior to plasma for mutation identification and genomic analysis of LMD (33).

In cases where CSF cytology and MRI finding are indeterminate, confirming the diagnosis of LMD is very difficult. Several studies have suggested that ctDNA can augment the diagnostic yield of CSF for prompt LMD

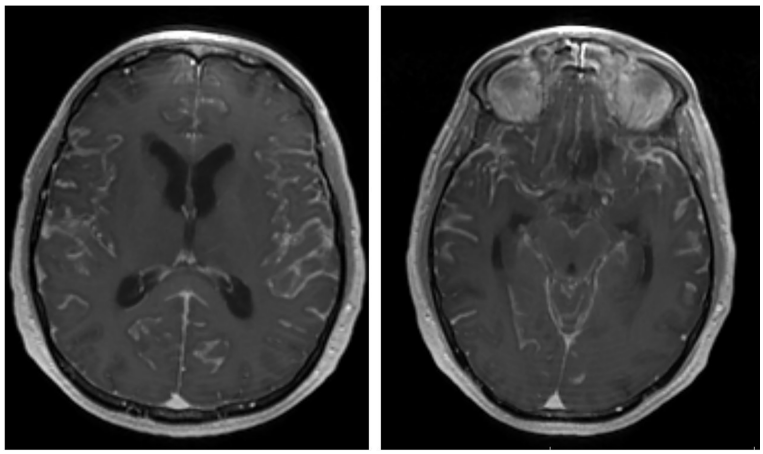

FIGURE 1 | Representative post-contrast brain MRI (axial) showing diffuse LMD with enhancement within the cerebral sulci.

diagnosis (34, 35). For example, Zhao et al. directly compared the sensitivity of imaging, CSF cytology and CSF ctDNA in the diagnosis of LMD. The authors evaluated CSF samples from 35 LMD cases across multiple primary malignancies (36). They reported that 71% of cases had positive CSF cytology and 63% had imaging features consistent with LMD while CSF ctDNA extraction and next-generation sequencing revealed cancer associated mutations in 100% of cases, highlighting the sensitivity of ctDNA. In a melanoma specific study, Ballester et al., utilized ddPCR and next-generation sequencing to evaluate the CSF-derived ctDNA of seven melanoma patients with LMD. First, this study confirmed the diagnostic power of ctDNA, as 30% of patients whose CSF samples were negative/indeterminate for malignant cells were positive for CSF ctDNA. Further, analysis of ctDNA showed the presence of melanoma associated mutations, and in two patients, they found a correlation between mutant allele fraction and radiographic tumor volume on MRI, suggesting that ctDNA could potentially aid in monitoring tumor burden (34). Since CSF can be collected serially at multiple time-points in the patients' treatment course, small studies have investigated the role of ctDNA in assessing and monitoring LMD tumor burden pre- and post-treatment (36–39). In a cohort of patients with EGFR mutated, NSCLC LMD, Zheng et al., evaluated if ctDNA could assess response to EGFR targeted therapy with osimertinib (tyrosine kinase inhibitor). The authors reported that CSF ctDNA revealed the genomic landscape of LMD in patients prior to treatment with osimertinib and following progression on treatment. They reported that overall detection of EGFR-sensitizing mutations was greater than 93% in patients with EGFR-mutated NSCLC LMD. Further, detection of EGFR 19 deletion and positive T790M (a point mutation in the EGFR tyrosine kinase domain) in the CSF was associated higher median intracranial progression free survival on osimertinib. Concurrent cell cycle alterations with EGFR-sensitizing mutations were associated lower median intracranial progression free survival. Additionally, analysis of a cohort of patients whose CSF was genotyped following progression post osimertinib treatment revealed multiple potential resistance mechanisms (37). In summary, the utility of ctDNA has been shown in three main categories: first, to aid in early diagnosis; second, to assess treatment course and tumor burden; and third, to potentially uncover actionable targets to optimize or introduce novel treatment strategies.

ROLE OF TARGETED THERAPY IN LMD

Historically, the treatment for LMD was divided into systemic therapy, radiation and intrathecal (IT) approaches. Until recently, systemic treatment options have been significantly limited due to the inability of chemotherapy to penetrate the blood brain barrier (BBB). However, recent advances in the treatment that may overcome this limitation, namely targeted therapy and checkpoint inhibitors, have brought some hope for patients with LMD. Moreover, while the vast majority of investigation in NSCLC, breast and melanoma is based on the systemically administered therapies, IT approaches are currently being investigated.

For NSCLC LMD, current therapies target EGFR mutations and anaplastic lymphoma kinase (ALK) rearrangement *via* tyrosine kinase inhibitors (TKIs). Targeting these molecular alterations has substantially impacted the prognosis of advanced NSCLC. Multiple studies have been published on systemic targeted therapy applications for patients with NSCLC LMD including case reports, retrospective and prospective studies, as well as phase 1 open label and phase 3 randomized controlled trials. In regards to EGFR inhibition, first generation and second generation TKIs such as gefitinib, erlotinib and afatinib were initially evaluated with some success but most have been challenged by limited CNS penetration (40–42). Magnification of therapy using higher concentrations or a pulsatile regimen has been proposed to increase the CSF concentrations (43–46). However, as a result of this limited BBB permeability, CNS recurrence following

treatment with first generation and second generation TKIs is as high as 40% (47). Based on multiple studies, third-generation TKI osimertinib has shown notable promise in the treatment of EGFR mutated LMD due to its higher BBB penetration (48–53). Yang et al. published a phase I study of 32 patients with LMD patients treated with osimertinib in which 87% of patients reported symptomatic improvement and 72% had a radiographic response (48). The follow-up study of 41 patients reported functional improvement in 57% of patients, a response rate of 41% and overall survival (OS) of 11 months [The BLOOM study (49)]. In a recent phase II study evaluating osimertinib in patients with brain metastasis and LMD, the authors reported an intracranial control rate of 92.5% (complete response in 12.5%) and a median OS of 13 months (53). Overall, based on these data, osimertinib is considered a viable treatment option for EGFR mutated NSCLC. An ongoing multicenter phase 2 trial [Osimertinib in Patients With a Lung Cancer With Brain or Leptomeningeal Metastases With EGFR Mutation (ORBITAL)] will assess CNS response rates to osimertinib as a single agent (NCT04233021). Another phase 2 trial is evaluating the safety and efficacy of osimertinib in combination with bevacizumab (NCT04425681 and NCT04148898).

AZD3759 is an alternative novel EGFR inhibitor that is capable of efficiently crossing the BBB. The safety of AZD3759 in patients with EGFR-mutant NSCLC, brain metastases and LMD was evaluated in a multicenter phase I study (54). Incidentally, the authors observed significant radiographic efficacy in three of four enrolled LMD patients. Another phase I study by Cho et al. reported that AZD3759 showed a reduction in EGFR expression in the majority of cases and stable disease in 50% (55). Nimotuzumab, another new generation TKI, has undergone limited evaluation, but a cases series with promising results and rapid responses has been reported (56).

ALK mutations are rare and can be found in approximately 3–7% of patients with NSCLC; targeting this mutation has been a notable step in the treatment of this patient population (57). The data specifically addressing the role of ALK inhibition in LMD is less robust than addressing EGFR inhibition, however, some small studies have been supportive of this approach and have demonstrated efficacy in CNS disease. Frost et al. reported the recent result of a German early access program with lorlatinib, a third-generation ALK inhibitor. This study included 52 patients who had progressed on first and second-line ALK inhibitors. The majority of the included patients had CNS disease [nine (17%) had LMD specifically], and the authors reported an intracranial response rate of 54% (58). A recent phase 3 clinical trial compared lorlatinib with first generation ALK inhibitor crizotinib in 296 patients with advanced *ALK*-positive NSCLC who had received no previous systemic treatment for metastatic disease. Intracranial response was a secondary end point and a complete intracranial response was achieved in 71% of cases, highlighting that later generation ALK inhibitors have relatively higher CNS efficacy. Case reports focused on LMD have shown impressive responses with ALK targeting (59, 60), but larger studies are still needed.

In breast cancer patients with LMD the majority of targeted therapy efforts have been focused on HER2+ patients. HER2 is a tyrosine kinase in the EGFR family; its overexpression has a known impact on patient prognosis and is associated with CNS dissemination (61). Among available agents, the HER2 antibody trastuzumab has received the most attention, as pivotal trials demonstrated its efficacy in HER+ breast cancer (62). However, the BBB penetration of trastuzumab is limited, making the CNS a frequent site of progression (63). In light of this, two arms of investigation have evolved to address HER2+ CNS disease (including LMD). First, new HER2 TKIs with better BBB penetration, including lapatinib, neratinib and tucatinib, are currently been evaluated. For example, lapatinib is a small molecule that binds HER2; it has shown limited CNS efficacy as a single agent (64), but encouraging results have been observed when used in combination with capecitabine (65–68). The recent HERCLIMB Trial (291 HER2+ patients with brain metastasis enrolled) evaluated the intracranial efficacy of tucatinib when combined with trastuzumab and capecitabine. This trial demonstrated that the combination of tucatinib, trastuzumab, and capecitabine significantly reduced the risk of intracranial progression or death (HR 0.32; $p<0.001$) and increased the intracranial response rate compared to control group (47 versus 20.0%; $p = 0.03$). However, this trial did not include LMD patients (69). For LMD specifically, Pellerino et al. reported the outcome of patients with HER2+ breast cancer LMD treated with neratinib. This study reported an OS of eight months, neurological improvement in 27% of cases, and stabilization of radiographic disease in 57% of cases (70). Second, to overcome the issue with BBB penetration, IT administration of HER2 targeted therapy has been explored in patients with HER2+ breast LMD. Of the available agents, IT administration of trastuzumab has been the most heavily evaluated. In a retrospective study by Figura et al., the authors compared the therapeutic efficacy of IT trastuzumab to IT methotrexate or whole brain radiation alone. IT trastuzumab resulted in significantly longer progression free survival and OS compared with the other treatment groups. Notably, 44% of patients treated with IT trastuzumab were alive at 6 months (71). A recent meta-analysis of 58 patients treated with IT trastuzumab reported radiological improvement in over 70% of patients and an OS of 13.2 months (72). Overall, IT trastuzumab is a potentially safe effective treatment of HER2+ LMD, but larger prospective studies needed.

Triple negative breast cancer (TNBC) presents a unique challenge as patients with this tumor type have limited targeted therapy options and a high risk of CNS dissemination. Poly adenosine diphosphate ribose polymerase enzymes (PARP enzymes) naturally repair the DNA breaks/damage that lead to apoptosis of tumor cells. BRCA (breast cancer susceptibility genes 1 or 2; BRCA) mutations impair the ability of PARP enzymes to repair damaged DNA. PARP inhibitors such as iniparib, olaparib, talazoparib and veliparib work by preventing tumor cells from repairing, allowing them to proceed to cell death. These inhibitors have been evaluated in patients with TNBC including those with brain metastasis. The use of PARP inhibitors has not yet been evaluated on a large scale in LMD,

however, limited case reports have shown good clinical and radiographic response with olaparib (73, 74).

Finally, in melanoma, approximately 40-50% of patients with melanoma harbor a mutation in the serine/threonine kinase BRAF (75). As such, therapies targeting BRAF and MEK has significantly impacted the natural history and outcome of patients with BRAF mutant melanoma, even in those with CNS metastases. However, for patients with LMD, no prospective clinical trial using BRAF/MEK inhibitors has been performed to date, and data is limited mainly to case reports. Some of these outcomes have been very encouraging, as patients had prolonged survival; however, all these patients were BRAF/MEK treatment naïve when they were diagnosed with LMD and started on targeted therapy. This is important when assessing the available data, as patients who develop LMD while on targeted therapy continue to face a dismal prognosis (70). In addition, recent analyses of two large cohorts of patients confirmed that despite the use of targeted therapy, overall survival remained poor (76, 77).

ROLE OF IMMUNOTHERAPY IN LMD

Recent advances in the field of immunotherapy, specifically the use of checkpoint inhibitors, has led to improved outcomes across multiple malignancies, including in patients with advanced disease. Importantly, checkpoint inhibitors have shown to provide improved outcomes in patients with brain metastases, specifically in patients with melanoma brain metastases (78–80). Until recently, patients with LMD have been excluded from trials for patients with brain metastases, and the limited data for systemic checkpoint inhibitor therapy was based on case reports only (81–83). The ABS trial focused primarily on the checkpoint inhibitor treatment (nivolumab) of melanoma patients with parenchymal brain metastases and also allowed patients with LMD to be enrolled into cohort C, which also included patients who had failed local therapy, were symptomatic and required steroids. None of the 4 patients with LMD obtained benefit from treatment with nivolumab (79). Two recent prospective trials were designed specifically for patients with cancer and LMD, and both of them used systemically administered pembrolizumab, another checkpoint inhibitor. The first one, a phase 2 trial, mainly enrolled patients with breast cancer (n=17), lung cancer (n=2) and ovarian cancer (n=1) (84). The primary endpoint was OS at 3 months, with secondary endpoints being toxicity and response. With a median follow-up of 6.3 months (range, 2.2-12.5 months) in surviving patients, the primary endpoint was met, and 12 out of 20 patients were alive 3 months after enrollment. No new safety signals were observed with the use of systemic pembrolizumab in this patient population. A second phase 2 study by Naidoo et al. enrolled 13 patients across multiple pathologies and reported a CNS response rate of 38% and a median OS of 4.9 months (85). Importantly, these patients were all treatment naïve to checkpoint inhibition with anti-PD1. TNBC, which has limited targeted therapy options, has ongoing trials evaluating the therapeutic efficacy of checkpoint inhibition, specifically PD-1 and PDL-1 inhibition, in combination with stereotactic radiosurgery (NCT03807765, NCT03449238, NCT03483012). In addition, another trial is evaluating the safety and dose limiting toxicity of combining avelumab in combination with whole brain radiation for patients with LMD and any type of solid tumor history (NCT03719768).

The effect of the combination of ipilimumab and nivolumab on survival has also been assessed in a phase II trial 18 patients with LMD (86). These patients [with breast cancer (n=8), melanoma (n=2), lung (n=2) and other primary tumors (n=6)] were treated with the combination of ipilimumab and nivolumab. Importantly, the majority of patients (78%) required corticosteroids for symptom management at treatment initiation or any point during the trial. Like the prior trial with single agent anti-PD1, this trial met its primary 3-month OS endpoint, as 8 patients (44%) were alive at that time point. Median survival for the whole group of patients was 2.9 months (90% CI: 1.6- 5 months). Six patients (33%) had grade 3 or 4 treatment related toxicities, which is slightly less than previous reports, but importantly, no new safety signals were seen.

In addition to systemic administration, IT approaches using various immunotherapies have been investigated for the treatment of LMD. In a retrospective review of 178 melanoma patients, the authors reported that patients treated with IT therapy were afforded significantly longer survival time (76). Interestingly, the IT use of immunotherapy dates back to the 1980s, when IT interleukin 2 (IL-2) was first assessed in patients with melanoma LMD. Two large cohorts (n=46 n=43) of patients with melanoma reported a median OS of 11.5 months (range 7-19), as well as 1-year, 2-year and 5-year OS rates of 36%, 26% and 13%, respectively, in patients that responded to IT IL-2 (87, 88). However, this approach is associated with significant toxicities the need for prolonged and intensive in-hospital monitoring, making this therapy an option for only a highly selected group of patients. To avoid the toxicity associated with IT IL-2, and based on the fact that systemic anti-PD1 administration leads to higher response rates than high dose IL-2 in patients with metastatic melanoma, a recent first-in-human trial assessed the safety and initial efficacy of using IT nivolumab in combination with IV nivolumab (NCT03025256). This allowed for a dose intensified approach, as it was shown that systemically administered nivolumab has very poor CSF penetration (89). Initial results for the first 25 patients treated showed a median OS of 4.9 months at a median follow-up of 20 weeks (range 5-147), with 3, 6 and 12 months OS rates of 65%, 47% and 35%, respectively. Importantly, the use of IT nivolumab was very well tolerated with no grade 3 or 4 toxicities observed, and the addition of IV nivolumab did not increase the expected toxicity from systemic anti-PD-1 administration. The trial is ongoing, with translational data expected in the near future (90).

CONCLUSION

LMD represents a subtype of CNS metastatic disease with few treatment options, and patients diagnosed with LMD, as well as their treating physicians, face major challenge in both prompt diagnosis and treatment. This condition commonly results in

rapid neurologic disability and death. Even with currently available therapies, prognosis remains grim. However, multiple avenues, including targeted and immunotherapy, are currently being explored to combat this challenging disease and gain a deeper insight into the underlying disease pathogenesis. Much more needs to be learned and done, but the initial results of these new approaches are promising.

AUTHOR CONTRIBUTIONS

SF: Conception, drafting of manuscript and review of final version. EF: Drafting of manuscript and review of final version. RG: Review of final version. IG: Conception, drafting of manuscript and review of final version. All authors contributed to the article and approved the submitted version.

REFERENCES

1. Nayar G, Ejikeme T, Chongsathidkiet P, Elsamadicy AA, Blackwell KL, Clarke JM, et al. Leptomeningeal Disease: Current Diagnostic and Therapeutic Strategies. *Oncotarget* (2017) 8(42):73312–28. doi: 10.18632/oncotarget.20272
2. Thomas KH, Ramirez RA. Leptomeningeal Disease and the Evolving Role of Molecular Targeted Therapy and Immunotherapy. *Ochsner J* (2017) 17 (4):362–78.
3. Herrlinger U, Förschler H, Küker W, Meyermann R, Bamberg M, Dichgans J, et al. Leptomeningeal Metastasis: Survival and Prognostic Factors in 155 Patients. *J Neurol Sci* (2004) 223(2):167–78. doi: 10.1016/j.jns.2004.05.008
4. Beauchesne P. Intrathecal Chemotherapy for Treatment of Leptomeningeal Dissemination of Metastatic Tumours. *Lancet Oncol* (2010) 11(9):871–9. doi: 10.1016/S1470-2045(10)70034-6
5. Groves MD. Leptomeningeal Disease. *Neurosurg Clin N Am* (2011) 22(1):67–78, vii. doi: 10.1016/j.nec.2010.08.006
6. Le Rhun E, Taillibert S, Chamberlain MC. Carcinomatous Meningitis: Leptomeningeal Metastases in Solid Tumors. *Surg Neurol Int* (2013) 4 (Suppl 4):S265–88. doi: 10.4103/2152-7806.111304
7. Taillibert S, Chamberlain MC. Leptomeningeal Metastasis. *Handb Clin Neurol* (2018) 149:169–204. doi: 10.1016/B978-0-12-811161-1.00013-X
8. Leal T, Chang JE, Mehta M, Robins HI. Leptomeningeal Metastasis: Challenges in Diagnosis and Treatment. *Curr Cancer Ther Rev* (2011) 7 (4):319–27. doi: 10.2174/157339411797642597
9. Li YS, Jiang BY, Yang JJ, Tu HY, Zhou Q, Guo WB, et al. Leptomeningeal Metastases in Patients With NSCLC With EGFR Mutations. *J Thorac Oncol* (2016) 11(11):1962–9. doi: 10.1016/j.jtho.2016.06.029
10. Abouharb S, Ensor J, Loghin ME, Katz R, Moulder SL, Esteva FJ, et al. Leptomeningeal Disease and Breast Cancer: The Importance of Tumor Subtype. *Breast Cancer Res Treat* (2014) 146(3):477–86. doi: 10.1007/s10549-014-3054-z
11. Griguolo G, Pouderoux S, Dieci MV, Jacot W, Bourgier C, Miglietta F, et al. Clinicopathological and Treatment-Associated Prognostic Factors in Patients With Breast Cancer Leptomeningeal Metastases in Relation to Tumor Biology. *Oncologist* (2018) 23(11):1289–99. doi: 10.1634/theoncologist.2018-0200
12. Niwińska A, Rudnicka H, Murawska M. Breast Cancer Leptomeningeal Metastasis: Propensity of Breast Cancer Subtypes for Leptomeninges and the Analysis of Factors Influencing Survival. *Med Oncol* (2013) 30(1):408. doi: 10.1007/s12032-012-0408-4
13. Brewster AM, Chavez-macgregor M, Brown P. Epidemiology, Biology, and Treatment of Triple-Negative Breast Cancer in Women of African Ancestry. *Lancet Oncol* (2014) 15(13):e625–34. doi: 10.1016/S1470-2045(14)70364-X
14. Yust-Katz S, Garciarena P, Liu D, Yuan Y, Ibrahim N, Yerushalmi R, et al. Breast Cancer and Leptomeningeal Disease (LMD): Hormone Receptor Status Influences Time to Development of LMD and Survival From LMD Diagnosis. *J Neurooncol* (2013) 114:229–35. doi: 10.1007/s11060-013-1175-6
15. Glass JP, Melamed M, Chernik NL, Posner JB. Malignant Cells in Cerebrospinal Fluid (CSF): The Meaning of a Positive CSF Cytology. *Neurology* (1979) 29(10):1369–75. doi: 10.1212/WNL.29.10.1369
16. Le Rhun E, Weller M, Brandsma D, Van den Bent M, de Azambuja E, Henriksson R, et al. EANO-ESMO Clinical Practice Guidelines for Diagnosis, Treatment and Follow-Up of Patients With Leptomeningeal Metastasis From Solid Tumours. *Ann Oncol* (2017) 28:iv84–99. doi: 10.1093/annonc/mdx221
17. Wasserstrom WR, Glass JP, Posner JB. Diagnosis and Treatment of Leptomeningeal Metastases From Solid Tumors: Experience With 90 Patients. *Cancer* (1982) 49(4):759–72. doi: 10.1002/1097-0142(19820215)49:4<759::AID-CNCR2820490427>3.0.CO;2-7
18. Brandsma D, Voest EE, de Jager W, Bonfrer H, Algra A, Boogerd W, et al. CSF Protein Profiling Using Multiplex Immuno-Assay: A Potential New Diagnostic Tool for Leptomeningeal Metastases. *J Neurol* (2006) 253 (9):1177–84. doi: 10.1007/s00415-006-0187-y
19. Straathof CS, de Bruin HG, Dippel DW. Vecht CJ The Diagnostic Accuracy of Magnetic Resonance Imaging and Cerebrospinal Fluid Cytology in Leptomeningeal Metastasis. *J Neurol* (1999) 246(9):810–4. doi: 10.1007/s004150050459
20. Van Oostenbrugge RJ, Twijnstra A. Presenting Features and Value of Diagnostic Procedures in Leptomeningeal Metastases. *Neurology* (1999) 53 (2):382–5. doi: 10.1212/WNL.53.2.382
21. Nayak L, Fleisher M, Gonzalez-Espinoza R, Lin O, Panageas K, Reiner A, et al. Rare Cell Capture Technology for the Diagnosis of Leptomeningeal Metastasis in Solid Tumors. *Neurology* (2013) 80(17):1598–605. doi: 10.1212/WNL.0b013e31828f183f
22. Subirá D, Serrano C, Castanón S, Gonzalo R, Illán J, Pardo J, et al. Role of Flow Cytometry Immunophenotyping in the Diagnosis of Leptomeningeal Carcinomatosis. *Neuro Oncol* (2012) 14(1):43–52. doi: 10.1093/neuonc/nor172
23. Bettegowda C, Sausen M, Leary R, Kinde I, Agrawal N, Bartlett B, et al. Detection of Circulating Tumor DNA in Early and Late Stage Human Malignancies. *Sci Transl Med* (2014) 6:224–224ra24. doi: 10.1126/scitranslmed.3007094
24. Canzoniero VL, Park BH. Use of Cell Free DNA in Breast Oncology. *Biochim Biophys Acta* (2016) 1865(2):266–74. doi: 10.1016/j.bbcan.2016.03.006
25. Newman AM, Bratman SV, To J, Wynne JF, Eclov NCW, Modlin LA, et al. An Ultrasensitive Method for Quantitating Circulating Tumor DNA With Broad Patient Coverage. *Nat Med* (2014) 20:5–548. doi: 10.1038/nm.3519
26. Creemers A, Krausz S, Strijker M, Mj VDW, Soer EC, Reinten RJ, et al. Clinical Value of ctDNA in Upper-GI Cancers: A Systematic Review and Meta-Analysis. *Biochim Biophys Acta* (2017) 1868(2):394–403. doi: 10.1016/j.bbcan.2017.08.002
27. Corrò C, Hejhal T, Poyet C, Sulser T, Hermanns T, Winder T, et al. Detecting Circulating Tumor DNA in Renal Cancer: An Open Challenge. *Exp Mol Pathol* (2017) 102(2):255–61. doi: 10.1016/j.yexmp.2017.02.009
28. Volik S, Alcaide M, Morin RD, Collins C. Cell-Free DNA (cfDNA): Clinical Significance and Utility in Cancer Shaped by Emerging Technologies. *Mol Cancer Res* (2016) 14(10):898–908. doi: 10.1158/1541-7786.MCR-16-0044
29. Lavon I, Refael M, Zelikovitch B, Shalom E, Siegal T. Serum DNA can Define Tumor-Specific Genetic and Epigenetic Markers in Gliomas of Various Grades. *Neuro Oncol* (2010) 12:173–80. doi: 10.1093/neuonc/nop041
30. Chen WW, Balaj L, Liau LM, Samuels ML, Kotsopoulos SK, Maguire CA, et al. BEAMing and Droplet Digital PCR Analysis of Mutant IDH1 mRNA in Glioma Patient Serum and Cerebrospinal Fluid Extracellular Vesicles. *Mol Ther Nucleic Acids* (2013) 2:e109. doi: 10.1038/mtna.2013.28
31. De Mattos-Arruda L, Mayor R, Ng CK, Weigelt B, Martínez-Ricarte F, Torrejon D, et al. Cerebrospinal Fluid-Derived Circulating Tumour DNA Better Represents the Genomic Alterations of Brain Tumours Than Plasma. *Nat Commun* (2015) 6:8839. doi: 10.1038/ncomms9839
32. Boisselier B, Gallego Perez-Larraya J, Rossetto M, Labussière M, Ciccarino P, Marie Y, et al. Detection of IDH1 Mutation in the Plasma of Patients With Glioma. *Neurology* (2012) 79:1693–169. doi: 10.1212/WNL.0b013e31826e9b0a
33. Ying S, Ke H, Ding Y, Liu Y, Tang X, Yang D, et al. Chen L Unique Genomic Profiles Obtained From Cerebrospinal Fluid Cell-Free DNA of non-Small Cell

Lung Cancer Patients With Leptomeningeal Metastases. *Cancer Biol Ther* (2019) 20(4):562–70. doi: 10.1080/15384047.2018.1538614
34. Ballester LY, Glitza Oliva IC, Douse DY, Chen MM, Lan C, Haydu LE, et al. Evaluating Circulating Tumor DNA From the Cerebrospinal Fluid of Patients With Melanoma and Leptomeningeal Disease. *J Neuropathol Exp Neurol* (2018) 77(7):628–35. doi: 10.1093/jnen/nly046
35. Momtaz P, Pentsova E, Abdel-Wahab O, Diamond E, Hyman D, Merghoub T, et al. Quantification of Tumor-Derived Cell Free DNA(cfDNA) by Digital PCR (DigPCR) in Cerebrospinal Fluid of Patients With BRAFV600 Mutated Malignancies. *Oncotarget* (2016) 7:85430–6. doi: 10.18632/oncotarget.13397
36. Zhao Y, He JY, Zou YL, Guo XS, Cui JZ, Guo L, et al. Evaluating the Cerebrospinal Fluid ctDNA Detection by Next-Generation Sequencing in the Diagnosis of Meningeal Carcinomatosis. *BMC Neurol* (2019) 19(1):331. doi: 10.1186/s12883-019-1554-5
37. Zheng MM, Li YS, Tu HY, Jiang BY, Yang JJ, Zhou Q, et al. Genotyping of Cerebrospinal Fluid Associated With Osimertinib Response and Resistance for Leptomeningeal Metastases in EGFR-Mutated NSCLC. *J Thorac Oncol* (2021) 16:250–8. doi: 10.1016/j.jtho.2020.10.008
38. Nevel KS, DiStefano N, Lin X, Skakodub A, Ogilvie SQ, Reiner AS, et al. A Retrospective, Quantitative Assessment of Disease Burden in Patients With Leptomeningeal Metastases From Non-Small-Cell Lung Cancer. *Neuro Oncol* (2020) 22:675–83. doi: 10.1093/neuonc/noz208
39. Pentsova EI, Shah RH, Tang J, Boire A, You D, Briggs S, et al. Evaluating Cancer of the Central Nervous System Through Next-Generation Sequencing of Cerebrospinal Fluid. *J Clin Oncol* (2016) 34:2404–15. doi: 10.1200/JCO.2016.66.6487
40. Jackman DM, Cioffredi LA, Jacobs L, Sharmeen F, Morse LK, Lucca J, et al. A Phase I Trial of High Dose Gefitinib for Patients With Leptomeningeal Metastases From Non-Small Cell Lung Cancer. *Oncotarget* (2015) 6:4527–36. doi: 10.18632/oncotarget.2886
41. Lee E, Keam B, Kim DW, Kim TM, Lee SH, Chung DH, et al. Erlotinib Versus Gefitinib for Control of Leptomeningeal Carcinomatosis in Non-Small-Cell Lung Cancer. *J Thorac Oncol* (2013) 8:1069–74. doi: 10.1097/JTO.0b013e318294c8e8
42. Yang H, Yang X, Zhang Y, Liu X, Deng Q, Zhao M, et al. Erlotinib in Combination With Pemetrexed/Cisplatin for Leptomeningeal Metastases and Cerebrospinal Fluid Drug Concentrations in Lung Adenocarcinoma Patients After Gefitinib Failure. *Targeting Oncol* (2015) 10:135–40. doi: 10.1007/s11523-014-0326-9
43. Grommes C, Oxnard GR, Kris MG, Miller VA, Pao W, Holodny AI, et al. "Pulsatile" High-Dose Weekly Erlotinib for CNS Metastases From EGFR Mutant non-Small Cell Lung Cancer. *Neuro Oncol* (2011) 13:1364–9. doi: 10.1093/neuonc/nor121
44. How J, Mann J, Laczniak AN, Baggstrom MQ. Pulsatile Erlotinib in EGFR-Positive Non-Small-Cell Lung Cancer Patients With Leptomeningeal and Brain Metastases: Review of the Literature. *Clin Lung Cancer* (2017) 18(4):354–63. doi: 10.1016/j.cllc.2017.01.013
45. Kawamura T, Hata A, Takeshita J, Fujita S, Hayashi M, Tomii K, et al. High-Dose Erlotinib for Refractory Leptomeningeal Metastases After Failure of Standard-Dose EGFR-TKIs. *Cancer Chemother Pharmacol* (2015) 75(6):1261–6. doi: 10.1007/s00280-015-2759-y
46. Jackman DM, Holmes AJ, Lindeman N, Wen PY, Kesari S, Borras AM, et al. Response and Resistance in a non–Small-Cell Lung Cancer Patient With an Epidermal Growth Factor Receptor Mutation and Leptomeningeal Metastases Treated With High-Dose Gefitinib. *J Clin Oncol* (2006) 24:4517–20. doi: 10.1200/JCO.2006.06.6126
47. Pellerino A, Brastianos PK, Rudà R, Soffietti R. Leptomeningeal Metastases From Solid Tumors: Recent Advances in Diagnosis and Molecular Approaches. *Cancers (Basel)* (2021) 13(12):2888. doi: 10.3390/cancers13122888
48. Yang JC, Cho BC, Kim D, Kim SW, Lee JS, Su WC, et al. Osimertinib for Patients (Pts) With Leptomeningeal Metastases (LM) From EGFR-Mutant non-Small Cell Lung Cancer (NSCLC): Updated Results From the BLOOM Study. *Proc Am Soc Clin Oncol* (2017) 35:2020. doi: 10.1200/JCO.2017.35.15_suppl.2020
49. Yang JCH, Kim SW, Kim DW, Lee JS, Cho BC, Ahn JS, et al. Osimertinib in Patients With Epidermal Growth Factor Receptor Mutation-Positive Non-Small-Cell Lung Cancer and Leptomeningeal Metastases: The BLOOM Study. *J Clin Oncol* (2020) 38:538–. doi: 10.1200/JCO.19.00457
50. Nanjo S, Hata A, Okuda C, Kaji R, Okada H, Tamura D, et al. Standard-Dose Osimertinib for Refractory Leptomeningeal Metastases in T790M-Positive EGFR-Mutant Non-Small Cell Lung Cancer. *Br J Cancer* (2018) 118:32–7. doi: 10.1038/bjc.2017.394
51. Ahn MJ, Chiu CH, Cheng Y, Han JY, Goldberg SB, Greystoke A, et al. Osimertinib for Patients With Leptomeningeal Metastases Associated With EGFR T790M-Positive Advanced NSCLC: The AURA Leptomeningeal Metastases Analysis. *J Thorac Oncol* (2020) 15:637. doi: 10.1016/j.jtho.2019.12.113
52. Lee J, Choi Y, Han J, Park S, Jung HA, Su JM, et al. Osimertinib Improves Overall Survival in Patients With EGFR-Mutated NSCLC With Leptomeningeal Metastases Regardless of T790M Mutational Status. *J Thorac Oncol* (2020) 15:1758–66. doi: 10.1016/j.jtho.2020.06.018
53. Park S, Lee MH, Seong M, Kim ST, Kang JH, Cho BC, et al. Multicenter, Two Cohort Study of 160 Mg Osimertinib in EGFR T790M-Positive Non-Small-Cell Lung Cancer Patients With Brain Metastases or Leptomeningeal Disease Who Progressed on Prior EGFR TKI Therapy. *Ann Oncol* (2020) 31:1397–404. doi: 10.1016/j.annonc.2020.06.017
54. Ahn MJ, Kim DW, Cho BC, Kim SW, Lee JS, Ahn JS, et al. Activity and Safety of AZD3759 in EGFR-Mutant Non-Small-Cell Lung Cancer With CNS Metastases (BLOOM): A Phase 1, Open-Label, Dose-Escalation and Dose-Expansion Study. *Lancet Respir Med* (2017) 5:891–902. doi: 10.1016/S2213-2600(17)30378-8
55. Cho BC, Ahn M, Lee J, Kim DW, Kim SW, John T, et al. Phase I Study (BLOOM) of AZD3759, a BBB Penetrable EGFR Inhibitor, in EGFRm NSCLC Patients With Leptomeningeal Metastasis (LM) Who Progressed After Other Anticancer Therapy. *J Clin Oncol* (2017) 35:2069. doi: 10.1200/JCO.2017.35.15_suppl.2069
56. Xu H, Zhou L, Lu Y, Su X, Cheng P, Li D, et al. Dual Targeting of the Epidermal Growth Factor Receptor Using Combination of Nimotuzumab and Erlotinib in Advanced Non-Small-Cell Lung Cancer With Leptomeningeal Metastases: A Report of Three Cases. *OncoTargets Ther* (2020) 13:647–56. doi: 10.2147/OTT.S230399
57. Gainor JF, Ou SH, Logan J, Borges LF, Shaw AT. The Central Nervous System as a Sanctuary Site in ALK-Positive Non-Small-Cell Lung Cancer. *J Thorac Oncol* (2013) 8(12):1570–3. doi: 10.1097/JTO.0000000000000029
58. Frost N, Christopoulos P, Kauffmann-Guerrero D, Stratmann J, Riedel R, Schaefer M, et al. Lorlatinib in Pretreated ALK- or ROS1-Positive Lung Cancer and Impact of TP53 Co-Mutations: Results From the German Early Access Program. *Ther Adv Med Oncol* (2021) 13:1758835920980558. doi: 10.1177/1758835920980558
59. Gaye E, Geier M, Bore P, Guilloïque M, Lucia F, Quéré G, et al. Intra-Cranial Efficacy of Brigatinib in an ALK-Positive Non-Small Cell Lung Cancer Patient Presenting Leptomeningeal Carcinomatosis. *Lung Cancer* (2019) 133:1–3. doi: 10.1016/j.lungcan.2019.04.013
60. Pellerino A, Buffoni L, Rudà R, Soffietti R. Complete Response of Spinal Metastases From Non-Small Cell Lung Cancer With ALK Inhibitors. *Neurology* (2019) 93:217–9. doi: 10.1212/WNL.0000000000007866
61. Palmieri D, Bronder JL, Herring JM, Yoneda T, Weil RJ, Stark AM, et al. Her-2 Overexpression Increases the Metastatic Outgrowth of Breast Cancer Cells in the Brain. *Cancer Res* (2007) 67:4190–8. doi: 10.1158/0008-5472.CAN-06-3316
62. Romond EH, Perez EA, Bryant J, Suman VJ, Geyer CEJr, Davidson NE, et al. Trastuzumab Plus Adjuvant Chemotherapy for Operable HER2-Positive Breast Cancer. *N Engl J Med* (2005) 353:1673–84. doi: 10.1056/NEJMoa052122
63. Lockman PR, Mittapalli RK, Taskar KS, Rudraraju V, Gril B, Bohn KA, et al. Heterogeneous Blood-Tumor Barrier Permeability Determines Drug Efficacy in Experimental Brain Metastases of Breast Cancer. *Clin Cancer Res* (2010) 16:5664–78. doi: 10.1158/1078-0432.CCR-10-1564
64. Lin NU, Diéras V, Paul D, Lossignol D, Christodoulou C, Stemmler HJ, et al. Multicenter Phase II Study of Lapatinib in Patients With Brain Metastases From HER2-Positive Breast Cancer. *Clin Cancer Res* (2009) 15:1452–9. doi: 10.1158/1078-0432.CCR-08-1080
65. Sutherland S, Ashley S, Miles D, Chan S, Wardley A, Davidson N, et al. Treatment of HER2-Positive Metastatic Breast Cancer With Lapatinib and

Capecitabine in the Lapatinib Extended Access Programme, Including Efficacy in Brain Metastases-the UK Experience. *Br J Cancer* (2010) 102:995–1002. doi: 10.1038/sj.bjc.6605586
66. Lin NU, Eierman W, Greil R, Campone M, Kaufman B, Steplewski K, et al. Randomized Phase II Study of Lapatinib Plus Capecitabine or Lapatinib Plus Topotecan for Patients With HER2-Positive Breast Cancer Brain Metastases. *J Neurooncol* (2011) 105:613–20. doi: 10.1007/s11060-011-0629-y
67. Metro G, Foglietta J, Russillo M, Stocchi L, Vidiri A, Giannarelli D, et al. Clinical Outcome of Patients With Brain Metastases From HER2-Positive Breast Cancer Treated With Lapatinib and Capecitabine. *Ann Oncol* (2011) 22:625–30. doi: 10.1093/annonc/mdq434
68. Bachelot T, Romieu G, Campone M, Diéras V, Cropet C, Dalenc F, et al. Lapatinib Plus Capecitabine in Patients With Previously Untreated Brain Metastases From HER2-Positive Metastatic Breast Cancer (LANDSCAPE): A Single-Group Phase 2 Study. *Lancet Oncol* (2013) 14:64–71. doi: 10.1016/S1470-2045(12)70432-1
69. Murthy RK, Loi S, Okines A, Paplomata E, Hamilton E, Hurvitz SA, et al. Tucatinib, Trastuzumab, and Capecitabine for HER2-Positive Metastatic Breast Cancer. *N Engl J Med* (2020) 382(7):597–609. doi: 10.1056/NEJMoa1914609
70. Pellerino A, Palmiero R, Bruno F, Mo F, Muscolino E, Franchino F, et al.Neratinib for Treatment of Leptomeningeal Metastases From HER2-Positive Breast Cancer in Extended Access Program: Preliminary Results. *Neuro-Onc* (2021) 23(2):supp_2, pg ii46. doi: 10.1093/neuonc/noab180.159.
71. Figura NB, Rizk VT, Mohammadi H, Evernden B, Mokhtari S, Yu HM, et al. Clinical Outcomes of Breast Leptomeningeal Disease Treated With Intrathecal Trastuzumab, Intrathecal Chemotherapy, or Whole Brain Radiation Therapy. *Breast Cancer Res Treat* (2019) 175:781–8. doi: 10.1007/s10549-019-05170-7
72. Zagouri F, Zoumpourlis P, Le Rhun E, Bartsch R, Zografos E, Apostolidou K, et al. Intrathecal Administration of Anti-HER2 Treatment for the Treatment of Meningeal Carcinomatosis in Breast Cancer: A Metanalysis With Meta-Regression. *Cancer Treat Rev* (2020) 88:102046. doi: 10.1016/j.ctrv.2020.102046
73. Bangham M, Goldstein R, Walton H, Ledermann JA. Olaparib Treatment for BRCA-Mutant Ovarian Cancer With Leptomeningeal Disease. *Gynecol Oncol Rep* (2016) 18:22–4. doi: 10.1016/j.gore.2016.10.004
74. Exman P, Mallery RM, Lin NU, Parsons HA. Response to Olaparib in a Patient With Germline BRCA2 Mutation and Breast Cancer Leptomeningeal Carcinomatosis. *NPJ Breast Cancer* (2019) 5:46. doi: 10.1038/s41523-019-0139-1
75. Arasaratnam M, Hong A, Shivalingam B, Wheeler H, Guminksi AD, Long GV, et al. Leptomeningeal Melanoma-A Case Series in the Era of Modern Systemic Therapy. *Pigment Cell Melanoma Res* (2018) 31:120–4. doi: 10.1111/pcmr.12652
76. Ferguson SD, Bindal S, Bassett RLJr, Haydu LE, McCutcheon IE, Heimberger AB, et al. Glitza IC Predictors of Survival in Metastatic Melanoma Patients With Leptomeningeal Disease (LMD). *J Neurooncol* (2019) 142(3):499–509. doi: 10.1007/s11060-019-03121-2
77. Chorti E, Kebir S, Ahmed MS, Keyvani K, Umutlu L, Kanaki T, et al. Leptomeningeal Disease From Melanoma-Poor Prognosis Despite New Therapeutic Modalities. *Eur J Cancer* (2021) 148:395–404. doi: 10.1016/j.ejca.2021.02.016
78. Tawbi HA, Forsyth PA, Algazi A, Hamid O, Hodi FS, Moschos SJ, et al. Combined Nivolumab and Ipilimumab in Melanoma Metastatic to the Brain. *N Engl J Med* (2018) 379(8):722–30. doi: 10.1056/NEJMoa1805453
79. Long GV, Atkinson V, Lo S, Sandhu S, Guminski AD, Brown MP, et al. Combination Nivolumab and Ipilimumab or Nivolumab Alone in Melanoma Brain Metastases: A Multicentre Randomised Phase 2 Study. *Lancet Oncol* (2018) 19(5):672–81. doi: 10.1016/S1470-2045(18)30139-6
80. Goldberg SB, Gettinger SN, Mahajan A, Chiang AC, Herbst RS, Sznol M, et al. Pembrolizumab for Patients With Melanoma or Non-Small-Cell Lung Cancer and Untreated Brain Metastases: Early Analysis of a non-Randomised, Open-Label, Phase 2 Trial. *Lancet Oncol* (2016) 17(7):976–83. doi: 10.1016/S1470-2045(16)30053-5
81. Bot I, Blank CU, Brandsma D. Clinical and Radiological Response of Leptomeningeal Melanoma After Whole Brain Radiotherapy and Ipilimumab. *J Neurol* (2012) 259(9):1976–8. doi: 10.1007/s00415-012-6488-4
82. Wu RC, Newman W, Patanowitz L, Branstetter BF, Amankulor N, Tarhini AA. Long-Term Control of Leptomeningeal Disease After Radiation Therapy and Nivolumab in a Metastatic Melanoma Patient. *Immunotherapy* (2020) 12(11):763–9. doi: 10.2217/imt-2019-0004
83. Glitza I, Bucheit A. Clinical Response of Central Nervous System Melanoma to Anti-PD1 Therapy in 2 Melanoma Patients. *Arch Immunol* (2017) 1(1):1–3. doi: 10.36959/885/364
84. Brastianos PK, Lee EQ, Cohen JV, Tolaney SM, Lin NU, Wang N, et al. Single-Arm, Open-Label Phase 2 Trial of Pembrolizumab in Patients With Leptomeningeal Carcinomatosis. *Nat Med* (2020) 26(8):1280–4. doi: 10.1038/s41591-020-0918-0
85. Naidoo J, Schreck KC, Fu W, Hu C, Carvajal-Gonzalez A, Connolly RM, et al. Pembrolizumab for Patients With Leptomeningeal Metastasis From Solid Tumors: Efficacy, Safety, and Cerebrospinal Fluid Biomarkers. *J Immunother Cancer* (2021) 9(8):e002473. doi: 10.1136/jitc-2021-002473
86. Brastianos PK, Strickland MR, Lee EQ, Wang N, Cohen JV, Chukwueke U, et al. Phase II Study of Ipilimumab and Nivolumab in Leptomeningeal Carcinomatosis. *Nat Commun* (2021) 12(1):5954. doi: 10.1038/s41467-021-25859-y
87. Papadopoulos NE, Moser RP, Grimm E, Gerber D, Myers C, Leavens M, et al. Intrathecal Use of Recombinant Interleukin-2 (rIL-2) in the Treatment of leptomeningeal Disease (LMD) From Metastatic Melanoma. *Proc Annu MeetAm Soc Clin Oncol* (1995) 14:A1307.
88. Glitza IC, Rohlfs M, Guha-Thakurta N, Bassett RLJr, Bernatchez C, Diab A, et al. Retrospective Review of Metastatic Melanoma Patients With Leptomeningeal Disease Treated With Intrathecal Interleukin-2. *ESMO Open* (2018) 3(1):e000283. doi: 10.1136/esmoopen-2017-000283
89. Pluim D, Ros W, van Bussel MTJ, Brandsma D, Beijnen JH, Schellens JHM. Enzyme Linked Immunosorbent Assay for the Quantification of Nivolumab and Pembrolizumab in Human Serum and Cerebrospinal Fluid. *J Pharm BioMed Anal* (2019) 164:128–34. doi: 10.1016/j.jpba.2018.10.025
90. Glitza IC, Brown C, Haymaker C, Bassett R, Rohlfs M, Richard J, et al. Davies MA Safety Data From a Single-Center Phase I/Ib Study of Concurrent Intravenous (IV) and Intrathecal (IT) Nivolumab (N) for Metastatic Melanoma (MM) Patients (Pts) With Leptomeningeal Disease (LMD). In: *Late Breaking Abstract*. Salt Lake City, Utah: Society Melanoma Research (SMR (2019).

Conflict of Interest: The authors declare that the research was conducted in the absence of any commercial or financial relationships that could be construed as a potential conflict of interest.

frontiers in Oncology

ORIGINAL RESEARCH
published: 14 January 2022
doi: 10.3389/fonc.2021.724769

The Prognostic Value of the Prognostic Nutritional Index in Operable High-Grade Glioma Patients and the Establishment of a Nomogram

Qian He[1], *Wei Zhao*[2] *and Qinglan Ren*[3]*

[1] Department of Oncology, Affiliated Dongguan People's Hospital, Southern Medical University, Dongguan, China,
[2] Department of Oncology, The Second Affiliated Hospital of Chongqing Medical University, Chongqing, China,
[3] Department of Oncology, The First Affiliated Hospital of Chongqing Medical University, Chongqing, China

Background: Studies confirmed the predictive value of the prognostic nutrition index (PNI) in many malignant tumors. However, it did not reach a consensus in glioma. Therefore, this study investigated the prognostic value of preoperative PNI in operable high-grade glioma and established a nomogram.

Methods: Clinical data of high-grade glioma patients were retrospectively analyzed. The primary endpoint was overall survival (OS). Survival analysis was conducted by the Kaplan–Meier method, log-rank test, and Cox regression analysis. A nomogram was established. The prediction effect of the nomogram covering PNI was verified by area under the curve (AUC).

Results: A total of 91 operable high-grade glioma patients were included. Kaplan–Meier analysis showed that among grade IV gliomas (n = 55), patients with higher PNI (>44) showed a trend of OS benefit (p = 0.138). In grade III glioma (n = 36), patients with higher PNI (>47) had longer OS (p = 0.023). However, the intersecting Kaplan–Meier curve suggested that there may be some confounding factors. Cox regression analysis showed that higher PNI was an independent prognostic factor for grade IV glioma (HR = 0.388, p = 0.040). In grade III glioma, there was no statistically relationship between PNI levels and prognosis. When evaluating the prognostic ability of PNI alone by ROC, the AUC in grade III and IV gliomas was low, indicating that PNI alone had poor predictive power for OS. Interestingly, we found that the nomogram including preoperative PNI, age, extent of resection, number of gliomas, and MGMT methylation status could predict the prognosis of patients with grade IV glioma well.

Conclusion: The PNI level before surgery was an independent prognostic factor for patients with grade IV glioma. The nomogram covering PNI in patients with grade IV glioma also proved the value of PNI. However, the value of PNI in grade III glioma needs to be further evaluated. More prospective studies are needed to verify this conclusion.

Keywords: prognostic nutritional index, high-grade glioma, prognostic, overall survival, nomogram

OPEN ACCESS

Edited by:
Liam Chen,
University of Minnesota, United States

Reviewed by:
Denis Aiudi,
Azienda Ospedaliero Universitaria Ospedali Riuniti, Italy
Andrea Salmaggi,
ASST Lecco, Italy

***Correspondence:**
Qinglan Ren
renqlwu@163.com

Specialty section:
This article was submitted to Neuro-Oncology and Neurosurgical Oncology, a section of the journal Frontiers in Oncology

Received: *14 June 2021*
Accepted: *23 December 2021*
Published: *14 January 2022*

Citation:
He Q, Zhao W and Ren Q (2022) The Prognostic Value of the Prognostic Nutritional Index in Operable High-Grade Glioma Patients and the Establishment of a Nomogram. Front. Oncol. 11:724769. doi: 10.3389/fonc.2021.724769

INTRODUCTION

The overall prognosis of patients with high-grade glioma is poor, and the survival of patients varied greatly, and their 5-year survival rate fluctuates between 5.5% and 75.2% (1). Therefore, it is very important to accurately predict the prognosis of patients. Research showed that the prognosis of patients with high-grade glioma was related to factors such as patient age, tumor characteristics, and treatment methods (1). Nevertheless, the accuracy in predicting the prognosis of high-grade gliomas is still limited. It is necessary to find more prognostic factors to comprehensively evaluate the prognosis of patients with high-grade glioma.

Studies showed that the nutritional status and inflammation of patients may affect the antitumor effect (2–5). The prognostic nutritional index (PNI) is based on the serum albumin count and lymphocyte count and is a comprehensive index for evaluating the nutritional status and inflammatory state of the body. Its calculation formula is serum albumin concentration (g/L) + 5× total lymphocyte count (10^9/l). More and more studies found that higher PNI can be used for independent factors for better prognosis of various malignant tumors, such as lung cancer (6), esophageal cancer (7), breast cancer (8), nasopharyngeal cancer (9), colorectal cancer (10), gastric cancer (11), and biliary tract cancer (12). However, there is no consensus on the role of PNI in glioma (13). Therefore, this study intended to explore the prognostic value of PNI in patients with operable high-grade glioma.

METHODS

Patients

The clinical data of operable high-grade glioma patients from December 2013 to December 2019 in the First Affiliated Hospital of Chongqing Medical University were analyzed retrospectively. The inclusion criteria include the following (1): patients underwent tumor resection (2); patients with high-grade glioma diagnosed according to the 2016 WHO classification and global standard classification (3); patients who completed the "STUPP" radiotherapy and chemotherapy protocol (4); regular follow-up; and (5) blood routine and serum albumin examination within 1 week before operation. The exclusion criteria include the following (1): incomplete clinical data (2); receiving other treatments before tumor resection; and (3) having infection or inflammatory disease during the last month.

Data Collection and Hematological Examination

Clinical data of patients were collected including age, gender, tumor grade, histological type, tumor site, tumor number, and extent of resection. The extent of surgical resection was determined according to the preoperative and postoperative MRI and the surgeon's intraoperative judgment. Postoperative MRI was obtained within 24–72 h after surgery. We used Carestream Vue PACS software to calculate the percentage of resection based on the preoperative MRI and postoperative MRI within 24–72 h and marked the tumor extent according to T1-enhanced sequence images. The percentage of tumor resection = (preoperative tumor volume-residual tumor volume)/ preoperative tumor volume * 100%. No tumor remaining was considered as gross total resection (GTR), tumor resection extent > 90% was considered as near total resection (NTR), tumor resection extent between 80% and 90% was considered as subtotal resection (STR), and tumor resection extent <80% was considered as partial resection (PR). Blood routine and serum albumin results before surgery were collected. The cutoff value of the optimal PNI was obtained by X-Tile software.

Follow-Up

The primary endpoint of the study was OS. OS was defined as the time from the day of surgery to the death of the patient or the final follow-up. There were 91 patients who met the inclusion and exclusion criteria and were successfully followed up. The follow-up ended on September 12, 2020.

Statistical Analysis

We used the independent sample T test or Mann–Whitney U test to compare continuous variables, and the chi-square test or Fisher's exact probability test to compare categorical variables. The Kaplan–Meier method, log-rank method, and Cox regression model were used for survival analysis. Survival was analyzed by calculating the hazard ratio (HR) and 95% confidence interval (CI). The prognostic ability of PNI was evaluated by the area under the curve (AUC) through the ROC curve. A nomogram covering the PNI was built, and the C index was calculated. The predictive effect of the nomogram was verified by the calibration curve through bootstrap sampling 1,000 times. The predictive ability of the nomogram covering PNI and the predictive model without PNI was compared by the ROC curve. SPSS version 25, X-Tile version 3.6.1, and R version 4.0.2 were used for data analysis. The statistical significance of the p value was set at 0.05 (double-sided).

RESULTS

Patient Characteristics

A total of 91 high-grade glioma patients (36 cases of grade III and 55 cases of grade IV) were enrolled. The median age was 50 years (range 18–79 years). **Table 1** showed the characteristics of grade III and grade IV glioma patients and their correlation with preoperative PNI. In patients with grade III and grade IV glioma, the best cutoff values of preoperative PNI were 47 and 44, respectively.

Survival Analysis

The median follow-up time for all patients was 21 months (95% CI: 23.4–31.4 months). The median OS for grade III glioma was 31 months (95% CI: 28.9–41.6 months), and the median OS for grade IV glioma was 17 months (95% CI: 17.5–27.1 months). Among patients with grade III glioma, the median OS of patients

TABLE 1 | Baseline patient characteristics stratified by preoperative PNI in grade III glioma and grade IV glioma.

Variables	Grade III glioma					Grade IV glioma				
	Total (n = 36)		PNI ≤47 (n = 9, 25%)	PNI >47 (n = 27, 75%)	p	Total (n = 55)		PNI ≤44 (n = 7, 12.7%)	PNI >44 (n = 48, 87.3%)	p
	n/mean ± SD	%	n/mean ± SD	n/mean ± SD		n/mean ± SD	%	n/mean ± SD	n/mean ± SD	
Age	48.4 ± 10.30		53.2 ± 10.95	46.7 ± 9.75	0.103	51.1 ± 14.26		51.7 ± 16.59	51.0 ± 14.08	0.906
Sex										
Female	14	38.9	3	11	1.000	29	52.7	4	25	1.000
Male	22	61.1	6	16		26	47.3	3	23	
Histology										
AA	21	58.3	5	16	0.681	NA				
AO	13	36.1	3	10		NA				
GBM	NA					55	100	7	48	NA
NOS	2	5.6	1	1		NA				
Main location										
Frontal	25	69.4	5	20	0.531	32	58.2	5	27	0.686
Parietal	4	11.1	1	3	1.000	18	32.7	2	16	1.000
Occipital	2	5.6	1	1	0.443	9	16.4	0	9	0.480
Temporal	9	25.0	3	6	0.824	12	21.8	2	10	1.000
Insular	1	2.8	1	0	0.250	2	3.6	0	2	1.000
No. of glioma										
Single	36	100	9	27	NA	49	89.1	6	43	0.577
Multiple	0	0.0	0	0		6	10.9	1	5	
Extent of resection										
PR	2	5.6	0	2	1.000	0	0.0	0	0	0.513
STR	3	8.3	1	2		6	10.9	0	6	
NTR	6	16.7	1	5		8	14.5	0	8	
GTR	25	69.4	7	18		41	74.5	7	34	
IDH mutation										
No	2	5.6	0	2	1.000	46	83.6	6	40	1.000
Yes	34	94.4	9	25		9	16.4	1	8	
MGMT methylation										
No	14	38.9	5	9	0.430	34	61.8	4	30	1.000
Yes	22	61.1	4	18		21	38.2	3	18	
1p19q deletion										
No	23	63.9	6	17	1.000	0	0	0	0	NA
Yes	13	36.1	3	10		0	0	0	0	
Ki-67	16.3 ± 14.44		22.2 ± 21.38	14.3 ± 11.12	0.311	27.6 ± 14.43		35.0 ± 18.03	26.5 ± 13.72	0.145
Epilepsy before surgery										
No	23	63.9	7	16	0.548	45	81.8	6	39	1.000
Yes	13	36.1	2	11		10	18.2	1	9	

AA, anaplastic astrocytomas; AO, anaplastic oligodendrogliomas; GBM, glioblastoma; GTR, gross total resection; n, number; NA, not applicable; No., number; NOS, not otherwise specified; NTR, near total resection; PNI, prognostic nutritional index; PR, partial resection; SD, Std. deviation; STR, subtotal resection.

in the preoperative low PNI (≤47) group and high PNI (>47) group was 22 and 37 months, respectively. In grade IV glioma, the median OS for the preoperative lower PNI (≤44) group and higher PNI (>44) group was 14 and 17.5 months.

The Kaplan–Meier survival curve and log-rank test were used to analyze the prognosis of patients in different PNI states. It was found that in grade III glioma, the OS of patients with preoperative high PNI status was significantly longer than that of preoperative low PNI status (**Figure 1A**, p = 0.023). However, the Kaplan–Meier curve intersected, suggesting that in grade III gliomas, there may be confounding factors that make patients with high PNI have longer OS, so we conducted a multivariate analysis. Grade IV glioma patients with higher preoperative PNI also showed a similar trend of obtain better prognosis (**Figure 1B**, p = 0.138).

Cox regression analysis showed that in grade IV glioma, preoperative PNI level, extent of resection, and MGMT methylation status were significantly correlated with OS (**Table 2**). Since primary and secondary grade IV gliomas were usually distinguished according to the wild type and mutant type of IDH (14), and the predictive value of preoperative PNI in patients with different types of grade IV gliomas may be different, we performed subgroup analysis on IDH wild-type grade IV glioma patients. The results showed that patients with higher preoperative PNI had a tendency to obtain OS benefits (HR = 0.476, p = 0.126, **Table 3**). We did not further analyze the role of PNI in secondary grade IV gliomas due to the small number of IDH mutated grade IV gliomas patients included (n = 9). In grade III glioma, age, histological type, extent of resection, MGMT methylation status, and Ki-67 level were independent

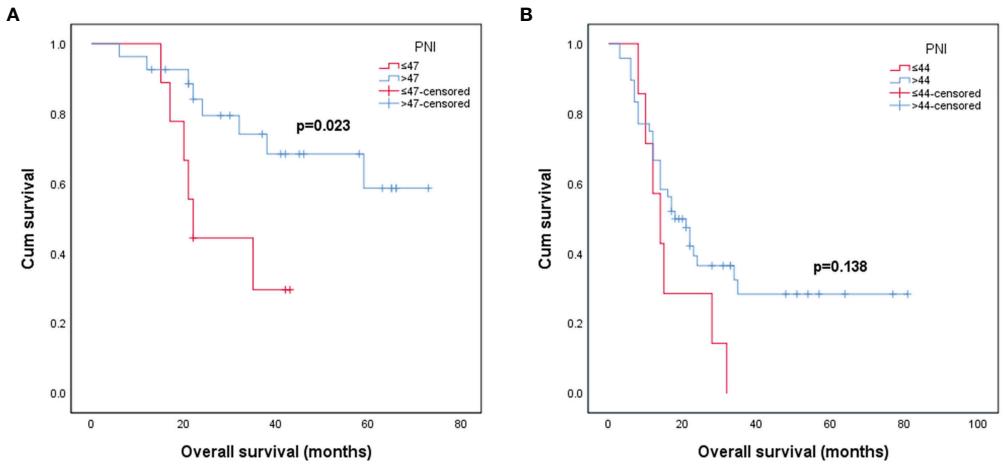

FIGURE 1 | Kaplan–Meier survival curves for patients stratified based on preoperative PNI in patients with grade III glioma **(A)** and patients with grade IV glioma **(B)**. (PNI, prognostic nutritional index).

prognostic factors that affect OS in patients (**Table 4**), and patients with higher preoperative PNI showed a better prognosis only in the univariate analysis (HR = 0.301, p = 0.032).

When assessing the prognostic ability of PNI in grade III and IV gliomas through the ROC curve, we found that the AUC was not high (0.65 and 0.50, respectively, **Figure 2**), which indicated that PNI alone had a limited effect of predicting OS in patients with high-grade glioma.

The Establishment of a Nomogram

Important factors associated with the prognosis of high-grade gliomas included age, extent of resection, number of gliomas, and MGMT methylation status. Since our study showed that preoperative PNI level was an independent prognostic factor in grade IV glioma patients, however, in grade III glioma, a significant correlation between PNI and OS was only shown in univariate analysis, and the number of patients with grade III glioma included was relatively small. Therefore, we only drew a nomogram in grade IV gliomas covering preoperative PNI, age, extent of resection, number of gliomas, and MGMT methylation status (**Figure 3**) and evaluated the predictive effect of the nomogram. The C-index of the nomogram was 0.771 (95% CI: 0.708–0.834). The calibration curves for the 1-, 2-, and 3-year survival of the patients showed that when predicting the 2-year survival rate, the agreement between the prediction and the observation results was the best (**Figures 4A–C**), indicating that the repeatability of the nomogram was reliable. ROC analysis showed that the AUC of the nomogram covering the

TABLE 2 | Univariate and multivariate Cox regression analyses for overall survival in grade IV glioma patients.

		Univariate Cox regression			Multivariate Cox regression		
Variable		**p value**	**HR**	**(95% CI)**	**p value**	**HR**	**(95% CI)**
Age		0.105	1.019	(0.996 -1.042)	0.382	1.010	(0.988 -1.032)
Sex	Female	ref					
	Male	0.537	1.222	(0.646 -2.313)			
No. of glioma	Single	ref			ref		
	Multiple	0.016[a]	3.321	(1.247 -8.847)	0.356	1.647	(0.571 -4.755)
Extent of resection	STR+PR	ref					
	GTR+NTR	0.001[a]	0.200	(0.078 -0.514)	0.002[a]	0.201	(0.073 -0.551)
IDH mutation	No	ref					
	Yes	0.004[a]	0.171	(0.051 -0.574)	0.096	0.320	(0.084 -1.223)
MGMT methylation	No	ref					
	Yes	0.001[a]	0.293	(0.14 -0.615)	0.036[a]	0.408	(0.177 -0.941)
Ki-67		0.580	1.006	(0.985 -1.028)	0.880	1.002	(0.977 -1.028)
Epilepsy before surgery	No	ref					
	Yes	0.197	0.528	(0.200 -1.392)			
PNI	≤44	ref			ref		
	>44	0.155	0.548	(0.239 -1.255)	0.040[a]	0.388	(0.158 -0.956)

CI, confidence interval; GTR, gross total resection; HR, hazard ratio; No., number; NTR, near total resection; PNI, prognostic nutritional index; PR, partial resection; ref, reference; STR, subtotal resection.

[a]*Statistically significant (p < 0.05).*

TABLE 3 | Univariate and multivariate Cox regression analyses for overall survival in the IDH wide-type IV glioma subgroup.

		Univariate Cox regression			Multivariate Cox regression		
Variable		**p value**	**HR**	**(95% CI)**	**p value**	**HR**	**(95% CI)**
Age		0.513	1.007	(0.985 1.030)	0.834	1.002	(0.980 -1.025)
Sex	Female	ref					
	Male	0.767	1.106	(0.568 -2.152)			
No. of glioma	Single	ref			ref		
	Multiple	0.058	2.568	(0.967 -6.822)	0.731	1.246	(0.356 -4.365)
Extent of resection	STR+PR	ref			ref		
	GTR+NTR	0.004[a]	0.254	(0.099 -0.652)	0.005[a]	0.234	(0.085 -0.645)
MGMT methylation	No	ref			ref		
	Yes	0.087	0.504	(0.230 -1.105)	0.087	0.479	(0.207 -1.112)
Ki-67		0.914	0.999	(0.977 -1.021)			
Epilepsy before surgery	No	ref			ref		
	Yes	0.012[a]	3.684	(1.338 -10.143)	0.246	2.129	(0.594 -7.626)
PNI	≤44	ref			ref		
	>44	0.369	0.666	(0.274 -1.617)	0.126	0.476	(0.184 -1.232)

CI, confidence interval; GTR, gross total resection; HR, hazard ratio; No., number; NTR, near total resection; PNI, prognostic nutritional index; PR, partial resection; ref, reference; STR, subtotal resection.

[a]*Statistically significant ($p < 0.05$).*

preoperative PNI was higher than the AUC of the prediction model without PNI (AUC = 0.716, 95% CI: 0.588–0.844 and AUC = 0.664, 95% CI: 0.501–0.827, respectively; **Figure 5**). This suggested that the nomogram could more accurately predict the prognosis of patients with grade IV glioma.

DISCUSSION

The nutritional status, inflammatory status, and immune function of patients with malignant tumors were often considered to be related to the prognosis (5, 15). Serum albumin levels were often used to assess the nutritional status of patients, and lymphocytes were often used to assess the immune function and inflammatory status of patients (16, 17). Many studies proved the prognostic value of serum albumin and lymphocytes in malignant tumors: lower albumin levels were linked to poor prognosis for cancer patients (13, 18), and high levels of lymphocytes may indicate a better prognosis (19–21). As an easily accessible index that could comprehensively evaluate the nutritional status and inflammatory status of patients, more and more studies confirmed its prognostic value in a variety of malignant tumors (9, 11, 22, 23). However, the prognostic value of PNI in glioma has not yet reached consensus (13, 24, 25).

TABLE 4 | Univariate and multivariate Cox regression analyses for overall survival in grade III glioma patients.

		Univariate Cox regression			Multivariate Cox regression		
Variable		**p value**	**HR**	**(95% CI)**	**p value**	**HR**	**(95% CI)**
Age		0.008[a]	1.078	(1.020 -1.139)	0.002[a]	1.137	(1.047 -1.234)
Sex	Female	ref					
	Male	0.914	1.062	(0.355 -3.181)			
Histology	AA	ref			ref		
	AO	0.525	0.682	(0.210 -2.220)	0.028[a]	0.114	(0.016 -0.789)
	NOS	0.875	1.183	(0.147 -9.483)	0.093	0.017	(0.000 -1.977)
Extent of resection	STR+PR	ref			ref		
	GTR+NTR	0.004[a]	0.195	(0.063 -0.599)	0.041[a]	0.237	(0.060 -0.941)
IDH mutation	No	ref			ref		
	Yes	0.848	0.819	(0.106 -6.311)	0.646	0.574	(0.053 -6.157)
MGMT methylation	No	ref			ref		
	Yes	0.187	0.487	(0.167 -1.418)	0.016[a]	0.128	(0.024 -0.687)
1p19q deletion	No	ref					
	Yes	0.503	0.672	(0.210 -2.149)			
Ki-67		0.018[a]	1.043	(1.007 -1.080)	0.037[a]	1.071	(1.004 -1.143)
Epilepsy before surgery	No	ref					
	Yes	0.081	0.318	(0.088 -1.151)			
PNI	≤47	ref			ref		
	>47	0.032[a]	0.301	(0.100 -0.904)	0.974	1.024	(0.239 -4.390)

AA, anaplastic astrocytomas; AO, anaplastic oligodendrogliomas; CI, confidence interval; GTR, gross total resection; HR, hazard ratio; NOS, not otherwise specified; NTR, near total resection; PNI, prognostic nutritional index; PR, partial resection; ref, reference; STR, subtotal resection.

[a]*Statistically significant (p lt 0.05).*

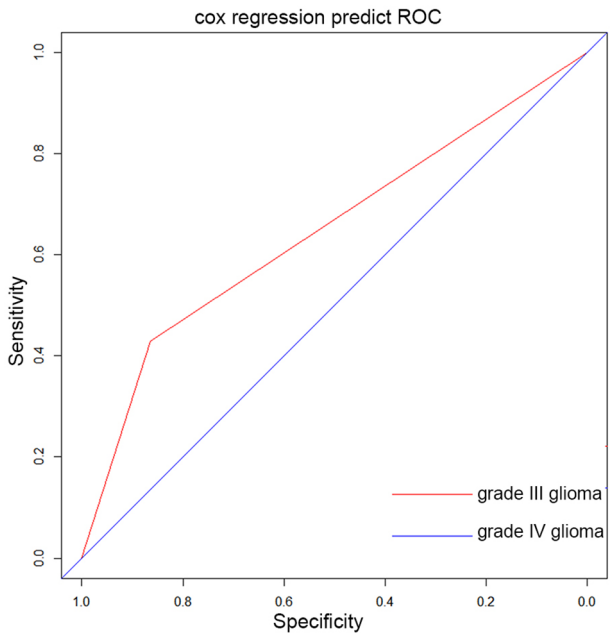

FIGURE 2 | The ROC curve of PNI for grade III and grade IV glioma patients.

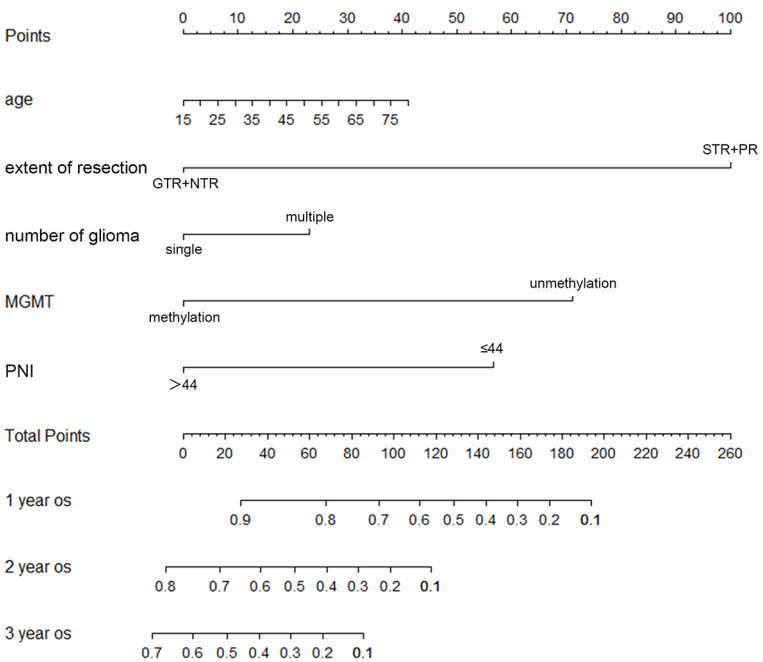

FIGURE 3 | The nomogram for survival of patients with grade IV glioma. (GTR, gross total resection; NTR, near total resection; PNI, prognostic nutritional index; PR, partial resection; STR, subtotal resection).

This study mainly explored the predictive value of preoperative PNI in patients with operable high-grade glioma. We only included patients with high-grade glioma who received standardized postoperative adjuvant radiotherapy and chemotherapy. After excluding the influence of treatment factors, it could better reflect the predictive ability of preoperative PNI. The IDH mutation frequency (94% and 16%, respectively) and MGMT methylation frequency (61%

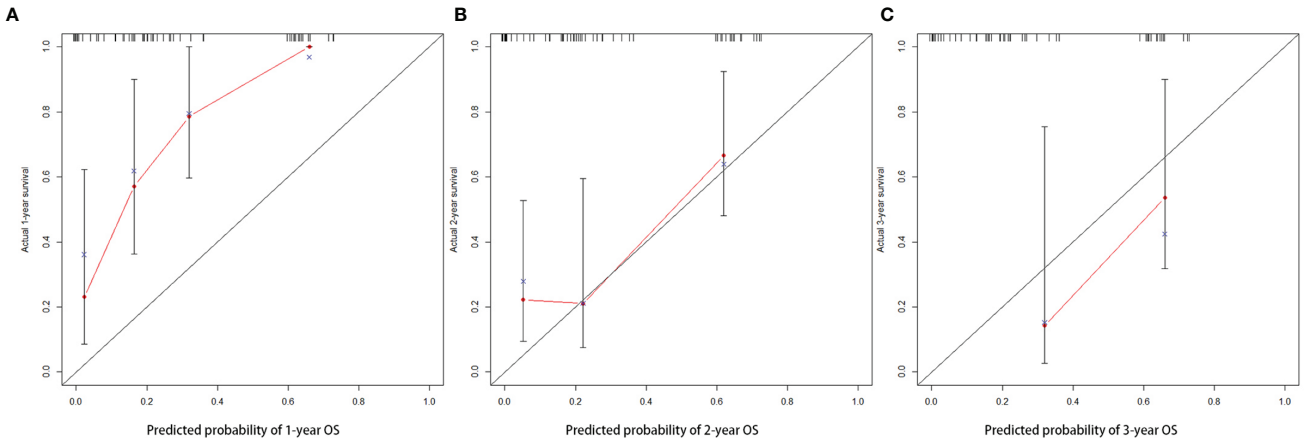

FIGURE 4 | The calibration curve of nomogram in patients with grade IV glioma at 1 **(A)**, 2 **(B)**, and 3 years **(C)**.

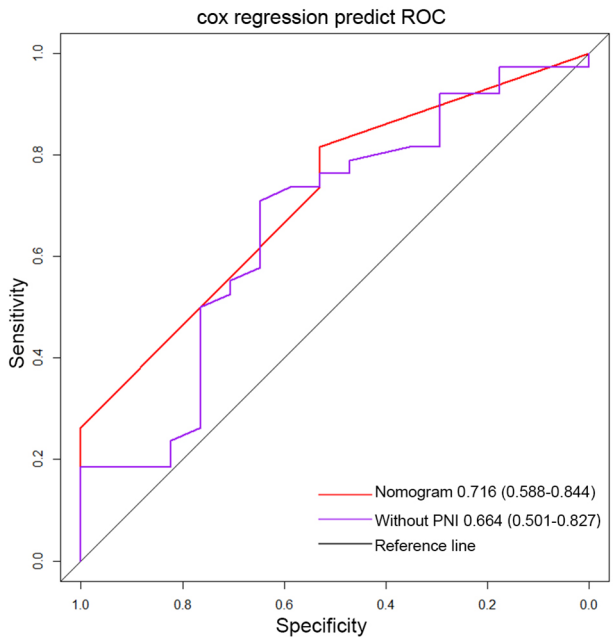

FIGURE 5 | The ROC curve of the nomogram covering PNI and the ROC curve of traditional markers in grade IV glioma. (PNI, prognostic nutritional index).

and 38%, respectively) of grade III and grade IV glioma reported in our study were consistent with the frequency reported in the past (26, 27). Some factors that affect the prognosis of patients with high-grade glioma, such as age, histological type, single or multiple gliomas, extent of resection, MGMT methylation status, and Ki-67 level, were verified in our results (27–32). However, the OS of patients with different IDH statuses did not show significant statistical differences. It may be related to the small number of IDH wild-type grade III glioma patients and IDH mutant grade IV glioma patients we included. Regarding PNI, consistent with most studies, we found that preoperative PNI showed a predictive value (13). Our study found that in grade III and grade IV gliomas, the median OS of patients with higher preoperative PNI was longer than that of patients with lower PNI. Preoperative PNI was an independent prognostic factor for grade IV glioma. However, in univariate analysis, patients with higher preoperative PNI only had trends to get better OS. This may be because OS was affected by other factors in addition to preoperative PNI. When a multivariate analysis was performed, the significance of preoperative PNI becomes apparent.

Furthermore, through ROC analysis, the nomogram covering PNI also showed a better prognostic value compared with the prediction model without PNI. In the IDH wild-type grade IV glioma subgroup, higher PNI only showed a trend for better OS. This may be due to the small number of IDH wild-type IV glioma patients included (n = 46). In this study, PNI did not show a good prognostic effect in grade III gliomas. Although our study showed that PNI in grade III gliomas was statistically significant in univariate Cox regression and Kaplan–Meier analysis, the intersecting Kaplan–Meier curves suggested that there might be confounding factors. Multivariate Cox analysis showed that the PNI was not an independent prognostic factor for grade III gliomas. This may be due to the strong heterogeneity of grade III gliomas, and a single indicator may not be used as a reliable independent prognostic factor. Moreover, the number of grade III gliomas patients we included was small (n = 36), which may be insufficient to support the inclusion of more indicators for multivariate analysis. In the future, we will follow more patients to evaluate the predictive value of PNI in grade III gliomas. In addition, we included 2 IDH wild-type grade III glioma patients. Some IDH wild-type grade III glioma patients may be classified as grade IV glioma with the development of molecular pathology (33). In the future, we would include more patients and evaluate the prognostic value of PNI in different subtypes of high-grade gliomas. Although, through the ROC curve, we found that in high-grade glioma, the predictive effect of PNI alone was limited, the nomogram based on PNI showed good predictive performance. The AUC of the nomogram covering PNI was higher than that of the prediction model without PNI. This showed that the nomogram covering preoperative PNI was better than traditional biomarkers. The molecular pathological diagnosis of patients may change with the advancement of molecular detection in the future. We will continue to include more patients and further optimize the nomogram to more accurately predict the OS of patients with high-grade glioma.

As a cheap and convenient indicator, PNI may affect the prognosis of patients with malignant tumors in many ways. Many studies found that the level of albumin was related to the nutritional status of patients and the immune system (34). Lower serum albumin levels indicated an increased nutritional risk for malignant tumor patients. In addition, lower albumin levels could also interfere with the body's immune response and reduce antitumor effects (34, 35). Lymphocytes were an important cell group for body immunity and an important factor for regulating immunity. Lymphocytes could limit tumor growth and metastasis through cytotoxicity and improve patient prognosis (36, 37). Therefore, high levels of PNI may often be associated with better prognosis in patients with malignant tumors. However, in high-grade gliomas, this conclusion was not always valid, and more clinical data were still needed to explore the prognostic value of PNI in high-grade gliomas. Due to the special microenvironment of glioma, its immune response was different from other solid tumors. First, most immune cells could not pass the blood–brain barrier smoothly, and high-grade gliomas were relatively "cold" tumors (38). Secondly, the ratio of CD4+ T cells, CD8+ T cells, regulatory T cells (Treg), and other types of T lymphocytes in the glioma microenvironment was different. Studies showed that the number of CD4+ T cells, CD8+ T cells, and Treg cells could affect the tumor immune response in gliomas (39–41). In addition, gliomas could also be divided into different subtypes according to the Tumor Genomics Atlas Project (TCGA), and the prognosis of different subtypes may be different (42, 43). These may be the reasons why the findings found in other malignant tumors did not necessarily exist in high-grade gliomas.

There was no doubt that this study had certain limitations (1). As a single-center, retrospective study, the number of patients included in this study was limited and the follow-up time was insufficient. Moreover, the number of people in the high-PNI and low-PNI groups was uneven. We will continue to follow up more patients to obtain more accurate results (2). The biomarker status of the tumor may affect the prognosis of patients with high-grade glioma. We would continue to follow up and include more patients with more accurate tumor molecular classification to verify our findings and optimize the nomogram (3). Patients with high-grade glioma may receive different treatments after surgery, such as tumor-treating fields and bevacizumab, and the duration of treatment may also be different. All of these may lead to bias in research results. More prospective clinical trials were needed to evaluate the prognostic value of PNI in patients with high-grade glioma (4). Although the OS predicted by the nomogram was in good agreement with the observed OS, the general applicability of the findings still needed to be confirmed by external verification.

CONCLUSIONS

Preoperative PNI level was an independent prognostic factor for patients with grade IV glioma. The nomogram covering PNI could predict the prognosis of patients with grade IV glioma more accurately than traditional markers. The value of PNI in grade III glioma needs to be further evaluated. More large-scale prospective clinical trials are needed to evaluate the prognostic value of preoperative PNI in high-grade gliomas.

DATA AVAILABILITY STATEMENT

The original contributions presented in the study are included in the article/**Supplementary Material**. Further inquiries can be directed to the corresponding author.

ETHICS STATEMENT

Ethical review and approval were not required for the study on human participants in accordance with the local legislation and institutional requirements. Written informed consent for

participation was not required for this study in accordance with the national legislation and the institutional requirements.

AUTHOR CONTRIBUTIONS

(I) Conception and design: all authors. (II) Administrative support: none. (III) Provision of study materials or patients: QH, QR. (IV) Collection and assembly of data: QH, WZ. (V) Data analysis and interpretation: QH, QR. (VI) Manuscript writing: all authors. (VII) Final approval of manuscript: all authors. All authors contributed to the article and approved the submitted version.

ACKNOWLEDGMENTS

Thanks are given for the data support provided by the First Affiliated Hospital of Chongqing Medical University.

SUPPLEMENTARY MATERIAL

The Supplementary Material for this article can be found online at: https://www.frontiersin.org/articles/10.3389/fonc.2021.724769/full#supplementary-material

REFERENCES

1. Ostrom QT, Cioffi G, Gittleman H, Patil N, Waite K, Kruchko C, et al. CBTRUS Statistical Report: Primary Brain and Other Central Nervous System Tumors Diagnosed in the United States in 2012-2016. *Neuro Oncol* (2019) 21 (Suppl 5):v1–100. doi: 10.1093/neuonc/noz150
2. Qian BZ. Inflammation Fires Up Cancer Metastasis. *Semin Cancer Biol* (2017) 47:170–6. doi: 10.1016/j.semcancer.2017.08.006
3. Hung RJ, Ulrich CM, Goode EL, Brhane Y, Muir K, Chan AT, et al. Cross Cancer Genomic Investigation of Inflammation Pathway for Five Common Cancers: Lung, Ovary, Prostate, Breast, and Colorectal Cancer. *J Natl Cancer Inst* (2015) 107(11). doi: 10.1093/jnci/djv246
4. Barahona Ponce C, Scherer D, Brinster R, Boekstegers F, Marcelain K, Gárate-Calderón V, et al. Gallstones, Body Mass Index, C-Reactive Protein, and Gallbladder Cancer: Mendelian Randomization Analysis of Chilean and European Genotype Data. *Hepatology* (2021) 73(5):1783–96. doi: 10.1002/hep.31537
5. Sasaki M, Miyoshi N, Fujino S, Ogino T, Takahashi H, Uemura M, et al. The Geriatric Nutritional Risk Index Predicts Postoperative Complications and Prognosis in Elderly Patients With Colorectal Cancer After Curative Surgery. *Sci Rep* (2020) 10(1):10744. doi: 10.1038/s41598-020-67285-y
6. Wang Z, Wang Y, Zhang X, Zhang T. Pretreatment Prognostic Nutritional Index as a Prognostic Factor in Lung Cancer: Review and Meta-Analysis. *Clin Chim Acta* (2018) 486:303–10. doi: 10.1016/j.cca.2018.08.030
7. Hao J, Chen C, Wan F, Zhu Y, Jin H, Zhou J, et al. Prognostic Value of Pre-Treatment Prognostic Nutritional Index in Esophageal Cancer: A Systematic Review and Meta-Analysis. *Front Oncol* (2020) 10:797. doi: 10.3389/fonc.2020.00797
8. Hua X, Long ZQ, Huang X, Deng JP, He ZY, Guo L, et al. The Value of Prognostic Nutritional Index (PNI) in Predicting Survival and Guiding Radiotherapy of Patients With T1-2n1 Breast Cancer. *Front Oncol* (2019) 9:1562. doi: 10.3389/fonc.2019.01562
9. Gao QL, Shi JG, Huang YD. Prognostic Significance of Pretreatment Prognostic Nutritional Index (PNI) in Patients With Nasopharyngeal Carcinoma: A Meta-Analysis. *Nutr Cancer* (2020) 73(9):1657–67. doi: 10.1080/01635581.2020.1810715
10. Sun G, Li Y, Peng Y, Lu D, Zhang F, Cui X, et al. Impact of the Preoperative Prognostic Nutritional Index on Postoperative and Survival Outcomes in Colorectal Cancer Patients Who Underwent Primary Tumor Resection: A Systematic Review and Meta-Analysis. *Int J Colorectal Dis* (2019) 34(4):681–9. doi: 10.1007/s00384-019-03241-1
11. Oh SE, Choi MG, Seo JM, An JY, Lee JH, Sohn TS, et al. Prognostic Significance of Perioperative Nutritional Parameters in Patients With Gastric Cancer. *Clin Nutr* (2019) 38(2):870–6. doi: 10.1016/j.clnu.2018.02.015
12. Lv X, Zhang Z, Yuan W. Pretreatment Prognostic Nutritional Index (PNI) as a Prognostic Factor in Patients With Biliary Tract Cancer: A Meta-Analysis. *Nutr Cancer* (2020) 73(10):1872–81. doi: 10.1080/01635581.2020.1817955
13. Liu M, Wang L. Prognostic Significance of Preoperative Serum Albumin, Albumin-to-Globulin Ratio, and Prognostic Nutritional Index for Patients With Glioma: A Meta-Analysis. *Med (Baltimore)* (2020) 99(27):e20927. doi: 10.1097/md.0000000000020927
14. Aldape K, Zadeh G, Mansouri S, Reifenberger G, von Deimling A. Glioblastoma: Pathology, Molecular Mechanisms and Markers. *Acta Neuropathol* (2015) 129(6):829–48. doi: 10.1007/s00401-015-1432-1
15. Zhang Y, Sun Y, Zhang Q. Prognostic Value of the Systemic Immune-Inflammation Index in Patients With Breast Cancer: A Meta-Analysis. *Cancer Cell Int* (2020) 20:224. doi: 10.1186/s12935-020-01308-6
16. Okugawa Y, Toiyama Y, Yamamoto A, Shigemori T, Ide S, Kitajima T, et al. Lymphocyte-C-Reactive Protein Ratio as Promising New Marker for Predicting Surgical and Oncological Outcomes in Colorectal Cancer. *Ann Surg* (2020) 272(2):342–51. doi: 10.1097/sla.0000000000003239
17. Eckart A, Struja T, Kutz A, Baumgartner A, Baumgartner T, Zurfluh S, et al. Relationship of Nutritional Status, Inflammation, and Serum Albumin Levels During Acute Illness: A Prospective Study. *Am J Med* (2020) 133(6):713–22.e7. doi: 10.1016/j.amjmed.2019.10.031
18. Haskins IN, Baginsky M, Amdur RL, Agarwal S. Preoperative Hypoalbuminemia Is Associated With Worse Outcomes in Colon Cancer Patients. *Clin Nutr* (2017) 36(5):1333–8. doi: 10.1016/j.clnu.2016.08.023
19. Zhao J, Huang W, Wu Y, Luo Y, Wu B, Cheng J, et al. Prognostic Role of Pretreatment Blood Lymphocyte Count in Patients With Solid Tumors: A Systematic Review and Meta-Analysis. *Cancer Cell Int* (2020) 20:15. doi: 10.1186/s12935-020-1094-5
20. Mei Z, Shi L, Wang B, Yang J, Xiao Z, Du P, et al. Prognostic Role of Pretreatment Blood Neutrophil-to-Lymphocyte Ratio in Advanced Cancer Survivors: A Systematic Review and Meta-Analysis of 66 Cohort Studies. *Cancer Treat Rev* (2017) 58:1–13. doi: 10.1016/j.ctrv.2017.05.005
21. Ethier JL, Desautels D, Templeton A, Shah PS, Amir E. Prognostic Role of Neutrophil-to-Lymphocyte Ratio in Breast Cancer: A Systematic Review and Meta-Analysis. *Breast Cancer Res* (2017) 19(1):2. doi: 10.1186/s13058-016-0794-1
22. Xue Y, Zhou X, Xue L, Zhou R, Luo J. The Role of Pretreatment Prognostic Nutritional Index in Esophageal Cancer: A Meta-Analysis. *J Cell Physiol* (2019) 234(11):19655–62. doi: 10.1002/jcp.28565
23. Zhang H, Shang X, Ren P, Gong L, Ahmed A, Ma Z, et al. The Predictive Value of a Preoperative Systemic Immune-Inflammation Index and Prognostic Nutritional Index in Patients With Esophageal Squamous Cell Carcinoma. *J Cell Physiol* (2019) 234(2):1794–802. doi: 10.1002/jcp.27052
24. Wang PF, Meng Z, Song HW, Yao K, Duan ZJ, Yu CJ, et al. Preoperative Changes in Hematological Markers and Predictors of Glioma Grade and Survival. *Front Pharmacol* (2018) 9:886. doi: 10.3389/fphar.2018.00886
25. Xu WZ, Li F, Xu ZK, Chen X, Sun B, Cao JW, et al. Preoperative Albumin-to-Globulin Ratio and Prognostic Nutrition Index Predict Prognosis for Glioblastoma. *Onco Targets Ther* (2017) 10:725–33. doi: 10.2147/ott.S127441
26. Ang SYL, Lee L, See AAQ, Ang TY, Ang BT, King NKK. Incidence of Biomarkers in High-Grade Gliomas and Their Impact on Survival in a Diverse SouthEast Asian Cohort - a Population-Based Study. *BMC Cancer* (2020) 20 (1):79. doi: 10.1186/s12885-020-6536-x
27. Aquilanti E, Miller J, Santagata S, Cahill DP, Brastianos PK. Updates in Prognostic Markers for Gliomas. *Neuro Oncol* (2018) 20(suppl_7):vii17–26. doi: 10.1093/neuonc/noy158
28. Pinson H, Hallaert G, van der Meulen J, Dedeurwaerdere F, Vanhauwaert D, Van den Broecke C, et al. Weak MGMT Gene Promoter Methylation Confers a Clinically Significant Survival Benefit in Patients With Newly Diagnosed

Glioblastoma: A Retrospective Cohort Study. *J Neurooncol* (2020) 146(1):55–62. doi: 10.1007/s11060-019-03334-5
29. Fuster-Garcia E, Lorente Estellés D, Álvarez-Torres MDM, Juan-Albarracín J, Chelebian E, Rovira A, et al. MGMT Methylation may Benefit Overall Survival in Patients With Moderately Vascularized Glioblastomas. *Eur Radiol* (2021) 31(3):1738–47. doi: 10.1007/s00330-020-07297-4
30. Bell EH, Pugh SL, McElroy JP, Gilbert MR, Mehta M, Klimowicz AC, et al. Molecular-Based Recursive Partitioning Analysis Model for Glioblastoma in the Temozolomide Era: A Correlative Analysis Based on NRG Oncology RTOG 0525. *JAMA Oncol* (2017) 3(6):784–92. doi: 10.1001/jamaoncol.2016.6020
31. Reifenberger G, Wirsching HG, Knobbe-Thomsen CB, Weller M. Advances in the Molecular Genetics of Gliomas - Implications for Classification and Therapy. *Nat Rev Clin Oncol* (2017) 14(7):434–52. doi: 10.1038/nrclinonc.2016.204
32. Nabors LB, Portnow J, Ahluwalia M, Baehring J, Brem H, Brem S, et al. Central Nervous System Cancers, Version 3.2020, NCCN Clinical Practice Guidelines in Oncology. *J Natl Compr Canc Netw* (2020) 18(11):1537–70. doi: 10.6004/jnccn.2020.0052
33. Weller M, van den Bent M, Preusser M, Le Rhun E, Tonn JC, Minniti G, et al. EANO Guidelines on the Diagnosis and Treatment of Diffuse Gliomas of Adulthood. *Nat Rev Clin Oncol* (2021) 18(3):170–86. doi: 10.1038/s41571-020-00447-z
34. Moujaess E, Fakhoury M, Assi T, Elias H, El Karak F, Ghosn M, et al. The Therapeutic Use of Human Albumin in Cancer Patients' Management. *Crit Rev Oncol Hematol* (2017) 120:203–9. doi: 10.1016/j.critrevonc.2017.11.008
35. Almasaudi AS, Dolan RD, Edwards CA, McMillan DC. Hypoalbuminemia Reflects Nutritional Risk, Body Composition and Systemic Inflammation and Is Independently Associated With Survival in Patients With Colorectal Cancer. *Cancers (Basel)* (2020) 12(7). doi: 10.3390/cancers12071986
36. Chapuis AG, Roberts IM, Thompson JA, Margolin KA, Bhatia S, Lee SM, et al. T-Cell Therapy Using Interleukin-21-Primed Cytotoxic T-Cell Lymphocytes Combined With Cytotoxic T-Cell Lymphocyte Antigen-4 Blockade Results in Long-Term Cell Persistence and Durable Tumor Regression. *J Clin Oncol* (2016) 34(31):3787–95. doi: 10.1200/jco.2015.65.5142
37. Lee YH, Martin-Orozco N, Zheng P, Li J, Zhang P, Tan H, et al. Inhibition of the B7-H3 Immune Checkpoint Limits Tumor Growth by Enhancing Cytotoxic Lymphocyte Function. *Cell Res* (2017) 27(8):1034–45. doi: 10.1038/cr.2017.90
38. Lim M, Xia Y, Bettegowda C, Weller M. Current State of Immunotherapy for Glioblastoma. *Nat Rev Clin Oncol* (2018) 15(7):422–42. doi: 10.1038/s41571-018-0003-5
39. Zhang W, Wu S, Guo K, Hu Z, Peng J, Li J. Correlation and Clinical Significance of LC3, CD68+ Microglia, CD4+ T Lymphocytes, and CD8+ T Lymphocytes in Gliomas. *Clin Neurol Neurosurg* (2018) 168:167–74. doi: 10.1016/j.clineuro.2018.02.044
40. Zhang M, Wang X, Chen X, Zhang Q, Hong J. Novel Immune-Related Gene Signature for Risk Stratification and Prognosis of Survival in Lower-Grade Glioma. *Front Genet* (2020) 11:363. doi: 10.3389/fgene.2020.00363
41. Long Y, Tao H, Karachi A, Grippin AJ, Jin L, Chang YE, et al. Dysregulation of Glutamate Transport Enhances Treg Function That Promotes VEGF Blockade Resistance in Glioblastoma. *Cancer Res* (2020) 80(3):499–509. doi: 10.1158/0008-5472.Can-19-1577
42. Hao Z, Guo D. EGFR Mutation: Novel Prognostic Factor Associated With Immune Infiltration in Lower-Grade Glioma; an Exploratory Study. *BMC Cancer* (2019) 19(1):1184. doi: 10.1186/s12885-019-6384-8
43. Pan YB, Zhang CH, Wang SQ, Ai PH, Chen K, Zhu L, et al. Transforming Growth Factor Beta Induced (TGFBI) Is a Potential Signature Gene for Mesenchymal Subtype High-Grade Glioma. *J Neurooncol* (2018) 137(2):395–407. doi: 10.1007/s11060-017-2729-9

Conflict of Interest: The authors declare that the research was conducted in the absence of any commercial or financial relationships that could be construed as a potential conflict of interest.

Publisher's Note: All claims expressed in this article are solely those of the authors and do not necessarily represent those of their affiliated organizations, or those of the publisher, the editors and the reviewers. Any product that may be evaluated in this article, or claim that may be made by its manufacturer, is not guaranteed or endorsed by the publisher.

frontiers in Neurology

REVIEW
published: 17 February 2022
doi: 10.3389/fneur.2021.784330

Natural Plant Compounds: Does Caffeine, Dipotassium Glycyrrhizinate, Curcumin, and Euphol Play Roles as Antitumoral Compounds in Glioblastoma Cell Lines?

Gabriel Alves Bonafé[1†‡], Matheus Negri Boschiero[1†‡], André Rodrigues Sodré[1†], Jussara Vaz Ziegler[2], Thalita Rocha[3†] and Manoela Marques Ortega[1†]*

[1] Laboratory of Cell and Molecular Tumor Biology and Bioactive Compounds, São Francisco University Medical School, São Paulo, Brazil, [2] Verdi Cosmetics LLC, São Paulo, Brazil, [3] Postgraduate Program in Biomaterials and Regenerative Medicine, Faculty of Medical Sciences and Health, Pontifical Catholic University of São Paulo, São Paulo, Brazil

Many plant-derived compounds are shown to be promising antitumor therapeutic agents by enhancing apoptosis-related pathways and cell cycle impairment in tumor cells, including glioblastoma (GBM) cell lines. We aimed to review four natural plant compounds effective in GBM cell lines as caffeine, dipotassium glycyrrhizinate (DPG), curcumin, and euphol. Furthermore, antitumoral effect of these plant compounds on GBM cell lines through microRNAs (miRs) modulation was investigated. However, only DPG and curcumin were found as effective on miR modulation. Caffeine arrests GBM cell cycle in G0/G1 phase by cyclin-dependent kinases (CDK) complex inhibition and by decreasing *BCL-2* and increasing *FOXO1* expression levels causing greater apoptotic activity. Caffeine can also directly inhibit IP3R3, p38 phosphorylation, and rho-associated protein kinase (ROCK), decreasing cell invasion and migration capacity or indirectly by inhibiting the tissue inhibitor metalloproteinase-1 (*TIMP-1*) and integrins β1 and β3, leading to lower matrix metalloproteinases, MMP-2 and MMP-9. DPG presents antitumoral effect in GBM cells related to nuclear factor kappa B (NF-κB) pathway suppression by *IRAK2* and *TRAF6*-mediating miR-16 and miR-146a, respectively. More recently, it was observed that DPG upregulated miR-4443 and miR-3620, responsible for post-transcriptional inhibition of the NF-κB pathway by *CD209* and *TNC* modulation, respectively leading to lower MMP-9 and migration capacity. Curcumin is able to increase miR-223-3p, miR-133a-3p, miR-181a-5p, miR-34a-5p, miR-30c-5p, and miR-1290 expression leading to serine or threonine kinase (AKT) pathway impairment and also it decreases miR-27a-5p, miR-221-3p, miR-21-5p, miR-125b-5p, and miR-151-3p expression causing p53-BCL2 pathway inhibition and consequently, cellular apoptosis. Interestingly, lower expression

OPEN ACCESS

Edited by:
Liam Chen, University of Minnesota, United States

Reviewed by:
Francisco Arenas-Huertero, Hospital Infantil de México Federico Gomez, Mexico
Parasuraman Aiya Subramani, Vels Institute of Science, Technology & Advanced Studies (VISTAS), India

***Correspondence:**
Manoela Marques Ortega
Email: manoela.ortega@usf.edu.br

†ORCID:
Gabriel Alves Bonafé
orcid.org/0000-0002-9280-0122
Matheus Negri Boschiero
orcid.org/0000-0002-2866-391X
André Rodrigues Sodré
orcid.org/0000-0002-3969-5386
Thalita Rocha
orcid.org/0000-0002-2731-9586
Manoela Marques Ortega
orcid.org/0000-0003-4609-7074

‡*These authors have contributed equally to this work*

Specialty section:
This article was submitted to Neuro-Oncology and Neurosurgical Oncology, a section of the journal Frontiers in Neurology

Received: *27 September 2021*
Accepted: *29 November 2021*
Published: *17 February 2022*

Citation:
Bonafé GA, Boschiero MN, Sodré AR, Ziegler JV, Rocha T and Ortega MM (2022) Natural Plant Compounds: Does Caffeine, Dipotassium Glycyrrhizinate, Curcumin, and Euphol Play Roles as Antitumoral Compounds in Glioblastoma Cell Lines? Front. Neurol. 12:784330. doi: 10.3389/fneur.2021.784330

of miR-27a by curcumin action enhanced the C/EBP homologous protein(CHOP) expression, leading to paraptosis. Curcumin can inhibit miR-21 expression and consequently activate apoptosis through caspase 3 and death receptor (DR) 4 and 5 activation. Autophagy is controlled by the LC-3 protein that interacts with Atg family for the LC3-II formation and autophagy activation. Euphol can enhance LC3-II levels directly in GBM cells or inhibits tumor invasion and migration through PDK1 modulation.

Keywords: caffeine, dipotassium glycyrrhizinate, curcumin, euphol, microRNAs, glioblastoma cell lines

INTRODUCTION

The central nervous system (CNS) tumors account for about 3% of all neoplasms (1). Glial tumors or gliomas comprise 50% of all CNS tumors and 80% of all brain-initiating malignant tumors (2). Gliomas are subdivided into astrocytomas, oligodendrogliomas, and ependymomas (3). Furthermore, according to the World Health Organization (WHO), astrocytomas are divided into four degrees of malignancy, which are based on histopathological criteria such as the presence of atypical cells, mitosis, endothelial proliferation, and necrosis; and molecular depending on the presence or absence of mutations in the isocitrate dehydrogenase 1 and 2 genes (*IDH1* and *IDH2*) (4).

Malignant gliomas are the most common primary brain tumor, representing 42% of CNS tumors (5). The most common aggressive glioma form is known as glioblastoma (GBM) or WHO grade IV has a 12–15-month medium survival rate. The lower-grade gliomas (WHO grades II and III) appear less aggressive at the time of diagnosis but eventually progress into a malignant phase within 5–10 years (6). Despite the surgical procedures and treatment regimens with radiation and chemotherapy, malignant gliomas remain incurable (6), due to their resistance to all conventional therapies and the diffuse infiltrative nature of the tumor cells.

Therefore, new therapies and therapeutic combinations need to be developed and quickly approved for use in patients. However, to gain approval, therapies need to be safe, effective, and able to penetrate the blood–brain barrier (BBB) (7). In that way, natural treatments might be new compounds that can eliminate GBM development and tumor expansion.

Many plant-derived compounds are shown to be promising antitumor therapeutic agents by enhancing apoptosis-related pathways in tumor cells through the regulation of microRNAs (miRs) expression (8, 9).

MicroRNAs are small molecules (on average about 22 nucleotides) of non-coding RNA that bind to complementary sequences in the 3'UTR portion of the transcribed mRNA target resulting in translational repression or gene degradation and silencing (10). The human species is able to synthetized ∼2,600 mature miRs (11), and more than 50% of these miRs are located in cancer-associated genomic regions (12).

The deregulation of miRs is associated with the development and progression of several types of tumors (13), including GBM (14), by inhibiting the translation of its target genes (10). Recent evidence suggests that miRs play an essential role in the etiology of GBM, as they are involved in several biological processes, such as cell growth, migration and invasion, apoptosis, and cell differentiation (15).

Therefore, in this study, we aimed to review four natural plant compounds that may be effective in enhancing apoptosis-related pathways and cell cycle impairment in GBM cell lines. Furthermore, antitumoral effect of these plant compounds on GBM cell lines through miR modulation was investigated, although only DPG and curcumin were found as effective on miR modulation.

METHODS

Following the recommendations from Preferred Reporting Items for Systematic Review and Meta-Analysis (PRISMA), a systematic review of the studies published in the PubMed (http://www.ncbi.nlm.nih.gov/pubmed) database in the last 10 years was conducted. Experimental studies that included natural plant compounds as caffeine, dipotassium glycyrrhizinate (DPG), curcumin, and euphol in gliomas were included (19 studies) (**Table 1**). In addition, studies related to these natural compounds and miR effects were also selected for the present review (7 studies) (**Table 2**).

DISCUSSION

Does Caffeine Play Role on GBMs?

Caffeine ($C_8H_{10}N_4O_2$) is a methylxanthine compound commonly found in coffee and tea (**Figure 1A**), which are the most ingested neuroactive substance in the world (34). Caffeine possesses antiinflammatory and antioxidant effect, as acetylcholinesterase inhibitors (35). Recently, it was reported that caffeine consumption might be associated with lower glioma risk (36). In fact, caffeine has been associated with rat glial cell (C6) and human GBM cell lines (U251 and U87MG) growth inhibition and apoptosis activation (16, 17, 19, 21).

Effects of Caffeine in Cell Cycle

The cell cycle checkpoints are controlled by cyclin and cyclin-dependent kinases (CDK) proteins. Generally, during final G1 phase, the cyclins D and E are synthetized, which associates with Cdk4 and/or Cdk6 and Cdk2 cyclins, respectively, forming CdkD/Cdk4,6 and CdkE/Cdk2 complexes (37). Both complexes participate in the phosphorylation and inactivation of the retinoblastoma protein (Rb). After phosphorylation, Rb unbound the transcription factor E2F protein, responsible for cyclin A and cyclin E synthesis (38) (**Figure 2A**). Caffeine effect on cell

TABLE 1 | The effects of the natural compounds on GBM cell lines (19–22, 41, 47, 49, 54, 63, 69, 83–87, 89, 92, 101).

Natural compounds	Cell lines	Studies	Assays	Effects	Pathways
Caffeine					
	C6/U87MG	Jiang et al. (16); Liu et al. (17)	*in vitro*	Cell cycle arrest; proliferation inhibition; apoptosis stimulation	G0/G1 phase arrest; S phase decreased; ↓Blc-2; ↑CytC e caspase 3
	U87MG/U178MG/ T98G/U373MG/M059K	Kang et al. (18)	*in vitro/ in vivo*	Migration and invasion inhibition	↓IP3R3-mediated Ca2+ release
	U87MG	Ku et al. (19)	*in vitro*	Cell cycle arrest; proliferation inhibition; apoptosis stimulation	G0/G1 phase arrest; ↓Rb phosphorylation; ↑caspase 3 and PARP activation; ↑GSK3β phosphorylation
	U87MG/GBM8401 /LN229	Cheng et al. (20)	*in vitro*	Migration and invasion inhibition	↑TIMP-1; ↓MMP-2; ↓p-ERK and integrins β1 and β3
	U251	Sun et al. (21)	*in vitro*	Apoptosis stimulation; proliferation inhibition	↑FoxO1 expression; ↑proapoptotic target Bim
AC derivatives					
PT93	T98G/U87MG /U251/HT22	Li et al. (22)	*in vitro*	Apoptosis stimulation; proliferation inhibition; migration inhibition	↓extracellular MMP-2 and MMP-9
FLVM/FLVZ	U87MG	Khan et al. (23)	*in vivo*	Apoptosis stimulation; proliferation inhibition; angiogenesis inhibition	↓tumor hypoxia (HIF-1α); ↓angiogenesis (CD34, VEGF, IL17A); ↓cell proliferation (Ki67); ↑Bax, caspase and FasL
GA					
	U251	Li et al. (24)	*in vitro*	Apoptosis stimulation; survival rate and colony formation inhibition;	↓NF-κB-p65 reduction
DPG					
	U87MG/T98G	Bonafé et al. (25)	*in vitro*	Apoptosis stimulation; proliferation inhibition; steam cells formation inhibition	↓NF-κB by *IRAK-2* and *TRAF6* reduction
	U251//U138MG	Unpublish data	*in vitro*	Apoptosis stimulation; proliferation inhibition; steam cells formation inhibition, migration inhibition	↓NF-κB by *CD209* and *TNC* modulation
Curcumin					
	U87MG	Wu et al. (26)	*in vitro*	Proliferation inhibition; apoptosis stimulation	↓NF-κB suppression
	U87MG	Li et al. (27)	*in vitro/in vivo*	Proliferation inhibition; apoptosis stimulation	↓MAPK pathway by phosphorylation of p38; ↑Bax and cytochrome C; ↓PCNA as reduction of cell proliferation
	U87MG/U251	Yin et al. (28)	*in vitro/ in vivo*	Proliferation inhibition; apoptosis stimulation; migration inhibition	SHH/GLI1 pathway has also been shown to regulate the stemness and invasiveness
	C6	Tan et al. (29)	*in vitro/ in vivo*	Apoptosis stimulation; tumor growth inhibition	↓*PDCD4* and *PTEN* inhibition
	GSC	Qian et al. (30)	*in vitro/ in vivo*	Apoptosis stimulation; cell growth inhibition	↑miR-145 results in increased cell growth inhibition and apoptosis to DC
	A172	Garrido-Armas et al. (31)	*in vitro*	Paraptosis	↑several miRs downregulate the AKT and p53-BCL2 pathways; ↓miR-27a expression reduced CHOP leading the cells to paraptosis

(Continued)

TABLE 1 | Continued

Natural compounds	Cell lines	Studies	Assays	Effects	Pathways
Euphol and its derivatives					
		Silva et al. (32)	*in vitro/ in vivo*	Proliferation and cell motility inhibition	↑autophagy-associated protein LC3-II and acidic vesicular organelle formation with Bafilomycin A1 potentiating cytotoxicity
IngA/IngB/IngC	12 human gliomas and GBM*	Silva et al. (33)	*in vitro*	Proliferation inhibition	Dose-dependent cytotoxic effects

*Cyt C, cytochrome C; AC, caffeic acid derivative; GA, glycyrrhizic acid; DPG, dipotassium glycyrrhizinate; DC, demethoxycurcumin; *, U87MG, U373, U251, GAMG, SW1783, SNB19; Cdk, cyclin-dependent kinases; ROCK, rho-associated protein kinase; p-p38, phosphorylated p38; TIMP-1, tissue inhibitor metalloproteinase-1; β, Integrins; MMP, matrix metalloproteinase; IngA, ingenol-3-transcinnamate; IngB, ingenol-3-hexanoate; IngC, ingenol-3-dodecanoate. The meaning of the symbols ↑, ↓ are up-regulated and down-regulated respectively.*

cycle might be associated with the suppression of CdkD/Cdk4,6 complex and subsequently phosphorylation (p) and inactivation of retinoblastoma (Rb) (39), preventing the E2F transcription factor unbound and the synthesis inhibition of important cell cycle proteins (40). In fact, it was observed that C6 (0.5 mM) and U87MG (1–5 mM) GBM cell lines presented lower S phase and G0/G1 phase arrested in a caffeine dose-dependent way (16, 17, 19, 21) (**Figure 2A**). Kaufmann et al. (41) have confirmed that caffeine actually targets the CdkD/Cdk4,6 complex required -for inactivation of pRB, in telomerase-expressing human fibroblasts.

In addition, the glycogen synthase kinase-3beta (GSK-3β) substrate phosphorylates the cyclin D1, leading to its degradation, decreasing Cdk4 activity, which leads to the S phase (19, 42). Hashimoto et al. (39) have suggested that the caffeine inhibitory effect on cell growth was mediated through GSK-3β by direct inhibition of PI3-kinase upstream. Interestingly, it was reported that caffeine, in combination with temozolomide (TMZ), revealed synergistic effects in U87MG cell line, since the combinational therapy TMZ suppressed the phosphorylation of ATM and p53 and downregulated p21 expression, thus releasing DNA-damaged cells from G2 arrest into premature mitosis. Cell cycle analysis demonstrated that the proportion of cells arrested in G2 phase decreased when caffeine was administered together with TMZ. In conclusion, the authors have demonstrated that caffeine enhanced the efficacy of TMZ through mitotic cell death by impeding ATM/p53/p21-mediated G2 arrest (43). The effects of caffeine on GBM cell cycle regulation are summarized in **Figure 2A**.

Effects of Caffeine in Apoptosis

It has been reported that caffeine has an anticancer apoptotic effect in various types of cancer such as gastric cancer (17), neuroblastoma (44), and GBM (16, 17, 19, 21).

The balance between the proapoptotic proteins, Bax, Bak, Bim, and Bad, and antiapoptotic proteins, Bcl-2 and Bcl-xL, regulates the apoptotic pathway (45). These proapoptotic and antiapoptotic proteins are responsible for cytochrome C (Cyt C) dissociation from the external mitochondrial membrane and prevent the Cyt C dissociation, respectively (46, 47). Therefore, the ratio Bax/Bcl-2 is an excellent indicative of apoptosis in tumor cells (46, 47) (**Figure 3A**).

Two studies have showed a decreased expression of antiapoptotic Bcl-2 and no changes on proapoptotic protein Bax, indicating an imbalance of Bax/Bcl-2 ratio and consequently, increased Cyt C dissociation and caspase 3 activation after caffeine exposure in GBM cell lines (C6 and U87MG). Caffeine at 1 mM reduced the cell viability of both cell lines to <70%. Therefore, to avoid any effects on cell viability, the maximal non-cytotoxic concentration of caffeine on both GBM cells was 0.5 mM (16, 17) (**Figure 3A**).

Maiese et al. (48) have demonstrated that caffeine also acts increasing the expression of *FOXO1*, important for cell survival and apoptosis regulation. However, the apoptosis mechanisms induced by *FOXO1* need to be elucidated (49, 50). One study has suggested that high *FOXO1* expression after caffeine treatment caused an increased proapoptotic Bim protein expression and, consequently, contributed for the apoptotic effect in U251 GBM cell line (21) (**Figure 3A**).

Effects of Caffeine in Tumor Cell Invasion and Migration

The tumor cell invasion is due to the actin polymerization and the intracellular cytoskeletal organization calcium-dependent proteins (51, 52). In GBM cells, the receptor-mediated calcium mechanism is an important factor for properly invasion, motility, and proliferation of tumor cells (53, 54).

Kang et al. (18) treated several GBM cell lines (U178MG, U87MG, and T98G) with caffeine, and the authors have observed inhibition of proliferation and invasion, in a dose-dependent manner (1-5-10 mM). It was noticed, especially in U178MG cells, the inhibition of IP_3R, an ion channel responsible for release of calcium from intracellular stores. Moreover, IP_3R_1 ion channel subtype was lower expressed in GBM cells, whereas IP_3R_3 subtype is more expressed. Caffeine seems to compete to IP_3R ATP binding even at lower concentrations (10-25-50mM), interfering its function (55, 56) (**Figure 2B**).

TABLE 2 | The natural compound effects on miRs in GBM cell lines (83–87, 89).

Natural compounds	Cell lines	Studies	Assays	miR effects	Pathways
DPG					
	U87MG/T98G	Bonafé et al. (25)	*in vitro*	↑miR-146a ↑miR-16	↓NF-κB by upregulating miR16 and miR146a, which downregulate its target genes, *IRAK2* and *TRAF6*
	U251/U138MG	Unpublished data	*in vitro*	↑miR-4443 ↑miR-3620	↑ miR-4443 and ↑miR-3620 induces post-transcriptional inhibition of the NF-κB by *CD209* and *TNC* genes modulation and leading to an antimigratory effect on GBM cells
Curcumin					
	U87MG	Wu et al. (26)	*in vitro*	↑miR-146a	↑miR-146a enhances apoptosis and suppressed NF-κB activation
	U87MG	Li et al. (27)	*in vitro/ in vivo*	↑miR-378	↑miR-378 enhances the response to curcumin by targeting *P-P38*
	A172	Garrido-Armas et al. (31)	*in vitro*	↑miR-223-3p ↑miR-1290 ↑miR-34a-5p ↑miR-181a-5p ↑miR-133a-3p ↑miR-30c-5p ↓miR-27a-3p ↓miR151-3p ↓miR-221-3p ↓miR-21-5p ↓miR-125b-5P	↑miRs downregulate the AKT and p53-BCL2 pathways; ↓miR-27a expression reduced CHOP leading the cells to paraptosis
	U87MG/U251	Yin et al. (28)	*in vitro/ in vivo*	↑miR-326	↑miR-326 enhances curcumin-inhibition by SHH/GLI1 and regulated the expression of p53 and stemness; tumor reduction
	C6	Tan et al. (29)	*in vivo/ in vitro*	↓miR-21	PDCD4 and PTEN were induced in the miR21ASO/DP and miR21ASO/DP-curcumin complex
	GSC	Qian et al. (30)	*in vitro/ in vivo*	↑miR-145	↑miR-145 is involved in enhancing chemosensitivity to miR-145 by targeting the SOX2-Wnt/β-catenin axis

miR21ASO/DP, miR-21 antisense oligonucleotide. The meaning of the symbols ↑, ↓ are up-regulated and down-regulated respectively.

The matrix metalloproteinase (MMP) proteins, especially MMP-2 and MMP-9, are related to cell invasion and angiogenesis (21, 57). Both are regulated by several factors, such as rho-associated protein kinase (ROCK) and ERK (58, 59). Thus, a study has tested caffeine in U87MG GBM cell line and *in vivo* and phosphorylated p38 (p-p38) and MMP-2 were observed as lower expressed. In contrast, the tissue inhibitor metalloproteinase-1 (TIMP-1) presented higher expression (20), which is an important inhibitor of MMP, and plays a crucial role in brain tumor invasion (60). Furthermore, cells exposed to caffeine presented lower levels of cathepsin B, which is responsible for the MMP activation, due to the integrins β1 and β3 inhibition (20) (**Figure 2B**). The results may explain the lower invasion and adhesion capacity of GBM cells after caffeine exposure (20). The effects of caffeine on GBM cells immigration and evasion are summarized in **Figure 2B**.

Compounds Derived From Caffeic Acid

PT93, a compound derived from caffeic acid (CA), has been evaluated regarding its effect on invasion and migration on GBM cell lines (T98G and U251) (22). The authors observed MMP-2 and MMP-9 inhibition in a dose-dependent way (3 and 10μM)

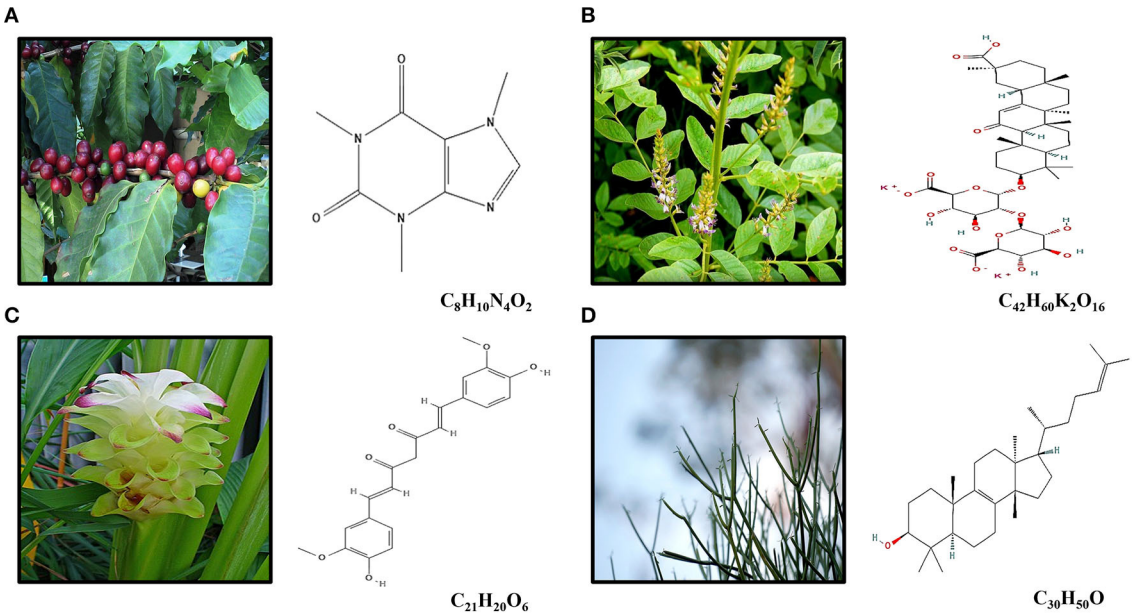

FIGURE 1 | (A) Caffeine ($C_8H_{10}N_4O_2$) is an alkaloid occurring naturally in some 60 plant species, of which cocoa beans, kola nuts, tealeaves, yerba maté, guarana berries, guayusa, yaupon holly, and coffee beans are the most well-known. The best-known source of caffeine is the coffee bean, the seed of the coffee plant. **(B)** Licorice root (*Glycyrrhiza glabra*) is widely used in traditional Chinese medicine for its pharmacological and physiological action as antiallergic, antibiotic, antiinflammatory, and antitumor effects. DPG ($C_{42}H_{60}K_2O_{16}$) is a dipotassium salt of GA, a compound isolated from licorice root. **(C)** Curcumin (diferuloylmethane; $C_{21}H_{20}O_6$) is the main compound found in turmeric, an Indian spice derived from *Curcuma longa Linn*, which presents antioxidant and antiinflammatory effects. **(D)** The euphol ($C_{30}H_{50}O$), a tetracyclic triterpene alcohol, is the main constituent of the *Euphorbia tirucalli* known as aveloz.

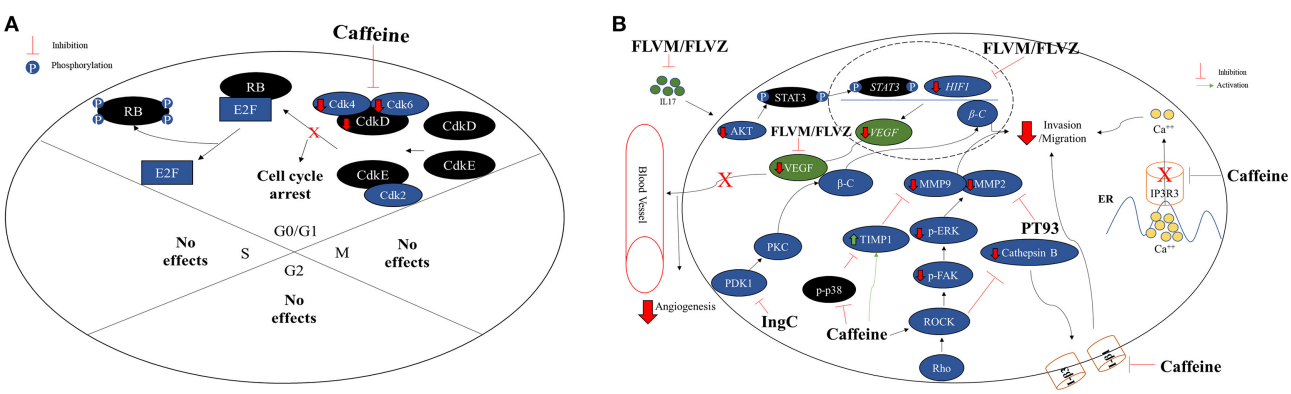

FIGURE 2 | (A) Caffeine arrests the cell cycle on G0/G1 phase in GBM cell lines. Normally, GO/G1 cell cycle phase is regulated by the CdkD and CdkE, which interacts with Cdk4, Cdk6 and Cdk2 forming CdkD/Cdk4,6 and CdkE/Cdk2 complexes. The CDK complexes are responsible for retinoblastoma (Rb) inactivation through phosphorylation and consequently, releasing the transcriptional factor E2F, retaining the cell cycle active. Caffeine appears to arrest the cell cycle in G0/G1 phase in GBM cell lines C6, U251, and U87MG by CDK complex inhibition. No caffeine effects were observed on S, G2, or M phases. **(B)** Effects of caffeine and compounds derived from caffeine on invasion/migration capacity and angiogenesis impairing in GBM cell lines. The caffeine can inhibit the IP3R3, an ER calcium receptor, which leads to a lower concentration of intracellular calcium, decreasing cell invasion and migration capacity. The rho-associated protein kinase (ROCK) cathepsin B/FAK/ERK pathway, associate with cellular invasion and migration, is also inhibited by caffeine through targeting phosphorylated p38 (p-p38) and ROCK proteins direct or by indirect inhibition through the TIMP-1 and integrins β1 (I-β1) and I-β3, leading to lower MMP-2 and MMP-9. In addition, PT93, a compound derived from CA, acts direct in the inhibition of MMP-2 and contributing to lower cellular invasion or migration capacity. In the same way, the CA derivatives FLVM/FLVZ can either inhibit IL17 and HIF-1, leading to VEGF inhibition and angiogenesis impairing. The euphol derivative (IngC), on the other hand, acts in PKC and Wnt/β-catenin (β-C) pathways, inhibiting the PDK1, leading to lower concentration of β-C, an effector protein, consequently inhibiting the tumor invasion and migration.

(**Figure 2B**). PT93, a selective MMP inhibitor, seems to present fewer side effects when compared to the first generation of MMP inhibitors *in vitro* studies (61–63), as Batimastat (BB-94) and Marimastat (BB-2516) (64).

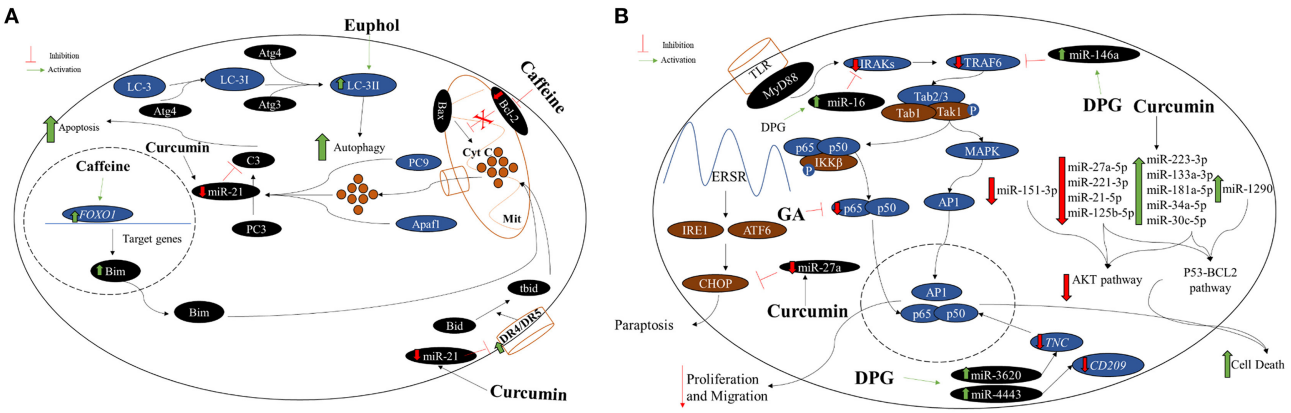

FIGURE 3 | (A) Caffeine, curcumin, and euphol antitumoral effect on GBM cell lines. Generally, the mitochondrial apoptotic pathway is regulated by the proapoptotic protein Bax, which acts in the dissociation of cytochrome C (Cyt C) in the mitochondria (Mit). Thus, Cyt C along the procaspase 9 (PC9) and Apaf1, activate procaspase 3 (PC3) into caspase 3 (C3) leading the cell to apoptosis. Moreover, the nuclear protein Foxo1 acts in the transcription of Bim, which contributes to the dissociation of Cyt C and apoptosis stimulation. Therefore, the ratio Bax/Bcl-2 is an excellent indicative of cellular apoptosis. Caffeine acts decreasing *BCL-2* and increasing *FOXO1* expression levels causing greater apoptotic activity. Curcumin can inhibit miR-21 expression and consequently activating apoptosis by caspase 3 and death receptor (DR) 4 and 5 activations. Autophagy, a misfolded proteins degradation and elimination and also damaged organelles, is control by the LC-3 protein that interacts with Atg family for the LC3-II formation and autophagy activation. Euphol is able to enhance LC3-II levels direct in GBM cell lines. **(B)** Effects of GA, DPG, and curcumin on apoptosis, migration, and paraptosis in GBM cell lines. GA, a compound isolated from licorice root, has presented inhibition effect on cell proliferation and colony formation in U251 GBM cell line. In addition, GA also presented apoptosis stimulation in these cells. The GA antitumoral effect is by direct p65 protein inhibition, responsible for nuclear factor kappa B (NF-κB) pathway activating. More recently, DPG, a dipotassium salt of GA, also has presented antitumoral effect related to NF-κB pathway suppression by *IRAK2* and *TRAF6*-mediating miR-16 and miR-146a, respectively, in U87MG and T98G cells. More recently, it was observed that DPG upregulated miR-4443 and miR-3620, responsible for post-transcriptional inhibition of the NF-κB pathway by *CD209* and *TNC* modulation, respectively, in U251 and U138MG, leading to lower MMP-9. The curcumin effect was able to increase miR-223-3p, miR-133a-3p, miR-181a-5p, miR-34a-5p, miR-30c-5p, and miR-1290 expression leading to serine or threonine kinase pathway (AKT) pathway impairment. Curcumin effect also decreased miR-27a-5p, miR-221-3p, miR-21-5p, miR-125b-5p, and miR-151-3p expression causing p53-BCL2 pathway inhibition and consequently, GBM cell death. Interestingly, lower expression of miR-27a by curcumin action enhanced the CHOP protein expression, leading to paraptosis.

In another study, an U87MG xenotransplant mouse has treated with two other CA derivatives, FLVM and FLVZ by targeting the normally overexpressed IL17A, HIF-1α and vascular endothelial growth factor (VEGF). The reduction of these cytokines leads to inhibition of U97MG GBM cell line, mainly because the angiogenesis is also inhibited. Interestingly, the inhibition of all described factors also provides nutrient partition, leading to a lower adipocyte storage due to the glucose, triglycerides, and fat oxidation metabolism reducing (23). In addition, FLVM and FLVZ provide a reduction in the glucose and adipocyte metabolism in the CNS, inhibiting GBM development (23) due to the adipocytes and blood vessel inhibition (65, 66).

DPG, a New Promising Compound on GBM

Licorice root (*Glycyrhiza glabra*) is widely used in traditional Chinese medicine for its pharmacological and physiological action as antiallergic, antibiotic, antiinflammatory, and antitumor effects (67, 68) (**Figure 1B**). Glycyrrhizic acid (GA) ($C_{42}H_{62}O_{16}$), a compound isolated from licorice root, has presented antiinflammatory and antitumor effects on several tumor cell lines such as human hepatoma (HLE), promyelocytic leukemia (HL-60), stomach cancer (KATO III), and prostate cancer (LNCaP e DU-145) by both DNA fragmentation and deregulating genes required for oxidative stress control (69–71). However, toxicity has been observed in *in vivo* models (72).

More recently, one study has exposure U251 GBM cell line to different concentrations of GA (1, 2, and 4 mM), and the authors have observed inhibition on cell proliferation and colony formation, apoptosis stimulation, and significantly decreasing in p65 protein, responsible for nuclear factor kappa B (NF-κB) pathway activating (24).

The NF-κB pathway is constantly activated in GBM, being responsible for the aggressiveness of the disease and regulation of the expression of antiapoptotic genes and cell adhesion and invasion factors (73). Thus, some studies have suggested inhibition of NF-κB pathway could decrease the resistance of tumor cells to chemotherapy and contribute to increase the survival of patients with GBM (74–77).

Following that idea, a recent study has evaluated the DPG ($C_{42}H_{60}K_2O_{16}$), a dipotassium salt of GA (**Figure 1B**), effects in GBM cell lines (25). The authors have demonstrated antitumoral effect in the GBM cell lines, U87MG and T98G, through a decrease of proliferation and an increase of apoptosis. Moreover, after both DPG and TMZ exposure, higher suppressed cell viability was observed in a dose-dependent way. Thus, even low TMZ concentration with half-maximal inhibitory concentration (IC50) of DPG was able to induce U87MG and T98G cell viability reduction (25, 50, 75, 100, 125, 150, 175, and 200 μM) for 6, 12, 18, and 24 h. Thus, a combinatorial therapy, DPG in combination with TMZ, showed a synergistic effect in U87MG and T98G cell lines (25). Interestingly, DPG was able to induce cell viability reduction even in T98G cell line, which presents both the hypermethylated *MGMT* promoter and mutated *P53* gene, making the phenotype more aggressive and resistant to the action of TMZ than the ones with wild-type *P53* (78), since p53

is fundamental in regulating the cell cycle arrest and the entry in the apoptotic process (79, 80).

In addition, DPG (18 mM and 24 mM for U87MG and T98G cells, respectively) antitumoral effect was related to NF-κB pathway suppression by *IRAK2* and *TRAF6*-mediating miR-16 and miR-146a, respectively (25) (**Figure 3B**), and consequently increasing the TMZ-induced apoptosis. Finally, the authors have also showed that DPG was able to inhibit the subpopulation of stem cells essential for tumor formation, survival, and recurrence (25). Further *in vivo* studies may elucidate the antitumor effect of DPG as an alternative treatment for GBM. The effects of GA and DPG on NF-κB pathway are presented in **Figure 3B**.

More recently, it was demonstrated that the cytotoxic effect of DPG was time- and dose-dependent also in U251 and U138MG and DPG (IC50: 32 mM and 20 mM for 48 h, respectively) inhibited cell viability by activating apoptosis, inhibiting cell proliferation and stem cell subpopulation formation through miR-4443 and miR-3620 upregulation. Both miRs are responsible for post-transcriptional inhibition of the NF-κB pathway by *CD209* and *TNC* modulation on U251 and U138MG cell lines. The authors have concluded that DPG presents an antimigratory effect on GBM cell lines by inhibition of cancer stem-like cells, evidenced by inhibition of neurosphere formation (unpublished data).

Curcumin, a Turmeric Compound With Antitumor Effect on GBM

Curcumin (diferuloylmethane; $C_{21}H_{20}O_6$) (**Figure 1C**) is the main compound found in turmeric, an Indian spice derived from *Curcuma longa Linn* (81). It has been demonstrated that the curcumin has present antioxidant and antiinflammatory effects (81), mainly in diabetes (82), Alzheimer's disease (83), and hepatitis (84).

Curcumin seems to play a role in a variety of pathways as proinflammatory cytokines (TNF-alpha, IL1, IL6, IL8) inhibition, wingless-related integration site (WNT) suppressing, mitogen-activated protein kinase pathway (MAPK) and Janus kinase/signal (JAK/STAT) activation (85–88). Furthermore, curcumin is highly lipophilic, which makes it permeable to the BBB (89, 90), making it further viable *in vivo* therapy.

A recent study has evaluated the curcumin effect over miRs in the GBM cell line, A172. Interestingly, the authors have observed that curcumin was able to downregulate the serine or threonine kinase pathway (AKT) and p53-BCL2 pathways by overexpressing several miRs such as miR-223-3p, miR-133a-3p, miR-181a-5p, miR-34a-5p, miR-30c-5p, and miR-1290 and also downregulating the expression of miR-27a-5p, miR-221-3p, miR-21-5p, miR-125b-5p, and miR-151-3p (31) (**Figure 3B**). AKT and p53-BCL2 pathways are related to proliferation and cellular growth, metabolism, apoptosis, and autophagy (31). In contrast, the authors also observed that in GBM curcumin-treated cells, the miR-27a expression level was reduced and its target gene, *CHOP,* was overexpressed leading the cells to paraptosis, mainly due to endoplasmatic reticulum (ER) instability (31) (**Figure 3B**).

Other studies have also observed that curcumin enhanced the expression of miR-326 (28), miR-378 (27), and miR-21 (29) in GBM cell lines. Thus, Yin et al. (28) have observed that U87MG and U251 cells presented a marked increase of curcumin-induced cytotoxicity and apoptosis and a decrease of proliferation and migration in GBM cells. Moreover, the authors have found that combination treatment of miR-326 mimics and curcumin caused significant inhibition of the SHH/GLI1 pathway in cells compared with either treatment alone, independent of p53 status. Furthermore, *in vivo*, the curcumin-induced miR-326 expression reduces tumor volume and prolonging the survival period compared with either treatment alone. The results support an important role of miR-326 in enhancing the chemosensitivity of glioma cells to curcumin. Similar results were observed in another study, in which the authors have evaluated the curcumin effect on U87MG cells stably expression miR-378. Cells were unable to form colonies compared with control cells, indicating a lower survival rate when treatment of curcumin and miR-378 was combined. In conclusion, curcumin can inhibit MAPK pathway activation by overexpressing miR-378 (27).

Tan et al. (29) have transfected deoxycholic acid-conjugated polyethylenimine (DP) micelles containing curcumin and miR-21 antisense oligonucleotide (ASO) into C6 GBM cell line, aiming knockdown the miR and enhance the expression of proapoptotic target genes. The authors have significantly observed cell viability decreases and apoptosis stimulation when compared to control cells (DP-curcumin). The anticancer effect of DP-curcumin-mir-21ASO complex was also evaluated in *in vivo* essays and it was noticed a significantly tumor growth decrease compared with miR-21ASO and curcumin alone in animals. Curcumin seems increasing miR-21 and consequently inhibiting *PDCD4* and *PTEN* target genes, resulting in cell death.

Glioma stem cells (GSCs) were transfected with lentivirus-GFP-miR-145, upregulating miR-145 and treated with demethoxycurcumin (DC), a curcumin compound. It was observed a greater inhibition in tumor growth and stimulation of apoptosis in both *in vivo* and *in vitro* when compared to control and to monotherapy (30). Combined lentivirus-GFP-miR-145 plus DC was able to inhibit miR-145 target gene *SOX2*, leading to downstream beta-catenin downregulation, responsible for transcriptional activation of *CCND1* and *C-MYC* (30).

Interestingly, curcumin appears to suppress AP-1 and NF-kB pathways leading to chemosensitization (91). Therefore, Wu et al. (26) have treated U87MG cells with curcumin and TMZ alone, and a higher expression of miR-146a was observed in curcumin-treated cells, in a dose-dependent way. The enhancement of miR-146a leads to inhibition of p65 and phosphorylation IκBα and consequently, suppressing NF-kB, increasing the TMZ-induced apoptosis (26).

The effects of curcumin on several pathways at GBM cell lines are summarized in **Figures 3A,B**. In addition, this study indicated that only DPG and curcumin have an antitumoral effect on GBM cell lines through miR modulation (**Table 2**, **Figure 3**).

Furthermore, curcumin in combination with radiation has presented a synergistic effect in U87MG and T98G GBM cell lines, using different concentrations (ranging from 5 to 25 μM and 3.25–26 μM in U87 and T98 cells, respectively) and dosages (2 Gy or 4 Gy of irradiation). In U87 cells, curcumin and radiation exerted synergism in most of the tested combinations,

and the highest synergy was monitored when curcumin was given at its IC50 (10 μM). In T98 cells, the highest levels of synergy were observed at higher curcumin concentrations, particularly at 26 μM, possibly due to the resistance of those cells to both chemotherapy and radiotherapy. The combinatorial treatment arrested both cell lines at the G2/M phase to a higher extent than radiation or curcumin treatment alone. In addition, it was also observed a synergistic effect of curcumin when combined with TMZ resulting in increased tumor cell death (92).

In accordance, Yin et al. (93) have treated U87MG cell line with curcumin in combination with TMZ. The authors have observed that apoptosis was enhanced, *in vitro* and *in vivo,* in the GBM cells by both generation of reactive oxygen species production and phosphorylated AKT and mTOR suppression. These data indicated that blockage of AKT/mTOR signaling appeared to contribute to the elevated apoptosis caused by the combination treatment of curcumin and TMZ. Further, in the U87MG xenograft mouse model, the combination treatment with curcumin and TMZ showed a significantly enhanced inhibition of tumor growth compared with single treatments. A similar trend was observed by the authors in the measurement of tumor weight.

An Overview of Euphol Antitumor Effect

In traditional medicine, the base extracts of species of the genus *Euphorbia* (*Euphorbiaceae*) are often used as a form of treatment for ulcers and warts (32, 94–96). The euphol ($C_{30}H_{50}O$), a tetracyclic triterpene alcohol, is the main constituent of the *Euphorbia tirucalli* known as aveloz (**Figure 1D**) and it has been observed to have antiinflammatory effects as antiviral, analgesic, and nociceptive properties. Recently, a potential antitumor activity has been also noticed by euphol (97–99). Thus, euphol was able to decrease cell viability in CS12 gastric cancer cell line (100, 101).

Silva et al. (32) have evaluated the euphol antitumor effect in 12 human gliomas and GBM cell lines comprising seven adults (U87MG, U373, U251, GAMG, SW1783, SNB19), five pediatric glioma cell lines (RES186, RES259, KNS42, UW479, and SF188), two primary cultures (HCB2 and HCB149), and one normal astrocyte cell line (NHA) for cytotoxic assays. The pediatric cell lines have showed more euphol sensibility than adult and primary cultures. Moreover, euphol had a higher selective cytotoxicity index (0.64-3.36) than TMZ (0.11-1.13). When combined, euphol and TMZ treatments seem to have a synergistic effect [combination index (CI $<$ 1) in 67% (8/12) of the glioma cell lines investigated (mean CI values: range: 0.48–0.96)]. However, no effect was found on cell cycle distribution, invasion, and colony cell formation (90). In addition, the authors have compared both drug-sensitive (GAMG) and drug-resistant (U373) cell lines using euphol dose at 15 μM, which was able to inhibit GAMG and U373 proliferation by 35.44 and 28.71%, respectively. Moreover, at 15 μM euphol suppressed cell viability of GAMG cells by 88.86% and U373 cells by 13.9%. These data suggest that euphol seems to have predominantly cytotoxic effects on the anchorage-dependent growth of both malignant glioma cell lines (32). Finally, euphol also exhibited antitumoral and antiangiogenic activity *in vivo*, using the chicken chorioallantoic membrane assay, with synergistic TMZ interactions in most above GBM cell lines (32). In conclusion, euphol exerted *in vitro* and *in vivo* cytotoxicity against glioma cells, through several cancer pathways. These findings provide experimental support for further development of euphol as a novel therapeutic agent for GBM.

In addition to euphol, the genus *Euphorbia* also has diterpenes as important bioactive constituents some already approved for precancerous conditions (33, 102–104). One diterpene that was approved for human use for the treatment of actinic keratosis, ingenol-3-angelate (I3A) (Picato®), from *Euphorbia peplus* demonstrated great antineoplastic potential evaluated in clinical trials for the effective treatment of basal cell carcinoma and squamous cell carcinoma through the modulation of PKC signaling (105–109). Some studies have also revealed diterpenes as promising modulators of multidrug resistance (MDR) in tumor cells and also showing *in vivo* antiinflammatory activity (110).

Recently, the cytotoxic potential of a new esters of semisynthetic ingenol from *E. tirucalli*, the derivative ingenol-3-dodecanoate (Ingenol C-IngC) was reported. IngC showed higher efficacy when compared to I3A and ingenol 3,20-dibenzoate (IDB) from E. esula L on esophageal cancer cell lines, two important ingenol diterpenes that can promote PKC activation and anticancer activity (33, 108, 111). In a panel of 11 glioma cell lines, IngC acted as a potent inhibitor of protein kinase C (PKC) activity by PDK1 inhibiting and consequently tumor invasion and migration impairment through Wnt/β-catenin (β-C) pathways by lower concentration the effector protein β-C (93) (**Figure 2B**). The different models of glioma cell lines exhibited a heterogeneous profile of response to IngC. At a fixed dose of 10 μM, 9.1% (1/11) of cell lines were resistant, 36.4% (4/11) were moderately sensitive, whereas 54.5% (6/11) were classified as highly sensitive. These findings identify IngC as a promising lead compound for the development of new cancer therapy and they may guide the search for additional PKC inhibitors.

Despite euphol's antitumor action, some reports have demonstrated that exposure to crude *Euphorbia tirucalli* may be a risk factor for Burkitt's lymphoma, as a result its performance as a genotoxic agent (97, 112) indicating that further studies are needed to define the potential therapeutic use of euphol. The effects of IngC and euphol on different GBM cell pathways are summarized in **Figures 2B**, **3A**, respectively.

AUTHOR CONTRIBUTIONS

GB, MB, AS, and MO: wrote the manuscript. GB, MB, AS, JZ, and TR: performed the research. MB and MO: designed the figures. MO: designed the research. All authors approved the submitted manuscript.

FUNDING

The financial support provided by the National Council for Scientific and Technological Development (CNPq) scholarship #149884/2019-2, #137689/2020-9, and #122513/2021-5 is gratefully acknowledged.

REFERENCES

1. Miranda-Filho A, Piñeros M, Soerjomataram I, Deltour I, Bray F. Cancers of the brain and cns: global patterns and trends in incidence. *Neuro-Oncol.* (2017) 19:270–80. doi: 10.1093/neuonc/now166
2. Wang H, Pan J-Q, Luo L, Ning X, Ye Z-P, Yu Z, et al. NF-κB Induces miR-148a to Sustain TGF-β/smad signaling activation in glioblastoma. *Mol Cancer.* (2015) 14:2. doi: 10.1186/1476-4598-14-2
3. Louis DN, Perry A, Reifenberger G, von Deimling A, Figarella-Branger D, Cavenee WK, et al. The 2016 world health organization classification of tumors of the central nervous system: a summary. *Acta Neuropathol (Berl).* (2016) 131:803–820. doi: 10.1007/s00401-016-1545-1
4. Badke GL, Panagopoulos AT, Aguiar GB de, Veiga JCE. Glioblastoma Multiforme em Idosos: uma Revisão Sobre seu Tratamento com Ênfase na Abordagem Cirúrgica. *Arq Bras Neurocir.* (2014) 33:199. doi: 10.1055/s-0038-1626199
5. Ashby LS, Ryken TC. Management of malignant glioma: steady progress with multimodal approaches. *Neurosurg Focus.* (2006) 20:E3. doi: 10.3171/foc.2006.20.4.3
6. Jovčevska I, Kočevar N, Komel R. Glioma and glioblastoma - how much do we (not) know? *Mol Clin Oncol.* (2013) 1:935–941. doi: 10.3892/mco.2013.172
7. Harder BG, Blomquist MR, Wang J, Kim AJ, Woodworth GF, Winkles JA, et al. Developments in blood-brain barrier penetrance and drug repurposing for improved treatment of glioblastoma. *Front Oncol.* (2018) 8:462. doi: 10.3389/fonc.2018.00462
8. Cassileth BR, Deng G. Complementary and alternative therapies for cancer. *Oncologist.* (2004) 9:80–9. doi: 10.1634/theoncologist.9-1-80
9. Cragg GM, Newman DJ. Plants as a source of anti-cancer agents. *J Ethnopharmacol.* (2005) 100:72–9. doi: 10.1016/j.jep.2005.05.011
10. Bartel DP. MicroRNAs: genomics, biogenesis, mechanism, and function. *Cell.* (2004) 116:281–97. doi: 10.1016/S0092-8674(04)00045-5
11. MiRBase. Available online at: https://Mirbase.org/Search.Shtml (accessed November 9, 2021).
12. Kawahara Y. Human diseases caused by germline and somatic abnormalities in microrna and microrna-related genes. *Congenit Anom.* (2014) 54:12–21. doi: 10.1111/cga.12043
13. Ventura A, Jacks T. MicroRNAs and cancer: short RNAs go a long way. *Cell.* (2009) 136:586–91. doi: 10.1016/j.cell.2009.02.005
14. Ma X, Yoshimoto K, Guan Y, Hata N, Mizoguchi M, Sagata N, et al. Associations between microrna expression and mesenchymal marker gene expression in glioblastoma. *Neuro-Oncol.* (2012) 14:1153–62. doi: 10.1093/neuonc/nos145
15. Jhanwar-Uniyal M, Labagnara M, Friedman M, Kwasnicki A, Murali R. Glioblastoma: molecular pathways, stem cells and therapeutic targets. *Cancers.* (2015) 7:538–55. doi: 10.3390/cancers7020538
16. Jiang J, Lan Y-Q, Zhang T, Yu M, Liu X-Y, Li L-H, et al. The *in vitro* effects of caffeine on viability, cycle cycle profiles, proliferation, and apoptosis of glioblastomas. *Eur Rev Med Pharmacol Sci.* (2015) 19:3201–7.
17. Liu J-D, Song L-J, Yan D-J, Feng Y-Y, Zang Y-G, Yang Y. Caffeine inhibits the growth of glioblastomas through activating the caspase-3 signaling pathway *in vitro*. *Eur Rev Med Pharmacol Sci.* (2015) 19:3080–8.
18. Kang SS, Han K-S, Ku BM, Lee YK, Hong J, Shin HY, et al. Inhibition of the Ca2+ Release channel, ip3r subtype 3 by caffeine slows glioblastoma invasion and migration and extends survival. *Cancer Res.* (2010) 70:1173–83. doi: 10.1158/0008-5472.CAN-09-2886
19. Ku BM, Lee YK, Jeong JY, Ryu J, Choi J, Kim JS, et al. Caffeine inhibits cell proliferation and regulates pka/gsk3β pathways in u87mg human glioma cells. *Mol Cells.* (2011) 31:275–9. doi: 10.1007/s10059-011-0027-5
20. Cheng Y-C, Ding Y-M, Hueng D-Y, Chen J-Y, Chen Y. Caffeine suppresses the progression of human glioblastoma *via* cathepsin B and MAPK signaling pathway. *J Nutr Biochem.* (2016) 33:63–72. doi: 10.1016/j.jnutbio.2016.03.004
21. Sun F, Han D-F, Cao B-Q, Wang B, Dong N, Jiang D-H. Caffeine-induced nuclear translocation of foxo1 triggers bim-mediated apoptosis in human glioblastoma cells. *Tumor Biol J Int Soc Oncodevelopmental Biol Med.* (2016) 37:3417–23. doi: 10.1007/s13277-015-4180-x
22. Li K, Tu Y, Liu Q, Ouyang Y, He M, Luo M, et al. PT93, a novel caffeic acid amide derivative, suppresses glioblastoma cells migration, proliferation and MMP-2/-9 expression. *Oncol Lett.* (2017) 13:1990–6. doi: 10.3892/ol.2017.5663
23. Khan MSS, Asif M, Basheer MKA, Kang CW, Al-Suede FS, Ein OC, et al. Treatment of Novel IL17A inhibitor in glioblastoma implementing 3rd generation co-culture cell line and patient-derived tumor model. *Eur J Pharmacol.* (2017) 803:24–38. doi: 10.1016/j.ejphar.2017.03.031
24. Li S, Zhu J-H, Cao L-P, Sun Q, Liu H-D, Li W-D, et al. Growth inhibitory in vitro effects of glycyrrhizic acid in u251 glioblastoma cell line. *Neurol Sci Off J Ital Neurol Soc Ital Soc Clin Neurophysiol.* (2014) 35:1115–20. doi: 10.1007/s10072-014-1661-4
25. Bonafé GA, Dos Santos JS, Ziegler JV, Umezawa K, Ribeiro ML, Rocha T, et al. Growth inhibitory effects of dipotassium glycyrrhizinate in glioblastoma cell lines by targeting micrornas through the NF-κB signaling pathway. *Front Cell Neurosci.* (2019) 13:216. doi: 10.3389/fncel.2019.00216
26. Wu H, Liu Q, Cai T, Chen Y-D, Wang Z-F. Induction of MicroRNA-146a is involved in curcumin-mediated enhancement of temozolomide cytotoxicity against human glioblastoma. *Mol Med Rep.* (2015) 12:5461–6. doi: 10.3892/mmr.2015.4087
27. Li W, Yang W, Liu Y, Chen S, Chin S, Qi X, et al. MicroRNA-378 enhances inhibitory effect of curcumin on glioblastoma. *Oncotarget.* (2017) 8:73938–46. doi: 10.18632/oncotarget.17881
28. Yin S, Du W, Wang F, Han B, Cui Y, Yang D, et al. MicroRNA-326 sensitizes human glioblastoma cells to curcumin *via* the SHH/GLI1 signaling pathway. *Cancer Biol Ther.* (2018) 19:260–70. doi: 10.1080/15384047.2016.1250981
29. Tan X, Kim G, Lee D, Oh J, Kim M, Piao C, et al. A Curcumin-loaded polymeric micelle as a carrier of a microrna-21 antisense-oligonucleotide for enhanced anti-tumor effects in a glioblastoma animal model. *Biomater Sci.* (2018) 6:407–17. doi: 10.1039/C7BM01088E
30. Qian C, Wang B, Zou Y, Zhang Y, Hu X, Sun W, et al. MicroRNA 145 enhances chemosensitivity of glioblastoma stem cells to demethoxycurcumin. *Cancer Manag Res.* (2019) 11:6829–40. doi: 10.2147/CMAR.S210076
31. Garrido-Armas M, Corona JC, Escobar ML, Torres L, Ordóñez-Romero F, Hernández-Hernández A, et al. Paraptosis in human glioblastoma cell line induced by curcumin. *Toxicol Vitro Int J Publ Assoc BIBRA.* (2018) 51:63–73. doi: 10.1016/j.tiv.2018.04.014
32. Silva VAO, Rosa MN, Miranda-Gonçalves V, Costa AM, Tansini A, Evangelista AF, et al. Euphol, a tetracyclic triterpene, from euphorbia tirucalli induces autophagy and sensitizes temozolomide cytotoxicity on glioblastoma cells. *Invest New Drugs.* (2019) 37:223–37. doi: 10.1007/s10637-018-0620-y
33. Silva VAO, Rosa MN, Martinho O, Tanuri A, Lima JP, Pianowski LF, et al. Modified ingenol semi-synthetic derivatives from euphorbia tirucalli induce cytotoxicity on a large panel of human cancer cell lines. *Invest New Drugs.* (2019) 37:1029–35. doi: 10.1007/s10637-019-00728-0
34. Morelli M, Frau L, Simola N. Alteration in the progression of dopamine neuron degeneration: may caffeine offer new perspective? *Exp Neurol.* (2012) 237:218–22. doi: 10.1016/j.expneurol.2012.05.023
35. Hosny EN, Sawie HG, Elhadidy ME, Khadrawy YA. Evaluation of antioxidant and anti-inflammatory efficacy of caffeine in rat model of neurotoxicity. *Nutr Neurosci.* (2019) 22:789–96. doi: 10.1080/1028415X.2018.1446812
36. Michaud DS, Gallo V, Schlehofer B, Tjønneland A, Olsen A, Overvad K, et al. Coffee and tea intake and risk of brain tumors in the european prospective investigation into cancer and nutrition (EPIC) cohort study. *Am J Clin Nutr.* (2010) 92:1145–50. doi: 10.3945/ajcn.2010.29876
37. Ohtsubo M, Theodoras AM, Schumacher J, Roberts JM, Pagano M. Human Cyclin E, a nuclear protein essential for the g1-to-s phase transition. *Mol Cell Biol.* (1995) 15:2612–24. doi: 10.1128/MCB.15.5.2612
38. Bode AM, Dong Z. The enigmatic effects of caffeine in cell cycle and cancer. *Cancer Lett.* (2007) 247:26–39. doi: 10.1016/j.canlet.2006.03.032
39. Hashimoto T, He Z, Ma W-Y, Schmid PC, Bode AM, Yang CS, et al. Caffeine inhibits cell proliferation by G0/G1 phase arrest in JB6 cells. *Cancer Res.* (2004) 64:3344–9. doi: 10.1158/0008-5472.CAN-03-3453
40. Weinberg RA. The retinoblastoma protein and cell cycle control. *Cell.* (1995) 81:323–30. doi: 10.1016/0092-8674(95)90385-2

41. Kaufmann WK, Heffernan TP, Beaulieu LM, Doherty S, Frank AR, Zhou Y, et al. Caffeine and human DNA metabolism: the magic and the mystery. *Mutat Res.* (2003) 532:85–102. doi: 10.1016/j.mrfmmm.2003.08.012
42. Diehl JA, Cheng M, Roussel MF, Sherr CJ. Glycogen synthase kinase-3beta regulates Cyclin D1 proteolysis and subcellular localization. *Genes Dev.* (1998) 12:3499–511. doi: 10.1101/gad.12.22.3499
43. Li N, Zhang P, Kiang KMY, Cheng YS, Leung GKK. Caffeine sensitizes u87-mg human glioblastoma cells to temozolomide through mitotic catastrophe by impeding G2 arrest. *BioMed Res Int.* (2018) 2018:5364973. doi: 10.1155/2018/5364973
44. Jang M-H, Shin M-C, Kang I-S, Baik H-H, Cho Y-H, Chu J-P, et al. Caffeine induces apoptosis in human neuroblastoma cell line SK-N-MC. *J Korean Med Sci.* (2002) 17:674–678. doi: 10.3346/jkms.2002.17.5.674
45. Heath-Engel HM, Shore GC. Regulated targeting of Bax and Bak to intracellular membranes during apoptosis. *Cell Death Differ.* (2006) 13:1277–80. doi: 10.1038/sj.cdd.4401961
46. Chipuk JE, Fisher JC, Dillon CP, Kriwacki RW, Kuwana T, Green DR. Mechanism of apoptosis induction by inhibition of the anti-apoptotic BCL-2 proteins. *Proc Natl Acad Sci U S A.* (2008) 105:20327–32. doi: 10.1073/pnas.0808036105
47. Kilbride SM, Prehn JHM. Central roles of apoptotic proteins in mitochondrial function. *Oncogene.* (2013) 32:2703–11. doi: 10.1038/onc.2012.348
48. Maiese K, Chong ZZ, Shang YC, Hou J. Clever cancer strategies with FoxO transcription factors. *Cell Cycle Georget Tex.* (2008) 7:3829–39. doi: 10.4161/cc.7.24.7231
49. Modur V, Nagarajan R, Evers BM, Milbrandt J. FOXO proteins regulate tumor necrosis factor-related apoptosis inducing ligand expression. implications for pten mutation in prostate cancer. *J Biol Chem.* (2002) 277:47928–37. doi: 10.1074/jbc.M207509200
50. Gilley J, Coffer PJ, Ham J. FOXO transcription factors directly activate bim gene expression and promote apoptosis in sympathetic neurons. *J Cell Biol.* (2003) 162:613–22. doi: 10.1083/jcb.200303026
51. Ridley AJ, Schwartz MA, Burridge K, Firtel RA, Ginsberg MH, Borisy G, et al. Cell migration: integrating signals from front to back. *Science.* (2003) 302:1704–9. doi: 10.1126/science.1092053
52. Yamazaki D, Kurisu S, Takenawa T. Regulation of cancer cell motility through actin reorganization. *Cancer Sci.* (2005) 96:379–86. doi: 10.1111/j.1349-7006.2005.00062.x
53. Berridge MJ, Lipp P, Bootman MD. The versatility and universality of calcium signaling. *Nat Rev Mol Cell Biol.* (2000) 1:11–21. doi: 10.1038/35036035
54. Ishiuchi S, Tsuzuki K, Yoshida Y, Yamada N, Hagimura N, Okado H, et al. Blockage of Ca(2+)-permeable ampa receptors suppresses migration and induces apoptosis in human glioblastoma cells. *Nat Med.* (2002) 8:971–8. doi: 10.1038/nm746
55. Brown GR, Sayers LG, Kirk CJ, Michell RH, Michelangeli F. The opening of the inositol 1,4,5-trisphosphate-sensitive Ca2+ channel in rat cerebellum is inhibited by caffeine. *Biochem J.* (1992) 282:309312. doi: 10.1042/bj2820309
56. Maes K, Missiaen L, De Smet P, Vanlingen S, Callewaert G, Parys JB, et al. Differential modulation of inositol 1,4,5-trisphosphate receptor type 1 and type 3 by ATP. *Cell Calcium.* (2000) 27:257–267. doi: 10.1054/ceca.2000.0121
57. Bello L, Lucini V, Carrabba G, Giussani C, Machluf M, Pluderi M, et al. Simultaneous inhibition of glioma angiogenesis, cell proliferation, and invasion by a naturally occurring fragment of human metalloproteinase-2. *Cancer Res.* (2001) 61:8730–6.
58. Park M-J, Park I-C, Hur J-H, Kim M-S, Lee H-C, Woo S-H, et al. Modulation of phorbol ester-induced regulation of matrix metalloproteinases and tissue inhibitors of metalloproteinases by SB203580, a specific inhibitor of p38 mitogen-activated protein kinase. *J Neurosurg.* (2002) 97:112–8. doi: 10.3171/jns.2002.97.1.0112
59. Caraballo-Miralles V, Cardona-Rossinyol A, Garcera A, Villalonga P, Soler RM, Olmos G, et al. SMN deficiency attenuates migration of U87MG astroglioma cells through the activation of RhoA. *Mol Cell Neurosci.* (2012) 49:282–9. doi: 10.1016/j.mcn.2011.12.003
60. Nasser JA, Falavigna A, Ferraz F, Duigou G, Bruce J. Transcription analysis of TIMP-1 and NM23-H1 genes in glioma cell invasion. *Arq Neuropsiquiatr.* (2006) 64:774–80. doi: 10.1590/S0004-282X2006000500014
61. Hadler-Olsen E, Winberg J-O, Uhlin-Hansen L. Matrix metalloproteinases in cancer: their value as diagnostic and prognostic markers and therapeutic targets. *Tumor Biol J Int Soc Oncodevelopmental Biol Med.* (2013) 34:2041–51. doi: 10.1007/s13277-013-0842-8
62. Dufour A, Overall CM. Missing the target: matrix metalloproteinase antitargets in inflammation and cancer. *Trends Pharmacol Sci.* (2013) 34:233–42. doi: 10.1016/j.tips.2013.02.004
63. Vandenbroucke RE, Libert C. Is there new hope for therapeutic matrix metalloproteinase inhibition? *Nat Rev Drug Discov.* (2014) 13:904–27. doi: 10.1038/nrd4390
64. Wojtowicz-Praga SM, Dickson RB, Hawkins MJ. Matrix metalloproteinase inhibitors. *Invest New Drugs.* (1997) 15:61–75. doi: 10.1023/A:1005722729132
65. Boutwell RK, Brush MK, Rusch HP. The stimulating effect of dietary fat on carcinogenesis. *Cancer Res.* (1949) 9:741–6.
66. Freedman LS, Clifford C, Messina M. Analysis of dietary fat, calories, body weight, and the development of mammary tumors in rats and mice: a review. *Cancer Res.* (1990) 50:5710–9.
67. Shibata N, Shimokawa T, Jiang Z, Jeong Y, Ohno T, Kimura G, et al. Characteristics of intestinal absorption and disposition of glycyrrhizin in mice. *Biopharm Drug Dispos.* (2000) 21:95–101. doi: 10.1002/1099-081X(200004)21:3<95::AID-BDD221>3.0.CO;2-9
68. Menegazzi M, Di Paola R, Mazzon E, Genovese T, Crisafulli C, Dal Bosco M, et al. Glycyrrhizin attenuates the development of carrageenan-induced lung injury in mice. *Pharmacol Res.* (2008) 58:22–31. doi: 10.1016/j.phrs.2008.05.012
69. Hibasami H, Iwase H, Yoshioka K, Takahashi H. Glycyrrhizin induces apoptosis in human stomach cancer KATO III and human promyelotic leukemia HL-60 cells. *Int J Mol Med.* (2005) 16:233–6. doi: 10.3892/ijmm.16.2.233
70. Hibasami H, Iwase H, Yoshioka K, Takahashi H. Glycyrrhetic acid (a metabolic substance and aglycon of glycyrrhizin) induces apoptosis in human hepatoma, promyelotic leukemia and stomach cancer cells. *Int J Mol Med.* (2006) 17:215–9. doi: 10.3892/ijmm.17.2.215
71. Thirugnanam S, Xu L, Ramaswamy K, Gnanasekar M. glycyrrhizin induces apoptosis in prostate cancer cell lines DU-145 and LNCaP. *Oncol Rep.* (2008) 20:1387–92. doi: 10.3892/or_00000157
72. Cosmetic Ingredient Review Expert Panel. Final report on the safety assessment of glycyrrhetinic acid, potassium glycyrrhetinate, disodium succinoyl glycyrrhetinate, glyceryl glycyrrhetinate, glycyrrhetinyl stearate, stearyl glycyrrhetinate, glycyrrhizic acid, ammonium glycyrrhizate, dipotassium glycyrrhizate, disodium glycyrrhizate, trisodium glycyrrhizate, methyl glycyrrhizate, and potassium glycyrrhizinate. *Int J Toxicol.* (2007) 26:79–112. doi: 10.1080/10915810701351228
73. Brassesco MS, Roberto GM, Morales AG, Oliveira JC, Delsin LEA, Pezuk JA, et al. Inhibition of NF- κ B by dehydroxymethylepoxyquinomicin suppresses invasion and synergistically potentiates temozolomide and γ -radiation cytotoxicity in glioblastoma cells. *Chemother Res Pract.* (2013) 2013:593020. doi: 10.1155/2013/593020
74. Smith D, Shimamura T, Barbera S, Bejcek BE. NF-KappaB controls growth of glioblastomas/astrocytomas. *Mol Cell Biochem.* (2008) 307:141–147. doi: 10.1007/s11010-007-9593-4
75. Galardi S, Mercatelli N, Farace MG, Ciafrè SA. NF-KB and c-Jun induce the expression of the oncogenic miR-221 and miR-222 in prostate carcinoma and glioblastoma cells. *Nucleic Acids Res.* (2011) 39:3892–902. doi: 10.1093/nar/gkr006
76. Zanotto-Filho A, Braganhol E, Schröder R, de Souza LHT, Dalmolin RJS, Pasquali MAB, et al. NFκB inhibitors induce cell death in glioblastomas. *Biochem Pharmacol.* (2011) 81:412–24. doi: 10.1016/j.bcp.2010.10.014
77. Westhoff M-A, Zhou S, Nonnenmacher L, Karpel-Massler G, Jennewein C, Schneider M, et al. Inhibition of NF-κB signaling ablates the invasive phenotype of glioblastoma. *Mol Cancer Res MCR.* (2013) 11:1611–23. doi: 10.1158/1541-7786.MCR-13-0435-T
78. Annovazzi L, Caldera V, Mellai M, Riganti C, Battaglia L, Chirio D, et al. The DNA damage/repair cascade in glioblastoma cell lines after chemotherapeutic agent treatment. *Int J Oncol.* (2015) 46:2299–308. doi: 10.3892/ijo.2015.2963

79. Hermisson M, Klumpp A, Wick W, Wischhusen J, Nagel G, Roos W, et al. O6-Methylguanine DNA methyltransferase and p53 status predict temozolomide sensitivity in human malignant glioma cells. *J Neurochem.* (2006) 96:766–76. doi: 10.1111/j.1471-4159.2005.03583.x
80. Bocangel DB, Finkelstein S, Schold SC, Bhakat KK, Mitra S, Kokkinakis DM. Multifaceted resistance of gliomas to temozolomide. *Clin Cancer Res Off J Am Assoc Cancer Res.* (2002) 8:2725–34. doi: 10.1016/j.gendis.2016.04.007
81. Sordillo LA, Sordillo PP, Helson L. Curcumin for the treatment of glioblastoma. *Anticancer Res.* (2015) 35:6373–8.
82. Meng B, Li J, Cao H. Antioxidant and antiinflammatory activities of curcumin on diabetes mellitus and its complications. *Curr Pharm Des.* (2013) 19:2101–13. doi: 10.2174/13816128113191 10011
83. Mishra S, Palanivelu K. The effect of curcumin (Turmeric) on Alzheimer's Disease: an overview. *Ann Indian Acad Neurol.* (2008) 11:13–9. doi: 10.4103/0972-2327.40220
84. Anggakusuma Null, Colpitts CC, Schang LM, Rachmawati H, Frentzen A, Pfaender S, et al. Turmeric curcumin inhibits entry of all hepatitis c virus genotypes into human liver cells. *Gut.* (2014) 63:1137–49. doi: 10.1136/gutjnl-2012-304299
85. Sordillo PP, Helson L. curcumin suppression of cytokine release and cytokine storm. a potential therapy for patients with ebola and other severe viral infections. *Vivo Athens Greece.* (2015) 29:1–4.
86. Leow P-C, Tian Q, Ong Z-Y, Yang Z, Ee P-LR. antitumor activity of natural compounds, curcumin and PKF118-310, as Wnt/β-catenin antagonists against human osteosarcoma cells. *Invest New Drugs.* (2010) 28:766–82. doi: 10.1007/s10637-009-9311-z
87. Elamin MH, Shinwari Z, Hendrayani S-F, Al-Hindi H, Al-Shail E, Khafaga Y, et al. Curcumin inhibits the sonic hedgehog signaling pathway and triggers apoptosis in medulloblastoma cells. *Mol Carcinog.* (2010) 49:302–14. doi: 10.1002/mc.20604
88. Alexandrow MG, Song LJ, Altiok S, Gray J, Haura EB, Kumar NB. Curcumin: a novel Stat3 pathway inhibitor for chemoprevention of lung cancer. *Eur J Cancer Prev Off J Eur Cancer Prev Organ ECP.* (2012) 21:407–12. doi: 10.1097/CEJ.0b013e32834ef194
89. Chiu SS, Lui E, Majeed M, Vishwanatha JK, Ranjan AP, Maitra A, et al. Differential distribution of intravenous curcumin formulations in the rat brain. *Anticancer Res.* (2011) 31:907–11.
90. Priyadarsini KI. The chemistry of curcumin: from extraction to therapeutic agent. *Mol Basel Switz.* (2014) 19:20091–112. doi: 10.3390/molecules191220091
91. Dhandapani KM, Mahesh VB, Brann DW. Curcumin suppresses growth and chemoresistance of human glioblastoma cells *via* AP-1 and NFkappaB transcription factors. *J Neurochem.* (2007) 102:522–38. doi: 10.1111/j.1471-4159.2007.04633.x
92. Zoi V, Galani V, Vartholomatos E, Zacharopoulou N, Tsoumeleka E, Gkizas G, et al. Curcumin and radiotherapy exert synergistic anti-glioma effect *in vitro*. *Biomedicines.* (2021) 9:1562. doi: 10.3390/biomedicines9111562
93. Yin H, Zhou Y, Wen C, Zhou C, Zhang W, Hu X, et al. Curcumin Sensitizes glioblastoma to temozolomide by simultaneously generating ros and disrupting AKT/MTOR signaling. *Oncol Rep.* (2014) 32:1610–16. doi: 10.3892/or.2014.3342
94. Akihisa T, Ogihara J, Kato J, Yasukawa K, Ukiya M, Yamanouchi S, et al. Inhibitory effects of triterpenoids and sterols on human immunodeficiency virus-1 reverse transcriptase. *Lipids.* (2001) 36:507–52. doi: 10.1007/s11745-001-0750-4
95. Dutra RC, Bicca MA, Segat GC, Silva K a. BS, Motta EM, Pianowski LF, et al. The antinociceptive effects of the tetracyclic triterpene euphol in inflammatory and neuropathic pain models: the potential role of PKCε. *Neuroscience.* (2015) 303:126–37. doi: 10.1016/j.neuroscience.2015.06.051
96. Dutra RC, de Souza PR de C, Bento AF, Marcon R, Bicca MA, Pianowski LF, et al. Euphol prevents experimental autoimmune encephalomyelitis in mice: evidence for the underlying mechanisms. *Biochem Pharmacol.* (2012) 83:531–42. doi: 10.1016/j.bcp.2011.11.026
97. Dutra RC, Campos MM, Santos ARS, Calixto JB. Medicinal plants in Brazil: pharmacological studies, drug discovery, challenges and perspectives. *Pharmacol Res.* (2016) 112:4–29. doi: 10.1016/j.phrs.2016.01.021
98. Franco-Salla GB, Prates J, Cardin LT, dos Santos ARD, Silva Jr WA da, da Cunha BR, et al. Euphorbia tirucalli modulates gene expression in larynx squamous cell carcinoma. *BMC Complement Altern Med.* (2016) 16:1115. doi: 10.1186/s12906-016-1115-z
99. Prakash E, Gupta DK. Cytotoxic activities of extracts of medicinal plants of euphorbiacae family studied on seven human cancer cell lines. *Univers J Plant Sci.* (2013) 1:113–7. doi: 10.13189/ujps.2013.010401
100. Chen N, Karantza V. Autophagy as a therapeutic target in cancer. *Cancer Biol Ther.* (2011) 11:157–68. doi: 10.4161/cbt.11.2.14622
101. Lin M-W, Lin A-S, Wu D-C, Wang SSW, Chang F-R, Wu Y-C, et al. Euphol From Euphorbia Tirucalli selectively inhibits human gastric cancer cell growth through the induction of ERK1/2-mediated apoptosis. *Food Chem Toxicol Int J Publ Br Ind Biol Res Assoc.* (2012) 50:4333–9. doi: 10.1016/j.fct.2012.05.029
102. Abreu CM, Price SL, Shirk EN, Cunha RD, Pianowski LF, Clements JE, et al. Dual role of novel ingenol derivatives from euphorbia tirucalli in HIV replication: inhibition of de novo infection and activation of viral LTR. *PloS One.* (2014) 9:E97257. doi: 10.1371/journal.pone.0097257
103. Vasas A, Rédei D, Csupor D, Molnár J, Hohmann J. Diterpenes from European euphorbia species serving as prototypes for natural-product-based drug discovery. *Eur J Org Chem.* (2012) 2012:5115–30. doi: 10.1002/ejoc.201200733
104. Béres T, Dragull K, Pospíšil J, Tarkowská D, Dančák M, Bíba O, et al. Quantitative analysis of ingenol in euphorbia species *via* validated isotope dilution ultra-high performance liquid chromatography tandem mass spectrometry. *Phytochem Anal PCA.* (2018) 29:23–9. doi: 10.1002/pca.2711
105. Lebwohl M, Swanson N, Anderson LL, Melgaard A, Xu Z, Berman B. Ingenol mebutate gel for actinic keratosis. *N Engl J Med.* (2012) 366:1010–9. doi: 10.1056/NEJMoa1111170
106. Berman B. New developments in the treatment of actinic keratosis: focus on ingenol mebutate gel. *Clin Cosmet Investig Dermatol.* (2012) 5:111–22. doi: 10.2147/CCID.S28905
107. Gillespie SK, Zhang XD, Hersey P. Ingenol 3-angelate induces dual modes of cell death and differentially regulates tumor necrosis factor-related apoptosis-inducing ligand-induced apoptosis in melanoma Cells. *Mol Cancer Ther.* (2004) 3:1651–8.
108. Hampson P, Chahal H, Khanim F, Hayden R, Mulder A, Assi LK, et al. PEP005, a selective small-molecule activator of protein kinase C, has potent antileukemic activity mediated *via* the delta isoform of PKC. *Blood.* (2005) 106:1362–8. doi: 10.1182/blood-2004-10-4117
109. Wang D, Liu P. Ingenol-3-angelate suppresses growth of melanoma cells and skin tumor development by downregulation of NF-κB-Cox2 signaling. *Med Sci Monit Int Med J Exp Clin Res.* (2018) 24:486–502. doi: 10.12659/MSM.906049
110. Duarte N, Gyémánt N, Abreu PM, Molnár J, Ferreira M-JU. new macrocyclic lathyrane diterpenes, from Euphorbia lagascae, as inhibitors of multidrug resistance of tumor Cells. *Planta Med.* (2006) 72:162–8. doi: 10.1055/s-2005-873196

111. Vigone A, Tron GC, Surico D, Baj G, Appendino G, Surico N. Ingenol derivatives inhibit proliferation and induce apoptosis in breast cancer cell lines. *Eur J Gynaecol Oncol.* (2005) 26:526–30.
112. MacNeil A, Sumba OP, Lutzke ML, Moormann A, Rochford R. Activation of the Epstein-Barr Virus Lytic Cycle by the Latex of the Plant Euphorbia Tirucalli. *Br J Cancer.* (2003) 88:1566–1569. doi: 10.1038/sj.bjc.6600929

Conflict of Interest: JZ is employed by Verdi Cosmetics LLC, Joanópolis, São Paulo, Brazil.

The remaining authors declare that the research was conducted in the absence of any commercial or financial relationships that could be construed as a potential conflict of interest.

Publisher's Note: All claims expressed in this article are solely those of the authors and do not necessarily represent those of their affiliated organizations, or those of the publisher, the editors and the reviewers. Any product that may be evaluated in this article, or claim that may be made by its manufacturer, is not guaranteed or endorsed by the publisher.

frontiers | Frontiers in Oncology

ORIGINAL RESEARCH
published: 27 April 2022
doi: 10.3389/fonc.2022.875521

Integrated Analysis of Transcriptome Data Revealed AURKA and KIF20A as Critical Genes in Medulloblastoma Progression

Bo Liang[1,2†], *Yan Zhou*[1†], *Jiji Jiao*[1†], *Lixia Xu*[3], *Yan Yan*[4], *Qiaoli Wu*[3], *Xiaoguang Tong*[3,5*] *and Hua Yan*[3,5*]

[1] Clinical College of Neurology, Neurosurgery and Neurorehabilitation, Tianjin Medical University, Tianjin, China, [2] Department of Neurosurgery, The Fifth Affiliated Hospital of Zhengzhou University, Zhengzhou, China, [3] Tianjin Neurosurgical Institute, Tianjin Key Laboratory of Cerebrovascular and Neurodegenerative Diseases, Tianjin Huanhu Hospital, Tianjin, China, [4] Clinical Laboratory, Tianjin Huanhu Hospital, Tianjin, China, [5] Department of Neurosurgery, Tianjin Huanhu Hospital, Tianjin, China

OPEN ACCESS

Edited by:
Liam Chen,
University of Minnesota, United States

Reviewed by:
Tung Nguyen-Thanh,
Hue University of Medicine and Pharmacy, Vietnam
Abhijeet R. Patil,
University of Pennsylvania, United States

***Correspondence:**
Hua Yan
yanhua20042007@sina.com
Xiaoguang Tong
tongxg@yahoo.com

[†]These authors have contributed equally to this work

Specialty section:
This article was submitted to Neuro-Oncology and Neurosurgical Oncology, a section of the journal Frontiers in Oncology

Received: 14 February 2022
Accepted: 29 March 2022
Published: 27 April 2022

Citation:
Liang B, Zhou Y, Jiao J, Xu L, Yan Y, Wu Q, Tong X and Yan H (2022) Integrated Analysis of Transcriptome Data Revealed AURKA and KIF20A as Critical Genes in Medulloblastoma Progression. Front. Oncol. 12:875521. doi: 10.3389/fonc.2022.875521

Medulloblastoma is the neuroepithelial tumor with the highest degree of malignancy in the central nervous system, accounting for about 8% to 10% of children's brain tumors. It has a high degree of malignancy and is easily transmitted through cerebrospinal fluid, with a relatively poor prognosis. Although medulloblastoma has been widely studied and treated, its molecular mechanism remains unclear. To determine which gene plays a crucial role in medulloblastoma development and progression, we analyzed three microarray datasets from Gene Expression Omnibus. Gene Ontology and Kyoto Encyclopedia of Genes and Genomes were used to detect and evaluate differentially expressed genes. Protein interaction network was established, and the hub genes were determined in cytoHubba through various assessment methods, while the target genes were screened out using survival analysis. Ultimately, human medulloblastoma samples were utilized to confirm target gene expression. In conclusion, This study found that aurora kinase A (AURKA) and kinesin family member 20A (KIF20A) may be involved in the initiation and development of medulloblastoma, have a close association with prognosis, and may become a potential therapeutic target and prognostic marker of MED.

Keywords: Medulloblastoma, Bioinformatics, Biomarker, AURKA, KIF20A

INTRODUCTION

Medulloblastoma is an embryonal cerebellar tumor most commonly seen in children as a malignant brain tumor, occupying 8% to 10% of all pediatric brain cancers and occurring extremely infrequently in adults. Wingless (WNT), sonic hedgehog (SHH), group 3 (G3), as well as group 4 (G4) medulloblastoma are four primary molecularly and histopathologically different categories of medulloblastoma (1). Multimodal therapy, which included surgery, radiation therapy, and chemotherapy, decreased the late death's cumulative incidence but raised the prevalence of recurrent tumors and critical, incapacitating chronic health disorders (2). Medulloblastoma research has also been on the leading edge of cancer genomics (3). According to current

molecular genetic evidence, many molecular abnormalities are linked to cell transformation in medulloblastoma. HER2 was reported to be present in 86% of medulloblastomas and to be co-expressed with HER4 in 54% of MEDs. Co-expression of HER2 and HER4 results in a bad prognosis. In sporadic medulloblastoma, oncogenic mutations in the β -catenin gene boost transcription of numerous genes, including cyclin D1, C-MYC, and T-cytokine (TCF-1).Mutations that activate β -catenin may cause cell transformation in a medulloblastoma subpopulation (4). Clinical sequencing can convey valuable information to help with the categorization and diagnosis of MED, and some gene variations are linked to distinct molecular subtypes. CTNNB1 mutations, for example, are a particular manifestation of the WNT molecular subtype and have diagnostic relevance (5, 6). SHH tumors exhibit mutations in SHH pathway mediators, including SUFU, PTCH1, or SMO. Complete or partial deletion of chromosome 6 is usually employed to establish the diagnosis of the WNT molecular population. A positive FISH result on homologous chromosome 17q may assist to more firmly designate malignancies as MB owing to its relatively high specificity (7). The use of appropriate targeted therapies for patients with specific genetic mutations is one direction of research for molecular therapy of medulloblastoma, Patients with phosphatase and tensin homologous (PTEN) or mammalian target of rapamycin (mTOR) or PIK3CA-activated mutations, for example, were given PI3K or mTOR inhibitors, while patients with BRAF V600E mutations were given BRAF inhibitors. Patients with fibroblast growth factor receptor (FGFR) activation mutations or fusions were given FGFR inhibitors (8). Some studies have found that tumor immune microenvironment is influential in supporting or preventing tumor advancement. Tumor-associated macrophages/microglia (TAMs) can accelerate the development of tumor in the medulloblastoma sonic hedgehog subgroup (SHH-MB), As TAMs generally rely on the colony-stimulating factor 1 receptor (CSF1R), the inhibition of CSF1R may have curative promise in SHH-MB patients (9). The downregulation of miR-204 was associated with low survival rates in the G4 medulloblastom, while, in medulloblastoma cells, tumor suppression of miR-204 and miR-30a is triggered by inhibition of autophagy. Autophagy inhibitors can effectively reduce cranial spinal radiation dose, thus significantly reducing treatment-related side effects, which has potential in the treatment of medulloblastoma (10, 11). OLIG2+ progenitors from the glial lineage initiate tumors during the carcinogenesis and relapse of medulloblastoma, indicating that oncogenic networks driven by OLIG2 might be therapeutic targets (12). However, the current mortality rate from MED remains high. In order to find valid diagnostic and treatment techniques, it is critical to figure out the precise molecular pathways behind MED occurrence, growth, and recurrence.

During the previous few decades, the development of microarray technology has triggered a molecular revolution in the field of biological science. With advanced high-throughput gene sequencing technology, we have the opportunity to re-understand the genesis and development of medulloblastoma from the whole genome level. Through these new technologies, more and more molecular mechanisms and effective biomarkers are being discovered. To find possible MED biomarkers, we ran a series of analysis using high-throughput sequencing data obtained from three different datasets GSE39182, GSE74195, and GSE86574 in Gene Expression Omnibus (GEO). We first identified common DEGs from three databases and performed gene Ontology (GO), Kyoto Encyclopedia of Genes and Genomes (KEGG) pathway enrichment and protein-protein interaction (PPI) network analyses to better comprehend the molecular underpinnings of cancer initiation and development. We confirmed that AURKA and KIF20A were associated with patient prognosis and could be used as biomarkers for MED. Then, immunohistochemistry was used to confirm its presence in patients. As for the screening of Hub genes in MED, compared with previous studies, we found two new Hub genes for the first time, and identified new biomarkers AURKA and KIF20A that are critical to the prognosis of patients combined with survival data. At the same time, we used experimental methods for the first time to verify that the expression of these two proteins in human medulloblastoma tissues is indeed significantly different from that in normal brain tissues.

In conclusion, our research identifies new possible prognostic indicators and therapeutic targets for MED.

MATERIALS AND METHODS

Immunohistochemistry

The tumor tissue of 10 medulloblastoma patients and part of cerebellar tissue of 4 cerebellar hemorrhage patients were paraformaldehyde fixed with a concentration of 4% for 24 hours before paraffin embedment. These sections were antigen-repaired with sodium citrate buffer and then sealed with goat serum. AURKA mouse monoclonal antibody (1:400, Proteintech, 66757-1-IG) and KIF20A rabbit polyclonal antibody (1:400, Proteintech, 15910-1-AP) were stained overnight at 4°C, and the second antibody was subjected to incubation for 1 hour at ambient temperature. The percentages of AURKA and KIF20A positive cells were calculated.

Microarray Data

As a publicly accessible functional genomics resource, GEO (https://www.ncbi.nlm.nih.gov/geo/) includes high-throughput gene expression data, chips, as well as microarrays (13, 14). We downloaded three gene expression datasets (GSE39182 (15), GSE74195 (16), GSE86574 (17)) from GEO (Illumina GPL6947, Agilent GPL6480, Affymetrix GPL570 platform). Founded on the platform-based annotation information, we transformed the probes into the matching gene symbol. The GSE74195 dataset was composed of 27 MED tissue samples and 5 noncancer samples. GSE86574 contained 16 MED tissue samples and 5 noncancer samples. GSE39182 was composed of 20 MED tissue samples and 5 noncancer samples. The above datasets altogether contain 63 MED tissue samples and 15 noncancer samples.

Identification of DEGs

GEO2R (http://www.ncbi.nlm.nih.gov/geo/geo2r) was utilized to filter the DEGs between MED and noncancer samples. GEO2R is an interactive online application for determining DEGs across test settings by comparing two or more datasets in one series of GEO. $P < 0.05$ and logFC > 1 or < –1 were taken as cut-off standards.

GO and KEGG Enrichment Analyses of DEGs

GO is a key bioinformatics tool, which can be used to annotate genes and analyze the corresponding biological processes. In contrast, KEGG is a huge database for studying high-level functions and biological systems derived from massive molecular datasets collected by high-throughput test techniques. We applied Metascape (http://metascape.org/gp/index.html#/main/step1) to conduct GO and KEGG analyses on DEGs to determine their function. Metascape is an analysis tool based on web, containing discovery and annotation features (18). Moreover, the data were analyzed using online tools from the DAVID website (https://david.ncifcrf.gov/home.jsp) to guarantee the results' legitimacy (19). The DAVID is an online bioinformatics database that includes a comprehensive biological knowledge base and analytical tools, as well as a large amount of annotation information concerning functions for genes and proteins, from which biological information may be extracted. $P < 0.05$ was taken as the cut-off standard.

PPI Network Construction and Screening of Hub Genes

The PPI network of DEGs or one single gene was established by utilizing STRING online database (http://string-db.org) (20), which can be adopted to analyze the functional protein–protein connections, and can explore the processes of disease formation or progression. Cytoscape is a free bioinformatics visualization software platform for visualizing interaction networks between molecules and finding hub genes (21). The Cytoscape plug-in cytoHubba is an APP for clustering a specific topology-based network based in order to locate highly linked sections (22). We identified the hub genes by three algorithms: DEGREE, MCC, and MNC in cytoHubba.

Target Gene Selection by Associating the Hub Gene Expression With the Survival of Patients with MED

To study the relationship between the hub gene expression and MED patients' prognosis, we screened two datasets (GSE30074 and GSE85217) containing patient survival information and gene expression information from GEO database. Then, we used GraphPad Prime software to conduct a survival analysis on the hub genes.

RESULTS

Identification of DEGs in MED

After the microarray results were standardized, DEGs (3470 in GSE39182, 1657 in GSE74195 and 3848 in GSE86574) were determined by GEO2R. The data were filtered by logFC ≥1 or ≤ –1 and $P < 0.05$. We analyzed the DEGs in each dataset separately and showed them in volcano map (**Figures 1A–C**). As indicated in the Venn diagram, the overlap between the three datasets includes 630 genes, with 299 upregulated genes (**Figure 1D**) and 331 downregulated genes (**Figure 1E**) between MED tissues and noncancer tissues.

GO and KEGG Enrichment Analyses of DEGs

To better understand DEGs' biological classification, Metascape online tools (http://metascape.org) were adopted for GO and KEGG pathway enrichment analyses. It is found that DEGs were predominantly enriched in the cell cycle, mitotic cell cycle process, chemical synaptic transmission, retinoblastoma gene in cancer, and neuronal system (**Figures 2A–D**). Afterwards, we conducted GO analysis by using the DAVID website. The biological process changes of DEGs were significantly concentrated in cell division, G1/S transition of mitotic cell cycle, mitotic nuclear, DNA replication, and sister chromatid cohesion (**Figure 2E**). The cell component (CC) changes of DEGs were mostly concentrated in nucleoplasm, cytosol, cytoplasm, cell junction, and postsynaptic density (**Figure 2F**). The molecular function (MF) changes of DEGs were mostly concentrated in protein biding, protein kinase binding, ATP binding, damaged DNA binding, as well as chromatin binding (**Figure 2G**). We investigated the DEG-enriched KEGG pathways further using the DAVID website. We discovered that the DEG genes were mostly concentrated in the cell cycle, DNA replication, oocyte meiosis, GABAergic synapse, and retrograde endocannabinoid signaling (**Figure 2H**).

PPI Network Construction and Screening of Hub Genes and Analysis

The PPI network of DEGs was built (**Figure 3A**), and the most important module was determined by the STRING online tool. Then, based on the DEGREE (**Figure 3B**), MCC (**Figure 3C**), and MNC (**Figure 3D**) in cytoHubba, we identified 12 hub genes. They were AURKA, BUB1B, CCNB1,CCNB2, CHEK1, KIF11, KIF20A, MAD2L1, MCM6, NCAPG, RFC4, and RRM2 (**Figure 3E** venn). The full names, abbreviations, as well as their functions for these hub genes are tabulated in **Table 1**. To visualize the findings of KEGG path analysis, we utilized the ClueGO plugin for Cytoscape. (**Figure 3F**).

Determination of AURKA and KIF20A as the Target Genes by Survival Analysis

To investigate the relationship between hub genes and MED patient's survival, we conducted a survival analysis of the hub genes by using survival data from GSE30074 (**Figures 4A–L**). We discovered that overexpressions of AURKA and KIF20A expression were linked with survival in MED patients. We then used the survival data of GSE85217 to verify these two genes again (**Figure 5**). Therefore, AURKA and KIF20A were selected as target genes. The different expressions of AURKA and KIF20A in the three databases were shown (**Figures 6A–F**).

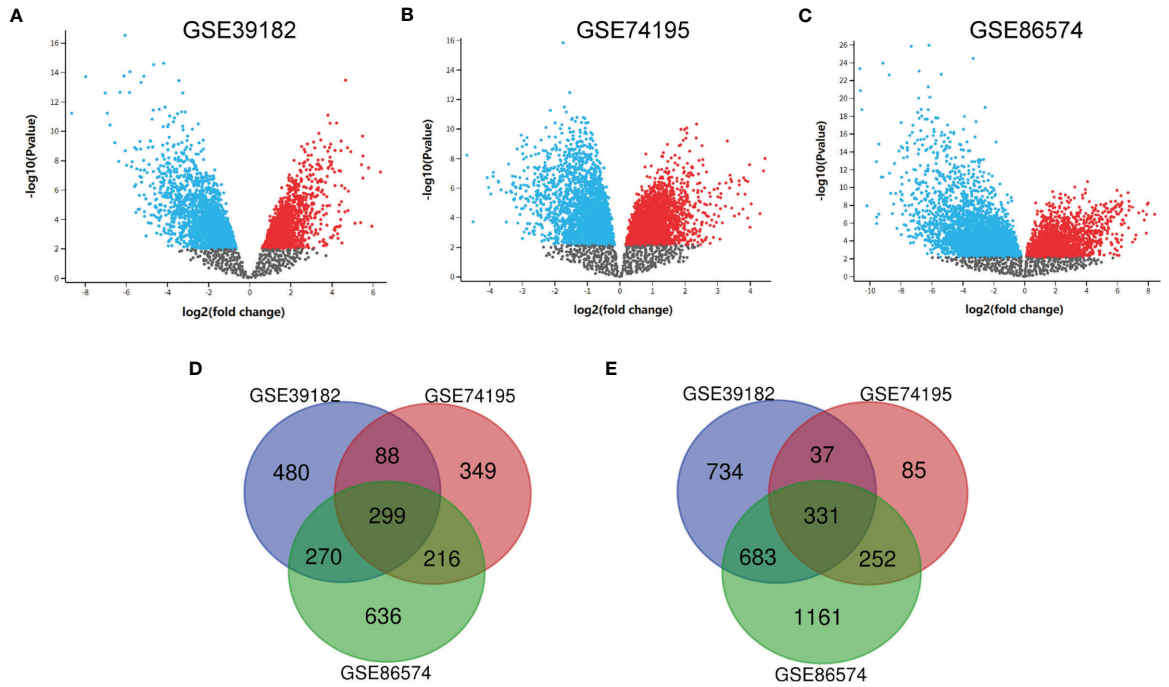

FIGURE 1 | Identification of DEGs shared between the three databases. **(A)** The volcano map of GSE39182, **(B)** The volcano map of GSE74195, **(C)** The volcano map of GSE86574, **(D)** A Venn diagram used to identify 299 upregulated target genes in MED. **(E)** A Venn diagram used to identify 331 downregulated target genes in MED.

The Biological Role of AURKA in Tumors

To study whether AURKA is used as a carcinogene in other tumors, we investigated the differential expression of AURKA in several tumors and healthy tissues using GEPIA (http://gepia.cancer-pku.cn/). We found that AURKA is upregulated in many tumors, such as BLCA and CHOL (**Figure 7A**). To investigate the underlying molecular processes of AURKA, we utilized the STRING website to identify genes owning a protein–protein interaction with AURKA (**Figure 7B**). Using Metascape online tools, we obtained the enrichment analysis results of AURKA and the top 20 interacting proteins pathways and biological processes (**Table 2**), and then we employed the ClueGO plugin for Cytoscape to visualize the findings of KEGG path analysis of these linked genes. It is discovered that AURKA-related genes are mostly concentrated in the cell cycle and p53 signaling pathway (**Figure 7C**). We discovered that AURKA has a significant coexpression relationship with CCNB1, PLK1, CDC20, TP53, and MDM2.

The Biological Role of KIF20A in Tumors

To study whether KIF20A is used as a carcinogene in other tumors, we analyzed the differential expression of KIF20A in several tumors and healthy tissues using GEPIA. We found that the KIF20A overexpression occurs in many tumors, such as BLCA and COAD (**Figure 8A**). To investigate the underlying molecular processes of KIF20A, we utilized the STRING website to identify genes owning a protein–protein interaction with KIF20A (**Figure 8B**). Using Metascape online tools, we obtained the enrichment analysis results of KIF20A and the top 20 interacting proteins pathways and biological processes (**Table 3**), and then we employed the ClueGO plugin for Cytoscape to visualize the findings of KEGG path analysis of these linked genes. It is discovered that KIF20A-related genes are mostly concentrated in the cell cycle, oocyte meiosis, and progesterone-mediated oocytematuration (**Figure 8C**). We discovered that KIF20A has a significant coexpression relationship with BUB1, BUB1B, CCNB1, MAD2L1, PLK1, AURKA and CDC25C.

The Expression level of AURKA and KIF20A in MED

To verify the expression of AURKA and KIF20A at the protein level, IHC staining was carried out, and it was discovered that AURKA and KIF20A expression levels in MED were substantially higher than in cerebellar tissue (**Figure 9**). AURKA and KIF20A were strongly positive in MED group, while in normal brain tissue, they were both expressed as weakly positive or negative.

DISCUSSION

Brain tumors cause the most fatalities related to cancer in children, and the most prevalent malignant juvenile brain tumor is medulloblastoma (MB). Medulloblastomas account

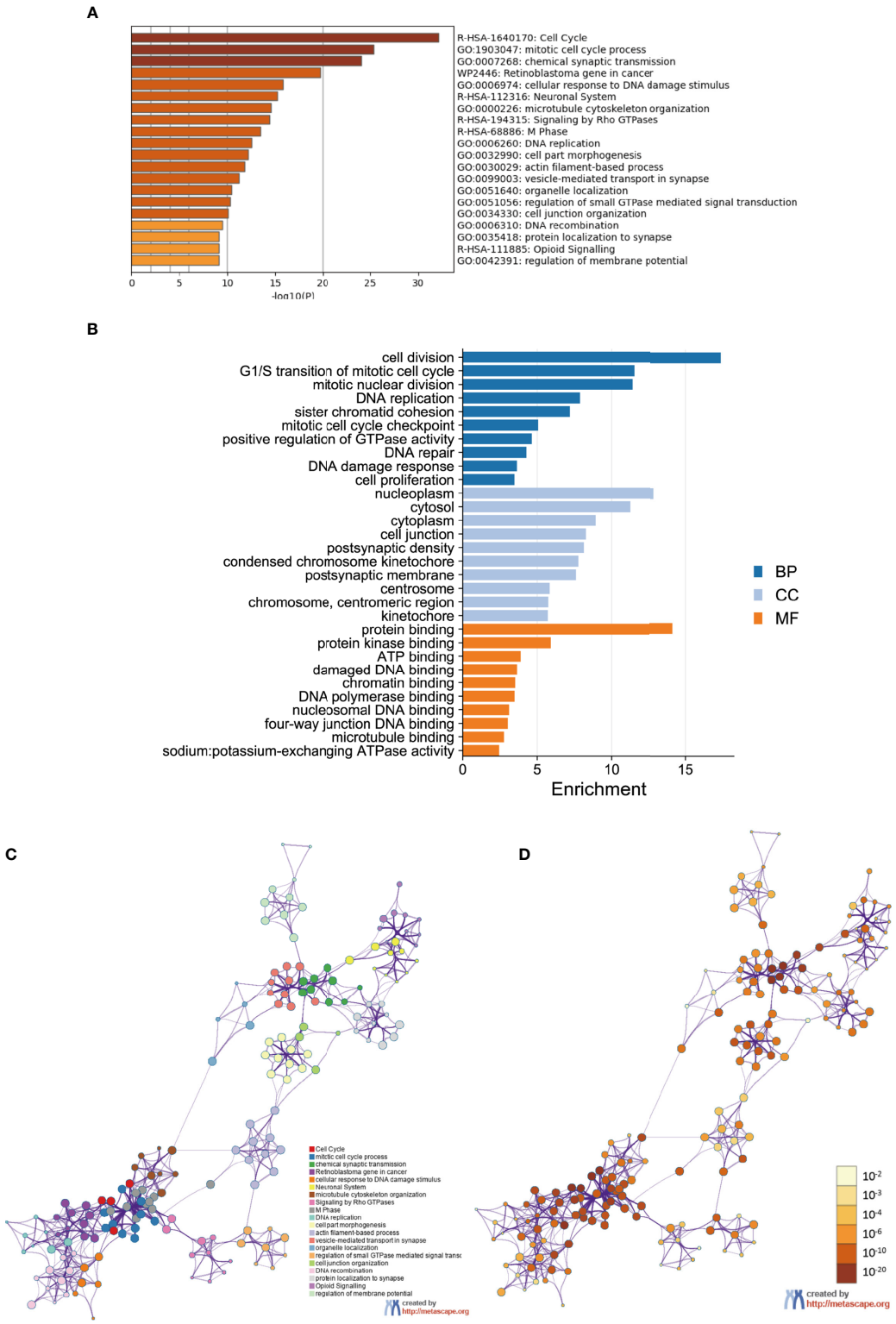

FIGURE 2 | Continued

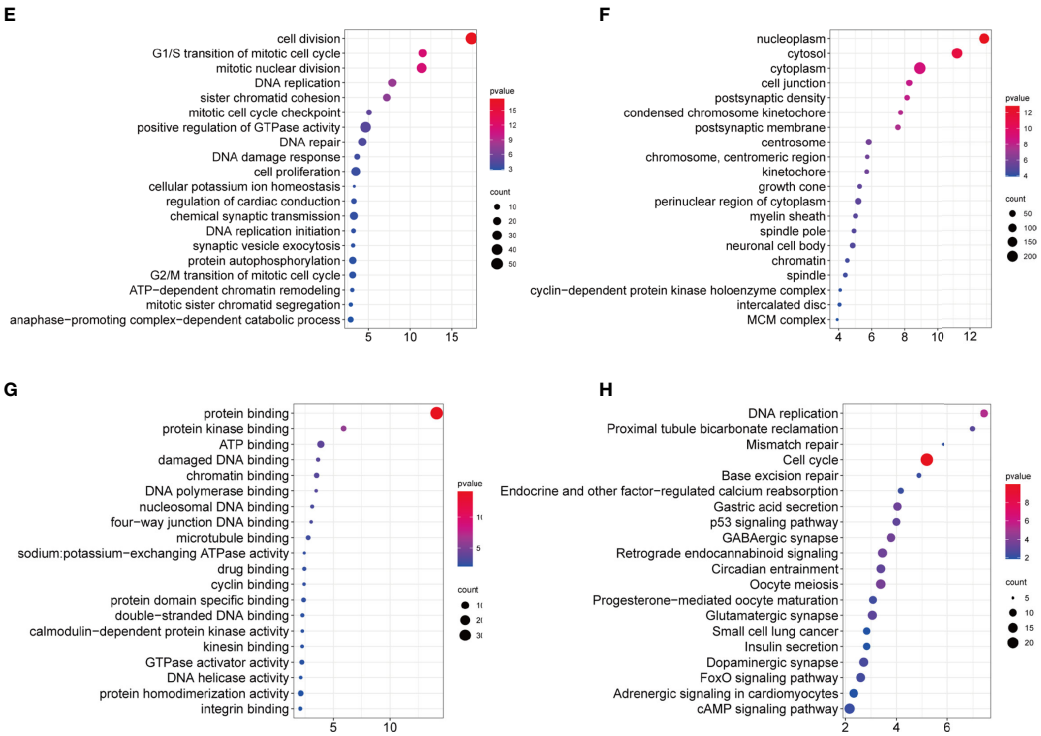

FIGURE 2 | GO analysis and KEGG pathway analysis of DEGs. **(A–D)** GO analysis and KEGG pathway analysis. Bubble diagram of BP **(E)**, CC **(F)**, MF **(G)** and KEGG **(H)** analysis for MED.

for 10% of all childhood brain tumors. These tumors occur only in the posterior fossa and have the possibility of mild meningeal spread (23). Surgical surgery, adjuvant chemotherapy, and craniospinal irradiation are the current therapeutic options (24). In spite of these advancements, 25–30% of patients still die from the condition, and those who survive have substantial long-range negative effects induced by intensive therapy (8), such as severe motor and cognitive deficits. As a result, it is urgent to discover new biomarkers and design new therapy procedures based on the presence of specific hub genes. Progresses in high-throughput chip technology and bioinformatics methods have helped us identify hub genes and provide a deeper understanding of childhood medulloblastoma.

In this study, DEGs between medulloblastoma tissue and healthy brain tissue were discovered analyzing three mRNA microarray datasets. The three datasets yielded 630 DEGs, comprising 299 upregulated genes and 331 downregulated genes. First, we performed GO (BP, CC and MF) analysis on 630 DEGs to study their biological functions. DEGs were mostly enriched in the cycle process, mitotic cell, cell cycle, chemical synaptic transmission, retinoblastoma gene in cancer, and neuronal system. Specifically, the changes in biological processes (BP) of DEGs were significantly enriched in Cell division, DNA replication, mitotic nuclear, G1/S transition of mitotic cell cycle, and sister chromatid cohesion. CC changes of DEGs were largely enriched in nucleoplasm, cytosol, cytoplasm, cell junction, and postsynaptic density. MF changes were largely enriched in protein binding, protein kinase binding, ATP binding, damaged DNA binding, and chromatin binding. These findings imply that these genes function in medulloblastoma cell mitosis, invasion, and metastasis. Based on KEGG pathway analysis results, DEGs were shown to be largely enriched in cell cycle, DNA replication, oocyte meiosis, GABAergic synapse and retrograde endocannabinoid signaling. Understanding the fundamental processes of MED proliferation and invasion, as well as predicting the course of MED, will be aided by research into these pathways.

We constructed a PPI network with these differential genes, and then screened out 12 hub genes: AURKA, BUB1B, CCNB1, CCNB2, CHEK1, KIF11, KIF20A, MAD2L1, MCM6, NCAPG, RFC4, and RRM2. KEGG analysis of these hub genes illustrated that they were largely enriched in DNA replication, cell cycle, progesterone-mediated oocyte maturation, and P53 signaling pathway. These hub genes can be potentially utilized as therapeutic targets for medulloblastoma. Then, based on the prognostic information of medulloblastoma patients in the GSE30074 and GSE85217 datasets. The expression levels of AURKA and KIF20A were discovered to be linked with the prognosis of medulloblastoma patients. Therefore, AURKA and KIF20A were selected as the target genes in this research.

To analyze the expression of AURKA and KIF20A in medulloblastoma at the protein level, we selected MED tissue samples and normal cerebellum tissues for immunohistochemical staining, and the findings proved that the expression of AURKA

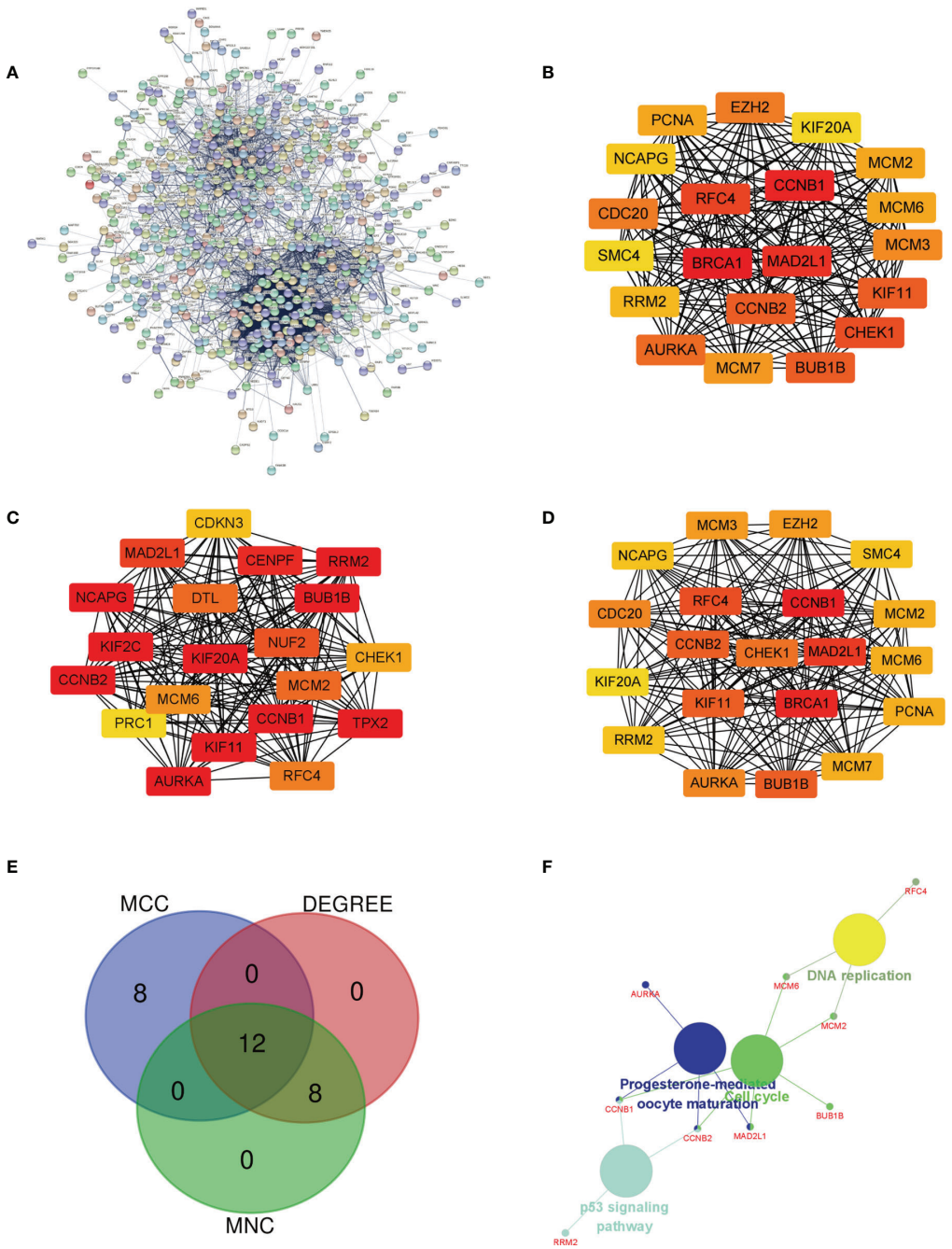

FIGURE 3 | Determination of the hub genes. **(A)** PPI network of DEGs in MED. **(B–D)** Three different metrics: DEGREE, MCC, and MNC. **(E)** In MED, 12 hub genes were identified using a Venn diagram, **(F)** The ClueGO plugin in Cytoscape software was used to visualize the findings of KEGG pathway analysis.

and KIF20A in cerebellum tissues was weakly positive or negative, while in MED, both AURKA and KIF20A were overexpressed, which was the same as their mRNA expression in MED. It was proved that AURKA and KIF20A can be used as biomarkers for MED.

KIF20A, also known as mitotic kinesin-like protein 2 (MKlp2) or rabkinesin6 (RAB6KIFL), is a kinesin-6 family 10 microtubule plus-end directed motor that is also necessary in the exit of mitosis for the final step of cytokinesis (25). KIF20A is found in the central spindle during mitosis, whose phosphorylation is necessary for cytoplasmic division (26). It has recently been reported that KIF20A knockout results in loss of neural precursor cells and neurons during cortical neurogenesis owing to premature cell cycle exit and neuronal differentiation (27).

TABLE 1 | Functional roles of 12 hub genes.

NO.	Gene symbol	Full name	Function
1	KIF20A	kinesin family member 20A	Mitotic kinesin is necessary for cytokinesis mediated by the chromosomal passenger complex (CPC).
2	AURKA	aurora kinase A	A cell cycle-regulated kinase that appears to be involved in the production and/or stability of microtubules at the spindle pole during chromosomal segregation.
3	BUB1B	threonine kinase B	Essential component of the mitotic checkpoint
4	RRM2	ribonucleotide reductase M2	Provides the precursors necessary for DNA synthesis.
5	KIF11	kinesin family member 11	During mitosis, a motor protein is essential for the formation of a bipolar spindle.
6	MAD2L1	MAD2 mitotic arrest deficient-like 1	A component of the spindle-assembly checkpoint that prevents anaphase from occurring until all chromosomes are correctly aligned at the metaphase plate.
7	CCNB1	cyclin B1	Belongs to the cyclin family and is required for cell cycle regulation during the G2/M (mitosis) transition.
8	RFC4	replication factor C4	Involved in the elongation of the multiprimed DNA template
9	NCAPG	non-SMC condensin I complex, subunit G	Condensin complex regulatory subunit, a complex essential for the conversion of interphase chromatin into mitotic-like condensed chromosomes.
10	CCNB2	cyclin B2	Belongs to the cyclin family and is required for cell cycle regulation during the G2/M (mitosis) transition.
11	MCM6	minichromosome maintenance complex component 6	one of the highly conserved mini-chromosome maintenance proteins (MCM) required for eukaryotic genome replication to begin
12	CHEK1	checkpoint kinase 1	Serine/threonine protein kinase that is necessary for checkpoint-mediated cell cycle arrest and DNA repair activation in the presence of DNA damage or unreplicated DNA.

The overexpression of KIF20A is linked to the onset, progression, and prognosis of different cancers. Recent researches have reported that KIF20A was upregulated in esophageal squamous cell carcinoma (28), lung adenocarcinoma (29), prostate cancer (30), cervical cancer (31), colorectal cancer (32), non-small cell lung cancer (33), gastric cancer (34), bladder cancer (35), renal clear cell carcinoma (36), breast cancer (37), hepatocellular carcinoma (38), nasopharyngeal carcinoma (39), ovarian cancer (40), leukemia (25), glioma (41), and soft tissue sarcoma (42). This is consistent with our analysis in the GEPIA online database. KIF20A overexpression is linked to HCC and NPC patient survival, and it can be utilized independently as a prognostic marker for HCC and NPC patients (38, 39). Furthermore, KIF20A is linked with chemotherapy resistance and radiation resistance of some tumors. For instance, in colorectal cancer, KIF20 is highly upregulated in oxaliplatin resistant cell lines, and has a close correlation with the survival of colorectal cancer patients. Silencing KIF20A increased the sensitivity of cells to oxaliplatin *in vivo* and *in vitro* (43). Forkhead box M1 (FOXM1), a transcription factor participating in cell proliferation as well as cycle progression, has been linked to chemotherapy sensitivity. High expression of FOXM1 may increase docetaxel resistance by promoting KIF20A expression (44). FOXM1 plays a role in regulating radiosensitivity in glioma and breast cancer cells, and FOXM1 may enhance radiation resistance in part by inducing KIF20A expression (45). In addition to the high expression of KIF20A in the above tumors, our study found that KIF20A was also highly upregulated in MED, and according to the prognostic survival analysis, KIF20A was shown to be directly linked to the prognosis of MED patients, and the overexpression of KIF20A illustrated a poor survival prognosis of MED patients. KEGG enrichment analysis of KIF20A revealed that KIF20A and its associated genes were shown to be highly enriched in the cell cycle, oocyte meiosis, and progesterone-mediated oocytematuration. The enrichment analysis results of KIF20A and the top 20 interacting proteins pathways and biological processes were shown in **Table 3**. Further study on these pathways will assist to reveal the mechanism of KIF20A in MED.

AURKA is a serine/threonine kinase whose activation is required for cell division through controlling mitosis. Under physiological conditions, AURKA controls cilia breakdown, neurite extension, cell movement, DNA replication, and aging procedures. It is found in mitochondria in a cancer-like environment, where mitochondrial dynamics and ATP generation are affected, actively promoting DNA repair and cell migration and invasion (46). Our analysis using the GEPIA database showed that AURKA was highly upregulated in various tumors. The function of AURKA substrates, some of which are mitotic regulators, tumor suppressors, or carcinogenes, is modulated by AURKA-mediated phosphorylation (47). Currently many researches have revealed that the activation of AURKA has a crucial role in multiple cancers, for example, gastric cancer (48), liposarcoma (49), neuroblastoma (50), pancreatic cancer (51), gastrointestinal cancer (52), hepatocellular carcinoma (53), leukemia (54), epithelial ovarian cancer (55), head and neck squamous cell carcinoma (56), prostate cancer (57), bladder cancer (58), upper gastrointestinal adenocarcinoma (59), fertile tumor of the bone marrow (60), oral squamous cell carcinoma (61), KIF20A was highly expressed. In most tumors, upregulation of KIF20A suggests a poor prognosis of patients, except for colon cancer, where it has been found that the AURKA upregulation in colon cancer suggests better prognosis of patients with colon cancer (62). AURKA overexpression contributed to oxaliplatin-induced death of colon cancer cells, while AURKA knockdown drastically reduced chemotherapy sensitivity of colon cancer cells to oxaliplatin. In terms of mechanism, AURKA inhibits DNA damage responses in a TP53-dependent manner by inhibiting the expression of multiple DNA damage repair genes, which may partly explain ARUKA's association with beneficial outcomes in colon cancer. In addition to the upregulation of AURKA in the above tumors, our study found that AURKA was also overexpressed in MED. According to the prognostic survival

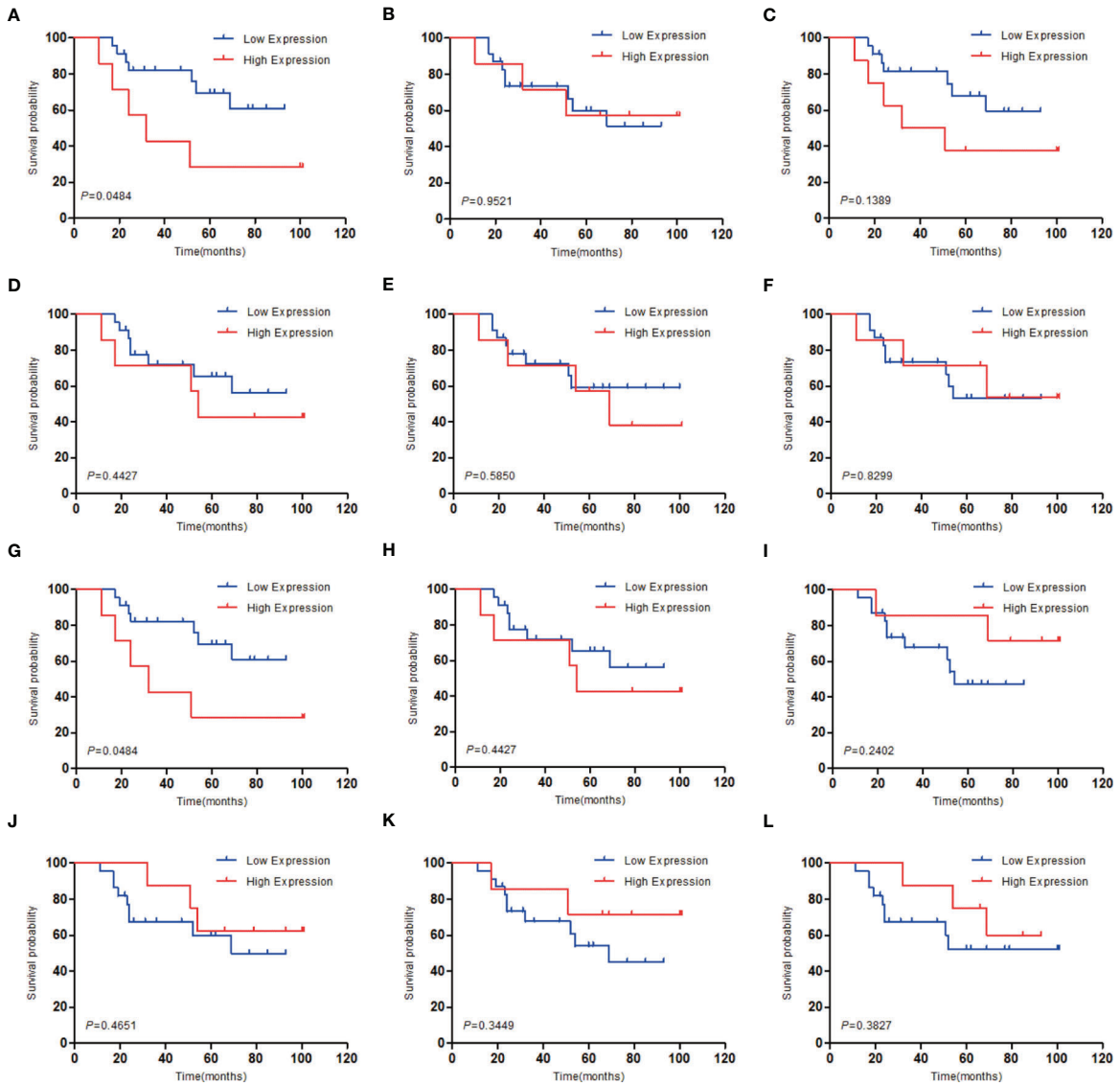

FIGURE 4 | Survival analysis of the 12 hub genes in MED based on the GSE30074 database. **(A)** AURKA, **(B)** BUB1B, **(C)** CCNB1, **(D)** CCNB2, **(E)** CHEK1, **(F)** KIF11, **(G)** KIF20A, **(H)** MAD2L1, **(I)** MCM6, **(J)** NCAPG, **(K)** RFC4, **(L)** RRM2; $P < 0.05$ was considered statistically significant.

analysis, AURKA was closely linked to the prognosis of MED patients, and the AURKA upregulation predicted a poor survival prognosis of MED patients. By KEGG enrichment analysis of AURKA and its interacting proteins, we found that these proteins affect typical carcinogenic pathways like the cell cycle and p53 signaling pathway. To better understand the biological functions of AURKA, enrichment analysis was performed using Metascape online tools, the enrichment analysis results of AURKA and the top 20 interacting proteins pathways and biological processes were shown in **Table 2**. All of these data points to AURKA as a potential target for cancer treatment, and various small compounds targeting AURKA have been found. These AURKA inhibitors (AKIs) have been studied in preclinical investigations, and some have been studied in clinical trials as monotherapies or in conjunction with traditional chemotherapy or other targeted medicines.

According to the latest research, we discussed the involvement of KIF20A and AURKA in the occurrence and development of MED and their close correlation with the prognosis of patients, implying that these genes might be used as promising biomarkers and therapeutic targets of MED. Despite the fact that our work adds to our understanding of the link between AURKA, KIF20A and MED, it has several limitations. First of all, the mRNA sequencing data of MED in this study only came from GEO database. As there were few sequencing data related to MED, our sample size was insufficient.

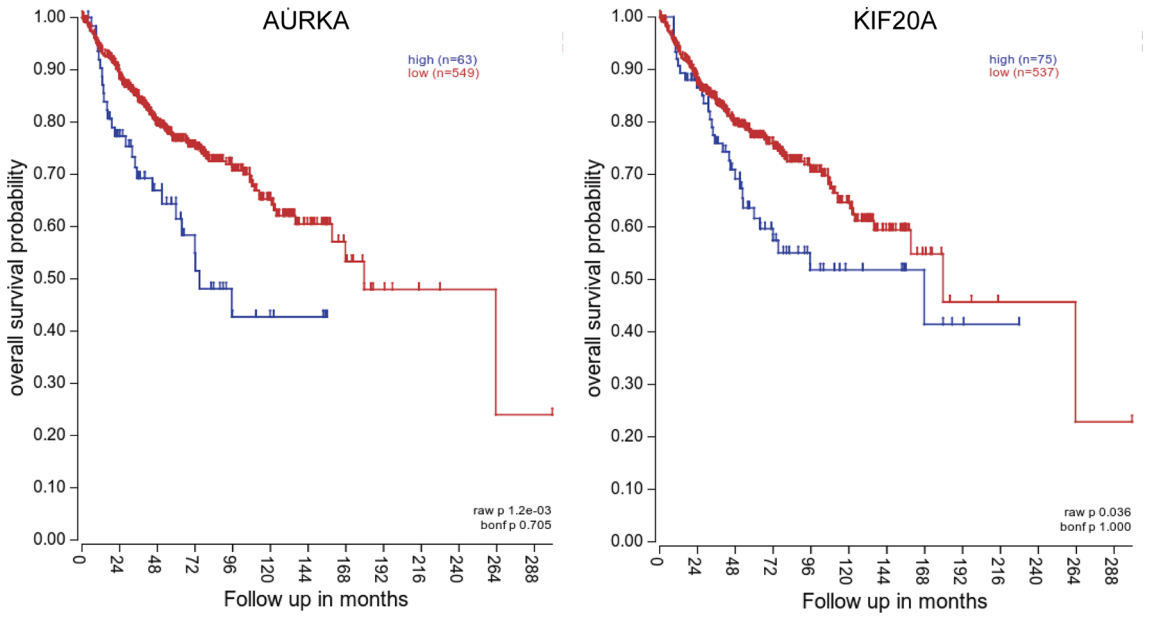

FIGURE 5 | Survival analysis of AURKA and KIF20A based on the GSE85217 database. **(A)** AURKA, **(B)** KIF20A. P < 0.05 was considered statistically significant.

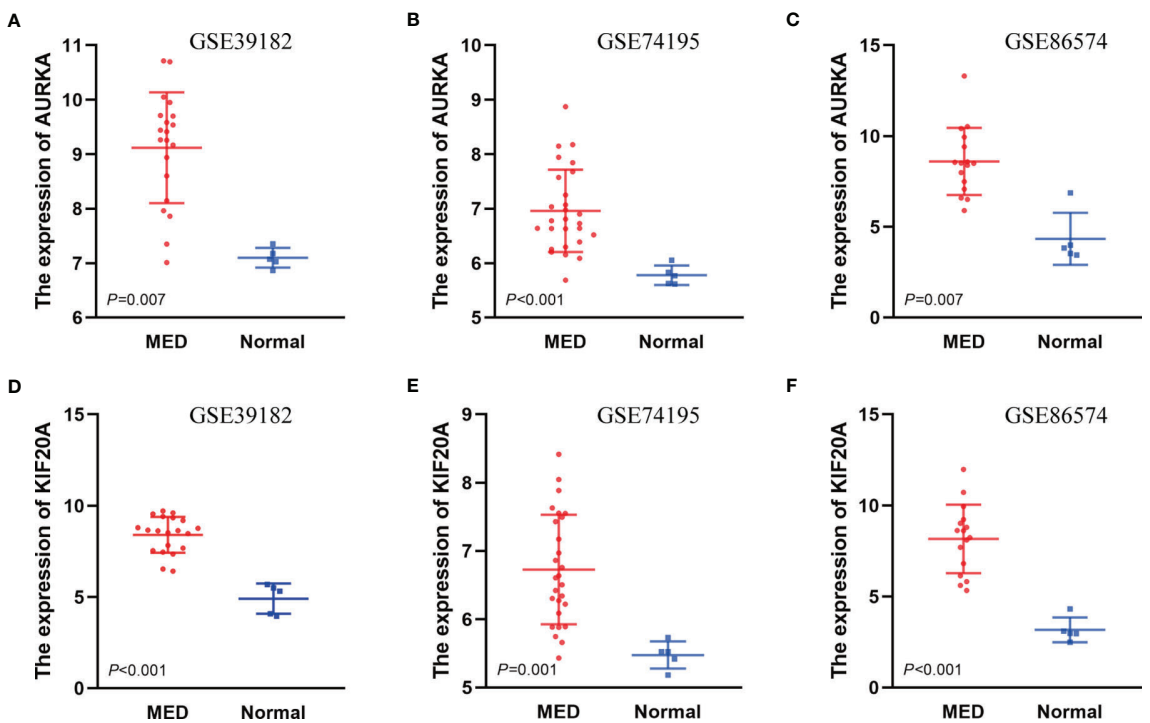

FIGURE 6 | The different expressions of AURKA and KIF20A in the three databases. **(A)** Expressions of AURKA in GSE39182, **(B)** Expressions of AURKA in GSE74195, **(C)** Expressions of AURKA in GSE86574, **(D)** Expressions of KIF20A in GSE39182, **(E)** Expressions of KIF20A in GSE74195, **(F)** Expressions of KIF20A in GSE86574.

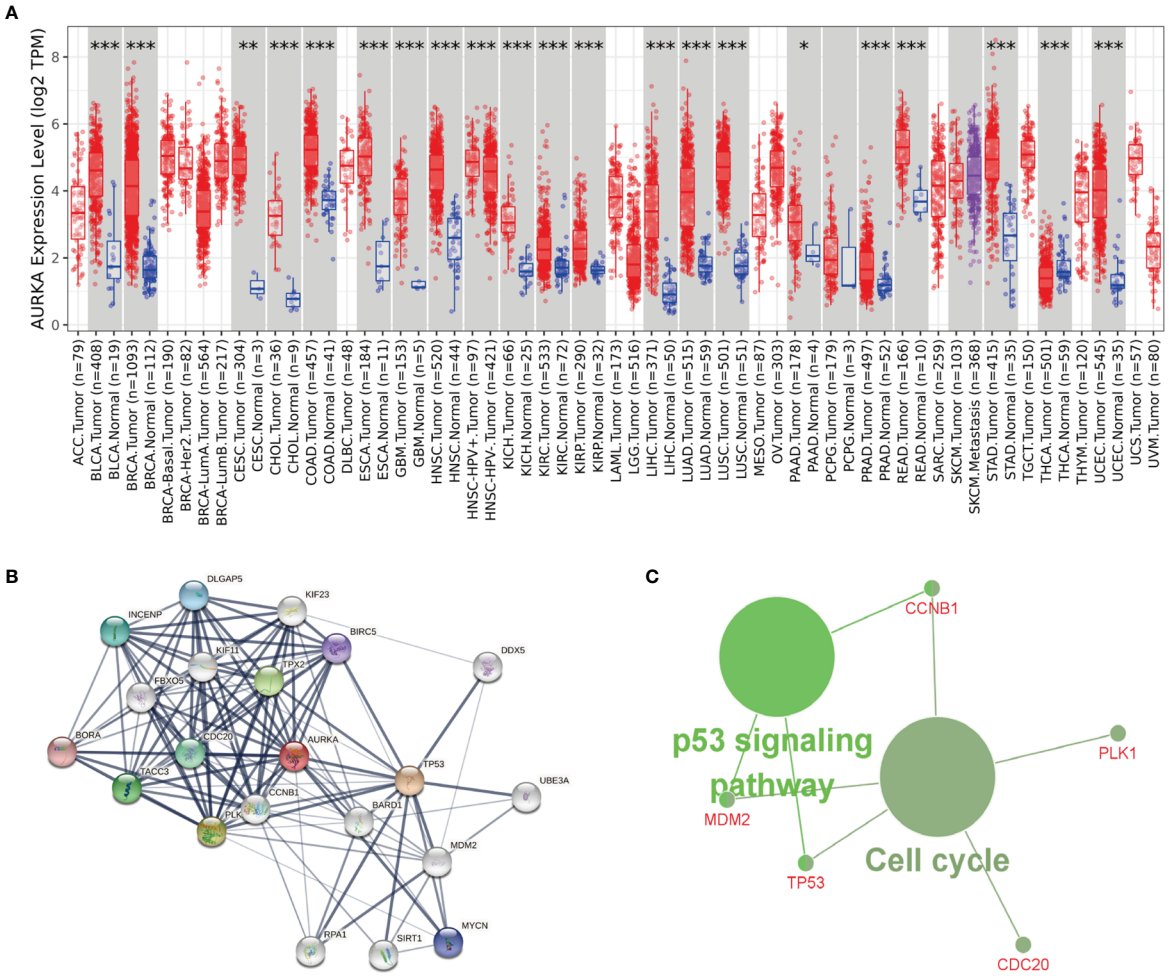

FIGURE 7 | AURKA's biological involvement in tumors. **(A)** AURKA expression in different tumors. **(B)** AURKA gene STRING interaction network preview of interacting proteins (showing top 20 STRING interactants). **(C)** Illustration of KEGG pathway analysis findings using the ClueGO plugin in Cytoscape. *P < 0.05, **P < 0.01, ***P < 0.001.

Secondly, the basic experiments of our verification and inspection are insufficient. Only IHC experiments are involved, and RT-qPCR validation in clinical samples is also required. *In vitro* and *in vivo* experiments are also our next research direction. Third, for these genes play a role in the mechanism is still not entirely clear, Our current study only stays at the transcriptional level and does not involve the upstream and downstream pathways of target gene related proteins, the

TABLE 2 | Pathway and process enrichment analysis of AURKA and top 20 interacting proteins.

GO	Category	Description	Count	-Log10(P)
M129	Canonical Pathways	PID PLK1 PATHWAY	12	29.03
M14	Canonical Pathways	PID AURORA B PATHWAY	11	26.91
GO:0051301	GO Biological Processes	cell division	17	26.77
R-HSA-69278	Reactome Gene Sets	Cell Cycle, Mitotic	17	25.8
GO:0051321	GO Biological Processes	meiotic cell cycle	8	11.64
GO:0061640	GO Biological Processes	cytoskeleton-dependent cytokinesis	6	10.37
hsa04914	KEGG Pathway	Progesterone-mediated oocyte maturation	6	10.18
CORUM:6184	CORUM	AuroraB-AuroraC-INCENP complex	3	9.54
GO:0051656	GO Biological Processes	establishment of organelle localization	7	8.64
GO:0051988	GO Biological Processes	regulation of attachment of spindle microtubules to kinetochore	3	7.08
GO:0001578	GO Biological Processes	microtubule bundle formation	3	4.13

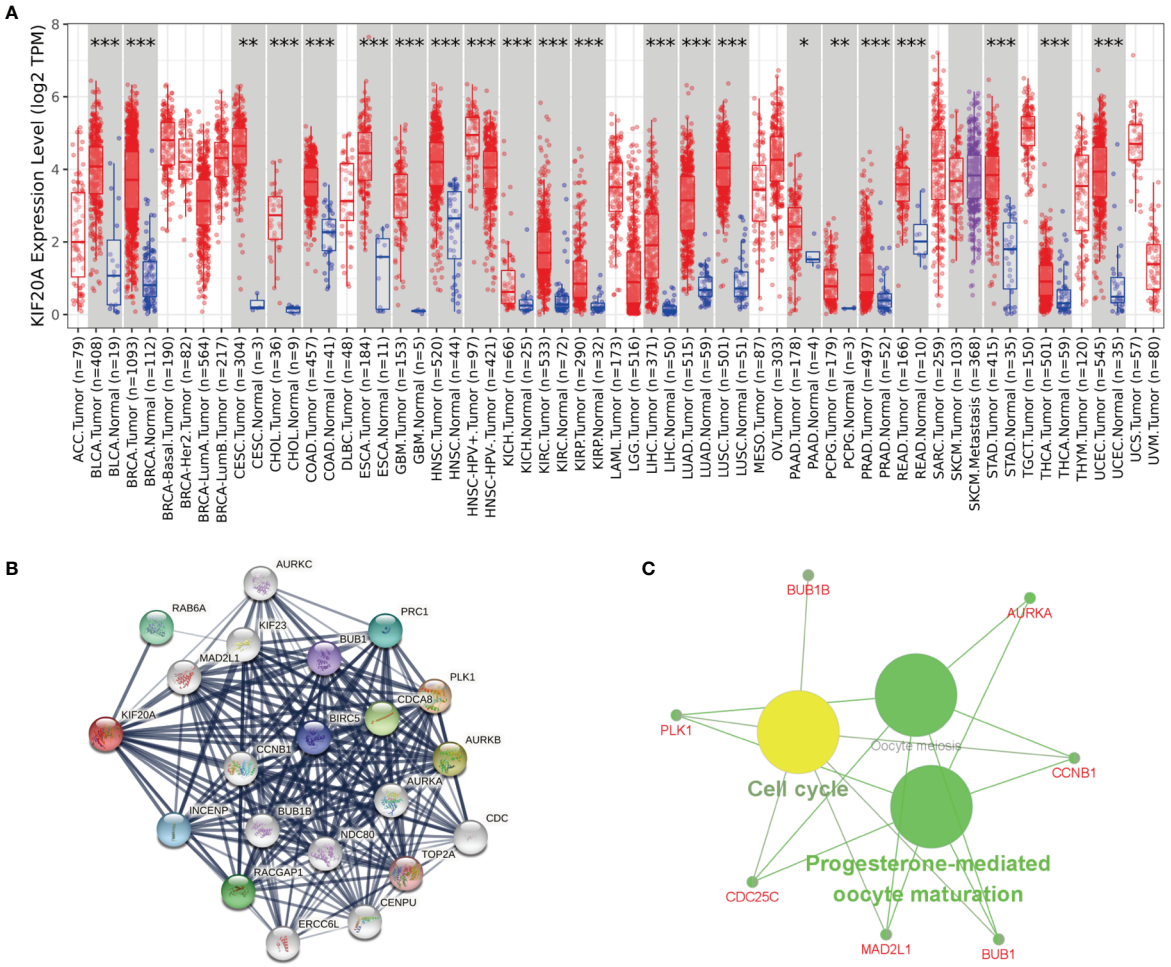

FIGURE 8 | KIF20A's biological involvement in tumors. **(A)** KIF20A expression in different tumors. **(B)** KIF20A gene STRING interaction network preview of interacting proteins (showing top 20 STRING interactants). **(C)** Illustration of KEGG pathway analysis findings using the ClueGO plugin in Cytoscape. *P < 0.05, **P < 0.01, ***P < 0.001.

TABLE 3 | Pathway and biological process enrichment analysis of KIF20A and top 20 interacting proteins.

GO	Category	Description	Count	-Log10(P)
GO:0007051	GO Biological Processes	spindle organization	11	19.88
R-HSA-1640170	Reactome Gene Sets	Cell Cycle	14	18.02
M129	Canonical Pathways	PID PLK1 PATHWAY	8	17.52
M242	Canonical Pathways	PID AURORA A PATHWAY	7	16.18
R-HSA-69620	Reactome Gene Sets	Cell Cycle Checkpoints	9	12.75
R-HSA-3108232	Reactome Gene Sets	SUMO E3 ligases SUMOylate target proteins	7	10.56
R-HSA-6804756	Reactome Gene Sets	Regulation of TP53 Activity through Phosphorylation	6	10.45
WP1984	WikiPathways	Integrated breast cancer pathway	6	9.07
GO:0060236	GO Biological Processes	regulation of mitotic spindle organization	4	7.86
GO:0030162	GO Biological Processes	regulation of proteolysis	8	7.7
GO:0090307	GO Biological Processes	mitotic spindle assembly	4	7.52
GO:1903800	GO Biological Processes	positive regulation of production of miRNAs involved in gene silencing by miRNA	3	7.2
GO:0051347	GO Biological Processes	positive regulation of transferase activity	7	7.18
GO:0010639	GO Biological Processes	negative regulation of organelle organization	4	4.12

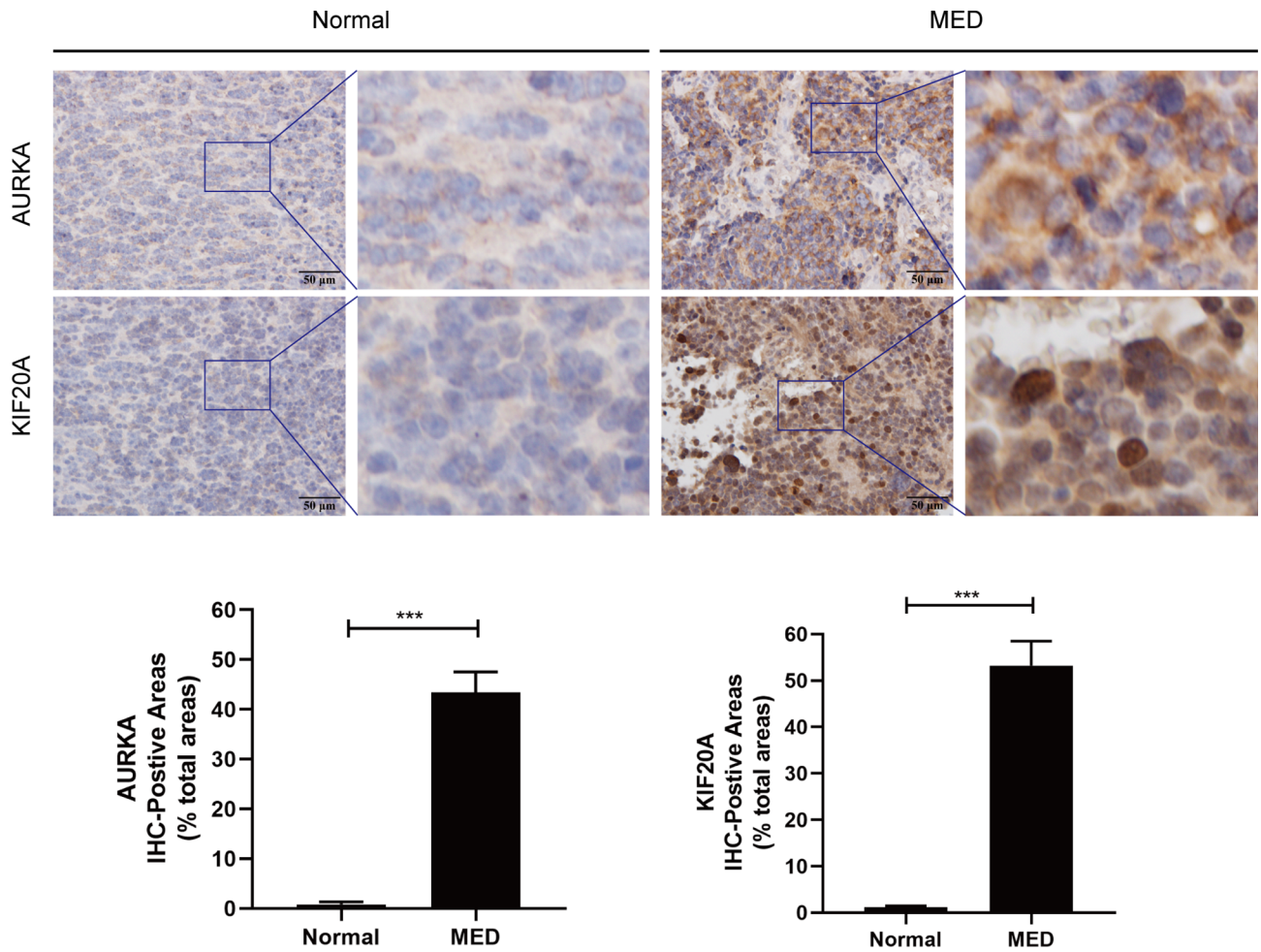

FIGURE 9 | Immunohistochemistry analysis of AURKA and KIF20A expression in Medulloblastoma tissues from Tianjin Huanhu Hospital (normal brain, n = 4; MED, n = 10). Scale bar = 50μm. Below is a list of statistical quantitative analyses. Data are mean ± SD. ***P < 0.001, one-way ANOVA.

next step we should take multiple omics research, including proteomics, metabolomics, and DNA methylation, autophagy and LncRNA, ceRNA, etc. Fourth, Immune infiltration is important in the growth of tumors. the immune microenvironment profoundly affected the prognosis of patients with tumor, because our data is limited, the present study did not show that the target gene influences the immune cell migration and invasion, the next step should be studied gradually AURKA, KIF20A biological function in immune microenvironment. Fifthly, our study is limited to MED. Next, we can carry out combinative analysis with a variety of tumors to explore the mechanism of action of AURKA and KIF20A in generalized cancer. Sixthly, to explore the correlation between target genes and patients' prognosis and survival, we need to consider multiple clinical factors and parameters, such as the details of patients' treatment. However, such information is lacking in the public database. We only included the information of two datasets, and the sample size is insufficient, which may lead to analysis bias, which is also the biggest problem of this study. In the next step, we should conduct a prospective study to avoid insufficient sample size due to the retrospective nature. At the same time, as many environmental factors and genetic factors including region, race, age, gender, family history were included as much as possible.

CONCLUSIONS

In conclusion, this study found that DEGs participate in the occurrence and development of MED through a public database study, and screened out two possible biomarkers, AURKA and KIF20A. Both genes may be new therapeutic targets. In addition, basic experiments on clinical patient specimens proved that these two genes were indeed upregulated in MED tissues. However, the biological function of these genes in MED remains to be further studied.

DATA AVAILABILITY STATEMENT

The original contributions presented in the study are included in the article/supplementary material. Further inquiries can be directed to the corresponding authors.

ETHICS STATEMENT

The studies involving human participants were reviewed and approved by Tianjin Huanhu Hospital Ethics Committee (Tianjin, China). Written informed consent to participate in this study was provided by the participants' legal guardian/next of kin. Written informed consent was obtained from the individual(s), and minor(s)' legal guardian/next of kin, for the publication of any potentially identifiable images or data included in this article.

AUTHOR CONTRIBUTIONS

BL, HY, and XT: study design. BL, YZ, and JJ: data collection. BL, LX, and QW: data analysis and interpretation. BL, YZ, and JJ: writing, review, polishing, and revision of the manuscript. All authors contributed to the article and approved the submitted version.

FUNDING

This study was financially supported by grants from the National Natural Science Foundation of China (No. 81972349), Tianjin Municipal Science and Technology Commission (No. 20JCQNJC00410), Tianjin Health Science and Technology Project (TJWJ2021MS030), and Applied basic research project of Tianjin Science and Technology Bureau (21JCZDJC00460).

ACKNOWLEDGMENTS

We gratefully appreciate Tianjin Huanhu Hospital, GEO and other databases and the funding of Tianjin Medical Key Disciplines (specialties) construction project.

REFERENCES

1. Roussel MF, Stripay JL. Epigenetic Drivers in Pediatric Medulloblastoma. *Cerebellum (London England)* (2018) 17:28–36. doi: 10.1007/s12311-017-0899-9
2. Menyhárt O, Győrffy B. Molecular Stratifications, Biomarker Candidates and New Therapeutic Options in Current Medulloblastoma Treatment Approaches. *Cancer Metastasis Rev* (2020) 39:211–33. doi: 10.1007/s10555-020-09854-1
3. Archer TC, Mahoney EL, Pomeroy SL. Medulloblastoma: Molecular Classification-Based Personal Therapeutics. *Neurother J Am Soc Exp Neurother* (2017) 14:265–73. doi: 10.1007/s13311-017-0526-y
4. Newton HB. Review of the Molecular Genetics and Chemotherapeutic Treatment of Adult and Paediatric Medulloblastoma. *Expert Opin Invest Drugs* (2001) 10:2089–104. doi: 10.1517/13543784.10.12.2089
5. Robinson G, Parker M, Kranenburg TA, Lu C, Chen X, Ding L, et al. Novel Mutations Target Distinct Subgroups of Medulloblastoma. *Nature* (2012) 488:43–8. doi: 10.1038/nature11213
6. Northcott PA, Buchhalter I, Morrissy AS, Hovestadt V, Weischenfeldt J, Ehrenberger T, et al. The Whole-Genome Landscape of Medulloblastoma Subtypes. *Nature* (2017) 547:311–7. doi: 10.1038/nature22973
7. Orr BA. Pathology, Diagnostics, and Classification of Medulloblastoma. *Brain Pathol* (2020) 30:664–78. doi: 10.1111/bpa.12837
8. Wang J, Garancher A, Ramaswamy V, Wechsler-Reya RJ. Medulloblastoma: From Molecular Subgroups to Molecular Targeted Therapies. *Annu Rev Neurosci* (2018) 41:207–32. doi: 10.1146/annurev-neuro-070815-013838
9. Tan IL, Arifa RDN, Rallapalli H, Kana V, Lao Z, Sanghrajka RM, et al. CSF1R Inhibition Depletes Tumor-Associated Macrophages and Attenuates Tumor Progression in a Mouse Sonic Hedgehog-Medulloblastoma Model. *Oncogene* (2021) 40:396–407. doi: 10.1038/s41388-020-01536-0
10. Bharambe HS, Paul R, Panwalkar P, Jalali R, Sridhar E, Gupta T, et al. Downregulation of miR-204 Expression Defines a Highly Aggressive Subset of Group 3/Group 4 Medulloblastomas. *Acta Neuropathol Commun* (2019) 7:52. doi: 10.1186/s40478-019-0697-3
11. Paul R, Bharambe H, Shirsat NV. Autophagy Inhibition Impairs the Invasion Potential of Medulloblastoma Cells. *Mol Biol Rep* (2020) 47:5673–80. doi: 10.1007/s11033-020-05603-3
12. Zhang L, He X, Liu X, Zhang F, Huang LF, Potter AS, et al. Single-Cell Transcriptomics in Medulloblastoma Reveals Tumor-Initiating Progenitors and Oncogenic Cascades During Tumorigenesis and Relapse. *Cancer Cell* (2019) 36:302–318.e7. doi: 10.1016/j.ccell.2019.07.009
13. Edgar R, Domrachev M, Lash AE. Gene Expression Omnibus: NCBI Gene Expression and Hybridization Array Data Repository. *Nucleic Acids Res* (2002) 30:207–10. doi: 10.1093/nar/30.1.207
14. Barrett T, Wilhite SE, Ledoux P, Evangelista C, Kim IF, Tomashevsky M, et al. NCBI GEO: Archive for Functional Genomics Data Sets–Update. *Nucleic Acids Res* (2013) 41:D991–5. doi: 10.1093/nar/gks1193
15. Valdora F, Banelli B, Stigliani S, Pfister SM, Moretti S, Kool M, et al. Epigenetic Silencing of DKK3 in Medulloblastoma. *Int J Mol Sci* (2013) 14:7492–505. doi: 10.3390/ijms14047492
16. de Bont JM, Kros JM, Passier MM, Reddingius RE, Sillevis Smitt PA, Luider TM, et al. Differential Expression and Prognostic Significance of SOX Genes in Pediatric Medulloblastoma and Ependymoma Identified by Microarray Analysis. *Neuro-oncology* (2008) 10:648–60. doi: 10.1215/15228517-2008-032
17. Amani V, Donson AM, Lummus SC, Prince EW, Griesinger AM, Witt DA, et al. Characterization of 2 Novel Ependymoma Cell Lines With Chromosome 1q Gain Derived From Posterior Fossa Tumors of Childhood. *J Neuropathol Exp Neurol* (2017) 76:595–604. doi: 10.1093/jnen/nlx040
18. Zhou Y, Zhou B, Pache L, Chang M, Khodabakhshi AH, Tanaseichuk O, et al. Metascape Provides a Biologist-Oriented Resource for the Analysis of Systems-Level Datasets. *Nat Commun* (2019) 10:1523. doi: 10.1038/s41467-019-09234-6
19. Huang da W, Sherman BT, Lempicki RA. Bioinformatics Enrichment Tools: Paths Toward the Comprehensive Functional Analysis of Large Gene Lists. *Nucleic Acids Res* (2009) 37:1–13. doi: 10.1093/nar/gkn923
20. Szklarczyk D, Gable AL, Lyon D, Junge A, Wyder S, Huerta-Cepas J, et al. STRING V11: Protein-Protein Association Networks With Increased Coverage, Supporting Functional Discovery in Genome-Wide Experimental Datasets. *Nucleic Acids Res* (2019) 47:D607–13. doi: 10.1093/nar/gky1131
21. Smoot ME, Ono K, Ruscheinski J, Wang PL, Ideker T. Cytoscape 2.8: New Features for Data Integration and Network Visualization. *Bioinformatics* (2011) 27:431–2. doi: 10.1093/bioinformatics/btq675
22. Chin CH, Chen SH, Wu HH, Ho CW, Ko MT, Lin CY. Cytohubba: Identifying Hub Objects and Sub-Networks From Complex Interactome. *BMC Syst Biol* (2014) 8 Suppl 4:S11. doi: 10.1186/1752-0509-8-S4-S11
23. Millard NE, De Braganca KC. Medulloblastoma. *J Child Neurol* (2016) 31:1341–53. doi: 10.1177/0883073815600866
24. Liu X, Ding C, Tan W, Zhang A. Medulloblastoma: Molecular Understanding, Treatment Evolution, and New Developments. *Pharmacol Ther* (2020) 210:107516. doi: 10.1016/j.pharmthera.2020.107516

25. Morita H, Matsuoka A, Kida JI, Tabata H, Tohyama K, Tohyama Y. KIF20A, Highly Expressed in Immature Hematopoietic Cells, Supports the Growth of HL60 Cell Line. *Int J Hematol* (2018) 108:607–14. doi: 10.1007/s12185-018-2527-y
26. Mandal K, Pogoda K, Nandi S, Mathieu S, Kasri A, Klein E, et al. Role of a Kinesin Motor in Cancer Cell Mechanics. *Nano Lett* (2019) 19:7691–702. doi: 10.1021/acs.nanolett.9b02592
27. Geng A, Qiu R, Murai K, Liu J, Wu X, Zhang H, et al. KIF20A/MKLP2 Regulates the Division Modes of Neural Progenitor Cells During Cortical Development. *Nat Commun* (2018) 9:2707. doi: 10.1038/s41467-018-05152-1
28. Zheng L, Li L, Xie J, Jin H, Zhu N. Six Novel Biomarkers for Diagnosis and Prognosis of Esophageal Squamous Cell Carcinoma: Validated by scRNA-Seq and qPCR. *J Cancer* (2021) 12:899–911. doi: 10.7150/jca.50443
29. Zhao X, Zhou LL, Li X, Ni J, Chen P, Ma R, et al. Overexpression of KIF20A Confers Malignant Phenotype of Lung Adenocarcinoma by Promoting Cell Proliferation and Inhibiting Apoptosis. *Cancer Med* (2018) 7:4678–89. doi: 10.1002/cam4.1710
30. Zhang Z, Chai C, Shen T, Li X, Ji J, Li C, et al. Aberrant KIF20A Expression Is Associated With Adverse Clinical Outcome and Promotes Tumor Progression in Prostate Cancer. *Dis Markers* (2019) 2019:4782730. doi: 10.1155/2019/4782730
31. Zhang W, He W, Shi Y, Gu H, Li M, Liu Z, et al. High Expression of KIF20A Is Associated With Poor Overall Survival and Tumor Progression in Early-Stage Cervical Squamous Cell Carcinoma. *PloS One* (2016) 11:e0167449. doi: 10.1371/journal.pone.0167449
32. Zhang Q, Di J, Ji Z, Mi A, Li Q, Du X, et al. KIF20A Predicts Poor Survival of Patients and Promotes Colorectal Cancer Tumor Progression Through the JAK/STAT3 Signaling Pathway. *Dis Markers* (2020) 2020:2032679. doi: 10.1155/2020/2032679
33. Xie F, He C, Gao S, Yang Z, Li L, Qiao L, et al. KIF20A Silence Inhibits the Migration, Invasion and Proliferation of Non-Small Cell Lung Cancer and Regulates the JNK Pathway. *Clin Exp Pharmacol Physiol* (2020) 47:135–42. doi: 10.1111/1440-1681.13183
34. Sheng Y, Wang W, Hong B, Jiang X, Sun R, Yan Q, et al. Upregulation of KIF20A Correlates With Poor Prognosis in Gastric Cancer. *Cancer Manage Res* (2018) 10:6205–16. doi: 10.2147/CMAR.S176147
35. Shen T, Yang L, Zhang Z, Yu J, Dai L, Gao M, et al. KIF20A Affects the Prognosis of Bladder Cancer by Promoting the Proliferation and Metastasis of Bladder Cancer Cells. *Dis Markers* (2019) 2019:4863182. doi: 10.1155/2019/4863182
36. Ren X, Chen X, Ji Y, Li L, Li Y, Qin C, et al. Upregulation of KIF20A Promotes Tumor Proliferation and Invasion in Renal Clear Cell Carcinoma and is Associated With Adverse Clinical Outcome. *Aging* (2020) 12:25878–94. doi: 10.18632/aging.202153
37. Nakamura M, Takano A, Thang PM, Tsevegjav B, Zhu M, Yokose T, et al. Characterization of KIF20A as a Prognostic Biomarker and Therapeutic Target for Different Subtypes of Breast Cancer. *Int J Oncol* (2020) 57:277–88. doi: 10.3892/ijo.2020.5060
38. Lu M, Huang X, Chen Y, Fu Y, Xu C, Xiang W, et al. Aberrant KIF20A Expression Might Independently Predict Poor Overall Survival and Recurrence-Free Survival of Hepatocellular Carcinoma. *IUBMB Life* (2018) 70:328–35. doi: 10.1002/iub.1726
39. Liu SL, Lin HX, Qiu F, Zhang WJ, Niu CH, Wen W, et al. Overexpression of Kinesin Family Member 20a Correlates With Disease Progression and Poor Prognosis in Human Nasopharyngeal Cancer: A Retrospective Analysis of 105 Patients. *PloS One* (2017) 12:e0169280. doi: 10.1371/journal.pone.0169280
40. Li Y, Guo H, Wang Z, Bu H, Wang S, Wang H, et al. And KIF20A, FOXM1 Target Genes, Increase Proliferation and Invasion of Ovarian Cancer Cells. *Exp Cell Res* (2020) 395:112212. doi: 10.1016/j.yexcr.2020.112212
41. Saito K, Ohta S, Kawakami Y, Yoshida K, Toda M. Functional Analysis of KIF20A, a Potential Immunotherapeutic Target for Glioma. *J Neuro-oncol* (2017) 132:63–74. doi: 10.1007/s11060-016-2360-1
42. Zhu Z, Jin Z, Zhang H, Zhang M, Sun D. Knockdown of Kif20a Inhibits Growth of Tumors in Soft Tissue Sarcoma *In Vitro* and *In Vivo*. *J Cancer* (2020) 11:5088–98. doi: 10.7150/jca.44777
43. Yang C, Zhang Y, Lin S, Liu Y, Li W. Suppressing the KIF20A/NUAK1/Nrf2/GPX4 Signaling Pathway Induces Ferroptosis and Enhances the Sensitivity of Colorectal Cancer to Oxaliplatin. *Aging* (2021) 13:13515–34. doi: 10.18632/aging.202774
44. Yu H, Xu Z, Guo M, Wang W, Zhang W, Liang S, et al. FOXM1 Modulates Docetaxel Resistance in Prostate Cancer by Regulating KIF20A. *Cancer Cell Int* (2020) 20:545. doi: 10.1186/s12935-020-01631-y
45. Xiu G, Sui X, Wang Y, Zhang Z. FOXM1 Regulates Radiosensitivity of Lung Cancer Cell Partly by Upregulating KIF20A. *Eur J Pharmacol* (2018) 833:79–85. doi: 10.1016/j.ejphar.2018.04.021
46. Bertolin G, Tramier M. Insights Into the Non-Mitotic Functions of Aurora Kinase A: More Than Just Cell Division. *Cell Mol Life Sci CMLS* (2020) 77:1031–47. doi: 10.1007/s00018-019-03310-2
47. Du R, Huang C, Liu K, Li X, Dong Z. Targeting AURKA in Cancer: Molecular Mechanisms and Opportunities for Cancer Therapy. *Mol Cancer* (2021) 20:15. doi: 10.1186/s12943-020-01305-3
48. Zhou X, Wang P, Zhao H. The Association Between AURKA Gene Rs2273535 Polymorphism and Gastric Cancer Risk in a Chinese Population. *Front Physiol* (2018) 9:1124. doi: 10.3389/fphys.2018.01124
49. Yen CC, Chen SC, Hung GY, Wu PK, Chua WY, Lin YC, et al. Expression Profile–Driven Discovery of AURKA as a Treatment Target for Liposarcoma. *Int J Oncol* (2019) 55:938–48. doi: 10.3892/ijo.2019.4861
50. Yang Y, Ding L, Zhou Q, Fen L, Cao Y, Sun J, et al. Silencing of AURKA Augments the Antitumor Efficacy of the AURKA Inhibitor MLN8237 on Neuroblastoma Cells. *Cancer Cell Int* (2020) 20:9. doi: 10.1186/s12935-019-1072-y
51. Xie Y, Zhu S, Zhong M, Yang M, Sun X, Liu J, et al. Inhibition of Aurora Kinase A Induces Necroptosis in Pancreatic Carcinoma. *Gastroenterology* (2017) 153:1429–1443.e5. doi: 10.1053/j.gastro.2017.07.036
52. Wang-Bishop L, Chen Z, Gomaa A, Lockhart AC, Salaria S, Wang J, et al. Inhibition of AURKA Reduces Proliferation and Survival of Gastrointestinal Cancer Cells With Activated KRAS by Preventing Activation of RPS6KB1. *Gastroenterology* (2019) 156:662–675.e7. doi: 10.1053/j.gastro.2018.10.030
53. Wang B, Hsu CJ, Chou CH, Lee HL, Chiang WL, Su CM, et al. Variations in the AURKA Gene: Biomarkers for the Development and Progression of Hepatocellular Carcinoma. *Int J Med Sci* (2018) 15:170–5. doi: 10.7150/ijms.22513
54. Park JW, Cho H, Oh H, Kim JY, Seo SB. AURKA Suppresses Leukemic THP-1 Cell Differentiation Through Inhibition of the KDM6B Pathway. *Mol Cells* (2018) 41:444–53. doi: 10.14348/molcells.2018.2311
55. Li T, Chen Y, Zhang J, Liu S. LncRNA TUG1 Promotes Cells Proliferation and Inhibits Cells Apoptosis Through Regulating AURKA in Epithelial Ovarian Cancer Cells. *Medicine* (2018) 97:e12131. doi: 10.1097/MD.0000000000012131
56. Lee JW, Parameswaran J, Sandoval-S3.33chaefer T, Eoh KJ, Yang DH, Zhu F, et al. (AURKA) and WEE1 Inhibition Demonstrates Synergistic Antitumor Effect in Squamous Cell Carcinoma of the Head and Neck. *Clin Cancer Res* (2019) 25:3430–42. doi: 10.1158/1078-0432.CCR-18-0440
57. Kivinummi K, Urbanucci A, Leinonen K, Tammela TLJ, Annala M, Isaacs WB, et al. The Expression of AURKA is Androgen Regulated in Castration-Resistant Prostate Cancer. *Sci Rep* (2017) 7:17978. doi: 10.1038/s41598-017-18210-3
58. Guo M, Lu S, Huang H, Wang Y, Yang MQ, Yang Y, et al. Increased AURKA Promotes Cell Proliferation and Predicts Poor Prognosis in Bladder Cancer. *BMC Syst Biol* (2018) 12:118. doi: 10.1186/s12918-018-0634-2
59. Gomaa A, Peng D, Chen Z, Soutto M, Abouelezz K, Corvalan A, et al. Epigenetic Regulation of AURKA by miR-4715-3p in Upper Gastrointestinal Cancers. *Sci Rep* (2019) 9:16970. doi: 10.1038/s41598-019-53174-6
60. Galusic D, Lucijanic M, Livun A, Radman M, Blaslov V, Vicelic Cutura L, et al. And PLK1 Expression are Associated With Inferior Overall Survival in Patients With Myelofibrosis. *Blood Cells Mol Dis* (2020) 81:102396. doi: 10.1016/j.bcmd.2019.102396
61. Dawei H, Honggang D, Qian W. AURKA Contributes to the Progression of Oral Squamous Cell Carcinoma (OSCC) Through Modulating Epithelial-to-Mesenchymal Transition (EMT) and Apoptosis *via* the Regulation of ROS. *Biochem Biophys Res Commun* (2018) 507:83–90. doi: 10.1016/j.bbrc.2018.10.170
62. Shan B, Zhao R, Zhou J, Zhang M, Qi X, Wang T, et al. AURKA Increase the Chemosensitivity of Colon Cancer Cells to Oxaliplatin by Inhibiting the

TP53-Mediated DNA Damage Response Genes. *BioMed Res Int* (2020) 2020:8916729. doi: 10.1155/2020/8916729

Conflict of Interest: The authors declare that the research was conducted in the absence of any commercial or financial relationships that could be construed as a potential conflict of interest.

Publisher's Note: All claims expressed in this article are solely those of the authors and do not necessarily represent those of their affiliated organizations, or those of the publisher, the editors and the reviewers. Any product that may be evaluated in this article, or claim that may be made by its manufacturer, is not guaranteed or endorsed by the publisher.

frontiers | Frontiers in Oncology

ORIGINAL RESEARCH
published: 08 July 2022
doi: 10.3389/fonc.2022.769895

Clinical Impact of the Histopathological Index and Neuroimaging Features Status in Primary Central Nervous System Diffuse Large B-Cell Lymphoma: A Single-Center Retrospective Analysis of 51 Cases

Zhou Qi[1], Lei Duan[1], Guoqiang Yuan[1], Jianli Liu[1,2], Jian Li[1], Guoqiang Li[1], Yue Yu[1], Yanlong Xu[1], Shangxian Ma[1], Yawen Pan[1†] and Yinian Zhang[3*†]*

[1] Department of Neurosurgery, Key Laboratory of Neurology, Gansu Province, Lanzhou University Second Hospital, Lanzhou, China, [2] Department of Medical Imaging, Lanzhou University Second Hospital, Lanzhou, China, [3] Neurosurgery center of Zhujiang Hospital of Southern Medical University, Guangzhou, China

OPEN ACCESS

Edited by:
Liam Chen,
University of Minnesota, United States

Reviewed by:
Yujie Chen,
Army Medical University, China
Shigeo Ohba,
Fujita Health University, Japan

***Correspondence:**
Yinian Zhang
ery_zhangyinian@lzu.edu.cn
Yawen Pan
panyawen666@sohu.com

†These authors have contributed equally to this work

Specialty section:
This article was submitted to Neuro-Oncology and Neurosurgical Oncology, a section of the journal Frontiers in Oncology

Received: *02 September 2021*
Accepted: *15 June 2022*
Published: *08 July 2022*

Citation:
Qi Z, Duan L, Yuan G, Liu J, Li J, Li G, Yu Y, Xu Y, Ma S, Pan Y and Zhang Y (2022) Clinical Impact of the Histopathological Index and Neuroimaging Features Status in Primary Central Nervous System Diffuse Large B-Cell Lymphoma: A Single-Center Retrospective Analysis of 51 Cases. Front. Oncol. 12:769895. doi: 10.3389/fonc.2022.769895

Primary central nervous system diffuse large B-cell lymphoma (PCNS-DLBCL) is an uncommon non-Hodgkin lymphoma subtype, and its clinical and pathological characteristics remain unclear. PCNS-DLBCL patient data were retrospectively evaluated to determine clinical and pathological characteristics and prognostic factors. Furthermore, prognoses were calculated by Kaplan–Meier and Cox regression models based on clinical observations. In total, 51 immunocompetent patients were enrolled. The median age was 55 (range, 16–82) years, and the male-to-female ratio was 3:2. Headache (n = 19; 37%) and the frontal lobe (n = 16; 31%) were the most common presenting symptom and location, respectively. The median follow-up was 33 (range, 3–86) months, and the median overall survival (OS) and progression-free survival (PFS) were 18 months [95% confidence interval (CI), 21.2–34.2] and 15 months (95% CI, 16.9–28.7), respectively. Ki-67, cluster of differentiation-3, and deep brain involvement were independent prognostic markers. Moreover, multifocal lesions and deep brain involvement were unfavorable independent prognostic markers for PFS. This study indicates that targeted drug development for adverse prognostic factors is possible and provides guidance for clinical treatment decision-making.

Keywords: primary central nervous system diffuse large B-cell lymphoma, pathological feature, survival rates, radiological features, molecular marker

Abbreviations: PCNS-DLBCL, primary central nervous system diffuse large B-cell lymphoma; OS, overall survival; PFS, progression-free survival, EOR, extent of resection; GTR, gross of resection.

INTRODUCTION

Diffuse large B-cell lymphoma (DLBCL) is the most common lymphoma subtype, accounting for 30%–40% of adult non-Hodgkin lymphoma diagnoses. Primary central nervous system diffuse large B-cell lymphoma (PCNS-DLBCL) is a rare subtype of B-cell lymphoma (BCL), representing <1% of all non-Hodgkin lymphomas (1). Moreover, the World Health Organization (WHO) classifies PCNS-DLBCL as a distinct entity of hematolymphoid tumors. PCNS-DLBCL mainly occurs among the elderly, especially those over the age of 60.

Over previous decades, the incidence of primary central nervous system lymphoma (PCNSL) has increased markedly in immunocompetent patients for unknown reasons, whereas the incidence of human immunodeficiency virus (HIV)-associated PCNSLs has declined, possibly due to the development of highly active antiretroviral therapies (2, 3). Recently, clinical trials with DLBCL patients have explored the prognostic effect and interdependence of the cell-of-origin (COO) classification and Hans algorithm, dual expression of MYC and BCL-2 proteins, and MYC, BCL-2, and BCL-6 translocations (4) using complementary DNA microarrays and immunohistochemical staining with various markers, including a cluster of differentiation (CD)10, BCL-6, and multiple myeloma-1/interferon regulatory factor-4 (MUM-1).

Previous studies have identified two DLBCL subtypes using the Hans algorithm: germinal center B-cell-like (GCB) and non-GCB (5–8). Many studies have also suggested that the clinical features of PCNS-DLBCL are particularly relevant. Thus, this study aimed to confirm the prognostic factors of PCNS-DLBCL by Kaplan–Meier and Cox regression models.

METHODS

Patients

All patients received surgical treatment between January 2012 and February 2021. Patients with HIV and immunodeficiency diseases were excluded. Clinical data were obtained from the medical records and follow-up, including sex, age, clinical symptoms, symptom duration, tumor location, laboratory reports, operative findings, and adjuvant therapy strategy. The PCNS-DLBCL diagnosis required microscopic and immunohistochemical evidence and was identified by two experienced neuropathologists (CD and LD) with no knowledge of the patient's clinical status. The same neuropathologists reexamined the tumor samples using the 2007 WHO classification guidelines (8).

Demographic and Clinical Data

Demographic and clinical data were retrospectively collected from patients' medical records. The location, number of lesions, tumor size, and deep brain involvement were evaluated using magnetic resonance imaging.

Histological Reexamination and Immunohistochemical Staining

Tissue specimens were fixed in a 10% buffered formaldehyde solution and embedded in paraffin wax. All specimens were cut into 3-mm-thick sections and stained with hematoxylin and eosin following the standard protocol. Specimens were also stained with periodic acid–Schiff with and without diastase, mucicarmine, and alcian blue (pH 2.5).

Immunohistochemical staining was performed using the Envision technique with monoclonal antibodies against CD20 (1:200), BCL-2 (1:100), BCL-6 (1:100), C-MYC (1:100), Ki-67 (1:100), CD3 (1:100), CD10 (1:100), and MUM-1 (1:100). All antibodies were obtained from Proteintech (Wuhan, China). Appropriate positive and negative controls for each antibody were run in parallel. Two observers jointly evaluated the immunohistochemical reactions that were descriptively evaluated according to the cellular compartment and cellular population expression of protein and used the cutoff values of > 0% and > 20% of neoplastic cells expressing CD20, BCL-2, BCL-6, C-MYC, Ki-67, CD3, CD10, and MUM-1 to determine positivity for these markers. The MIB-1 labeling index was calculated in regions of maximal activity and expressed as the percentage of stained nuclear area.

Outcome Data

Follow-up data were obtained from patient records or by telephone. Progression-free survival (PFS) and overall survival (OS) were the primary endpoints. The last follow-up day was 8 February 2021. OS was assessed from the first diagnosis date until the date of the last follow-up or death. PFS was calculated from the date of the first diagnosis to the date of progression, relapse, death, or last contact.

Ethics Committee Approval

The surgical procedures and clinical follow-up were conducted under the guidelines and terms of all relevant local legislation and received approval from the Lanzhou University Second Hospital's ethics committee (number 2021A-524). All patients signed informed consent before the operation.

Statistical Analyses

The potential prognostic factors were age, sex, lactate dehydrogenase (LDH) level, tumor size, number of lesions, the extent of resection, histopathology, immunohistochemistry, and survival rates or progression rates and analyzed by the Kaplan–Meier method. All variables with a p-value of <0.10 in the univariate analysis were included in the Cox proportional hazards multivariate analysis, used to further investigate the prognostic factor relationships. The chi-squared test was used to compare the survival rate differences among PCNS-DLBCL patients with and without GCB. Bivariate associations between survival or recurrence and the prognostic factors were tested using the log-rank test. All differences were considered statistically significant at a p-value of <0.05. Statistical analyses were performed using SPSS for Windows (version 18.0; IBM SPSS Statistics, IBM Corporation, Armonk, NY, USA).

RESULTS

Supplementary Table S1 and **Table 1** summarize patient clinical information. The study included 30 men and 21 women with a median age of 55.0 (range, 16–82) years; three patients were aged

TABLE 1 | Initial presentations of the 51 PCNS-DLBCL patients at diagnosis.

Presentation	n=51 (%)
Headache	19 (37.2%)
Dizziness	17 (33.3%)
Motor symptoms	16 (31.3%)
Visual symptoms	12 (23.5%)
Hemiplegia and aphasia	10 (19.6%)
Incidental	5 (9.8%)
Cognitive symptoms	4 (7.8%)
Epilepsy	4 (7.8%)
Decreased consciousness	3 (5.8%)
Nausea/vomiting	3 (5.8%)

<18 years upon initial diagnosis. The most common presenting symptom was headache (n = 19). Other presenting symptoms included motor symptoms (n = 16), vision loss (n = 12), epilepsy (n = 3), hemiplegia (n =10, aphasia (n = 10), and cognitive symptoms (n = 4). The main postoperative complication was venous thrombosis of the lower extremities.

Table 2 presents the tumor characteristics. At the initial operation, the tumors occurred in different locations, including the frontal lobe (n = 16), temporal lobe (n = 9), parietal lobe (n = 9), occipital lobe (n = 5), ventricular region (n = 10), basal ganglia and thalamus (n = 4), cerebellopontine angle area (n = 3), cerebellum (n = 3), brainstem (n = 2), and pineal gland (n = 2). Notably, the tumor in case number 47 was in the hypothalamus. There were 17 cases with multifocal lesions and deep brain involvement, involving important structures such as the lateral ventricle, basal ganglia, thalamus, and hippocampus (**Figures 1A–H**). At the same time, we also found that two cases were very special; patient 1 is the youngest reported case of PCNS-DLBCL, and patients 1 and 2 were of great clinical value and significance in analysis, diagnosis, and differential diagnosis of PCNS-DLBCL (**Figures 2A–D**). The tumors ranged from 15 to 150 mm (median, 60 mm) in maximal diameter. In total, 31 (61%) patients underwent gross total resection, and 20 patients (39%) underwent stereotactic biopsy.

Histology and Immunohistochemistry

We obtained specimens from 51 PCNS-DLBCL patients. Histopathological examination revealed tumor tissue composed of lymphoid cells with irregular morphology. The tumor cells displayed abundant eosinophilic cytoplasm, frequent mitoses, and necrotic foci. Most tumor tissues were accompanied by the proliferation of small blood vessels. Furthermore, some lymphoid cells around the blood vessels had apparent proliferation, forming the "cuff" and "starry sky" phenomena. Reed–Sternberg cells were also found in a small number of tumor tissues (**Figure 2A**). All 51 PCNS-DLBCL patients met the 2007 WHO diagnostic criteria (9).

All 51 PCNS-DLBCL patients were identified in the pathology database. All were HIV negative and without an immunosuppressive disease. Furthermore, all patients were strongly positive for CD20 and CD79a, and neoplastic cells expressed pan-B-cell markers, such as CD20, CD79a, and paired box 5 (i.e., PAX5). Seventy percent (36/51) stained positively for MUM-1, 73% (37/51) stained positively for BCL-6, 57% (29/51) stained positively for BCL-2, 31% (16/51) stained positively for CD10, 49% (25/51) stained positively for CD3, and 18% (9/51) stained >90% positive for Ki-67. The Hans algorithm indicated that 32 cases (63%; 32/51) were non-GCB, and 19 (37%; 19/51) were GCB. Finally, 33% (17/51) had BCL-2 and C-MYC coexpression.

TABLE 2 | Mass location of the 51 PCNS-DLBCL patients (63 lesions) at diagnosis.

Location	n=63 (%)
Frontal lobe	16 (31.4%)
Parietal lobe	9 (17.6%)
Temporal lobe	9 (17.6%)
Occipital lobe	5 (9.8%)
Ventricular region	10 (19.6%)
Basal ganglia and thalamus	4 (7.8%)
Cerebellopontine angle	3 (5.9%)
Cerebellum	3 (5.9%)
Brainstem	2 (3.9%)
Pineal gland	2 (3.9%)

Treatments

All patients had available treatment information. No one received radiotherapy only as an initial treatment because diagnosing PCNS-DLBCL based on only imaging data (i.e., without pathological examination) is very difficult. Moreover, no one received chemotherapy only as an initial treatment or autologous stem cell transplantation. Of those who received postoperative chemotherapy, all received high-dose methotrexate (HD-MTX ≥3.5 g/m2). When their diagnosis was not clear, two patients (4%) received rituximab, and another two patients received treatment options included rituximab and cyclophosphamide, Adria MYC, vincristine, and prednisone (i.e., CHOP)-like regimens as part of their initial therapy, but when their diagnosis was established, HD-MTX therapy was performed.

Prognostic Factors and Overall Survival

All patients had sufficient follow-up data for the analysis. The median follow-up was 33 (range, 3–86) months, and the median OS was 18.0 months [95% confidence interval (CI), 21.2–34.2]. The 1-, 3-, and 5-year OS probability rates were 75% (95% CI, 71–79), 31% (95% CI, 27–35), and 12% (95% CI, 8–15), respectively. **Table 3** summarizes the independent univariate analyses performed for each potential prognostic factor. Ki-67 positivity >90% (p = 0.001), CD3 positivity (p = 0.002), tumor size >5 cm (p = 0.003), less than two lesions (p = 0.029), AB blood type (p = 0.011), BCL-2 and C-MYC coexpression (p = 0.036), and deep brain involvement (p = 0.017) were significantly related to a worse OS (**Figures 3A, C, D, G**, **4A, C**). Patients with gross total resection (GTR) had a greater median OS (32 months; 95% CI, 16.5–47.4) than those with residual tumor after surgery (30 months; 95% CI, 16.2–43.7; p = 0.292). Cox regression analyses revealed that Ki-67 and CD3 were independent prognostic factors for improved OS [Ki-67: p = 0.001, hazard ratio (HR) = 0.135, 95% CI, 0.045–0.411; CD3: p = 0.004, HR = 3.697; 95% CI, 1.145–11.940].

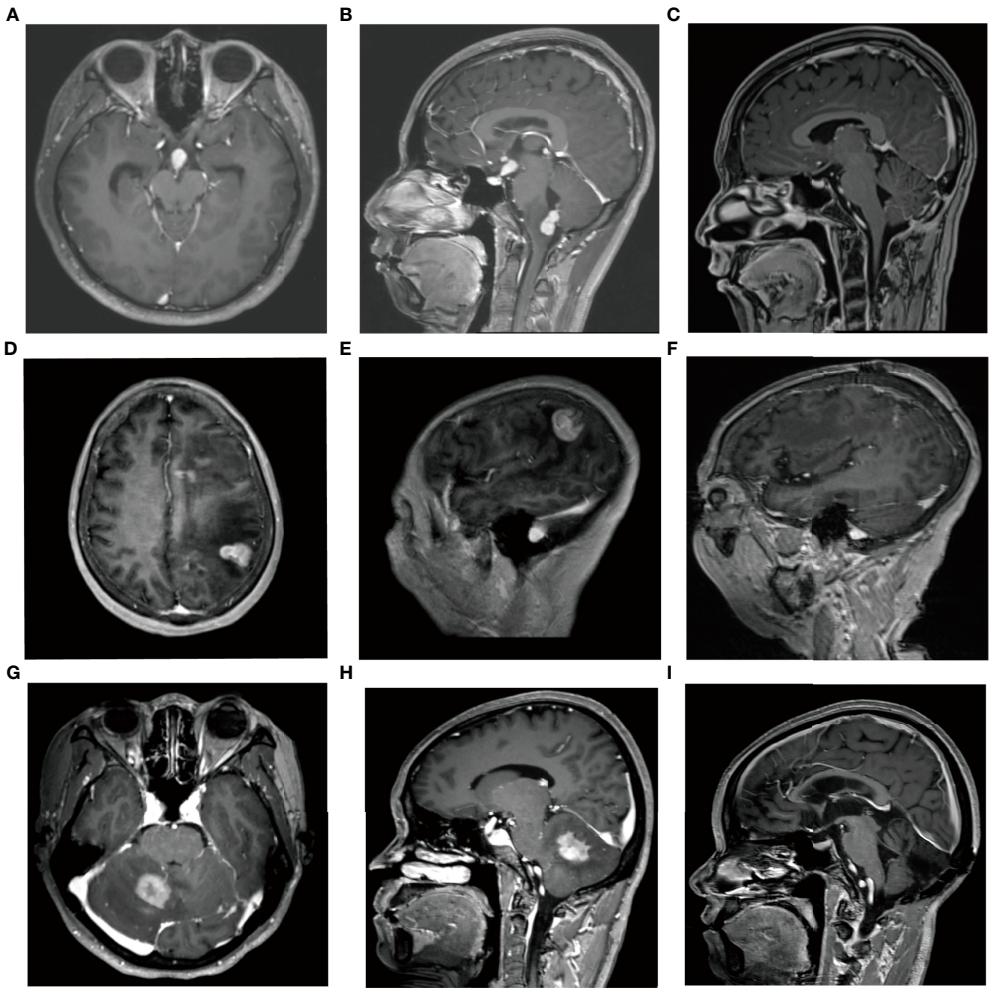

FIGURE 1 | Case 1, male, 16 years old. **(A, B)** MRI-enhanced images showed homogeneous enhancement of tumors in the dorsal side of the brainstem, around the fourth ventricle, and in the pineal region. **(C)** Postoperative MRI showed gross total resection of brainstem lesions. **(D, E)** Case 2, female, 52 years old. Sagittal-enhanced images showed significantly enhanced tumor masses in the left parietal lobe. **(F)** The tumor was totally resected. **(G, H)** Case 38, female, 48 years old, right cerebellar hemisphere aera displayed homogeneous enhancement. **(I)** Postoperative MRI revealed surgery combined with radiotherapy and chemotherapy obtained a good therapeutic effect.

Prognostic Factors and Progression-Free Survival

At the final follow-up, 37 patients experienced progression, defined as aggravation, recurrence, and death. The median PFS was 17.0 months (95% CI, 13.6–20.4). Progression occurred in 18 of 30 male PCNS-DLBCL patients and 18 of 21 female PCNS-DLBCL patients. Men with PCNS-DLBCL had an 18.7% 5-year PFS rate, and women had a rate of 6.8%, but log-rank tests indicated no association between sex and PFS ($p = 0.167$). Progression occurred in 26 of 36 PCNS-DLBCL patients younger than 60 and 11 of 15 PCNS-DLBCL patients over 60. Patients younger than 60 had a 14.4% 5-year PFS rate, and patients older than 60 had a 22.5% rate, but age and PFS were also not associated (log-rank test; $p = 0.281$).

Progression occurred in 7 of 9 (77.7%) PCNS-DLBCL patients with Ki-67 positivity >90% and 12 of 42 (28.5%) with Ki-67 positivity <90%. Those with Ki-67 positivity >90% had a 0% 5-year PFS rate, and those with Ki-67 positivity <90% had a 19.5% rate. Log-rank tests indicated a significant relationship between Ki-67 and PFS ($p = 0.001$).

Progression occurred in 8 of 25 (32%) PCNS-DLBCL patients with CD3 positivity and 6 of 26 (23%) with CD3 negativity. CD3-positive patients had a 30% 5-year PFS rate, but CD3-negative patients had a 0% rate; CD3 and PFS were significantly associated (log-rank test; $p = 0.007$).

Progression occurred in 10 of 34 (29.4%) PCNS-DLBCL patients with less than two lesions and 4 of 17 patients (23.5%) with more than two lesions. Patients with less than two lesions had a 19% 5-year PFS rate, and patients with more than two lesions had a 0% rate; the lesion number and PFS were significantly associated (log-rank test; $p = 0.024$).

Progression occurred in 8 of 31 (25.8%) PCNS-DLBCL patients receiving GTR and 6 of 20 (30.0%) patients receiving

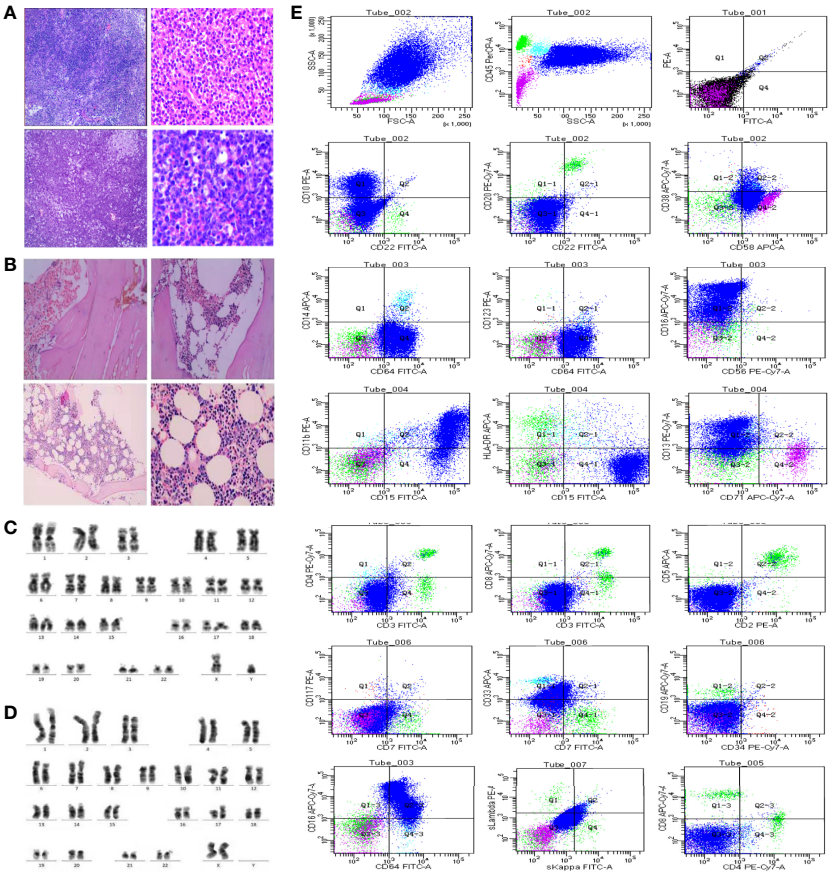

FIGURE 2 | **(A)** HE staining pictures of patients 1 and 2. The above two pictures show patient 1; the bottom two pictures show patient 2 (left: 10×10, right: 10×40). **(B)** Histopathological examination of the bone marrow of patients 1 and 2: the above two pictures showed patient 1; the bottom two picture showed patient 2. **(C, D)** Chromosome karyotype analysis of the two patients. **(E)** Flow cytometry analysis showed that lymphocytes accounted for 9.5% of nuclear cells, and the proportion decreased in patient 1. The proportion of B lymphocytes increased. However, no obvious light chain restriction was found. Primitive region cells account for about 0.5% of nuclear cells.

partial excision. Patients with GTR had a 20.3% 5-year PFS rate, and patients receiving partial excision had a 5% rate. Importantly, PCNS-DLBCL patients with BCL-2 and C-MYC coexpression had a 0% 5-year PFS rate, whereas patients with BCL or C-MYC expression had a 20% rate. Ki-67 positivity >90% ($p = 0.001$), CD3 positivity ($p = 0.007$), two or more lesions ($p = 0.024$), BCL-2 and C-MYC coexpression ($p = 0.019$), partial excision ($p = 0.051$), and deep brain involvement ($p = 0.004$) were significantly associated with worse PFS (**Figures 3B, E, F, H**, **4B, D**). **Table 4** summarizes the other factors.

DISCUSSION

The fifth edition of the WHO Classification of Tumors of the Central Nervous System (CNS), published in 2021, has emphasized molecular diagnostics for CNS tumor classification (10). This study investigated the role of clinicopathological features and molecular diagnostic factors in predicting patient prognosis. We found seven prognostic factors that significantly correlated with OS and six that significantly related to PFS. We also found that BCL-2 and C-MYC coexpression can act as a hazard factor of PCNS-DLBCL, and smaller tumors had shortened survival times. Deep tumor involvement or multifocal lesions were also significantly associated with OS and PFS, and CD3 was related to good PCNS-DLBCL outcomes as a T-cell marker. Together, these results suggest that molecular pathological diagnosis may play a vital role in the prognosis of PCNS-DLBCL patients.

In our study, more PCNS-DLBCL patients were <60 years old, contrary to a previous study (11) that reported a median age at PCNSL diagnosis of 66 years. Occurrence in children is very rare. However, in our series, one patient (1/51) was younger than 18 years old upon initial diagnosis, and the age of 16 was the youngest case of PCNS-DLBCL found in China.

In our study, the smaller the tumor, the shorter the survival time. It is possible that the tumor tissue was deep, which may destroy the deep brain conduction bundle, leading to a considerably shorter survival time and higher recurrence risk. At the same time, deep brain involvement was an independent

TABLE 3 | Univariate and multivariate analyses of risk factors for overall survival.

Prognostic factor		Univariate analysis		Multivariate analysis	
		No (%n=51)	p-value (log-rank test)	p-value (cox regression)	Relative risk (95% CI)
Gender	Female	21 (41.2%)	0.297		
	Male	30 (58.8%)			
Age	≥60	15 (29.4%)	0.362		
	<60	36 (70.6%)			
Ki-67	≥90%	9 (17.6%)	<0.001	0.001	0.176 (0.061–0.505)
	<90%	42 (82.4%)			
Bcl-2	Positive	29 (56.8%)	0.538		
	Negative	22 (43.2%)			
C-myc	Positive	28 (54.9%)	0.203		
	Negative	23 (45.1%)			
Bcl-6	Positive	37 (72.5%)	0.456		
	Negative	14 (27.5%)			
MUM-1	Positive	36 (70.5%)	0.292		
	Negative	15 (29.5%)			
CD3	Positive	25 (49.1%)	0.002	0.004	3.490 (1.498–8.831)
	Negative	26 (50.9%)			
CD10	Positive	16 (31.3%)	0.817		
	Negative	35 (68.7%)			
HANS	GCB	19 (37.2%)	0.955		
	NGCB	32 (62.8%)			
Size	≤2cm	4 (7.8%)	0.003	0.069	0.356 (0.139–0.910)
	2–5cm	38 (74.5%)			
	>5cm	9 (17.7%)			
Number of lesions	1	34 (66.6%)	0.029	0.255	1.496 (0.449–4.981)
	≥2	17 (33.4%)			
EOR	GTR	31 (60.7%)	0.391	0.705	1.377 (0.458–4.135)
	PR	20 (39.3%)			
Blood type	A+	17 (33.3%)	0.011	0.298	1.071 (0.721–1.592)
	B+	19 (37.2%)			
	AB+	5 (9.8%)			
	O+	10 (19.7%)			
LDH	≤215U/L	36 (70.5%)	0.839		
	>215U/L	36 (29.5%)			
BCL-2 and C-myc	co-expression	17 (33.3%)	0.036	0.626	0.642 (0.108–3.816)
	one-expression	34 (66.6%)			
KPS score	>70	31(60.8%)	0.988		
	≤70	20(39.2%)			
Deep brain involment	present	20 (39.2%)	0.017	0.090	0.560 (0.152–2.061)
	absent	31 (60.8%)			

GCB, germinal center B cell; LDH, lactate dehydrogenase, EOR, extent of resection; GTR, gross total resection; PR, partial resection.

risk factor in multivariate analysis, but another study reported no difference in deep brain involvement between patients with and without recurrence (12). It is generally believed that PCNS-DLBCL is highly sensitive to chemotherapy and radiotherapy, and surgical treatment is limited to diagnostic biopsies. However, in our study, the extent of resection may correlate with PFS. Technical advances in neurosurgery have increased the safety of PCNSL surgical resections (13, 14). Therefore, we propose reconsidering tumor removal to treat a single lesion amenable to resection.

The GCB-like DLBCL subtype has a better prognosis than the activated B-cell-like subtype (15, 16). It is well known that PCNS-DLBCL has a variety of molecular characteristics, and the primary factors closely related to prognosis are BCL-2/MYC double expression, BCL-2/C-MYC double aberrations (17), and BCL-6 rearrangements, which are often recognized using cytogenetic fluorescence *in situ* hybridization (FISH) studies (18). C-MYC/BCL-2 double-hit lymphoma has been recognized as a chromosomal break involving MYC and BCL-2, which is very rare, representing 3% of all DLBCL cases (19). In our series, 33% (17/51) of patients had C-MYC/BCL-2 coexpression, and coexpression was correlated with OS and PFS. C-MYC and BCL-2 have also been associated with resistance, a poor response to therapy, and a worse survival rate in PCNS-DLBCL patients (16, 20). We also found C-MYC/BCL-2 as a new predictive factor, correlating with survival time and occurrence independent of the COO subtype and Hans algorithm. In our study, 53% of cases had C-MYC expression, which was significantly lower than that reported by Gill et al. (73%) (21) and Brunn et al. (92%) (22). Additionally, the MYC FISH study provided crucial information for differentiating PCNS-DLBCL from other lymphoma subtypes. As a result, FISH staining should be performed as soon as possible to observe chromosomal site mutations (18).

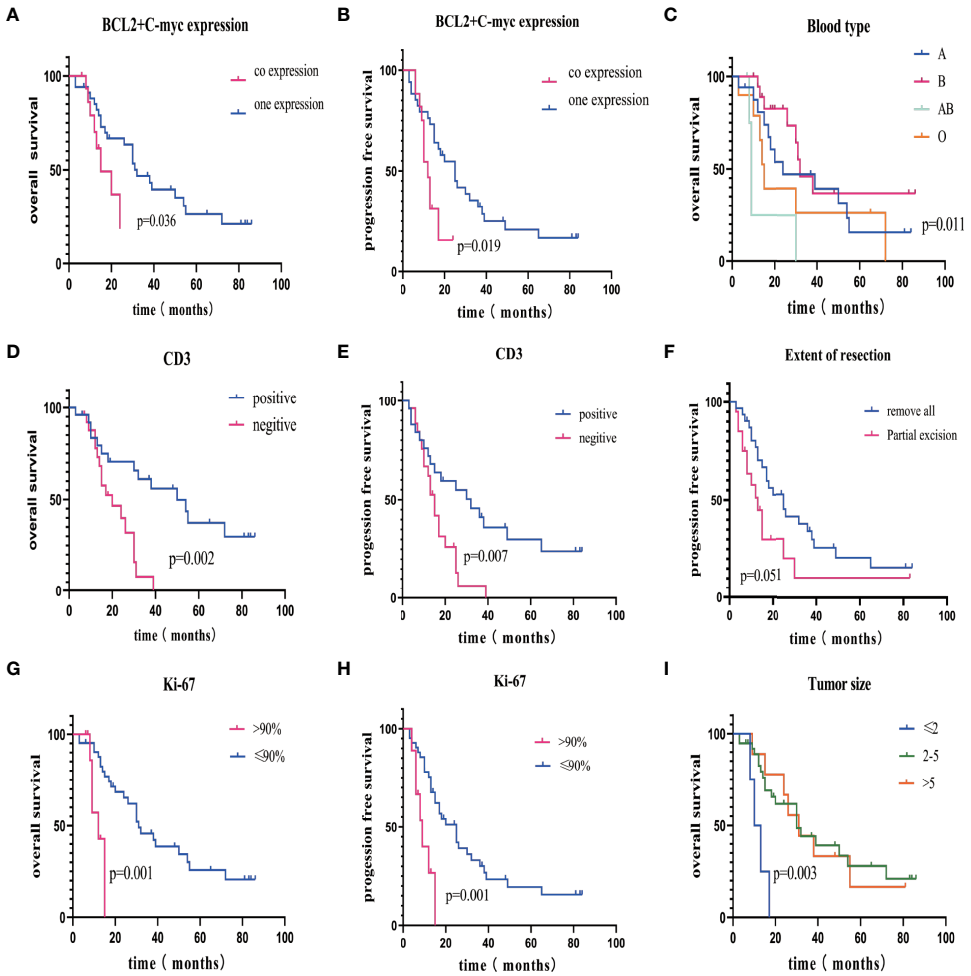

FIGURE 3 | Kaplan–Meier overall survival curve stratified by various risk factors. **(A)** OS in patients with BCL-2 and C-myc coexpression (red line) or one expression (blue line). **(B)** PFS in patients with positive C-myc combined with positive Bcl-2 (red line) or the other conditions (blue line). **(C)** OS in patients with different blood types, there was a significant difference in OS between different blood types. **(D, E)** OS/PFS in patients with positive CD3 (red line) or negative CD3(blue line). **(F)** PFS in patients with GTR (red line) and PR (blue line). **(G, H)** OS/PFS in patients with Ki-67 >90% (red line) or Ki-67 <90% (blue line). **(I)** OS in patients with different tumor size. PFS, progression-free survival; OS, overall survival.

Although some studies determined that MUM-1, CD10, and BCL-6 were favorable prognostic markers (23), other studies and ours did not find a correlation between these factors and prognosis (24, 25). As a T-cell marker, CD3-positive PCNS-DLBCL is very rare. In our cohort study, we found that CD3 positivity was associated with a significantly better median OS than CD3 negativity in univariate and multivariate analyses. Interestingly, blood type was a prognostic factor for OS in the univariate analysis. Thus, we are the first to demonstrate that blood types significantly correlate with the prognosis of PCNS-DLBCL. In our study, the AB blood type was the least represented, and type AB patients had the worst prognosis, which deserves further investigation. Multivariate analysis identified Ki-67 and CD3 as independent prognostic factors for survival time. Moreover, Ki-67, CD3, and deep brain involvement were independent prognostic factors for PFS.

Limitations

There are some limitations to this study. First, our study was a retrospective study; therefore, potential bias is inevitable. Second, the median follow-up time was not sufficiently long, <3 years in several cases. Third, the postoperative imaging data were not complete. Moreover, the small cohort in this study might not be well suited to an assessment of our treatment policy.

CONCLUSION

This retrospective study spanned 9 years and analyzed the demographic and clinicopathological features of PCNS-DLBCL patients.

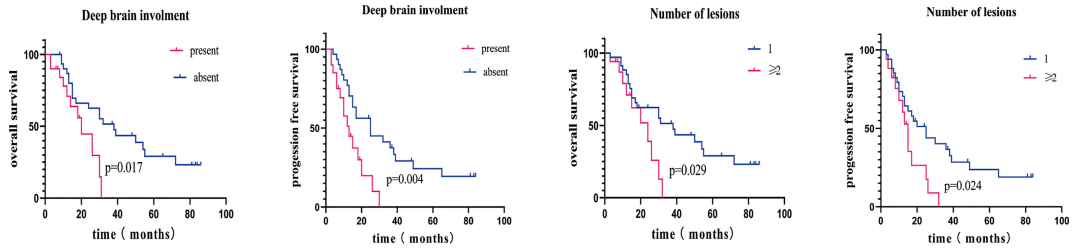

FIGURE 4 | Kaplan–Meier overall survival curve stratified by various risk factors. **(A, B)** OS and PFS in patients with deep brain involvement (red line) or absent deep brain involvement (blue line). **(C, D)** OS/PFS in patients with multifocal lesions (red line) or one lesion (blue line).

TABLE 4 | Univariate and multivariate analyses of risk factors for progression-free survival.

Prognostic factor		Univariate analysis		Multivariate analysis	
		No (%n=51)	p-value (log-rank test)	p-value (Cox regression)	Relative risk (95% CI)
Gender	Female	21 (41.2%)	0.167		
	Male	30 (58.8%)			
Age	≥60 years	15 (29.4%)	0.281		
	<60 years	36 (70.6%)			
Ki-67	≥90%	9 (17.6%)	0.001	0.005	0.256 (0.100–0.657)
	<90%	42 (82.4%)			
Bcl-2	Positive	29 (56.8%)	0.858		
	Negative	22 (43.2%)			
C-myc	Positive	28 (54.9%)	0.187		
	Negative	23 (45.1%)			
Bcl-6	Positive	37 (72.5%)	0.958		
	Negative	14 (27.5%)			
MUM-1	Positive	36 (70.5%)	0.097	0.441	0.925 (0.308–2.782)
	Negative	15 (29.5%)			
CD3	Positive	25 (49.1%)	0.007	0.009	2.591 (0.923–7.271)
	Negative	26 (50.9%)			
CD10	Positive	16 (31.3%)	0.548		
	Negative	35 (68.7%)			
HANS	GCB	19 (37.2%)	0.298		
	NGCB	32 (62.8%)			
Size	≤2cm	4 (7.8%)	0.086	0.442	0.765 (0.312–1.873)
	2~5cm	38 (74.5%)			
	>5cm	9 (17.7%)			
Number of lesions	1	34 (66.6%)	0.024		
	≥2	17 (33.4%)			
EOR	GTR	31 (60.7%)	0.051	0.088	1.926 (0.751–4.942)
	PR	20 (39.3%)			
Blood type	A+	17 (33.3%)	0.283		
	B+	19 (37.2%)			
	AB+	5 (9.8%)			
	0+	10 (19.7%)			
LDH level	≤215U/L	36 (70.5%)	0.929		
	>215U/L	15 (29.5%)			
BCL-2 and C-myc	Coexpression	17 (33.3%)	0.019	0.532	0.620 (0.133–2.898)
	One expression	34 (66.6%)			
KPS score	>70	31(60.8%)	0.543		
	≤70	20(39.2%)			
Deep brain involment	Present	20 (33.3%)	0.004	0.008	0.373 (0.179–0.775)
	Absent	31 (66.7%)			

GCB, germinal center B cell; LDH, lactate dehydrogenase, EOR, extent of resection; GTR, gross total resection; PR, partial resection.

For OS, CD3 positivity was an independent favorable prognostic factor, and Ki-67 positivity>0%, tumor size <2 cm, multifocal lesions, BCL-2 and C-MYC coexpression, and deep brain involvement were independent adverse prognostic factors.

For PFS, the extent of resection was an important prognostic factor. Therefore, we recommend GTR for a single lesion. Furthermore, Ki-67 positivity>0%, multifocal lesions, BCL-2 and C-MYC coexpression, and deep brain involvement were independent adverse prognostic factors. The diagnosis and differential diagnosis of PCNS-DLBCL are very difficult. Therefore, it is important to diagnose PCNS-DLBCL based on molecular characteristics and FISH staining. Furthermore, early postoperative chemotherapy and radiotherapy may play a vital role in preventing recurrence.

DATA AVAILABILITY STATEMENT

The original contributions presented in the study are included in the article/**Supplementary Material**. Further inquiries can be directed to the corresponding authors.

ETHICS STATEMENT

The studies involving human participants were reviewed and approved by the Lanzhou University Second Hospital's ethics committee. Written informed consent to participate in this study was provided by the participants' legal guardian/next of kin. Written informed consent was obtained from the minor(s)' legal guardian/next of kin for the publication of any potentially identifiable images or data included in this article.

AUTHOR CONTRIBUTIONS

Conception and design: ZQ. Acquisition of data: all authors. Analysis and interpretation of data: ZQ and YZ. Drafting the article: ZQ, LD, GY, JL, YP, and YZ. Critically revising the article: YZ. Reviewed submitted version of manuscript: ZQ and YZ. Approved the final version of the manuscript on behalf of all authors: YZ. Statistical analysis: ZQ. Study supervision: YZ. All authors contributed to the article and approved the submitted version.

FUNDING

This work was supported by the National Natural Science Foundation of China (81771297), Research Innovation Group Project of Gansu Province (21JR7RA432), and Gansu Province Health Industry Research Project (GSWSKY2018-01).

ACKNOWLEDGMENTS

We thank Professor Chi Dong and Professor Li Dong for providing patient information.

SUPPLEMENTARY MATERIAL

The Supplementary Material for this article can be found online at: https://www.frontiersin.org/articles/10.3389/fonc.2022.769895/full#supplementary-material

Supplementary Table S1 | Clinicopathological features of 51 primary PCNS-DLBCL cases.

REFERENCES

1. Schlegel U. Primary CNS Lymphoma. *Ther Adv Neurol Disord* (2009) 2 (2):93–104. doi: 10.1177/1756285608101222
2. Corn B, Marcus S, Topham A, Hauck W, Curran W. Will Primary Central Nervous System Lymphoma be the Most Frequent Brain Tumor Diagnosed in the Year 2000? *Cancer* (1997) 79(12):2409–13. doi: 10.1002/(SICI)1097-0142(19970615)79:12<2409::AID-CNCR17>3.0.CO;2-V
3. Kadan-Lottick N, Skluzacek M, Gurney J. Decreasing Incidence Rates of Primary Central Nervous System Lymphoma. *Cancer* (2002) 95(1):193–202. doi: 10.1002/cncr.10643
4. Staiger A, Ziepert M, Horn H, Scott D, Barth T, Bernd H, et al. Clinical Impact of the Cell-Of-Origin Classification and the MYC/ BCL2 Dual Expresser Status in Diffuse Large B-Cell Lymphoma Treated Within Prospective Clinical Trials of the German High-Grade Non-Hodgkin's Lymphoma Study Group. *J Clin Oncol* (2017) 35(22):2515–26. doi: 10.1200/JCO.2016.70.3660
5. Myklebust J, Brody J, Kohrt H, Kolstad A, Czerwinski D, Wälchli S, et al. Distinct Patterns of B-Cell Receptor Signaling in non-Hodgkin Lymphomas Identified by Single-Cell Profiling. *Blood* (2017) 129(6):759–70. doi: 10.1182/blood-2016-05-718494
6. Kurtz D, Scherer F, Jin M, Soo J, Craig A, Esfahani M, et al. Circulating Tumor DNA Measurements As Early Outcome Predictors in Diffuse Large B-Cell Lymphoma. *J Clin Oncol* (2018) 36(28):2845–53. doi: 10.1200/JCO.2018.78.5246
7. Merdan S, Subramanian K, Ayer T, Van Weyenbergh J, Chang A, Koff J, et al. Gene Expression Profiling-Based Risk Prediction and Profiles of Immune Infiltration in Diffuse Large B-Cell Lymphoma. *Blood Cancer J* (2021) 11(1):2. doi: 10.1038/s41408-020-00404-0
8. Hans C, Weisenburger D, Greiner T, Gascoyne R, Delabie J, Ott G, et al. Confirmation of the Molecular Classification of Diffuse Large B-Cell Lymphoma by Immunohistochemistry Using a Tissue Microarray. *Blood* (2004) 103(1):275–82. doi: 10.1182/blood-2003-05-1545
9. Grimm K, O'Malley D. Aggressive B Cell Lymphomas in the 2017 Revised WHO Classification of Tumors of Hematopoietic and Lymphoid Tissues. *Ann Diagn Pathol* (2019) 38:6–10. doi: 10.1016/j.anndiagpath.2018.09.014
10. Louis DN, Perry A, Wesseling P, Brat DJ, Cree IA, Figarella-Branger D, et al. The 2021 WHO Classification of Tumors of the Central Nervous System: A Summary. *Neuro Oncol* (2021) 23(8):1231–51. doi: 10.1093/neuonc/noab106
11. Grommes C, DeAngelis LM. Primary CNS Lymphoma. *J Clin Oncol* (2017) 35 (21):2410–8. doi: 10.1200/JCO.2017.72.7602
12. Yuan X, Huang Y, Yu T, Xu Y, Liang Y, Zhang X, et al. Primary Central Nervous System Lymphoma in China: A Single-Center Retrospective Analysis of 167 Cases. *Ann Hematol* (2020) 99(1):93–104. doi: 10.1007/s00277-019-03821-9

13. Cloney MB, Sonabend AM, Yun J, Yang J, Iwamoto F, Singh S, et al. The Safety of Resection for Primary Central Nervous System Lymphoma: A Single Institution Retrospective Analysis. *J Neurooncol* (2017) 132(1):189–97. doi: 10.1007/s11060-016-2358-8
14. Yun J, Yang J, Cloney M, Mehta A, Singh S, Iwamoto FM, et al. Assessing the Safety of Craniotomy for Resection of Primary Central Nervous System Lymphoma: A Nationwide Inpatient Sample Analysis. *Front Neurol* (2017) 8:478. doi: 10.3389/fneur.2017.00478
15. Alizadeh AA, Eisen MB, Davis RE, Ma C, Lossos IS, Rosenwald A, et al. Distinct Types of Diffuse Large B-Cell Lymphoma Identified by Gene Expression Profiling. *Nature* (2000) 403(6769):503–11. doi: 10.1038/35000501
16. Rosenwald A, Wright G, Chan WC, Connors JM, Campo E, Fisher RI, et al. The Use of Molecular Profiling to Predict Survival After Chemotherapy for Diffuse Large-B-Cell Lymphoma. *N Engl J Med* (2002) 346(25):1937–47. doi: 10.1056/NEJMoa012914
17. Yin W, Xia X, Wu M, Yang H, Zhu X, Sun W, et al. The Impact of BCL-2/MYC Protein Expression and Gene Abnormality on Primary Central Nervous System Diffuse Large B-Cell Lymphoma. *Int J Clin Exp Pathol* (2019) 12 (6):2215–23.
18. Swerdlow S. Diagnosis of 'Double Hit' Diffuse Large B-Cell Lymphoma and B-Cell Lymphoma, Unclassifiable, With Features Intermediate Between DLBCL and Burkitt Lymphoma: When and How, FISH Versus IHC. *Hematol Am Soc Hematol Educ Program* (2014) 2014(1):90–9. doi: 10.1182/asheducation-2014.1.90
19. Hu S, Xu-Monette ZY, Tzankov A, Green T, Wu L, Balasubramanyam A, et al. MYC/BCL2 Protein Coexpression Contributes to the Inferior Survival of Activated B-Cell Subtype of Diffuse Large B-Cell Lymphoma and Demonstrates High-Risk Gene Expression Signatures: A Report From The International DLBCL Rituximab-CHOP Consortium Program. *Blood* (2013) 121(20):4021–31. doi: 10.1182/blood-2012-10-460063
20. Akyurek N, Uner A, Benekli M, Barista I. Prognostic Significance of MYC, BCL2, and BCL6 Rearrangements in Patients With Diffuse Large B-Cell Lymphoma Treated With Cyclophosphamide, Doxorubicin, Vincristine, and Prednisone Plus Rituximab. *Cancer* (2012) 118(17):4173–83. doi: 10.1002/cncr.27396
21. Gill KZ, Iwamoto F, Allen A, Hoehn D, Murty VV, Alobeid B, et al. MYC Protein Expression in Primary Diffuse Large B-Cell Lymphoma of the Central Nervous System. *PLoS One* (2014) 9(12):e114398. doi: 10.1371/journal.pone.0114398
22. Brunn A, Nagel I, Montesinos-Rongen M, Klapper W, Vater I, Paulus W, et al. Frequent Triple-Hit Expression of MYC, BCL2, and BCL6 in Primary Lymphoma of the Central Nervous System and Absence of a Favorable MYC(low)BCL2 (Low) Subgroup may Underlie the Inferior Prognosis as Compared to Systemic Diffuse Large B Cell Lymphomas. *Acta Neuropathol* (2013) 126(4):603–5. doi: 10.1007/s00401-013-1169-7
23. Levy O, Deangelis LM, Filippa DA, Panageas KS, Abrey LE. Bcl-6 Predicts Improved Prognosis in Primary Central Nervous System Lymphoma. *Cancer* (2008) 112(1):151–6. doi: 10.1002/cncr.23149
24. Liu J, Wang Y, Liu Y, Liu Z, Cui Q, Ji N, et al. Immunohistochemical Profile and Prognostic Significance in Primary Central Nervous System Lymphoma: Analysis of 89 Cases. *Oncol Lett* (2017) 14(5):5505–12. doi: 10.3892/ol.2017.6893
25. Raoux D, Duband S, Forest F, Trombert B, Chambonnière ML, Dumollard JM, et al. Primary Central Nervous System Lymphoma: Immunohistochemical Profile and Prognostic Significance. *Neuropathology* (2010) 30(3):232–40. doi: 10.1111/j.1440-1789.2009.01074.x

Conflict of Interest: The authors declare that the research was conducted in the absence of any commercial or financial relationships that could be construed as a potential conflict of interest.

frontiers | Frontiers in Oncology

ORIGINAL RESEARCH
published: 03 August 2022
doi: 10.3389/fonc.2022.819599

Anti-Migratory Effect of Dipotassium Glycyrrhizinate on Glioblastoma Cell Lines: Microarray Data for the Identification of Key MicroRNA Signatures

Gabriel Alves Bonafé[1,2†], *Jéssica Silva dos Santos*[1,2†], *Anna Maria Alves de Piloto Fernandes*[3], *Jussara Vaz Ziegler*[4], *Fernando Augusto Lima Marson*[1,2†], *Thalita Rocha*[5†], *Patricia de Oliveira Carvalho*[3†] *and Manoela Marques Ortega*[1,2*†]

[1] Laboratory of Cell and Molecular Tumor Biology and Bioactive Compounds, Post Graduate Program in Health Science, São Francisco University, Bragança Paulista, São Paulo, Brazil, [2] Laboratory of Human and Medical Genetics, Post Graduate Program in Health Science, São Francisco University, Bragança Paulista, São Paulo, Brazil, [3] Multidisciplinary Research Laboratory, Post Graduate Program in Health Science, São Francisco University, Bragança Paulista, São Paulo, Brazil, [4] Verdi Cosmetics Limited Liability Company, Joanópolis, São Paulo, Brazil, [5] Post Graduate Program in Biomaterials and Regenerative Medicine, Faculty of Medical Sciences and Health, Pontifical Catholic University of São Paulo, Sorocaba, São Paulo, Brazil

The nuclear factor kappa B (NF-κB) pathway has been reported to be responsible for the aggressive disease phenomenon observed in glioblastoma (GBM). Dipotassium glycyrrhizinate (DPG), a dipotassium salt of glycyrrhizic acid isolated from licorice, has recently demonstrated an anti-tumoral effect on GBM cell lines U87MG and T98G through NF-κB suppression by *IRAK2*- and *TRAF6*-mediating microRNA (miR)-16 and miR-146a, respectively. Thus, the present study aimed to evaluate the expression profiles of miRNAs related to NF-κB suppression in T98G GBM cell line after DPG exposure using miRNA microarray (Affymetrix Human miRNA 4.0A), considering only predicted miRNAs as NF-κB regulator genes. Additional assays using U251 and U138MG cells were performed to validate the array results. DPG cytotoxicity was determined by (4,5-dimethylthiazol-2-yl)-2,5-diphenyl tetrazolium bromide assay, and cellular apoptosis was quantified by DNA fragmentation and terminal deoxynucleotidyl transferase dUTP nick-end labeling (TUNEL) assay. The anti-proliferative effect was observed by cell proliferation and wound-healing assays, and the sphere formation assay examined whether DPG reduced stem cell subpopulation formation. The most over-expressed miRNAs were miR-4443 and miR-3620. The cytotoxic effect of DPG in U251 and U138MG was observed with an IC50 of 32 and 20 mM for 48 h, respectively. The IC50 of each cell line was used in all further assays. DPG treatment-induced apoptosis is observed by DNA fragmentation and increased TUNEL-positive cells. Cell proliferation and wound-healing assays showed an anti-proliferative and anti-migratory effect by DPG on the evaluated cell lines. In addition, DPG treatment led to a 100% reduction in sphere formation. The qPCR results in U251 and U138MG cells showed that DPG increased miR-4443 (2.44 *vs*. 1.11, *p*-value = 0.11;

OPEN ACCESS

Edited by:
Liam Chen,
University of Minnesota, United States

Reviewed by:
Gerardo Caruso,
University Hospital of Policlinico G. Martino, Italy
Ari Meerson,
Migal - Galilee Research Institute, Israel

***Correspondence:**
Manoela Marques Ortega
manoela.ortega@usf.edu.br

†ORCID:
Gabriel Alves Bonafé
orcid.org/0000-0002-9280-0122
Jéssica Silva dos Santos
orcid.org/0000-0002-3733-6734
Patricia de Oliveira Carvalho
orcid.org/0000-0002-2681-7022
Thalita Rocha
orcid.org/0000-0002-2731-9586
Fernando Augusto Lima Marson
orcid.org/0000-0003-4955-4234
Manoela Marques Ortega
orcid.org/0000-0003-4609-7074

Specialty section:
This article was submitted to Neuro-Oncology and Neurosurgical Oncology, a section of the journal Frontiers in Oncology

Received: *21 November 2021*
Accepted: *06 June 2022*
Published: *03 August 2022*

Citation:
Bonafé GA, dos Santos JS, Fernandes AMAdP, Ziegler JV, Marson FAL, Rocha T, Carvalho PdO and Ortega MM (2022) Anti-Migratory Effect of Dipotassium Glycyrrhizinate on Glioblastoma Cell Lines: Microarray Data for the Identification of Key MicroRNA Signatures. Front. Oncol. 12:819599. doi: 10.3389/fonc.2022.819599

8.27 *vs*. 1.25, *p*-value = 0.04) and miR-3620 expression (1.66 vs. 1.00, *p*-value = 0.03; 8.47 *vs*. 1.01, *p*-value = 0.03) and decreased *CD209* (0.44 *vs*. 1.10, *p*-value = 0.03; 0.49 *vs*. 1.07, *p*-value = 0.04) and *TNC* (0.20 *vs*. 1.03, *p*-value = 0.001; 0.39 *vs*. 1.06, *p*-value = 0.01) mRNA levels compared to controls. Our results suggest that DPG inhibits cell viability by activating apoptosis and inhibiting cell proliferation and stem cell subpopulation formation through miR-4443 and miR-3620 upregulation. Both miRNAs are responsible for the post-transcriptional inhibition of NF-κB by *CD209* and *TNC* modulation.

Keywords: glioblastoma, dipotassium glycyrrhizinate, nuclear factor kappa B pathway, microRNA signature, miR-4443 and miR-3620, metastasis formation inhibition

INTRODUCTION

Glioblastoma (GBM) cells have a high capacity to invade and infiltrate normal surrounding brain tissue aggressively, hindering complete surgical resection (1). In addition, GBM cell tumors are very resistant to radiation and cytotoxic chemotherapy (2). GBM molecular subtyping, over the past two decades, has provided predictions of evolution, common disease pathways, and better treatment options (3–8). In addition, single-cell RNA sequencing revealed that multiple subtypes could exist within a single tumor, underscoring the substantial inter- and intra-tumor heterogeneity of GBM (9). MicroRNAs (miRNAs), a class of small non-coding RNA species, have critical functions across various biological processes associated with the pathogenesis of GBM (10). The miR expression signatures also characterize the phenotypic diversity of GBM subclasses through their ability to regulate developmental growth and differentiation (10, 11). Moreover, miRNAs have been previously proven to be promising diagnostic biomarkers in GBM (11–13).

Dipotassium glycyrrhizinate (DPG, $C_{42}H_{60}K_2O_{16}$), a dipotassium salt of glycyrrhizic acid ($C_{42}H_{62}O_{16}$) isolated from licorice (*Glycyrrhiza glabra*), has recently demonstrated an anti-tumoral effect on GBM cell lines U87MG and T98G through a decrease of proliferation and an increase of apoptosis. In addition, DPG anti-tumoral effect seems to be related to nuclear factor kappa B (NF-κB) pathway suppression by *IRAK2*- and *TRAF6*-mediating miR-16 and miR-146a, respectively (14). In fact, one study supported the role of miRNAs in NF-κB regulation (15).

In the present study, the expression profile of miRNAs in T98G GBM cells, a temozolomide (TMZ)-resistant cell line, after DPG exposure was obtained using microarrays. Interestingly, the most over-expressed miRNAs were miR-4443 and miR-3620. Additional cellular studies using other GBM cell lines were performed to validate the array results. Moreover, DPG decreased the viability and sphere formation of the cultured stem cell-enriched populations of established GBM cell lines.

Abbreviations: CAS, chemical abstracts service; CD209, cluster of differentiation 209; DMEM, Dulbecco's modified Eagle's medium; FCS, fetal calf serum; DMSO, dimethyl sulfoxide; GA, glycyrrhizic acid; DPG, dipotassium glycyrrhizinate; *IRAK2*, interleukin-1 receptor-associated kinase 2; qPCR, quantitative polymerase chain reaction; NF-κB, nuclear factor kappa B; miRNAs, microRNAs; MTT, (4,5-dimethylthiazol-2-yl)-2,5-diphenyl tetrazolium bromide; PBS, phosphate-buffered saline; SD, standard deviation; *TNC*, tenascin; TMZ, temozolomide; *TRAF6*, TNF receptor-associated factor; TUNEL, terminal deoxynucleotidyl transferase (TdT) dUTP nick-end labeling.

MATERIALS AND METHODS

Cell Culture and Treatments

U87MG, T98G, U251, and U138MG were kindly donated by Dr. Adriana da Silva Santos Duarte, Hemocenter, University of Campinas, Campinas, São Paulo, Brazil, and were cultured at 37°C in Dulbecco's modified Eagle's medium (DMEM) high glucose supplemented with 10% fetal calf serum (FCS) and 1% penicillin/streptomycin (Cultilab, Campinas, São Paulo, Brazil) at 37°C in a 5% CO_2 atmosphere. For all experiments, the cells were seeded and grown for 72 h before the experimental treatments. The cells were passaged by Trypsin 0.25% (Cultilab) until the seventh passage after thawing.

DPG (chemical abstracts service number 68797-35-3) was obtained from Verdi Cosmetics LLC (Joanópolis, São Paulo, Brazil). For the cell line treatments, DPG was diluted in DMEM to prepare a 2,000-μM stock solution. All treatment assays were performed in the presence of 10% FCS and 1% P/S.

Ultraperformance Liquid Chromatography

The composition of DPG was determined by ultraperformance liquid chromatography–mass spectrometry using an Acquity UPLC system (Waters Co., Milford, MA, USA) coupled with an Acquity TQD mass spectrometer (Micromass; Waters Co.) as described in Franco et al. (16).

Determination of Cellular Metabolic Activity (Cell Viability)

Adherent GBM cells (U251 and U138MG) were seeded in 96-well flat-bottomed tissue culture plates (0.2×10^6 cells/plate). After 24 h of incubation at 37°C in a 5% CO_2 environment, various concentrations (5, 8, 12, 15, 18, 20, 24, 28, 32, and 36 mM) of DPG were used to treat the GBM cell lines based on a previous study (14). The cells were cultured for 24, 48, and 72 h prior to (4,5-dimethylthiazol-2-yl)-2,5-diphenyl tetrazolium bromide incubation (Sigma, St. Louis, MO, United States). The cells were incubated for 4 h at 37°C in a 5% CO_2 environment. Following incubation, formazan crystals were solubilized with 100 μL of dimethyl sulfoxide. Cell viability was determined by

measuring the optical density at 550 nm using a microplate spectrometer (Thermo Fisher, Waltham, MA, USA). The cell survival rates were expressed as percentages of the value of normal cells. Untreated control cells were analyzed in all experiments, and all DPG dose treatments were performed in triplicate.

Determination of DPG Effects on Cell Viability

U251 and U138MG cells (0.4×10^6 cells/well) were cultured in 24-well tissue culture plates for 24 h at 37°C in a 5% CO_2 environment and further exposed to 32 and 20 mM of DPG, respectively. The cells were washed in phosphate-buffered saline (PBS), and the viable cells were counted by trypan blue dye exclusion assay for 4 days. Untreated cells were used as a control, and the experiments were performed in triplicate.

Evaluation of the Effect of DPG on Cell Death by DNA Fragmentation

U251 and U138MG cells were cultured in 6-well tissue culture plates for 24 h at 37°C in a 5% CO_2 environment and further exposed to 32 and 20 mM of DPG for 48 and 72 h, respectively. The TMZ-resistant U251 was also exposed for 96 h. DNA was isolated using lithium chloride extraction (17). The purity of DNA was analyzed in a spectrophotometer at 260/280 nm, and the ratio was confirmed to be between 1.7 and 1.9. DNA samples were then electrophoresed on 1.5% agarose gel and visualized with ethidium bromide staining under ultraviolet illumination.

Evaluation of DPG Effect on Cell Death by TUNEL Assay

U251 and U138MG cells were cultured in 96-well tissue culture plates for 24 h at 37°C in a 5% CO_2 environment and further exposed to 32 and 20 mM of DPG for 72 h, respectively. Cellular apoptosis was evaluated after treatment with DPG by *in situ* terminal deoxynucleotidyl transferase dUTP nick-end labeling (TUNEL) assay using *in situ* cell death detection kit, fluorescein (Roche Applied Science, Mannheim, Germany), according to the manufacturer's protocols. Apoptotic indexes were calculated by scoring four randomly selected fields and counting the number of apoptotic cells over the total of viable cells, representing a quota compared to untreated cells. The cells were directly analyzed under a fluorescence microscope (Axio Vert. A1 ZEISS, Germany).

Wound Healing Assay

U251 and U138MG cells were seeded in 6-well plates (1×10^6 cells/well) and grown overnight at 37°C in a 5% CO_2 environment to confluence. The monolayer of cells was scratched with a 200-mL pipette tip to create a wound, and the plates were washed twice with PBS and cultured with DPG (32 mm and 20 mM, respectively). Afterward, cells migrating from the leading edge were photographed at 0, 24, 48, and 72 h under an inverted microscope (Axio Vert. A1 ZEISS). Untreated cells were used as a control. The distance of the scratch closure was examined using ImageJ software (National Institutes of Health, Bethesda, MD, United States). Each value is derived from the same selected fields, and results are expressed as the mean of migrating cell numbers per field.

Sphere-Cultured Stem Cell-Enriched GBM Populations

U251 and U138MG cells (1×10^4 cells/well) were cultured at 37°C in a 5% CO_2 environment in serum-free DMEM/F12 supplemented with N_2 supplement (StemCell, Vancouver, Canada) containing epidermal growth factor (20 ng/mL) (Peprotech, Ribeirão Preto, São Paulo, Brazil), basic fibroblast growth factor (20 ng/mL) (Peprotech), and 1% penicillin/streptomycin (120 mg/mL) (Thermo Fisher) for at least 6 days. For the subsequent DPG treatment (32 and 20 mM, respectively), 75-μm neuro-spheres were cultured for 24 and 48 h. Cells without DPG were cultured as controls. Cells were observed and photographed under an inverted microscope (Axio Vert. A1 ZEISS).

miRNA and Gene Expression Arrays

miRNA expression profiles were conducted in T98G cell line DPG exposure (24 mM; 48 h of DPG treatment) (14) and control cells. Analyses were performed using Affymetrix® GeneChip miRNA 2.0 array (Affymetrix, Santa Clara, CA, USA), which detects 2,578 known human miRNAs (miRBase v.15; Affymetrix). Total RNA was labeled with FlashTag Biotin HSR, hybridized with the arrays, then washed with PBS, stained, and scanned according to Affymetrix GeneChip Command Console software. The miRNA QC Tool software (Affymetrix) was used for data summarization, normalization, and quality control.

Identification of miRNA Target Genes

The analysis of miRNA differential expression profile was performed considering only 91 miRNAs previously selected and predicted as regulators of genes involved in the NF-κB pathway (**Supplementary Table S1)**. Conventional online programs, including miRanda (http://www.microrna.org), TargetScan (http://www.targetscan.org), and Findtar (http://bio.sz.tsinghua.edu.cn), were used to predict the targets of miRNAs. To identify the most likely targets, mRNA and miRNA expression data obtained on the same biological samples using Microsoft Excel tools were integrated. Twofold upregulated miRNA and corresponding 2fold downregulated mRNA targets were selected for further investigation.

Total RNA Isolation

For the U87MG and T98G cells, the half-maximal inhibitory concentration (IC50) used is based on a previous study using DPG as a therapeutic compound in GBM cell lines (14). Total RNA was isolated from U87MG, T98G, U251, and U138MG cells after DPG exposure (18, 24, 32, and 20 mM for 48 h, respectively) and control cells using TRIzol® reagent (Thermo Fisher), according to the manufacturer's instructions. Total RNA quantification was performed using the ND-1000 spectrophotometer (Nanodrop; Thermo Fisher).

Validation of miRNA and mRNA Expression Levels

cDNA conversion was performed using the High-Capacity cDNA Reverse Transcription Kit (Applied Biosystems, Foster City, CA, USA). qPCR was performed on a 7500 Fast Real-Time PCR system (Applied Biosystems) using SYBR-Green PCR Master Mix (Applied Biosystems). Each sample was examined in triplicate, and the expression of each gene was normalized by control gene expression (*GAPDH*) and calculated by applying the $2^{-\Delta\Delta Ct}$ method (18). The expression value of each gene was represented as fold change. The primer sequences used for amplification by qPCR with SYBRGreen dye (Applied Biosystems) are as follows: *CD209* 5′-CATGTCTAACTCCCAGCGG-3′ (sense) and 5′-GAAA GTCCCATCCAGGTGAAG-3′ (anti-sense), *TNC* 5′-CACT ACAC AGCC AAGATCCAG-3′ (sense) and 5′-TCGT GTCT CCATT CAGC ATTG-3′ (anti-sense), and *GAPDH* (forward) 5′- CCAC TTG ATTTTGGAGGGAT-3′ and (reverse) 5′-GCA CCGT CAAG GCTGAGAAC-3′.

miRNA expression analysis was validated using the MicroRNA Assay kit (Applied Biosystems), which incorporates a target-specific stem-loop reverse transcription primer to provide specificity for mature miRNA target. U6 served as an endogenous control for the normalization of RNA input. Specific primers for mRNA expression analysis and the endogenous control were provided by Thermo Fischer (miR-4443: assay 463010_mat; miR-3620: assay CTKA3MT; and U6: assays 001973 and 03928990_g1). The specificity of the PCR products was tested by dissociation curves. Relative values of transcripts were calculated using the equation $2^{-\Delta\Delta Ct}$, where ΔCt is equal to the difference in threshold cycles for target and reference genes. Each experiment was performed in triplicate.

Statistical Analysis

A two-tailed *T*-test was performed for all two sets of numerical data (treated and non-treated cells), and *P*-value ≤0.05 was considered statistically significant. The results are expressed as mean ± SD from experiments repeated at least three times. Statistical analysis was performed using the Statistical Package for the Social Sciences software (IBM SPSS Statistics for Macintosh, version 27.0.).

RESULTS

DPG Analysis by Liquid Chromatography

Mass spectrometry (UPLC-QTOF, Waters) was applied to evaluate the presence of DPG in the sample used for the present study. The signals from $[M-H]^-$ and $[M-2H]^{-2}$ anions as well as the mass measurement accuracy and the adequacy of the simulated isotopic standard for $[M-H]^-$ ion confirmed the presence of the DPG (**Supplementary Figure S1A**).

DPG Inhibits Cell Viability and Proliferation

The antitumor effect of DPG was evaluated by using two GBM cell lines (U251 and U138MG). Based on these findings, the cytotoxic effect of DPG was time and dose dependent, and the IC50 in U251 and U138MG was 32 and 20 mM for 48 h, respectively (**Figures 1A, D**). For all further assays, IC50 was adopted. Moreover, it was observed that cells presented nuclear morphological changes after 48 h of DPG treatment (**Figures 1B, E**). Furthermore, cell proliferation assay showed a significantly anti-proliferative effect by DPG on the same cell lines starting after 24 h of treatment (p-value = 2.6×10^{-5} and p-value = 2.2×10^{-8}, respectively) until 96 h later (p-value = 2.8×10^{-15} and p-value = 2.6×10^{-15}, respectively) (**Figures 1C, F**).

DPG Induces Apoptosis

To investigate cellular apoptosis, DNA fragmentation was quantified by TUNEL assay. As expected, DPG was also able to induce cellular apoptosis by DNA fragmentation (**Figures 2A, C**), which was confirmed by increased TUNEL-positive cells when compared to untreated cells (**Figures 2B, D**), mostly on the U138MG cell line (p-value = 0.023).

DPG Inhibits Invasion and Migration

Furthermore, to investigate the effect of DPG on the migration ability of U251 and U138MG, both cell lines were treated with DPG for 24, 48, and 72 h, and a wound-healing motility assay was performed simultaneously. The results showed that cells exposed to DPG migrated significantly slower than DPG-free control cells starting after 24 h of treatment (p-value = 1×10^{-5} and p-value = 1×10^{-5}, respectively) until 96 h later (p-value = 2×10^{-5} and p-value = 9×10^{-7}, respectively) (**Figures 3A, B**).

DPG Effect on GBM Stem-Like Cells

The phenotypic plasticity of cancer cells grown as neurospheres to elucidate the influence of DPG on GBM stem-like cells was also investigated. Thus, it was observed that DPG promoted a 100% reduction in neurosphere formation compared to untreated cells, starting after 24 h of DPG exposure (p-value ≤ 0.05) (**Figures 3C, D**), characterizing DPG as an antitumor compound.

Identification of miRNAs With Differential Expression

Global miRNA expression changes in T98G cells were evaluated after 48 h of treatment with 24 mM of DPG. No treated T98G cells were evaluated as control. A total of 11 miRNAs with DE-miRNAs were identified after comparing DPG-treated and control samples (among 91 predicted miRNAs as NF-κB regulator genes) (**Supplementary Figure S2A**). The number of upregulated and downregulated DE-miRNAs is shown in **Tables 1**, **2**, respectively. Furthermore, a new analysis was performed considering the expression values, mRNA volume, and target genes predicted to be involved in GBM pathogenesis, and most DE-miRNAs were found to be miR-4443 and miR-3620 (**Supplementary Figure S2B**) and their respective target genes *CD209* and *TNC*.

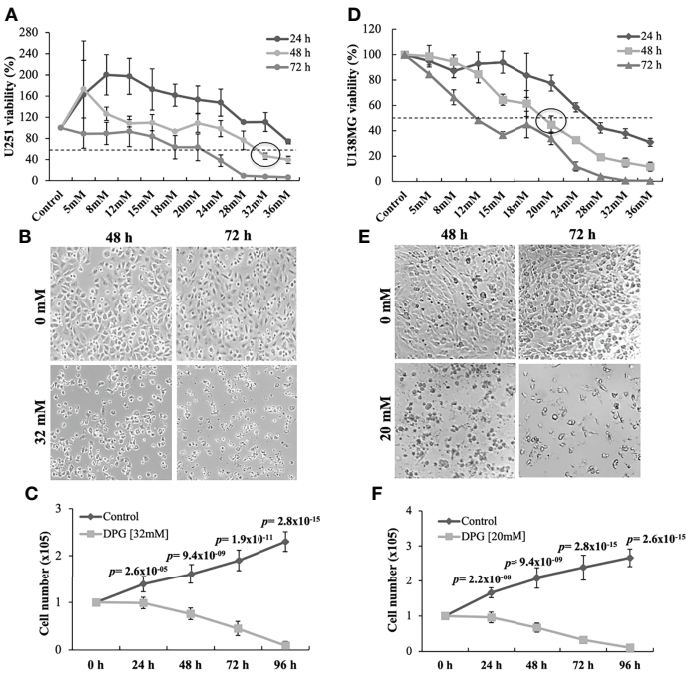

FIGURE 1 | Dipotassium glycyrrhizinate (DPG) reduces cell viability and changes morphology in glioblastoma cell lines. **(A)** U251 cells were treated with different concentrations of DPG for 24, 48, and 72 h and evaluated by the 4,5-dimethylthiazol-2-yl)-2,5-diphenyl tetrazolium bromide (MTT) assay to determine the IC50 (32 mM for 48 h). **(B)** Morphological and nuclear changes were observed in U251 cells, especially after 72 h of exposure to DPG, when compared to untreated cells. **(C)** The DPG treatment also significantly inhibited the rate of proliferation in U251 cells in a time-dependent way compared to untreated cells. **(D)** U251 cells were treated with different concentrations of DPG for 24, 48, and 72 h and evaluated by the MTT assay to determine the IC50 (20 mM for 48 h). **(E)** Morphological and nuclear changes were observed in U138MG cells, especially after 72 h of exposure to DPG, when compared to untreated cells. **(F)** The DPG treatment significantly inhibited the rate of proliferation in U138MG cells in a time-dependent way compared to untreated cells. The data presented are the mean ± standard deviation of the experiments performed in triplicate. The *T*-test indicated *p*-values ≤0.05.

Validation of miRNA and mRNA Expression Levels

The expression of both miRNAs and their predicted target genes was evaluated by qPCR using U87MG, T98G, U251, and U138MG cell lines after exposure to DPG. Untreated cells were used as controls. In accordance with the global analysis, the mean mRNA expression level was significantly higher in DPG-treated T98G cells when compared to control cells for miR-4443 (2.44 *vs.* 1.17, *p*-value = 0.03) (**Figure 4A**) and miR-3620 (7.50 *vs.* 1.19, *p*-value = 0.007) (**Figure 4B**). In addition, qPCR showed that DPG increased the level of miR-4443 (2.44 *vs.* 1.11, *p*-value = 0.11; 8.27 *vs.* 1.25, *p*-value = 0.04; 1.64 *vs.* 1.00, *p*-value = 0.05) (**Figure 4A**) and miR-3620 expression (1.66 *vs.* 1.00, *p*-value = 0.03; 8.47 *vs.* 1.00, *p*-value = 0.03; 2.08 *vs.* 1.04, *p*-value = 0.05) in U251, U138MG, and U87MG cell lines (**Figure 4B**).

On the other hand, the *CD209* and *TNC* expression levels were lower in DPG-treated cells when compared to controls (**Figures 4C, D**). Thus, decreased *CD209* (0.06 *vs.* 1.07, *p*-value = 0.007; 0.32 *vs.* 1.04, *p*-value = 0.002; 0.44 *vs.* 1.11, *p*-value = 0.03; 0.49 *vs.* 1.07; *p*-value = 0.04) (**Figure 4C**) and *TNC* (0.24 *vs.* 1.03, *p*-value = 0.03; 0.05 *vs.* 1.15, *p*-value = 0.03; 0.20 *vs.* 1.03, *p*-value = 0.001; 0.39 *vs.* 1.06; *p*-value = 0.01) (**Figure 4D**) mRNA levels were observed in U87MG, T98G, U251, and U138MG when compared to control cells.

DISCUSSION

In the present study, we demonstrated first that DPG, under *in vitro* conditions, was able to significantly reduce the number of viable cells in GBM cell lines U251 and U138MG, inhibiting cell growth and adhesion. This finding corroborates with previous results using the GBM U87MG and T98G cell lines (14). In addition, this previous study has suggested alterations in miRNA expression after DPG treatment in GBM cell lines U87MG and T98G (14), which were able to modulate NF-κB genes. Thus, here a global analysis evaluated potentially over-expressed miRNAs responsible for the NF-κB pathway in GBM cells. The choice of T98G for array analysis was based on hypermethylated *MGMT* promoter and mutated *P53* gene. In fact, cell lines with a hypermethylated *MGMT* promoter and mutated *P53* gene appeared more resistant to the action of TMZ than the ones with wild-type *P53* (19) since p53 protein is fundamental in regulating the cell cycle arrest and the entry in the apoptotic

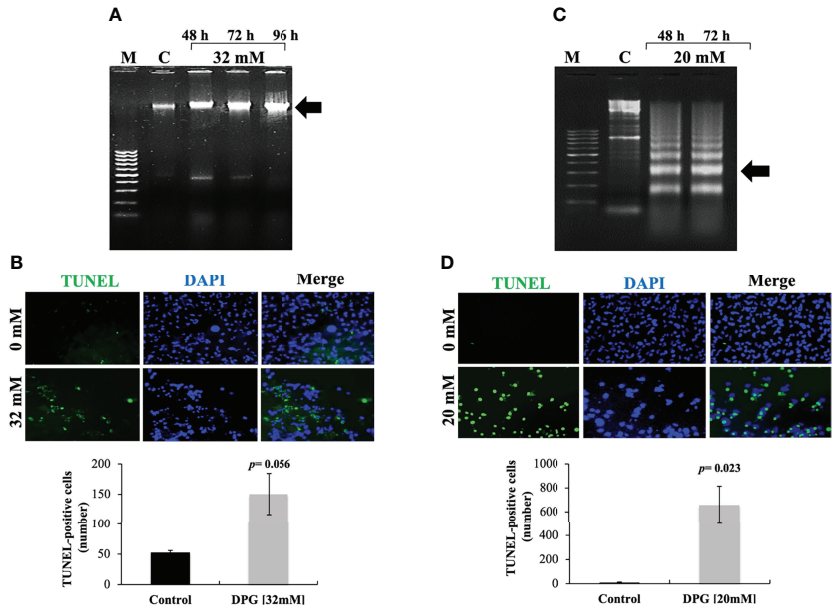

FIGURE 2 | Apoptotic effects of dipotassium glycyrrhizinate (DPG) on glioblastoma cell lines. **(A)** U251 cells were incubated with 32 mM of DPG for 48, 72, and 96 h. Genomic DNA was isolated and analyzed on 1.5% agarose gel stained with ethidium bromide. M, DNA marker 100 base pairs; C, untreated control cells. **(B)** U251 cells were treated with DPG (32 mM for 96 h). After incubation with DPG, TUNEL-positive cells were quantified by the ImageJ computer program. **(C)** U138MG cells were incubated with 20 mM of DPG for 48 and 72 h. Genomic DNA was isolated and analyzed on 1.5% agarose gel stained with ethidium bromide. M, DNA marker 100 base pairs; C, untreated control cells. **(D)** U138MG cell lines were treated with DPG (20 mM for 72 h). After incubation with DPG, TUNEL-positive cells were quantified by the ImageJ computer program. The data presented are mean ± standard deviation of the experiments performed in triplicate. The results showed that treatment with DPG increased the number of cells undergoing apoptosis compared to untreated control cells (U251: *p*-value = 0.056; U138MG: *p*-value = 0.023).

process (20, 21). Besides this, it was observed previously that the effect of DPG on T98G decreased cell proliferation and increased migration and invasion at a concentration of 24 mM (14).

Few studies have focused on miRNAs involved in the NF-κB pathway, which is known as continuously active (22) in GBM (14, 23–28). Thus, the large-scale global approach evaluated 91 miRNAs previously selected and predicted as regulators of genes involved in the NF-κB pathway in T98G lineage exposed to DPG action. Among the 11 DE-miRNAs reported in the present study, none has been previously evaluated in GBM cells. Besides, 2 miRNAs (miR-4443 and mir-3620-5p) were further validated using 4 GBM cell lines. Both miRNAs are predicted to be responsible for *TNC* and *CD209* modulation, respectively. Those genes are known as post-transcriptional target genes for the NF-κB pathway.

Thus, our study revealed, for the first time, that both miR-4443 and mir-3620-5p are upregulated on GBM cell lines after DPG exposure. miR-4443 was first identified by Xun et al. (29) in enterovirus-71-infected cells. In addition, it has been shown that miR-4443 plays a role in acquiring drug resistance in breast cancer (30) and inhibits cell proliferation and metastasis in colon cancer (31). In addition, miR-4443 is decreased in metastatic and serous samples from ovarian cancer (32). In the study of Gao et al. (33), the authors have found that long non-coding RNAs (lncRNAs) MNX1-AS1 were upregulated in GBM tissues and cell lines. The knockdown of MNX1-AS1 significantly inhibited the proliferation, migration, and invasion of GBM cells. In addition, the overexpression of miR-4443 significantly inhibited the expression of MNX1-AS1 and *vice versa*. Moreover, there was an inverse correlation between the expression levels of MNX1-AS1 and miR-4443 in GBM tissues. The overexpression of miR-4443 also inhibited the proliferation, migration, and invasion of GBM cells. In contrast, the inhibition of miR-4443 reversed the effects of MNX1-AS1 knockdown on GBM cell proliferation, migration, and invasion. MNX1-AS1 promoted the proliferation, migration, and invasion of GBM cells by inhibiting miR-4443. miR-3620 was able to reverse claudin-4 upregulation in gastric cancer cell lines, which is responsible for reinforcing proliferation, invasion, and epithelial–mesenchymal transition in gastric cancer and with poor prognosis (34).

TNC and *CD209* genes play an important role in the progression of GBM by regulating the migration, adhesion, and invasion of tumor cells into adjacent tissues (35, 36). The *TNC* gene was evaluated in tumor tissues and primary cultures of patients with GBM, and its increased expression was associated with the process of carcinogenesis and invasion (35, 37). A recent survey of tumor tissues from patients with GBM correlated the infiltrative character of GBM malignant cells with an increased expression of *CCL15*, *CCL17*, *CD209*, and *TNF*-α genes (36). In the GBM cell line (U87MG), *CD209* gene interacts with TGF-β1 gene, stimulating cell invasion and metastasis (38). In addition, the results of the cell proliferation assay and wound healing in the present study corroborate with what was observed previously regarding *CD209* and *TNC* genes, both involved in cell metastasis process. Both genes

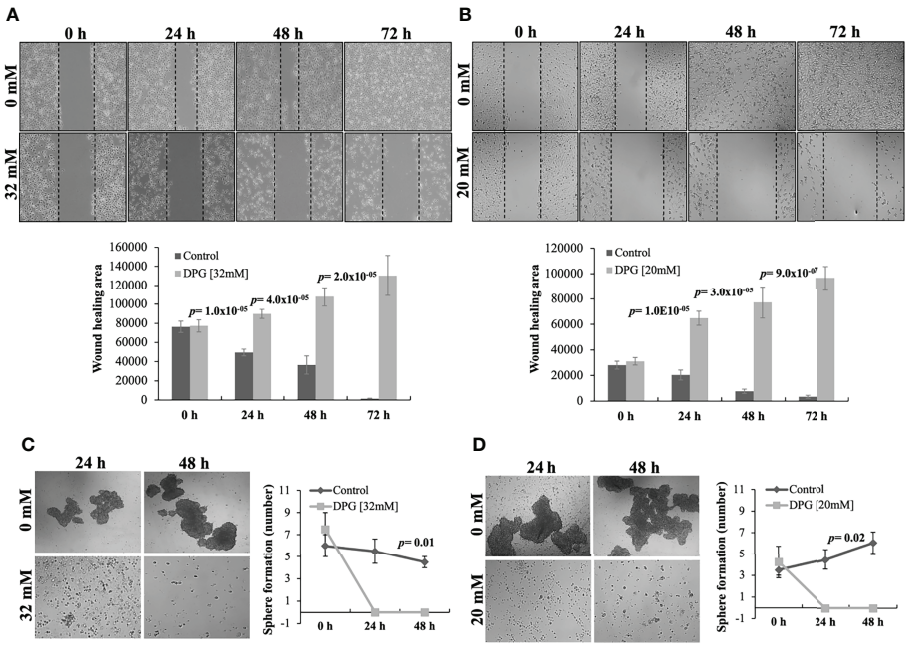

FIGURE 3 | Dipotassium glycyrrhizinate (DPG) inhibits cell migration and cancer stem-like cells in glioblastoma cell lines. **(A)** U251 and **(B)** U138MG cell lines treated with DPG fill the wound area (the area between the two dotted lines) more slowly at 24, 48, and 72 h when compared to untreated control cells (p-value ≤ 0.001). The wound-healing assay was quantified using the ImageJ computer program by measuring the relative area of the wound after treatment with DPG. Loss of sphere-forming capacity of cell lines **(C)** U251 (p-value = 0.01) and **(D)** U138MG (p-value = 0.02) after 24 and 48 h of treatment with DPG when compared to untreated control cells. The data presented are the mean ± standard deviation of the experiments performed in triplicate.

showed a significant decrease in expression due to the overexpression of miR-4443 and miR-3620, respectively, after the DPG effect in the evaluated GBM cell lines in the study.

Therefore, DPG-modulated miRNAs are involved in the post-transcriptional inhibition of the NF-κB pathway. Interestingly, in a previous study, DPG inhibited the NF-κB pathway by modulation of miR-16 and miR-146a, which inhibited the expression of its target genes *IRAK2* and *TRAF6*, respectively (14). It appears that the antitumor action of DPG can inhibit genes that belong to the NF-κB signaling pathway and genes downstream by the overexpression of miRNAs.

In accordance with the results observed in the present study, another recent study has suggested that DPG has an apoptotic, anti-proliferative, and anti-migratory effect on the melanoma cell line (SK-MEL-28) bearing the *BRAF* mutation. DPG was also able to inhibit cancer stem-like cells that may cause cerebral tumor formation (39). In addition, DPG treatment has shown that SK-MEL-28 cells also presented a significantly higher level of miR-4443 and miR-3620 expression than control cells. In contrast, their predicted genes, *CD209* and *TNC*, significantly presented reduced mRNA levels after DPG compared to untreated cells. Furthermore, the migration of SK-MEL-28 cells stimulated by 12-O-tetradecanoylphorbol-13-acetate (TPA) was attenuated by adding DPG by wound-healing assay. In addition, the MMP-9 expression level was inhibited by DPG in melanoma cells stimulated by TPA and compared to only TPA-treated cells (39).

Therefore, in the present study, the potential inhibition by DPG was verified on miR-4443 and miR-3620, possible

TABLE 1 | The most upregulated microRNAs (FC ≥-2) after dipotassium glycyrrhizinate (DPG) treatment in the glioblastoma T98G cell line by global miRNA microarrays.

	MicroRNAs	FC	mRNA volume	Target genes (>99%)[a]	Function
1	miR-4448	16.70	2.01	*CASP4*	Apoptosis—caspase
2	miR-1587	3.88	3.60	*TNC*	Cell adhesion—control of cell growth, migration, and adhesion by the ECM protein
3	miR-3620-5p	2.04	6.68	*TNC*	Cell adhesion—control of cell growth, migration, and adhesion by the ECM protein
4	miR-4443	2.10	7.12	*CD209*	Cell adhesion—dendritic cell surface by leptin C
5	miR-7111-5p	2.66	2.71	*MAP4K1*	Stress response—activator of the stress-induced protein kinase pathway
6	miR-3148	6.79	2.93	*S100A4*	Miscellaneous—tumor suppressor

FC, fold change; mRNA volume, $\sqrt{\text{normalized control value} \times \text{normalized DPG value}}$.
[a]*Prediction according to TargetScan database.*

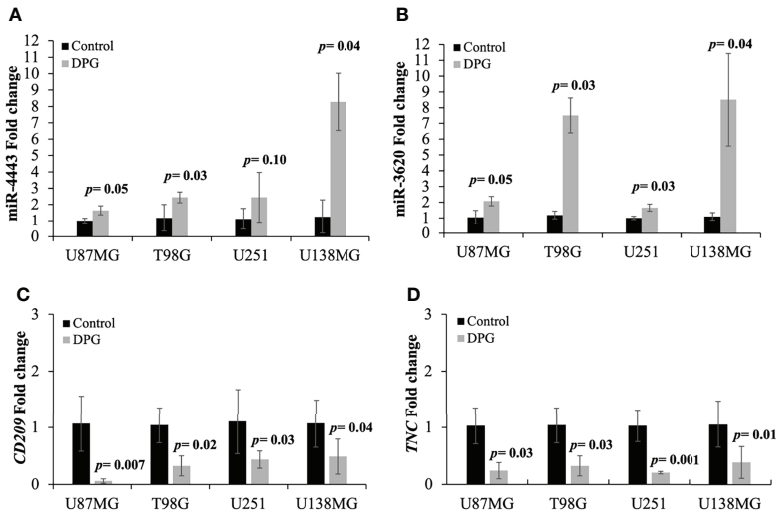

FIGURE 4 | Dipotassium glycyrrhizinate (DPG) modulated the expression of selected miRNAs and their respective target genes in glioblastoma cell lines (GBM). **(A)** U87MG (1.64 *vs*. 1.00, *p*-value = 0.05), T98G (2.44 *vs*. 1.17, *p*-value = 0.03), U251 (2.44 *vs*. 1.11, *p*-value = 0.11), and U138MG 8.27 *vs*. 1.25, *p*-value = 0.04) cell lines treated with DPG showed an increased level of miR-4443 expression compared to untreated control cells. **(B)** U87MG (2.08 *vs*. 1.04, *p*-value = 0.05), T98G (7.50 *vs*. 1.19, *p*-value = 0.007), U251 (1.66 *vs*. 1.00, *p*-value = 0.03), and U138MG (8.47 *vs*. 1.00, *p*-value = 0.03) cell lines exposed to DPG showed increased miR-3620 expression levels compared to untreated control cells. **(C)** Decreased *CD209* (0.06 *vs*. 1.07, *p*-value = 0.007; 0.32 *vs*. 1.04, *p*-value = 0.002; 0.44 *vs*. 1.11, *p*-value = 0.03; 0.49 *vs*. 1.07; *p*-value = 0.04) and **(D)** *TNC* (0.24 *vs*. 1.03, *p*-value = 0.03; 0.05 *vs*. 1.15, *p*-value = 0.03; 0.20 *vs*. 1.03, *p*-value = 0.001; 0.39 *vs*. 1.06; *p*-value = 0.01) mRNA levels were observed in U87MG, T98G, U251, and U138MG treated with DPG compared to control cells. The data presented are mean ± standard deviation of the experiments performed in triplicate.

TABLE 2 | The most downregulated microRNAs (FC ≥-2) after dipotassium glycyrrhizinate (DPG) treatment in the glioblastoma T98G cell line by global miRNA microarrays.

	MicroRNAs	FC	mRNA volume	Target genes[a]	Function
1	miR-27b-3p	-2.22	4.21	*BCL3*	Transcription—coactivator for NF-κB p50 and p52
2	miR-106a-5p	-6.13	4.97	*MMP3*	Enzymes—related to metastasis
3	miR-17-5p	-4.09	5.39	*MMP3*	Enzymes—related to metastasis
4	miR-20a-5p	-4.38	3.61	*MMP3*	Enzymes—related to metastasis
5	miR-22-3p	-2.46	5.06	*PTEN*	Miscellaneous—tumor suppressor

FC, fold change; mRNA volume, $\sqrt{\text{normalized control value} \times \text{normalized DPG value}}$.
[a]*Prediction according to TargetScan database.*

therapeutic targets for GBM. In addition, the results obtained in the present study may contribute to the development of future *in vivo* studies to target GBM cells by DPG, which is a promising approach to restrict tumor cell growth.

DATA AVAILABILITY STATEMENT

The raw data supporting the conclusions of this article will be made available by the authors, without undue reservation.

AUTHOR CONTRIBUTIONS

Conception and design: MMO; acquisition of data: GAB, JSS, and JVZ; analyses and interpretation of data: MMO and GAB; statistical analyses: FALM; drafting of the manuscript: MMO; mass spectrometer analyses: POC and AMAPF; TUNEL analysis: GAB and TR; study supervision: MMO. All authors contributed to the article and approved the submitted version.

FUNDING

The fInancial support provided for this work by the São Paulo Research Foundation (FAPESP) scholarships #2018/05930-0 and grant #2015/03870-1 and by Coordination for the Improvement of Higher Education Personnel (CAPES) scholarship #88887.464813/2019-00 is gratefully acknowledged.

ACKNOWLEDGMENTS

We are thankful to JZ, Verdi Cosméticos LTDA (Joanópolis, São Paulo, Brazil), for the dipotassium glycyrrhizinate donation (chemical abstracts service number 68797-35-3).

SUPPLEMENTARY MATERIAL

The Supplementary Material for this article can be found online at: https://www.frontiersin.org/articles/10.3389/fonc.2022.819599/full#supplementary-material

Supplementary Figure 1 | Mass spectrum of dipotassium glycyrrhizinate (DPG). The presence of the ion $[M-H]^-$ (the anion of the DPG) and the ion $[M-2H]^{-2}$ is highlighted. The error observed for measuring the ion $[M-H]^{-1}$ (DPG anion) was -1.83 ppm.

Supplementary Figure 2 | Identification of microRNAs (miRNAs) with differential expression (DE-miRNAs) in glioblastoma T98G cell line. **(A)** Scatter plot of 11 DE-miRNAs identified after comparing dipotassium glycyrrhizinate (DPG)-treated and control T98G cell line (among 91 predicted miRNAs as NF-κB regulator genes). The gray and red dots represent each predicted miRNA. The red dots represent those that presented |fold change, FC ≥ 2|, according to the analysis of the computer program Affymetrix GeneChip® Command Console™. The dots above and below the dashed line represent those up- and downregulated miRNAs after DPG treatment, respectively. **(B)** Volume graph of the most overexpressed miRNAs among the 11 DE-miRNAs in T98G cell line exposure to DPG. Each gray, blue, and red dot represents one DE-miRNA. The red dots represent those miRNAs that presented both |FC ≥ 2| and increased volume of mRNA detected and quantified by the Affymetrix GeneChip® Command Console™ software. The dots above and below the dashed line represent those up- and downregulated miRNAs after DPG treatment, respectively.

Supplementary Table 1 | List of the 91 selected microRNAs predicted as NF-κB modulators and their predicted target genes (above 99%, according to TargetScan database) belonging to the NF-κB signaling pathway.

REFERENCES

1. Hambardzumyan D, Bergers G. Glioblastoma: Defining Tumor Niches. *Trends Cancer* (2015) 1:252–65. doi: 10.1016/j.trecan.2015.10.009
2. Stupp R, Mason WP, van den Bent MJ, Weller M, Fisher B, Taphoorn MJ, et al. Radiotherapy Plus Concomitant and Adjuvant Temozolomide for Glioblastoma. *N Engl J Med* (2005) 352:987–96. doi: 10.1056/NEJMoa043330
3. The Cancer Genome Atlas Research Network. Comprehensive Genomic Characterization Defines Human Glioblastoma Genes and Core Pathways. *Nature* (2008) 455:1061–8. doi: 10.1038/nature07385
4. Verhaak RG, Hoadley KA, Purdom E, Wang V, Qi Y, Wilkerson MD, et al. Integrated Genomic Analysis Identifies Clinically Relevant Subtypes of Glioblastoma Characterized by Abnormalities in PDGFRA, IDH1, EGFR, and NF1. *Cancer Cell* (2010) 17:98–110. doi: 10.1016/j.ccr.2009.12.020
5. Snuderl M, Fazlollahi L, Le LP, Nitta M, Zhelyazkova BH, Davidson CJ, et al. Mosaic Amplification of Multiple Receptor Tyrosine Kinase Genes in Glioblastoma. *Cancer Cell* (2011) 20:810–7. doi: 10.1016/j.ccr.2011.11.005
6. Szerlip NJ, Pedraza A, Chakravarty D, Azim M, McGuire J, Fang Y, et al. Intratumoral Heterogeneity of Receptor Tyrosine Kinases EGFR and PDGFRA Amplification in Glioblastoma Defines Subpopulations With Distinct Growth Factor Response. *Proc Natl Acad Sci U.S.A.* (2012) 109:3041–6. doi: 10.1073/pnas.1114033109
7. Brennan CW, Verhaak RG, McKenna A, Campos B, Noushmehr H, Salama SR, et al. The Somatic Genomic Landscape of Glioblastoma. *Cell* (2013) 155:462–77. doi: 10.1016/j.cell.2013.09.034
8. Sottoriva A, Spiteri I, Piccirillo SG, Touloumis A, Collins VP, Marioni JC, et al. Intratumor Heterogeneity in Human Glioblastoma Reflects Cancer Evolutionary Dynamics. *Proc Natl Acad Sci U.S.A.* (2013) 5:4009–14. doi: 10.1073/pnas.1219747110
9. Patel AP, Tirosh I, Trombetta JJ, Shalek AK, Gillespie SM, Wakimoto H, et al. Single-Cell RNA-Seq Highlights Intratumoral Heterogeneity in Primary Glioblastoma. *Science* (2014) 344:1396–401. doi: 10.1126/science.1254257
10. Ahir BK, Ozer H, Engelhard HH, Lakka SS. MicroRNAs in Glioblastoma Pathogenesis and Therapy: A Comprehensive Review. *Crit Rev Oncol Hematol* (2017) 120:22–33. doi: 10.1016/j.critrevonc.2017.10.003
11. Kim TM, Huang W, Park R, Park PJ, Johnson MD. A Developmental Taxonomy of Glioblastoma Defined and Maintained by MicroRNAs. *Cancer Res* (2011) 71:3387–99. doi: 10.1158/0008-5472.CAN-10-4117
12. Henriksen M, Johnsen KB, Olesen P, Pilgaard L, Duroux M. MicroRNA Expression Signatures and Their Correlation With Clinicopathological Features in Glioblastoma Multiforme. *Neuromolecular Med* (2014) 16:565–77. doi: 10.1007/s12017-014-8309-7
13. Huang SW, Ali ND, Zhong L, Shi J. MicroRNAs as Biomarkers for Human Glioblastoma: Progress and Potential. *Acta Pharmacol Sin* (2018) 39:1405–13. doi: 10.1038/aps.2017.173
14. Bonafé GA, Dos Santos JS, Ziegler JV, Umezawa K, Ribeiro ML, Rocha T, et al. Growth Inhibitory Effects of Dipotassium Glycyrrhizinate in Glioblastoma Cell Lines by Targeting MicroRNAs Through the NF-κb Signaling Pathway. *Front Cell Neurosci* (2019) 13:216. doi: 10.3389/fncel.2019.00216
15. Baud V, Karin M. Is NF-kappaB a Good Target for Cancer Therapy? Hopes and Pitfalls. *Nat Rev Drug Discovery* (2009) 8:33–40. doi: 10.1038/nrd2781
16. Franco EPD, Contesini FJ, Lima da Silva B, Alves de Piloto Fernandes AM, Wielewski Leme C, Gonçalves Cirino JP, et al. Enzyme-Assisted Modification of Flavonoids From Matricaria Chamomilla: Antioxidant Activity and Inhibitory Effect on Digestive Enzymes. *J Enzyme Inhib Med Chem* (2020) 35(1):42–9. doi: 10.1080/14756366.2019.1681989
17. Woodhead JL, Fallon R, Figueredo H, Langdale J, Malcom ADB. Alternative Methodology of Gene Diagnosis. In: KE Davies, editor. *Human Genetic Diseases: A Practical Approach*. Oxford: IRL Press Limited (1986). p. 51–64.
18. Livak KJ, Schmittgen TD. Analysis of Relative Gene Expression Data Using Real-Time Quantitative PCR and the 2(-Delta Delta C(T)) Method. *Methods* (2001) 25:402–8. doi: 10.1006/meth.2001.1262
19. Annovazzi L, Caldera V, Mellai M, Riganti C, Battaglia L, Chirio D, et al. The DNA Damage/Repair Cascade in Glioblastoma Cell Lines After Chemotherapeutic Agent Treatment. *Int J Oncol* (2015) 46:2299–308. doi: 10.3892/ijo.2015.2963
20. Hermisson M, Klumpp A, Wick W, Wischhusen J, Nagel G, Roos W, et al. O6-Methylguanine DNA Methyltransferase and P53 Status Predict Temozolomide Sensitivity in Human Malignant Glioma Cells. *J Neurochem* (2006) 96:766–76. doi: 10.1111/j.1471-4159.2005.03583.x
21. Bocangel DB, Finkelstein S, Schold SC, Bhakat KK, Mitra S, Kokkinakis DM. Multifaceted Resistance of Gliomas to Temozolomide. *Clin Cancer Res* (2002) 8:2725–34.
22. Brassesco MS, Roberto GM, Morales AG, Oliveira JC, Delsin LE, Pezuk JA, et al. Inhibition of NF- κ B by Dehydroxymethylepoxyquinomicin Suppresses Invasion and Synergistically Potentiates Temozolomide and γ -Radiation Cytotoxicity in Glioblastoma Cells. *Chemother Res Pract* (2013) 2013:593020. doi: 10.1155/2013/593020
23. Galardi S, Mercatelli N, Farace MG, Ciafrè SA. NF-kB and C-Jun Induce the Expression of the Oncogenic miR-221 and miR-222 in Prostate Carcinoma and Glioblastoma Cells. *Nucleic Acids Res* (2011) 39:3892–902. doi: 10.1093/nar/gkr006
24. Yang TQ, Lu XJ, Wu TF, Ding DD, Zhao ZH, Chen GL, et al. MicroRNA-16 Inhibits Glioma Cell Growth and Invasion Through Suppression of BCL2 and the Nuclear Factor-κb1/MMP9 Signaling Pathway. *Cancer Sci* (2014) 105:265–71. doi: 10.1111/cas.12351
25. Yang G, Han D, Chen X, Zhang D, Wang L, Shi C, et al. MiR-196a Exerts its Oncogenic Effect in Glioblastoma Multiforme by Inhibition of Iκbα Both *In Vitro* and In Vivo. *Neuro Oncol* (2014) 16:652–61. doi: 10.1093/neuonc/not307
26. Rajbhandari R, McFarland BC, Patel A, Gerigk M, Gray GK, Fehling SC, et al. Loss of Tumor Suppressive microRNA-31 Enhances TRADD/NF-κb

Signaling in Glioblastoma. *Oncotarget* (2015) 6:17805–16. doi: 10.18632/oncotarget.4596
27. Wang H, Pan JQ, Luo L, Ning XJ, Ye ZP, Yu Z, et al. NF-κb Induces miR-148a to Sustain TGF-β/Smad Signaling Activation in Glioblastoma. *Mol Cancer* (2015) 14:2. doi: 10.1186/1476-4598-14-2
28. Wu H, Liu Q, Cai T, Chen YD, Wang ZF. Induction of microRNA-146a is Involved in Curcumin-Mediated Enhancement of Temozolomide Cytotoxicity Against Human Glioblastoma. *Mol Med Rep* (2015) 12:5461–6. doi: 10.3892/mmr.2015.4087
29. Xun M, Ma CF, Du QL, Ji YH, Xu JR. Differential Expression of miRNAs in Enterovirus 71-Infected Cells. *Virol J* (2015) 12:56. doi: 10.1186/s12985-015-0288-2
30. Chen X, Zhong SL, Lu P, Wang DD, Zhou SY, Yang SJ, et al. miR-4443 Participates in the Malignancy of Breast Cancer. *PloS One* (2016) 11:e0160780. doi: 10.1371/journal.pone.0160780
31. Meerson A, Yehuda H. Leptin and Insulin Up-Regulate miR-4443 to Suppress NCOA1 and TRAF4, and Decrease the Invasiveness of Human Colon Cancer Cells. *BMC Cancer* (2016) 16:882. doi: 10.1186/s12885-016-2938-1
32. Ebrahimi SO, Reiisi S. Downregulation of miR-4443 and miR-5195-3p in Ovarian Cancer Tissue Contributes to Metastasis and Tumorigenesis. *Arch Gynecol Obstet* (2019) 299:1453–8. doi: 10.1007/s00404-019-05107-x
33. Gao Y, Xu Y, Wang J, Yang X, Wen L, Feng J. lncRNA MNX1-AS1 Promotes Glioblastoma Progression Through Inhibition of miR-4443. *Oncol Res* (2019) 27(3):341–7. doi: 10.3727/096504018X15228909735079
34. Song YX, Sun JX, Zhao JH, Yang YC, Shi JX, Wu ZH, et al. Non-Coding RNAs Participate in the Regulatory Network of CLDN4 *via* ceRNA Mediated miRNA Evasion. *Nat Commun* (2017) 8:289. doi: 10.1038/s41467-017-00304-1
35. Xia S, Lal B, Tung B, Wang S, Goodwin CR, Laterra J. Tumor Microenvironment Tenascin-C Promotes Glioblastoma Invasion and Negatively Regulates Tumor Proliferation. *Neuro Oncol* (2016) 18:507–17. doi: 10.1093/neuonc/nov171
36. Gabrusiewicz K, Rodriguez B, Wei J, Hashimoto Y, Healy LM, Maiti SN, et al. Glioblastoma-Infiltrated Innate Immune Cells Resemble M0 Macrophage Phenotype. *JCI Insight* (2016) 1:e85841. doi: 10.1172/jci.insight.85841
37. Sivasankaran B, Degen M, Ghaffari A, Hegi ME, Hamou MF, Ionescu MC, et al. Tenascin-C is a Novel RBPJkappa-Induced Target Gene for Notch Signaling in Gliomas. *Cancer Res* (2009) 69:458–65. doi: 10.1158/0008-5472.CAN-08-2610
38. Bryukhovetskiy I, Shevchenko V. Molecular Mechanisms of the Effect of TGF-β1 on U87 Human Glioblastoma Cells. *Oncol Lett* (2016) 12:1581–90. doi: 10.3892/ol.2016.4756
39. Bonafé GA, Santos JS, Ziegler JV, Marson FAL, Rocha T, Ortega MM. Dipotassium Glycyrrhizinate on Melanoma Cell Line: Inhibition of Cerebral Metastases Formation by Targeting NF-kB Genes-Mediating microRNA-4443 and microRNA-3620. *Int J Mol Sci* (2022) 23, 7251. doi: 10.3390/ijms23137251

Conflict of Interest: Author JZ is employed by Verdi Cosmetics LLC, Joanópolis, São Paulo, Brazil.

The remaining authors declare that the research was conducted without any commercial or financial relationships that could be construed as a potential conflict of interest.

Publisher's Note: All claims expressed in this article are solely those of the authors and do not necessarily represent those of their affiliated organizations, or those of the publisher, the editors and the reviewers. Any product that may be evaluated in this article, or claim that may be made by its manufacturer, is not guaranteed or endorsed by the publisher.

frontiers | Frontiers in Oncology

TYPE Original Research
PUBLISHED 16 August 2022
DOI 10.3389/fonc.2022.901647

OPEN ACCESS

EDITED BY
Liam Chen,
University of Minnesota, United States

REVIEWED BY
Olga Vasiljeva,
CytomX Therapeutics Inc,
United States
Parandzem Khachatryan,
Yerevan State Medical University,
Armenia

*CORRESPONDENCE
Yiming Mu
muyiming@301hospital.com
Weijun Gu
guweijun301@163.com

SPECIALTY SECTION
This article was submitted to Neuro-Oncology and Neurosurgical Oncology, a section of the journal Frontiers in Oncology

RECEIVED 22 March 2022
ACCEPTED 27 July 2022
PUBLISHED 16 August 2022

CITATION
Liu H, Zhang S, Wu T, Lv Z, Ba J, Gu W and Mu Y (2022) Expression and clinical significance of Cathepsin K and MMPs in invasive non-functioning pituitary adenomas.
Front. Oncol. 12:901647.
doi: 10.3389/fonc.2022.901647

Expression and clinical significance of Cathepsin K and MMPs in invasive non-functioning pituitary adenomas

Hongyan Liu[1,2], Saichun Zhang[2], Ting Wu[1,2], Zhaohui Lv[1,2], Jianming Ba[2], Weijun Gu[1,2]* and Yiming Mu[1,2]*

[1]The Chinese PLA Medical School, Beijing, China, [2]Department of Endocrinology, The First Medical Center of Chinese PLA General Hospital, Beijing, China

Background: Cathepsin K (CTSK) is a protease that degrades type I collagen and extracellular matrix, thereby contributing to bone resorption and tumor invasion. Some pituitary adenomas (PAs) could invade the sphenoid sinus (SS) and cavernous sinus (CS).

Purpose: This retrospective cohort study aimed to study the expression of tumoral biomarkers (CTSK, MMP9, MMP2, TIMP2, and PTTG1) and evaluate their clinical significance in non-functioning pituitary adenomas (NFPAs) with different invasion patterns.

Methods: We assessed the expression levels of candidate invasion-specific protein biomarkers CTSK, MMP9, MMP2, TIMP2, and PTTG1 by immunohistochemical staining in paraffin-embedded NFPA tumor tissues. Variations in staining intensity were analyzed in cases with SS and CS invasion and non-invasive NFPAs.

Results: We found that the levels of CTSK were higher in PA cases with SS invasion than that in PA cases with CS invasion (95.57 ± 31.57 vs. 65.29 ± 29.64, $P < 0.001$), and the expression of MMP9 and MMP2 was higher in CS-invasive cases than that in SS-invasive cases (145.02 ± 49.25 vs. 111.80 ± 51.37, $P = 0.002$, and 138.67 ± 52.06 vs. 108.30 ± 41.70, $P = 0.002$). Multiple Cox regression demonstrated that higher CTSK expression (P=0.011), subtotal resection (P<0.001), invasion (P=0.037), and larger tumor diameter (P=0.001) were independent risk factors for recurrence. A positive correlation was observed between CTSK expression and tumor size (r=0.671, p<0.001). There was no significant difference in TIMP2 and PTTG1 levels between CS-and SS-

invasive cases (97.42± 39.80 vs. 102.10± 43.22, P = 0.58 and 13.89 ± 4.59 vs. 12.56 ± 3.96, P = 0.14).

Conclusion: Our data indicated that CTSK has the potential as a marker for SS invasion of PAs, whereas MMP9 and MMP2 may be markers for CS invasion. And CTSK may play an important role in tumor relapse.

KEYWORDS

Cathepsin K, sphenoid sinus, pituitary adenomas, invasion

Introduction

Pituitary adenomas (PAs) are one of the most common intracranial tumors, with an overall community-based prevalence of 68-116 per 100 000 population (1–7), with the increasing annual incidence rate mainly due to incidentalomas. They are usually benign and slow-growing, causing symptoms because of excess hormone secretion or compression of close-by structures. However, they may become locally invasive, namely invasive PAs (IPAs), resulting in infiltration within the sphenoid sinus (SS; the destruction of the sellar floor is the first step in this process), cavernous sinus (CS), or suprasellar structures, especially nonfunctioning PAs (NFPAs) because of a lack of typical clinical symptom. The main clinical manifestations of NFPAs are compression effects, such as visual disturbance, headache, and hypopituitarism. It is difficult to achieve a total resection of the tumor tissues for IPA patients and they are associated with a higher rate of recurrence and a lower rate of remission.

Abundant articles have analyzed and hypothesized the mechanisms involved in the invasion process of PAs. Many studies have investigated the correlation between the invasion of PAs and several biological markers, including matrix metalloproteinase-9 (MMP9), matrix metalloproteinase-2 (MMP2), tissue inhibitor of metalloproteinases-2 (TIMP2), and pituitary tumor transforming gene 1 protein (PTTG1, also called securin) (8–13). Our previous meta-analysis has shown that MMP9 and MMP2 expression in IPAs was distinctly higher than that in noninvasive PAs (non-IPAs) (14). Chen, K. et al. reported that epithelial-mesenchymal transition (EMT)-related markers in serum exosomes were associated with invasion of PAs (15). However, the established mechanisms still need to be explored. Some researchers believe that PAs extending into CS are not invasive, and the extension into the CS occurs due to its medial wall weakness, and sometimes defect (10, 16). To our knowledge, no study has investigated the protein expression in SS invasion only or compared the expression levels in SS- and CS-invasive PAs.

Cathepsin K (CTSK), one of the papain-like cysteine proteases (17), is expressed predominantly in activated osteoclasts. CTSK, having high matrix-degrading activity, could degrade collagens, especially type I collagen (18), which is the main component (90%) of bone collagen fibers, and plays a crucial role in bone resorption. Beyond the osteoclasts, CTSK is highly expressed in various malignant tumors, such as breast carcinomas, lung cancers, melanomas, ovarian carcinomas, and prostate cancers (19–24). Besides, a higher level of CTSK expression was found in patients with bone metastasis or invasive tumor than that in patients with primary tumors (22, 25, 26). The bone metastases in breast carcinomas or prostate cancers are predominantly osteolytic (27, 28). *In vitro* experiments, animal models and clinical trials have evaluated the efficiency of several CTSK inhibitors (CatKi). *In vitro* experiments of Liang, W. et al. showed that CatKi reduced tumor invasion of prostate cancers and bone resorption induced by conditioned media of prostate cancers (29). They further conducted experiments in the animal models and found that CatKi prevented and reduced prostate cancer establishment and bone metastasis. Similarly, Le Gall et al. observed a reduction in osteolytic lesions in nude mice with bone metastatic breast cancer after being administered with CatKi AFG-495 (25). Moreover, a clinical randomized controlled trial (RCT) by Jensen et al. found that for breast cancer patients with bone metastases, the efficacy and safety of CatKi odanacatib were similar to that of zoledronic acid (ZOL), a standard therapeutic option for breast cancer bone metastases, after 4 weeks of treatment (30). Like bone metastases of breast carcinomas or prostate cancers, PAs with SS or clivus invasion lead to osteolytic lesions (31). Thus, we hypothesized that CTSK may play a role in SS or clivus invasion of PAs, which has been published previously (32). The present study aimed to verify our hypothesis, study the clinical significance of CTSK, and investigate the differential expression of MMP9, MMP2, TIMP2, and PTTG1 in SS and CS invasion of NFPAs.

Materials and methods

Patients

NFPAs were used in our study only because we could not determine whether the abnormal hormone secretion in functioning PAs will affect the expression of CTSK. Of the patients undergoing surgery for resection of PAs at the Chinese PLA General Hospital (Beijing, P.R. China) between 2011 and 2018, 176 cases met the following criteria: 1) transsphenoidal surgery; 2) no radiotherapy, chemotherapy, or any other medical interventions before the surgery; 3) complete clinical and radiological information in the database; 4) NFPAs. The diagnosis of the tumor and its functional status was according to its clinical, biochemical and radiological features, and was verified by immunohistological staining for prolactin (PRL), growth hormone (GH), adrenocorticotropic hormone (ACTH), thyroid-stimulating hormone (TSH), follicular stimulating hormone (FSH), and luteinizing hormone (LH). IHC criteria for NFPAs are silent gonatotropinomas and null-cell adenomas. The following criteria were used to define invasion: (1) preoperative images showed that Knosp/Hardy grades were 3 or 4; (2) intraoperative inspection of tumor infiltration within the SS (destruction of sellar floor or clivus only were included) and CS. The invasion was diagnosed only when both of the above criteria are met. 176 cases included 44 PAs invading SS only, 50 PAs invading CS only, 2 PAs invading both SS and CS, and 80 non-IPAs. Finally, Paraffin-embedded tissues of 174 patients including PAs invading SS only (n =44), PAs invading CV only (n = 50), and noninvasive PAs (n = 80) were used for immunohistochemical staining. In the SS invasion group, there were 20 women and 24 men, with a mean age of 50.2 ± 12.0 years (range 19-81 years). In the CS invasion group, there were 28 women and 22 men, with a mean age of 52.4 ± 14.8 years (range 19-78 years). In the non-invasion group, there were 40 women and 40 men, with a mean age of 48.1 ± 12.9 years (range 10-75 years). Micro-adenomas were defined as the largest tumor diameter (LTD) < 1cm and macro-adenomas were defined as the LTD ≥1cm, among which the LTD > 3cm were defined as large adenomas and the LTD > 4cm were defined as giant adenomas. There were 52 patients with large adenomas and 18 patients with giant adenomas.

Postoperative follow-up

Postoperative telephone or outpatient follow-up was conducted every 6 months until December 2021. MR scans were used to evaluate tumor relapse. Tumor relapse is defined as tumor recurrence after gross-total resection (GTR) or an increase of residual tumor more than 2-mm in at least one dimension after subtotal resection (STR) according to contrast-enhanced (CE) T1WI (33). This study was approved by the Ethics Committee of the Chinese (People's Liberation Army (PLA) General Hospital.

Antibodies and dilutions

The following antibodies and kits were used: rabbit monoclonal primary antibody to human CTSK (ab207086, dilution 1:1,000), mouse monoclonal primary antibody to human MMP9 (ab58803, 1:500), mouse monoclonal primary antibody to human MMP2 (ab86607, 1:200), mouse monoclonal primary antibody to human TIMP2 (ab1828, 1:50), mouse monoclonal primary antibody to human PTTG1 (ab3305, 1:100), and mouse and rabbit specific HRP/DAB (ABC) detection IHC Kit (ab64264, including biotinylated goat anti-polyvalent, streptavidin peroxidase, 50×DAB chromogen, DAB substrate, and hydrogen peroxide block). All antibodies were purchased from Abcam (Cambridge, MA USA).

Immunohistochemical staining procedure

Paraffin sections (4 μm-thick) were deparaffinized in xylene and rehydrated through graded ethanol (100% I, 100% II, 90%, and 80%). For antigen retrieval, the sections were heated at 100 ° C in a microwave in 1× citrate buffer, pH 6.0 (MMP9, MMP2, and TIMP2 staining) or an EDTA solution, pH 9.0 (CTSK and PTTG1 staining) for 2.5 min. To block the endogenous peroxidase activity, the slides were immersed in 3% hydrogen peroxide (H_2O_2) in methanol for 15 min and then washed three times with 1× phosphate-buffered saline (PBS) for 5 min. The slides were then incubated with the primary antibodies indicated above, overnight at 4 °C in a humidified chamber, and then washed with PBS. Biotinylated goat anti-polyvalent and streptavidin peroxidase were then added and incubated for 10 min at 20-25°C, in succession. After washing with PBS, the slides were treated with 3,3'-diaminobenzidine (DAB) substrate for 15 min at 20-25°C. The slides were then washed two times with water, lightly counterstained with hematoxylin, and finally, mounted with coverslips and DPX after dehydration through an ethanol gradient (80%, 90%, 100% II, and 100% II) (34).

Analysis of immunohistochemical results

For each case, 2 slides were analyzed. For each slide, 5 microscopic fields were counted. The intensity of expression was scored as 0 (negative staining), 1 (weak staining), 2 (moderate staining), or 3 (strong staining). The extent of expression was calculated using the Image Pro-Plus (IPP) software (Media Cybernetic, USA) (35).

For CTSK, MMP9, MMP2, and TIMP2, the final score was calculated as follows: (1×% of weak staining) + (2×% of moderate staining) + (3×% of strong staining). For PTTG1, the final score was calculated as follows: percentage of weak staining + percentage of moderate staining + percentage of strong staining (36). The expression of final score was described as numbers without %.

Taking the tertile 1 (Q1) value of expression as the boundary line, patients could be separated into high expression and low expression groups.

The assessment of protein expression was conducted independently by two pathologists. To constrain bias, both pathologists were blinded to whether the images were from invasive cases or non-invasive cases.

Statistical analyses

Continuous variables are expressed as the mean ± standard deviation (SD) or median (inter-quartile range, IQR) (for data not conforming to normal distribution) and categorical variables are expressed as frequency and percentage. Continuous variables were compared using the Student's T-test (for data conforming to normal distribution and homogeneity of variance) or Wilcoxon test or Kruskal-Wallis H test (for data not conforming to normal distribution or homogeneity of variance). Categorical variables were compared using the Chi-square test. Pearson analysis was used for correlation analysis of all possible pairwise combinations of CTSK, MMP9, MMP2, TIMP2, and PTTG1 proteins' expression and correlation analysis of CTSK expression and tumor size. $P < 0.05$ was considered statistically significant. The Cox regression model was used to investigate factors related to recurrence of PAs. The SPSS software (version 25.0, IBM) and GraphPad Prism 8 (GraphPad Software Inc., San Diego, CA, USA) were used to perform all analyses.

Results

Expression and invasion

CTSK and invasion

Representative images of CTSK staining were showed in Figure 1A. CTSK was expressed in 91% of the PA cases with SS invasion, 78% of the PA cases with CS invasion, and 51% of the non-invasive PA cases. Additionally, CTSK expression was higher in invasive than in non-invasive PA cases (79.46 ± 33.98 vs. 48.09 ± 19.50, $P < 0.001$), and in SS-invasive cases than in CS-invasive cases (95.57 ± 31.57 vs. 65.29 ± 29.64, $P < 0.001$, Figure 1B).

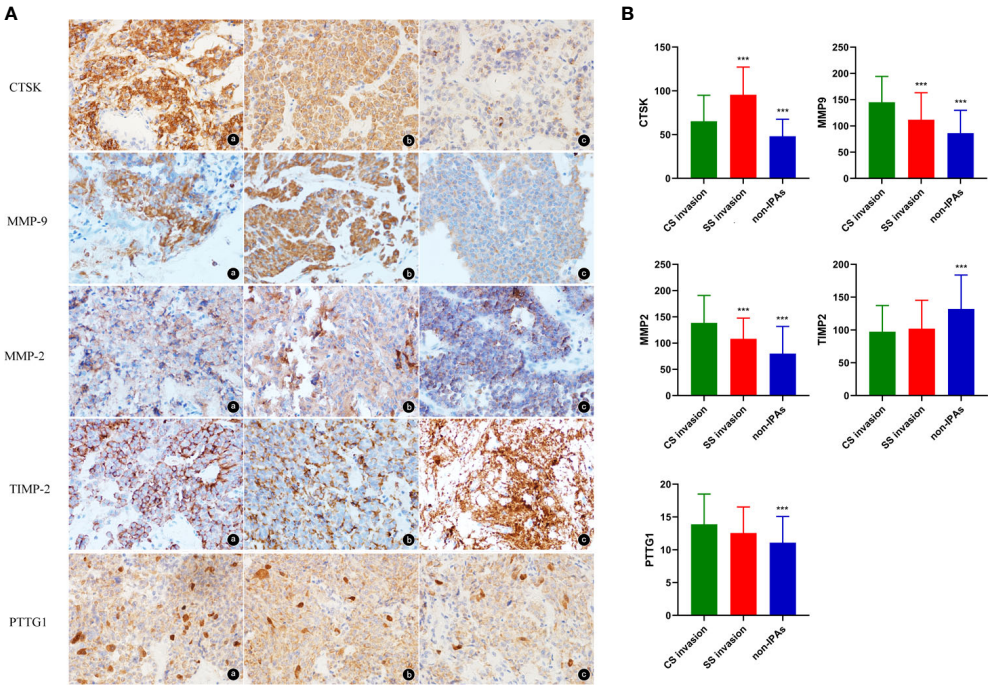

FIGURE 1
(A) Representative images of CTSK, MMP9, MMP2, TIMP2, and PTTG1 staining of PAs (magnification, 40×). a: PAs with SS invasion, b: PAs with CS invasion, c: non-IPAs. **(B)** Expression levels (%) (mean ± SD) of CTSK, MMP9, MMP2, TIMP2, and PTTG1 (Student's t-test: ***p<0.001). SD: standard deviation.

MMP9 and invasion

MMP9 was expressed primarily in the cytoplasm (Figure 1A). MMP9 was expressed in 100% of the SS-invasive cases, 100% of the CS-invasive cases, and 85% of the non-invasive PA cases. MMP9 expression was higher in invasive cases than in non-invasive cases (129.47 ± 52.69 vs. 86.35 ± 43.44, P < 0.001), and in CS-invasive cases than in SS-invasive cases (145.02 ± 49.25 vs. 111.80 ± 51.37, P = 0.002, Figure 1B).

MMP2 and invasion

MMP2 was expressed primarily in the cytoplasm (Figure 1A). MMP2 was expressed in 100% of the SS-invasive cases, 100% of the CS-invasive cases, and 90% of the non-invasive cases. MMP2 levels were higher in invasive than in non-invasive PA cases (124.46 ± 50.11 vs. 79.99 ± 51.87, P < 0.001), and in CS-invasive cases than in SS-invasive cases (138.67 ± 52.06 vs. 108.30 ± 41.70, P = 0.002, Figure 1B).

TIMP2 and invasion

TIMP2 was expressed primarily in the cytoplasm (Figure 1A). TIMP2 expression was lower in invasive cases than in non-invasive cases (99.61 ± 41.28 vs. 132.15± 51.64, P < 0.001). There was no significant difference in TIMP2 levels between CS-and SS-invasive cases (97.42± 39.80 vs. 102.10± 43.22, P = 0.58, Figure 1B).

PTTG1 and invasion

PTTG1 was expressed both in cytoplasm and nuclei (Figure 1A). PTTG1 expression was higher in invasive than in non-invasive cases (13.27 ± 4.34 vs. 11.08 ± 4.00, P = 0.001). There was no significant difference in PTTG1 expression between CS- and SS-invasive cases (13.89 ± 4.59 vs. 12.56 ± 3.96, P = 0.14, Figure 1B).

Expression and tumor size

The mean LTD in invasive and non-invasive cases were 3.41 ± 0.67 cm and 2.40 ± 0.52 cm, respectively (p<0.001, Figure 2A). The mean LTD in SS invasive and CS invasive cases were 3.64 ± 0.68 cm and 3.21 ± 0.60 cm, respectively (p=0.002, Figure 2B).

The mean LTD in CTSK high-expression cases and CTSK low-expression cases were 3.04 ± 0.82 cm and 2.76 ± 0.69 cm, respectively (p=0.028). A positive correlation was observed between CTSK expression and tumor size (r=0.671, p<0.001) (Figure 2C). There was no significant difference in the mean LTD between different MMP9, MMP2, TIMP2, and PTTG1-expression groups (all p>0.05, Additional file 1).

Expression and clinical features of patients

The postoperative follow-up time was 45.74 ± 20.33 months (range from 2.17 to 70.6 months). In total, 63 (36.2%) patients had tumor relapse and the average time to recurrence was 26.59 ± 11.24 months. 40 of 94 (42.6%) IPA patients recurred with an average time of 24.34 ± 9.91 months.

The Cox regression model was used to further investigate the factors related to tumor relapse. Univariate Cox analysis demonstrated that the older [HR: 2.22 (1.22-4.02), p=0.009], higher CTSK expression [HR: 2.22 (1.22-4.02), p=0.009], STR [HR: 0.27 (0.16-0.44), p<0.001], invasion [HR: 1.32 (1.02-1.70), p=0.036], and

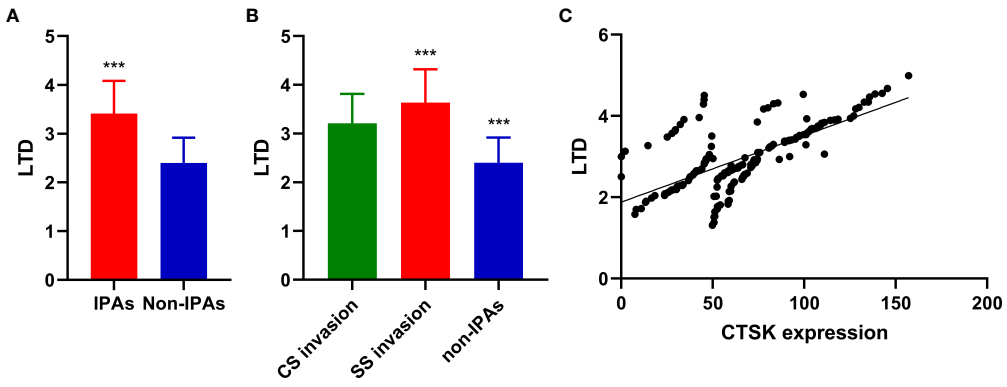

FIGURE 2
Correlations between PAs invasion, CTSK expression, and tumor size. **(A)**: Tumor size (cm) (mean ± SD) in in invasive and non-invasive PAs (Student's t-test: ***p<0.001). **(B)** Tumor size (cm) (mean ± SD) in CS invasive PA, SS invasive PAs, and non-IPAs (Student's t-test: ***p<0.001). **(C)** Correlations between CTSK expression (%) and tumor size (cm). (r=0.671, p<0.001). SD: standard deviation.

larger LTD [HR: 2.87 (1.72-4.78), p<0.001] were associated with recurrence. Multiple Cox analysis demonstrated that higher CTSK expression [HR: 2.31 (1.22-4.39), P=0.011], STR [HR: 0.34 (0.21-0.57), P<0.001], invasion [HR: 0.65 (0.44-0.97), P=0.037], and larger LTD [HR: 3.60 (1.68-7.75), P=0.001] were independent risk factors for recurrence (Table 1). Kaplan–Meier curve demonstrated that higher CTSK expression, STR, invasion, and larger LTD group had worse recurrence-free survival (RFS) (Figure 3). Regarding the surgical resection degree, 42 (24.1%) patients had a residual tumor in the CTSK high-expression group while only 9 cases (5.2%) had a residual tumor in the low-expression group. However, this difference was not statistically significant (p=0.06). Compression symptoms are the main clinical manifestations of NFPAs. Patients with compression symptoms had a higher CTSK expression than those without (p=0.001). No evident correlation was found between expression levels of CTSK and other clinical features of PAs, including gender, age, pituitary apoplexy, and tumor texture. Detailed clinical features were summarized in Table 2. No evident correlation was found between expression levels of MMP9, MMP2, TIMP2, and PTTG1 and clinical features of PAs, including gender, age, compression symptoms, pituitary apoplexy, tumor texture, resection degree, and recurrence. Detailed clinical features were summarized in Additional file 2.

TABLE 1 Factors related to pituitary adenoma recurrence by Cox regression analysis.

	Univariate Cox regression		Multiple Cox regression	
	HR (95%)	P value	HR (95%)	P value
Age[1]	1.02 (1.00-1.04)	**0.038**	1.02 (0.99-1.04)	0.06
Sex[2]	1.03 (0.63-1.68)	0.920		
Tumor texture[3]	reference			
	3.23 (0.44-23.52)	0.247		
	3.45 (0.47-25.63)	0.225		
MMP9 expression[4]	0.98 (0.58-1.64)	0.930		
MMP2 expression[4]	1.22 (0.71-2.08)	0.477		
TIMP2 expression4	1.36 (0.79-2.35)	0.270		
PTTG1 expression[4]	1.29 (0.76-2.20)	0.339		
CTSK expression[4]	2.22 (1.22-4.02)	**0.009**	2.31 (1.22-4.39)	**0.011**
Resection degree[7]	0.27 (0.16-0.44)	**<0.001**	0.34 (0.21-0.57)	**<0.001**
Invasion[6]	1.32 (1.02-1.70)	**0.036**	0.65 (0.44-0.97)	**0.037**
LTD[5]	2.87 (1.72-4.78)	**<0.001**	3.60 (1.68-7.75)	**0.001**

[1]age as a continuous variable. [2]male vs. female, [3]cystic vs. solid vs. cystic & solid, [4]high expression vs. low expression, [5]>3cm vs. ≤3cm, [6]IPAs vs. non-IPAs, [7]GTR vs. STR. LTD, the largest tumor diameter; IPAs, invasive pituitary adenomas; non-IPAs, non-invasive pituitary adenomas. GTR, gross-total resection; STR, subtotal resection. The bold values mean p<0.05.

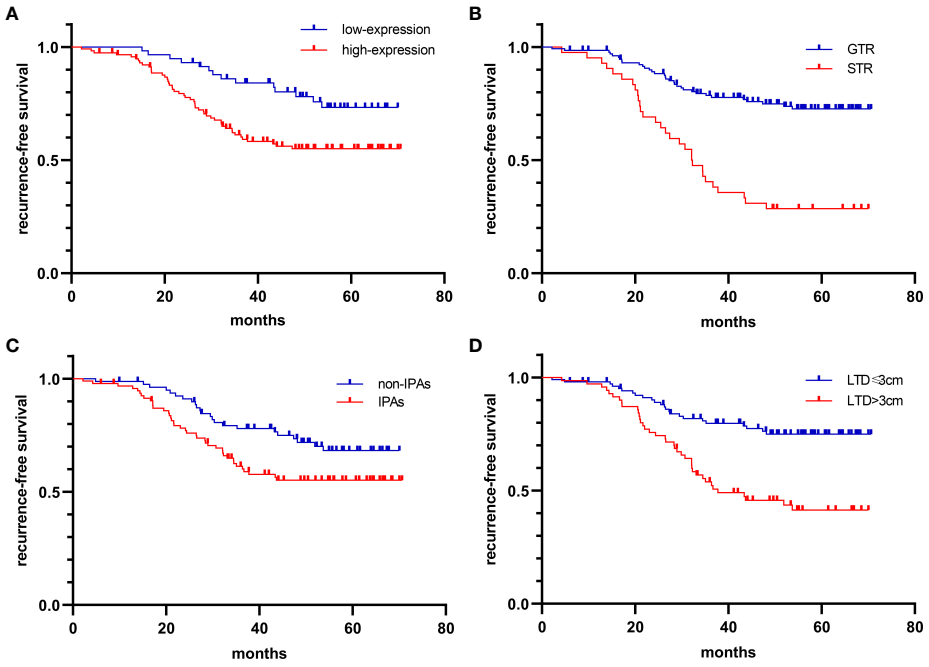

FIGURE 3
Kaplan-Meier curves for the recurrence-free interval. **(A)** high-CTSK expression vs. low-CTSK expression [HR: 2.31 (1.22-4.39), P=0.011], **(B)** GTR vs. STR [HR: 0.34 (0.21-0.57), P<0.001], **(C)** IPAs vs. Non-IPAs [HR: 0.65 (0.44-0.97), P=0.037], **(D)** LTD>3cm vs. LTD ≤ 3cm [HR: 3.60 (1.68-7.75), P=0.001].

TABLE 2 Relationship between CTSK expression and clinical features of patients.

Clinical features	N	CTSK expression		X^2	p
		High 116	Low 58		
Sex					
Male	86	54	32	1.15	0.284
Female	88	62	26		
Age (year)					
<50	90	59	31	0.104	0.748
≥50	84	57	27		
LTD					
≤3cm	104	62	42	5.784	**0.016**
>3cm	70	54	16		
Invasiveness					
IPAs	94	80	14	31.283	**0.000**#
SS-IPAs	44	42	2	6.988	**0.008***
CS-IPAs	50	38	12		
non-IPAs	80	36	44		
Compression symptoms					
Yes	112	85	27	12.04	**0.001**
No	62	31	31		
Pituitary apoplexy					
Yes	30	18	12	0.725	0.395
No	144	98	46		
Tumor texture					
Cystic	7	3	4		
Solid	110	74	36	0.23	0.88
Cystic & solid	57	39	18		
Resection degree					
Total	132	83	49	3.531	0.06
Residual	42	33	9		
Recurrence					
Yes	63	49	14	5.486	**0.019**
No	111	67	44		

#P-value for comparison of IPAs and Non-IPAs, *P value of comparison of SS-IPAs and CS-IPAs. LTD, the largest tumor diameter; SS, sphenoid sinus; CS, cavernous sinus; IPAs, invasive pituitary adenomas; non-IPAs, non-invasive pituitary adenomas. The bold values mean p<0.05.

Relationship between CTSK, MMP-9, MMP-2, TIMP-2, PTTG1 Protein expression

A positive correlation was observed between MMP9 and MMP2 expression (r=0.824, p<0.001). There is a negative correlation between MMP9 and TIMP2 (r=-0.743, p<0.001) and MMP2 and TIMP2 (r=-0.700, p<0.001). No significant correlation was found between the expression of others (Figure 4).

Discussion

To our knowledge, this is the first study that investigates the difference in the expression of MMP9, MMP2, TIMP2, and PTTG1 in PAs with SS and CS invasion and explores the expression of CTSK in SS invasion of PAs. Our results showed that PAs with SS invasion express significantly higher levels of CTSK compared with PAs with CS invasion and non-invasive controls, confirming our hypothesis. CTSK is expressed predominantly in osteoclasts, and can also be expressed in thyroid epithelial cells and skin fibroblasts (37). Christensen et al. have reported that CTSK, besides degrading type I collagen, can cleave and activate MMP9 in acidic environments such as those seen in tumors and during bone resorption (38), therefore contributing to the degradation of type I collagen and other matrix proteins and facilitating bone metastases. A similar bone resorption mechanism (*via* CTSK expression) might be involved in the SS invasion of PAs.

We also found that the higher CTSK expression was associated with higher rate of compression symptoms and large adenomas. It is well known that oversized tumors were responsible for compression symptoms of PAs. *In vitro* experiments of Yang, H. et al. demonstrated that CTSK high-expression contributed to the proliferation and migration of human non-small cell lung cancer (NSCLC) cells by activating the mammalian target of rapamycin (mTOR) signaling pathway (39). *In vitro* experiments of Gu, X. et al. found that down-

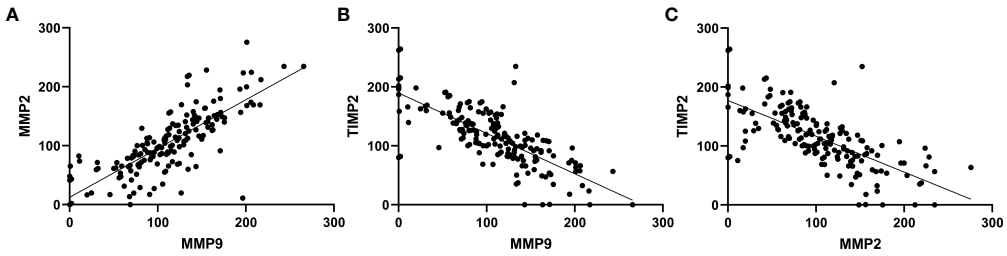

FIGURE 4
Correlations between expression of MMP9, MMP2 and TIMP2. **(A)** MMP9 and MMP2 (r=0.824, p<0.001). **(B)** MMP2 and TIMP2 (r=-0.700, p<0.001). **(C)** MMP9 and TIMP2 (r=-0.743, p<0.001).

regulation of CTSK expression could inhibit the proliferation and migration of breast cancer cells (40). Thus, we consider that CTSK may have a potential role in the proliferation of PA cells.

Our results show that IPA tissues express significantly higher levels of MMP9 and MMP2 compared with non-IPA tissues. Additionally, PA tissues with CS invasion express higher levels of MMP9 and MMP2 compared with PA tissues with SS invasion, indicating the important role of MMP9 and MMP2 in CS invasion. MMP9 and MMP2 degrade primarily collagen type IV, which is the prominent component of the basement membrane, pituitary capsule, medial wall of the cavernous sinus, and reticular fiber roof of the hypophysis (41), and it is also the key component of the dura mater. Notably, Deryugina et al. have found that MMP9 and MMP2 can contribute to tumor angiogenesis, which is important in tumor invasion and metastasis (42).

Our results show that IPA tissues express significantly higher levels of PTTG1 compared with non-IPA tissues. Malik *et al.* have reported that PTTG1 contributes to tumor growth and metastasis by increasing the expression of MMP-2 (43). Similarly, Lim et al. have found that PTTG1 can inhibit trophoblast invasion by regulating the expression and secretion of MMP9 and MMP2 (44). Liu et al. have found that folate receptor α (FRα)-targeted liposomes loaded with doxorubicin (F-L-DOX) have the anti-invasive ability in NFPAs by suppressing the secretion of MMP9 and MMP2 (45). Additionally, Barreiros et al. have reported that Toll-like receptor 2 (TLR2) and myeloid differentiation factor 88 (MyD88) are associated with apical periodontitis progression, possibly through the modulation of MMP9 and MMP2 (46). Besides, some proteins related to PA invasion, such as the discoidin domain receptor-1 (DDR1) (47), and β-catenin (48), have been reported to function by regulating the levels of MMP9 and MMP2. These data indicate that MMP9 and MMP2 play an important role in the invasion of PAs, particularly in CS invasion, and other related proteins may act through the regulation of MMP9 and MMP2 or in an MMP-independent manner.

We found that IPA tissues expressed significantly lower levels of TIMP2 compared with non-IPA tissues; this data differs from that obtained by Gültekin et al. (8). TIMP2 inhibits MMP activity by forming noncovalent complexes with the MMP protease active site. TIMP2 was initially shown to prohibit cell proliferation and migration *via* inhibiting the function of MMPs (49), and many studies found that TIMP2 could also be predictive of better prognosis in several cancer types, such as breast cancer (50), gastric cancer (51), colorectal cancer (52), and non-small cell lung cancer (49). However, TIMP2 can also act as an activator of MMPs, by forming the complex MT1-MMP/TIMP2 (53). Stetler-Stevenson *et al.* have found that TIMP2 can play other roles in an MMP-independent manner (54). Therefore, the function of TIMP2 is complex, and additional studies are needed to investigate the relationship between TIMP2 expression and tumor invasion.

Our results showed that the recurrence rate of NFPAs was 36.2% after surgical resection. Many articles have reported that larger LTD, invasion, and STR are related to a higher risk of recurrence (55–57). Similarly, a significant association of larger LTD, invasion, and STR, and with recurrence was observed in our study. We also found that higher CTSK expression, not MMP9, MMP2, TIMP2, and PTTG1 expression, was a risk factor for recurrence. Up to now, this is the first study to explore the relationship between CTSK expression and the recurrence of PAs. However, the relationship between CTSK expression and the recurrence of other cancers has been studied. Cordes, C. et al. reported that in patients with NSCLC, a high expression of CTSK was associated with a substantial increase of recurrence and mortality (21).

In conclusion, our data indicated that CTSK has the potential as a marker for SS invasion of PAs, whereas MMP9 and MMP2 may be markers for CS invasion. And CTSK may play an important role in tumor relapse. In the future, CTSK is expected to be as a predictor of bone invasion and recurrence of NFPAs in clinical practice. Our results provide insights to explore and understand the mechanisms involved in the invasion of PAs and seek new therapies for patients with IPAs. In the next future, we plan to perform studies on animal models, to investigate the function of CatKi in SS invasion of PAs.

Data availability statement

The original contributions presented in the study are included in the article/Supplementary Material. Further inquiries can be directed to the corresponding author.

Ethics statement

The studies involving human participants were reviewed and approved by Ethics Committee of the Chinese PLA General Hospital. The patients/participants provided their written informed consent to participate in this study.

Author contributions

HL experimented and analyzed the data. She was a major contributor to writing the manuscript. SZ, WG, and TW supervised the histological examination. ZL and JB made substantial contributions to conception and design, or acquisition of data, or analysis and interpretation of data, and have been involved in revising it critically for important intellectual content. WG and YM were the superior advisors. They gave final approval of the version to be published and agreed to be accountable for all aspects of the work in ensuring that questions related to the accuracy or integrity of any part of

the work are appropriately investigated and resolved. All authors read and approved the final manuscript.

Acknowledgments

The authors thank all of the patients at the Chinese People's Liberation Army General Hospital who formed part of the treatment groups.

Conflict of interest

The authors declare that the research was conducted in the absence of any commercial or financial relationships that could be construed as a potential conflict of interest.

Publisher's note

Supplementary material

The Supplementary Material for this article can be found online at: https://www.frontiersin.org/articles/10.3389/fonc.2022.901647/full#supplementary-material

References

1. Daly AF, Rixhon M, Adam C, Dempegioti A, Tichomirowa MA, Beckers A. High prevalence of pituitary adenomas: a cross-sectional study in the province of liege, Belgium. *J Clin Endocrinol Metab* (2006) 91(12):4769–75. doi: 10.1210/jc.2006-1668

2. Fontana E, Gaillard R. [Epidemiology of pituitary adenoma: results of the first Swiss study]. *Rev Med Suisse* (2009) 5(223):2172–4.

3. Fernandez A, Karavitaki N, Wass JA. Prevalence of pituitary adenomas: a community-based, cross-sectional study in Banbury (Oxfordshire, UK). *Clin Endocrinol (Oxf)* (2010) 72(3):377–82. doi: 10.1111/j.1365-2265.2009.03667.x

4. Raappana A, Koivukangas J, Ebeling T, Pirilä T. Incidence of pituitary adenomas in northern Finland in 1992-2007. *J Clin Endocrinol Metab* (2010) 95 (9):4268–75. doi: 10.1210/jc.2010-0537

5. Gruppetta M, Mercieca C, Vassallo J. Prevalence and incidence of pituitary adenomas: a population based study in Malta. *Pituitary* (2013) 16(4):545–53. doi: 10.1007/s11102-012-0454-0

6. Agustsson TT, Baldvinsdottir T, Jonasson JG, Olafsdottir E, Steinthorsdottir V, Sigurdsson G, et al. The epidemiology of pituitary adenomas in Iceland, 1955-2012: a nationwide population-based study. *Eur J Endocrinol* (2015) 173(5):655–64. doi: 10.1530/eje-15-0189

7. Day PF, Loto MG, Glerean M, Picasso MF, Lovazzano S, Giunta DH. Incidence and prevalence of clinically relevant pituitary adenomas: retrospective cohort study in a health management organization in Buenos Aires, Argentina. *Arch Endocrinol Metab* (2016) 60(6):554–61. doi: 10.1590/2359-3997000000195

8. Gültekin GD, Çabuk B, Vural Ç, Ceylan S. Matrix metalloproteinase-9 and tissue inhibitor of matrix metalloproteinase-2: Prognostic biological markers in invasive prolactinomas. *J Clin Neurosci* (2015) 22(8):1282–7. doi: 10.1016/j.jocn.2015.02.021

9. Knappe UJ, Hagel C, Lisboa BW, Wilczak W, Lüdecke DK, Saeger W. Expression of serine proteases and metalloproteinases in human pituitary adenomas and anterior pituitary lobe tissue. *Acta Neuropathol* (2003) 106 (5):471–8. doi: 10.1007/s00401-003-0747-5

10. Yokoyama S, Hirano H, Moroki K, Goto M, Imamura S, Kuratsu JI. Are nonfunctioning pituitary adenomas extending into the cavernous sinus aggressive and/or invasive? *Neurosurgery* (2001) 49(4):857–862; discussion 862-853. doi: 10.1097/00006123-200110000-00014

11. Turner HE, Nagy Z, Esiri MM, Harris AL, Wass JA. Role of matrix metalloproteinase 9 in pituitary tumor behavior. *J Clin Endocrinol Metab* (2000) 85(8):2931–5. doi: 10.1210/jcem.85.8.6754

12. Xiao JQ, Liu XH, Hou B, Yao Y, Deng K, Feng M, et al. Correlations of pituitary tumor transforming gene expression with human pituitary adenomas: a meta-analysis. *PloS One* (2014) 9(3):e90396. doi: 10.1371/journal.pone.0090396

13. Kum SJ, Lee HW, Kim SG, Park H, Hwang I, Kim SP. Association of PTTG1 expression with invasiveness of non-functioning pituitary adenomas. *J Pathol Transl Med* (2022) 56(1):22–31. doi: 10.4132/jptm.2021.08.31

14. Liu HY, Gu WJ, Wang CZ, Ji XJ, Mu YM. Matrix metalloproteinase-9 and -2 and tissue inhibitor of matrix metalloproteinase-2 in invasive pituitary adenomas: A systematic review and meta-analysis of case-control trials. *Med (Baltimore)* (2016) 95(24):e3904. doi: 10.1097/md.0000000000003904

15. Chen K, Li G, Kang X, Liu P, Qian L, Shi Y, et al. EMT-related markers in serum exosomes are potential diagnostic biomarkers for invasive pituitary adenomas. *Neuropsychiatr Dis Treat* (2021) 17:3769–80. doi: 10.2147/ndt.S339067

16. Dietemann JL, Kehrli P, Maillot C, Diniz R, Reis MJr., Neugroschl C, et al. Is there a dural wall between the cavernous sinus and the pituitary fossa? anatomical and MRI findings. *Neuroradiology* (1998) 40(10):627–30. doi: 10.1007/s002340050653

17. Rawlings ND, Waller M, Barrett AJ, Bateman A. MEROPS: the database of proteolytic enzymes, their substrates and inhibitors. *Nucleic Acids Res* (2014) 42 (Database issue):D503–509. doi: 10.1093/nar/gkt953

18. Garnero P, Ferreras M, Karsdal MA, Nicamhlaoibh R, Risteli J, Borel O, et al. The type I collagen fragments ICTP and CTX reveal distinct enzymatic pathways of bone collagen degradation. *J Bone Miner Res* (2003) 18(5):859–67. doi: 10.1359/jbmr.2003.18.5.859

19. Littlewood-Evans AJ, Bilbe G, Bowler WB, Farley D, Wlodarski B, Kokubo T, et al. The osteoclast-associated protease cathepsin K is expressed in human breast carcinoma. *Cancer Res* (1997) 57(23):5386–90.

20. Duong LT, Wesolowski GA, Leung P, Oballa R, Pickarski M. Efficacy of a cathepsin K inhibitor in a preclinical model for prevention and treatment of breast cancer bone metastasis. *Mol Cancer Ther* (2014) 13(12):2898–909. doi: 10.1158/1535-7163.Mct-14-0253

21. Cordes C, Bartling B, Simm A, Afar D, Lautenschläger C, Hansen G, et al. Simultaneous expression of cathepsins b and K in pulmonary adenocarcinomas and squamous cell carcinomas predicts poor recurrence-free and overall survival. *Lung Cancer* (2009) 64(1):79–85. doi: 10.1016/j.lungcan.2008.07.005

22. Brubaker KD, Vessella RL, True LD, Thomas R, Corey E. Cathepsin K mRNA and protein expression in prostate cancer progression. *J Bone Miner Res* (2003) 18(2):222–30. doi: 10.1359/jbmr.2003.18.2.222

23. Xu H, Ma Y, Zhang Y, Pan Z, Lu Y, Liu P, et al. Identification of cathepsin K in the peritoneal metastasis of ovarian carcinoma using *in-silico*, gene expression analysis. *J Cancer* (2016) 7(6):722–9. doi: 10.7150/jca.14277

24. Petricevic SJ, Pavlovic A, Capkun V, Becic K, Durdov MG. Cathepsin K expression in melanoma is associated with metastases. *Histol Histopathol* (2017) 32 (7):711–6. doi: 10.14670/hh-11-833

25. Le Gall C, Bellahcène A, Bonnelye E, Gasser JA, Castronovo V, Green J, et al. A cathepsin K inhibitor reduces breast cancer induced osteolysis and skeletal tumor burden. *Cancer Res* (2007) 67(20):9894–902. doi: 10.1158/0008-5472.Can-06-3940

26. Kleer CG, Bloushtain-Qimron N, Chen YH, Carrasco D, Hu M, Yao J, et al. Epithelial and stromal cathepsin K and CXCL14 expression in breast tumor progression. *Clin Cancer Res* (2008) 14(17):5357–67. doi: 10.1158/1078-0432.Ccr-08-0732

27. Loberg RD, Gayed BA, Olson KB, Pienta KJ. A paradigm for the treatment of prostate cancer bone metastases based on an understanding of tumor cell-microenvironment interactions. *J Cell Biochem* (2005) 96(3):439–46. doi: 10.1002/jcb.20522

28. Gaculenko A, Gregoric G, Popp V, Seyler L, Ringer M, Kachler K, et al. Systemic PPARγ antagonism reduces metastatic tumor progression in adipocyte-rich bone in excess weight Male rodents. *J Bone Miner Res* (2021) 36(12):2440–52. doi: 10.1002/jbmr.4422

29. Liang W, Wang F, Chen Q, Dai J, Escara-Wilke J, Keller ET, et al. Targeting cathepsin K diminishes prostate cancer establishment and growth in murine bone. *J Cancer Res Clin Oncol* (2019) 145(8):1999–2012. doi: 10.1007/s00432-019-02950-y

30. Jensen AB, Wynne C, Ramirez G, He W, Song Y, Berd Y, et al. The cathepsin K inhibitor odanacatib suppresses bone resorption in women with breast cancer and established bone metastases: results of a 4-week, double-blind, randomized, controlled trial. *Clin Breast Cancer* (2010) 10(6):452–8. doi: 10.3816/CBC.2010.n.059

31. Zhu H, Guo J, Shen Y, Dong W, Gao H, Miao Y, et al. Functions and mechanisms of tumor necrosis factor-α and noncoding RNAs in bone-invasive pituitary adenomas. *Clin Cancer Res* (2018) 24(22):5757–66. doi: 10.1158/1078-0432.Ccr-18-0472

32. Liu H, Wang G, Gu W, Mu Y. Cathepsin K: The association between cathepsin K expression and sphenoid sinus invasion of pituitary adenomas. *Med Hypotheses* (2016) 97:88–9. doi: 10.1016/j.mehy.2016.10.013

33. Brochier S, Galland F, Kujas M, Parker F, Gaillard S, Raftopoulos C, et al. Factors predicting relapse of nonfunctioning pituitary macroadenomas after neurosurgery: a study of 142 patients. *Eur J Endocrinol* (2010) 163(2):193–200. doi: 10.1530/eje-10-0255

34. Yang K, Zhang Z, Li Y, Chen S, Chen W, Ding H, et al. Expression and distribution of HIF-1α, HIF-2α, VEGF, VEGFR-2 and HIMF in the kidneys of Tibetan sheep, plain sheep and goat. *Folia Morphol (Warsz)* (2020) 79(4):748–55. doi: 10.5603/FM.a2020.0011

35. López C, Callau C, Bosch R, Korzynska A, Jaén J, García-Rojo M, et al. Development of automated quantification methodologies of immunohistochemical markers to determine patterns of immune response in breast cancer: a retrospective cohort study. *BMJ Open* (2014) 4(8):e005643. doi: 10.1136/bmjopen-2014-005643

36. Costantini V, Sidoni A, Deveglia R, Cazzato OA, Bellezza G, Ferri I, et al. Combined overexpression of urokinase, urokinase receptor, and plasminogen activator inhibitor-1 is associated with breast cancer progression: an immunohistochemical comparison of normal, benign, and malignant breast tissues. *Cancer* (1996) 77(6):1079–88. doi: 10.1002/(sici)1097-0142(19960315)77:6<1079::aid-cncr12>3.0.co;2-z

37. Saftig P, Hunziker E, Wehmeyer O, Jones S, Boyde A, Rommerskirch W, et al. Impaired osteoclastic bone resorption leads to osteopetrosis in cathepsin-k-deficient mice. *Proc Natl Acad Sci U.S.A.* (1998) 95(23):13453–8. doi: 10.1073/pnas.95.23.13453

38. Christensen J, Shastri VP. Matrix-metalloproteinase-9 is cleaved and activated by cathepsin K. *BMC Res Notes* (2015) 8:322. doi: 10.1186/s13104-015-1284-8

39. Yang H, Heyer J, Zhao H, Liang S, Guo R, Zhong L. The potential role of cathepsin K in non-small cell lung cancer. *Molecules* (2020) 25(18) 4136. doi: 10.3390/molecules25184136

40. Gu X, Peng Y, Zhao Y, Liang X, Tang Y, Liu J. A novel derivative of artemisinin inhibits cell proliferation and metastasis *via* down-regulation of cathepsin K in breast cancer. *Eur J Pharmacol* (2019) 858:172382. doi: 10.1016/j.ejphar.2019.05.011

41. Ceylan S, Anik I, Koc K, Kokturk S, Ceylan S, Cine N, et al. Microsurgical anatomy of membranous layers of the pituitary gland and the expression of extracellular matrix collagenous proteins. *Acta Neurochir (Wien)* (2011) 153 (12):2435–2443; discussion 2443. doi: 10.1007/s00701-011-1182-3

42. Deryugina EI, Quigley JP. Tumor angiogenesis: MMP-mediated induction of intravasation- and metastasis-sustaining neovasculature. *Matrix Biol* (2015) 44-46:94–112. doi: 10.1016/j.matbio.2015.04.004

43. Malik MT, Kakar SS. Regulation of angiogenesis and invasion by human pituitary tumor transforming gene (PTTG) through increased expression and secretion of matrix metalloproteinase-2 (MMP-2). *Mol Cancer* (2006) 5:61. doi: 10.1186/1476-4598-5-61

44. Lim SM, Jang HY, Lee JE, Shin JS, Park SH, Yoon BH, et al. Alteration of pituitary tumor transforming gene-1 regulates trophoblast invasion *via* the Integrin/Rho-family signaling pathway. *PloS One* (2016) 11(2):e0149371. doi: 10.1371/journal.pone.0149371

45. Liu X, Ma S, Dai C, Cai F, Yao Y, Yang Y, et al. Antiproliferative, antiinvasive, and proapoptotic activity of folate receptor α-targeted liposomal doxorubicin in nonfunctional pituitary adenoma cells. *Endocrinology* (2013) 154 (4):1414–23. doi: 10.1210/en.2012-2128

46. Barreiros D, Nelson PF, Paula-Silva FWG, Oliveira KMH, Lucisano MP, Rossi A, et al. MMP2 and MMP9 are associated with apical periodontitis progression and might be modulated by TLR2 and MyD88. *Braz Dent J* (2018) 29(1):43–7. doi: 10.1590/0103-6440201801731

47. Yoshida D, Teramoto A. Enhancement of pituitary adenoma cell invasion and adhesion is mediated by discoidin domain receptor-1. *J Neurooncol* (2007) 82 (1):29–40. doi: 10.1007/s11060-006-9246-6

48. Zhao C, Zhang M, Liu W, Wang C, Zhang Q, Li W. β-catenin knockdown inhibits pituitary adenoma cell proliferation and invasion *via* interfering with AKT and gelatinases expression. *Int J Oncol* (2015) 46(4):1643–50. doi: 10.3892/ijo.2015.2862

49. Zhu L, Yu H, Liu SY, Xiao XS, Dong WH, Chen YN, et al. Prognostic value of tissue inhibitor of metalloproteinase-2 expression in patients with non-small cell lung cancer: a systematic review and meta-analysis. *PloS One* (2015) 10(4): e0124230. doi: 10.1371/journal.pone.0124230

50. Chen WQ, Yang SJ, Xu WX, Deng F, Wang DD, Tang JH. Bioinformatics analysis revealing prognostic significance of TIMP2 gene in breast cancer. *Med (Baltimore)* (2021) 100(42):e27489. doi: 10.1097/md.0000000000027489

51. Li Z, Jing Q, Wu L, Chen J, Huang M, Qin Y, et al. The prognostic and diagnostic value of tissue inhibitor of metalloproteinases gene family and potential function in gastric cancer. *J Cancer* (2021) 12(13):4086–98. doi: 10.7150/jca.57808

52. Wang W, Li D, Xiang L, Lv M, Tao L, Ni T, et al. TIMP-2 inhibits metastasis and predicts prognosis of colorectal cancer *via* regulating MMP-9. *Cell Adh Migr* (2019) 13(1):273–84. doi: 10.1080/19336918.2019.1639303

53. Sato H, Takino T. Coordinate action of membrane-type matrix metalloproteinase-1 (MT1-MMP) and MMP-2 enhances pericellular proteolysis and invasion. *Cancer Sci* (2010) 101(4):843–7. doi: 10.1111/j.1349-7006.2010.01498.x

54. Stetler-Stevenson WG. The tumor microenvironment: regulation by MMP-independent effects of tissue inhibitor of metalloproteinases-2. *Cancer Metastasis Rev* (2008) 27(1):57–66. doi: 10.1007/s10555-007-9105-8

55. Li C, Zhu H, Zong X, Wang X, Gui S, Zhao P, et al. Experience of trans-nasal endoscopic surgery for pituitary tumors in a single center in China: Surgical results in a cohort of 2032 patients, operated between 2006 and 2018. *Clin Neurol Neurosurg* (2020) 197:106176. doi: 10.1016/j.clineuro.2020.106176

56. Zielinski G, Ozdarski M, Maksymowicz M, Szamotulska K, Witek P. Prolactinomas: Prognostic factors of early remission after transsphenoidal surgery. *Front Endocrinol (Lausanne)* (2020) 11:439. doi: 10.3389/fendo.2020.00439

57. Omar AT, DG M, Goguen J, JM L, Rotondo F, Kovacs K, et al. Resection of the medial wall of the cavernous sinus in functioning pituitary adenomas: Technical note and outcomes in a matched-cohort study. *Clin Neurol Neurosurg* (2020), 200: 106306. doi: 10.1016/j.clineuro.2020.106306

Frontiers in Oncology

Advances knowledge of carcinogenesis and tumor progression for better treatment and management

The third most-cited oncology journal, which highlights research in carcinogenesis and tumor progression, bridging the gap between basic research and applications to imrpove diagnosis, therapeutics and management strategies.

Discover the latest Research Topics

See more →

Frontiers

Avenue du Tribunal-Fédéral 34
1005 Lausanne, Switzerland
frontiersin.org

Contact us

+41 (0)21 510 17 00
frontiersin.org/about/contact